DEPARTMENT OF TRANSPORTATION

Long-term Testing and Analysis on Asphalt Mix RA Field Sections

Jo E. Sias, Principal Investigator
Department of Civil and Environmental Engineering
University of New Hampshire

April 2025

Final Report NRRA202404

National Road Research Alliance

To get this document in an alternative format or language, please call 651-366-4720 (711 or 1-800-627-3529 for MN Relay). You can also email your request to ADArequest.dot@state.mn.us. Please make your request at least two weeks before you need the document.

Technical Report Documentation Page

1. Report No. NRRA202404	2.	3. Recipients Accession No.
4. Title and Subtitle Long-term Testing and Analysis on Asphalt Mix RA Field Sections		5. Report Date April 2025 6.
7. Author(s) Wang, Z., Sias, J., Dave, E., Hanz, A., Reinke, G.		8. Performing Organization Report No.
9. Performing Organization Name and Address Department of Civil and Environmental Engineering W183, 33 Academic Way Kingsbury Hall University of New Hampshire Durham, NH 03824		10. Project/Task/Work Unit No. 11. Contract (C) or Grant (G) No. (c) 1036343 (wo)1
12. Sponsoring Organization Name and Address Minnesota Department of Transportation Office of Research & Innovation 395 John Ireland Boulevard, MS 330 St. Paul, Minnesota 55155-1899		13. Type of Report and Period Covered Final Report 14. Sponsoring Agency Code
15. Supplementary Notes http://mdl.mndot.gov/		

16. Abstract (Limit: 250 words)

Asphalt rejuvenators, or recycling agents (RA), are used to incorporate higher amounts of Reclaimed Asphalt Pavement (RAP) in Hot Mix Asphalt (HMA) without detrimentally impacting the long-term performance of the pavement. The National Road Research Alliance (NRRA) Flexible Team constructed field test sections as part of a mill and overlay project in northern Minnesota in August of 2019. These field sections included wearing courses with 40% RAP that incorporate seven different RA products, with the dosage determined by the supplier to meet a target extracted and recovered performance grade (PG) of XX-34. In addition to the RA test sections, there were control sections with 40% RAP and 30% RAP (the maximum level allowed on the remainder of this project). The objective of this research project was to evaluate the effectiveness of the seven RA products over time and evaluate their performance as compared to the control mixtures. This was accomplished through a combination of binder (chemical and rheological) and mixture characterization and performance testing using different laboratory aging levels, field core testing, and performance monitoring of the field sections over time. This report documents the results after four years in service with cores taken annually. The study showed that all RAs exhibit improved rheological properties in 1-year field cores. However, the benefits of RA diminish with field aging, and after four years, some RAs show comparable properties with controls. In terms of mixture properties, the inclusion of RA enhances both rheological properties and fracture and fatigue crack resistance initially.

17. Document Analysis/Descriptors Recycled materials, Rejuvenators, Reclaimed asphalt pavements, Pavement performance		18. Availability Statement No restrictions. Document available from: National Technical Information Services, Alexandria, Virginia 22312	
19. Security Class (this report) Unclassified	20. Security Class (this page) Unclassified	21. No. of Pages 266	22. Price

Long-term Testing and Analysis on Asphalt Mix RA Field Sections

Final Report

Prepared by:

Zheng Wang
Jo E. Sias
Eshan V. Dave
Department of Civil and Environmental Engineering
University of New Hampshire

Andrew Hanz
Gerald Reinke
MTE Services, Inc.

April 2025

Published by:
Minnesota Department of Transportation
Office of Research & Innovation
395 John Ireland Boulevard, MS 330
St. Paul, Minnesota 55155-1899

TABLE OF CONTENTS

LIST OF FIGURES

LIST OF TABLES

LIST OF ABBREVIATIONS

$\|G^*\|$	Complex Shear Modulus
1-Year FC	1-Year Field Core
C=O	Carbonyl Ratio
DCT	Disk-shaped Compact Tension
DSR	Dynamic Shear Rheometer
DTCF	Direct Tension Cyclic Fatigue
E*	Dynamic Modulus
FST	Fracture Strain Tolerance
FTIR	Fourier-transform Infrared Spectroscopy
G_f	Fracture Energy
G_{mm}	Maximum Specific Gravity
$G\text{-}R_m$	Mixture Glover-Rowe Parameter
HWTT	Hamburg Wheel Tracking Test
LTA	Long Term Aging
SVECD	Simplified Viscoelastic Continuum Damage Theory
PAV	Pressure Aging Vessel
RAP	Reclaimed Asphalt Pavement
RA	Recycling Agents
RPM	Reheated Plant Mixture
RTFO	Rolling Thin Film Oven
S_{app}	Fatigue Damage Capacity Index
SARA	Saturates, Aromatics, Resins, and Asphaltenes
STA	Short term Aging
δ	Phase Angle

Executive Summary

Asphalt rejuvenators are used to incorporate higher amounts of Reclaimed Asphalt Pavement (RAP) in Hot Mix Asphalt (HMA) without detrimentally impacting the long-term performance of the pavement. There are many different rejuvenation agents (RAs) products marketed to transportation agencies. However, most of these products have limited field and laboratory test data available to support their effectiveness over time. To address this need, the Minnesota Department of Transportation (MnDOT) and National Road Research Alliance (NRRA) Flexible Team constructed field test sections as part of a mill and overlay project on Trunk Highway 6 (TH6) located in Emily, MN in August of 2019. These field sections include wearing courses with 40% RAP that incorporate seven different RA products, with the dosage determined by the supplier to meet a target extracted and recovered performance grade (PG) of XX-34. In addition to the RA test sections, there were control sections with 40% RAP and 30% RAP (the maximum level allowed on remainder of this project).

The objective of this research project was to evaluate the effectiveness of the seven RA products over time and evaluate their performance as compared to the control mixtures. Samples were collected during construction, cores were taken annually, and distress surveys were conducted for each test section to facilitate binder and mixture characterization and performance testing at different laboratory aging levels.

Significant findings from this research include a detailed examination of the effects of reclaimed asphalt (RA) on binder properties, mixture properties, and field performance. The study shows that all RAs exhibit improved rheological properties in 1-year field cores. However, the benefits of RA diminish with field aging, and after four years, some RAs show comparable properties with controls. In terms of mixture properties, the inclusion of RA enhances both rheological properties and fracture and fatigue crack resistance initially. These benefits decrease with both laboratory and field aging. After four years or extended aging of loose mixes, some RAs lose their improvement in crack resistance and perform comparably to the 30% control. Regarding field performance, distress in the first four years is primarily composed of transverse cracking. Only a few instances of longitudinal cracking appeared in the fourth year and they are believed to be reflective cracking from underlying distress. The ride quality and rutting values are minimal. Regarding Lab-Field Correlations, both the monitored mixture cracking parameter D^R, S_{app} and G-R_m from field cores show a fairly good correlation with field cracking performance. Among binder properties, the cracking properties ΔT_c and G-R parameter, as well as rheological properties like R-Value and glassy modulus, outperform PG grading and exhibit a more significant correlation with field thermal cracking performance. Compared to the physical binder properties, chemical composition parameters show less correlation with field performance. However, %resin and %aromatics demonstrate potential correlation with thermal cracking performance.

Chapter 1: Introduction and Scope

Recycling agents (RAs) are intended to be used to incorporate high amounts of reclaimed asphalt pavement (RAP) in asphalt mixtures without detrimentally impacting the long-term performance of the pavement. RAs are relatively new in the asphalt industry and there are many different products marketed to transportation agencies. However, most of these products have limited field and laboratory test data available to support their effectiveness over time. Several recent research efforts have shown that some products, while effective immediately after production, show rapid decrease in effectiveness with aging (Mohammadafzali et al., 2017; Ziari et al., 2019; Sias et al., 2019; Christensen et al., 2019). Therefore, there is a need for a better understanding of how various RAs perform over time through both laboratory and field evaluations to help guide engineers on the appropriate use of these materials.

The National Road Research Alliance (NRRA) constructed field test sections as part of a mill and overlay project on Trunk Highway 6 (TH6) located in Emily, MN, in August 2019. These field sections include wearing courses with 40% RAP that incorporated seven different RA products, with the dosage determined by the supplier to meet a target extracted and recovered performance grade (PG) of XX-34. In addition to the RA test sections, there were control sections with 40% RAP and 30% RAP (the maximum level allowed on the remainder of this project).

The objective of this research project was to evaluate the effectiveness of the seven RA products over time and evaluate their performance as compared to the control mixtures. This was accomplished through a combination of binder and mixture characterization and performance testing using different laboratory aging levels, field core testing, and performance monitoring of the field sections over time. The outcome of this project is anticipated to provide NRRA with guidance for assessment and use of RAs in asphalt mixtures.

This serves as the final report for the project, summarizing the research testing results analysis and outcomes from this project. Chapter 1 introduces the project background, research motivation, and objective. Chapter 2 provides a literature review of current knowledge and practice for the recycling agents and RA-treated binder blends. Chapter 3 provides a literature review of current knowledge and practice for evaluating RA-treated mixtures and long-term aging protocols. Chapter 4 presents an overview of the full-scale pavement test sections as well as the aging protocols that were applied in this research project. Chapter 5 presents the detailed methodology and data analysis approach performed in this research. Chapters 6 and Chapter 7 summarize the key laboratory results from all previous project tasks, including testing on binder and mixture materials. Chapter 8 presents the monitored field performance, simulated field performance and lab-field correlation analysis. And finally, Chapter 9 summarizes the project findings and main conclusions as well as recommendations for Phase II of this research.

Chapter 2: Literature Review of RA Treated Binder Blends

A literature review was conducted by the research team, concentrating on the current laboratory evaluation methods used on the RA treated asphalt mixtures. This chapter provides an overview of the definition and various types of RAs, as well as the key factors that affect the performance of the RAs.

2.1 Definition Of Recycling Agents

Asphalt Institute (1986) provided the initial definition of RA as the “organic material with chemical and physical characteristics selected or designed to restore/rejuvenate the properties of aged asphalt to desired specifications”. Typically, RAs are added to binders/mixtures with recycled asphalt material (RAM) for the following purposes: (a) restore the aged binder by decreasing the stiffness for construction purposes and mixture field performance; (b) restore the recycled mixture in terms of durability or resistance to cracking by increasing the flexibility of the binder; (c) provide sufficient additional binder to coat the recycled and base aggregates; and (d) provide sufficient additional binder to satisfy mix design volumetrics requirements (Epps et al. 1980; Newcomb and Epps 1981; Newcomb et al. 1984; Kandhal and Mallick 1997; Epps Martin et al., 2020).

The use of asphalt recycling agents is motivated by economic and environmental benefits: From the economic perspective, using recycling agents reduces costs by replacing expensive virgin binder with cheaper old binder from higher content RAP, and by decreasing the need for natural aggregates and transportation expenses (Willis, J R, et al. 2012). While there are additional costs associated with milling and rejuvenators, some studies suggest that utilizing rejuvenator with high percent RAP can lower the total cost: Based on an economic analysis， increasing the RAP content from 16% to 19% showed a cost reduction of $7.1 per ton, which represents about a 16% cost saving (Im et al.,2014); Increasing RAP content from 20% to 40% resulted in a cost savings of about $10.00 per ton of asphalt mixture, equating to approximately 15% of the production cost. (Epps Martin et al.,2020); Similarly, increasing the RAP content from 0% to 50%, can lower total costs by up to around 35%. (Veeraragavan 2016; Rathore, et al. 2019).

From the environmental perspective, RAP contributes to sustainability by conserving natural resources, reducing landfill use and material waste. Although high-RAP mixtures can generate emissions, advancements in asphalt production technology and modern air pollution controls mitigate these effects, supporting a more sustainable approach to road construction (Hansen, et al., 2011; Zaumanis, et al., 2015).

2.2 Types Of Recycling Agents

Various types of RA have different impacts on the chemical and physical properties of an aged binder, and thus restoring properties of aged binder is a function of the RA type (Little et al. 1981; Lin et al. 2011; Mogawer et al. 2013; Zaumanis et al. 2014a, 2014b). Common sources of RAs that satisfy the purpose of adding RAs include (Epps Martin et al., 2020):

- Aliphatic, Naphthenic, and Paraffinic Rubber Processing Oils—These by-products of lube oil production are not very volatile, are likely compatible with binders at lower concentrations, and are likely low in wax content.
- Maltenes and Resins from Solvent De-Asphalting—These potential RAs are left after butane or propane precipitates the asphaltenes from refinery vacuum tower bottoms.
- Re-refined Waste Lube Oils—While lube oils themselves are cost prohibitive, recovered and recycled lube oils from diesel train engines are potential RAs as long as compatibility is assessed, especially at higher concentrations in highly aromatic binders.
- Derivatives of Lipid-Based Bio-Oils—Bio-based oils from plants such as soybeans, sunflowers, palm and pine trees. They may be either waste vegetable oil products or chemical derivatives of vegetable and/or tall oil.

Early efforts from Rostler and co-workers at Witco/Golden Bear (Rostler and White 1959; Kari et al. 1980) had led to the ASTM D4552 (Standard Classification for Hot-Mix Recycling Agents) specification for RAs, which has been recently revised. This current D4552 specification includes seven different RA grades (RA 0, RA 1, RA 5, RA 25, RA 75, RA 250 and RA 500) defined primarily on the viscosity of the RA. The choice of the recycling agent group usually depends on the hardness/stiffness (typically refers to viscosity or penetration) of the recycled/aged binder; RA 0, RA 1, RA 5, RA 25, and RA 75 are typically considered suitable for mixtures/binders with high quantities of RAM.

A different classification system for recycling agents that is based on the source or chemical composition of the RA was developed by the National Center for Asphalt Technology (NCAT) (2014). The categories in this system are shown in **Table 2-1** with examples of commercially available products for each category.

Table 2-1 Common Types of Recycling Agents

Category	Generic Types (Examples)	Description
Paraffinic Oils	Waste Engine Oil (WEO) Waste Engine Oil Bottoms (WEOB) (Valero VP 165®, Storbit®)	Refined used lubricating oils
Aromatic Extracts	Aromatic Oils (Hydrolene®, Reclamite®, Cyclogen L®, ValAro 130A®)	Refined crude oil products with polar aromatic oil components
Napthenic Oils	(SonneWarmix RJ™, Ergon HyPrene®)	Engineered hydrocarbons for asphalt modification
Triglycerides & Fatty Acids	Waste Vegetable Oil Waste Vegetable Grease Brown Grease Oleic Acid	Derived primarily from vegetable oils
On purpose bio-based products	(Sylvaroad™ RP1000, Hydrogreen® Anova®, CA4®)	Derived from vegetable oils and/or tall oil, a paper industry by-product.

2.3 Factors Affect Performance of Recycling Agents

There are several important factors identified from the literature review that can significantly impact the performance of RA treated asphalt blends and mixtures including the type of RA, appropriate selection of RA dosage, dispersion, and diffusion of the RA into the RAM.

2.3.1 RA Type

RA type plays a significant role in determining the properties of RAs in the binder blends and mixtures. Zaumanis et al. (2013) evaluated the effectiveness of nine different RAs, categorized by their origin (organic blend, refined tallow, paraffinic base oil, aromatic extract, naphthenic flux oil, WEO, WEOB, WEO + Fischer- Tropsch [FT] wax, and distilled tall oil), in restoring the properties of RAP binders by means of evaluating the penetration and the kinematic viscosity of binder blends. Penetration results indicated that the effect of the RA on RAP binders varied significantly among the different products. The use of refined tallow increased the penetration level of the blend to the same level of the base binder with a dosage of 9.7%, while naphthenic flux oil, WEO + FT wax, and WEO bottoms were found to be ineffective at reducing the viscosity of the aged asphalt within the tested dosage rates. Kinematic viscosity test results showed the same trend. In another study, Zaumanis et al. (2014) concluded that bio-based RAs require much lower dosage rates as compared to petroleum-based RAs to reduce the PG grade. Therefore, the appropriate selection of the RA type is of great importance in defining the properties of the RA treated asphalt blends/mixtures.

Another important factor with regard to RA type is compatibility. Compatibility problems may occur when aged binders are blended with base binders and RAs since different types of RAs may not be compatible with the composition of the aged binders (Epps and Holmgreen, 1980; Holmgreen et al. 1982, Epps Martin et al., 2020). Therefore, high compatibility should be sought when combining RAs with base binder and recycled materials in order to ensure good diffusion and restoration (O'Sullivan 2011). The typical methods and tools that can be employed to determine the right RA types for the binders/mixtures containing recycled materials are discussed in detail in chapters 3 and 4.

2.3.2 RA Dosage

When using RAs, it is important to determine the dosage required to restore, as close as possible, the aged binder properties that meet the desired performance properties.

Typically, as the dosage of a RA increases, the impact on the aged binder increases as well. However, that does not mean that adding more RA will always result in good or improved performance. Adding RAs exceeding reasonable dosages will be costly and even potentially detrimental to the performance of the asphalt material. Using high doses of RAs will soften the aged binders to a large extent, which will likely be beneficial with respect to the cracking resistance of the asphalt mixtures. However, that also may negatively impact the mixture's resistance to rutting and permanent deformation, as well as increase the potential for moisture damage. Therefore, the dosage should be carefully optimized. Normally, the dosage of an RA is recommended by the manufacturers based on their experience, and small dosages (typically <5% of total weight of asphalt binder in mixture) are preferred. However, the dose for a particular recycling agent type cannot be the same for mixtures with different types and quantities of recycled materials, since factors such as the base binder source and grade, the level of aging of the recycled materials, and their proportion in the mixture have an effect and should be considered (Arámbula-Mercado et al., 2018).

To determine the suitable RA dose, previous research efforts have evaluated the blending between base binders, recycled binders, and recycling agents, and have developed blending charts. Typically changes in the penetration, viscosity, or PG of the recycled binder blends with increasing doses of the RAs are evaluated and plotted in blending charts (Kaseer et al., 2018). Two types of methods are available in the literature: a) Using blending charts based on the traditional viscosity and/or penetration of the RA treated binder blends with various amounts of RAs to select the appropriate dose to meet the desired viscosity and penetration levels (Little et al., 1981; Zaumanis et al., 2013; Yan et al., 2014; Ali, 2015; Rodríguez-Fernández et al., 2019); and b) Using the PG system: a minimum dose can be determined to ensure sufficient low-temperature cracking resistance (low-temperature PG (PGLT)), while a maximum dose is set to ensure adequate rutting resistance (high-temperature PG (PGHT)) (Shen et al., 2002; Shen et al., 2007; Tran et al., 2012; Zaumanis et al., 2014b; Zhou et al., 2015; Karki et al., 2016; Arámbula-Mercado et al., 2018; Epps Martin et al., 2020).

Figure 2-1 shows an example of using a blending chart to determine the appropriate RA dosage to meet the desired PG grade for a binder blend. As illustrated in **Figure 2-1,** base binder high and low temperature PG (PGHT and PGLT) are plotted in the primary y-axis while the high and low temperature

PGs for RAP binders are indicated in the secondary y-axis, and x-axis shows the increase of the RAP content in the binder blend. Using the blending chart, the PGHT and the PGLT of the binder blend can be estimated based on the RAP content as shown in equation below:

$$PGHT/PGLT_{Blend} = PGHT/PGLT_{Virgin} + (PGHT/PGLT_{RAP} - PGHT/PGLT_{Virgin}) \times RAP_{Content} \quad (2.1)$$

A similar concept can be employed to develop the RA blending chart as illustrated in **Figure 2-2**. The improvement of the RA on the PGLT can be estimated while the PGHT of the binder blend can be also evaluated. NCHRP Project 09-58 has comprehensively evaluated the complex binder blends with various source base binders, recycled materials, and different types of RAs and developed **Equation 2.2** as a reference guideline for estimation of the initial RA dose. Blending charts together with Equation 2.2 can be used to evaluate the RA dosage effect on the PG of binder blend and further determine the appropriate RA dosage for the binder blend. As shown in **Figure 2.2**, the selected dosage of the example binder blend is 9.5% by the binder weight, which provides a good low temperature performance with ΔTc (difference between the critical temperature determined by creep stiffness (S) and the relaxation rate (m)) = -3.0 ˚C, while also meeting the target PGHT of 70 ˚C.

$$\text{Recycling Agent Dosage} = (PGHT_{Blend} - PGHT_{Target})/1.7 \quad (2.2)$$

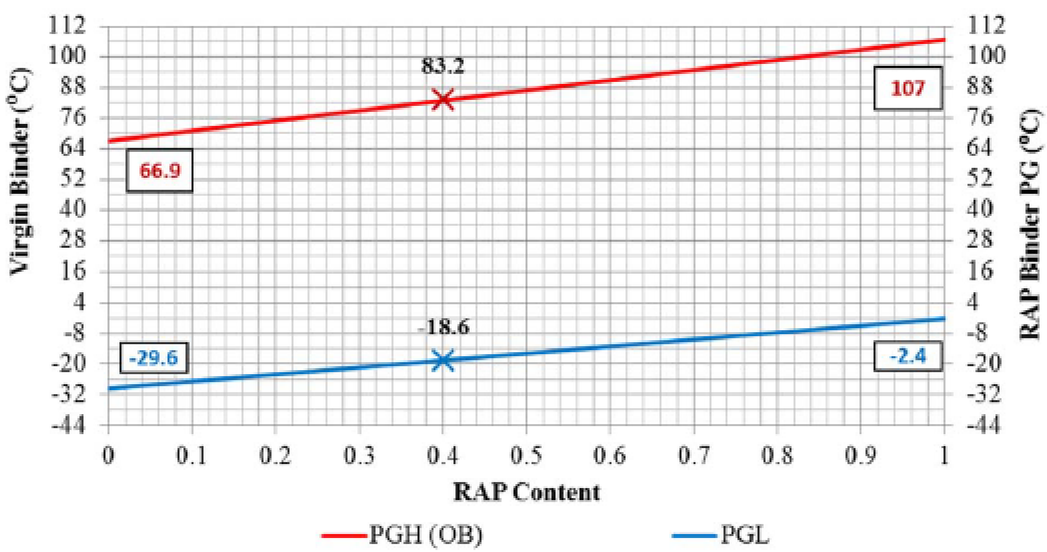

Figure 2-1 Example of a RAP Blending Chart (Munoz et al., 2018)

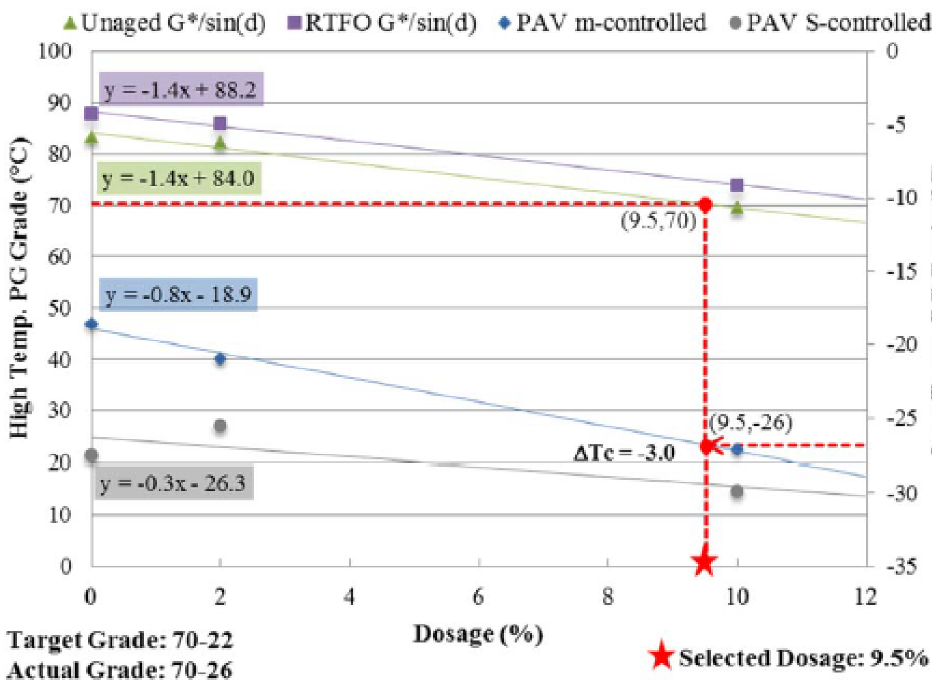

Figure 2-2 Example of a RA Blending Chart (Munoz et al., 2018)

The method of using blend charts to meet binder penetration, viscosity and PG specification provides agencies and researchers a valuable way to determine the RA dosage, but such an approach is limited to assessing the effects of RAs on binders' experimental or rheological properties. Due to the complexity in current asphalt binders and mixtures that contain binders from various sources, recycled asphalt material from different locations and regions, various type of asphalt binder modifiers, potential uses of re-refined engine oil bottom (REOB) and bio-additives, these methods based only on the traditional binder tests (e.g. penetration and Dynamic Shear Rheometer (DSR) temperature and frequency sweeps) may not be sufficient to fully reflect the behavior of complex asphalt blends and mixtures for determination of the appropriate RA type and dosage. Therefore, other methods and tools have been developed or employed to evaluate the asphalt blends and mixtures containing recycled asphalt materials and RAs. They have been used on a limited basis to determine appropriate RA types and RA dosages. These methods and tools are discussed in detail in chapters 3 and 4.

2.3.3 Dispersion and Diffusion of RAs

The effectiveness or performance of the RA also relies on the working mechanism when adding the RAs into the blends and mixtures. In general, the working mechanism of RAs depends on the following processes (Tran et al. 2012):

- Uniform dispersion of the RA within the binder or mixture.
- Diffusion of the RA into the film of the aged binder.

Dispersion is mixing caused by physical processes. The RA will uniformly be dissipated throughout the base binder and the mixture by mechanical mixing. Thus, the efficiency of the RA in terms of dispersion in asphalt mixtures is a function of mixing time. The longer the mixing time the better the dispersion of the RA in the blends or mixtures (Lee et al. 1983; Epps Martin et al. 2020).

The second important factor for determining RA efficiency is diffusion. Diffusion is the process where a constituent moves from a higher concentration to a lower concentration. For the diffusion mechanism, the RA spreads into the aged binder in the following four steps (Carpenter and Wolosick 1980):

1. The RA forms a very low viscosity layer that surrounds the aged binder that is coating the recycled material particles.
2. The RA begins to penetrate into the aged binder layer, softening the aged binder. The amount of the RA surrounding the recycled material particles decreases as penetration continues.
3. Penetration of the RA into the aged binder continues, decreasing the viscosity of the inner layer and increasing the viscosity of the outer layer of the recycled material particle.
4. Equilibrium is approached after a certain time.

Studies (Oliver, 1975; Wang et al., 2017) have reported that rate of diffusion can be accelerated with increased mixing and compaction temperatures. In addition, the diffusion process is also affected by the type and dose of the RA, method of RA introduction into mix (such as, pretreating RAP, blending method of RA with base binder [terminal blended versus in-line blended at plant] or direct addition of RA into mixing drum), and the rheological and chemical properties of the aged binder. The diffusion of a less viscous RA added in high dose to a softer aged binder is expected to be better than the diffusion of a highly viscous recycling agent added in low dose to an extremely aged binder. It is also important to highlight that the method of adding the RA in the asphalt mixture has an influence on its diffusion, and thus its effectiveness in the asphalt mixture. Better diffusion of the RA is expected when it is mixed with the recycled materials before combining them with the base binder and aggregate because there is direct contact with the recycled material to facilitate diffusion into the aged binders (Epps Martin et al. 2020). However, it is also important to note that this process is difficult to practically implement in an asphalt plant where typically the RA is added to the base binder, and subsequently, the blend is added to the combination of base aggregate and the recycled materials (Tran et al., 2012).

In summary, the efficiency of the RA depends on both dispersion and diffusion processes. The recycling agent should be properly diffused and dispersed into the base and RAP/RAS binders after it is added. If the RA is not evenly distributed in the recycled mixture, the mixture may have poor rutting performance at high temperature, poor cracking resistance at low temperature, and/or high moisture susceptibility. Better diffusion of the RA is expected when it is mixed directly with the recycled materials, as compared to adding the RA to the base binder, and the rate of diffusion can be accelerated with increased mixing and compaction temperatures.

2.4 Current Methods and Practices for Evaluation of RA Treated Binder Blends

2.4.1 Analytical Methods

2.4.1.1 Measurement of the Colloidal Indices

To determine chemical or colloidal composition of binders and binder blends, column chromatography or the SARA separation method can be performed on the binder samples. In this method, asphaltenes are precipitated in n-heptane and separated from n-heptane soluble petrolenes. Afterward, petrolenes are fractionated into saturates, aromatics and resins by descending in a glass chromatographic column. Finally, eluted fractions are recovered by removing the solvent before weighing (Mansourkhaki et al., 2020). **Figure 2-3** shows the typical process for SARA fractionation test.

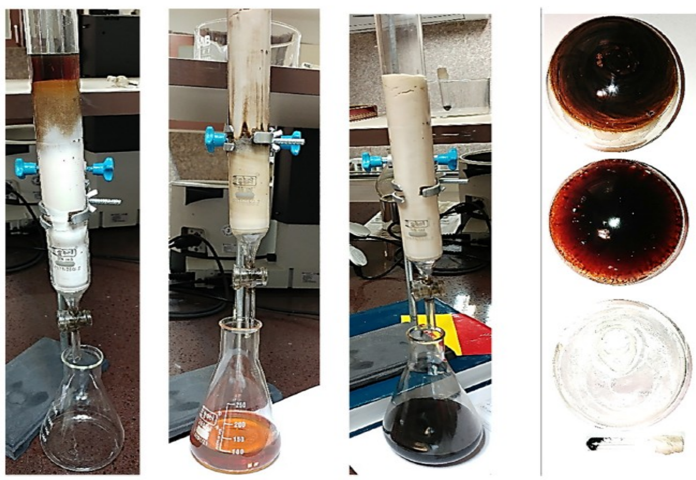

Figure 2-3 SARA Fractionation Test (Column Chromatography) (Mansourkhaki et al., 2020)

Figure 2-4 below shows an example of using SARA analysis to evaluate the diffusion of a recycling agent (petroleum-based) into an aged binder. The SARA tests were conducted on diffused asphalt part at 1 cm (depth of binder sample) location at temperatures of 120 and 140 °C to study the change of binder components during the diffusion process. It can be seen from **Figure 3-2** that aromatic content of asphalt at 1 cm location increased obviously at 120 °C, which showed aromatic component was easier to diffuse into aged asphalt because of lower molecular polarity and moderate molecular weight. At temperature of 140 °C, the aromatic fraction diffuses faster because of quicker Brownian movement (quantity is constantly undergoing small, random fluctuations). Meanwhile, the resin component increased to some extent because of lower viscosity. The saturates component increased slightly with time.

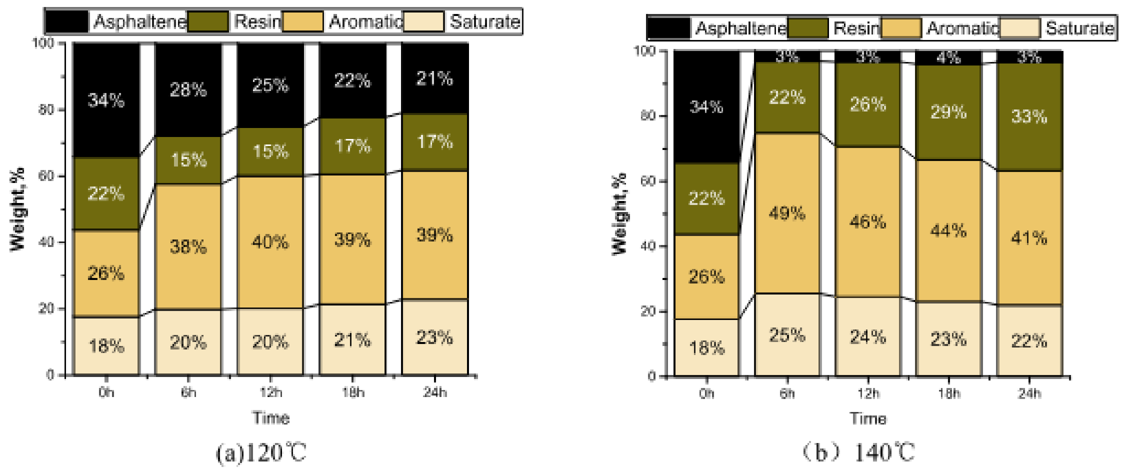

Figure 2-4 SARA Test at 1cm Location at Various Time with (a) 120 °C and (b) 140 °C (Xu et al., 2020)

To characterize the binder colloidal system, several indices such as asphaltene Index (I_A) and Gaestel Index (I_C) have been proposed. These two indices are calculated by Equations 3.1 and 3.2 (Oyekunle et al., 2006; Paliukaite et al., 2014).

$$I_A = (A_S + R)/(A_R + S) \quad (3.1)$$

$$I_C = (A_S + S)/(A_R + R) \quad (3.2)$$

Where:

A_S = denotes the asphaltene content;
S = saturate content;
R = resin content; and
A_R = Aromatic content.

Gaestel Index (I_C), also known as the colloidal index (CI) or colloidal instability index (CII), is one of the most common indices to demonstrate binder colloidal compatibility and stability. If the I_C increases, the colloidal compatibility of the system decreases. A colloidal stable binder has an I_C value between 0.22 and 0.50; the binder is considered unstable for I_C values between 0.5 and 2.7 (Paliukaite et al., 2014; Oliver, 2009). Gaestel Index itself can be used to evaluate and compare the compatibility of different binders and blends, the trend of changing the I_c with change of additives (e.g. RAs) can be also used to evaluate the change of the compatibility of the binder blends (Mansourkhaki et al., 2020).

Figure 2-5 shows the CI values for virgin, aged, and bio-based RA treated asphalts (5% and 10% dosage; added to the PAV aged binder). For both the PEN 70 and SBS modified binder, the CI value of the PAV-aged asphalt is higher than the base binder due to the increase in asphaltene content caused by aging. The CI values of the two bio-RA binders are significantly lower than the PAV aged (control) binder, even lower than the base binder, showing the effectiveness of the adding the RA into the aged binder.

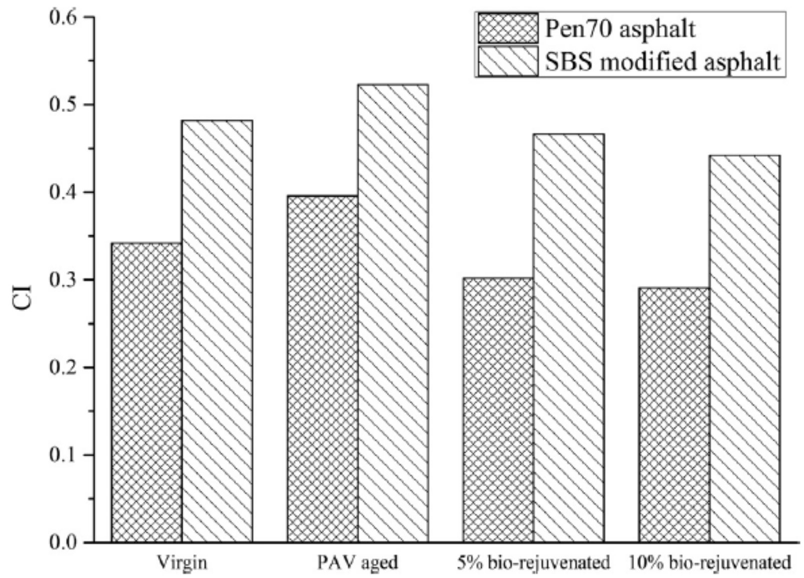

Figure 2-5 Colloidal Index Values of Different Asphalt Binders (Zhu et al., 2017)

Figure 2-6 shows an example of using the Gaestel Index to evaluate the change of the compatibility or stability of complex binder blends with change of RAP content. As shown in the figure, blends modified with softer binder (SB) and polymer modified binder (PMB) tend to move toward upper boundary area (unstable zone) with the increase in RAP content. By adding RAP up to 50%, the colloidal system of the binder modified with SB is still in the stable area. However, for the RA treated binder the trend is not the same. As can be seen in **Figure 2-6,** I_C increases with an increase in RAP content from 25 to 50%. Further increase in RAP content causes a decrease in Gaestel Index, resulting in incompatible blended binders.

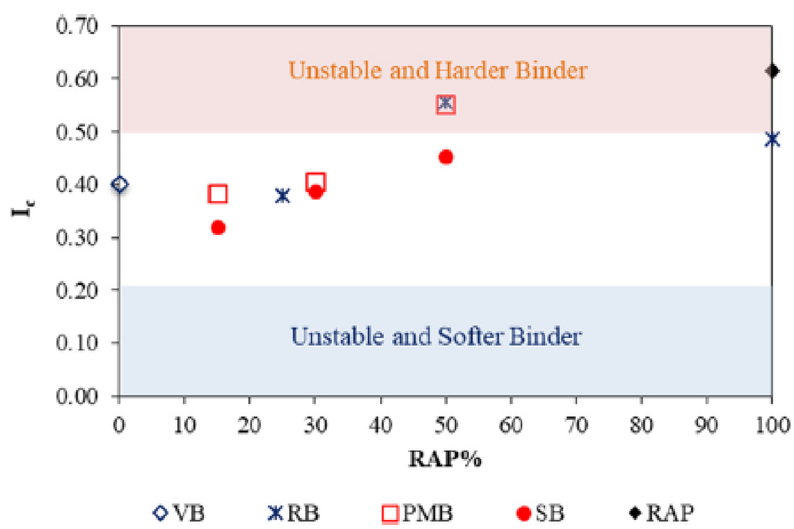

Figure 2-6 I_C Versus RAP Content for RAP Binder, base Binder (VB) and Blends Modified with Soft Binder (SB), RA treated Binder (RB), Polymer Modified Binder (PMB) (Mansourkhaki et al., 2020)

2.4.1.2 Chromatography Analysis

Chromatography is a laboratory technique for separation of a mixture. There are two popular methods in the field of chemistry: the Size Exclusion Chromatography (SEC) and High-performance Liquid Chromatography (HPLC). Size-exclusion chromatography is also called gel-filtration or gel-permeation chromatography (GPC). This method uses porous particles to separate molecules of different sizes. It is generally used to separate biological molecules and to determine molecular weights and molecular weight distributions of polymers, and the separation of molecules which is also called fractionation. HPLC is a technique in analytical chemistry used to separate, identify, and quantify each component in a mixture. It relies on pumps to pass a pressurized liquid solvent containing the sample mixture through a column filled with a solid adsorbent material. HPLC has also been used for separating the components of a complex biological sample or of similar synthetic chemicals from each other.

Chromatography analysis has been recently employed in the asphalt materials field to evaluate the molecular weight and molecular-weight distribution of complex binder blends (Churchill et al., 1995; Geng et al., 2014; Zhu et al., 2017; Cong et al., 2020; Barghabany et al., 2022). **Figure 3-5** below shows an example output from a GPC measurement. From the GPC analysis, a large molecular size (LMS) fraction, a medium molecular size fraction (MMS) and a small molecular size fraction (SMS) are generally divided by molecular weight distribution of asphalt, using the method developed by Daly et al. (2013). The binder component is divided into fractions including the maltenes (molecular weight less than 3,000 g/mol), asphaltenes (molecular weight from 3,000 to 19,000 g/mol), and polymers (molecular weight greater than 19,000 g/mol). The peak of LMS (%) difference was always found around 3,000 g/mol and was considered as the large molecule threshold. The LMS fraction was selected for the components with molecular weights greater or equal to 3,000 g/mol, while the SMS fraction consisted of the proportions with molecular weights less than 1,000 g/mol. The proportion of the fraction is calculated by the ratios of the fraction area to the total area of the chromatogram. A representative chromatogram based on molecular weights is plotted in **Figure 2-7** (Zhao et al., 2019). A RAP/RAS binder typically has a higher proportion of LMS fraction while the base binder and the RA treated binder generally show lower LMS fraction (Daly et al., 2013; Zhao et al., 2019; Ma et al., 2020; Cong et al., 2020).

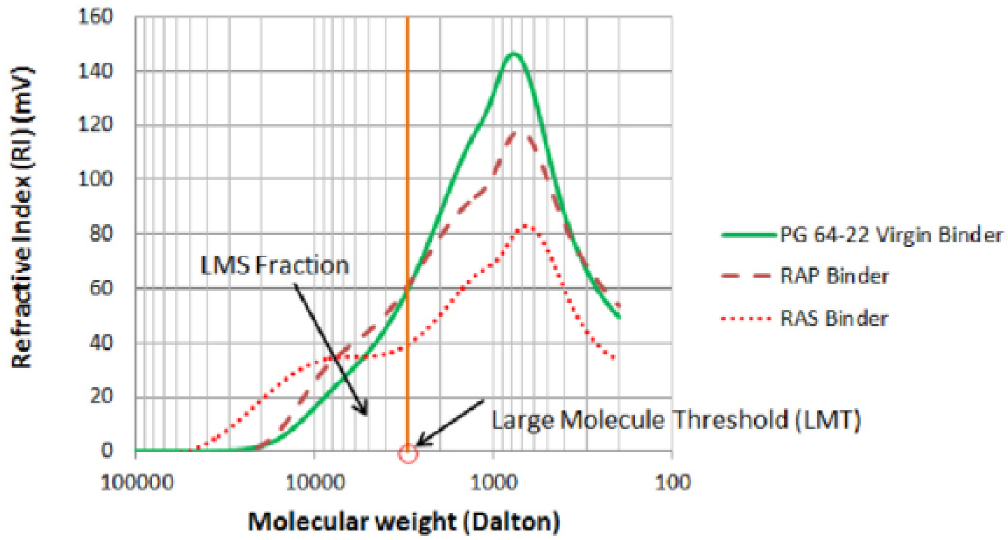

Figure 2-7 GPC Chromatogram Based on Molecular Weights (1 Dalton = 1 g/mol) (Zhao et al., 2019)

Figure 2-8 below shows the measured molecular size distributions for the various binder samples studied by (Huang et al., 2021). As can be seen from the figure below, the 100% RAP binder (AB) shows the highest LMS fraction and the lowest SMS fraction, while the 100% base binder shows the lowest LMS fraction and the highest SMS fraction. Comparing the blends of base binder and RAP binder (S30: 70% virgin+30% RAP; S50: 50% virgin+50% RAP; S80: 20% virgin+80% RAP) and the blends of base binder and RAP binder, and with RA added (bio-based) (B30: 70% virgin+30% RAP+RA; B50: 50% virgin+50% RAP+RA; B80: 20% virgin+80% RAP+RA), at the same RAP content level, the RA treated binder blend clearly shows the lower LMS fraction but higher MMS and SMS fractions.

Figure 2-8 Molecular size distributions of bitumen samples (Huang et al., 2021)

2.4.1.3 Fourier-Transform Infrared (FTIR) Spectroscopy

A Fourier-transform infrared spectrometer emits infrared photons at the sample. These photons can be absorbed by the sample, exciting parts of the molecule to vibrate or rotate. Different molecules absorb different wavelengths of photons depending on their structure and the types of bonds and functional groups in the molecule. Thus, the infrared peak intensities measured from FTIR analysis have been widely used for identifying and characterizing important elements and functional groups in asphalt, such as modified asphalt binder (Lamontagne et al., 2001), base binder mixed with RAP (Pieri et al., 1996; Kudva et al., 1998; Lima et al., 2004; Pasandín et al., 2015; Barghabany et al., 2021), as well as RA treated asphalt binders (Lamontagne et al., 2001; Gulmine et al., 2002; Canto et al., 2006; Pasandín et al., 2015; Cong et al., 2020; Barghabany et al., 2021).

Figure 2-9 below shows an example from the FTIR measurement from Zhu et al. (2017). **Figure 2-9a** shows the FTIR spectra while **Figure 2-9b** shows the functional groups identified from the FTIR analysis for the binders. The oxidation reaction of the chemical components of the asphalt typically generates oxygenic functional groups. The peak-area intensity of the oxygenated groups (C=O and S=O) can be used to reflect the degree of aging and rejuvenation of the asphalt blends. The functional groups indices including carbonyl index and sulfoxide index are calculated as follows (Chen et al., 2014; Gong et al., 2016).

$$I_{C=O} = \frac{Carbonyl\ Peak\ Area\ (1700\ cm^{-1})}{Peak\ Area\ (\sum 2000\ and\ 600\ cm^{-1})} \tag{2.3}$$

$$I_{S=O} = \frac{Sulfoxide\ Peak\ Area\ (1030\ cm^{-1})}{Peak\ Area\ (\sum 2000\ and\ 600\ cm^{-1})} \tag{2.4}$$

Figure 2-9b shows the carbonyl and sulfoxide index values of virgin, aged, and the bio-based RA treated and SBS modified asphalts (5% and 10% dosage of RA; added to the PAV aged binder). Both indices of the PAV-aged asphalt are higher than the base binder due to the aging effect. The index values of the two bio-RA binders are significantly lower than the PAV aged (control) binder, showing the effectiveness of adding the RA into the aged binder.

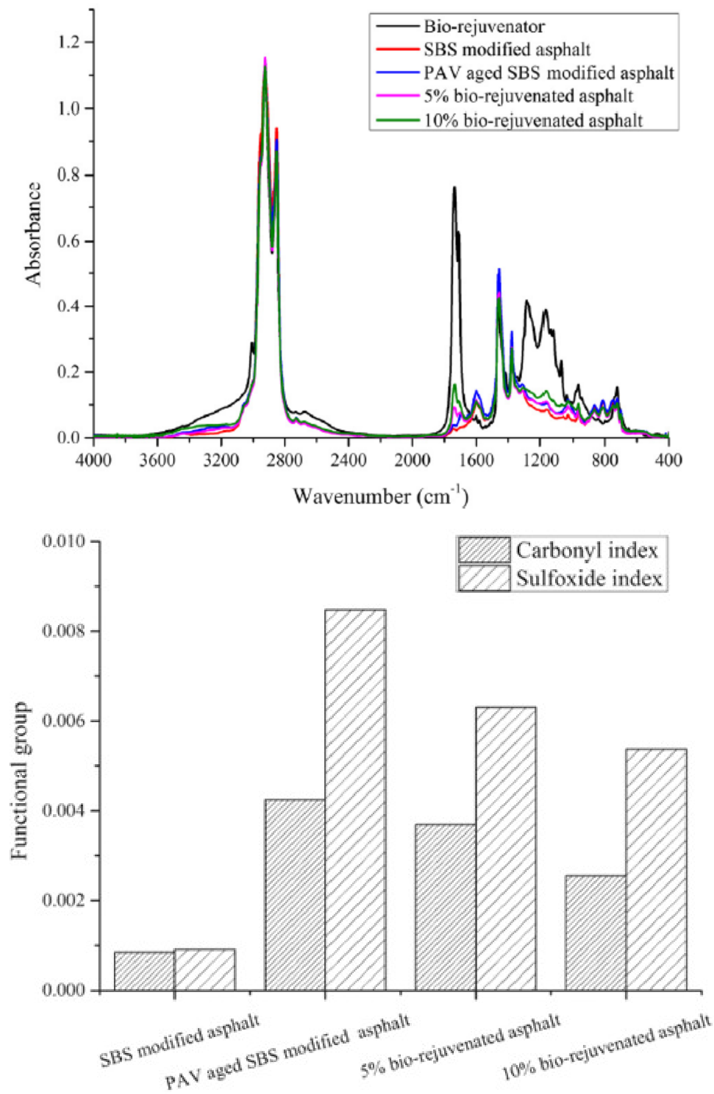

Figure 2-9 (a) Spectra; and b) Carbonyl and Sulfoxide Indexes of Virgin, Aged, and Bio-based RA Treated Asphalts (Zhu et al., 2017)

In addition to the carbonyl index and sulfoxide index, other indices derived from FTIR analysis have been used to characterize the effect of addition of RAs on binder properties. These include the Aliphatic Index

(I_{Al}) and Aromatic Index (I_{Ar}), as well as the Aromatic to Aliphatic Ratio (AAR) (I_{Ar}/I_A). The calculation of these parameters is shown below:

$$I_{Al} = \frac{Aliphatic\ Peak\ Area\ (1460\ cm^{-1}\ and\ 1377\ cm^{-1})}{Peak\ Area\ (\sum A)} \tag{2.5}$$

$$I_{Ar} = \frac{Aromatic\ Peak\ Area\ (1600\ cm^{-1})}{Peak\ Area\ (\sum A)} \tag{2.6}$$

Figure 2-10 below shows an example of using the carbonyl index and sulfoxide index, as well as the I_{Al} and I_{Ar} to evaluate the effects of different RAs on binder properties for a Nebraska Department of Transportation study by Haghshenas et al., 2016. There are seven different binder samples shown, including the control binder(C), blend of the RAP-extracted binder (RAB) and control binder (CR), binder CR with different RAs (R1: Soybean Oil; R2: Hydrolene; R3: Hydrogreen) named as CRR1; CRR2 and CRR3 respectively, and binder blends of RA treated binders with WMA additive (Evotherm) indicated as CWRR1 and CWRR2. As can be seen from **Figure 3-8**, after blending the RAB into the control binder (resulting into binder CR), the two oxidation indices (carbonyl and sulfoxide) and aromatic index increase, whereas aliphatic index decreases. Introducing R1 and R2 to the binder CR results in a decrease in the carbonyl, sulfoxide and aromatic indices and an increase in aliphatic index, which indicates that R1 and R2 can restore the chemical compositions of the CR binder. The impact of R3 is different from the other two RAs; the carbonyl index of CRR3 is greater than that of CR, which is opposite from the binders mixed with the other two RAs. The aliphatic index of the CRR3 decreases as compared to CR; however, the two other RAs increase the aliphatic index of the CR.

In addition, the efficiency of diffusion between RAs and binder including the new binder and aged/recycled binder is a key factor in producing high quality recycled asphalt materials. Oliver et al. (1974) and Karlsson et al. (2003, 2007) have conducted laboratory experiments using FTIR to study the RA diffusion in the RAP binder. The results showed that FTIR was also suitable for analyzing the diffusion process (Karlsson et al., 2003). In addition, the methyl-methylene stretch absorption bands as well as the carbonyl stretch bands were found as potential indices to characterize the RA's diffusion degree in asphalt (Karlsson et al., 2003).

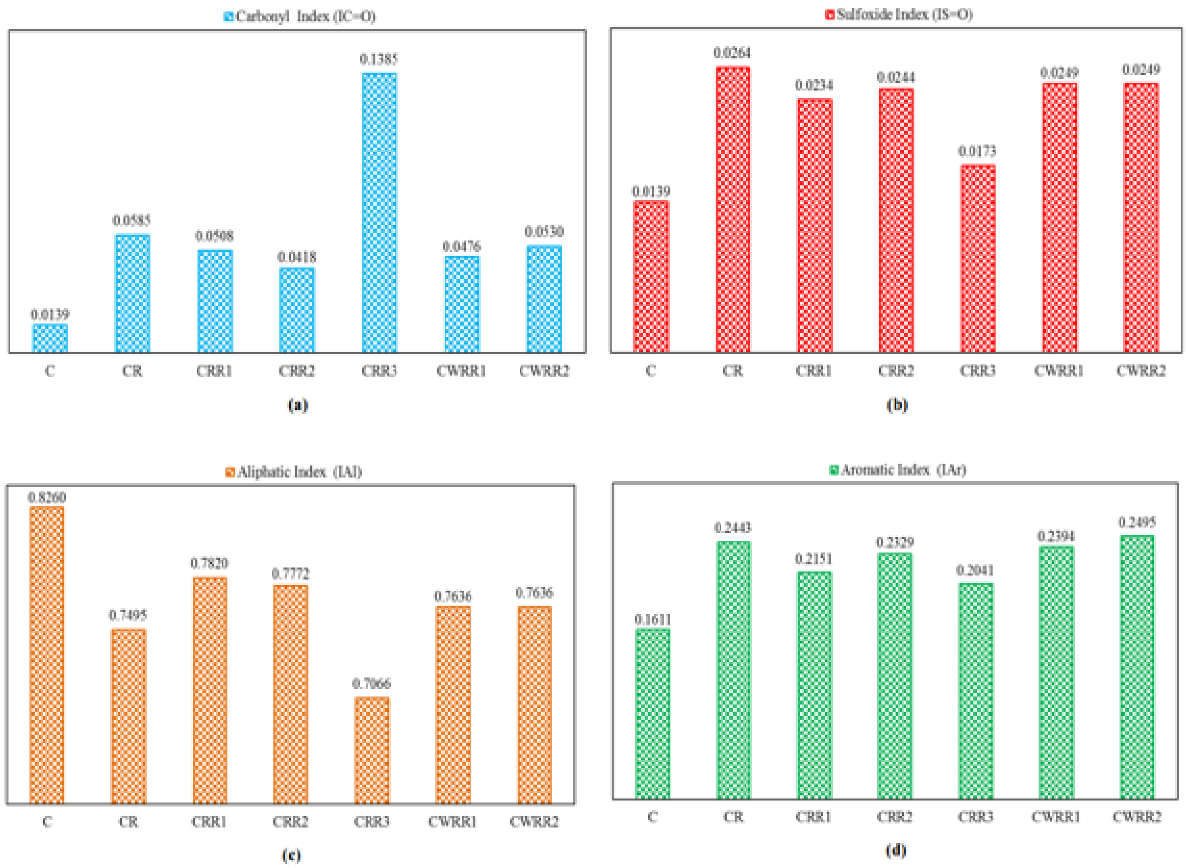

Figure 2-10 FTIR Structural Index: (a) Carbonyl, (b) Sulfoxide, (c) Aliphatic, and (d) Aromatic (Haghshenas et al., 2016)

Recent experience by the research team (MTE services, Inc.) has also shown that in order to better characterize the effect of RAs on binder properties, especially for the bio-based RA, the traditional integration region or peak area for binder samples should be extended by increasing the sulfoxide peak region to lower wavenumbers while moving or extending the carbonyl peak area to higher wavenumbers. **Figure 2-11** below shows an example result measured by the research team. As can be seen from the figure, comparing the two binder samples (unaged and 60 hrs. PAV aged binders indicated by the red and purple curve respectively) and the two bio-based RA (Soy oil and Invigorate indicated by the green and blue curve respectively), the bio-based RA clearly show the higher wavenumber of the carbonyl peak and the lower wavenumber of the sulfoxide peak, and their corresponding integration areas are also slightly shifted. This indicates the importance of revising the traditional FTIR analysis methods for better evaluation of the RA treated binder blends, especially for those with bio-based RA.

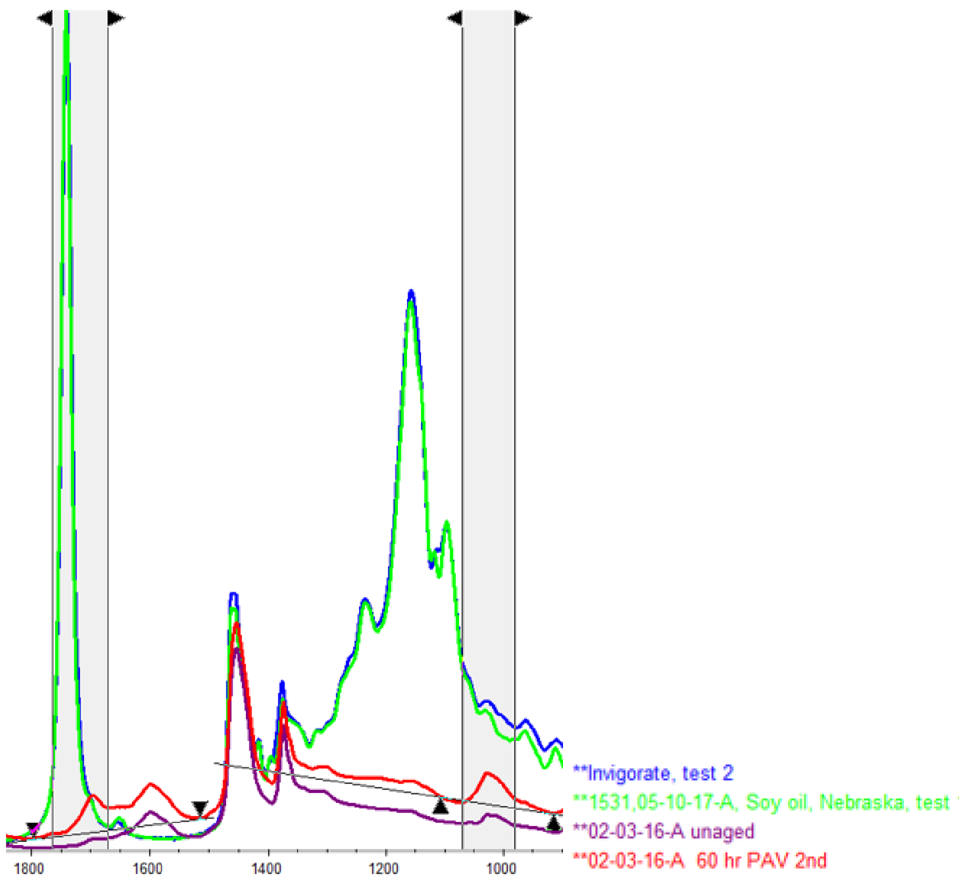

Figure 2-11 Comparisons of the Carbonyl and Sulfoxide Peak/Area of the Bio-based RA with Binder Samples from FTIR Scans

Overall, FTIR analysis has been widely used as a valuable analytical tool to evaluate the infrared peak intensities for identifying and characterizing the key elements and functional groups in complex binder blends.

2.4.1.4 Other Advanced Analytical Methods

There are also many recently developed analytical methods that have been employed to evaluate the properties of complex binder blends and have the potential to be used to characterize binders with RAs. These include X-Ray Fluorescence (XRF), Nuclear Magnetic Resonance (NMR) and Inductively Coupled Plasma Atomic Emission Spectroscopy (ICP-AES).

X-Ray Fluorescence (XRF) is a simple and widely accepted technique for the quantitative analysis of elements, typically from Sodium to Uranium in the Periodic Table. It is very useful to determine the presence of certain elements to help fingerprint the sources of various binders/RAP/RAs from different locations or projects. An energy-dispersive X-ray fluorescence analyzer emits high energy (40 keV) X-ray photons at a sample and measures the energy of the fluorescent photons emitted by the sample (Hesp and Shurvell, 2010). Because samples contain different elements in different proportions, their spectra are different. The XRF technique has been used by many studies in the asphalt field to identify and detect the composition of binders (Barborak et al., 2016; Arnold, 2017). **Figure 2-12** below shows an example of using XRF to detect the amount of recycled engine oil bottoms (REOB) (estimated from the zinc and molybdenum peak heights in the XRF spectrum) within different binder samples.

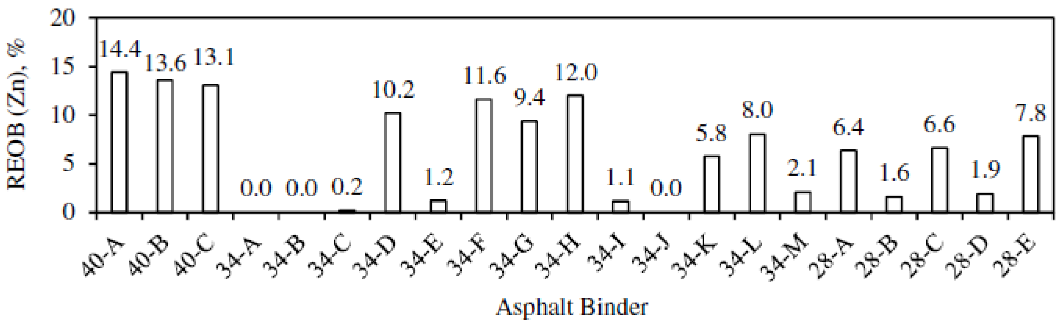

Figure 2-12 REOB Contents in Samples using X-Ray Fluorescence Spectra (Hesp and Shurvell, 2010)

Nuclear magnetic resonance (NMR) involves emitting radio waves at a sample to cause a change in the alignment of nuclei with respect to an applied magnetic field. The signal varies slightly depending on the other atoms and bonds surrounding the NMR active nucleus, which affect the local magnetic field. Results are measured relative to a standard in parts per million (ppm); this measurement is called chemical shift (Paliukaitė et al. 2017). For a binder sample that contains specific elements or organic molecules, the protons in these molecules have different bonds and nuclei surrounding them, and thus will have different chemical shifts as measured by NMR. The NMR technique has been also widely employed for analyzing the effect of aging (Menapace et al., 2015), impact of modifiers (Miknis et al., 1998) and RAs (Menapace et al., 2018) on base binder properties.

Inductively coupled plasma atomic emission spectroscopy (ICP-AES) involves using a nebulizer to spray the sample into an argon plasma as a mist, where the atoms in the sample are excited. When the atoms return to a ground state, they emit photons. Each element has its own characteristic radiation signature, and thus it emits photons at unique wavelengths. This radiation is measured by a detector and can be used to determine the concentrations of each element in the sample. ICP-AES analysis has been used in the asphalt materials field to primarily identify and track the sources of various binders, RAP and RAs for evaluation of the complex binder blends (Zhou et al., 2013; Kaskow et al., 2018).

2.4.2 Morphology Analysis (Microscopy Techniques)

With the progress of research and development of microscopy technology, many techniques have been applied to the microscopic study of asphalt binders, including ultraviolet, infrared and fluorescence microscopy, scanning electron microscopy (SEM), atomic force microscopy (AFM) and so on. In contrast to other technologies, the microscopic technique is instrumental in the observation and quantitative analysis of the asphalt microscale morphology, because of its high resolution and ability to obtain nanomechanical properties (Wang et al., 2014&2015). Ultraviolet (UV) microscopy is a type of light microscopy that utilizes UV light to generate a magnified image of the sample being analyzed. While Infrared (IR) microscopy, also known as infrared microspectroscopy, is a type of light microscopy that uses a source that transmits infrared wavelengths of light to view an image of the sample. Fluorescence microscopy is an optical microscopy technique that uses the emission of fluorescence to study properties of organic or inorganic substances. AFM is an advanced surface structure technology developed on the basis of scanning tunneling microscopy (STM). AFM can obtain surface topography by the interaction between probes and samples of the tested material. As compared to other microcopy techniques, AFM can measure both topography and nanomechanical properties of the given binder samples.

Many recent research efforts (Masson et al., 2006&2007; De Moraes et al., 2010; Dourado et al., 2012; Fischer et al., 2013; Jahangir et al., 2015; Naha et al., 2014; Roy, 2018; Roy et al., 2019) have employed the morphological technique to characterize the surface morphology and estimate nanomechanical properties of various binder blends. They observed three distinct phases (Catana, Peri-phase, and Para-phase) for binder blends, which can be described by the three distinct morphological clusters, namely dispersed, interstitial, and matrix (as indicated in **Figure 3-11a**). The dispersed phase, which is also well-known as the ‘‘bee structures”, are highly visible and stiff with a rippled topography (Leober et al. 1996). The phase around the dispersed phase is the interstitial phase that is less stiff than the dispersed phase. The phase next to the interstitial phase is softer and is called the matrix phase. The dispersed phase along with the interstitial phase of the asphalt binder is colloidally dispersed in a medium of suspension in the matrix system. By investigation of the phase distribution of the binder sample, the compatibility between the binder blend components as well as the diffusion effectiveness of the additives (e.g. modifiers and RAs) into the base binder can be investigated and evaluated.

As seen in **Figure 2-13**, the results from an AFM test indicate the changes of the morphological and nanomechanical properties of the binder sample S1PG64-22+RAP1(40)U (PG 64-22 binder with 40% RAP) before (**Figure 2-13 (a) and (c)**) and after (**Figure 2-13 (b) and (d)**) the application of RA. For these four figures, the top two are morphology, and the bottom two are DMT Modulus calculated based on AFM analysis (Derjaguin et al., 1975; Fischer et al., 2013; Nahar et al., 2014). The effect of RA on morphology was observed from **Figure 2-13 (a) and (b)**. The 40% RAP blend contained several bees of varying sizes. After application of the RA, the bees disappeared completely. By adding the RA, elevated areas were observed from **Figure 2-13 (b)**, which were not exactly so-called ‘‘bee structures,” but might have developed from the ‘‘bees.” The effect of RA was also observed in the modulus maps. The modulus maps shown in **Figure 2-13 (c) and (d)** indicated that overall modulus of 40% RAP blend decreased due to the addition of RA in the RAP binder.

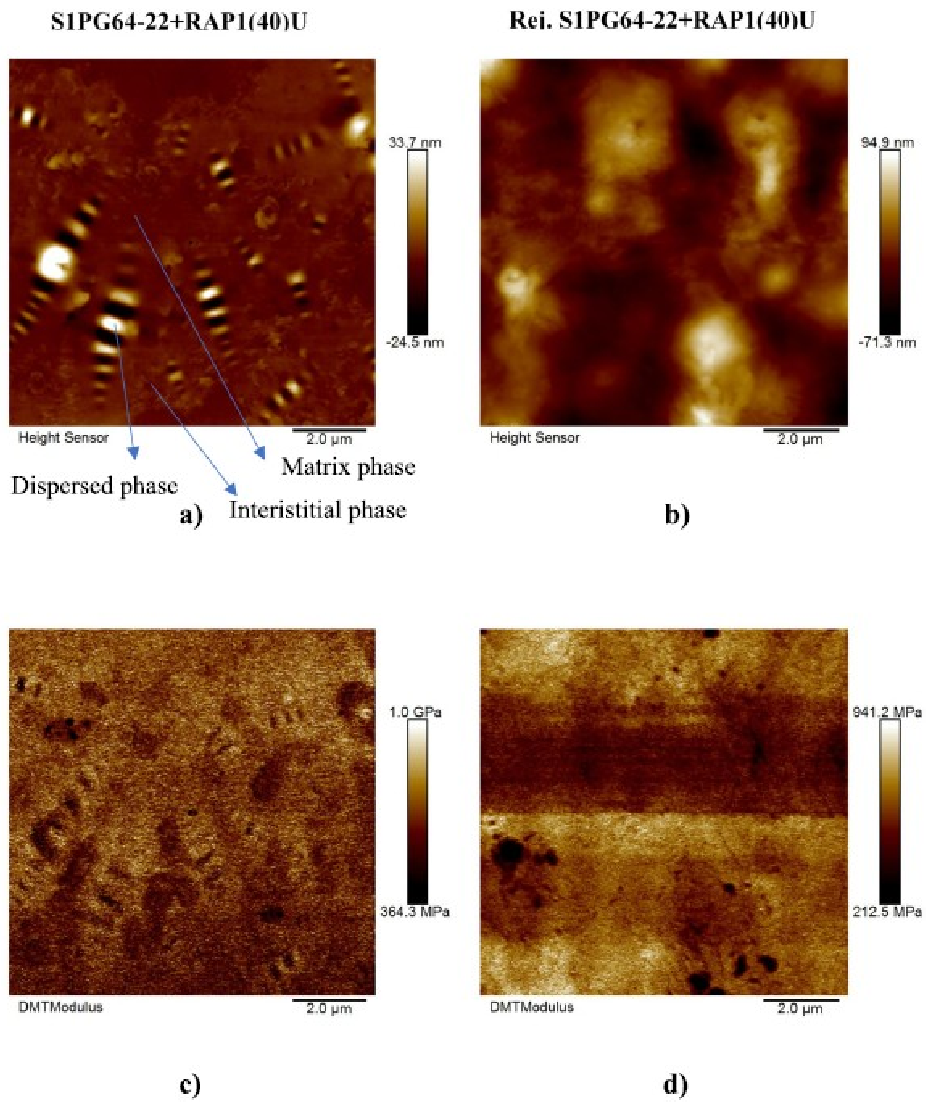

Figure 2-13 AFM-based Maps for base Binder with 40% RAP1 and Its RA Treated Binder Blends: (a)-(b) Surface Morphology; and (c)-(d) DMT Modulus (Hossain et al., 2019)

2.4.3 Thermal Analysis

Use of solvents can affect and modify the molecular association, therefore confounding results of compatibility analysis carried out using analytical methods (discussed in section 3.1) that study asphalt in solution. Thermal analysis methods avoid this issue and have shown promise as a means of investigating various binder properties (Kriz, et. al., 2008).

2.4.4 Differential Scanning Calorimetry (DSC)

Differential scanning calorimetry (DSC) is the most widely used approach to determine the enthalpy related transitions of asphalt binders and of polymeric materials (Harrison et. al., 1992; Planche et. al., 1998). DSC monitors the endothermic or exothermic heat flow of a sample under a controlled temperature program, considering that the heat generation and its rate is proportional to the reaction rate when crosslinking polymers are studied (DiBenedetto et al., 1987) and to thermal events, such as glass transition (Kamal et al., 1973).

DSC analyses have been used successfully to evaluate the glass transition temperature (T_g) of asphalt binders of different origins as well as the effect of various asphaltic fractions (Claudy et. al., 1991&1992; Jimenez-Mateos et. al., 1996), modifiers (Turner et. al., 1997; Adams et. al., 2019; Apostolidis, et. al., 2019) and recycling agents (Lei et. al., 2015) on their glass temperature region. The T_g can be used to interpret thermal-related defects in asphalt pavements, such as thermal cracking. For instance, binders with low T_g accumulate less thermal stress under a given thermal history and thus are more resistant to low temperature cracking.

Figure 2-14 shows the heating flow curve for a control and RA treated binders from the DSC scans. A wide glass transition region was observed for all the binders. A shift in the glass transition region towards lower temperatures occurred for the RA treated binders compared to the control binder. **Table 2-2** lists the glass transition temperature (T_g) and glass transition onset temperature for the various binders evaluated. All RA treated binders showed a decrease in their glass transition temperatures and onset temperatures compared to that of the control binder.

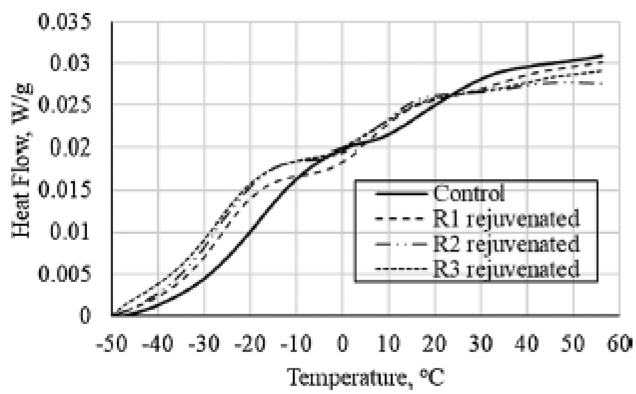

Fig. 8. DSC scan of heating cycle.

Figure 2-14 Glass Transition Regions of Different Binder Samples (Elkashef et al., 2019)

Table 2-2 Binder Testing Plan (Elkashef et al., 2019)

Binder Type	Control	PG58-28 6% R1	PG58-28 6% R2	PG58-28 6% R3
Tg, °C	−20.8	−28.2	−28.6	−29.1
Onset, °C	−35.4	−36.7	−39.9	−40.2

In addition to the glass transition region/temperature, the crystalized fraction (wax crystallization/ precipitation) C(T) can be calculated from the DSC measurement and has been used to evaluate the performance of asphalt binders. Waxy constituents of binders are significant contributors to their temperature sensitivity. At only a few percent by weight, waxes significantly lower viscosity when molten but solidify (gel) the binder when crystalline at cold temperatures (Thomas et al., 1933; Le Guern et al., 2010; Polacco et al., 2012; Rebelo et al., 2014). Higher contents of solid wax in asphalt binder usually contribute to poor performance of the asphalt pavement. Crystallized wax in the asphalt binder generally promotes phase separation (incompatibility between blend components) (Traxler et al., 1952; Romberg et al., 1959; Hesp et al., 2007; Schmets et al., 2010), which can directly lead to lower cracking resistance (Redelius et al., 2015). Further, wax acts as a flocculant for the asphaltenes that are dispersed in the maltenes, so the colloidal system is easily destabilized at cold temperatures, and/or in old age when asphaltene contents increase (Thomas et al., 1933; Rebelo et al., 2014).

Several researchers have also used the Ozawa exponent (n) calculated from the Ozawa function (theory) (by fitting the heat flow curves measured from DSC), typically used to analyze the non-isothermal kinetics for crystallizing systems, to evaluate the performance of asphalt binders. Generally, smaller values of Ozawa exponent (n) indicated slower rates of hardening through crystallization, and the binder is believed to have good thermal stability and is expected to show better thermal cracking performance. **Figure 2-15** below shows a consistent trend between the Ozawa exponent n and the measured thermal cracking on different asphalt pavement sections.

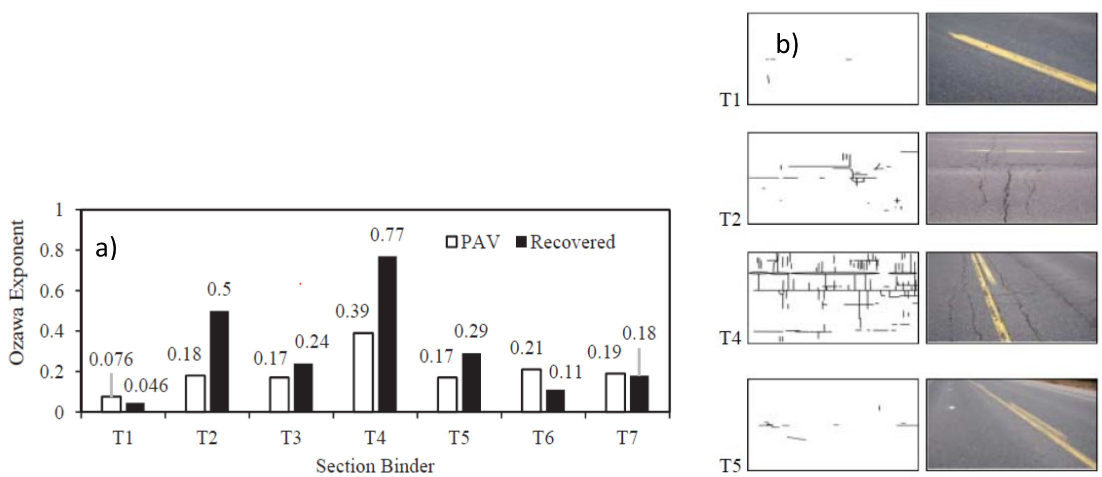

Figure 2-15 (a) Ozawa DSC Exponents Determined on PAV Residues and Recovered Asphalt Samples; (b) Crack Maps and Photographs for Corresponding Sections (Rigg et al., 2017)

In summary, DSC measurement together with the corresponding output parameters have been shown to be a powerful tool to evaluate the thermal-related properties of asphalt binders, especially for complex binder blends.

2.4.5 Thermogravimetric Analysis (TGA)

Thermogravimetric analysis (TGA) is another popular method of characterizing the thermal behavior of polymeric materials. TGA is a process of determining material weight with respect to a combination of temperature and time (Das et al., 2019). Generally, two types of plot are evaluated. A plot of specimen weight against temperature (TGA curve) provides thermal decomposition temperatures with residue amount as a function of temperature. The second plot, a derivative of the TGA curve, indicates mass loss rate depending on an increase in temperature. These curves can also be used to derive other parameters, such as the kinetics of the reaction. Since the thermogravimetric analysis is a powerful technique for the measurement of the thermal stability and weight reduction of polymer composites and biomass, it is also expected to be able to assess the stability of binders under temperature changes, as well as provide estimates volatility of various fractions within the bitumen (volatilization spectra) which is an important factor that impacts the property of the binders (Pauli et al., 1998&1999; Petersen, 2009; Cong et al., 2020).

Figure 2-16 shows example thermal-decomposition (TGA) curves **(Figure 2-16 (a))** and derivative thermogravimetric (DTG) curves **(Figure 2-16 (b))** measured using the TGA method for control and RA treated binders (indicated as R1, and R2 and R3) (Elkashef et al., 2019). The TGA curves, shown in **Figure 2-16 (a)**, were compared to assess the effect of the RAs on the oxidative stability of the binders. The differences between the binders were not considerable at this stage, however the performance of the binder with R2 was very similar to that of the control binder, while at temperatures above 340 °C, the binder with R3 showed better oxidative stability compared to the other two RA treated binders due to the low rate of mass loss. The DTG curves, as shown in **Figure 2-16 (b)**, indicate four peaks at which the rate of mass loss is maximized. The first peak denoting the initial decomposition stage has the least intensity and occurs around 300 °C. The second and third peaks occur above 300 °C and 400 °C. The peaks corresponding to the R3 treated binders are slightly shifted towards higher temperatures compared to the other two RA treated binders, due to the low mass loss rate and the higher oxidative aging stability. The fourth and final peak occurring above 500 °C is due to burning off the remaining char residue of the binders.

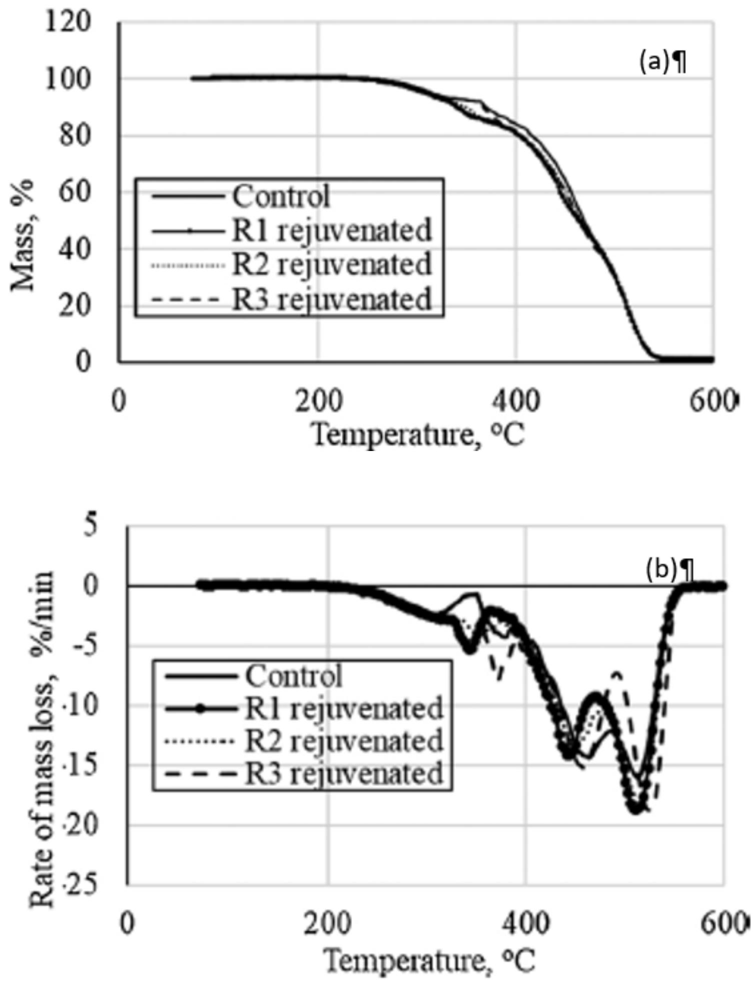

Figure 2-16 (a) Thermogravimetric Curves; and (b) Derivative Thermogravimetric Curves for Study Binders (Elkashef et al., 2019)

2.4.6 Frequency and Temperature Sweep Test by Dynamic Shear Rheometer (DSR) with a 4mm plate

The thermal properties of asphalt binders can also be measured using a Dynamic Shear Rheometer (DSR) with a 4 mm plate (Glaser et al., 2015). This test covers a wide range of temperatures (-40 °C to 50 °C, usually in 3 degree increments near the low temperature PG, and the increased increment of 6-10 °C when the test temperature is above 0 °C), and frequencies (15 frequencies from 100 rad/sec to 0.2 rad/sec), by using the appropriate strain level at each combination of test temperature and frequency. The isotherm tests are conducted from the coldest to the warmest temperature and from the highest to the lowest frequencies. The complex shear modulus and phase angle master curves can be constructed, and multiple rheological parameters can be then calculated and evaluated, including: (1) critical temperatures determined by creep stiffness ($T_c(S)$) and the relaxation rate ($T_c(m)$); (2) performance grade low temperature (PGLT); (3) critical temperature difference (ΔT_c); (4) Glover-Rowe (G-R) parameter; (5) R-value, which can be calculated using either an assumed glassy modulus of 1 x 10^9 Pa or the actual calculated gassy modulus (Anderson et al., 2011; Sui et al., 2011; Elwardany et al., 2019; Zhang, 2020).

In addition to these rheological parameters, the transition temperatures (glass transition temperature (T_g); viscoelastic (crossover) transition temperature (T_t); and the intermediate region temperature range (ΔT_{IR})) can be also measured from the 4 mm DSR test and have correlated well with the measurements from DSC method (Elwardany at el., 2019). These three temperatures are typically calculated from the storage and loss modulus master curves in the temperature domain with a frequency of 10 rad/s or 1.59 Hz (as shown in **Figure 2-17**). The viscoelastic transition temperature (T_t) is the temperature where loss modulus is equal to storage modulus in between the intermediate and terminal region (this temperature is close to the point of gelation, thus can be potentially used to evaluate the compatibility of different component of binder blends). The Intermediate Region Temperature (ΔT_{IR}) is the difference between the viscoelastic temperature and the glassy transition temperature, indicating the "length" of the intermediate "transition" region. Recent studies (Zhang et al., 2019&2020) have employed this method to evaluate the thermal behaviors of the different binder blends. Zhang et al. (2019&2020) proposed that a binder with ΔT_{IR} larger than 60 °C should be avoided due to its high susceptibility to thermal cracking.

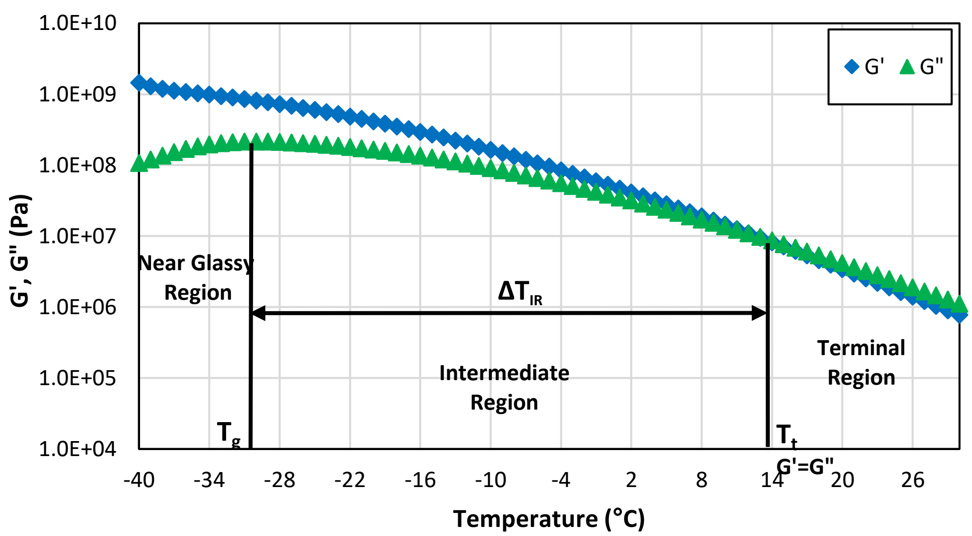

Figure 2-17 T_g, T_t and T_{IR} in G' and G" Master Curve (Temperature Domain)

2.4.7 Binder Performance Tests

Binder performance tests can be directly employed to measure the physical (and mechanical) properties of asphalt materials and to address the primary concerns of the asphalt pavement.

2.4.7.1 Traditional Tests in Superpave Binder Grading System

Common parameters and criteria that are directly measured from the traditional binder tests in the Superpave specification have often been employed for assessing the properties of RA treated binders and comparing the effects of different types and dosages of RA products. These include the ΔT_c

parameter (defined as the difference in critical temperature for the creep stiffness (S) and relaxation rate (m value) passing temperatures from bending beam rheometer (BBR) test), indices from Black space plots which are two dimensional representations of dynamic modulus and phase angle of viscoelastic materials measured from temperatures and frequencies sweep tests performed on the DSR (e.g. the binder Glover-Rowe (G-R) parameter), and master curve shape parameters (such as R-value, the difference between the glassy modulus and equilibrium modulus in logarithmic scale). The advantages of employing these parameters are: (1) They have been extensively used in recent decades and are valuable tools for characterizing binder properties; (2) Studies have proposed threshold values for these parameters through field validation (e.g. ΔT_c = -2.5 °C is typically used as a crack warning limit and ΔT_c = -5.0 °C as the cracking limit; G-R = 180 kPa is proposed as a crack warning limit, G-R = 600 kPa for the development of significant cracking), thus, it is simpler and more convenient for researchers and agencies to evaluate different asphalt materials in a "pass" or "fail" manner.

Figure 2-18 below shows an example illustrating the typical direction of the shifts observed in Black space with the inclusion of recycled materials, RAs, and aging for typical binders without polymer modification (Epps Martin et al., 2020). The Black space shown in the figure is constructed at the temperature and frequency of 15 °C at 0.005 rad/s. A new or base asphalt binder has a relatively low |G*| and high δ, therefore it is located in the lower right corner of the Black space diagram. The inclusion of recycled materials (labeled as recycling in **Figure 2-18**) generally results in an increase in stiffness (|G*|) and reduction in relaxation capability (δ), similar to the effect of laboratory and/or field aging. Conversely, application of the RA (labeled as rejuvenation) as the partial reversal of the impact of aging on asphalt binders from a rheological standpoint, typically leads to the reduction in |G*| and increase in δ as an indication of improved ductility.

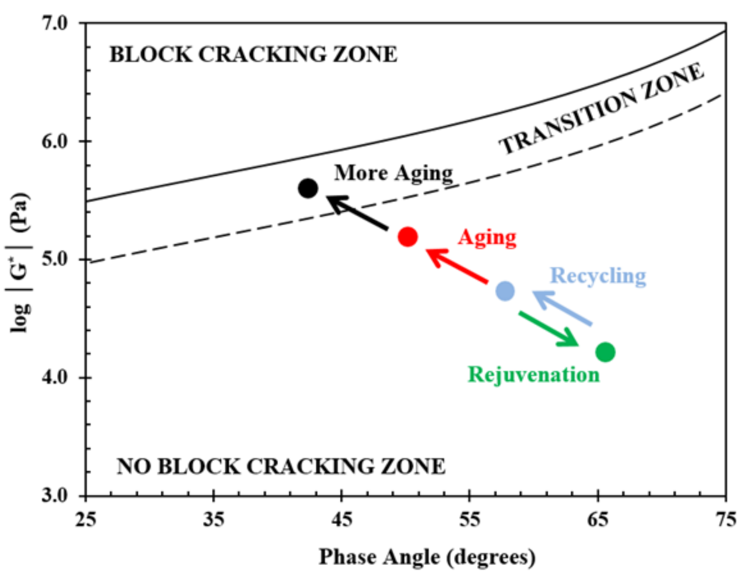

Figure 2-18 Illustration of |G*| and δ Changing with Recycling, Aging, and Rejuvenation in Black Space at 15 °C and 0.005 rad/s (Epps Martin et al., 2020)

Figure 2-19 below shows an example of combining ΔTc and G-R parameter to evaluate the thermal and durability cracking susceptibility of asphalt binders with aging (three conditions included: STA, 5 days@95 °C and 12 days@95 °C) (Zhang et al., 2020). The two red dashed lines represent the cracking warning values for ΔTc and G-R parameter (-2.5 °C for ΔTc ; 180 kPa for G-R parameter) respectively, while the solid red lines represent the cracking limit values for ΔTc and G-R parameter (-5.0 °C for ΔTc ; 600 kPa for G-R parameter). The threshold lines also cut the plot into four zones: safe zone where both ΔTc and G-R parameter are smaller than the significant cracking limit; durability cracking zone where the ΔTc parameter is within the limit, however, the G-R parameter is larger than the limit value; thermal cracking zone where the G-R parameter is within the limit, however, the ΔTc parameter is larger than the limit value; failure zone/significant cracking zone where both parameter exceed the significant cracking limit values. As can be seen from **Figure 2-19**, binder samples gradually move to top left corner (failure zone), indicating the increase in cracking susceptibility after aging. This type of plot could also be used to track the rejuvenation of binders (similar to **Figure 2-19**).

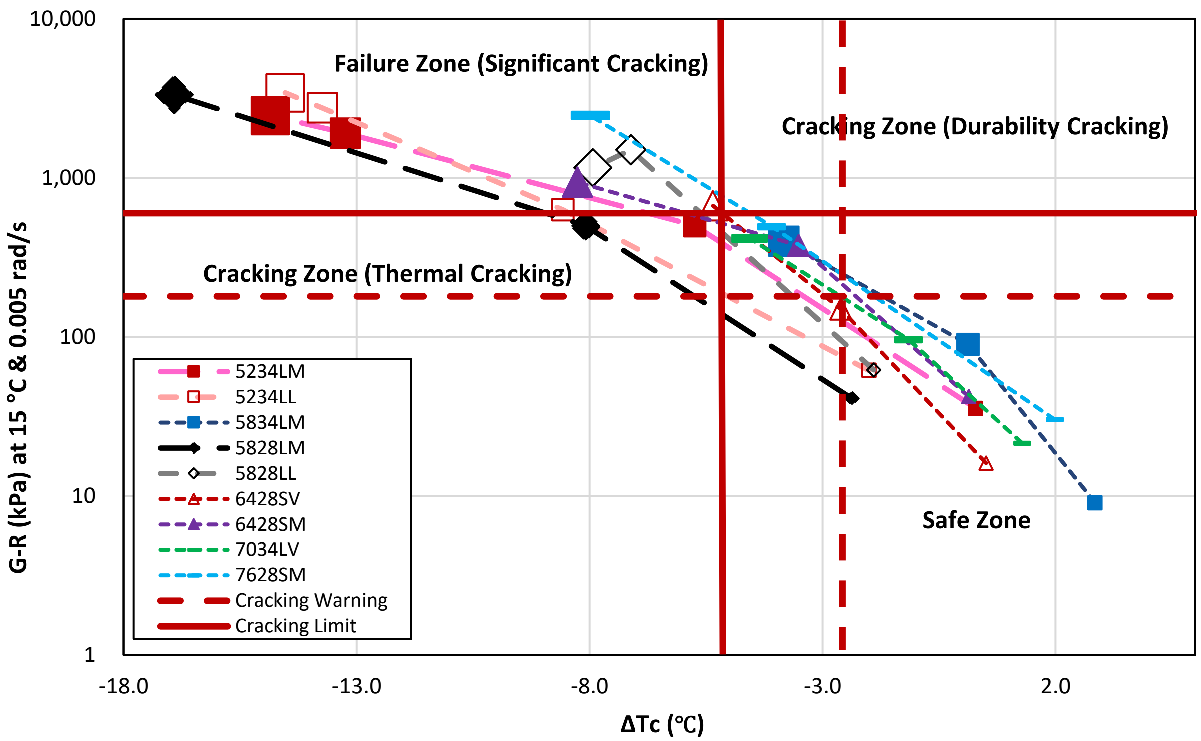

Figure 2-19 Combination of ΔTc and G-R Criteria (marker size increases with increase of aging conditions)（Zhang et al., 2020)

2.4.7.2 Linear Amplitude Sweep (LAS) Test

The LAS test evaluates the ability of the asphalt binder to resist fatigue damage. The LAS test (AASHTO TP101) consists of two steps: first, a frequency sweep is performed to get information about undamaged material properties and evaluate the rheological characteristics of the binder. Second, the damage characteristics of the binder are measured by employing a linear amplitude strain sweep test. Studies (Zhou et al., 2012; Clopotel et al., 2012) have shown that the LAS test is an effective test method to evaluate binder fatigue properties and has been shown to correlate fairly well with the Long-Term Pavement Performance (LTPP) field fatigue cracking data (Hintz et al., 2011).

From the test, the relationship between the number of cycles to failure and the applied strain level can be calculated using the equation below:

$$N_f = A(r_{max})^B \tag{2.7}$$

where *A* and *B* are VECD (viscoelastic continuum damage) model coefficients that depend on the material characteristics, r_{max} is the applied strain. **Figure 2-20** shows the fatigue life of different asphalt binders as obtained from the LAS test from the study conducted by Daryaee et al. (2020). It can be seen from **Figure 2-20**, the RAB (binder extracted and recovered from RAP) has lower fatigue life as compared to other asphalt binders at various strain levels. The '30%RAB +WPMB (waste polymer modified binder)" binder compound exhibits fatigue behavior like that of the control (neat) bitumen. As shown in **Figure 2-20**, use of WPMB alone cannot significantly improve the fatigue performance of the 50%RAB binder blend, however, the combination of WPMB and the oil-based RA can significantly enhance the fatigue performance of the 50%RAB binder as illustrated by the higher N_f value for binder "50%RAB+Rej+WPMB".

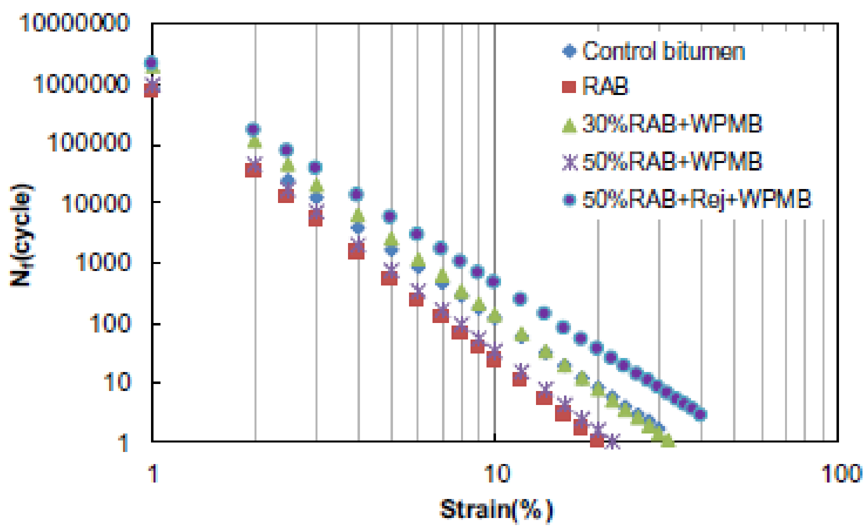

Figure 2-20 Fatigue Life of Different Binder Compounds in the LAS Test (Daryaee et al., 2020)

Zhang et al. (2020) recently developed new parameters from the LAS test to better evaluate the fatigue properties of asphalt binders by incorporating the effect of aging and polymer modifiers on binder properties. These parameters include the Average Reduction in Integrity up to Failure (I_R), Stain Tolerance up to Failure (ε_T) and Strain Energy Tolerance (E_f). The I^R parameter was developed based on the Viscoelastic Continuum Damage (VECD) principle for characterizing material behavior under the repeated loading condition, while the ε_T and E_f parameters were developed from the stress versus strain curve during the test to evaluate the effect of additives more appropriately on binder behavior under the loading conditions. These parameters can be also employed to evaluate the binder blends with different RAs.

2.4.7.3 Multiple Stress Creep Recovery (MSCR) Test

The Multiple Stress Creep Recovery (MSCR) test is the latest improvement to the Superpave Performance Graded (PG) Asphalt Binder specification - providing a new high temperature binder specification methodology that more accurately indicates the rutting performance of the asphalt binder and is blind to modification. A major benefit of the MSCR test, specified as AASHTO M 332, is that it eliminates the need to run tests such as elastic recovery, toughness and tenacity, and force ductility, procedures designed specifically to indicate polymer modification of asphalt binders. A single MSCR test can provide information on both performance and formulation of the asphalt binder.

There are two important parameters that are generally measured from the MSCR test: the non-recoverable creep compliance (Jnr) and MSCR percent (%) recovery. The Jnr is a measure of the amount of residual strain left in the specimen after repeated creep and recovery, relative to the amount of stress applied. The MSCR % recovery is a measure of how much the sample returns to its previous shape after being repeatedly stretched and relaxed. In recent years, this test has been shown to be an effective tool to capture the field rutting performance of the asphalt materials (Anderson et al., 2010; Horan et al., 2011; Zelelew et al., 2011; Morea et al., 2012).

Figure 2-21 below shows an example of MSCR analysis from the study conducted by Wang et al. (2020).

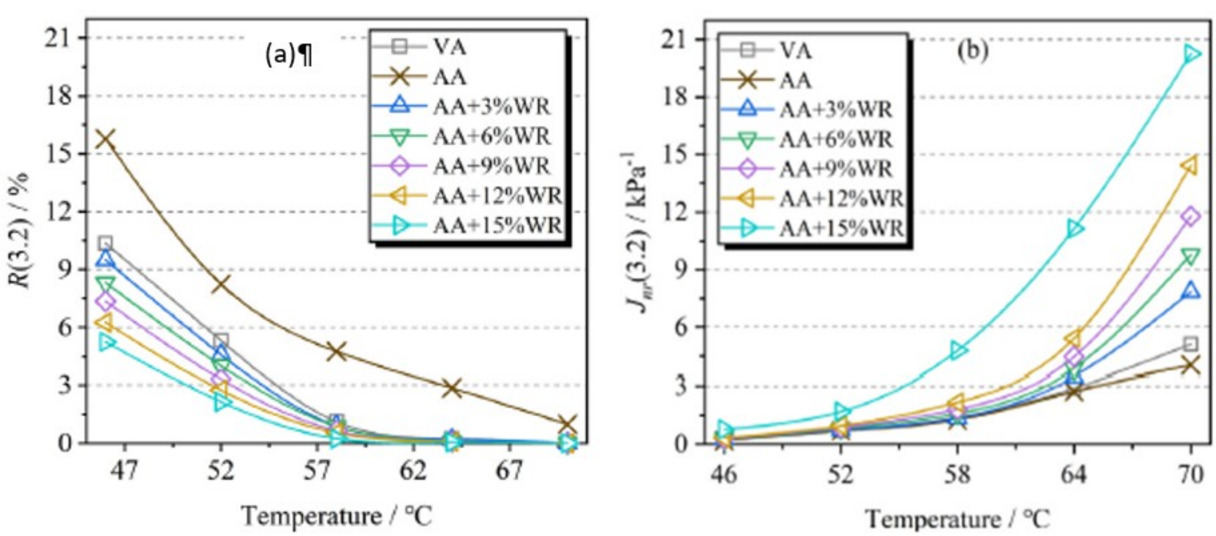

Figure 2-21 **2-21 (a)** presents percent recovery (R) values of various binders at various temperature under stress level of 3.2 kPa. As expected, for all binders (virgin binder (VA), RAP binder (AA), RA binder with different dosages of WR (waste oil extracted from petroleum distillate), percent recovery value decreases as the temperature or stress level increases. As indicated in **Figure 2-21 (a)**, binder AA shows the largest relative R-value due to the aging effect. Obvious reduction in percent recovery can be found for the aged asphalt with an addition of WR, which indicates that the WR has a significant influence on elastic recovery of asphalt binders. When the addition of WR is more than 3%, percent recovery value of aged asphalt could be reduced to a level that is even lower than base asphalt (VA).

Figure 2-21 (b) presents non-recoverable creep compliances (Jnr) of asphalt binder to evaluate its strain response to the stress. This parameter has been widely used to assess deformation resistance under repeated loading at high temperature. As evident in the **Firgure 2-21 (b)**, Jnr value increases as the temperature or stress level increases. Generally, a larger Jnr value corresponds to lower rutting resistance. Aged asphalt (AA) showed the lowest Jnr value, whereas binders with WR addition exhibited a higher Jnr value. When the addition of WR is more than 12%, Jnr value was remarkably increased, which concludes that excessive addition of WR has an adverse effect on the rutting resistance of the RAP binder.

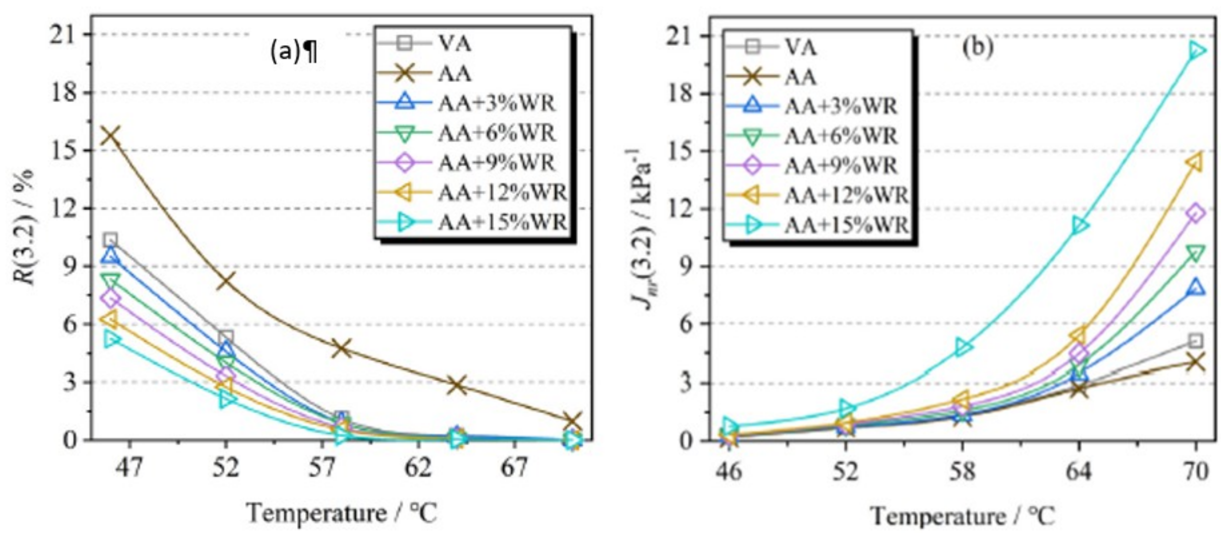

Figure 2-21 (a) Variation of Percent Recovery vs. Temperature; and (b) Variation of Non-Recoverable Creep Compliance vs. Temperature at 3.2 kPa (Wang et al., 2020)

2.4.7.4 Asphalt Binder Cracking Device (ABCD)

The Asphalt Binder Cracking Device has been employed to investigate the low temperature cracking resistance of base asphalts, aged asphalts and RA treated asphalts. The ABCD runs the sample under a gradually reduced temperature, which induces the development of micro-strains caused by temperature stresses (Kim, 2005&2007&2010; Yao et al, 2016). The thermal strains of the virgin, aged and RA treated asphalts during temperature reduction are measured and the crack temperatures (T_c defined as the temperature at which sample fails at a given cooling rate) are determined after a progressive temperature drop. The average cooling rate is typically set as 20 °C/h. The fracture stress of asphalt binders at cracking temperature can be also calculated based on Eq. 3.9.

$$\delta_{AC} = \frac{K * F_{ABCD}}{A_{AC}} = (K * \varepsilon * E_{ABCD} * A_{ABCD})/A_{AC} \quad (2.8)$$

Where:

δ_{AC} = the fracture stress at the cracking temperature, (MPa);

K = the stress concentration factor (approximately 2.0 for the dimensions of ABCD specimen and protrusion);

F_{ABCD} = the thermal force in the ABCD ring, (N);

A_{AC} = the cross-sectional area of the asphalt binder, (m^2);

ε = strain jump, (με);

E_{ABCD} = the modulus of elasticity of the ABCD ring, (Pa);

A_{ABCD} = the cross-sectional area of the ABCD ring, (m^2).

Figure 2-22 shows an example of the crack temperature and fracture stress of asphalts (PG 58-28 base binder (control), 20 hrs PAV aged binder, 20 hrs PAV aged binder with 10%, 15% and 20% bio-RA) measured from the ABCD test. It is found that the application of the bio-RA can increase the fracture stress significantly as compared to the control binders, which indicates that bio-based RA treated asphalts can endure higher thermal stress caused by cooling of asphalt. Comparing the crack temperatures of the study binders, aging increases the crack temperature of asphalt significantly, indicating worse low temperature cracking resistance. However, the application of the bio-RA decreases the crack temperature of aged asphalt to the level of base asphalts or even lower. This can be because the higher content of aromatic components in the bio-oil balances the chemical components of aged asphalt binders, which improves the resistance to cracking at low temperatures.

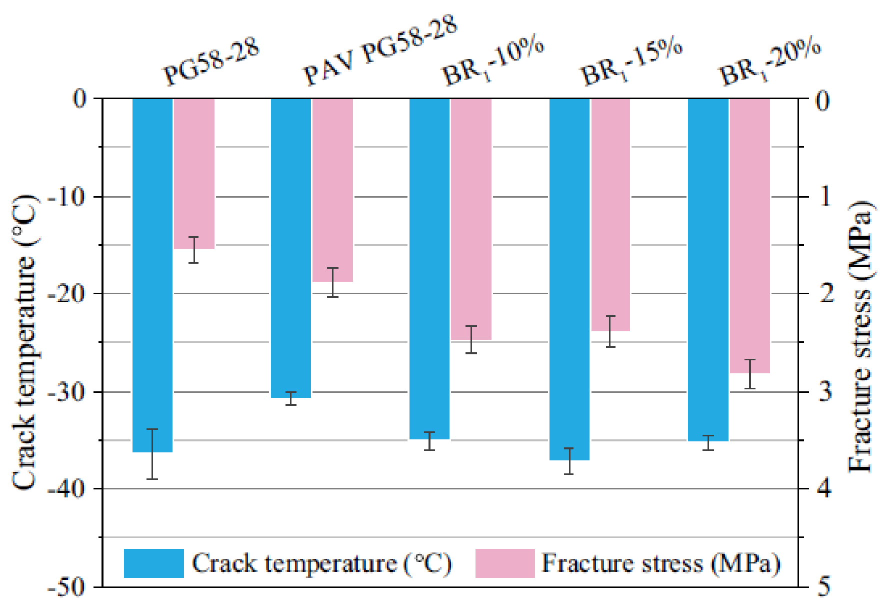

Figure 2-22 Cracking Temperature and Fracture Stress of Asphalts with Base Binder PG 58-28 (Zhang et al., 2019)

The recent NCHRP 09-60 project proposes a novel method to evaluate the thermal performance of asphalt material using the ΔT_c parameter from the BBR measurement and the ΔT_f parameter (difference between $T_C(S)$ from BBR test and T_c from ABCD test). Generally, a binder with a higher value of both parameters is desired. **Figure 2-23** shows an example of how the ΔT_c and ΔT_f measured from the BBR/DSR measurement and ABCD test can be used to evaluate the low temperature performance of asphalt binders. Most modified binders (in red) perform better compared to unmodified binders (in blue). PMAs with poor performance are related to poor compatibility between the modifiers and the base binders (Elwardany et al., 2019).

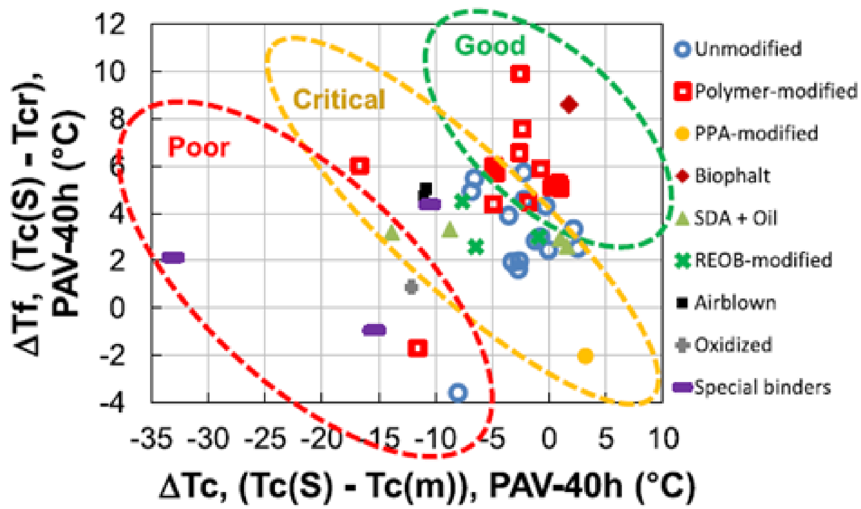

Figure 2-23 Analysis Approach Developed from NCHRP 09-60 for Evaluation of Various Binders after PAV 40h Aging (Elwardany et al., 2019)

2.4.7.5 Other Methods and Tools

In the literature, there are also other tests that could be employed to evaluate the properties of complex binder blends such as the Extended Bending Beam Rheometer (EBBR) and the Double-edge-notched Tension (DENT) test.

Over the past 10 years, significant research has shown that physical hardening is able to explain vast performance differences considering the material design, climate, and aging conditions (Hesp et al., 2007&2009; Erskine et. al., 2012). The EBBR protocol is thus specifically designed to assess a binder's tendency to physically harden during conditioning. The test procedure conditions samples for one, 24 and 72 h at $T_d + 10$ and $T_d + 20$, where T_d is the temperature of the pavement design limit. The continuous grade is obtained as the warmest of all temperatures measured for the two conditioning temperatures and three conditioning times. The grade loss from the one-hour result at Td + 10 (roughly equal to the AASHTO M 320 grade) is calculated and serves as a measure of durability. A 6 °C loss in low temperature grade reduces the reliability that no damage occurs in any given winter from the intended 98% to around 50%. A 12 °C loss reduces this to less than 10% reliability. The low temperature grade and the grade loss after 72 hours of conditioning measured from EBBR test have been shown to correlate well with the long–term pavement performance (Hesp et al., 2007&2009; Erskine et. al., 2012; Johnson et al., 2014).

The DENT test is designed to measure ductility of asphalt materials in a more fundamental and refined framework. The DENT test is created to control fatigue-type cracking distress (Andriescu et al., 2004&2009). It is based on a fundamental essential work of ductile failure (EWF) analysis by Cotterell and Reddel (1977). The DENT test is conducted at a relatively fast rate of 50 mm/min and moderate temperature of 15 °C. These conditions were chosen to correspond to significantly slower speeds at lower temperatures around the freeze–thaw regime, where significant cracking is believed to occur. The test is typically conducted on three DENT specimens with varying notch depths, providing ligaments of 5, 10 and 15 mm. The most important output parameter from DENT test is the crack tip opening displacement (CTOD). The CTOD is the amount by which a tiny fiber (fibril) of asphalt cement can be stretched under severe constraint in the ductile state until it fails. A higher CTOD allows the pavement to flex more under traffic and therefore provide better resistance to cracking.

Figure 2-24 shows an example of using CTOD measured from the DENT test to evaluate the different binder samples. As shown in the figure, binders 5% SBS D1192 and 3% SBS D1192+8% REOB initially have high CTOD values, however, after adding 20% RAP, the CTOD value significantly decreases. One of the potential reasons provided by the researchers is that this significant deterioration of failure properties can be attributed to the incompatibility between the SBS and the RAP used in this study.

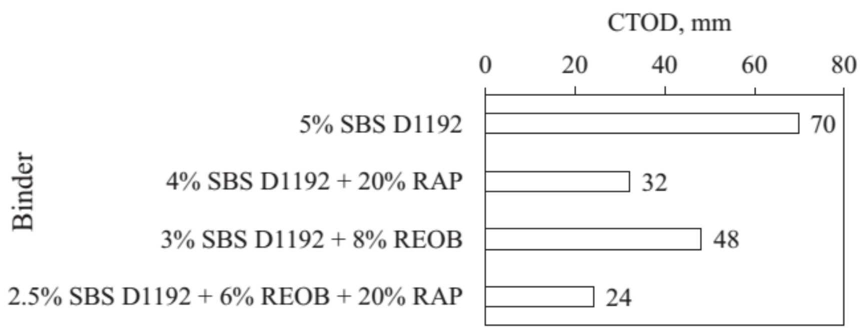

Figure 2-24 Measured CTOD (Paliukaite et al., 2016)

Chapter 3: Literature Review of RA Treated Asphalt Mixtures

A literature review was conducted by the research team as part of Task 1, concentrating on the testing methods and long-term aging approaches that are used on RA treated asphalt mixtures. The review in this chapter first summarizes the common tools and methods for characterizing asphalt mixtures with RAs (RA-treated asphalt mixtures). The current concerns are discussed regarding the long-term performance of asphalt materials with recycled asphalt and RAs based on the results of the literature review. Then, a summary of the available laboratory conditioning methods and tools (focusing on the mixture conditioning methods) to simulate the long-term aging of asphalt mixtures in the field is presented.

3.1 Viscoelastic Parameters

An asphalt mixture is a typical viscoelastic material that exhibits both viscous and elastic characteristics when undergoing deformation. The fundamental viscoelasticity of asphalt mixtures is the most commonly used property for conducting pavement analysis and modelling and is usually described or characterized by complex modulus (including dynamic modulus and phase angle), creep compliance, and relaxation modulus, which can be interconverted using the mathematic methods (e.g. Laplace and Fourier Transform) and mechanical models (e.g. Prony-series Models). Laboratory measurement of complex modulus is commonly done at different temperature and frequency combinations using AASHTO T 342 procedure, while creep compliance and relaxation modulus can be measured following AASHTO T 322 specification. These tests have been also widely used to evaluate the effect of various RAs on the viscoelasticity of asphalt mixtures (Mallick et al., 2010; O'Sullivan, 2011; Tran et al., 2012; Mogawer et al, 2013; Im et al., 2014; Haghshenas et al., 2016).

Based on the results measured from dynamic modulus testing, Mallick et al. (2010) found that an RA can drop the stiffness of a 100% RAP mixture at high loading frequencies (5 and 10 Hz) but increase the stiffness at lower loading frequencies (1 and 0.1 Hz) at the highest testing temperature (54.4 °C). Uzarowski et al. (2010), O'Sullivan (2011) and Im et al. (2014) reported that the evaluated RAs can significantly drop the stiffness of recycled mixtures, evenly below the stiffness of the control (virgin) mixtures. Mogawer et al (2013) concluded that recycled mixture with RAS and RAP/RAS showed less significant reduction in stiffness after incorporating an RA, as compared to RAP only mixtures. Haghshenas et al. (2016) proposed that the petroleum-based RAs had more impact in reducing dynamic modulus than soybean oil and tall oil.

Figure 3-1 below shows an example of using a Black space diagram to evaluate the viscoelastic properties of the RA treated asphalt mixtures. There are two points for each set of mixtures, indicating the two aging conditions (short-term aging and long-term aging following AASHTO R 30). RBR represents the recycled binder ratio in the mix, V2 indicates the modified vegetable oil used in the study. As shown in **Figure 3-1**, the use of the lower dose of RA (1.2% V2) with higher (0.31) RBR resulted in rheological performance similar to that of the DOT control mixture at lower (0.22) RBR, but the use of the softer base binder (PG 52-34) resulted in improved performance with a shorter aging path (smaller magnitude) and steeper slope. At the higher RA doses (5.5% for 0.31 RBR, 9% for 0.5 RBR), the resulting mixtures were even softer and less brittle (higher phase angle) with longer aging paths (larger magnitude) and steeper slopes compared to the DOT control mixture.

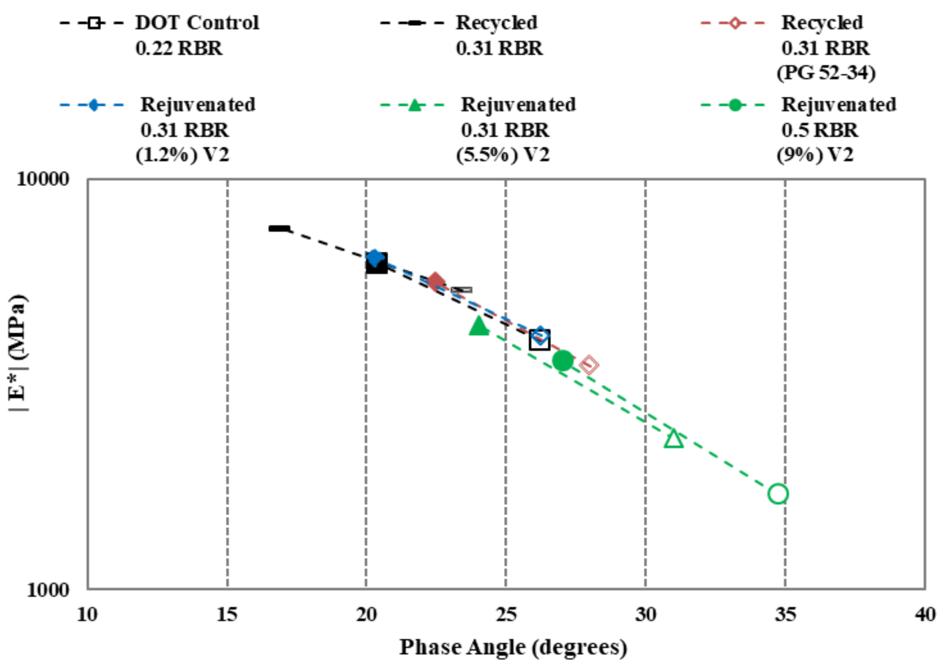

Figure 3-1 Complex Modulus Test Results in Mixture Black Space for Different Mixtures (Epps Martin et al., 2020)

3.2 Permanent Deformation

Rutting or permanent deformation is one of the major distresses in asphalt pavements. Resistance to rutting is a critical part of performance in the field, and testing for it is an important consideration. There are different tests available to assess the rutting resistance of asphalt mixtures. Currently the most common type of standardized laboratory rutting tests include the Hamburg Wheel Tracking Test (HWTT) following AASHTO T 324 procedure, Asphalt Pavement Analyzer (APA) following AASHTO T 340, Flow Number (FN) following AASHTO TP 79-15, Superpave Shear Tester (SST) (AASHTO T 320-07) and Triaxial Stress Sweep (TSS) Test (AASHTO TP 116-15), and the recently developed Stress Sweep Rutting (SSR) test (Kim et al., 2017). Among these, the FN test, HWTT and APA test have been widely used to evaluate the rutting performance of RA treated mixtures as identified from the literature review.

By conducting HWTT, Shen et al. (2004) found that an RA can significantly decrease stability by a range of 20% to 50% depending on RA dosage (2-7.4%). Based on the APA result, Uzarowski et al. (2010) and Tran et al. (2012) found that the RAs increase the susceptibility to rutting. Shen et al. (2007) reported that RA addition and softer binder usage decrease the rut depth, but the rut depths of recycled mixtures with RA are smaller than those using a softer base binder. Based on the HWTT results, Mogawer et al

(2013), Im et al. (2014) and Espinoza-Luque et al. (2018) reported that RAs increase the susceptibility to rutting and moisture damage for RAP/RAS mixtures. However, Cooper et al. (2018) and Zhang et al. (2021) found that RA addition did not negatively affect the rutting susceptibility of the mixtures containing RAM as evaluated by the HWTT test. Based on the FN testing result, Al-Badr et al. (2021) reported that when adding the RA (corn oil) with the SBS polymer modifier together at the appropriate dosage, the rutting performance of the modified mixture with RA is significantly better than the control mixture (FN value for modified mixture is ten times of the control mixture).

Figure 3-2 below shows the example result (rut-depth progression against the number of passes for the short-term aged (STA, following AASHTO R 30) samples measured from the HWTT (Arturo et al., 2018). Evaluating the entire span of the test (20,000 passes), rut depth increases with increasing levels of rejuvenation (RA is a heavy paraffinic distillate solvent extract with the appearance and viscosity of a dark brown lubricating oil). As the RA dosage increases, the rut progression curves deteriorate more rapidly, as compared to previous lower dosages. For the different samples, the mixture with 9% RA concentration shows the most severe rutting deterioration curve.

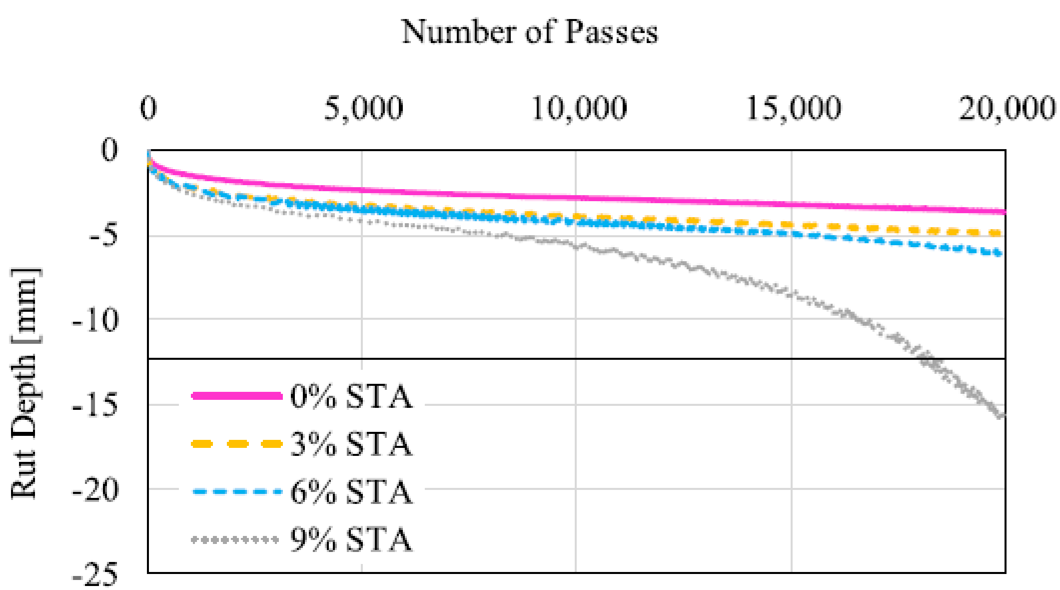

Figure 3-2 Rut-depth Progression vs. Number of Passes for Samples (Arturo et al., 2018)

Figure 3-3 presents an example of APA test results. The three types of asphalt mixtures, mixture containing 50% RAP (designated as R), mixture containing RA and 50% RAP (designated as R + R), and WMA containing 50% RAP (designated as W) were evaluated in the study (Song et al., 2018). It can be clearly observed that the rutting depth of R + R was the largest, indicating that study RA degraded the rutting resistance, which may be due to the fact that RA could soften the RAP asphalt binder. By utilizing molecular dynamics modeling, research from Ding et al. (2016) indicated that the RA could accelerate the diffusion of aged asphalt in base asphalt, which mitigated the stiffness of the RAP binder at the macro level and may result in the higher rutting susceptibility as compared to the control (RAP) mixture.

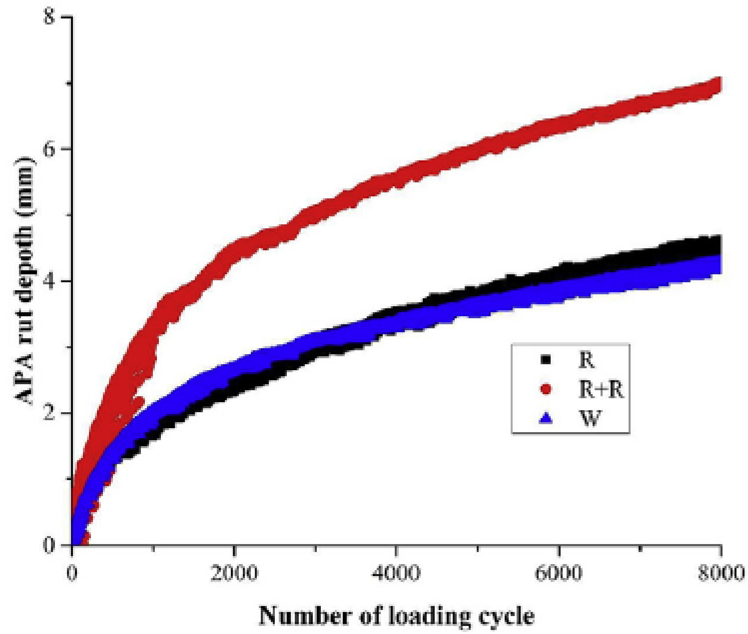

Figure 3-3 Rut-depth vs. Loading Cycle (Song et al., 2018)

3.3 Cracking Properties

This section focuses on available methods and tools to evaluate the cracking properties of asphalt mixtures, especially for RA treated mixtures. It is organized into two sub-sections with respect to the cracking types including low-temperature cracking properties and intermediate-temperature cracking properties.

3.3.1 Low-Temperature Cracking Properties

Asphalt pavement low-temperature cracking or thermal cracking is tied to the climatic conditions of either a slow temperature differential developed seasonally along with contraction and expansion cycles in very cold climates or due to large diurnal temperature differentials in arid climates with a fast temperature differential over a short period of time. Asphalt mixtures with high RAM content typically appear to develop thermal stresses more quickly than base asphalt mixtures, and therefore have less resistance to thermal cracking. The incorporation of RAs is believed to be helpful in improving the low-temperature cracking resistance of the mixtures (Tran et al. 2012; Mogawer et al. 2013; Booshehrian, et al. 2013; Yan et al. 2014). Current methods and practices to evaluate the thermal cracking properties of asphalt mixtures, especially for those with recycled materials and RAs, include the Disk-Shaped Compact Tension (DCT) Test (ASTM D7313-13), Semi-Circular Bend (SCB) Test at low temperature (AASHTO TP 105-13), Indirect Tensile (IDT) Test at low-temperature (AASHTO T 322), and the Thermal Stress Restrained Specimen Test (TSRST) (Jung and Vinson 1994) or the modified version of TSRST - Uniaxial Thermal Stress and Strain Test (UTSST) (Hajj et al. 2010).

Based on the TSRST results, Shen et al. (2004), Mogawer et al (2013) and Hajj et al. (2013) found that RAs can significantly improve the low-temperature fracture properties of asphalt mixtures containing RAP/RAS, while Cooper et al. (2018) reported that the RA adversely affects the low temperature properties of the recycled mixtures with RAS. By conducting the low temperature IDT test, Tran et al. (2012) proposed that addition of the RA can reduce the critical failure temperature of RAP/RAS mixtures, thus improving their low temperature cracking properties. Zaumanis et al. (2013) reported that RA addition increases indirect tensile strength and fracture energy, depending on RA type. RA addition can also increase the low-temperature creep compliance (and thus reduced low-temperature cracking potential) of a 100% RAP mixture. Lee et al. (2018), Mohamed and Christopher (2017), Arabzadeh et al. (2021) performed DCT tests to evaluate the low-temperature cracking properties of control (RAP) mixtures and RA treated asphalt mixtures. DCT results indicate that RAs, when applied at optimum dosage rates to high RAP mixtures, helped to enhance low-temperature cracking properties.

Figure 3-4 shows example results measured from a DCT test to evaluate the effect of RAs on mixtures with RAP material. As can be seen from **Figure 4-4(a)**, RA “A” (extracted from petroleum oil) and RA “B” (extracted from refined tall oil) significantly increased the fracture energy of the mixtures with 27.6% RAP even slightly higher than that of base asphalt. However, RA “C” (extracted from vegetable oil) decreased the fracture energy of the RAP mixture. Similar results can be also observed for the mixtures containing 70% RAP (**Figure 4-4(b))**.

Figure 3-5 shows example results measured from a UTSST test to evaluate the effect of RAs on RAP mixtures, while also considering aging conditions (short-term oven aging (STOA) and long-term oven aging (LTOA) following AASHTO R 30). CRI_{Env} is the Environmental Cracking Resistance Index calculated from the UTSST test, and a higher value generally indicates the mixture has better thermal cracking properties. Comparing the three mixtures with same RBR (0.31) in **Figure 3-5**, RA “T2” does not seem to be effective in increasing the CRI_{Env} value, while RA “A2” clearly shows improvement of the thermal cracking properties of the 0.31 RBR mixture.

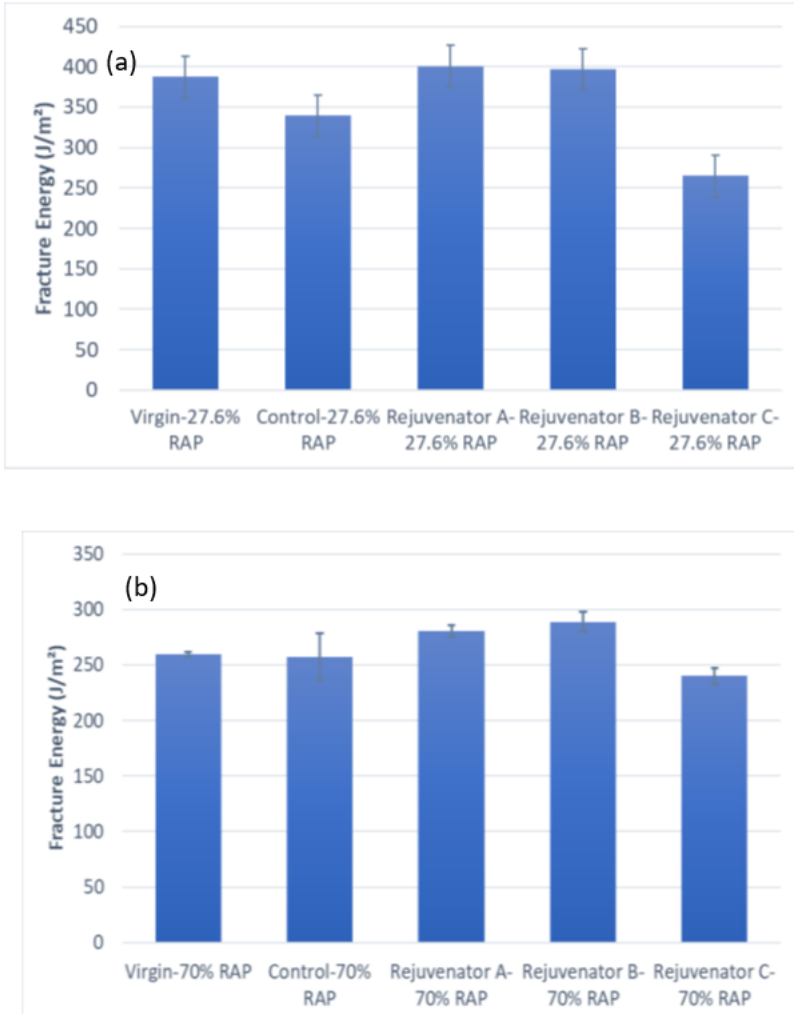

Figure 3-4 DCT Results for (a) 27.6% RAP Lab Compacted Mixtures; and (b) DCT Results For 70% RAP Lab Compacted Mixtures (Lee et al., 2018)

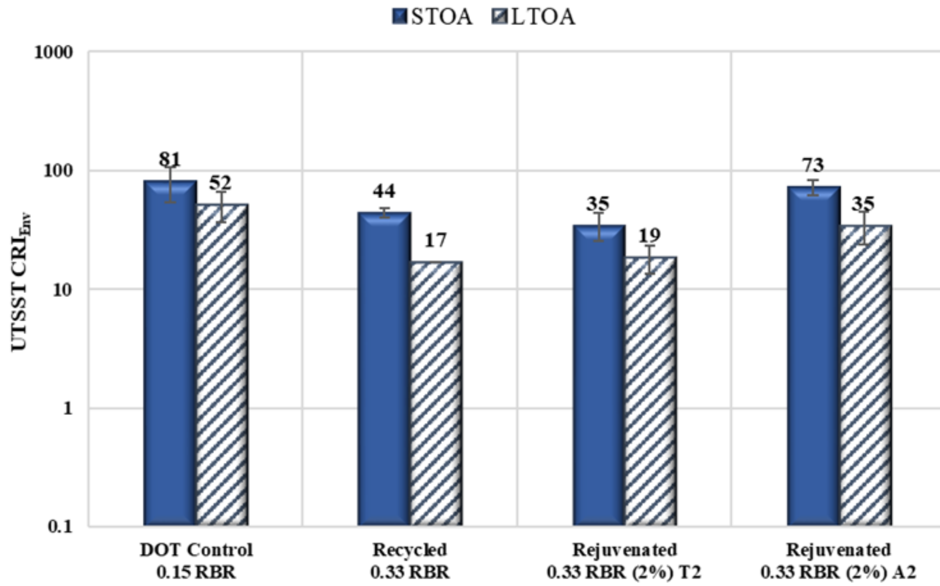

Figure 3-5 CRI$_{Env}$ Results for Mixtures (Epps Martin et al., 2020)

3.3.2 Intermediate-Temperature Cracking Properties

Asphalt pavement intermediate-temperature cracking, primarily fatigue cracking, is a major distress mode considered in asphalt mixtures and pavement structural design. Many tests have been developed to evaluate and characterize the intermediate-temperature cracking properties of asphalt mixtures, including the traditional indirect tensile strength (IDT) test and 4-point flexural bending beam (FBB) test (AASHTO T 321) (Tangella et al., 1990; Tayebali et al., 1994&1995). Newer tests with more mechanical and simulative background include the Cracking Tolerance Index (CT-Index/ Ideal-CT, ASTM D8225) test, Semi-Circular Bend (SCB) at intermediate temperature for Illinois flexibility index measurement (AASHTO T393) and Louisiana Transportation Research Center SCB (ASTM D8044), simplified viscoelastic continuum damage (S-VECD) test (AASHTO TP 107) (Lee and Kim 1998, Daniel and Kim 2002, and Underwood et al. 2006), Texas Overlay Test (Texas OT, Tex-248-F), the University of Florida Indirect Tension test (UF-IDT) (Roque et al. 2004), and asphalt mixture direct tension (DT) test (Luo et al. 2013; Lytton et al. 2013). These tests have been widely used to evaluate the cracking properties of the mixtures with RAP/RAS, and/or recycling agents and modifiers (Chehab et al. 2002, Bodin et al. 2004, Christensen and Bonaquist 2005, Underwood et al. 2006., Kim et al. 2009, Roque et al. 2010, Zhang 2019&2020).

Tran et al. (2012) found that addition of an RA can improve the fatigue properties of RAP mixtures as measured by the UF-IDT testing. By conducting the FBB test, Yan et al. (2014) proposed that the fatigue life of 30%-50% RAP mixtures was significantly improved by adding RAs, and the mixtures containing RA with higher CII (colloidal stability index) had better fatigue properties than others. Mogawer et al (2013), Im et al. (2014) and Asli (2015) concluded that the Texas OT test was able to identify the properties difference between the control mixtures (mixtures with RAM) and the RA treated mixtures. The RAs increased the average OT number of cycles to failure from approximately 110% to 300%, depending on

RA type. By means of the SCB test, Cooper et al. (2015) found that the Flexibility Index (FI) increased with the addition of RA, and the mixtures with naphthenic oil exhibited better fracture resistance at intermediate temperature than those treated with vegetable oil. Nabizadeh et al. (2017) proposed that addition of RA can increase the FI value, and aromatic extract was more effective than tall oil and soybean oil. Based on the CT-Index test, Al-Badr et al. (2021) and Zhang et al. (2021) proposed that the addition of RAs can significantly improve the intermediate-temperature cracking properties of control mixtures.

Figure 3-6 below shows an example of using the CT-Index test to evaluate the effect of RAs on the intermediate-temperature cracking properties of asphalt mixtures (Al-Badr et al., 2021). There are four different types of mixtures evaluated in the study, including the control mixture, mixture with 7.5% SBS and 7% RA (corn oil) (labelled as 7SA+7.5SBS), mixture with 7.5% SBS and 14% RA and mixture with 10% SBS and 14% RA (labelled as 14SA+7.5SBS and 14SA+10SBS respectively). Three aging conditions are also included in this study: STA (following AASHTO R 30); Long-term aging (LTA) (8 hrs@135 °C) and Extended long-term aging (16 hrs@135 °C). As can be seen from **Figure 4-6**, the CT-Index value for the three modified mixtures are significantly higher than the control mixture after STA, indicating the improvement of the cracking properties by adding the SBS modifier and RA. Comparing mixtures 7SA+7.5SBS and 14SA+7.5SBS after STA, addition of excessive RA results in a decrease of the CT-Index value, showing degradation of the cracking properties. Interestingly, even though the modified mixtures have higher CT-Index value after STA, they show a drastic/significant drop in cracking properties as compared to the control mixture after the two Long-Term Aging (LTA) conditions.

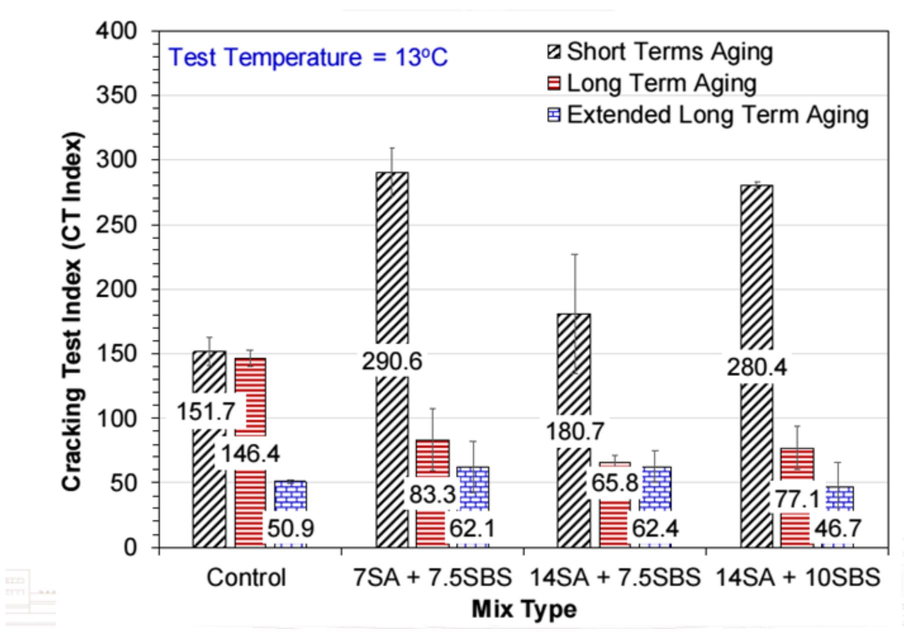

Figure 3-6 CT-Index Criteria for Different Mixtures (Al-Badr et al., 2021)

Figure 3-7 presents an example of the SCB (I-FIT) results for laboratory-mixed, laboratory-compacted (LMLC) and reheated plant-mixed, laboratory-compacted (RPMLC) specimens after STA and LTOA (following AASHTO R 30), as well as field cores at construction. For each mixture, the darker shaded stacked column represents the FI value after STOA (at construction for the field cores), and the hatched lighter shaded stacked column represents the FI after LTOA (at one year after construction for the field cores). As shown in **Figure 3-7**, for all three types of material (LMLC, RPMLC and field cores), addition of the RA (1.2% V2(modified vegetable oils)) and using the softer base binder (PG 52-34) can increase the FI of the mixture with 0.31 RBR, thus improving the cracking properties of mixtures.

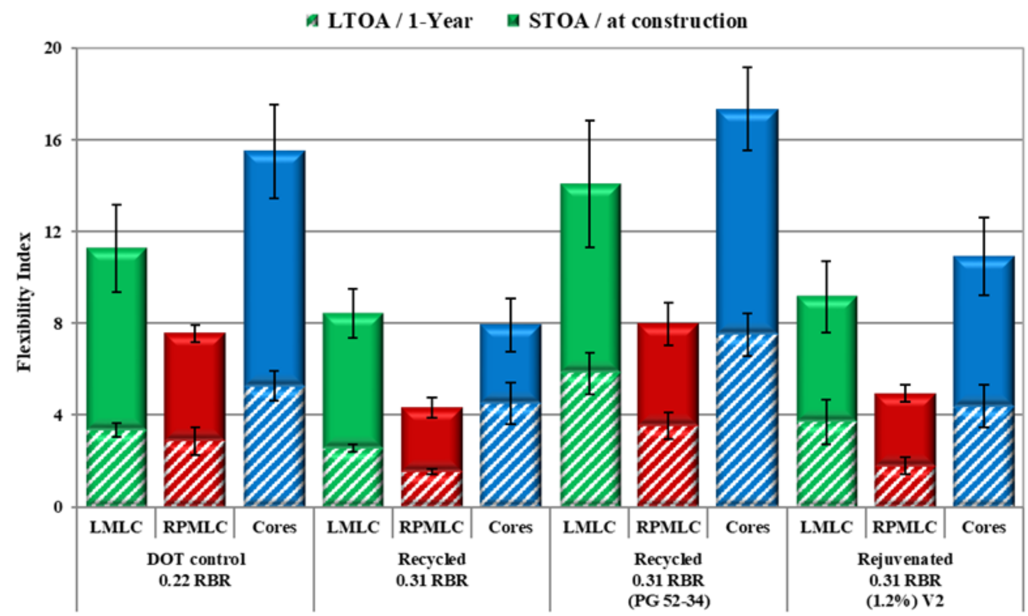

Figure 3-7 SCB Test Results for Mixtures with Different Specimen Types (Epps Martin et al., 2020)

Figure 3-8 below shows an example of conducting the S-VECD test to evaluate the effect of RAs on the fatigue properties of asphalt mixtures. Two failure criteria were employed: (1) the rate of pseudo strain energy release (G^R) and (2) the average reduction in pseudo stiffness up to failure (D^R). D^R represents the damage tolerance of the asphalt mixture before failure (Wang, 2017), while G^R characterizes the rate of damage accumulation during load application with higher N_f value when G^R is equal to 100 indicating better fatigue resistance (Sabouri et al., 2013). As shown in **Figure 3-8**, both S-VECD failure criteria (D^R and G^R) show an improvement with the addition of the RA (1.2% V2 (modified vegetable oils)) and with the use of a softer base binder (PG 52-34) compared to the 0.31 RBR recycled control mixture.

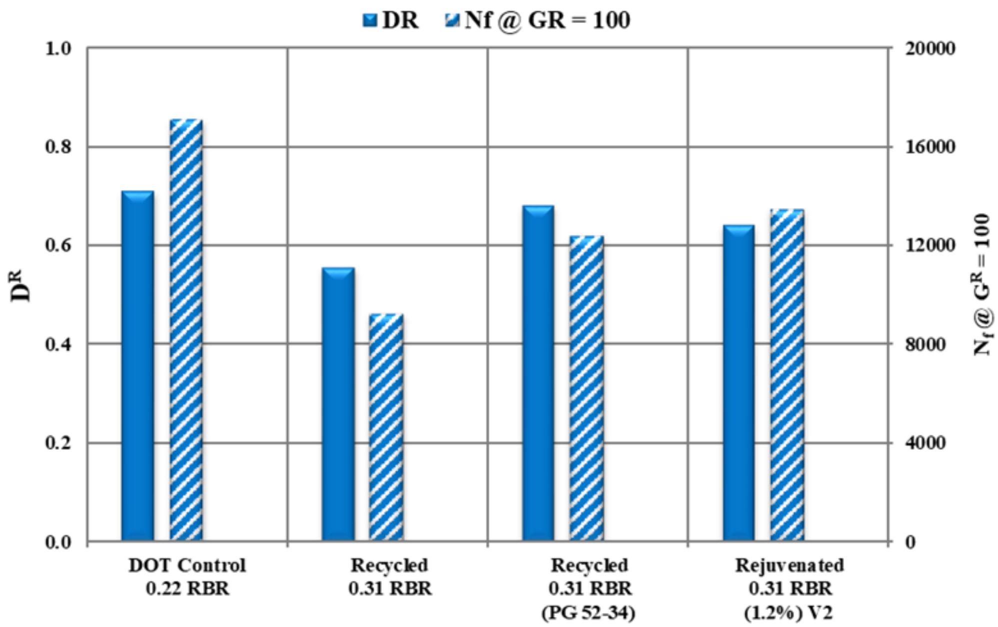

Figure 3-8 S-VECD Criteria for Different Mixtures (Epps Martin et al., 2020)

3.4 Moisture Susceptibility

Moisture damage is another primary distress in some climates and for some material sources and combinations. For asphalt mixtures that are susceptible to moisture, the internal bond between the binder and aggregate is weakened in the presence of water, which may lead to stripping and further significant damage of asphalt pavement. To characterize moisture susceptibility, the boiling test (ASTM D 3625), coatability test (suggested by NCHRP 09-53),raveling test (ASTM D7196) and the Tensile Strength Ratio (TSR) test (ASTM D4867) are the quickest, but purely empirical tests. The Hamburg Wheel Tracking Test (HWTT) (AASHTO T 324) and Asphalt Pavement Analyzer (APA) (AASHTO T 340), as well as the Modulus (e.g. complex modulus (E*) and Resilient modulus (Mr)) Ratio tests (Dave et al., 2018) are simulative and mechanically based and have been widely accepted in recent years.

Many studies (Shen et al., 2007; Hajj et al. 2009; Zhao et al. 2012) have indicated that HMA and WMA mixtures containing recycled materials have acceptable moisture resistance. This is related to the fact that the aggregate in the recycled materials is covered and protected by the aged binder and the bonds between aggregate and aged binder are stronger than those between aggregate and base binder, making the recycled mixture less vulnerable to moisture damage. However, studies have found that the rutting and moisture susceptibility of recycled asphalt mixtures containing RAs would be higher as compared to recycled asphalt mixtures without RAs, since RAs can reduce the stiffness (Shen et al., 2007; Mogawer et al., 2013; Zhang et al., 2021). But not all mixtures with RAs will show the higher moisture susceptibility as compared to conventional mixtures with and/or without recycled materials (Tran et al. 2012). In fact, some studies have shown that adding RAs to HMA and/or WMA mixtures containing high RBR improves their rutting resistance and moisture susceptibility as compared to control mixtures (Im and Zhou 2014; Zaumanis et al. 2014; Yan et al. 2014).

Figure 3-9 below shows an example of using the TSR test and the resilient modulus ratio (MMR) measured from the M_R test to evaluate the effect of RAs on moisture resistance of different mixtures. As seen in **Figure 3-9**, mixtures containing RAP have higher TSR and MMR value than the control mixture. Comparison of the RAP-containing mixtures with (50%RAP+Rej) and without RA (50%RAP) showed that the RA enhanced the TSR and MMR values and improved the moisture susceptibility of the mixtures. Therefore, the RAP mixtures with RA, because of high adhesion between aggregate and bitumen, had better resistance to moisture. In addition, comparison of ‘‘50%RAP+SB”, ‘‘50%RAP+WPMB” and ‘‘50%RAP+Rej+WPMB” mixtures showed that the combination of waste polymer (WPMB) with soft bitumen and RA enhanced moisture resistance of RAP mixtures.

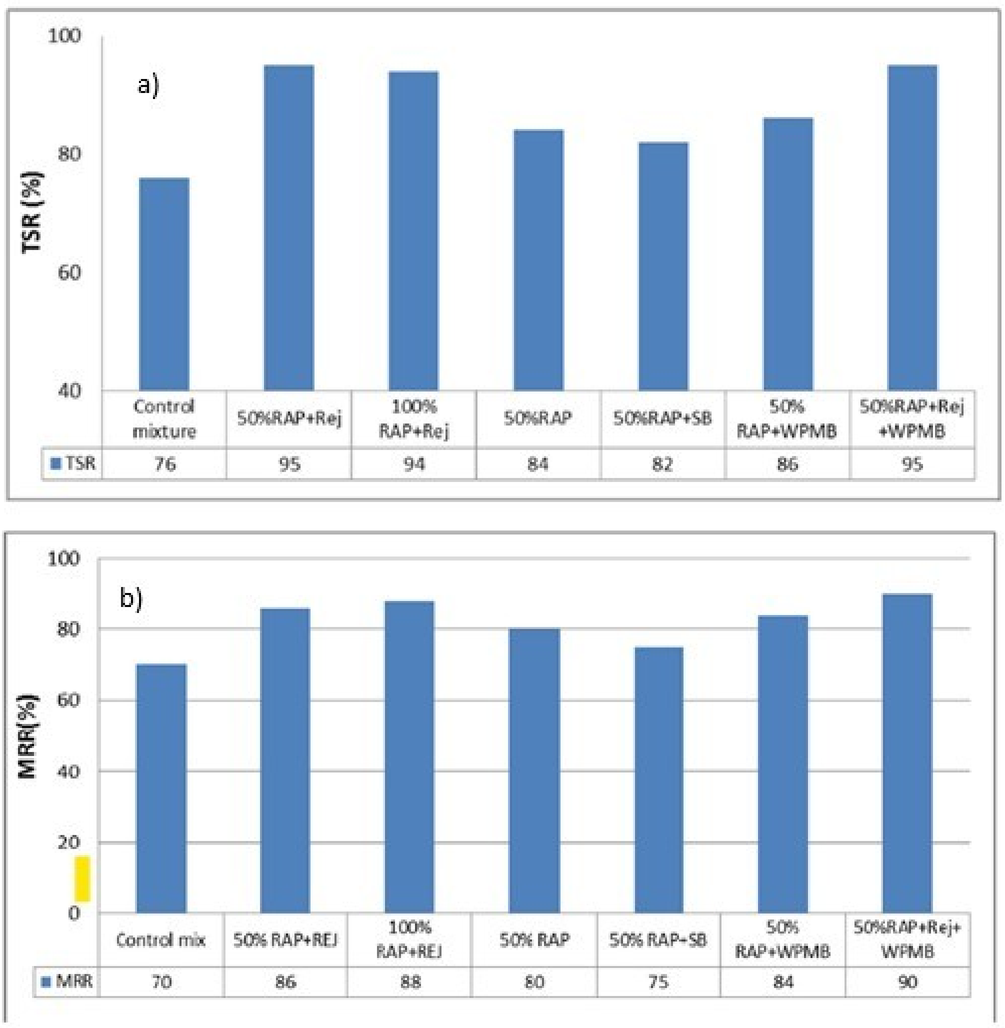

Figure 3-9 (a) Tensile Strength Ratio (TSR) values; (b) Resilient Modulus Ratio (MMR) of Different Asphalt Mixtures (Daryaee et al., 2020)

Figure 3-10 below shows example results from the HWTT test for characterization of the moisture susceptibility of asphalt mixtures. **Figure 4-10a** shows the stripping number (SN), and the LC_{SN} parameter (number of load cycles to the point of SN) parameters to evaluate the moisture susceptibility of asphalt mixtures; higher values are preferred (Yin et al., 2014). As shown in **Figure 3-10b**, addition of RAs designated as KU, KA and K1 can significantly decrease the moisture resistance of the mixtures by dropping the LC_{SN} values.

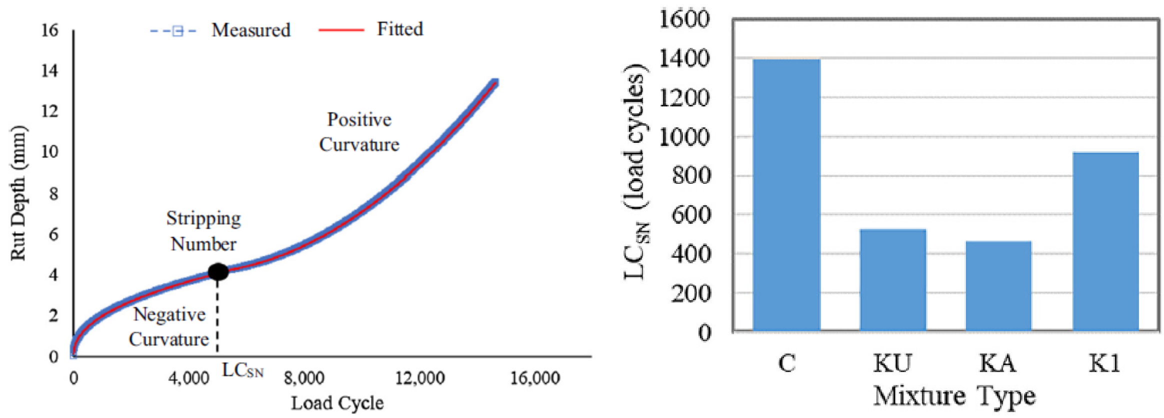

Figure 3-10 (a) HWTT stripping number determination; (b) LC_{SN} for different mixtures. (Lee et al., 2019)

3.5 Concerns Of Long-Term Performance of RA Treated Asphalt Materials

Many recent research efforts have shown that some RAs, while effective immediately after production, show rapid decrease in effectiveness with aging. Cavalli et al. (2018) and Ongel et al. (2015) show that compared with other binder samples, the RA treated RAP binder is more susceptible to aging as evaluated by the FTIR and SARA tests. They concluded that considering the effect of aging is vital in identifying how RAs affect the RAP binder chemically and mechanically. Mohammadafzali et al. (2017) investigated the aging of RA treated asphalt binders compared with base binders. The authors found that the paraffinic RA slowed the aging process compared to the base binder while the re-refined used oils accelerated the aging process. Critical PAV time was used to evaluate the RA's impact. Critical PAV time was defined as the PAV aging time to increase the high-temperature PG from the base binder (70 ˚C in this study) to 95 ˚C. Paraffinic RA showed positive correlation between increasing RA dosage and the critical PAV time while the re-refined used oils demonstrated an inverse correlation.

Based on dynamic modulus testing results, Tran et al. (2012) observed that after short-term aging, the use of RA dropped the stiffness of RAP/RAS mixtures closer to the base mixture, while mixtures with RA appeared to age faster than the RAP/RAS mixtures without RA after long-term aging. Cai et al. (2019), Grilli et al. (2017) and Yang et al. (2017) proposed that although RAs can improve the rheological and physical properties of the aged asphalt binders, RA treated binders are usually more susceptible to aging than base binders. This behavior is mainly reported for the bio-RAs, which might be due to the higher amount of oxygen in bio-oils than petroleum asphalt. Other Studies (Mohammadafzali et al., 2017; Ziari et al., 2019; Sias et al., 2019; Christensen et al., 2019; Al-Badr et al. 2021) also noted that the beneficial effects of RAs are diminished with subsequent aging.

However, other studies have reported that RAs did not deteriorate the aging resistance of the asphalt material containing RAM. Bennert et al. (2015) tested mixtures using the Thermal Stress Restrained

Specimen Test (TSRST) device to determine the cracking behavior of mixtures at low temperature. The properties of RAP mixtures with and without RAs were relatively similar for both STOA and LTOA, which indicates that RAs did not cause a notable effect on the aging resistance of the RAP mixtures. In addition, polymer/ SBS-modified asphalt binders treated with RAs have been reported to show better aging resistance than RA treated binders (Elkashef et al., 2017; Cai et al., 2019).

3.6 General Trend for Change of Binder/Mixture Properties with Aging

Many studies related to aging of asphalt binders have proposed that the change of any aging index property (AIP), follows a similar trend with increase of aging conditions (Herrington et al., 1994; Lau et al., 1992; Davison et al., 1994; Liu et al., 1996; Domke et al., 2000; Glover et al., 2014; Glaser et al., 2013&2015; Elwardany et al., 2017; Zhang, 2020). All asphalt materials exhibit relatively similar kinetics consisting of an initial fast reaction period, also known as spurt, followed by a slower reaction period that has an approximately constant rate. These two reaction periods are known to be made up of fundamentally different chemical reactions (Petersen et al., 2011). Petersen et al. (2011) explains that during the spurt, sulfoxides are the major oxidation product and cause an increase in stiffness. During the slower reaction period, ketones are the major product that cause the increase in stiffness. The two reaction periods are illustrated in **Figure 3-11** below.

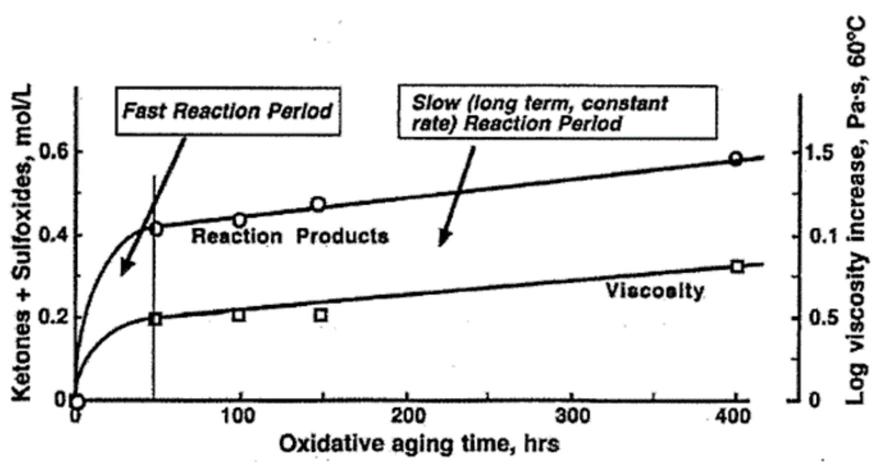

Figure 3-11 Dual Oxidation Mechanisms for Asphalt Binder (Petersen et al., 2011).

A recent study conducted by Zhang (2020) has shown that the change of mixture cracking properties, as indicted by the mixture Glover-Rowe parameter, with increase of aging follows this general trend as well. Zhang (2020) proposed a mixture aging model based on this general trend to predict the mixture cracking properties over time, while also considering mixture variables, such as binder PG grade and mixture RAP content. **Figure 3-12** below shows the developed aging model from Zhang (2020).

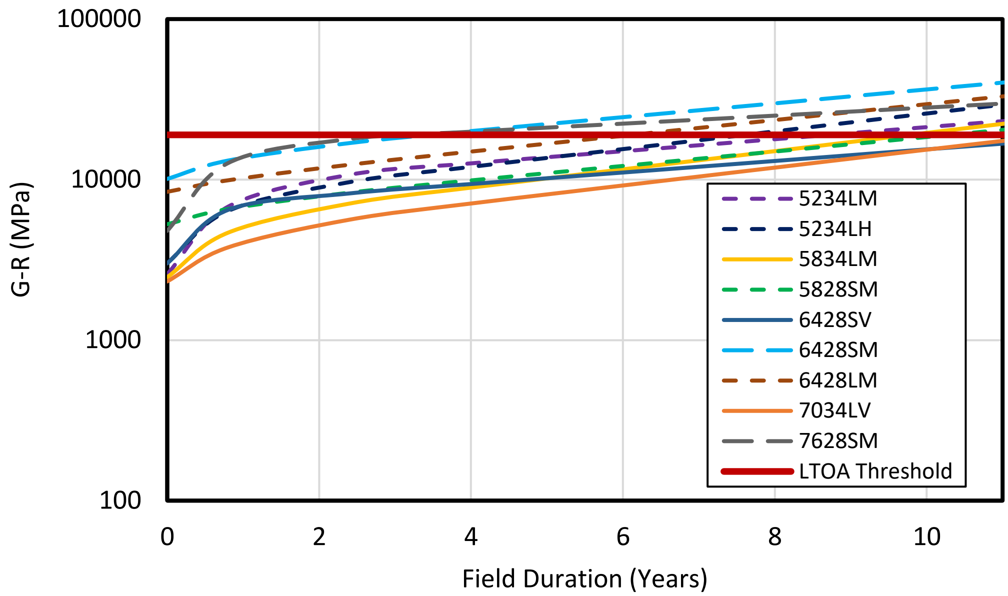

Figure 3-12 Change **of Mixture Glover-Rowe Parameter over Pavement Service Life (Zhang, 2020).**

3.7 Summary of Available Characterization Methods

As summarized in the literature review, the key factors that affect the performance of asphalt binders and mixtures with RAs include the dispersion and diffusion of the RAs in the binder blends and mixtures, and the appropriate selection of the RA type and dosage. Increase of the mixing time and temperature can significantly improve the dispersion and diffusion process of the RAs into the recycled material. Selection of the right RA type and proper RA dosage needs to be determined by means of the different testing and evaluation tools and methods. The most popular methods for selecting the RA type and dosage are to either use the blending charts based on the traditional viscosity and/or penetration of the RA treated binder blends or develop the blending charts and the associated equations based on the rheological measures used in Superpave grading system to meet the PG requirement.

Other methods have been developed and are currently employed to evaluate complex asphalt binders and mixtures containing the recycled material and RAs. These methods can be used to evaluate the different properties and performance of RA treated asphalt material and can be employed to determine the appropriate RA type and dosage from different perspectives; for instance, the binder colloidal stability and compatibility, binder microstructure and nanomechanical properties, mixture properties and pavement distress types. A summary of these available methods and tools is presented in tabular form (**Table 3-1** for binder and **Table 3-2** for mixture) below. These methods are organized into different categories based on the evaluation purpose and their corresponding key outputs that can be used to evaluate the properties of RA treated asphalt materials are discussed in the table. It needs to be noted that for study of the complex asphalt materials, coupling methods can be used to comprehensively evaluate the material from various perspectives. This is important and has been considered by the research team when finalizing the testing plan.

Table 3-1 Summary of Common Binder Evaluation Tools and Methods

Methods	Tests	Corresponding Outputs from the Testing
Analytical Method	SARA separation	Colloidal Indices (asphaltene Index (IA) and Gaestel Index (IC) or Colloidal Instability Index (CII))
	Chromatography Analysis	Determining molecular weights and size distribution (agglomeration or aggregation of the sample)
	Fourier-Transform Infrared (FTIR) Spectrometer	Infrared peak intensities for identifying and characterizing the important elements and functional groups;
	X-Ray Fluorescence (XRF)	Detecting the specific elements or organic molecules in binder blends to help identify and track the binder source/RAP/RAs/Modifier
	Nuclear Magnetic Resonance (NMR)	
	Inductively Coupled Plasma Atomic Emission Spectroscopy (ICP-AES)	
Morphology Analysis (Microscopy Technique)	Ultraviolet, Infrared Microscopy	Mapping the micro-structure and evaluating the blending/diffusion effectiveness
	Fluorescence Microscopy	
	Scanning Electron Microscopy (SEM)	
	Atomic Force Microscopy (AFM)	
Thermal Analysis	Differential Scanning Calorimetry (DSC)	Measure the glass transition temperature (Tg); wax crystallization/ precipitation (C(t)); Ozawa exponent (n)
	Thermo-gravimetric Analysis (TGA)	Thermal decomposition curves; derivative of the decomposition curve
	Frequency and Temperature Sweep Test by Dynamic Shear Rheometer (DSR) with a 4 mm plate	Transition Regions and Temperatures
Binder Performance Tests	Traditional Tests in Superpave Specification	Rheological characterization; ΔTc parameter; Glover-Rowe Parameter; R-value; Black space diagram etc.
	Linear Amplitude Sweep (LAS) Test	Load cycles versus strain curve; fatigue failure criteria
	Multiple Stress Creep Recovery (MSCR) Test	Non-recoverable creep compliance (Jnr) and MSCR %recovery
	Asphalt Binder Cracking Device (ABCD)	Crack temperatures (Tc); Fracture stress (δ)
	Extended Bending Beam Rheometer (EBBR)	Low temperature grade and the grade loss after 72 hours of conditioning
	Double-edge-notched Tension (DENT) Test	Crack tip opening displacement (CTOD)

Table 3-2 Summary of Common Mixture Evaluation Tools and Methods

Methods and Tests		Typical Output Parameters
Stiffness/Rheology	Resilient Modulus (M_r Test)	M_r
	Complex Modulus (E* Test)	Linear Viscoelastic Characterization (complex modulus and phase angle, rheological indices)
Fatigue Cracking	Cracking Tolerance Index (CT-Index)	CT_{Index}
	Illinois Flexibility Index Test (I-FIT)	Fracture Energy; Flexibility Index
	Louisiana Transportation Research Center-Semi-Circular Bend (LTRC-SCB)	Critical Value of Fracture Resistance (J_c)
	Flexural Bending Beam Fatigue Test (BBF)	Cycles to Failure; Energy-based Parameters (e.g. Plateau Value (PV))
	Direct Tension Cyclic Fatigue (S-VECD)	Damage Characteristic Curve; Fatigue Parameters (GR; DR; Sapp)
Thermal Cracking	Disk-Shaped Compact Tension Test (DCT)	Fracture Energy; Fracture Strain Tolerance
	Semi-Circular Bend (SCB) Test at low temperature	Fracture Energy
	Uniaxial Thermal Stress and Strain Test (UTSST)	Fracture Temperature; Fracture Strength; Cracking Resistance Index
	Thermal Stress Restrained Specimen Test (TSRST)	Failure Temperature
Moisture Susceptibility	Tensile Strength Ratio (TSR)	Tensile Strength Ratio; Wet IDT Strength
	Modulus (E*, Mr) Ratio	M_R Ratio
Moisture& Rutting	Hamburg Wheel Tracking Test (HWTT)	Rut Depth; Load Cycles to Certain Depth (e.g. 12.5mm); Stripping Inflection Point; Stripping Number
	Asphalt Pavement Analyzer (APA)	
Rutting	Flow Number (FN)	FN value

3.8 Available Laboratory Conditioning Methods to Simulate the Field Aging of Asphalt Pavement (Mixture Conditioning)

To capture the performance more accurately and effectively, especially the long-term performance of RAs included in this project, several aging levels should be evaluated to characterize how the properties of the binders and mixtures change with age. Several asphalt mixture laboratory conditioning procedures to simulate the long-term aging of asphalt pavement in the field are documented in the literature. These procedures can be further classified based on state of mixture during aging: (a) compacted specimen (b) loose mix.

3.8.1 Aging of compacted specimen

Experimental results from Bell et al. (1989&1994) recommended the compacted specimen be conditioned at 85 °C for 2 days or 100 °C for 1 day duration to simulate around 1 to 3 years field aging condition. A longer conditioning time (4 to 8 days for 85 °C or 2 to 4 days for 100 °C) was needed to simulate 9-10 years field aging. A higher conditioning temperature (100 °C) was not recommended because conditioning the mixtures at this temperature could cause damage to the specimens. The outcome of these studies (part of the SHRP project) was standardized as AASHTO R 30 for the long-term aging of compacted asphalt specimens in the laboratory, which can approximately represent five to ten years of aging in the field (Harrigan et al., 2007). Houston et al. (2005) conditioned compacted asphalt specimens at 5 days at multiple temperatures (80, 85 and 90 °C) to simulate the LTA for different sites across the United States with the different aggregates and binders. High variability was observed from the data, and due to this variability and inability to account for different variables including the environmental conditions and mix properties, the researchers were not able to standardize a new long-term conditioning procedure for asphalt mixtures. It was concluded that the current standard procedure is not sufficient to truly simulate and predict the long-term aging of asphalt mixtures in the field. A new laboratory conditioning procedure that accounts for different environmental conditions and asphalt mixture properties is highly desirable.

Several other procedures for conditioning compacted mixture specimens have also been proposed in the literature. A summary of these methods is provided in **Table** 3-3**.**

Table 3-3 Studies on Accelerated Laboratory Aging Procedures Developed for Compacted Asphalt Specimens

References	Laboratory Conditioning Method	Key Findings	Validation Test/ Parameter
AASHTO R 30	5 days at 85 °C	can approximately represent five to ten years of aging in the field	|E*|
Brown and Scholz (2000)	4 and 5 days at 85 °C	1. 5 days at 85 °C can simulate long-term aging of asphalt pavements in UK; 2. 4 days at 85 °C simulates 15 years old pavement in the US	|E*|

References	Laboratory Conditioning Method	Key Findings	Validation Test/ Parameter
Harrigan (2007); Houston et al. (2005)	5 days at 80, 85 and 90 °C	5 days at 85 °C simulates 7–10 years of field aging	|E*|
Epps Martin et al. (2014)	1 to 16 weeks at 60 °C	4–8 weeks at 60 °C simulates first year of field aging	IDT, TSR, MR, HWTT
NCHRP 09-52 (Newcomb et al., 2015)	weeks at 60 °C; days at 85 °C	1. 2 weeks at 60 °C can simulate around 9,600 CDD (cumulative degree-days) of field aging; and 7-12 months field aging; 2. 5 days at 85 °C can simulate around 1,7500 CDD of field aging; and 12-23 months field aging;	MR |E*| HWTT DSR BBR FTIR
Sirin et al. (2020)	0, 3, 7, 15, 30, 45, 60, 90, and 120 days at 85 °C	45 and 75 days at 85 °C simulate 5 years field aging in Middle East condition for wearing and base course, respectively	|E*| DSR MSCR
Nicholls (2006)	2 days at 60 °C	Simulates around 1-year aging in the field	|E*|
Van den Bergh (2011)	16 hours at 110-120 °C	The method can simulate around 20 years of aging in field	DSR SARA
MTE Services, Inc. (Hanz & Reinke, 2016), (Reinke & Hanz, 2018)	5 days and 10 days at 85 °C	5 days can simulate around 2 years field aging, while 10 days can simulate less than 6 years field aging	|E*| RAS DSR
Al-Qadi et al. (2019)	3 days at 95 °C (SCB sample); 5 days at 85 °C	1. 3 days at 95 °C aging is equal to 5 days at 85 °C aging (AASHTO R 30); 2. 3 days at 95 ° aging can simulate up to 10 years field aging.	IFIT-SCB

However, research (Collop et al., 2004; Kim et al., 2013; Elwardany et al., 2017; Zhang et al., 2019) has shown that aging on the compacted specimen leads to a change in air void distribution (Reed, 2010) and the development of an aging gradient from the specimen's center to its periphery and can result in different aging extents for different specimen geometries. This variability complicates the interpretation of results from different lab testing on the aged mixtures.

3.8.2 Aging of loose mix

Studies have recommended aging loose mixtures in the laboratory to simulate the aging of asphalt pavements instead of aging compacted specimens (Van den Bergh et al., 2011; Mollenhauer et al., 2011). The primary advantages of loose mixture aging over compacted specimen aging are: (1) problems associated with the conditioning of compacted specimen (e.g., change in air void distribution and aging gradient) during laboratory aging may be reduced; (2) air and heat can easily circulate inside the loose asphalt mixture, which not only allows for uniform aging throughout the mix but also significantly shortens the conditioning time needed due to a larger area of the binder surface being exposed to oxygen.

Several aging procedures for loose mixture conditioning have been proposed in the literature. A summary of these methods is provided in **Table 3-4.**

Table 3-4 Studies on Accelerated Laboratory Aging Procedures Developed for Loose Asphalt Specimens

References	Laboratory Aging Condition	Key Findings	Validation Test/ Parameter
Asphalt Institute (2010)	24 hours at 135 °C	This method can simulate 7 to 10 years of aging in the field	ITS HWTT
Von Quintus (1989); Van den Bergh (2009; 2011)	8, 16, 24, and 36 hours at 135 °C	1. STA at 130 °C for 3 hours following LTA at 90 °C for 168 hours; 2. STA at 134 °C for 4 hours following LTA at 85 °C for 168 hours 3. Two methods can be used to simulate 7 to 10 years field aging	DSR RAS FTIR
Yin et al. (2017)	2 weeks at 60 °C; 3 days at 85 °C; and 5 days at 85 °C	1. 2 weeks at 60 °C simulates 7 to 12 months field aging; 2. 5 days at 60 °C simulates 12 to 23 months field aging	MR HWTT
Islam et al. (2015)	1, 5, 10, 15, 20, and 25 days of oven aging at 85 °C	1 day laboratory aging is close to 1 year of field aging	ITS
RILEM TC ATB TG5 (2009)	7-9 days at 85 °C	1. Laboratory aging of loose mix provides an appropriate way to produce RAP material; 2. A more homogenous aged mix obtained from aging of loose mix	--
Mollenhauer and Mouillet (2011)	90 °C with 2.1 MPa pressure for 20 hours; 85 °C for nine days	Both can simulate 11 to 12 years field aging	Penetration FTIR
Reed (2010)	Loose mix at 85 °C for 5 days; Compacted sample at 85 °C for 14 days	1. Uniform aging of the asphalt around each aggregate particle in the laboratory-aged loose mix; 2. Significant changes in air void content during the long-term aging of the compacted specimens	DSR |E*| Beam Fatigue
Yousefi et al. (2018); NCHRP 09-54 (Kim et al., 2018)	Loose mix at 70 °C, 85 °C and 95 °C for different durations; Loose mix at 135 °C with different durations	Aging asphalt at temperatures above 100 °C may: 1. disrupt polar molecular associations, which leads to the thermal decomposition of sulfoxides in asphalt binders; 2. lead to significantly different cracking properties results compared to the material testing and pavement simulations for aging below 95 °C	DSR FTIR |E*| DTCF
MTE Services, Inc. (Hanz & Reinke, 2016), (Reinke, G., & Hanz, A, 2018)	135 °C for up to 24 hours and 95 °C up to 20 days;	1. There is a universal exponential relationship exists between colloidal Index and ΔTc; 2. Strong linear relationship exists between carbonyl ratio and R-value. 3. Aging asphalt at temperatures above 100 °C may not impact the relationship between the binder chemical make-up and the binder rheology	DSR

References	Laboratory Aging Condition	Key Findings	Validation Test/ Parameter
NCAT Chen et al. (2018)	Loose mix at 95 °C for different durations; Loose mix at 135 °C with different durations	1. Correlate the hrs.@135 °C aging conditions with field aging based on 70,000 CDD (cumulative degree-days) 2. 8 hrs.@135 °C can simulate an equivalent aging level as 5 days@95 °C; 3. Both can simulate around 70,000 CDD of field aging	DSR BBR FTIR

In addition, the recent findings of the National Cooperative Highway Research Program (NCHRP) 09-54 project on long term aging of asphalt mixtures suggest 95 °C as an optimal temperature for aging loose mix (Kim et al., 2018). The aging time varies with the geographical location of the pavement and should be adjusted based on climate conditions and pavement depth. Also, a climatic aging index (CAI), based on a simplification of the aging kinetics model, was developed from NCHRP 09-54 project to determine laboratory aging durations at 95 °C for asphalt mixtures that best reflect the time, climate, and pavement depth for a given pavement location in the United States using Enhanced Integrated Climatic Model (EICM) hourly pavement temperature data. Zhang et al. (2019&2020) proposed that 5days@95 °C can simulate around 4 years field aging while 12 days@95 °C can simulate approximately 10 years field aging based on New Hampshire historical climatic condition.

3.8.3 Determination Of Suitable Laboratory Long-Term Conditioning Method

Based on the discussion between the research team and the TAP, as well as the findings observed in the literature review, the multi-days at 135 °C recommended by Asphalt Institute and multi-days at 95 °C suggested by NCHRP 09-54 project are selected as the laboratory loose mix aging protocols in this project. 6 hours at 135 °C was selected as the first mixture LTA protocol in the Task-2 for mixture testing, the aging duration for 95 °C protocol was determined based on the discussion of the obtained results in the Task-2.

As a rapid approach to achieve this aim, two RA mixes and one control mix were selected for evaluation. Two aging durations were chosen for investigation: 7 days at 95°C and 10 days at 95°C, to serve as trial conditions. Dynamic Shear Rheometer (DSR) tests were then performed on the binders extracted and recovered from the loose mixes aged for 7 days and 10 days at 95°C, respectively.

Chapter 4: Overview of Materials and Pavement Test Sections

This chapter summarizes the information for asphalt binder and mixture materials, as well the 10 full-scale test sections evaluated in this research project. In the following sections, detailed information is provided in terms of test sections locations, cross section structures, material type and mix design.

4.1 Full-Scale Pavement Test Sections

4.1.1 Location and Traffic

As shown in the Figure 4-1, the full-scale test sections were located on Trunk Highway 6 near Emily, MN. Before the construction of the test section, this segment incorporated an existing bituminous layer, averaging 5 inches in thickness, which rests on a 6-inch aggregate base. This configuration was the result of ongoing resurfacing and rehabilitation activities conducted from 1957 to 2004. From existing conditions and construction history, this section had seen minimal invasive maintenance, primarily focusing on surface treatments that did not significantly alter the structural integrity of the pavement system. Before the current resurfacing, past strategies included periodic milling and overlays, with more substantial reconstructions being performed only where necessary, such as at deteriorated joints or severely damaged panels. The existing mainline lanes, shoulders, and turn lanes within the project limits had undergone various treatments since their initial construction, with records indicating regular maintenance activities dating back to the 1970s.

Figure 4-1 Locations of Evaluated Full-Scale Pavement Test Sections

The MnDOT developed a detailed traffic forecast for the test sections. The field section of TH 6 has projected AADT volumes for 2020 of 2,050. For design purposes, it has been assumed that the 2020 and

2040 AADT volumes are 2,050 and 2,250, respectively. Based on the 20-year projected AADT, the Bituminous Equivalent Single Axle Load (BESAL) forecast for bituminous design is 869,000. The MnDOT report the Heavy Commercial Annual Average Daily Traffic (HCAADT) on the testing section for year 2023 is 180 vehicles/year (Minnesota Department of Transportation, n.d.). For this section, the 20-year projected Concrete Equivalent Single Axle Load (CESAL) forecast is 1,371,000. The real traffic volume is higher than the prediction as shown in **Table 4-1**.

Table 4-1 Predicted Traffic on Field Section Lanes from 2020 to 2050

Year	Service Year	AADT (Unit/Day)	Annual Traffic (Vehicle)	Cumulative Traffic (Vehicle)
2019	0	2700	985500	0
2020*	1	***2635***	961775	985500
2021	2	2586	943890	1947275
2022	3	2560	934400	2891165
2023	4	2546	929290	3825565

4.1.2 Test Section Profile

In 2019, a series of ten overlay pavement test sections were constructed on Trunk Highway 6, each serving a specific purpose in evaluating the properties of different mixtures. As shown in **Figure 4-2**, the construction encompassed a bituminous preservation and resurfacing. The top 2 inches of the existing 5-inch asphalt layer were milled and refilled with new asphalt mixture. Then, a 1.5 inch wearing course containing the 40% RAP recycled from the milled asphalt layer was placed in accordance with MnDOT Specifications. Specific focus areas included improving ride quality and pavement condition of existing pavement while reducing future maintenance needs.

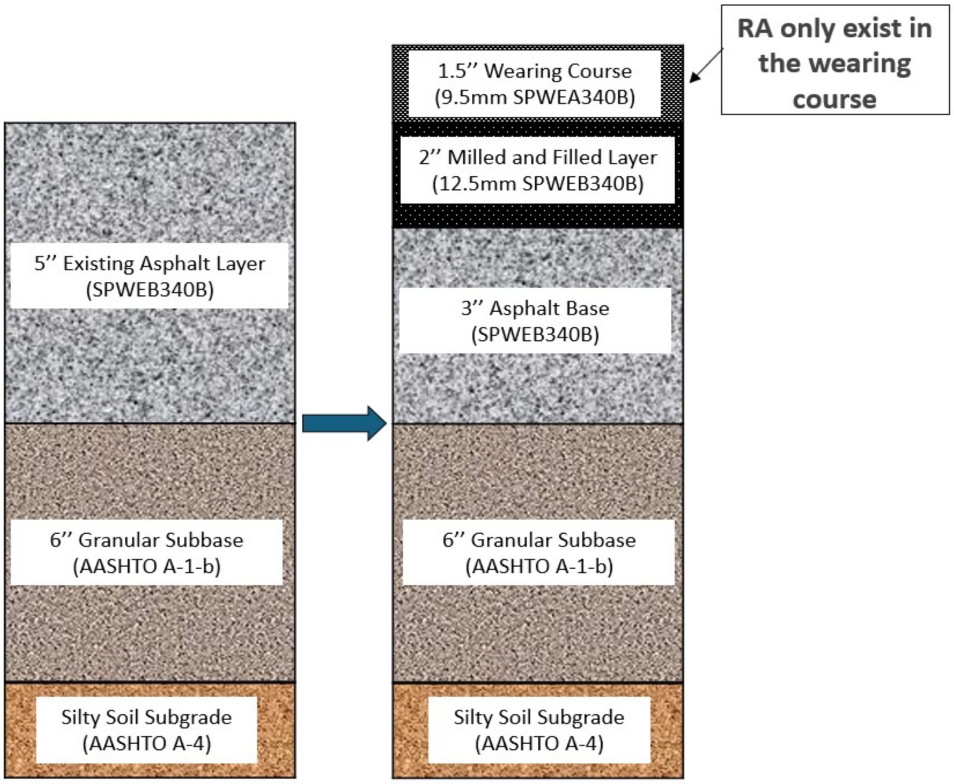

Figure 4-2 Typical Cross-Section of Full-Scale Pavement Test Sections

4.1.3 Materials Information

Table 4-2 below shows the detailed material information of the 10 testing sections evaluated in this project (RAP content is the ratio of the weight of RAP to the total mixture weight). The sole distinction among the 10 testing sections lies in the 1.5-inch wearing course, where varying RAP content and recycling agents were incorporated into the mixture materials. The overlays of these sections comprised seven blends of 40% RAP mixtures incorporating various RAs (6001-6007) and three control mixtures (6010-6012). The construction of these test sections spanned over three days. Control section 6010 with 30% RAP was placed on Day 0 (8/27/2019), followed by the test sections with RA-treated RAP mixes 6001, 6002, 6003, and 40% RAP Day1 control section 6011 on Day 1. The test sections with RA treated RAP mix 6004- 6007 and Day2 control section 6012 with 40% RAP were constructed on Day 2 (8/29/2019).

Note that the asterisk (*) indicates significant issues identified in the construction of the 40% RAP control test section on Day 2, leading to anomalous results. A chemical composition analysis of the extracted and recovered binder confirmed these inconsistencies. To ensure the integrity and reliability of the study's findings, the test results from the 40% RAP Day 2 control sections were excluded from the discussion.

Table 4-2 Information for Plant-Produced and Field Core Mixtures

Mixture ID	RA Supplier	As-extracted Performance Grade (PG)	RAP Content (%)	Production Day
6001 (D1)	Cargill	58.1-37.6	40%	Day 1
6002 (D1)	Poet	61.4-38.8	40%	Day 1
6003 (D1)	US Soybean	54.9-38.4	40%	Day 1
6004 (D2)	Ingevity	62.6-33.7	40%	Day 2
6005 (D2)	Kraton	61.7-34.7	40%	Day 2
6006 (D2)	Asphalt and Wax Innovations	66.8-30.5	40%	Day 2
6007 (D2)	Georgia Pacific	70.5-33.2	40%	Day 2
30% RAP (D0)	--	64.1-31.5	30%	Day 0
40% RAP (D1)	--	65.5-31.6	40%	Day 1
40% RAP (D2)*	--	60.8-33.7	40%	Day 2

Each RA supplier determined the necessary dosage required to attain the target Performance Grade (PG) of XX-34 at low temperatures for the 40% RAP mixture, with no restrictions placed on the high-temperature PG. In terms of the blending methods, six RA products (6001-6006) were added in-line at the plant, while one (6007) was blended at the terminal. All test sections used a PG 58-28 base binder, and samples from the mixed binders, as well as the control and RA-modified mixtures, were collected during production.

All pavement test sections had the same structure, the 40% RAP mixtures had the same mix design, were produced at the same hot-mix plant, and constructed by the same paving contractor. Detailed mix design information for the 30% and 40% RAP mixtures is available in the Appendix. The 30% RAP mixture was designated as the standard mixture, tailored to the traffic and environmental conditions at the project location. As shown in the gradation curves in the **Figure 4-3** below, adjustments to the aggregate stockpile for the 40% RAP was performed to ensured consistent gradation and mix design across all test sections.

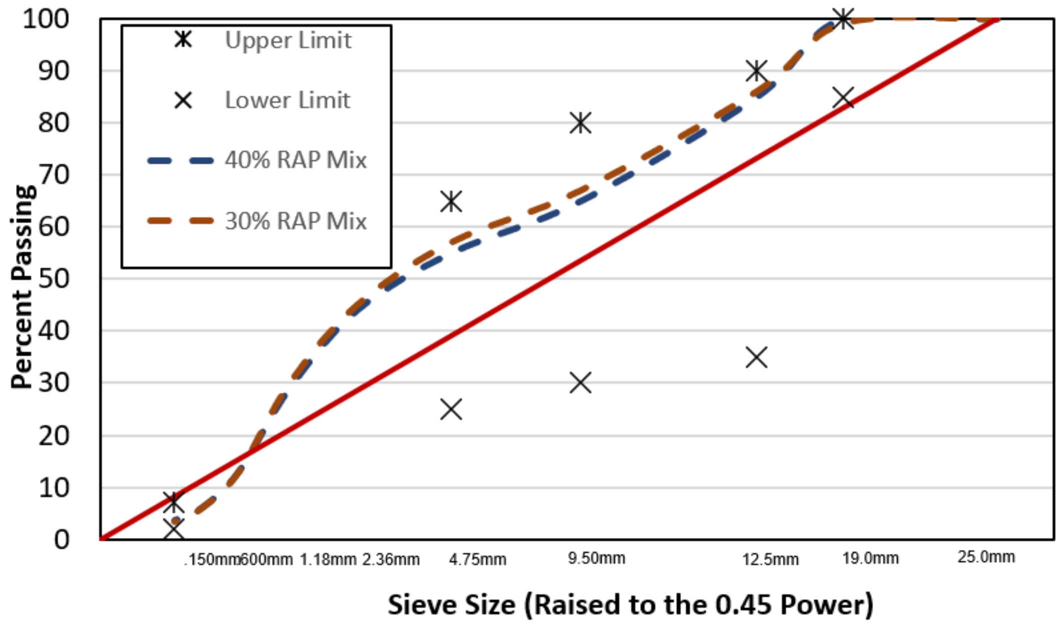

Figure 4-3 Gradation Curves for Mixtures

4.2 Field Performance Indices

After construction, the field performance of the 10 field test sections was monitored by MnDOT. The field monitoring of the test section was conducted twice every year at the time of coring and at the conclusion of each winter. The assessment of field performance encompasses cracking resistance, ride quality, and rutting resistance. To characterize this overall field performance over a four-year service period, three indices: TC-Total, Rut-Total, and IRI-Total were calculated.

4.2.1 Pavement Cracking Performance

For long-term evaluation of cracking performance, most highway agencies utilized varying pavement distress indices, largely determined by the pavement management system they've implemented. Given that the only visible pavement distress observed in the received road survey was transverse cracking, it would be more appropriate to use a cracking performance index that specifically addresses this type of distress. Based on the TAP's suggestion, the distress deduct curves originally proposed for South Dakota, and now adopted by LTPP data base and several other agencies, were employed to characterize the pavement cracking. The distress deduct values were determined using the formulas presented in equations 4.1 through 4.5 for each severity level. The magnitude of pavement distress for each severity level was summed up based on pavement distress deduct values.

$$D_L = 3.4082 * P_L^{0.514} \tag{4.1}$$

$$D_M = 4.4575 * P_M^{0.6107} \tag{4.2}$$

$$D_H = 5.2064 * P_H^{0.6956} \tag{4.3}$$

$$D_T = D_L + D_M + D_H \tag{4.4}$$

$$PCI_T = 100 - D_T \tag{4.5}$$

Where:
P_L, P_M, P_H= percentage of low, moderate, high severity level distress
D_L, D_M, D_H= deduct value at low, moderate, high severity level
D_T= transverse cracking deduct value
PCI_T = pavement condition index for transverse cracking (Range from 0~100)

In order to accurately quantify the cracking performance of the testing sections for the entire 4-year monitoring period, it is important to take the performance degradation rate and overall performance in the service life into account. Therefore, another performance index used in this study is TC-Total, which was proposed to quantify the total field cracking performance across the evaluated service life (Dave et al., 2016). The TC-Total Index employs the notion of cracking work, which involves calculating the cumulative and normalized area of the curve between transverse cracking percentages and the lifespan of the pavement, relative to the most recent recorded service time. A higher TC-Total number indicates that the test section exhibits a greater average annual percentage of transverse cracking performance during the entire service period, from construction to the latest survey.

$$\text{TC-Total} = \frac{\text{Transeverse Cracking Work}}{\text{Life at Latest Survey}^2} \quad (4.6)$$

Another pavement performance index used to quantify pavement distress is the Pavement Surface Rating (SR), which is adopted and recommended by MnDOT. To assess this, distresses are quantified within these 500-foot sections, with each type assigned a weighted percentage based on severity. More serious distresses receive higher weights. These weighted percentages are then aggregated to compute the Total Weighted Distress (TWD). The SR is subsequently calculated from the TWD using the following exponential formula. The SR ranges from 0 to 4, with a higher value indicating better pavement conditions. which quantifies the overall road serviceability and provides a consistent, objective assessment of roadway conditions.

$$SR = e^{(1.386-(0.04)(TWD))} \quad (4.7)$$

4.2.2 Pavement Roughness Performance

The ride quality or roughness was surveyed by MnDOT three times every year, immediately after the construction, mid of the service year, end of the service year. The international Roughness Index (IRI) was utilized to quantify the pavement roughness and translate it into the Ride Quality Index (RQI) for a more relatable assessment of road quality from the public's perspective. The IRI was calculated from data collected by lasers mounted on a Digital Inspection Vehicle (DIV) equipped with lasers and 3D imaging technology which measured the longitudinal profile of the pavement. This profile captured the changing variation in vertical direction as the vehicle moves at highway speeds. The IRI, reflecting vertical movement over a mile (inches/mile), was then correlated to the RQI using a rating panel method. This panel comprised citizens who rate the ride quality of different pavement sections, ensuring the RQI accurately reflects public perception of pavement smoothness.

$$For\ Bituminous\ Pavements: RQI = 5.697 - 0.264 * \sqrt{IRI} \quad (4.8)$$

4.2.3 Pavement Rutting Performance

The Digital Inspection Vehicle also collected detailed data on rutting depth by scanning road surfaces at surveyed intervals along both left and right lanes. Rutting Data was collected twice a year, immediately after the pavement is laid and routinely thereafter to monitor changes. The system captured rutting traces every ¼ inch over 50-foot sections. This data was then analyzed using a Visual Basic macro, which calculated the maximum rut depth(mm) for each test section. A higher Rut Depth indicates that the test section has higher rutting susceptibility with severe permanent deformation.

Chapter 5: Laboratory Testing and Analysis Methods

This chapter provides an overview of the methodologies employed in the laboratory testing of asphalt binders and mixtures. The selection of tests was informed by the comprehensive literature review conducted in Chapter 2 and Chapter 3, as well as consultations with TAP. By drawing from established approaches and expert input, this chapter also outlines the necessary data processing methods and technical details used to assess the characteristics of asphalt binders and mixes.

The summary of the testing methods is presented below in **Table 5-1** below. These methods are organized by material form and aging conditions.

Table 5-1: Summary of Mixture and Binder Tests with Different Material Sources and Aging Conditions

Testing		Loose Mix			Field Cores				In-line Sampled Binder			Extracted and Recovered Binder		
		RPM	135°C LTA	95°C LTA	1-Year	2-Year	3-Year	4-Year	Virgin	RTFO	1xPAV	1xPAV	2xPAV	3xPAV
Mixture Testing	Complex Modulus (E*)	✓	✓	✓	✓	✓	✓	✓						
	Direct Tension Cyclic Fatigue (DTCF)	✓	✓	✓	✓	✓	✓	✓						
	Disk-shaped Compact Tension (DCT)	✓	✓	✓										
	Hamburg Wheel Tracking (HWTT)	✓												
	Tensile Strength Ratio (TSR)	✓	✓											
	Cracking Tolerance Index (CT-Index)	✓	✓											
	Illinois Flexibility Test (I-FIT)	✓	✓	✓		✓	✓							
Binder Testing	Dynamic Shear Rheometer (DSR)	✓	✓	✓	✓	✓	✓	✓	✓	✓	✓	✓	✓	✓
	Fourier-Transform Infrared (FTIR)	✓	✓	✓	✓	✓	✓	✓	✓	✓	✓	✓	✓	✓
	Asphalt Fractionation (SARA)	✓	✓	✓	✓	✓	✓	✓	✓	✓	✓	✓	✓	✓

5.1 Aging Protocols and Specimen Fabrication

5.1.1 Overview Of Materials and Aging Levels

The overview of all materials with various aging levels that are evaluated in this research project is shown in **Figure 5-5**. This research encompasses an extensive array of mixture test results derived from field cores over four years. Furthermore, the research incorporates three distinct loose mix aging levels, each designed to simulate varying degrees of oxidative aging. These include short-term aging achieved through reheating plant-produced mixes to mixing temperature at 135°C (RPM), as well as more long-term aging protocols involving 6 hours at 135°C loose mixes aging (6 hrs. at 135°C LTA) and 7 days at 95°C loose mixes aging (7 days at 95°C LTA). In addition to these mixture evaluations, this research also presents a thorough summary of the testing results pertaining to in-line sampled binder at various aging levels, including original, RTFO (Rolling Thin Film Oven), and PAV (Pressure Aging Vessel) conditions. The study further examines extracted and recovered binders subjected to different PAV aging cycles, as well as those retrieved from field cores and loose mix aged mixture.

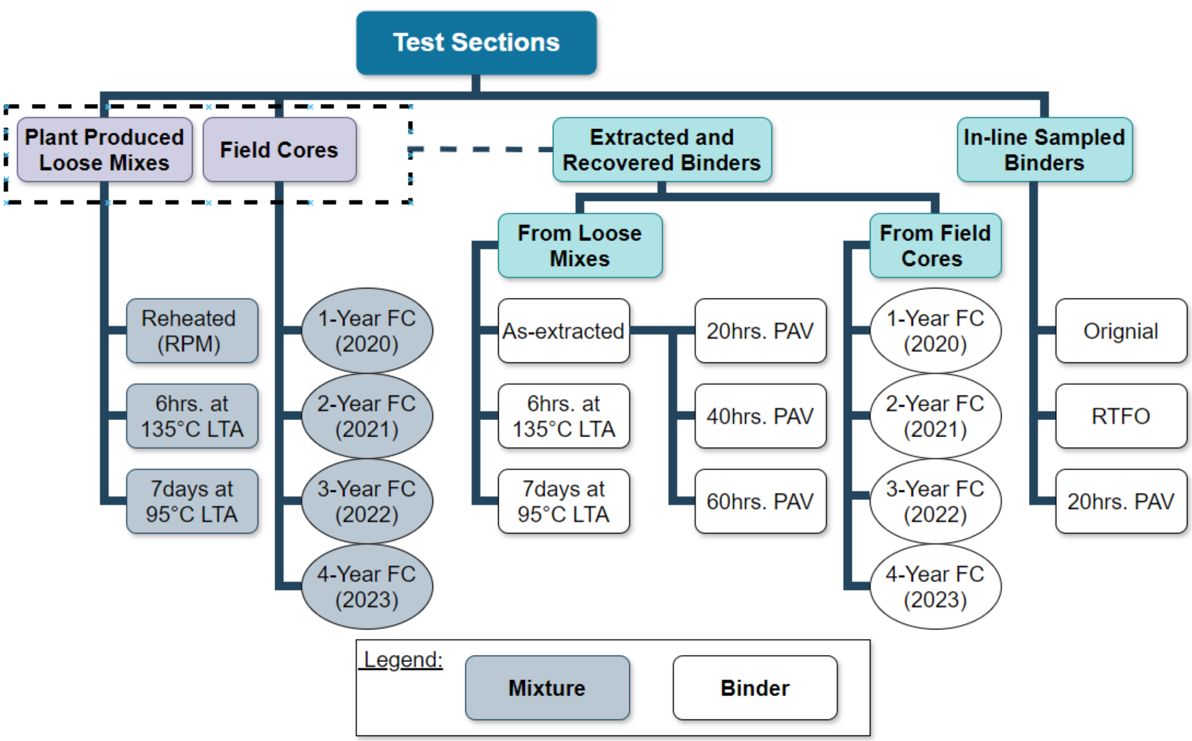

Figure 5-1 Overview Flow Chart of Materials and Aging Levels

5.1.2 Aging Protocols on Sampled Binder and Extracted Binder

For the base and binder blends sampled during production, the tests are conducted on binder samples with the original (unaged), RTFO (Rolling Thin-Film Oven) and standard 20 hrs. PAV (Pressure Aging

Vessel) conditions. For the binders extracted and recovered from the ten mixtures/sections, the tests are performed on binders recovered from production mix (as extracted) and then also after PAV aging (20hr, 40hr, 60hr). Binders are also extracted and recovered from mixture after long-term aging (LTA) (6 hrs. @ 135C), 1-year field cores, and 2-year field cores. The six-hour LTA mix aging condition was the first studied based on agency interest to evaluate an efficient method to obtain aged mixed properties.

5.1.3 Aging Protocols on Loose Mix and Specimen Fabrication

5.1.3.1 Reheated Plant Mix and Loose Mix Aging at 135°C

To produce the RPM mixtures, the plant produced loose mixes were reheated to the compaction temperature at 135°C (about 40~50min) and then compacted to fabricate test specimens. The 6-hour aging at 135°C for loose mix was selected as the primary long-term aging (LTA) protocol in this study. Agency interest is the reason that the 6 hour, 135°C protocol was the first loose mix aging method evaluated in this study. This procedure emulates an estimated 70,000 cumulative degree-days (CDD) in the field, a point at which pavements typically begin to exhibit prominent top-down cracking issues (Chen et al., 2020). For this LTA conditioning process, the loose mix was uniformly spread in steel pans to an approximate depth of 25 mm. It was then heated in the oven at 135°C for 6 hours without any stirring.

5.1.3.2 Loose Mix Aging at 95°C

The additional long-term aging protocol selected for this study is 7-day aging at 95°C. Prior to aging, the loose mix was uniformly distributed in steel pans to a depth of about 25 mm, roughly twice of mixture NMAS. The following efforts were implemented to ensure consistent and even aging of the loose mix:

1. The pans were staggered in the oven to facilitate even circulation of the heated air through each pan.
2. The loose mixes in the pans were fully stirred every day at a consistent time. The loose mix is fully stirred with the gardener's shovel to break the oxidized and hardened asphalt mix cluster to avoid partial aging or uneven aging of the asphalt.
3. The position of each mix pan was rotated to the subsequent quadrant as indicated by white arrows in Figure 5-2.

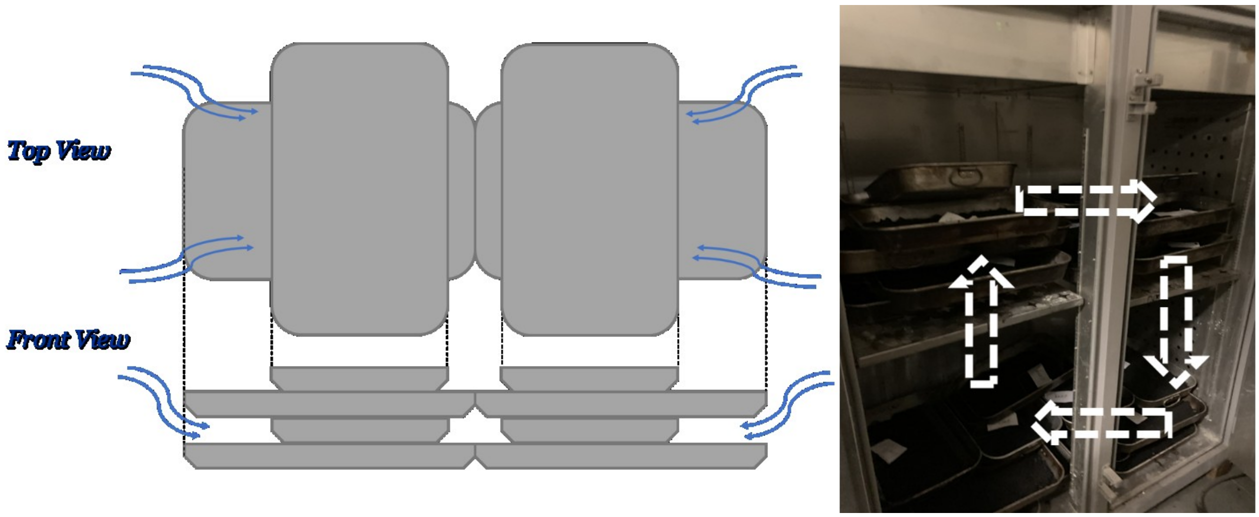

Figure 5-2 Lab Practice of 95°C Loose Mix Aging Protocol

After the aging process, the aged mixtures were compacted using a Superpave gyratory compactor. The objective was to produce final test specimens with air void contents of 7 ± 0.5%.

5.1.4 Pavement Field Cores

Field cores were sampled from the 10 field sections of TH6. All test specimens from the field cores were extracted from the top two inches of the pavement surface. For the mixture testing, the small-scale complex modulus test geometry is adopted to characterize the rheological properties of the field cores. The top two inches of the field cores were cut, and the air void contents measured on the resulting disks. As shown in Figure 5-3 the small cylinder specimens were then cored horizontally to fabricate test specimens. Figure 5-4 below shows the air void contents measured on the field cores as well as the test small cylinder specimens drilled from near the top of the field cores. The air void content generally decreases with the increasing service years for all 10 sections.

The 1-Year, 2-Year, and 4-Year FC field core binders were extracted and recovered from the top half inch of each field core after the small specimens were attained. The 3-Year FC field binder was extracted and recovered from the small-scale mixture testing specimens because the cored shells were contaminated.

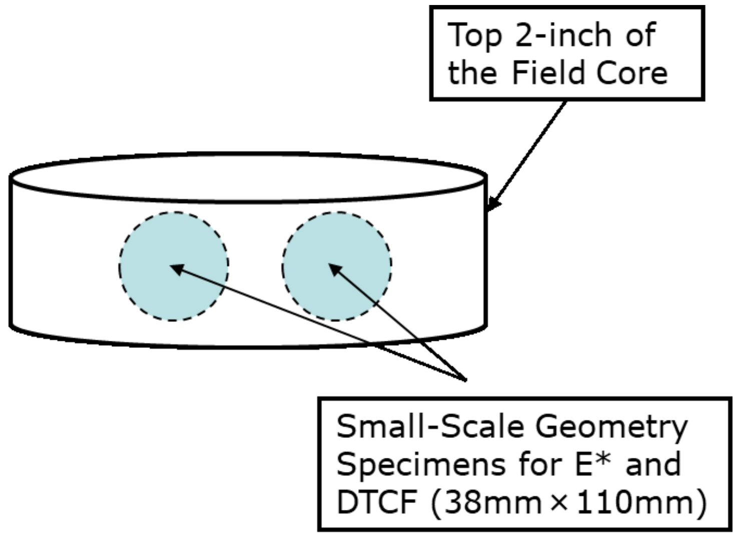

Figure 5-3 Coring Method of Field Core for Small-Scale Specimens

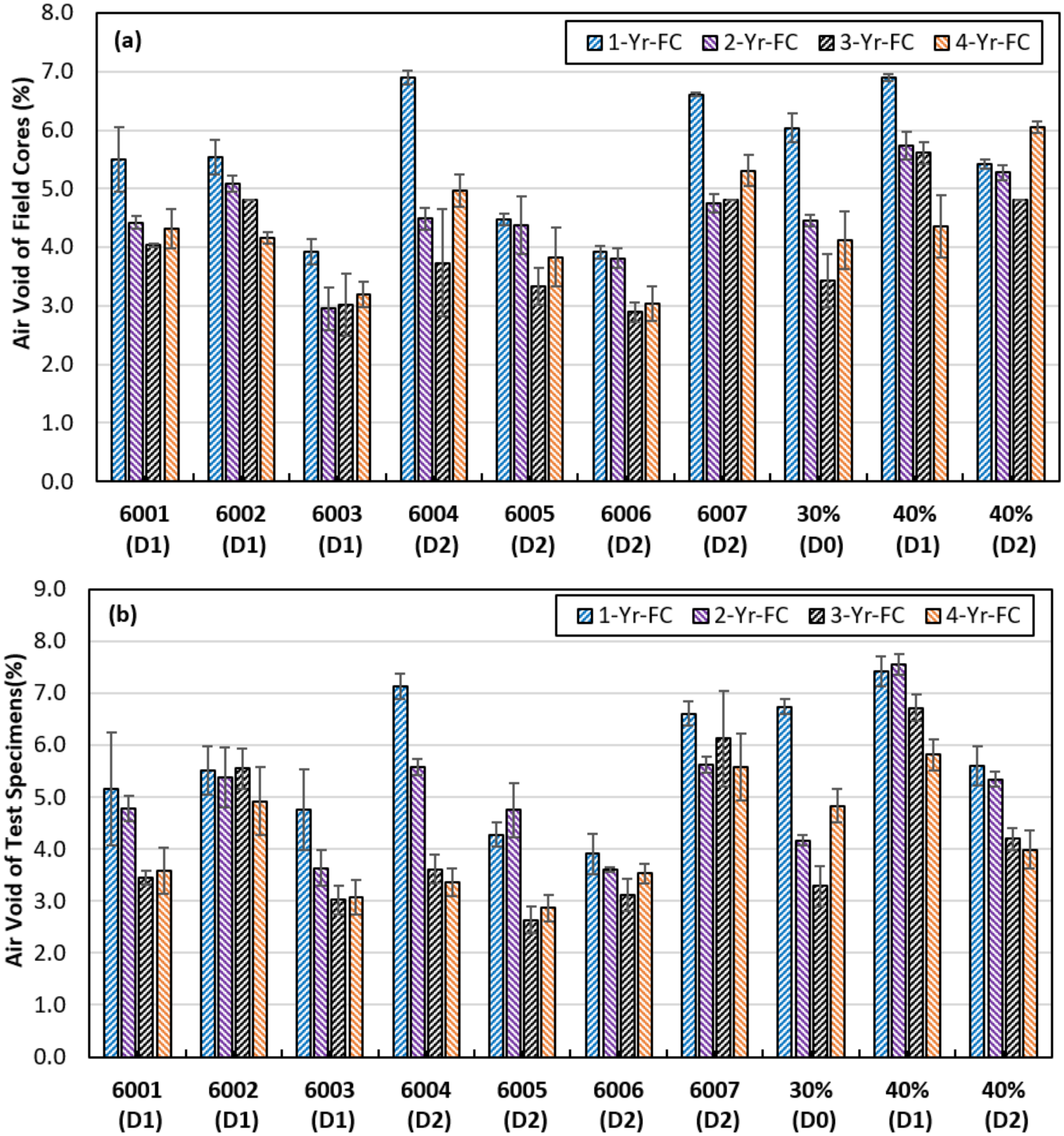
(a)
1-Yr-FC
2-Yr-FC
3-Yr-FC
4-Yr-FC
Air Void of Field Cores (%)
0.0
1.0
2.0
3.0
4.0
5.0
6.0
7.0
8.0
6001 (D1)
6002 (D1)
6003 (D1)
6004 (D2)
6005 (D2)
6006 (D2)
6007 (D2)
30% (D0)
40% (D1)
40% (D2)
(b)
1-Yr-FC
2-Yr-FC
3-Yr-FC
4-Yr-FC
Air Void of Test Specimens(%)
0.0
1.0
2.0
3.0
4.0
5.0
6.0
7.0
8.0
9.0
6001 (D1)
6002 (D1)
6003 (D1)
6004 (D2)
6005 (D2)
6006 (D2)
6007 (D2)
30% (D0)
40% (D1)
40% (D2)

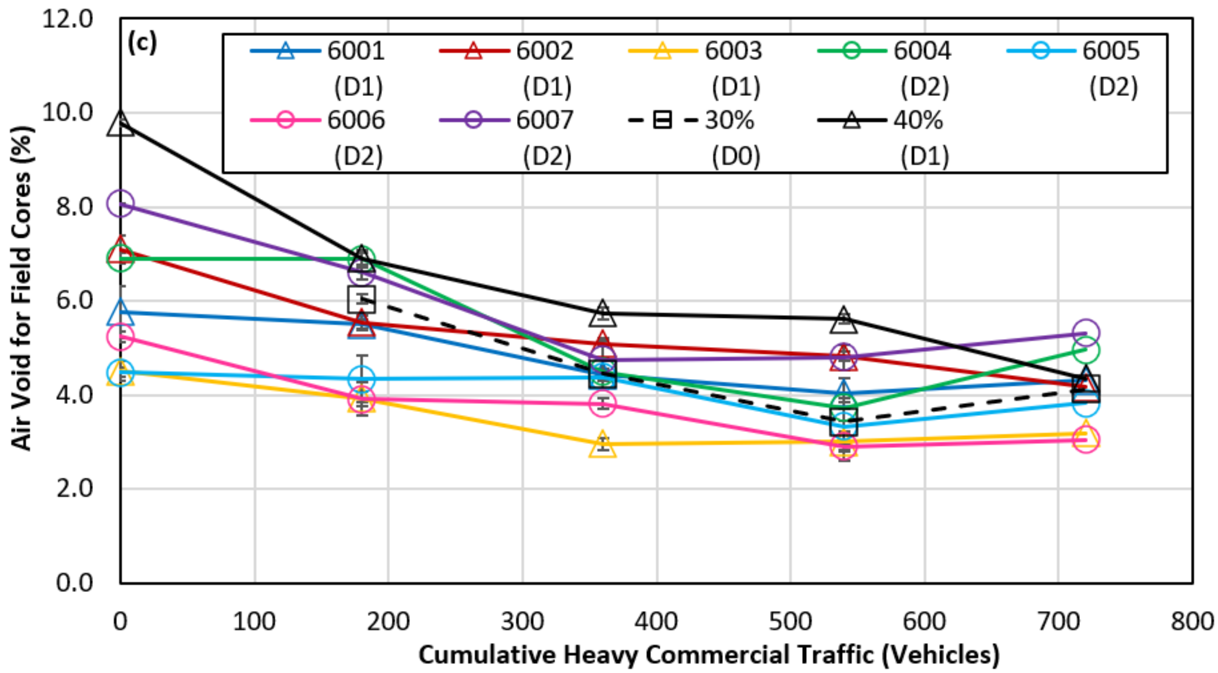

Figure 5-4 Air Void over Time for (a) Field Cores and (b) Test Specimens (c) Field Core Air Void vs. Heavy Traffic

5.2 Binder Testing and Analysis Methods

5.2.1 Binder Extraction and Recovery

Asphalt binder was extracted (ASTM D2172 - centrifuge) and recovered (ASTM D7906) with the rotary evaporator. The solvent used was toluene. The binder samples were extracted from the following asphalt mixture:

- Sampled plant-produced loose mix. Binder was recovered then aged in the pressure aging vessel for 20, 40, and 60 hrs.
- Field sampled loose mix from construction. The loose mixes aged at a nominal thickness of 1.5" for 6 hours at 135°C, and 7 days at 95°C.
- Field cores after years in-service. Nominally the top ½" of the field core was cut and used for recovery.

5.2.2 Complex Shear Modulus Testing

The rheological properties of asphalt binders were measured using a Dynamic Shear Rheometer (DSR) using the parallel plate testing geometry. DSR testing with 8 mm and 25 mm plates was done according to AASHTO T315. The 4mm parallel plate geometry was used to construct complex modulus and phase angle master curves. Testing was conducted at temperatures ranging from -40°C to 50°C and frequencies from 0.2 to 100 rad/s. Strain levels were adjusted at different isotherms to maintain material response remained in the linear visco-elastic region. Tests were conducted from the coldest to the warmest temperature and from the highest to the lowest frequencies. The complex shear modulus master curve is constructed at 25°C in this study and fit by the Christensen-Anderson-Marasteanu model (CAM, as shown in following Equations) using the RHEA software.

$$G^*(w) = \frac{G_g}{\left[1+(w_0/w)^{\beta}\right]^{k/\beta}} \tag{5.1}$$

$$\beta = log2/R \tag{5.2}$$

Where:
$G^*(w)$: complex shear modulus at a given frequency (Pa);
G_g: glassy asymptote (modulus) (Pa);
w: frequency (rad/s);
w_0: crossover frequency (rad/s);
k: fitting coefficient.
R: difference between the logarithmic glassy modulus and the logarithmic equilibrium modulus of the binder, simplified as Log |G*| at glassy asymptote (approximately 1E9 Pa) minus Log |G*| at the crossover frequency.

As shown in the following Equation, the R-value requires estimation of the glassy modulus. RHEA uses an extrapolated value of glassy modulus, which can result in values significantly higher than the 1E9 Pa generally assumed. For example, the average glassy modulus from the data generated in this study was 2.2E9, range 1.7E9 to 3.1E9. The variation can confound interpretation of trends in R-value for different samples or aging conditions. An alternative method of calculating R-Value from NCHRP 9-59 is provided in **Equation 5.3** (Christensen & Tran, 2022).

$$R = \log(2)\frac{log\left(|G^*|/1\times10^9\right)}{log(1-\delta/90)} \tag{5.3}$$

Where:
R = Christensen-Anderson R-value (rheological index)
|G*|= dynamic complex modulus, in Pascal (Pa)
δ = binder phase angle at the same temperature and frequency as |G*|

Calculation of R-value using **Equation 5.3** requires a complex modulus value of at least 10 MPa. For this study the modulus and phase angle at a frequency of 1 rad/s from the last isotherm that exceeded a modulus of 10 MPa was used.

R-value calculated by **Equation 5.2** and **Equation 5.3** are compared in **Figure 5-5**. Two methods of calculating R-value were investigated. The first is the traditional R-value calculation from the CAM model which uses an extrapolated Glassy modulus value, the second is the method using a single modulus and phase angle value, given the modulus is above 10 MPa. For this study a frequency of 1 rad/s was used. The comparison between the two methods provided in **Figure 5-5** shows that with increasing R-value there is more deviation from the line of equality. Higher R-values represent more brittle or aged asphalt binder property and have an increased potential for a higher value of extrapolated glassy modulus. The Christensen method for calculating R-value was used in preparation of the proceeding plots to remove potential confounding effects of extrapolated glassy modulus on interpreting trends in R-values within the dataset.

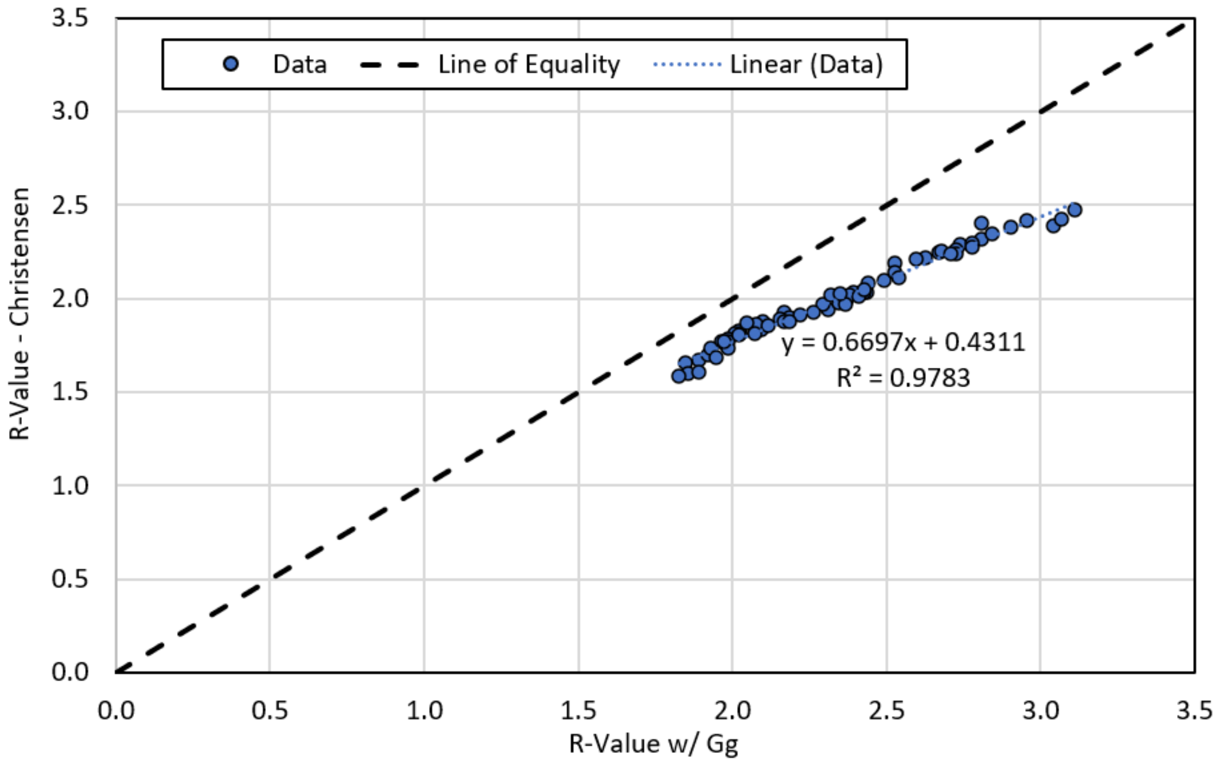

Figure 5-5: Comparison of R-Value Calculated by Christensen NCHRP 9-59 Method and Extrapolated Glassy Modulus

The 4mm frequency sweep data was used to estimate intermediate and low temperature grades for all field and lab aging conditions. Estimating low temperature PG using the 4mm DSR requires converting from the frequency domain, $G^*(\omega)$, to the time domain, $G(t)$ master-curve and using empirical relationships to determine critical BBR critical values (Sui C. , Farrar, Harnsberger, Tuminello, & Turner, 2011), (Sui C. , Farrar, Tuminello, & Turner, 2010). The BBR to 4mm conversion factors used in this study were S(60) = 300 MPa, G(60) = 143 MPa, and m(60) BBR = 0.300, m(60) 4mm = 0.275. These values were adjusted slightly from original conversion factors published based on internal testing at MTE. Results presented in **Figure 5-6** for S-Critical temperature show agreement. The 4mm DSR estimate consistently predicts m-critical values 1°C warmer than the BBR (**Figure 5-7**).

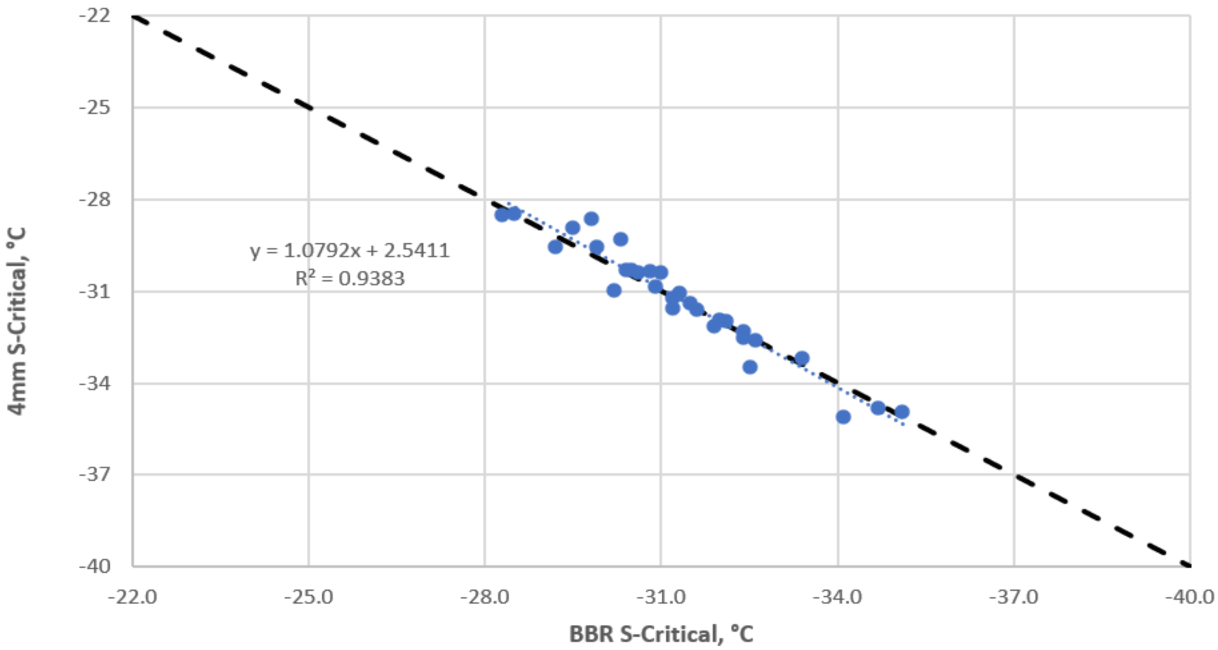

Figure 5-6: Comparison of 4mm S-Critical Temperature Estimate to BBR Results

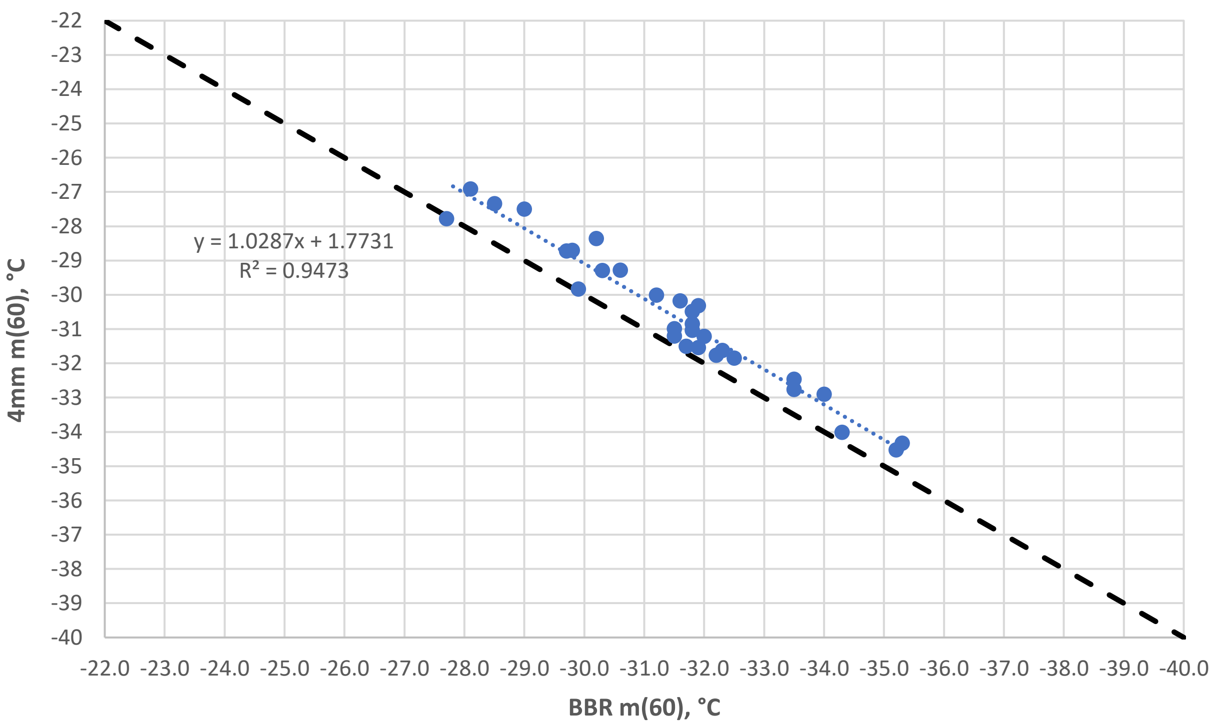

Figure 5-7: Comparison of 4mm m-Critical Temperature Estimate to BBR Results

The ΔTc parameter is an important parameter that provides insight into asphalt binder relaxation properties under aging (Robertson et al., 2001; Anderson et al., 2011). It can be calculated from critical values from BBR or 4mm DSR measurements. ΔTc is defined as the difference between the temperature at which the stiffness (S(t) or G(t) and m-value critical criteria from the BBR or 4mm testing are met, as shown in **Equation 5.4**.

$$\Delta T_c = T_{(stiffness)} - T_{(m\text{-}slope)} \tag{5.4}$$

Where:
$T_{(stiffness)}$: critical low temperature at which S(60) =300 MPa (BBR) or G(60) = 143 MPa (4mm);
$T_{(m\text{-}slope)}$: critical low temperature at which m(60) = 0.300 (BBR) or m(60) =0.275 (4mm).

When the ΔT_c value is positive, the binder grade is controlled by the creep stiffness (S-controlled); when the ΔT_c value is negative, the binder grade becomes m-controlled. S-controlled binders typically have better stress relaxation capability and are therefore typically less prone to cracking. Threshold values for cracking warning and failure limits of ΔT_c = -2.5°C and ΔT_c = -5.0°C were proposed when the parameter was introduced (Anderson, King, Hanson, & Blankenship, 2011). Recent research recommended no changes to the threshold values. (Al-Badr et al., 2021; Christensen et al., 2019).

The complex modulus master curve from the DSR test allows for determination of the binder Glover-Rowe parameter (Anderson, King, Hanson, & Blankenship, 2011; Christensen et al., 2019). The binder G-R parameter is calculated at the temperature and frequency combination of 15°C and 0.005rad/sec, as shown in **Equation 5.5**. A lower G-R parameter indicates better capability to resist durability cracking. A limiting value of 180 kPa is proposed as a crack warning limit, a second value of 600 kPa is suggested for the development of significant cracking (block cracking).

$$G - R = \frac{|G^*|(cos\delta)^2}{sin\delta} \tag{5.5}$$

Where:
δ: phase angle of the binder;
G^* = Complex modulus of the binder.

5.2.3 Asphalt Fractionation (SARA)

Asphalt binder composition was measured by SARA (Saturates, Asphaltenes, Resins, and Aromatics) using an internal standard operating procedure (SOP) developed by MTE Services. Asphaltenes were precipitated from the maltenes using n-heptane as a solvent. The maltene solution is tested with the IATRSOCAN which uses a combination of thin layer chromatography and flame ionization detection to quantify the relative proportions of saturates, resins, and aromatics. The Colloidal Index, defined as the ratio of the dispersed constituents (resins + aromatics) to flocculated constituents (asphaltenes + saturates) was used to quantify changes in composition (Loeber, 1998). The calculation of Colloidal Index is provided in the following Equations.

$$CI = \frac{Resins+Aromatics}{Asphaltenes+Saturates} \tag{5.6}$$

$$CI = \frac{A_R+R}{A_S+S} \tag{5.7}$$

Where:
A_S = denotes the asphaltene content;
S = saturate content;
R = resin content; and,
A_R = Aromatic content.

5.2.4 Fourier-Transform Infrared Spectrometer (FTIR)

A Fourier-transform infrared spectrometer emits infrared photons at the sample. These photons can be absorbed by the sample, exciting parts of the molecule to vibrate or rotate. Different molecules absorb different wavelengths of photons depending on their structure and the types of bonds and functional groups in the molecule. Thus, the infrared peak intensities measured from FTIR analysis have been widely used for identifying and characterizing key functional groups in asphalt (Lima et al., 2004; Pasandín et al 2015).

The peak-area intensity of the oxygenated groups (C=O and S=O) can be used to reflect the degree of aging and rejuvenation of the asphalt blends, thus are calculated for evaluation of the study binder blends. The functional groups indices including carbonyl index and sulfoxide index can be determined from the following equations (Marsac et al., 2014; Hofko et al., 2017).

$$I_{C=O} = \frac{Carbonyl\ Peak\ Area\ (around\ 1700\ cm^{-1})}{Asphaltic\ Peak\ Area(\ 1350\text{–}1500\ \ cm^{-1})} \tag{5.8}$$

$$I_{S=O} = \frac{Sulfoxide\ Peak\ Area\ (around\ 1030\ cm^{-1})}{Asphaltic\ \ Peak\ Area\ (\ 1350\text{–}1500\ \ cm^{-1})} \tag{5.9}$$

$$Peak\ Area = \int_L^U A(w)dw - \frac{A(U)+L(L)}{2} * (U - L) \tag{5.10}$$

Where: Peak Area represents the integral between the absorbance curve and the baseline intensities

Modern infrared spectrometers have operating software that not only generates infrared spectra but also provide functionality to set the baseline range and the wavenumber integration range and to calculate the areas under the regions of interest.

The asphaltic peak area always shows good stability within the same asphalt binder and shows little variation across most asphalt binder materials; it can be used as the stable reference for both carbonyl index and sulfoxide index. However, wave numbers that define the carbonyl range are not always fixed, and they might vary with the different material compositions (Hofko et al., 2018). Based on the research team's experience, the traditional quantification function should be adjusted with a carbonyl peak area defined by an extended range and baseline. The reason behind this adjustment is related to the addition of bio-based RA, where esters show high concentrations in the FTIR result for the study RA additives. The baseline region is shown in **Figure 5-8.** **Figure 5-9** shows absorbance peaks of carboxylic acids (centered at 1700 cm^{-1}) for the 40 hour and 60-hour PAV samples of the Day 1 control binder from the project. **Figure 5-10** shows IR scans from mix 6003 on as-recovered binder and after 20-, 40-, and 60-hour PAV aging. Visual inspection of the plot shows increasing IR intensity values for both esters and carboxylic acids. Because both types of carbonyl functional groups increase with aging the total area for both are included in total carbonyl determination.

Equation 5.11 shows the adjusted equation for carbonyl group characterization that will be used in this study; the quantification area is expanded to include wavelengths from 1676 cm^{-1} to 1763 cm^{-1} and the baseline is expanded to include 1525 cm^{-1} to 1800 cm^{-1}. The carbonyl wavelengths reported may vary slightly from sample to sample, final determination is based on location of the peaks in the IR scans.

$$I'_{C=O} = \frac{Carbonyl\ Peak\ Area\ (1676\text{–}\ 1763\ cm^{-1})}{Stable\ Region\ Peak\ Area\ (1350\text{–}1500\ \ cm^{-1})} \tag{5.11}$$

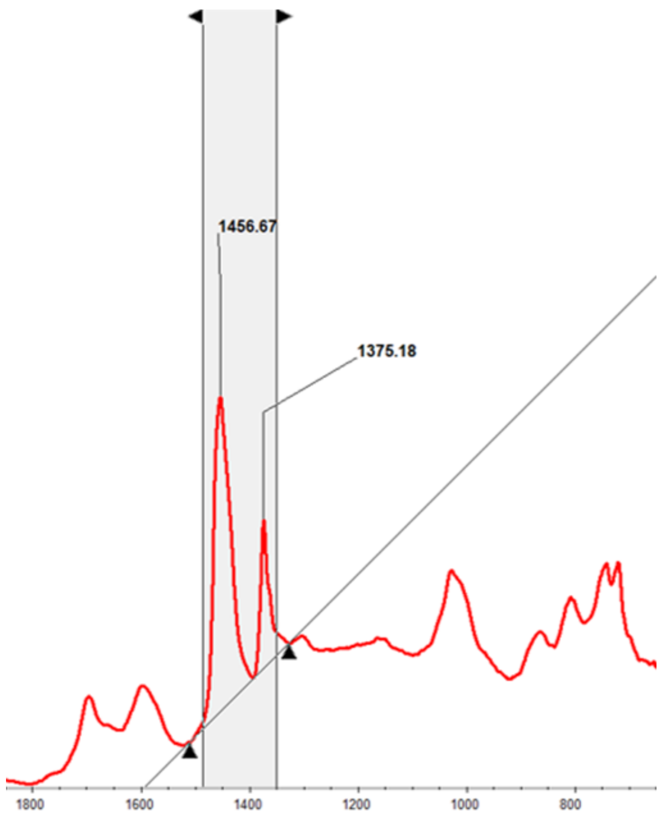

Figure 5-8 Stable Region Baseline 1500-1328 cm^{-1}, Peaks centered at 1456 and 1375 cm^{-1}

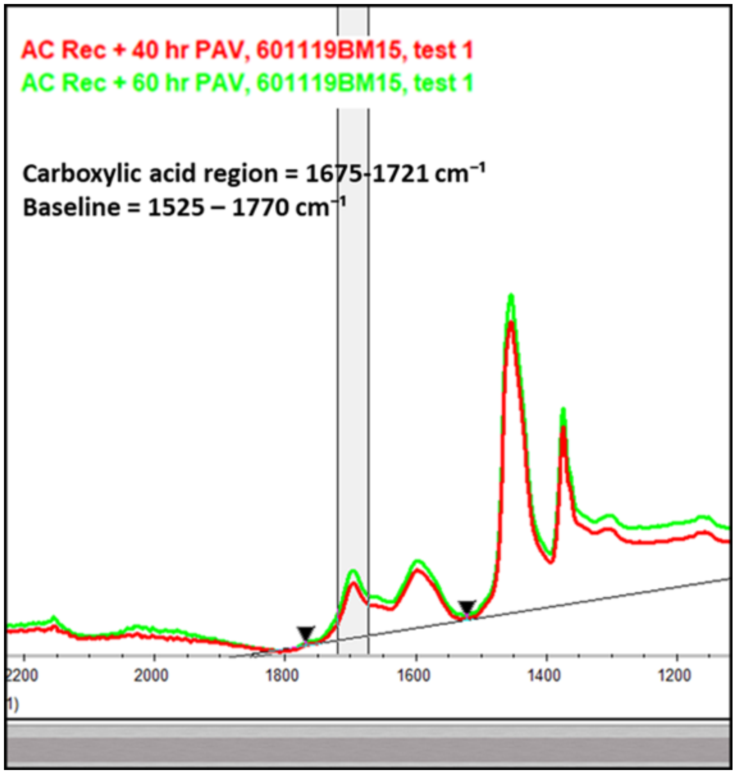

Figure 5-9 IR Scan Showing a Typical Carboxylic Acid Region

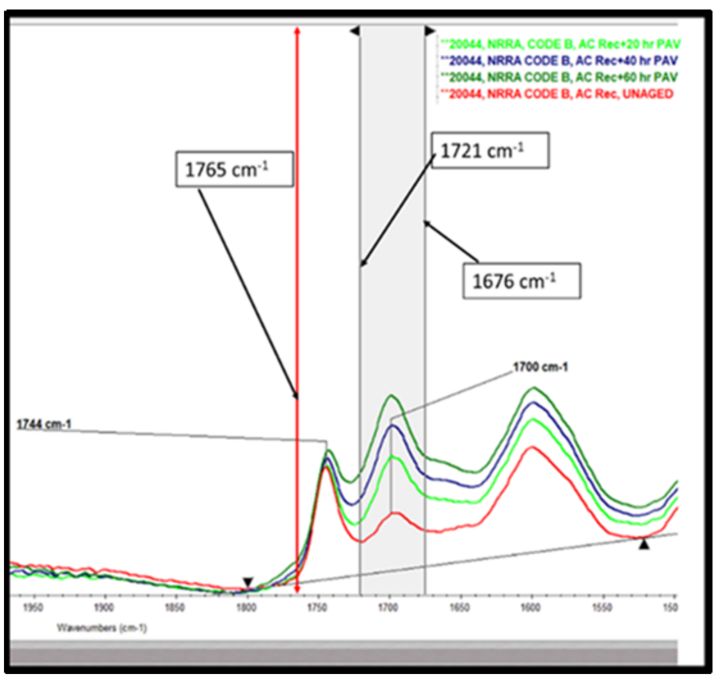

Figure 5-10 IR Scan Showing Both the Carboxylic Acid Region Centered at 1700 cm^{-1} and Ester Region Centered at 1740 cm^{-1}

5.3 Mixture Testing and Analysis Methods

This section outlines various testing methods used to analyze the properties of asphalt mixtures and field cores. This section delves into comprehensive mixture laboratory tests including Complex Modulus Test, Direct Tension Cyclic Fatigue Test, Hamburg Wheel Tracking Test, Illinois Flexibility Index Test, Cracking Tolerance Index Test, Disk-Shaped Compact Tension Test and Tensile Strength Test. Each test is described in detail with respect to the methods used to evaluate the properties of the RA-treated asphalt mixes.

5.3.1 Complex Modulus Testing

The rheological properties of the field core mixtures were measured following the AASHTO T-342 procedure at various temperatures (2.9, 18.0, 30.0°C) and frequencies (0.1, 0.5, 1.5, 10, 25 Hz) using an Asphalt Mixture Performance Tester (AMPT). Dynamic modulus (|E*|) and phase angle (δ) master curves were constructed using Abatech RHEA® software. The mixture Glover-Rowe ($G\text{-}R_m$) parameter, which indicates the general cracking resistance (Mensching et al., 2017) were computed from the complex modulus data. Generally, a lower $G\text{-}R_m$ value indicates better cracking resistance while a higher CMRI value indicates better rutting resistance.

The dynamic modulus can be characterized using the following sigmoidal model, where the shape parameters for lower and upper asymptotes can capture the viscoelastic properties in a wide frequency range.

$$\log|E^*| = \delta + \frac{\alpha}{1+e^{\beta+\gamma\log(\omega)}} \tag{5.12}$$

Where:
$|E^*|$ = dynamic modulus.
ω = reduced frequency shifted by Time-temperature Superposition Principle (TTSP).
α = upper asymptotic value of the master curve.
δ = lower asymptotic value of the master curve.
γ = the width of the s-shape zone.
β = the position of the reflection point.

The phase angle can be expressed as the Lorentzian Peak function:

$$\log|\delta| = \frac{(d\cdot b^2)}{((\log(\omega)-c)^2+b^2)} \tag{5.13}$$

Where:
b = growth rate
c = critical point
d = peak value of the function

The mixture Glover-Rowe (G-R$_m$) parameter (Glover et al., 2015) was initially developed as a parameter to evaluate the cracking resistance of binders. The mixture G-R$_m$ parameter was shown to have good relationship with the mixture cracking properties (Mensching et al., 2017). The G-R$_m$ parameter has a similar format as binder G-R parameter and can be expressed as Eq. 3:

$$G - R_m = \frac{|E^*|(cos\delta)^2}{sin\delta} \quad (5.14)$$

Where:

$|E^*|$, δ= dynamic modulus and phase angle (21.1°C at 5Hz suggested by NCHRP 09-58).

5.3.1.1 Adjustment of Field Core Master Curves

In this project, a comparison is required between complex modulus testing results from field core specimens and laboratory-compacted specimens. However, mixture test properties are influenced by the air void content of the specimen. To allow for direct comparison of complex modulus testing results from laboratory-compacted (controlled to 7% ± 0.5) and field core (variable air void content) specimen, the field core master curve data was adjusted to 7%. The adjustment procedure uses the Hirsch model (Equation 10) and the process shown in **Figure 2-11**. The |E*| master curve, phase angle master curve and in-situ volumetric properties are used with the Hirsch model to back-predict |G*| values using nonlinear regression methods. The back-predicted |G*|values are then used with the volumetric properties at the target air void level (7%) to calculate the adjusted master curve. **Figure 5-12** shows an example of dynamic modulus and phase angle master curves before and after adjustment. In this example, the dynamic modulus master curves of the field cores dropped, and phase angle master curves increased after adjusted from in-situ air void level to target air void level (7%).

$$\begin{aligned} |E^*_{\text{mix}}| = & P_c\left[4{,}200{,}000(1 - VMA/100) + 3|G^*|_{\text{binder}}\left(\frac{VFA \times VMA}{10{,}000}\right)\right] \\ & + (1 - P_c)\left[\frac{1 - VMA/100}{4{,}200{,}000} + \frac{VMA}{3VFA|G^*|_{\text{binder}}}\right] \end{aligned} \quad (5.15)$$

$$\delta_{mix} = -9.5(\log Pc)^2 - 39\log Pc + 9.6 \quad (5.16)$$

$$P_c = \frac{\left(20 + \frac{VFA \times 3|G^*|_{\text{binder}}}{VMA}\right)^{0.58}}{650 + \left(\frac{VFA \times 3|G^*|_{\text{binder}}}{VMA}\right)^{0.58}} \quad (5.17)$$

Where:
P_c= contact volume parameter
$|G^*|_{\text{binder}}$ = binder shear modulus
$|E^*|_{mix}$= mixture dynamic modulus
δ_{mix} = mixture phase angle
VMA = voids in the mineral aggregate
VFA = voids filled with asphalt

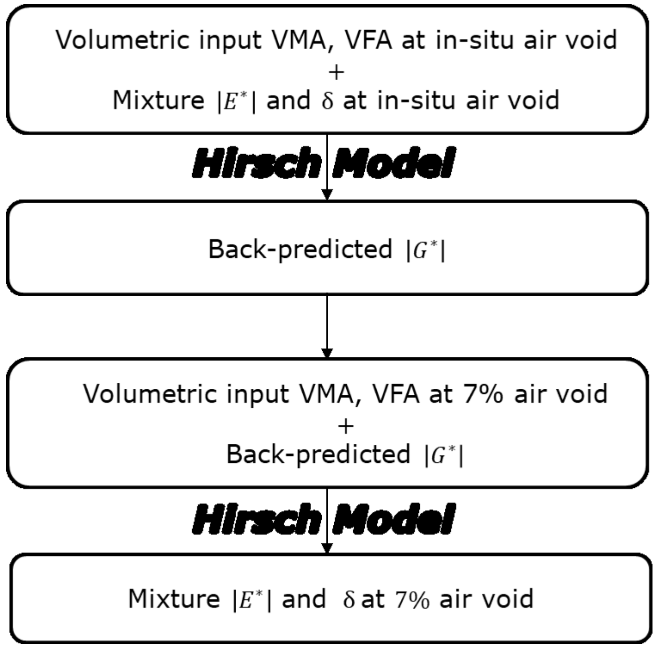

Figure 5-11 Process for Adjusting Field Core |E*| and Phase Angle Master Curves with Hirsch Model

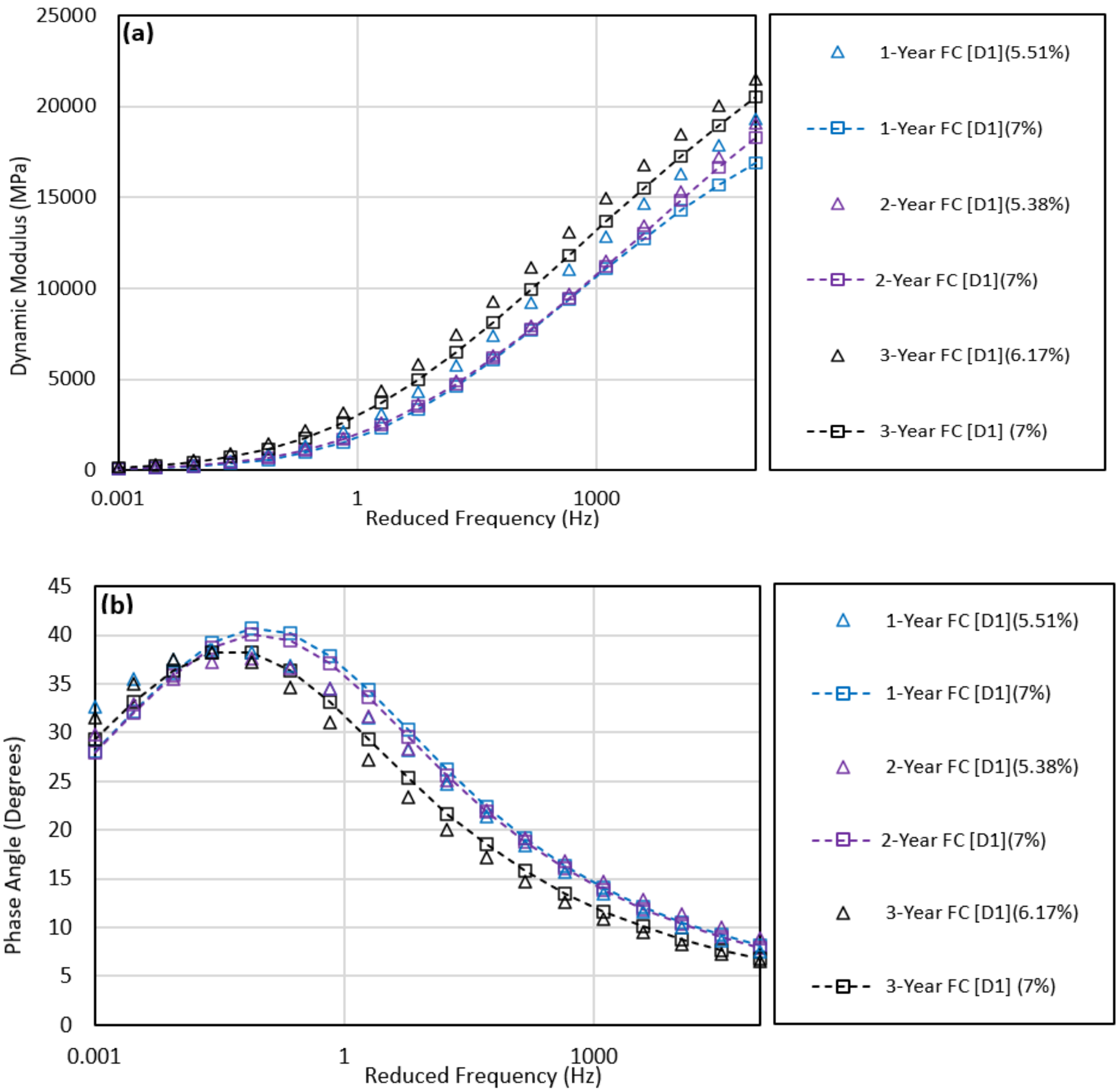

Figure 5-12 Example Master Curves Before and After Air Void Adjustment (a) Dynamic Modulus; (b) Phase Angle

5.3.2 Direct Tension Cyclic Fatigue Test (DTCF)

The uniaxial Direct Tension Cyclic Fatigue (DTCF) Test was conducted in accordance with AASHTO TP 107 to evaluate the fatigue properties for all aging conditions. The test was conducted at a constant temperature of 11°C determined based on the continuous PG of the binders extracted and recovered from the mixtures. The simplified viscoelastic continuum damage (S-VECD) approach was used for the data analysis. There are two fatigue property parameters: D^R (fatigue failure parameter) and S_{app} (apparent fatigue damage resistance capacity) that are used to evaluate the ability of the mixtures to resist fatigue cracking in this study.

The fatigue failure parameter D^R is a constant defined as the average loss of integrity per loading cycle before the specimens reach failure. (Wang et al, 2017) The D^R values can be determined using **Equation 5.18** From the definition, a higher value of D^R indicates higher resistance to cyclic loading.

$$D^R = \frac{\int_0^{N_f} (1-C)dN}{N_f} = \frac{\sum(1-C)}{N_f} \tag{5.18}$$

Where:
N = number of load cycles.
N_f = maximum number of load cycles up to failure.
C = normalized pseudo-stiffness, which decreases from the value of 1 as the damage gets cumulated.

Mixture fatigue parameter S_{app} is defined as the accumulated damage when C (pseudo stiffness) is equal to 1-D^R (Wang et al., 2018). The S_{app} is expressed in **Equation 5.19** and captures both stiffness and toughness information of the material. Mixtures with higher S_{app} value are expected to have higher fatigue damage resistance.

$$S_{app} = \frac{1}{10000} \times \left(\frac{1}{C_1} \times D^R\right)^{\frac{1}{C_2}} \tag{5.19}$$

Where:

C_1 ,C_2 = the model coefficients in C-S curve determined from S-VECD theory.

5.3.3 Disk-shaped Compact Tension Test (DCT)

The Disk-shaped Compacted Tension (DCT) testing (ASTM D 7313) was conducted to compare the fracture properties at low temperatures for the study mixtures. The test temperature is 10°C warmer than the PG of the base binder. As following equations 14 and 15, The measured data were analyzed to calculate the fracture energy (G_f) and fracture strain tolerance (FST) parameter (Zhu et al., 2017).

$$G_f = \frac{U_f}{t \cdot ligam} \tag{5.20}$$

$$FST = \frac{G_f}{P} \tag{5.21}$$

Where:
t = specimen thickness.
$(W - a)$ = initial ligament length.
P = peak strength before failure.
U_f = work of fracture that represents the area under the load-CMOD curve.

The Minnesota Department of Transportation (MnDOT) has introduced the Post Peak Index (PPI) for interpreting low-temperature test results using the DCT test. Following equations 22 and 23, this index normalizes the fracture energy with the post peak slope m_n at decreasing percentages of peak load (n=90%, 80%, 70%...20% etc.). The PPI is determined by taking the average of all normalized Index values. Generally, a higher value is preferred for all three parameters, indicating better ability to resist cracking.

$$Index_n = \frac{t}{62} \times \frac{G_f}{|m_n|} \times \left(\frac{l_n}{ligam}\right) \tag{5.22}$$

$$DCT_{\text{Index}} = S \times \frac{\sum_{n=10}^{90} Index_n}{n} \tag{5.23}$$

Where:
S = scaling parameter 700,
$|m_n|$ = slope of post-peak curve at n% of peak load,
l_n = CMOD at n% of peak load.

5.3.4 Illinois Flexibility Index Test (I-FIT)

The Semi-Circular Bending (SCB) testing was conducted on RPM and LTA mixtures at an intermediate temperature of 25°C following AASHTO T393. The load-displacement curves are used to calculate the flexibility index (FI) parameter. FI is a dimensionless cracking parameter developed to capture the crack growth velocity and the brittleness of the mixtures. As shown in the following equation, the FI is defined as the ratio between the fracture energy and the slope of inflection point at post-peak stage of the load-displacement curve. A higher value of FI is generally preferred, indicating a better ability to resist cracking. The Illinois DOT I-FIT flexibility index cracking limit for LTA applications is $FI = 4.0$ for non-SMA plant produced mixtures.

$$FI = A \times \frac{G_\mathrm{f}}{|\mathrm{m}|} \tag{5.24}$$

Where,
G_f $=$ fracture energy
$|\mathrm{m}|$ $=$ slope at the post-peak inflection point
A $=$ the unit correction coefficient taken as 0.01

5.3.5 Cracking Tolerance Index Test (CT-Index)

The Cracking Tolerance Index Test (CT_{Index}) (ASTM D8225) was conducted room temperature (25°C) following the ASTM D8225 procedure with a monotonic loading rate of 50 mm/minute of cross-headed displacement. A mix cracking property index parameter called Cracking Tolerance Index (CT_{Index}), that combines total energy dissipation during test with post-peak shape of load-displacement curve, was calculated using Eq. 9. Generally, a higher CT_{Index} value indicates better cracking resistance.

$$CT_{\text{Index}} = \frac{G_f}{|m_{75}|} \times \left(\frac{l_{75}}{D}\right) \tag{5.25}$$

Where:
G_f = fracture energy (total shaded area under load-displacement curve)
l_{75} = displacement at 75 percent point
$|m_{75}|$ =slope at 75 percent point
D = specimen diameter (mm)

5.3.6 Hamburg Wheel Tracking Test (HWTT)

The Hamburg Wheel Tracking Test (HWTT) was conducted following AASHTO T-324 specification, at a temperature of 50°C. HWTT was only conducted on RPM. The cumulative rut depth was then computed with the increase of the loading cycles (to 20,000 cycles). The pass-fail screening criterion used in this study is the number of passes at 12.5 mm rut depth.

In addition, the Stripping Inflection Point (SIP) was calculated from the HWTT measurements to evaluate the ability of the mixtures to resist moisture damage. The parameter LC_{SN} developed by Yin et al. (2014), which represents the maximum number of load cycles that the asphalt mixture can resist before the adhesive fracture between binder and aggregate occurs, was also calculated in this study using the following equation:

$$\mathrm{LC_{SN}} = \mathrm{LC_{ult}} \exp\left(-\frac{\beta+1}{\beta}\right) \tag{5.26}$$

Where:

$\mathrm{LC_{ult}}$, β = shape parameters determined by fitting function of rutting depth-load cycle.

Mixtures with higher SIP and LC_{SN} values are expected to have lower moisture susceptibility. Mixtures that do not exhibit a stripping phase during the test are expected to have a robust moisture resistance.

5.3.7 Tensile Strength Ratio Test (TSR)

The Tensile Strength Ratio (TSR) test was conducted in accordance with the ASTM D4867 procedure to evaluate moisture susceptibility of RPM and LTA mixtures. As shown in the equation below, TSR values are expressed as the ratio of the test result from dry and wet condition. A higher TSR value indicates better resistance of the asphalt mixture to moisture.

$$TSR = \left(\frac{ITS_{\mathrm{wet}}}{ITS_{\mathrm{dry}}}\right) * 100 \tag{5.27}$$

Where:
TSR_{wet} = average indirect tensile strength of wet conditioned specimens.
TSR_{dry} = average indirect tensile strength of unconditioned specimens.

5.4 Evaluating Control Sections and Data Summary Approach

Significant differences were observed in control sections placed on Day 1, 6010 (30% RAP) and 6011 (40% RAP), relative to the 40% RAP control section placed on Day 2. Following the conclusions from the Task 4 report and considerations about variations in results between 2 construction days, all RA treated binders in this analysis are benchmarked against the Day 1 40% control. While the Day 2 40% control results will still be presented for completeness, they are not used as a benchmark in the evaluation of RA materials. This decision is made to address the unknown issues associated with the Day 2 40% control section, ensuring a more reliable comparison and interpretation of the data.

Examples of variations on two 40% controls on extracted binder properties are presented in **Figure 5-13** through **Figure 5-15**. Specifically, recovered binder from mix 6012 on mix sampled after construction (LM-As recovered) had a high temperature grade 3° to 5°C lower and a m-critical value 3°C lower than the 40% D1 controls. Similar differences were also observed on 6 hour aged loose mix and field cores from Year 1,2 and 3. Regarding composition asphaltenes were 2% lower on binder recovered from field sampled loose mix for mix 6012 relatives to 6010 and 6011. The asphaltenes after 6-hour loose mix aging were also different for the two 40% RAP sections, however similar values were observed between all three control mixes for Year 1 and 2 field cores. Furthermore, all control mixes have statistically similar PGHT, m-Critical and asphaltene after 7 days at 95°C loose mix aging. As a result of these observations the decision was made to use 40% Day1 control instead of 40%Day 2 controls to remove any potential bias caused by changes during construction.

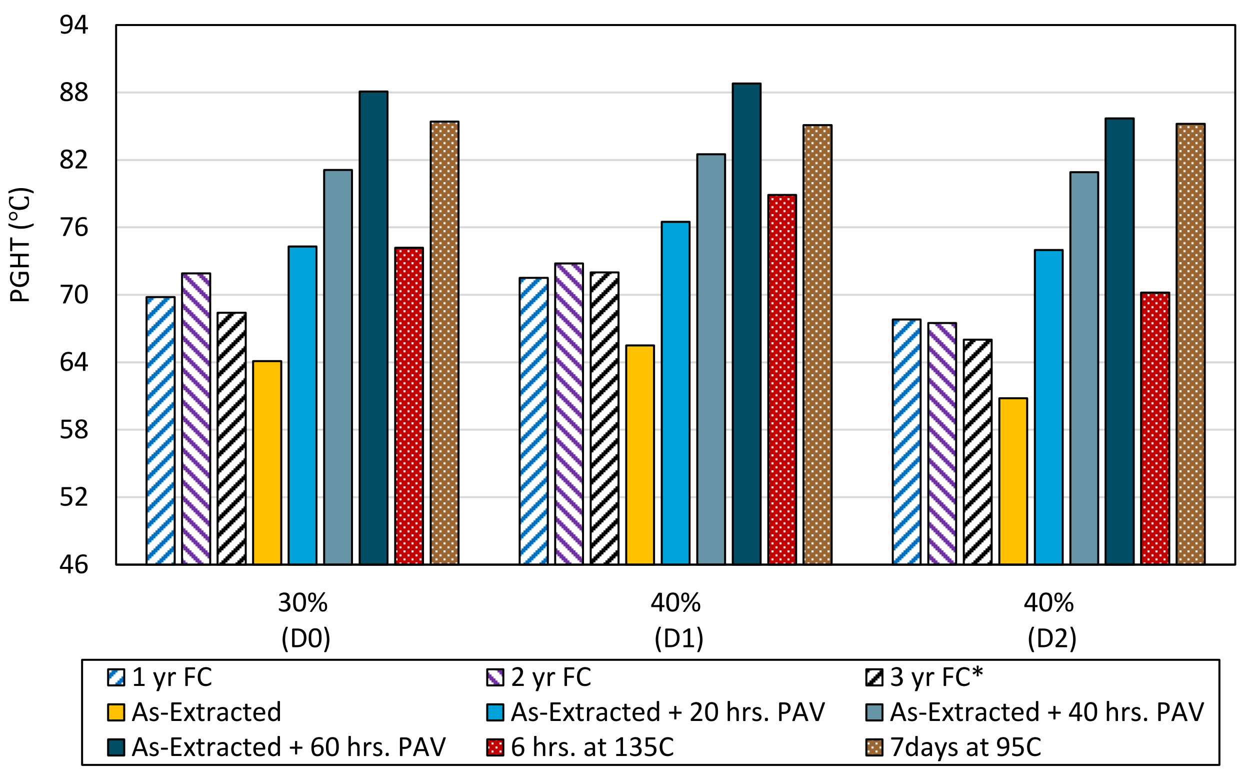

Figure 5-13: High Temperature PG Grade at Various Aging Conditions – Control Sections

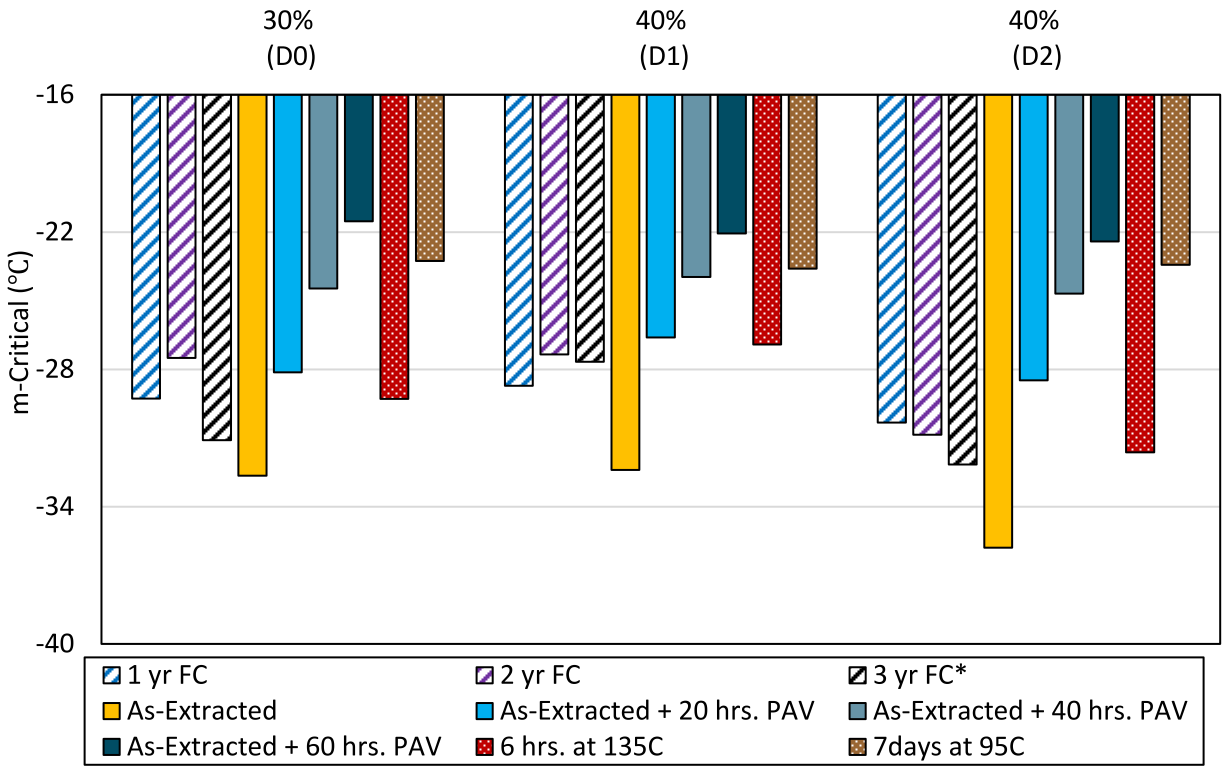

Figure 5-14: m-Critical Temperature Various Aging Conditions – Control Sections

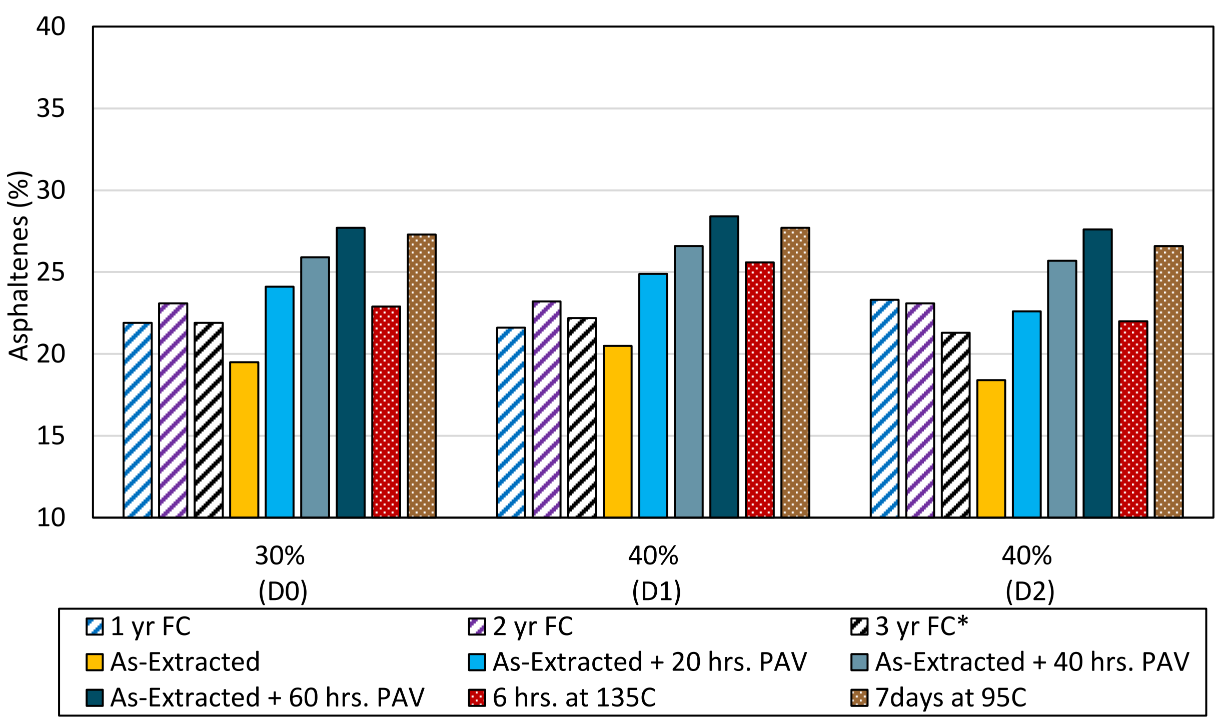

Figure 5-15: Percent Asphaltenes at Various Aging Conditions – Control Sections

Chapter 6: Binder Test Results

This chapter presents the comprehensive results of binder tests conducted on samples derived from various aging protocols as part of this project. The presentation of results follows a structured order: 1. The in-line sampled binders processed through STA and LTA binder aging protocols (RTFO and PAV). 2. The binders extracted and recovered from unaged loose mixes with multiple PAV aging cycles, 3. The binders extracted and recovered from different loose mix aging protocols. The analysis of each protocol is organized by examining the rheological properties, chemical composition, functional groups, and exploring how these properties evolve under laboratory aging conditions. This structured approach ensures a comprehensive comparison of the binder properties between RA treated binders and control binders.

6.1 In-Line Sampled Binder Results

Based on the conclusion in Section 5.3, all RA sections on both days of construction are only compared to the 30% RAP control and 40% RAP D1 control to evaluate RA effectiveness.

6.1.1 Performance Grading

Table 6-1 provides the continuous performance grade and AASHTO M320 performance grade for the study binders sampled in-line during production. For sections 6001 – 6007 in-line samples consist of base binder and RA at the supplier targeted dosage. The three base binders have similar grades with binder N having slightly lower temperatures than the other two. Base binders O1 and O2 are from the same source and were sampled from the asphalt plant storage tank on subsequent days of production. All RA binders (6001-6007) meet the project requirement of decreasing the PGLT of the base binder (-28°C) to -34°C. The PGHT for all the RA sections dropped 8-12°C (the equivalent of two grades) due to the addition of the RAs.

Table 6-1 Continuous PG Temperatures Grade of In-line Sampled Binders

Binder ID (production day[1])	Continuous PG Temperatures (°C)		Performance Grade (°C)
	PGHT	PGLT	
6001 (D1)	51.1	-36.1	46-34
6002 (D1)	51.5	-35.8	46-34
6003 (D1)	48.8	-37.1	46-34
6004 (D2)	50.6	-34.3	46-34
6005 (D2)	49.8	-37.3	46-34
6006 (D2)	46.3	-36.7	46-34
6007 (D2)	47.7	-38.5	46-34
O1 (D1)	59.9	-28.5	58-28
O2 (D2)	59.9	-28.3	58-28
N (D2)	59.4	-29.6	58-28

[1]D1: Produced on day 1; D2: Produced on day 2

6.1.2 Rheological Properties

Figure 6-1 to **Figure 6-3** show the complex shear modulus and phase angle master curves for the study binders with different aging conditions at the reference temperature of 25°C. The three base binders have very similar stiffness (as indicated by norm of complex modulus) and relaxation capability (as indicated by phase angle). All RA binders have lower complex modulus and higher phase angle as compared to the base binders, indicating lower cracking susceptibility.

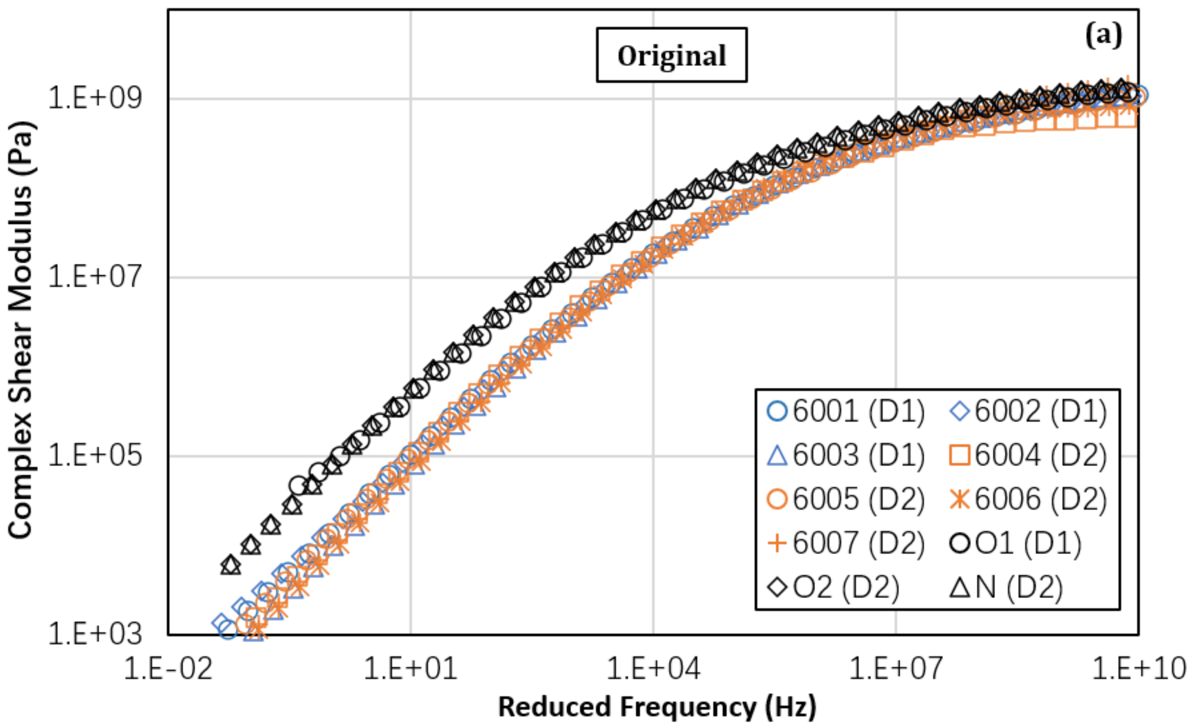

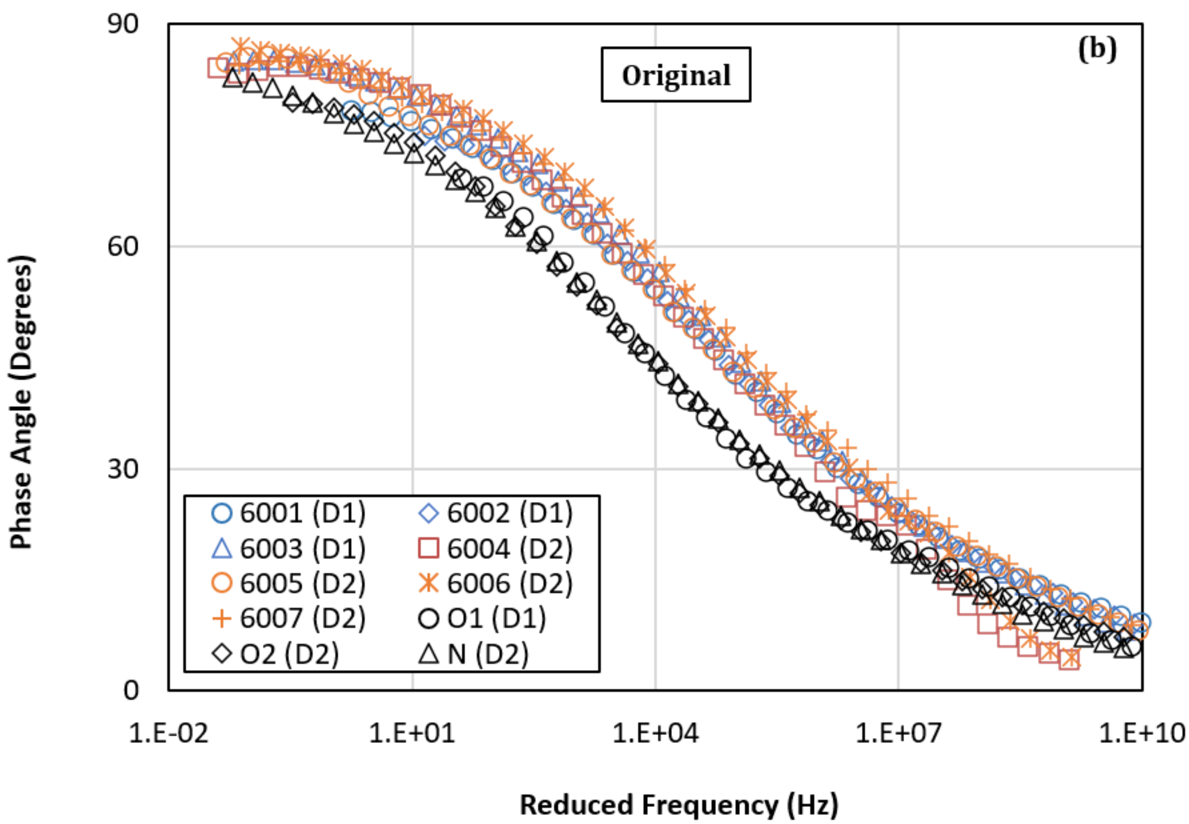

Figure 6-1 Master Curves of (a) Complex Modulus and (b) Phase Angle for Original Binders (Ref. 25°C)

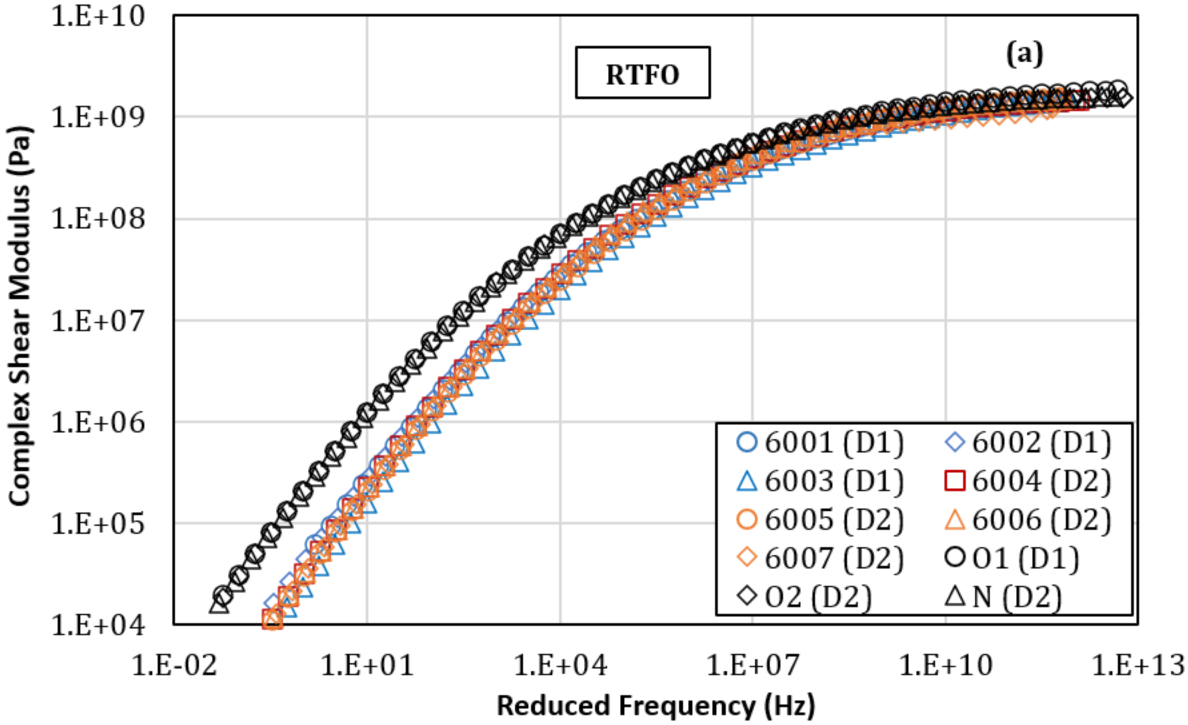

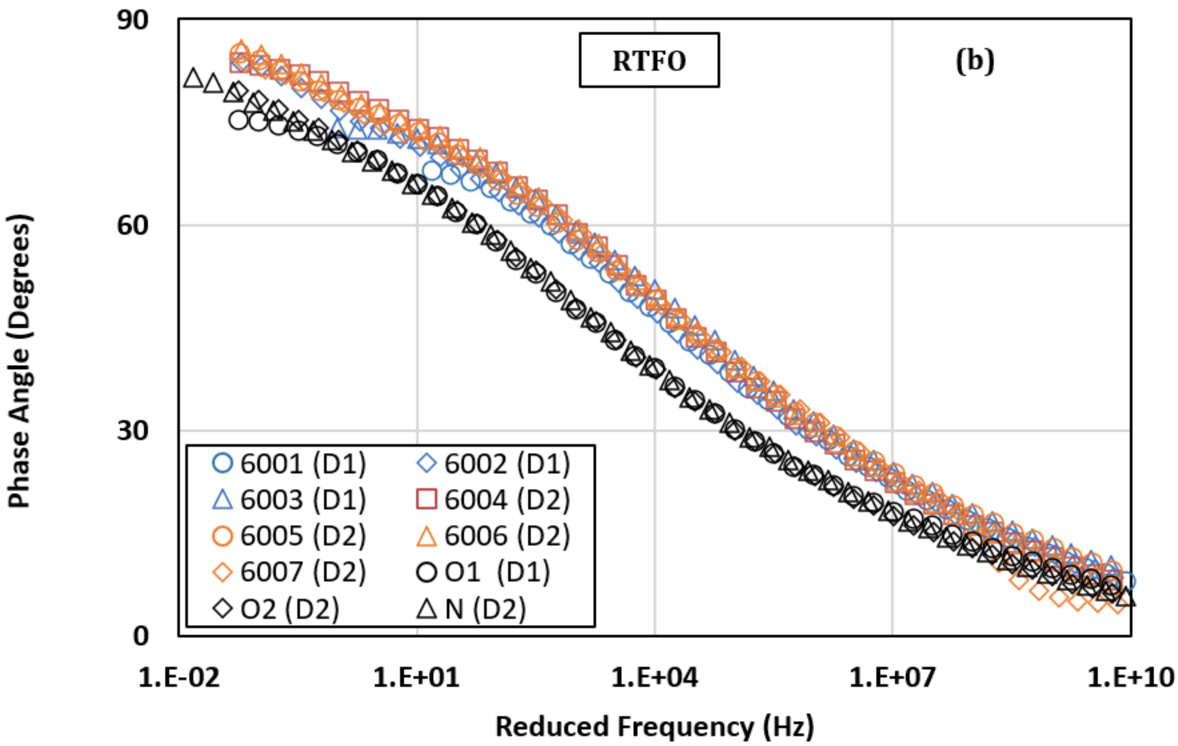

Figure 6-2 Master Curves of (a) Complex Modulus and (b) Phase Angle for RTFO Aged Binders (Ref. 25°C)

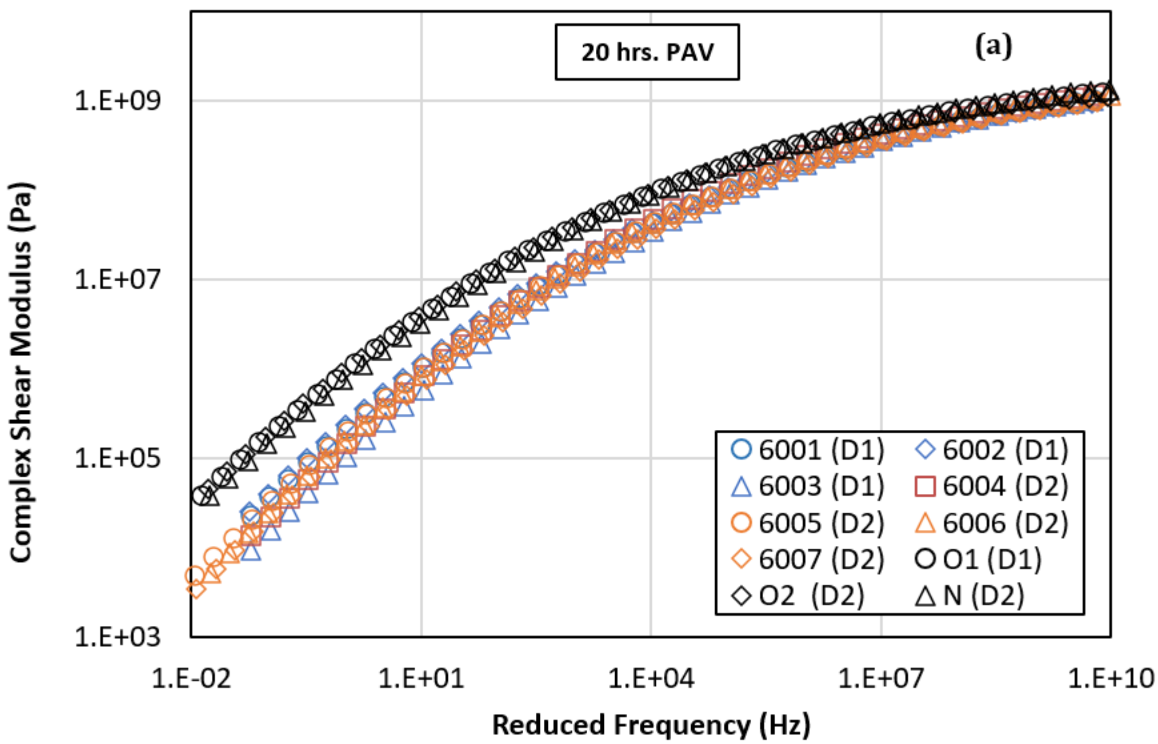

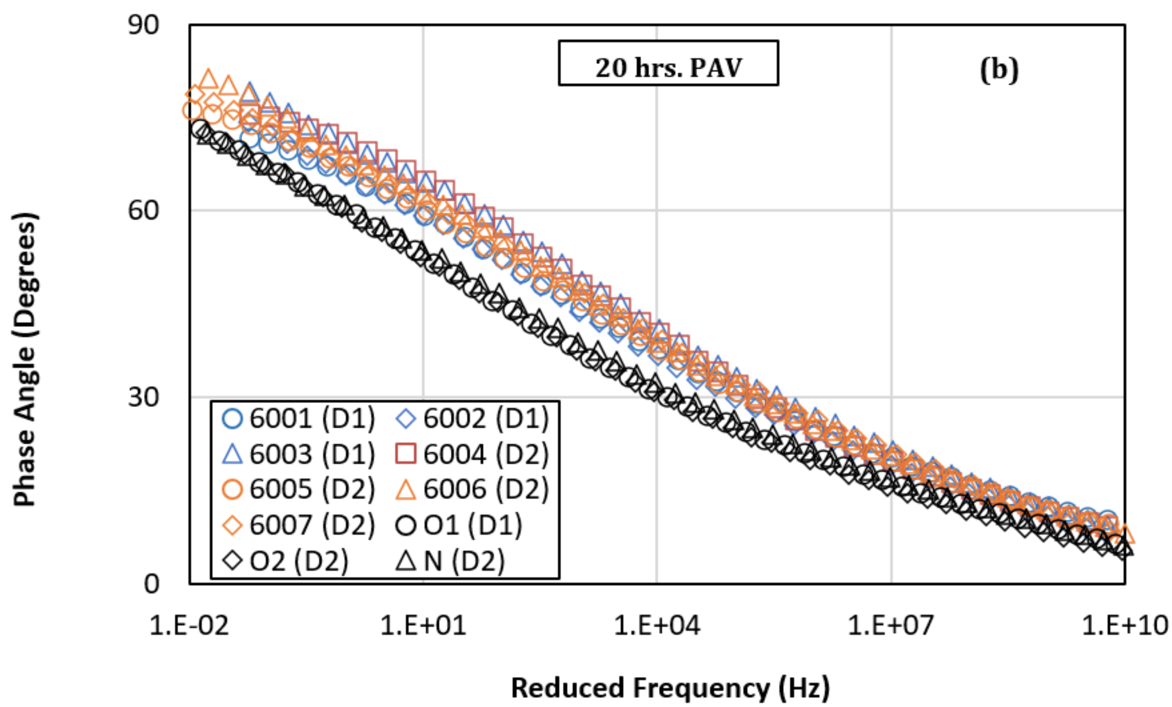

Figure 6-3 Master Curves of (a) Complex Modulus and (b) Phase Angle for 20 hrs. PAV Aged Binders (Ref. 25°C)

Figure 6-4 below shows how the R-value for the in-line sampled binders changes with aging. The three base binders have a similar R-value after each aging condition. With the exception of 6005 Original condition, all RA binders have lower R-value than their corresponding base binder after each aging condition.

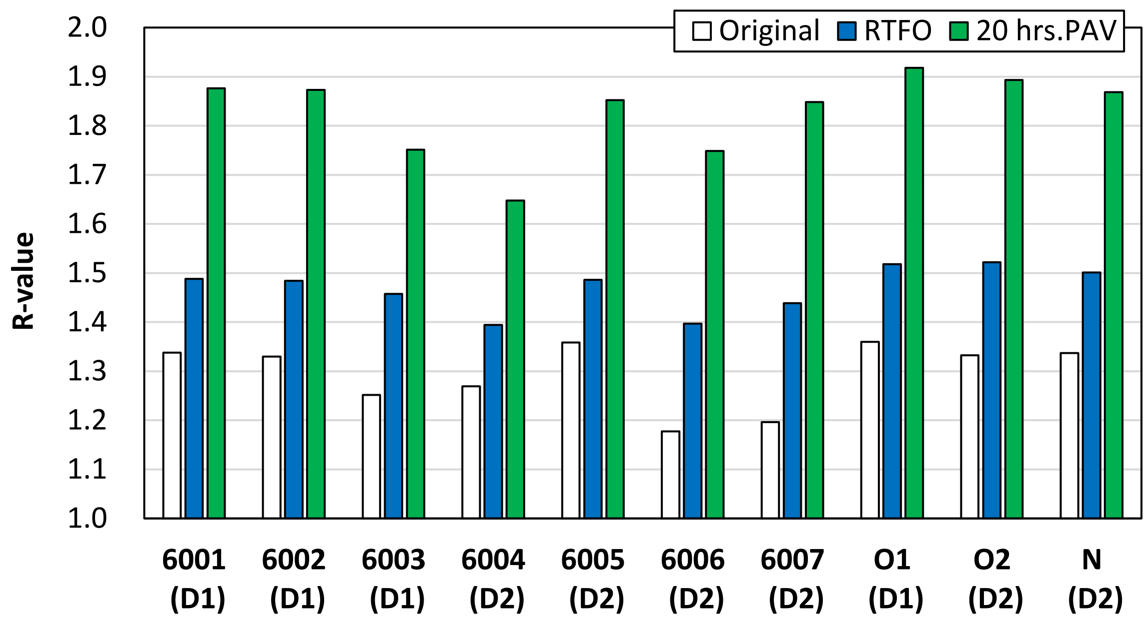

Figure 6-4 R-values for In-line Sampled Binders

Figure 6-5 below shows the ΔT_c values for the in-line sampled binders with different aging conditions. The ΔT_c value for most of the binders with different aging conditions is positive, indicating these binders are primarily S-controlled. After aging, all binders still meet the cracking threshold value of -2.5°C. Base binders are similar in original and RTFO condition, while binder N retains a positive ΔT_c value after PAV aging. Comparing the RA binders with their base binder, binder 6001 and 6003 consistently show higher ΔT_c value than the base binder O1 after each aging condition. Binder 6002 originally has a higher ΔT_c value than base binder O1 but lower value after the RTFO and 20 hrs. PAV conditions. RA binders 6004, 6005 and 6006 generally have higher ΔT_c values than the O2 base binder. Binder 6007 has significantly higher ΔTc value than the base binder N with unaged and RTFO condition, but their ΔT_c value becomes similar after 20 hrs. PAV aging.

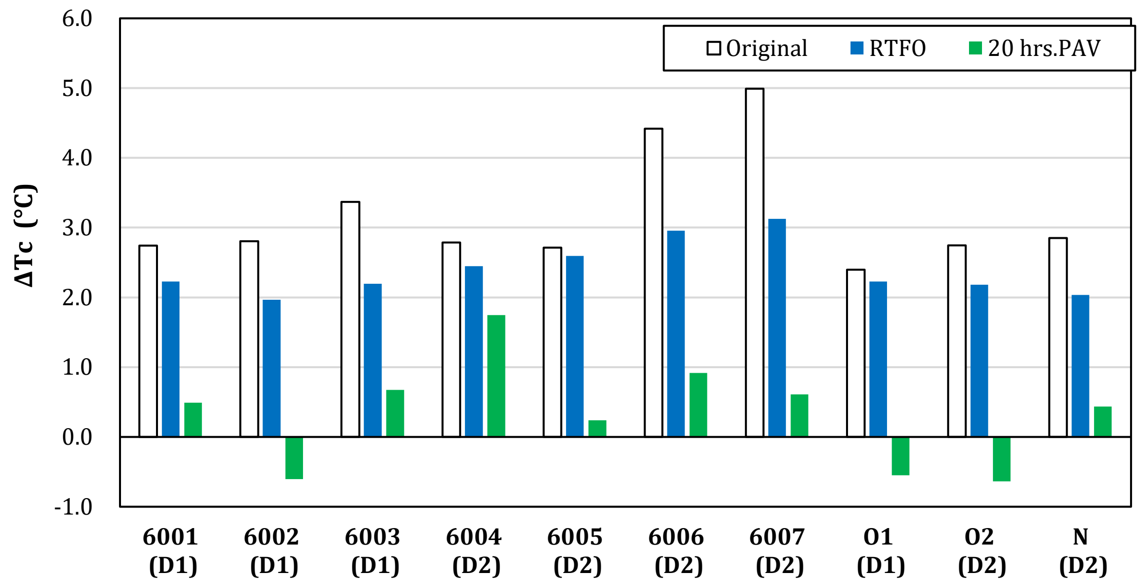

Figure 6-5 ΔTc Values for In-line Sampled Binders

Figure 6-6 below shows that all binders still meet the G-R cracking warning threshold value of 160kPa after aging. The three base binders have similar G-R values with unaged and RTFO conditions, while binder N has a lower G-R value after 20 hrs. PAV condition. All RA binders have a lower G-R value than their corresponding base binder after each aging condition.

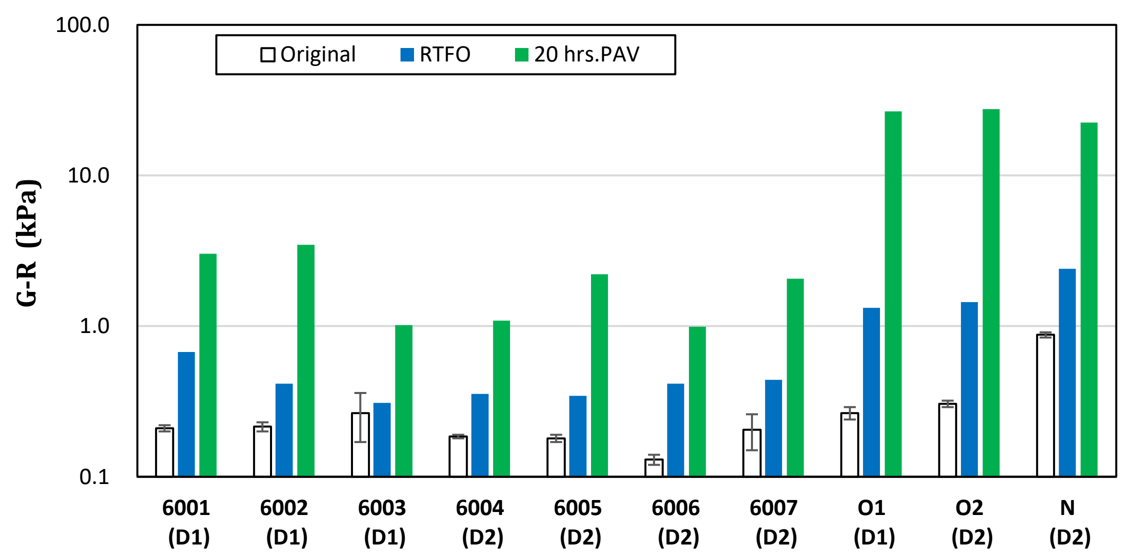

Figure 6-6 G-R Values at 15°C and 0.05 rad/s for In-line Sampled Binders

6.1.3 Chemical Compositions

Aging causes a decrease in CI value for all binders due to the increase of the asphaltene content and decrease of the light fractions, as shown in **Figure 6-7**. The base binders O1 and O2 have similar CI values after each aging condition, while binder N has a lower CI value. All RA binders have higher CI value as compared to their corresponding base binder after each aging condition, indicating improvement of the colloidal structure through addition of the study RAs.

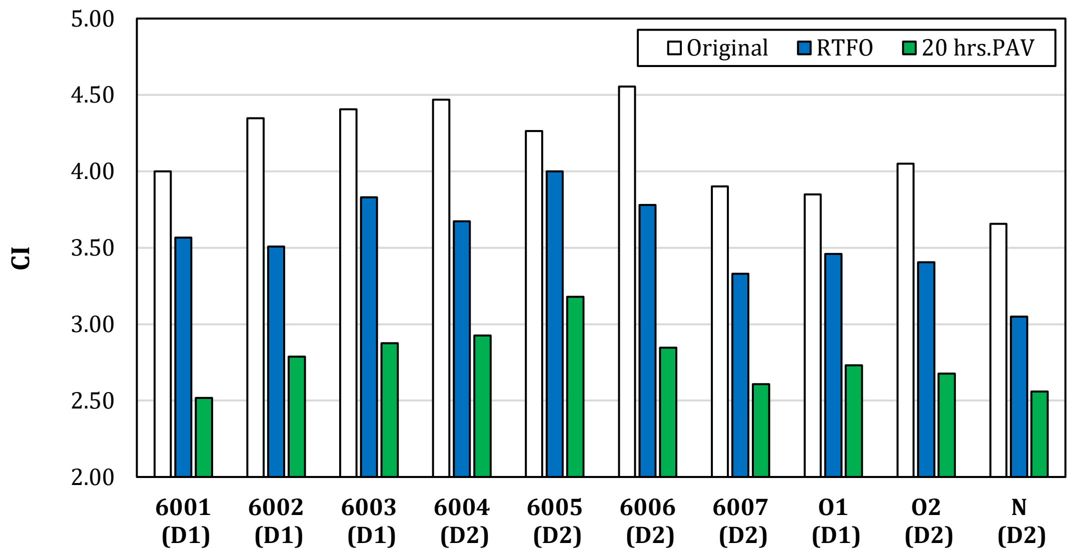

Figure 6-7 CI Values for In-line Sampled Binders

Aging causes an increase in carbonyl ratio ($I_{C=O}$) and sulfoxide ratio ($I_{S=O}$) for all binders as shown in **Figure 6-8**. The base binders O1 and O2 generally have similar $I_{C=O}$ and $I_{S=O}$ values after each aging condition (O1 has a higher $I_{S=O}$ value after PAV aging), while binder N has a slightly higher $I_{C=O}$ but lower $I_{S=O}$ value. All RA binders have higher $I_{C=O}$ value as compared to the base binders after each aging condition. In terms of the $I_{S=O}$ parameter, RA binders 6001, 6002 and 6003 have a lower value than the base binder O1 after each aging condition. RA binders 6004 and 6005 typically have a higher $I_{S=O}$ value than the base binder O2 after each aging condition, while binder 6006 has a lower value with original and RTFO condition but higher value after PAV aging. Binder 6007 originally has a higher $I_{S=O}$ value as compared to the base binder N, but the value is comparable after RTFO and PAV aging.

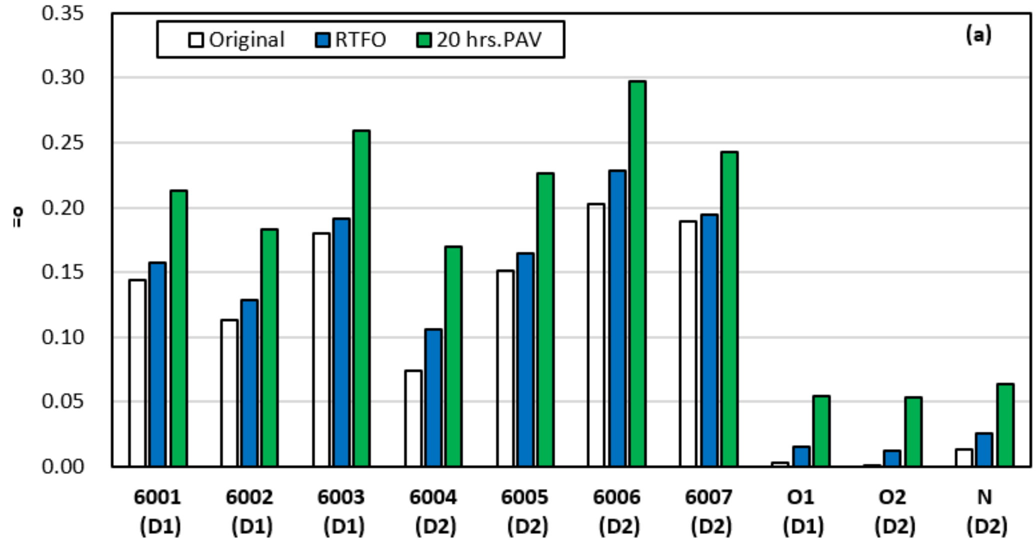

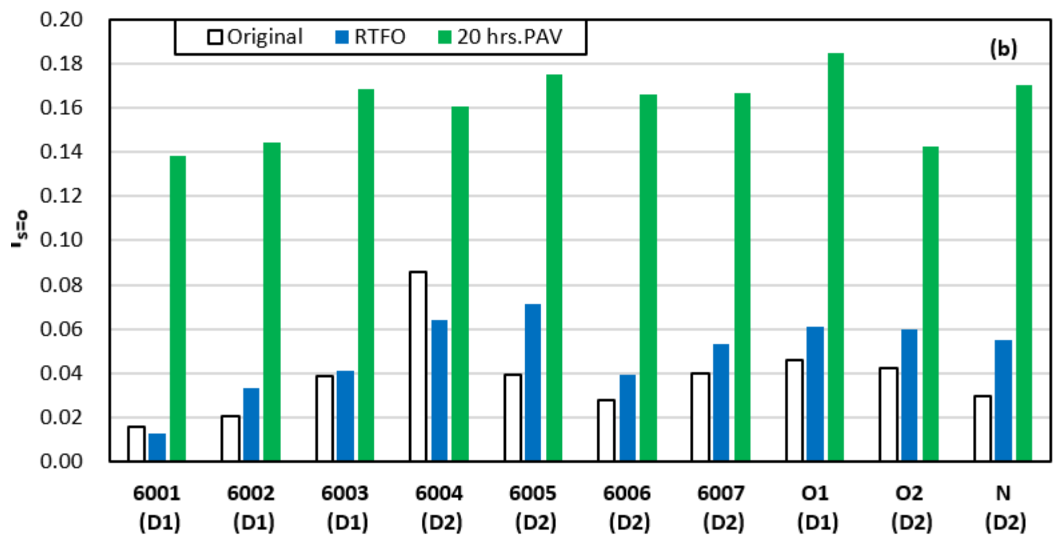

Figure 6-8 (a) $I_{C=O}$; and (b) $I_{S=O}$ Values for In-line Sampled Binders

6.2 Extracted and Recovered Binders from Production Mixes

This section presents the results of binders extracted from sampled plant loose mixes during production. Due to the conclusion in section 5.3, all RA sections on both days of construction are compared only to the 40% RAP D1 control.

6.2.1 Performance Grading

6.2.1.1 Effect of Binder Extraction and Recovery on PG

Table 6-2 below summarizes the performance grades for the binder samples extracted and recovered from the sampled plant produced mixtures. For the binders with as-extracted condition, 30% D0 and 40% D1 control binders have similar grades. Both PGHT and PGLT for RA binders 6001 and 6002 are lower (by over a full grade) than their control mix and the 30% mix, while binder 6003 PGHT drops over 10^{o}C, resulting in a drop of two grades. RA binders 6004 and 6005 have slightly higher continuous PGHT, but same PG as the corresponding control mix; binder 6005 PGLT decreases just enough to change grade. RA binders 6006 and 6007 have PGHT increases over 6^{o}C.

Table 6-2 Performance Grades of Binders Extracted and Recovered from Sampled Mixtures

Binder ID	Continuous PG (°C)		PG (°C)
	PGHT	PGLT	
	As extracted	As extracted	As extracted
6001 (D1)	58.1	-37.6	58-34
6002 (D1)	61.4	-38.8	58-34
6003 (D1)	54.9	-38.4	52-34
6004 (D2)	62.6	-33.7	58-28
6005 (D2)	61.7	-34.7	58-34
6006 (D2)	66.8	-30.5	64-28
6007 (D2)	70.5	-33.2	70-28
30% Control (D0)	64.1	-31.5	64-28
40% Control (D1)	65.5	-31.6	64-28
40% Control (D2)	60.8	-33.7	58-28

D0: Produced on the day before day 1; D1: Produced on day 1; D2: Produced on day 2.

Table 6-3 compares PG grading results from in-line sampled binders presented previously to extracted binders from plant-produced loose mix sampled at the time of construction. For in-line sampled binders' high temperature PG grade was derived from RTFO aged material, low temperature grade from PAV aged material. For recovered binders from plant-produced loose mixtures high and low temperature grade were derived from as-recovered and as-recovered + PAV aged binders respectively. Note that plant-produced recovered PG was based on recovered binder with no additional aging. Low temperature grades reported in **Table 4-1** will be warmer than those reported in **Table 6-1**. Reported values for in-line sampled binders in **Table 6-3** will match results in **Table 6-1**. The control field sampled binders (O1 and O2 from Table 31) had similar PG grade, the average of all three samples was PG 59.9-28.4. The average PG from the field sampled binders was compared to recovered binder grading from the 30% and 40% control loose mixes. Changes in grading follow expected trends due to the presence of RAP and increasing RAP content for the 30% RAP and 40% RAP Day 1 mixtures. The 30% RAP had a stiffening effect of approximately 3°C for high temperature grade and 1°C for low temperature grade. Additional stiffening of 1°C to 2°C was observed when RAP content was increased to 40%. However, the 40% RAP Day 2 mixture shows little change to the high temperature grade and slight improvement in the low temperature grade. Overall, the change in grade between field sampled binders and recovered binders from loose mixtures for the RA sections (6001 – 6007) was higher than the differences observed for the control sections. Significant differences in change between field sampled binders and loose mixtures were also observed between Day 1 and Day 2 production. For Day 2 production the change from binder to loose mix was on the order of 2 to 3 PG grades. Furthermore, grading for 6006 was comparable with 40% Day 1 control. There were no reported issues with additive dosing for 6006 at the asphalt plant, additive 6007 was dosed at the terminal prior to delivery. It is unclear if the differences observed are related to changes in plant temperature, changes to the properties of the RAP stockpile, or other production related factors.

AASHTO M320 grading results at all aging conditions are provided in Table 6-4. Low and intermediate temperature grades were determined using the 4mm DSR because 8mm DSR and BBR data was not available for all materials/aging conditions. Data was summarized using bar charts and plots with aging time to determine aging rates. Bar charts in this and subsequent sections will follow a similar format.

Table 6-3: Comparison of Field Sampled Binder and Loose Mix Recovered PG

Binder ID (production day[1])	Continuous PG, °C		Change in PG (Mix-Binder), °C	
	In-Line Sampled Binders	Plant Produced Mix Recovery	HT PG	LT PG
6001 (D1)	51.2-36.1	58.1-31.9	+6.9	+4.2
6002 (D1)	52.6-35.8	61.4-33.8	+8.8	+2.0
6003 (D1)	48.9-37.1	54.9-33.8	+6.0	+3.3
6004 (D2)	50.6-34.3	62.6-28.3	+12.0	+6.0
6005 (D2)	50.2-37.3	61.7-30.2	+11.5	+7.1
6006 (D2)	48.5-36.7	66.8-25.8	+18.3	+10.9
6007 (D2)	49.3-38.5	70.5-28.4	+21.2	+10.1
30% RAP Control	59.9-28.4[2]	64.1-28.1	+4.2	+0.3
40% RAP Control (D1)	59.9-28.5	65.5-26.6	+5.6	+1.9
40% RAP Control (D2)	59.9-28.3	60.8-28.5	+0.9	-0.2

[1]D1: Produced on day 1; D2: Produced on day 2.

[2] Binder not sampled, average of O1 and O2 control binders used for analysis

Table 6-4: Summary of PG Test Results and Grading for Extracted and Recovered Binders

Sample ID	Description	Aging	Test Data					Grading	
			HT PG, °C	IT PG, °C	S critical, °C	m critical, °C	ΔTc	Continuous PG	M320 PG
6001	Loose Mix	As Recovered	58.1	11.2	-37.6	-39.1	1.5	58.1-37.6	58-34
	Loose Mix	20 hr. PAV	70.2	18.8	-32.3	-31.9	-0.4	70.2-31.9	70-28
	Loose Mix	40 hr. PAV	76.3	20.7	-31.5	-29.1	-2.4	76.3-29.1	76-28
	Loose Mix	60 hr. PAV	82.9	23.1	-30.2	-26.7	-3.5	82.9-26.7	82-22
6002	Loose Mix	As Recovered	61.4	9.6	-38.8	-40.5	1.7	61.4-38.8	58-34
	Loose Mix	20 hr. PAV	67.7	17.2	-33.8	-34.1	0.3	67.7-33.8	64-28
	Loose Mix	40 hr. PAV	76.1	20.9	-32.6	-30.6	-2	76.1-30.6	76-28
	Loose Mix	60 hr. PAV	81	22.6	-31.4	-27.5	-3.9	81.0-27.5	76-22
6003	Loose Mix	As Recovered	54.9	9.5	-38.4	-39.9	1.5	54.9-38.4	52-34
	Loose Mix	20 hr. PAV	65.9	16.1	-33.8	-34	0.2	65.9-33.8	64-28
	Loose Mix	40 hr. PAV	72.9	20	-31.5	-30.2	-1.3	72.9-30.2	70-28
	Loose Mix	60 hr. PAV	81.1	24.5	-29.5	-26.1	-3.4	81.1-26.1	76-22
6004	Loose Mix	As Recovered	62.6	15.6	-33.7	-34.4	0.7	62.6-33.7	58-28
	Loose Mix	20 hr. PAV	72.2	22	-29	-28.3	-0.7	72.2-28.3	70-28
	Loose Mix	40 hr. PAV	78.1	23.5	-29	-26	-3	78.1-26.0	76-22
	Loose Mix	60 hr. PAV	84.4	27.1	-27.3	-23.7	-3.6	84.4-23.7	82-22
6005	Loose Mix	As Recovered	61.7	14.5	-34.7	-35.7	1	61.7-34.7	58-34
	Loose Mix	20 hr. PAV	72.7	20.2	-31.3	-30.2	-1.1	72.7-30.2	70-28
	Loose Mix	40 hr. PAV	77.9	22.1	-30.9	-27.8	-3.1	77.9-27.8	70-22
	Loose Mix	60 hr. PAV	84.5	25.1	-29.7	-24.7	-5	84.5-24.7	82-22

Table 6-4: Summary of PG Test Results and Grading for Extracted and Recovered Binders (Continued)

Sample ID	Description	Aging	Test Data					Grading	
			HT PG, °C	IT PG, °C	S critical, °C	m critical, °C	ΔTc	Continuous PG	M320 PG
6006	Loose Mix	As Recovered	66.8	19.3	-30.9	-30.5	-0.4	66.8-30.5	64-28
	Loose Mix	20 hr. PAV	76.9	24.4	-27.8	-25.8	-2	76.9-25.8	76-22
	Loose Mix	40 hr. PAV	82.6	27.4	-26.6	-22.9	-3.7	82.6-22.9	82-22
	Loose Mix	60 hr. PAV	88.6	30.3	-26	-19.3	-6.7	88.6-19.3	88-16
6007	Loose Mix	As Recovered	70.5	16.5	-33.3	-33.4	0.1	70.5-33.3	70-28
	Loose Mix	20 hr. PAV	74.8	21.9	-30.1	-28.4	-1.7	74.8-28.4	70-28
	Loose Mix	40 hr. PAV	81.8	25.6	-28.2	-24.3	-3.9	81.8-24.3	76-22
	Loose Mix	60 hr. PAV	89	28.3	-27.1	-21.5	-5.6	89.0-21.5	88-16
6010	Loose Mix	As Recovered	64.1	17.9	-31.5	-32.6	1.1	64.1-31.5	64-28
	Loose Mix	20 hr. PAV	74.3	22.7	-28.7	-28.1	-0.6	74.3-28.1	70-28
	Loose Mix	40 hr. PAV	81.1	25.7	-27.3	-24.5	-2.8	81.1-24.5	76-22
	Loose Mix	60 hr. PAV	88.1	28.8	-25.7	-21.5	-4.2	88.1-21.5	88-16
6011	Loose Mix	As Recovered	65.5	18.8	-31.6	-32.4	0.8	65.5-31.6	64-28
	Loose Mix	20 hr. PAV	76.5	23.8	-28.1	-26.6	-1.5	76.5-26.6	76-22
	Loose Mix	40 hr. PAV	82.5	26.4	-27.5	-24	-3.5	82.5-24.0	82-22
	Loose Mix	60 hr. PAV	88.8	28.3	-26.5	-22.1	-4.4	88.8-22.1	88-22
6012	Loose Mix	As Recovered	60.8	14.6	-33.6	-35.8	2.2	60.8-33.6	58-28
	Loose Mix	20 hr. PAV	74	21.8	-30.1	-28.5	-1.6	74.0-28.5	70-28
	Loose Mix	40 hr. PAV	80.9	26.2	-27.1	-24.7	-2.8	80.9-24.7	76-22
	Loose Mix	60 hr. PAV	85.7	28	-26.8	-22.4	-4.4	85.7-22.4	82-22

High temperature continuous grade, determined at G*/sinδ = 2.2 kPa, for all PAV aging conditions evaluated is provided in **Figure 6-9.** The initial grade, as recovered from loose mix sampled during construction ranged from 55.0 °C (6003) to 70.5°C (6007) for the RA test sections and 60.8°C to 65.5°C for the controls.

Intermediate temperature PG grade based on a G*sinδ limit of 5000 kPa for various PAV aging conditions is presented in **Figure 6-10**. The target IT PG for PG 58S-28 base binder is 19.0°C after 20-hour PAV aging. Due to the presence of RAP, the control mixes exceed this limit by approximately 3°C. For day 1 control mix production (6010 and 6011) the increase in RAP from 30% to 40% resulted in an increase in IT PG of ~1°C. Performance of the RA sections relative to the IT PG target of 19°C after 20-hour PAV aging varied. Sections 6001-6003 were below the target IT grade and thus met requirements. Sections 6006 and 6007 exceeded the threshold and in most cases did not have properties substantially different than the controls.

S-critical and m-critical values are provided in **Figure 6-11** and **Figure 6-12**. In general, because relaxation properties are more sensitive to aging than stiffness, the m-value becomes the controlling parameter in determining low temperature grade. As shown in **Figure 6-13**, ΔT_c is positive for recovered plant mix, then near zero or negative for all other PAV aging conditions studied. For the majority of the data set low temperature grade is m-controlled. The target m-critical temperature was defined as -28°C after 20-hour PAV aging of the binder recovered. The 30% RAP control (6010) and Day 2 40% RAP control (6012) met this criterion, the Day 1 40% RAP control (6010) was slightly warmer than the target grade (-26.6°C). RA sections 6001-6005 and 6007 met the -28°C benchmark by varying degrees. Sections 6001-6003 maintained an m-critical value lower than -28°C after 40-hour PAV aging of the recovered binder. Section 6006 did not meet requirements and had properties equal to or worse than the Day 1 40% RAP control.

The ΔTc cracking warning limit is not exceeded until 40-hour PAV (6004, 6005, 6006, 6007, 6010, 6011) or 60-hour PAV (6001, 6002, 6003, 6012) aging condition. Three RA sections (6005, 6006, 6007) exceed the cracking failure limit after 60-hour PAV aging. Initial ΔTc values for the controls were all positive, with the highest value observed for Section 6012, with additional aging similar values of ΔTc were observed. In general, Sections 6001 – 6004 maintained equal or better ΔTc values for all aging conditions studied. Differences between Sections 6005-6007 and the controls increased with aging.

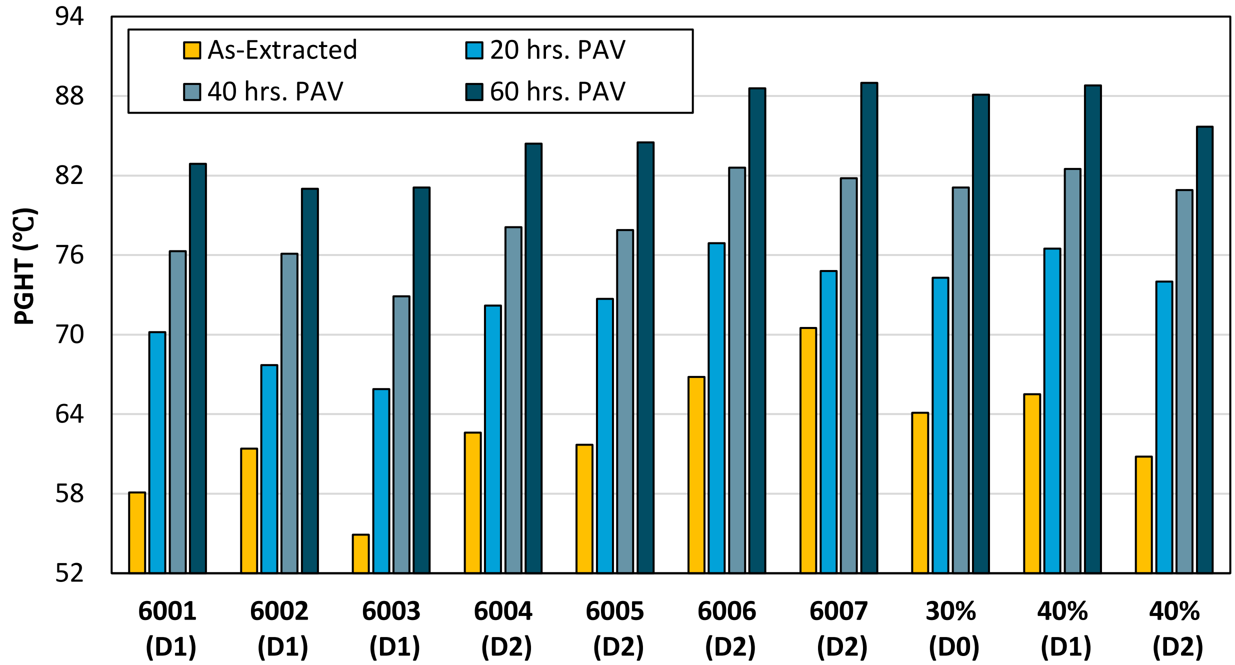

Figure 6-9 High Temperature Grade at Various Aging Conditions

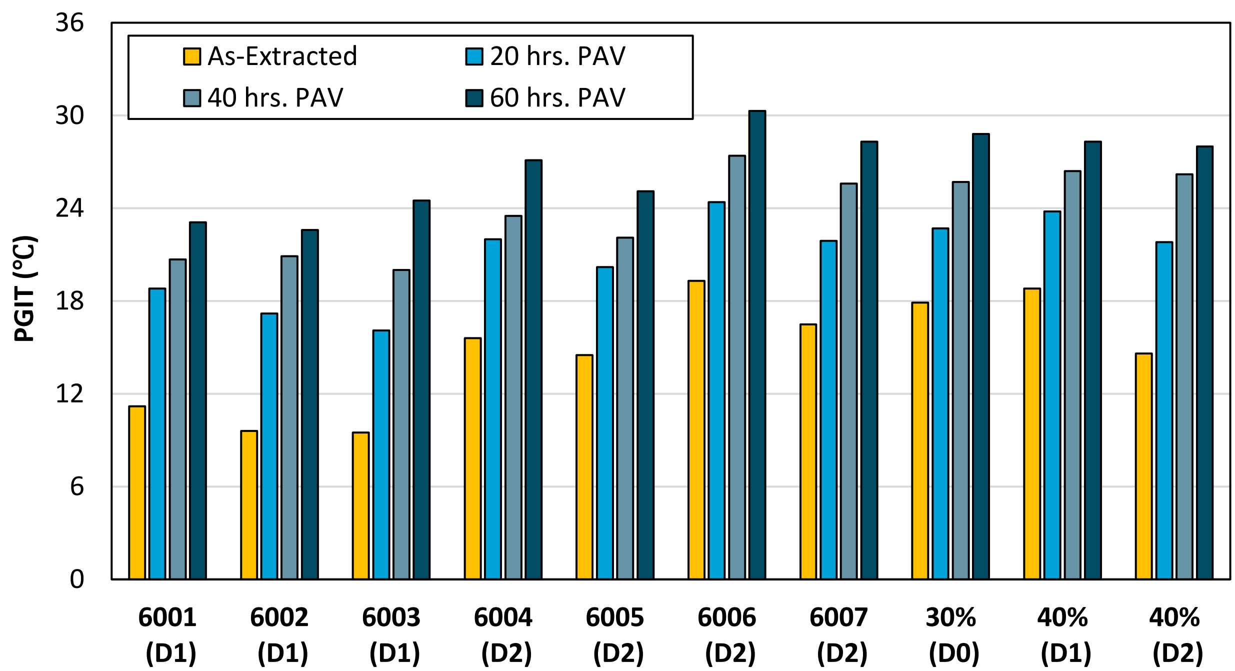

Figure 6-10 Intermediate Temperature Grade at Various Aging Conditions

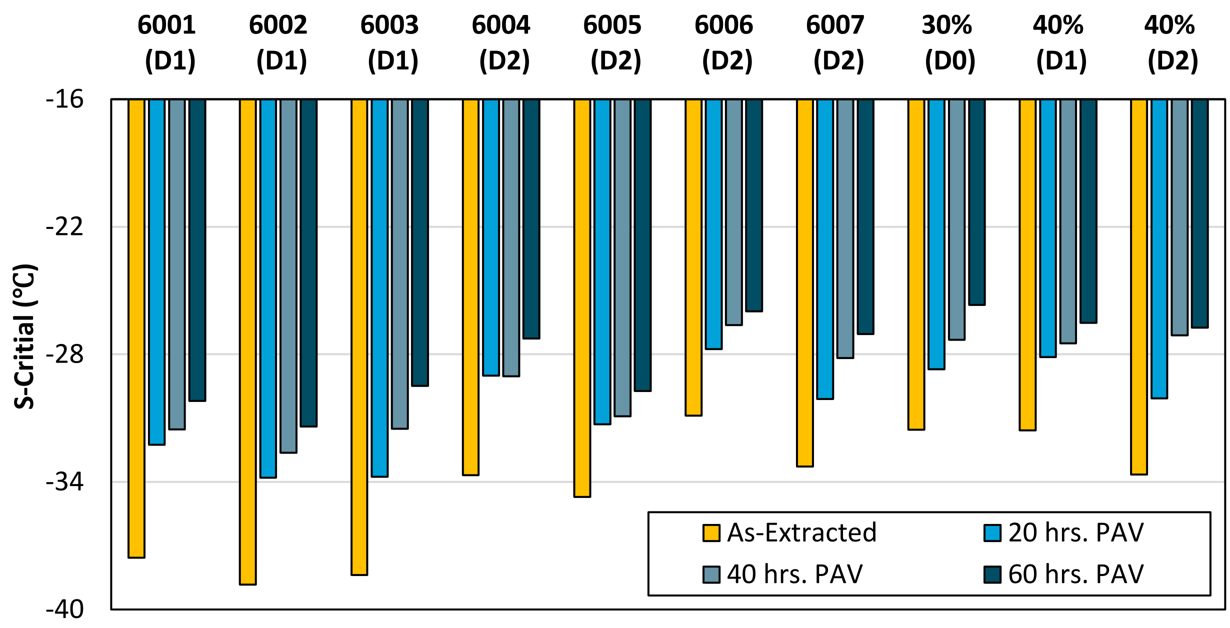

Figure 6-11: 4mm S-Critical Temperature at Various Aging Conditions

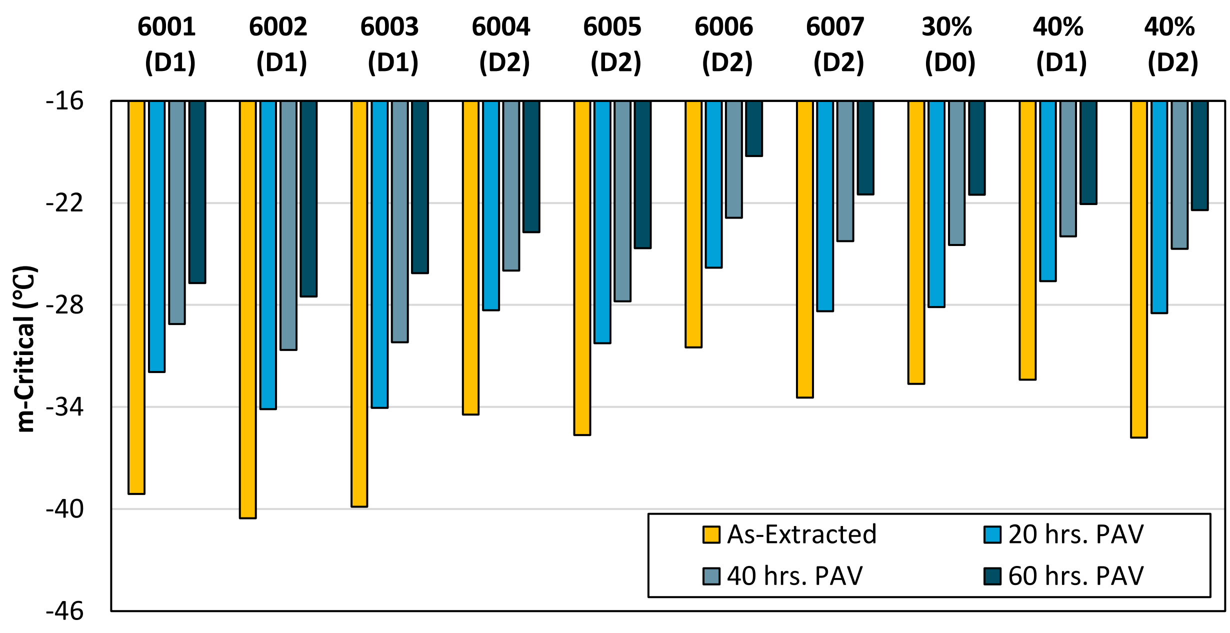

Figure 6-12: 4mm m-Critical Temperature at Various Aging Conditions

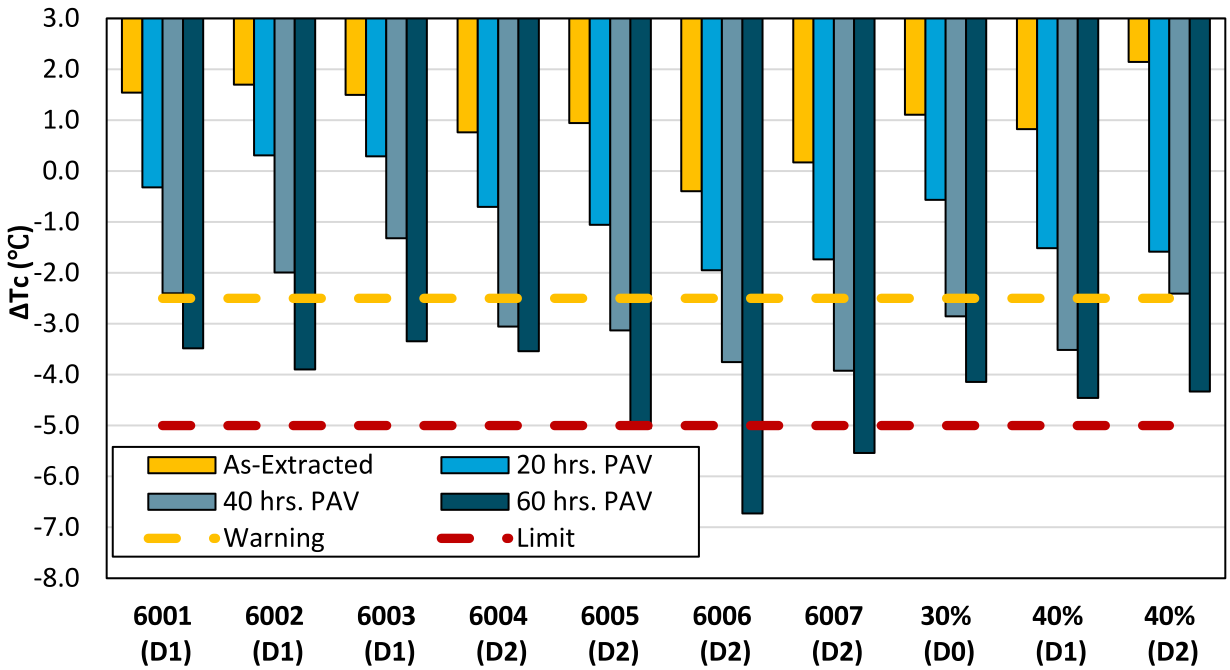

Figure 6-13: 4mm ΔTc at Various Aging Conditions Binder Aging susceptibility

Aging susceptibility and how it is influenced by different RAs is a primary concern in evaluating the mixes with increased recycled asphalt content. For this portion of the study, aging susceptibility was evaluated using binder recovered from loose mix then PAV aged for 20, 40, and 60 hours. The as-recovered material was considered 0 PAV aging hours. For this analysis, a linear trendline was fit to each test section for a given PG property, model coefficients and R^2 values are summarized in **Table** 6-5 and **Table 6-6**. Aging susceptibility was evaluated based on the slope of the linear trendlines. In the table the highest slope is highlighted in red, lowest in blue.

High temperature grade was most sensitive to aging with a slope value approximately double that of intermediate temperature grade and m-critical. The range in high temperature PG grade at 0 PAV aging hours was reduced from 14°C at 0 PAV aging hours to 7.7°C after 60 PAV aging hours. The average aging slope for the 40% control sections is 0.39°C/PAV hour, no significant difference was observed for the 30% RAP control section. Two RA sections (6001 and 6003) have aging slopes equal to or higher than the controls, these are also the sections with the lowest initial PG indicating a higher dose of additive may have been used. The remaining data set is segregated into two categories, sections 6004-6006 have aging slopes moderately less than the respective control (~9%), whereas a significant reduction in aging slope was observed for sections 6002 and 6007 (~18%).

Intermediate temperature and m-critical grades had similar aging slopes. The change in spread between results at 0 PAV hours and 60 PAV hours was also similar. S-critical had a significantly lower slope and thus less spread in data from the unaged to 60 PAV aged conditions. The data range for intermediate temperature grade reduced from 9.1°C to 7.7°C due to aging. For m-critical the data range reduced from 9.5°C to 8.3°C. For both properties, significant differences were observed in aging slopes between 40% RAP D1 and D2 results, with the 40% RAP D1 mix having the lowest aging slope across the entire data set. The difference between control sections influences evaluation of the RA sections. Regardless of the reference used Section 6003 has the highest aging slope and ages at a rate 35% to 56% faster than Section 6011 (40% Day 1 Control). The other RA sections had similar aging slopes that aged at a rate 5% to 30% faster relative to the Day 1 40% control.

Table 6-5: Linear Fit Equation Parameters for HT and IT Grade

Section	HT PG			IT PG		
	Slope	Constant	R^2	Slope	Constant	R^2
6001	0.40	59.8	97.1	0.19	12.8	89.1
6002	0.34	61.5	99.1	0.21	11.2	91.1
6003	**0.43**	55.9	99.1	**0.25**	10.9	98.6
6004	0.36	62.6	98.6	0.18	16.7	93.6
6005	0.37	63.1	97.3	0.17	15.4	95.0
6006	0.36	68.1	98.0	0.18	20.0	97.9
6007	***0.31***	69.9	98.8	0.20	17.2	97.6
6010 (30% RAP)	0.39	65.1	99.0	0.18	18.4	98.6
6011 (40% RAP D1)	0.38	66.9	97.7	***0.16***	19.7	95.0
6012 (40% RAP D2)	0.41	63.1	99.5	0.22	15.7	93.2
Average	**0.37**	**63.6**		**0.19**	**15.8**	
Min	**0.31**	**55.9**		**0.16**	**10.9**	
Max	**0.43**	**69.9**		**0.25**	**20.0**	

Table 6-6: Linear Fit Equation Parameters for S-Critical and m-critical

Section	S-Critical			m-critical		
	Slope	Constant	R^2	Slope	Constant	R^2
6001	0.11	-36.3	83.1	0.20	-37.7	92.5
6002	0.12	-37.7	86.4	0.21	-39.6	96.8
6003	***0.14***	-37.6	95.6	***0.23***	-39.3	99.0
6004	*0.09*	-32.6	81.4	***0.17***	-33.3	93.0
6005	0.07	-33.9	85.6	0.18	-34.9	96.7
6006	0.08	-30.2	88.4	0.18	-30.1	99.2
6007	0.10	-32.7	95.3	0.20	-32.2	98.3
6010 (30% RAP)	0.09	-31.2	97.3	0.19	-32.2	99.1
6011 (40% RAP D1)	0.08	-30.8	86.0	0.17	-31.3	93.3
6012 (40% RAP D2)	0.12	-32.9	90.9	0.22	-34.3	93.6
Average	**0.10**	**-33.6**		**0.19**	**-34.5**	
Min	**0.07**	**-37.7**		**0.17**	**-39.6**	
Max	**0.14**	**-30.2**		**0.23**	**-30.1**	

6.2.1.2 Comparison of Binder Aging with Loose Mix Aging

Relationships between laboratory and field aging have been the focus of multiple national and state research efforts as a means to better understand mixture cracking and durability. The current research project presents an opportunity to add two mix aging protocols (135°C and 95°C loose mix aging) to this knowledge base. Specifically, state agencies have expressed interest in loose mix aging at 135°C to allow for evaluation of aging in a reasonable timeframe. Agency interest is the reason that the 6 hour, 135°C loose mix aging condition was the first evaluated in this study. Data presented in **Table 6-7** and **Table 6-8** show the change in properties for a given aging condition relative to 6 hours loose mix aging at 135°C. The table was constructed as (Property at aging condition X – property at 6 hours, 135°C). The two aging conditions where the difference switches from positive to negative are highlighted in red and bold.

6 hours 135°C mix aging produces high and intermediate temperature PG results between as-recovered binder and 20-hour PAV (6010, 6012) or 20 hour and 40-hour PAV (6011) for the control sections. Relative performance of the RA sections differs based on the property evaluated. For high temperature PG most sections (6001-6004, 6007) are between the 20 and 40 hr PAV aging conditions. Conversely only two sections fall within the 20/40 PAV aging range for intermediate temperature grade (6001 and 6002). For high temperature grade Year 1 and Year 2 field core result remained negative for most sections, indicating that the field aged mix had values below (better) than the 6 hours 135°C loose mix aged material. Most differences for intermediate temperature grade did not change sign indicating that the loose mix aging resulted in lower (positive sign) or warmer (negative sign) for both Year 1 and Year 2 cores.

For m-critical the 6 hours 135°C aging protocol produced results between recovered and 20-hour PAV aged binder for all three control mixes (6010 – 6012) and a majority of the RA sections (6003-6007). Negative differences observed for Year 1 and Year 2 field cores for sections 6006, 6007 and 6011 indicate that these results had warmer m-critical grades than the aged loose mix. Differences for all other sections remained positive indicating that field aging had not yet reached the extent of laboratory loose mix aging.

The 6 hours 135°C loose mix aging protocol produced results between 20-hour and 40-hour PAV for seven of 10 sections evaluated, including two of the three controls (6001, 6002, 6003, 6006, 6007, 6010, and 6012). The remaining sections had results between recovered binder and 20-hour PAV (6004, 6005, 6011). The loose mix aging procedure also produced results between Year 1 and Year 2 field cores for two sections (6001 and 6010).

Table 6-7: Change in HT PG and IT PG Relative to Loose Mix Aging – 6 hours at 135°C

Section	HT PG				IT PG			
	Rec. AC	20 hr PAV	40 hr PAV	60 hr PAV	Rec. AC	20 hr PAV	40 hr PAV	60 hr PAV
6001	-16	-3.9	2.2	8.8	-8.9	-1.3	0.6	3
6002	-10.8	-4.5	3.9	8.8	-7.7	-0.1	3.6	5.3
6003	-14.2	-3.2	3.8	12	-6.5	0.1	4	8.5
6004	-10.3	-0.7	5.2	11.5	-4.1	2.3	3.8	7.4
6005	-8.5	2.5	7.7	14.3	-2.2	3.5	5.4	8.4
6006	-8.5	1.6	7.3	13.3	-2.1	3	6	8.9
6007	-7.6	-3.3	3.7	10.9	-4.6	0.8	4.5	7.2
30% RAP	-10.1	0.1	6.9	13.9	-3.6	1.2	4.2	7.3
40% RAP D1	-13.4	-2.4	3.6	9.9	-5.2	-0.2	2.4	4.3
40% RAP D2	-9.4	3.8	10.7	15.5	-4.8	2.4	6.8	8.6

Table 6-8: Change in m-critical and ΔT_c Relative to Loose Mix Aging – 6 hours at 135°C

Section	m-critical				ΔTc			
	Rec. Ac	20 hr PAV	40 hr PAV	60 hr PAV	Rec. AC	20 hr PAV	40 hr PAV	60 hr PAV
6001	-7.6	***-0.4***	***2.4***	4.8	2.3	***0.4***	***-1.6***	-2.7
6002	-6.5	***-0.1***	***3.4***	6.5	2.8	***1.4***	***-0.9***	-2.8
6003	***-5.3***	***0.5***	4.3	8.4	1.8	***0.6***	***-1.0***	-3.1
6004	***-2.9***	***3.2***	5.6	7.8	***1.2***	***-0.3***	-2.6	-3.1
6005	***-1.3***	***4.1***	6.5	9.7	***1.5***	***-0.5***	-2.5	-4.5
6006	***-1.2***	***3.5***	6.4	10.0	1.9	***0.4***	***-1.4***	-4.4
6007	***-3.6***	***1.5***	5.6	8.3	2.3	***0.4***	***-1.8***	-3.4
30% RAP	***-3.4***	***1.2***	4.8	7.8	2.1	***0.4***	***-1.9***	-3.2
40% RAP D1	***-5.5***	***0.3***	2.9	4.8	2.8	***0.5***	***-1.5***	-2.5
40% RAP D2	***-4.2***	***3.1***	6.9	9.2	**2.1**	***1.6***	*-2.4*	-4.4

Table 6-9 and **Table 6-10** show the change in properties for a given aging condition relative to 7 days of loose mix aging at 95°C. 7 days of mix aging at 95°C produces comparable ΔTc results to 60 hours of PAV binder aging. For performance grades, mix aging produces slightly higher grades than 60 hours. PAV binder aging for most RA binders. While produce lower grades than the 60 hrs. PAV for the control binders. This could imply that the addition of RA to asphalt binders makes them more susceptible to mix aging than binder aging in terms of rheological characteristics.

Table 6-9: Change in HT PG and IT PG Relative to Loose Mix Aging – 6 hours at 135°C

Section	HT PG				IT PG			
	Rec. AC	20 hr PAV	40 hr PAV	60 hr PAV	Rec. AC	20 hr PAV	40 hr PAV	60 hr PAV
6001	-27.5	-15.4	-9.3	-2.7	-15.1	-7.5	-5.6	-3.2
6002	-23.3	-17.0	-8.6	-3.7	-16.1	-8.5	-4.8	-3.1
6003	-27.8	-16.8	-9.8	-1.6	-14.6	-8.0	*-4.1*	*0.4*
6004	-22.8	-13.2	-7.3	-1.0	-12.3	-5.9	-4.4	-0.8
6005	-22.5	-11.5	*-6.3*	*0.3*	-11.1	-5.4	-3.5	-0.5
6006	-24.9	-14.8	-9.1	-3.1	-11.9	-6.8	-3.8	-0.9
6007	-18.8	-14.5	-7.5	-0.3	-11.7	-6.3	*-2.6*	*0.1*
30% RAP	-21.3	-11.1	*-4.3*	*2.7*	-9.9	-5.1	*-2.1*	*1.0*
40% RAP D1	-19.6	-8.6	*-2.6*	*3.7*	-8.9	-3.9	*-1.3*	*0.6*
40% RAP D2	-24.4	-11.2	*-4.3*	*0.5*	-12.4	-5.2	*-0.8*	*1.0*

Table 6-10: Change in m-critical and ΔT_c Relative to Loose Mix Aging – 6 hours at 135°C

Section	m-critical				ΔTc			
	Rec. Ac	20 hr. PAV	40 hr PAV	60 hr PAV	Rec. AC	20 hr PAV	40 hr PAV	60 hr PAV
6001	-15.4	-8.2	-5.4	-3.0	6.0	4.2	2.1	1.0
6002	-16.5	-10.1	-6.6	-3.5	6.7	5.3	3.0	1.1
6003	-14.1	-8.3	-4.4	-0.3	4.9	3.7	2.1	0.1
6004	-12.4	-6.2	-3.9	-1.7	5.6	4.1	1.8	1.3
6005	-11.1	-5.6	-3.2	-0.1	5.7	3.7	*1.6*	*-0.3*
6006	-13.6	-8.9	-5.9	-2.3	7.4	5.9	4.0	1.1
6007	-12.3	-7.3	-3.2	-0.4	5.4	3.5	*1.4*	*-0.3*
30% RAP	-9.4	-4.9	*-1.2*	*1.7*	5.2	3.5	*1.2*	*-0.1*
40% RAP D1	-8.8	-3.0	*-0.4*	*1.5*	4.8	2.4	*0.4*	*-0.5*
40% RAP D2	-12.4	-5.1	*-1.3*	*1.0*	6.0	2.3	*1.4*	*-0.5*

6.2.2 Rheological Properties

Figure 6-14 below shows the R values for the different study binders. Binder 30% and 40% D2 have lower R values than binder 40% D1 after each aging condition. Most of the RA binders 6001~6006 have lower R values than the 40% control binder and the 30% RAP binder. RA binder 6007 has higher R values as extracted, but similar values to the control after PAV aging.

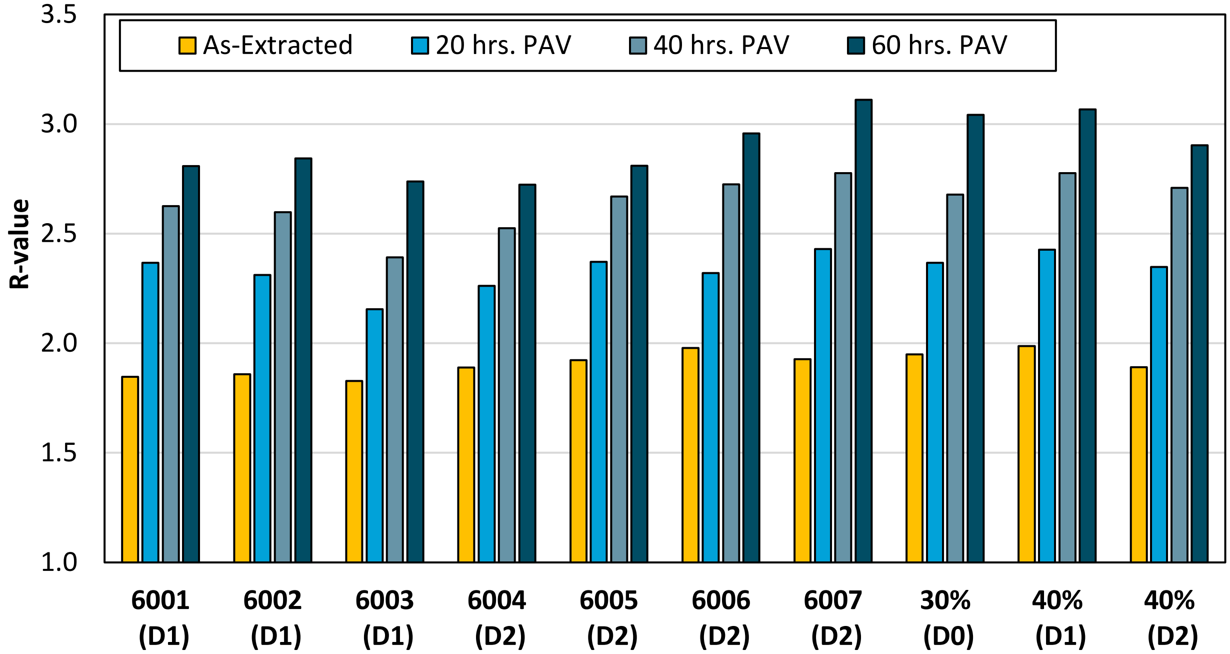

Figure 6-14 R Values for Extracted and Recovered Binders

Figure 6-15 below shows the ΔTc values for the different study binders with different aging conditions; all binders still meet the cracking warning threshold value of -2.5°C after 20 hrs. PAV condition, but all binders fail the threshold after 60 hrs. PAV. The 40% D2 binder has the warmest ΔTc value with as-extracted condition while the 30% D0 has the warmest value after PAV aging condition. There is a large difference in the ΔTc values between the two 40% control mixtures (6011 and 6012) in the as-extracted condition. RA binders 6001, 6002, 6003, and 6005 have warmer ΔTc values than 40% D1 control binders. RA binders 6006 and 6007 have a lower ΔTc value than the 40% D1 control after each aging condition. RA binders 6001, 6002 and 6003 have warmer ΔTc values than the 30% control mixture as well.

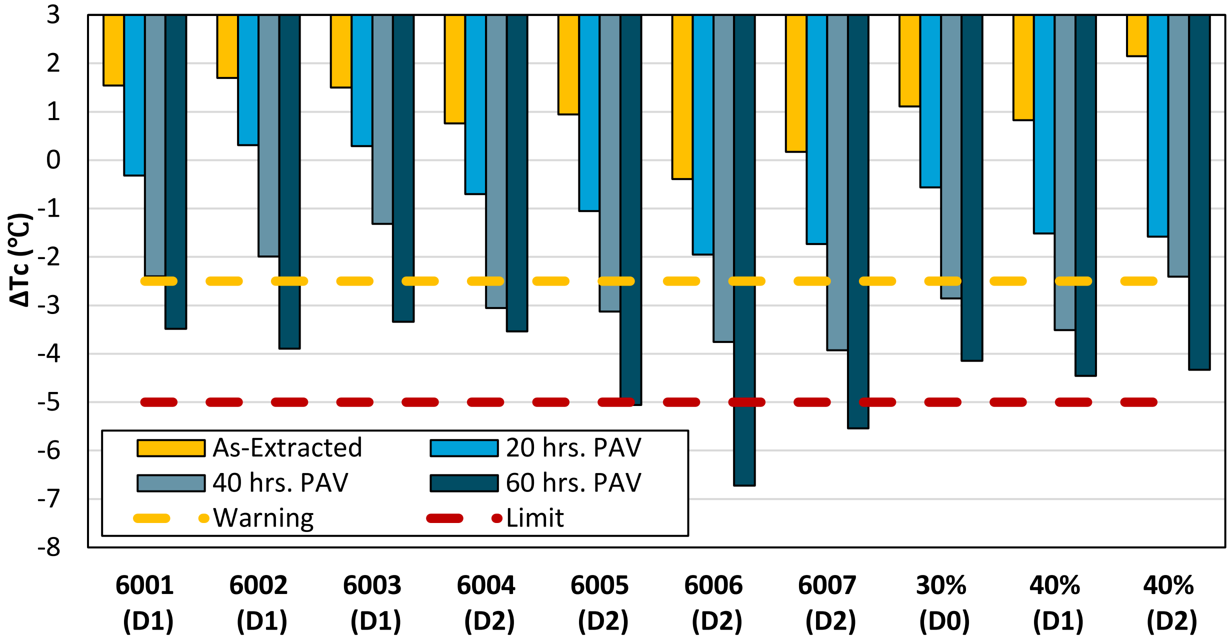

Figure 6-15 ΔTc Values for Extracted and Recovered Binders

Figure 6-16 below shows that all the recovered binders meet the G-R cracking warning threshold value of 180kPa after 20 hrs. PAV condition. After 60 hrs. PAV, binder 6006, 6007, 30% D0 and 40% D1 Control fail the cracking limit at 480kPa. There is a difference in G-R values for the two 40% binders at both aging conditions. RA binders 6001, 6002, 6003, 6004, and 6005 have lower G-R values than 40% D1 control binder and the 30% RAP binder. RA binders 6006 and 6007 have similar extracted G-R values as compared to 40% D1 control binder; however, they have higher values after PAV aging.

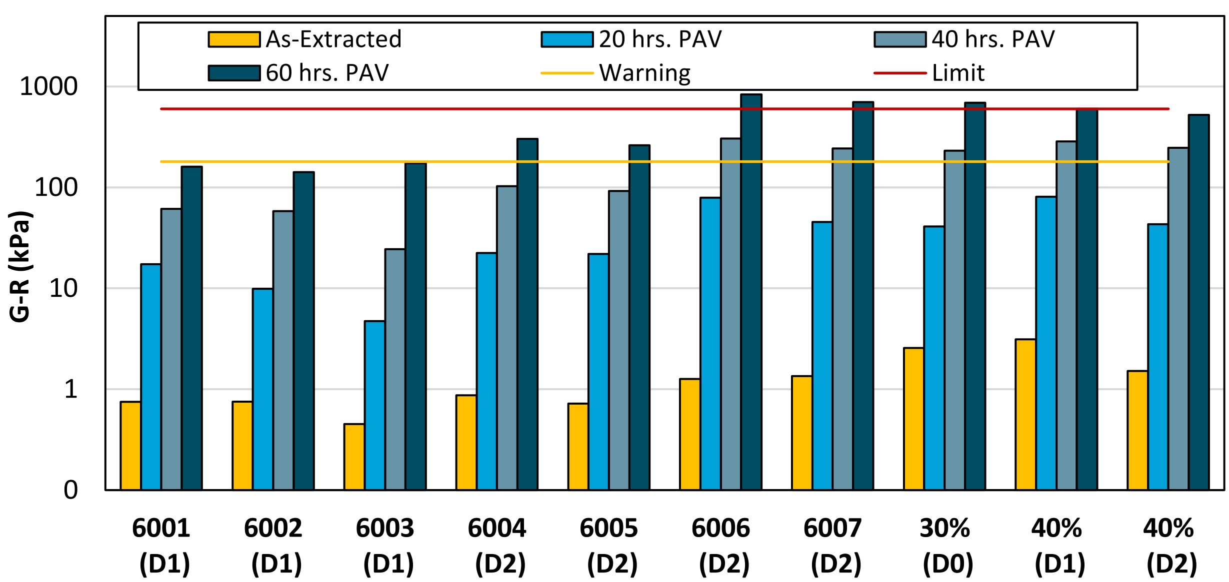

Figure 6-16 G-R Values at 15°C and 0.05 rad/s for Extracted and Recovered Binders

6.2.3 Chemical Compositions

Figure 6-17 below shows the CI values for the different study binders. There is a large difference in CI value between binder 40% D1 and 40% D2 with as-extracted condition, indicating potential variability during production. RA binders 6001, 6002 and 6003 typically have higher CI values than 40% control binder after each aging condition, indicating improvement of the colloidal structure by adding the RA products. RA binders 6006 and 6007 all have lower CI values than 40% control binder after each aging condition. Compared to the 30% control binder, RA binders 6005 and 6006 have lower CI values.

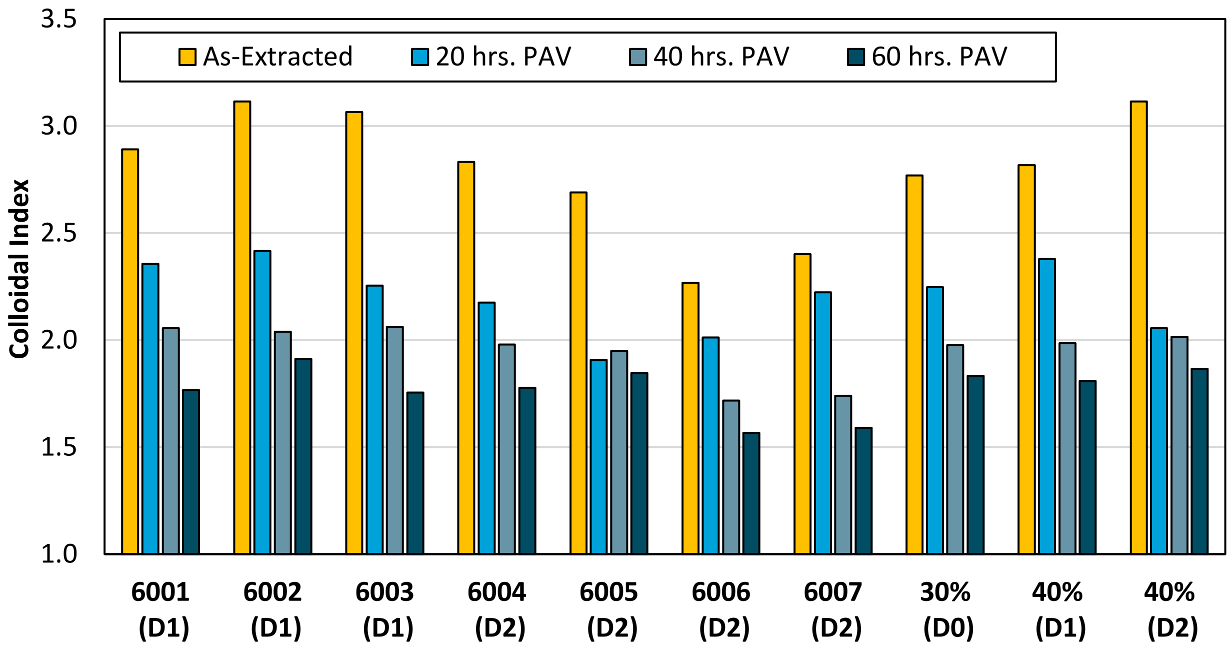

Figure 6-17 CI Values for Extracted and Recovered Binders

Figure 6-18 shows the carbonyl ratio ($I_{C=O}$) and sulfoxide ratio ($I_{S=O}$) for all binders. The $I_{C=O}$ parameter increases with aging, while there isn't a consistent trend for change of $I_{S=O}$ parameter with aging. Generally, there is a large difference in both $I_{C=O}$ and $I_{s=O}$ values between binder 40% D1 and 40% D2 (40% D1 and 40% D2 have similar $I_{C=O}$ values with as-extracted condition). All RA binders have higher $I_{C=O}$ value as compared to the control binders after each aging condition. In terms of the $I_{S=O}$ parameter, RA binders 6001, 6002 and 6003 have a lower value than the control binder 40% D1 with as-extracted condition but higher value after PAV aging. RA binders 6004, 6005, 6006 and 6007 all have higher $I_{S=O}$ parameter than the control binder 40% D2 as well as binder 30% D0.

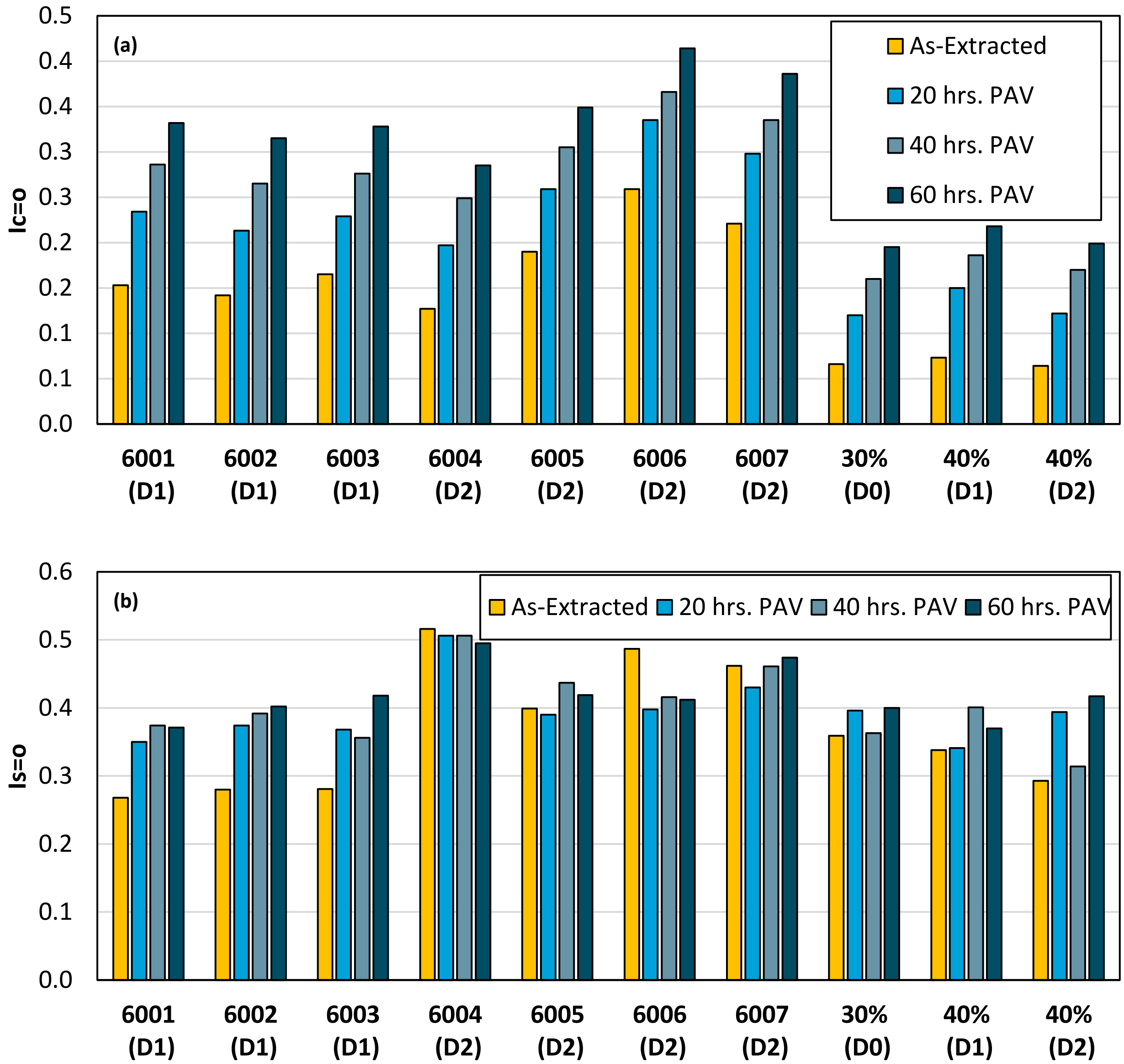

Figure 6-18 (a) $I_{C=O}$; and (b) $I_{S=O}$ Values for Extracted and Recovered Binders

The linear fits of asphaltenes and Colloidal Index vs. PAV aging hours to compare aging profiles of the control and RA sections were done. Coefficients and R^2 for the linear model used to fit the data are provided in **Table 6-11.** Initial Colloidal Index (CI) ranged from 2.27 – 3.12, Section 6012 (40% RAP Control – D2) had the highest CI value, another indicator of a potential issue during production of the 6012 mixes. Based on the design of the experiment it was expected Sections 6011 and 6012, 40% RAP Controls Day 1 and Day 2, would have similar composition. Five of the RA sections (6001-6005) had equal to or higher CI values relative to the controls, sections 6006 and 6007 were the worst performers in the data set. Aging is necessary to determine if variations in initial properties observed are due to dilution effect of the additive or represent an improvement in properties. Loose mix aging (6 hrs. at 135°C) results show differing trends. The 30% control (6010) has a higher CI value than the 40% Day 1 control (6011), initial CI values were similar. After aging all RA sections had CI values equal to or higher than the control (6011) and ranking changed. Sections 6003-6005 have the best performance, whereas aging caused a significant decrease in CI for 6001 and 6002. Sections 6006-6007 now have CI values equal to the control and had the least change in CI due to aging in the data set. The importance of aging is also demonstrated by the field core data. Year 1 Field Cores have a range in CI from 2.22 to 2.68, the range for Year 2 Field Cores is 2.16 to 2.32.

Table 6-11: Linear Model Coefficients for Asphaltenes and CI vs. PAV Aging Time

Section	Asphaltenes			Colloidal Index		
	Slope	Constant	R^2	Slope	Constant	R^2
6001	0.159	19.4	99.5	-0.018	2.823	97.7
6002	0.163	18.8	94.8	-0.020	2.944	88.2
6003	0.161	19.0	99.1	-0.021	2.967	96.6
6004	0.143	20.8	95.1	-0.017	2.726	94.0
6005	0.120	21.3	92.2	-0.014	2.579	89.7
6006	0.121	24.7	98.8	-0.012	2.209	95.7
6007	0.132	23.7	97.3	-0.014	2.342	96.2
6010 (30% RAP D1)	0.132	20.3	93.7	-0.015	2.659	91.6
6011 (40% RAP D1)	0.127	21.9	93.9	-0.016	2.707	92.9
6012 (40% RAP D2)	0.154	19.0	97.3	-0.021	2.960	90.6

6.3 Extracted and Recovered Binders from Field Core and Lab Aged Mixes

6.3.1 Performance Grading

Performance grade according to AASHTO M320 for binders recovered from loose mix sampled during construction, aged loose mix, and field cores are presented in **Table 6-12** to **Table 6-14**. Low temperature grading data for the as-recovered field mix was taken from 4mm DSR testing as insufficient material was available to conduct BBR testing. A comparison of 4mm DSR and BBR test data will be provided in subsequent sections of the report. This data was included to provide a comparison to other aging conditions and compare trends for a specific mix type and between mix types. The asterisk in the notation "3-Year FC*" signifies that the 3-Year FC recovered binders are extracted from the small cylinder test specimens rather than the top half-inch of the field cores.

The 30% and 40% control had essentially the same continuous PG grade (PG 64.5-31.5) a marginal increase in high temperature PG grade was observed for the 40% RAP section, but the higher RAP content did not affect low temperature grade or ΔTc. Different results were observed for the Production Day 2 control and RA test sections. The 40% Day 2 mix (6012) was ½ grade softer than the control mix produced with 30% RAP. Again, the observation led us to choose the 40% Day1 mix as the D2 control, rather than using the 40% Day2 control. For RA binders on Day 1, addition of RAs for Sections 6001 through 6003 caused softening ranging in 0.5 (3°C) to 1.5 (9°C) in high and low temperature grade. The field sampled loose mix from the RA sections also had similar low temperature PG grades of approximately -38°C. After 6 hours of loose mix aging the change in high temperature PG was consistent across all test sections and more severe relative to changes in low temperature grade. Low temperature grade change due to aging was ~3°C for the control sections and ranged from 4°C to 6°C for the RA sections. Low temperature failure remained S-controlled or slightly m-controlled for all test sections.

After 6 hours of loose mix aging, the change in high temperature PG was consistent across all test sections and more severe relative to changes in low temperature grade. Low temperature grade change due to aging was ~3°C for the control sections and ranged from 4°C to 6°C for the RA sections. Low temperature failure remained S-controlled or slightly m-controlled for all test sections. At 6hrs. at 135°C aging levels, the low temperature grades for 6005 and 6006 were slightly lower than the as-extracted material. This result is attributed to use of the 4mm DSR for the as-extracted material and BBR testing for the aged material and will be investigated in more detail later in the report.

After 7 days of loose mix aging at 95°C, all control mixtures have similar PG as 64-22. The Day1 mixtures' HTPG increased by approximately 15-17°C, while the LTPG decreased by roughly 5-17°C. It shows all failures at low temperatures have transitioned to being m-controlled as a result of significant aging of the binders. Although all RA mixtures are marginally softer in continuous PG than the controls, they ultimately align with the same PG (64-22) as the control mixtures. In general, all field core grading results fall between the loose mix as recovered and loose mix aged for 6 hours at 135°C. Section 6002 is an outlier, both field core results were stiffer than the 6 hrs. 135°C loose mix aging conditions tested but still softer than the 7days at 95°C loose mix aging.

Table 6-12: Summary of PG Test Results and Grading –Day 1 RA Sections, Control (D010), and Day 1 Control (6011)

Sample ID	Description	Aging	Test Data					Grading	
			HT PG, °C	IT PG, °C	S critical, °C	m critical, °C	ΔTc	Continuous PG	M320 PG
6001	Field Core	1 yr FC	68.2	16.2	-31.4	-31.2	-0.15	68.2-31.2	64-28
6001	Field Core	2 yr FC	70.9	18.1	-30.3	-28.7	-1.62	70.9-28.7	64-28
6001	Field Core	3 yr FC	68.2	15.8	-31	-30.7	-0.25	68.2-30.7	64-28
6001	Field Core	4 yr FC	75.1	24.4	21.1	-26.3	-2.2	75.1-21.1	64-22
6001	Loose Mix	As-Extracted	58.1	15.3	-37.6	-39.1	1.54	58.1-37.6	58-34
6001	Loose Mix	6 hrs. at 135C	74.1	16.7	-32.3	-31.5	-0.76	74.1-31.5	64-28
6001	Loose Mix	7 days at 95C	85.6	23.2	-28.2	-23.7	-4.48	85.6-23.7	64-22
6002	Field Core	1 yr FC	69.7	17.2	-30.4	-30	-0.36	69.7-30.0	64-28
6002	Field Core	2 yr FC	72.5	19.1	-28.6	-27.8	-0.85	72.5-27.8	64-22
6002	Field Core	3 yr FC	73.1	19.8	-29.2	-27.7	-1.56	73.1-27.7	64-22
6002	Field Core	4 yr FC	75.4	24.3	21.7	-26.4	-1.9	75.4-21.7	64-22
6002	Loose Mix	As-Extracted	61.4	14.2	-38.8	-40.5	1.7	61.4-38.8	58-34
6002	Loose Mix	6 hrs. at 135C	72.2	14	-35.1	-34	-1.09	72.2-34.0	64-34
6002	Loose Mix	7 days at 95C	84.7	22.8	-29	-24	-5	84.7-24.0	64-22
6003	Field Core	1 yr FC	64.6	14.2	-32.6	-32.9	0.34	64.6-32.6	64-28
6003	Field Core	2 yr FC	66.9	15.7	-31.6	-31.2	-0.36	66.9-31.2	64-28
6003	Field Core	3 yr FC	62.1	12.3	-33.5	-34.4	0.89	62.1-33.5	58-28
6003	Field Core	4 yr FC	71.7	21.7	18.8	-28.6	-1.7	71.7-18.8	64-22
6003	Loose Mix	As-Extracted	54.9	12.8	-38.4	-39.9	1.5	54.9-38.4	52-34
6003	Loose Mix	6 hrs. at 135C	69.1	13.4	-34.8	-34.5	-0.28	69.1-34.5	64-34
6003	Loose Mix	7 days at 95C	82.7	21.1	-29.2	-25.8	-3.45	82.7-25.8	64-22

Table 6-13: Summary of PG Test Results and Grading – Control (D010), Day 2 Control (6012), and Day 2 RA Sections

Sample ID	Description	Aging	Test Data					Grading	
			HT PG, °C	IT PG, °C	S critical, °C	m critical, °C	ΔTc	Continuous PG	M320 PG
6004	Field Core	1 yr FC	68.1	17.2	-30.9	-31	0.14	68.1-30.7	64-28
6004	Field Core	2 yr FC	70.2	18.7	-29.3	-28.4	-0.95	70.2-28.4	64-28
6004	Field Core	3 yr FC	67.6	17	-31.2	-31.2	-0.03	67.6-31.1	64-28
6004	Field Core	4 yr FC	72.8	23.3	-20.1	-27.5	-1.5	72.8-20.1	64-16
6004	Loose Mix	As Extracted	62.6	17.6	-33.7	-34.4	0.76	62.6-33.7	58-28
6004	Loose Mix	6 hrs. at 135C	72.9	16.7	-32	-31.5	-0.42	72.9-31.5	64-28
6004	Loose Mix	7 days at 95C	85.4	24.2	-26.9	-22.1	-4.83	85.4-22.1	64-22
6005	Field Core	1 yr FC	65.9	15.3	-32.5	-32.5	-0.06	65.9-32.5	64-28
6005	Field Core	2 yr FC	68.6	17	-31	-30.2	-0.85	68.6-30.2	64-28
6005	Field Core	3 yr FC	63.7	13.5	-34.1	-34.9	0.88	63.7-34.1	58-34
6005	Field Core	4 yr FC	73.6	22.9	-20	-27.3	-1.9	73.6-20	64-16
6005	Loose Mix	As Extracted	61.7	16	-34.7	-35.7	0.94	61.7-34.7	58-34
6005	Loose Mix	6 hrs. at 135C	70.2	13.2	-34.9	-34.3	-0.58	70.2-34.3	64-34
6005	Loose Mix	7 days at 95C	84.2	22.4	-29.3	-24.6	-4.72	84.2-24.6	64-22
6006	Field Core	1 yr FC	68.1	16.5	-31.2	-31	-0.18	68.1-31.0	64-28
6006	Field Core	2 yr FC	67.8	16.4	-30.4	-30.5	0.1	67.8-30.4	64-28
6006	Field Core	3 yr FC	67.4	16.2	-30.8	-30.3	-0.51	67.4-30.3	64-28
6006	Field Core	4 yr FC	66.1	17.2	15.1	-32.5	0.3	66-15.1	64-16
6006	Loose Mix	As Extracted	66.8	20.8	-30.9	-30.5	-0.39	66.8-30.5	64-28
6006	Loose Mix	6 hrs. at 135C	75.3	16	-33.2	-31.8	-1.31	75.3-31.8	64-28
6006	Loose Mix	7 days at 95C	91.7	28.8	-24.7	-16.9	-7.8	91.7-16.9	64-16
6007	Field Core	1 yr FC	68.8	16.3	-32.1	-31.8	-0.37	68.8-31.8	64-28
6007	Field Core	2 yr FC	66.4	14.9	-33.5	-32.8	-0.72	66.4-32.8	64-28
6007	Field Core	3 yr FC	70.1	17.1	-30.6	-30.5	-0.17	70.1-30.3	64-28
6007	Field Core	4 yr FC	75.8	25.2	-21	-26.2	-1.9	75.8-21	64-16
6007	Loose Mix	As Extracted	70.5	19.2	-33.3	-33.4	0.17	70.5-33.2	64-28
6007	Loose Mix	6 hrs. at 135C	78.1	19.1	-31.9	-29.8	-2.09	78.1-29.8	64-28
6007	Loose Mix	7 days at 95C	89.3	25.1	-26.4	-21.1	-5.28	89.3-21.1	64-16

Table 6-14: Summary of PG Test Results and Grading – Control (D010), Day 2 Control (6012), and Day 2 RA Sections

Sample ID	Description	Aging	Test Data					Grading	
			HT PG, °C	IT PG, °C	S critical, °C	m critical, °C	ΔTc	Continuous PG	M320 PG
30%	Field Core	1 yr FC	69.8	18.4	-29.6	-29.3	-0.28	69.8-29.2	64-28
30%	Field Core	2 yr FC	71.9	19.5	-28.5	-27.5	-0.99	71.9-27.5	64-22
30%	Field Core	3 yr FC	68.4	17.9	-31.1	-31.1	0	68.4-31.0	64-28
30%	Field Core	4 yr FC	75.8	25.2	22.5	-25	-1.8	75.8-22.5	64-22
30%	Loose Mix	As Extracted	64.1	19	-31.5	-32.6	1.11	64.1-31.5	64-28
30%	Loose Mix	6 hrs. at 135C	74.2	18.3	-30.3	-29.3	-0.99	74.2-29.3	64-28
30%	Loose Mix	7 days at 95C	85.4	23.7	-27.3	-23.3	-4.05	85.4-23.3	64-22
40% D1	Field Core	1 yr FC	71.5	19.3	-29.6	-28.7	-0.84	71.5-28.7	64-28
40% D1	Field Core	2 yr FC	72.8	19.9	-28.5	-27.3	-1.12	72.8-27.3	64-22
40% D1	Field Core	3 yr FC	72	19.4	-28.7	-27.7	-1	72.0-27.7	64-22
40% D1	Field Core	4 yr FC	76.1	25.5	18.7	-25.3	-1.8	76.1-18.7	64-16
40% D1	Loose Mix	As Extracted	65.5	20.2	-31.6	-32.4	0.82	65.5-31.6	64-28
40% D1	Loose Mix	6 hrs. at 135C	78.9	21.1	-28.9	-26.9	-2	78.9-26.9	64-22
40% D1	Loose Mix	7 days at 95C	85.1	24.7	-27.6	-23.6	-3.95	85.1-23.6	64-22
40% D2	Field Core	1 yr FC	67.8	16.7	-30.4	-30.3	-0.03	67.8-30.3	64-28
40% D2	Field Core	2 yr FC	67.5	16.7	-30.9	-30.9	-0.1	67.5-30.9	64-28
40% D2	Field Core	3 yr FC	66	15.6	-31.7	-32.2	0.51	66-31.7.0	64-28
40% D2	Field Core	4 yr FC	76.1	25.5	18.7	-25.3	-1.8	76.1-18.7	64-16
40% D2	Loose Mix	As Extracted	60.8	18.2	-33.7	-35.8	2.14	60.8-33.7	58-28
40% D2	Loose Mix	6 hrs. at 135C	70.2	17	-31.6	-31.6	0.03	70.2-31.6	64-28
40% D2	Loose Mix	7 days at 95C	85.2	23.6	-27.3	-23.4	-3.86	85.2-23.4	64-22

6.3.2 Rheological Properties

Bar charts in this section will follow a similar format. For a given mix/section the first three bars have a patterned fill and represent recovered binder properties from field cores. The next four bars have solid fill and represent the loose mix sampled from construction then subsequently aged for multiple PAV cycles. The last two bars have pattern fill and represent results from loose mix aged for 6 hours at 135°C and 7 days at 95°C respectively.

High temperature continuous grading is presented in **Figure 6-19** and **Figure 6-20.** RA sections on both days of construction are only compared to 30% RAP control and 40% RAP D1 Control. For all samples high temperature grade was determined based on $G^*/\sin\delta = 2.2$ kPa. For Day 1 production the 6-hour loose mix aging at 135°C condition is similar to or falls between grading results after 20 and 40 hrs. PAV aging. Field core results generally have lower PG grades than the six hours loose mix aging condition, except for 6002 which is approximately equal to the grade of the aged loose mix. In all cases an increase in grade was observed for 1-Year and 2-Year field cores.

The 4-year field core results generally have comparable PGHT values to the 20 hrs. PAV and 6 hours at 135°C loose mix aging condition. 6001, 6002 and 6007 FC show comparable PG grades with 30% and 40% control. The other RA field cores, exhibit lower PG grades compared to the 40% control. This indicates that these RAs still impart a softening effect on the asphalt binders.

After 6 hours of loose mix aging at 135°C, the condition is similar or intermediate to the results obtained after 20 and 40 hours of PAV aging. RA 6001 ~6005 show a lower PGHT than both controls, while 6006 and 6007 fall between 30% control and 40% control.

After 7 days of loose mix aging at 95°C, the high-temperature grade generally aligns with the results from the 60-hour PAV aging. All RA mixtures show higher values than the 60-hour PAV, whereas control mixtures exhibit values below the 60-hour PAV results. This may suggest that the RA is more sensitive to loose mix aging compared to binder PAV aging. When contrasted with the two control mixtures, most of RA mixtures either match or are slightly lower in terms of high-temperature grade. However, RA mixtures 6006 and 6007 show higher high temperature grade than the controls.

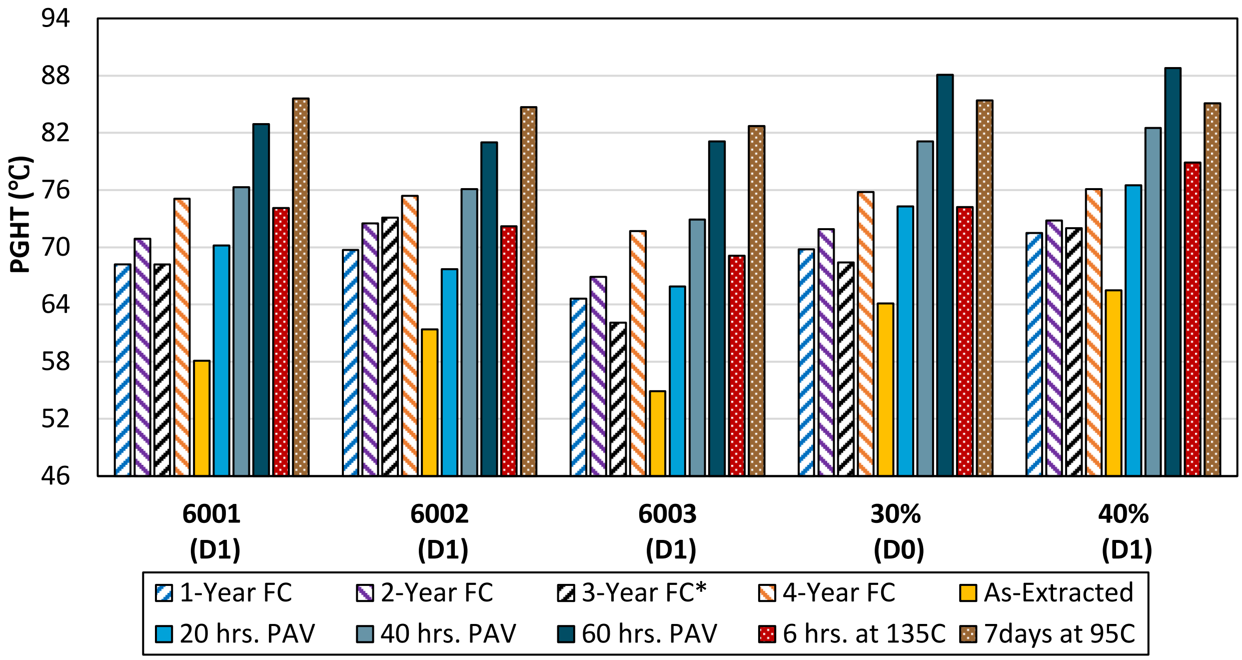

Figure 6-19: High Temperature Grade at Various Aging Conditions - Day 1 RA Sections and Controls

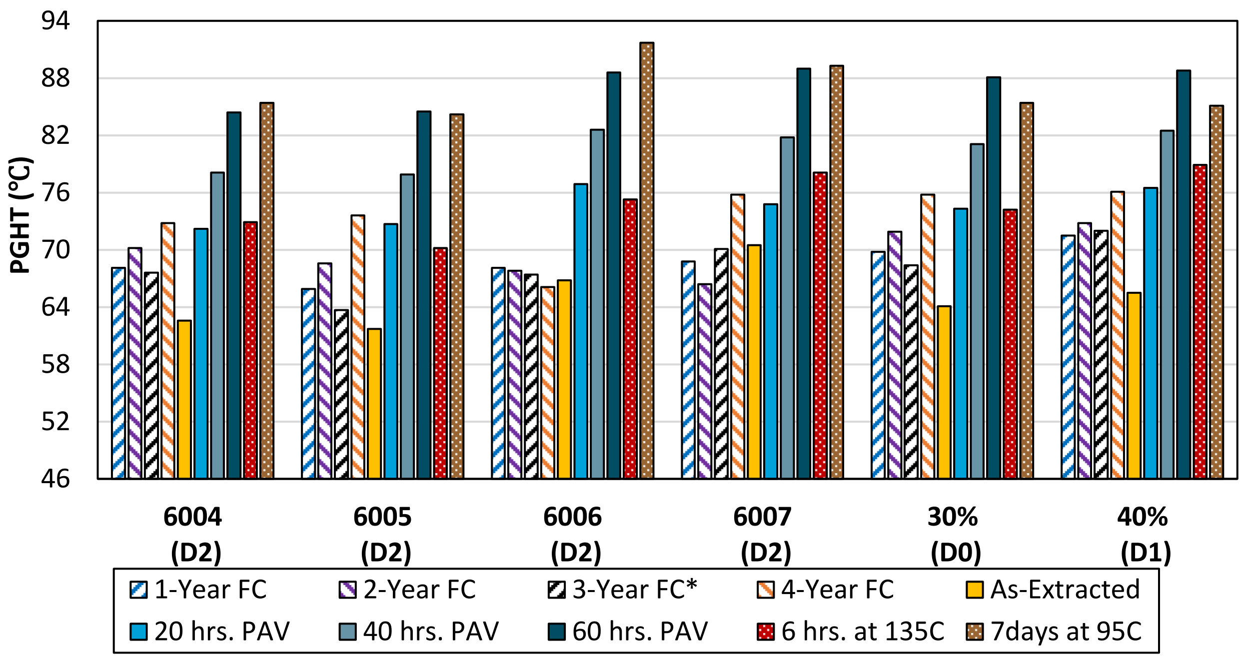

Figure 6-20: High Temperature Grade at Various Aging Conditions- Day 2 RA Sections and Controls

Day 1 production m-critical and ΔTc values for various lab and field aging conditions are presented in **Figure 6-21** through **Figure 6-24** . M-critical values of the binder recovered from loose mix sampled after construction were approximately 8°C lower for the three RA sections relative to the controls. The RA sections also maintained a m-critical temperature lower than -28°C after 40-hour PAV aging, whereas both control sections were 4°C warmer.

All field core results were similar except for Section 6003 which had m-critical values approximately 3°C lower. ΔTc values stayed above the cracking failure limit (-5.0°C) for all materials and aging conditions tested. The only exception is 6002, which have a ΔTc lower than failure limit after 7 days of loose mix aging at 95°C. Values were above warning limit (-2.5°C) for 6 hrs at 135°C loose mix aged and field core results, but all of the sections overpass warning after 60-hour PAV aging and 7 days at 95 °C aging.

For the 4-year field cores, the 40% control exhibited comparable ΔTc with its 30% counterpart. In contrast to the control mixes, most of the 3-year RA FCs maintained a lower m-critical and a warmer ΔTc, however, 4-year FC suggesting the continued influence of RA on the asphalt binders is dissipating. For example, 6001, 6002, and 6007 had similar m-critical values compared to the 40% control. 6001, 6002, 6003, 6005 and 6007 show comparable ΔTc compared to the 40% control. This indicates the diminishing softening effect of RA, accompanied by the reduced crack resistance.

The 6 hours at 135°C loose mix aged material was similar to as-recovered binder + 20-hour PAV aging and matched well with the Year 1~2 Field cores for 6001, 6003, 30% and 40% Control. All 3 Day 1 RA binders show warmer m-critical than controls, while all RAs show comparable values with controls after 7 days at 95 °C aging.

After 7 days of loose mix aging at 95°C, the properties of the aged materials for 6003 and the two controls were comparable to those of the as-extracted binders with 60-hour PAV aging. In terms of both m-critical and ΔTc values, the two control mixtures showed similar results. When assessing the RA and control mixtures, 6001 and 6002 aligned closely with the controls in m-critical, whereas 6003 showed a softer m-critical value compared to the controls. For ΔTc values, both 6001 and 6002 showed lower vales than the controls, but 6003 showed improvement.

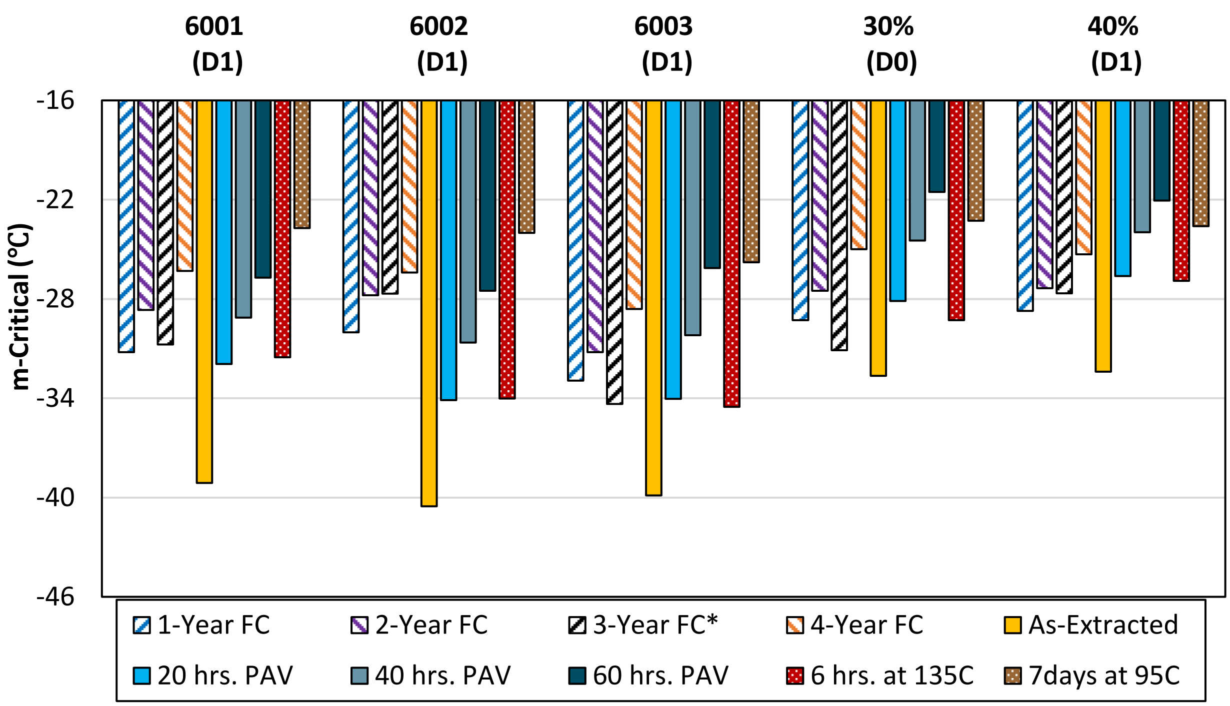

Figure 6-21: 4mm m-Critical Temperature at Various Aging Conditions – Day 1 RA Sections and Controls

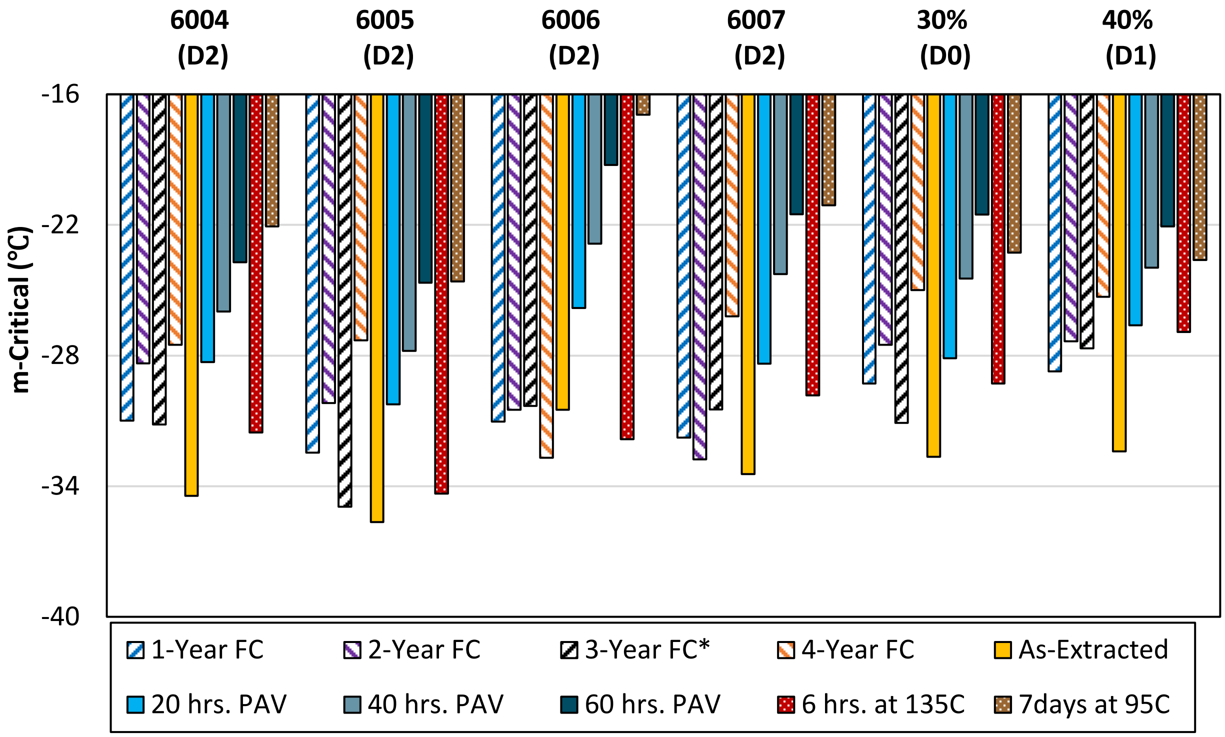

Figure 6-22: 4mm m-Critical Temperature at Various Aging Conditions – Day 2 RA Sections and Controls

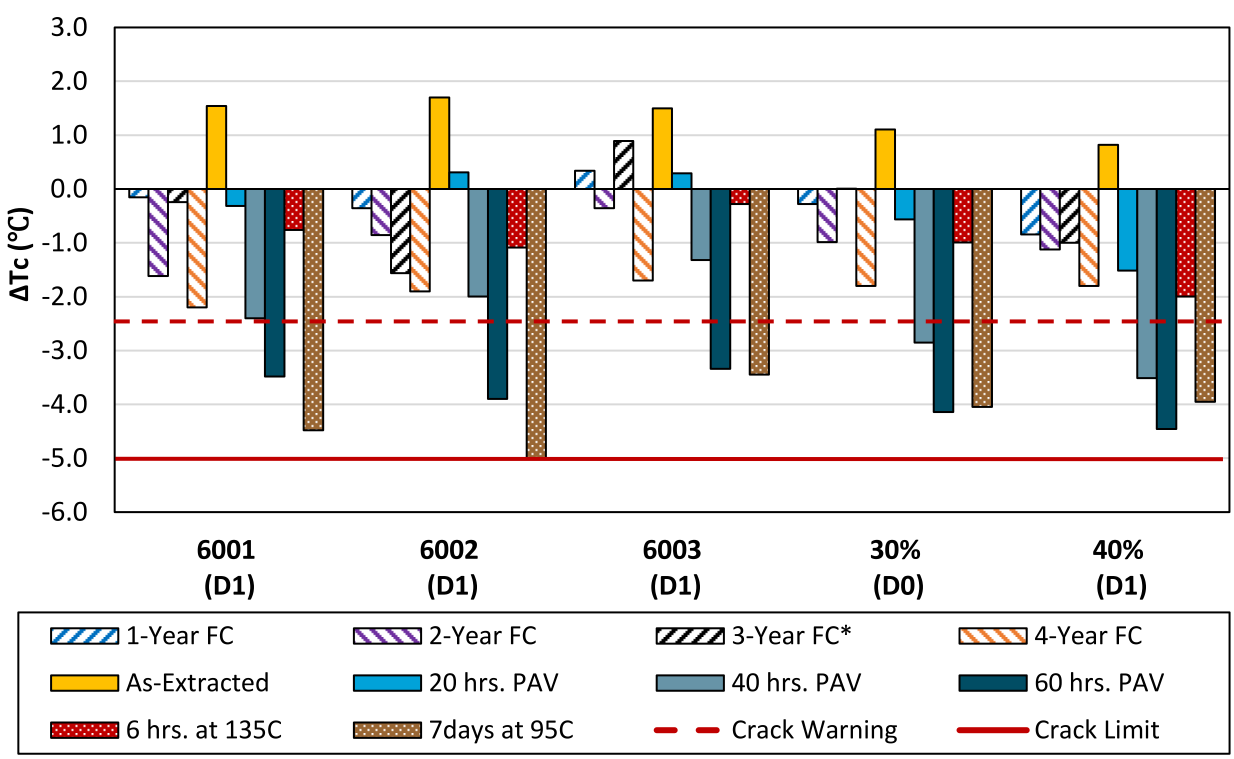

Figure 6-23: 4mm ΔTc at Various Aging Conditions – Day 1 RA Sections and Controls

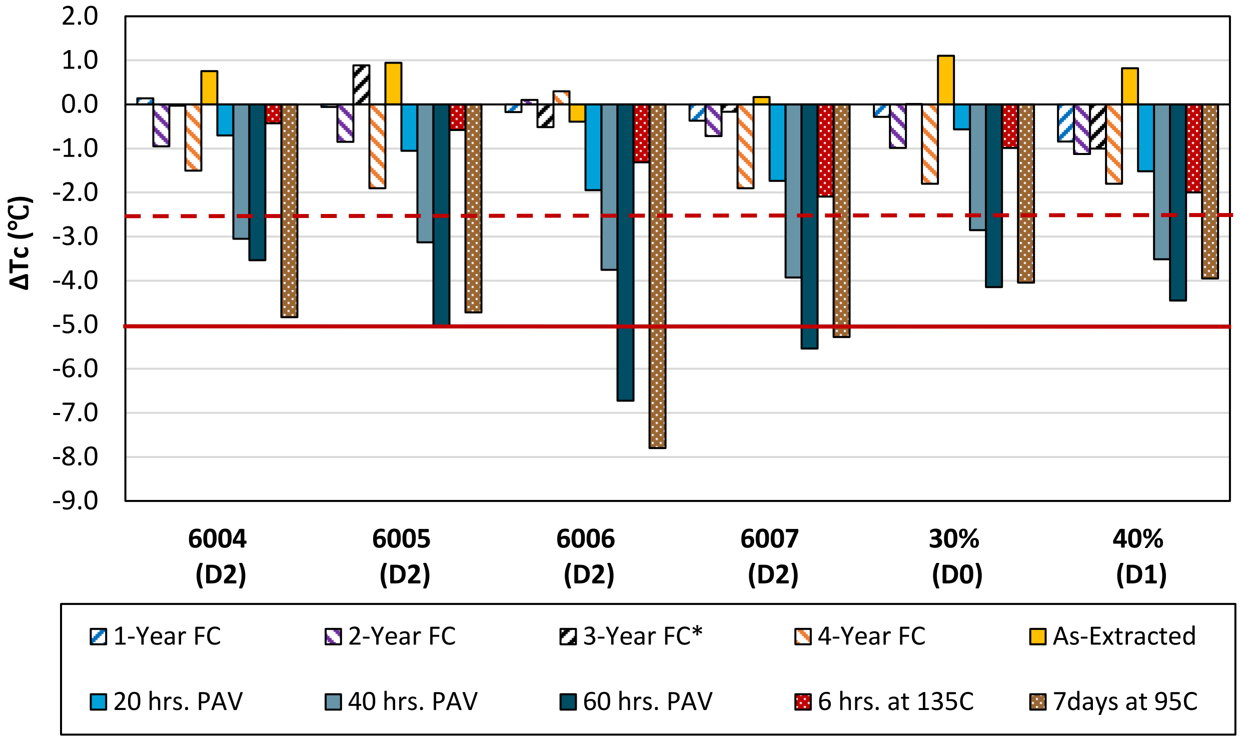

Figure 6-24: 4mm ΔTc at Various Aging Conditions – Day 2 RA Sections and Controls

As stated in Chapter 3, The Christensen method for calculating R-value was used in calculation of the R-values. The R-values for Day 1 control and RA sections are provided in **Figure 6-25**. For loose mix sampled after construction and subsequently aged for multiple cycles in the PAV R-values between all test sections remain relatively similar (within ~0.10) for a given aging condition. The outlier is the 40-hour PAV 6003 result which is lower than the rest of the data set. R-values for the 6 hours at 135°C loose mix aged material fall between 20- and 40-hour PAV results. An increase in R-value between Year 3 and Year 4 field cores was also observed.

4-Year Field core data R-values are comparable with the 6 hours at 135°C aged loose mix and 20-hour aged PAV binder. For both 6 hrs. at 135°C aging 7 days at 95°C aging, all RA shows comparable results with controls. This indicates the R-values are hard to differentiate between RA binders and control binders.

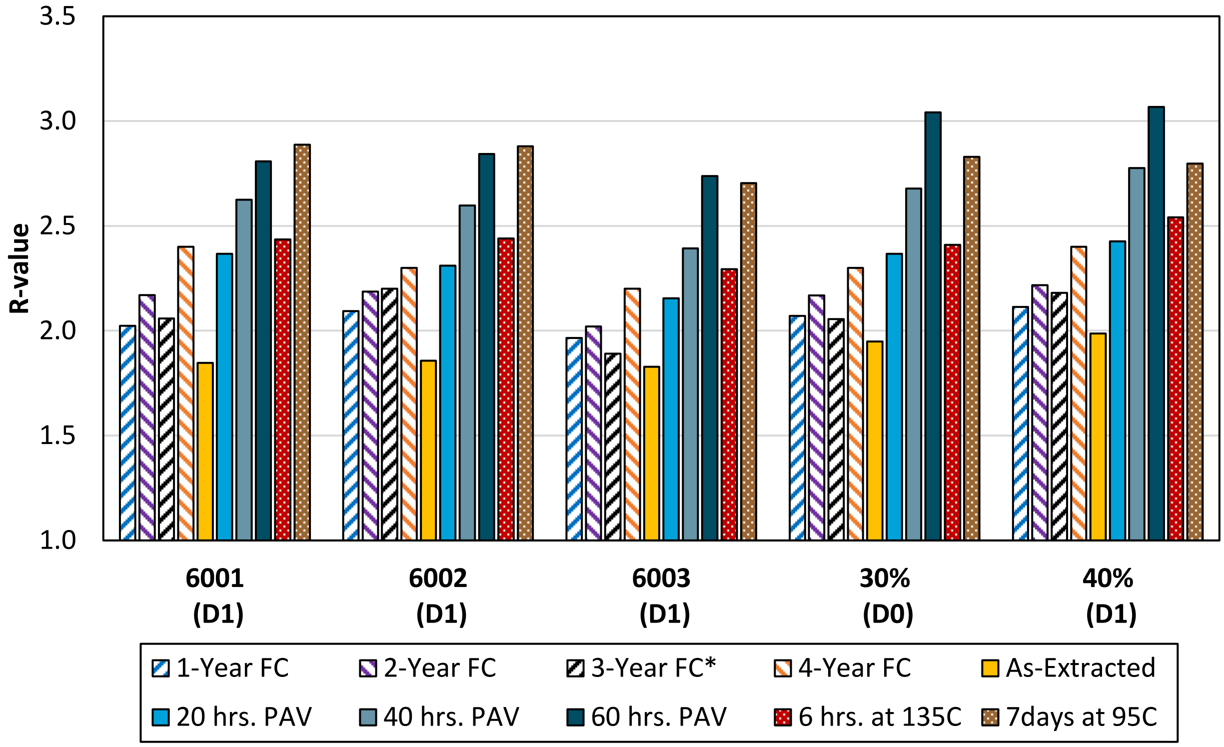

Figure 6-25: Comparison of R-Value Calculated by Christensen NCHRP 9-59 for Day 1 Control and RA Sections

The R-values for Day 2 control and RA sections are presented in **Figure 6-26.** In contrast to Day 1 results the R-values were similar to or higher than both the 30% and 40% RAP control sections. The notable difference being the recovered binder + 20-hour PAV aging for section 6004. Similar to the Day 1 results presented the 6-hour loose mix aged samples fell between 20- and 40-hour PAV aged, recovered binder for most sections tested, but in general were closer to 20-hour PAV results. R-values for Year 1 and Year 2 field cores were significantly lower than the 6-hour loose mix aged material and are comparable to as-recovered or as-recovered + 20-hour PAV results.

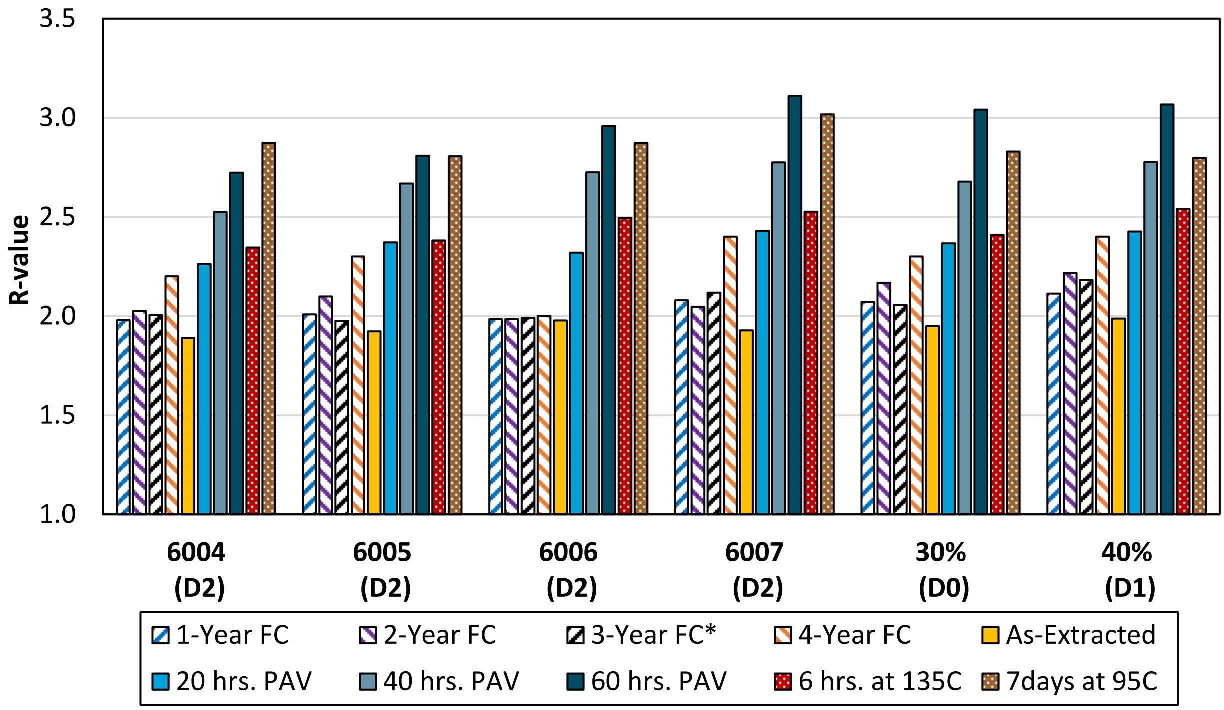

Figure 6-26: Comparison of R-Value Calculated by Christensen NCHRP 9-59 for Day 2 Control and RA Sections

The Glover-Rowe Parameter and Black Space plot with Glover-Rowe cracking warning and failure limits for are provided in **Figure 6-27** and **Figure 6-28**. Across all binder aging, loose mix aging, and field core samples the G-R parameter is lower relative to both controls. As a result, all three RA sections are below the cracking warning line of G-R = 180 kPa at most aging conditions (field cores, as-extracted binder + 40-hour PAV, 6 hrs. at 135°C loose mix aging). The control mixes approach or exceed the cracking warning and cracking limits at 40-hour and 60-hour PAV respectively. Consistent with other parameters presented in this report the 6-hour loose mixed aged condition most closely matches the as-extracted binder + 20-hour PAV aging. Low values of the G-R parameter were observed for the aged loose mix and field cores relative to the cracking warning at 180 kPa.

For the 4-year field cores, all RA sections are still lower than the crack warning threshold and 30% control and 40% control show comparable G-R values. Compared to the 40% control mix, while 6001 and 6007 are close with controls, most of the RA sections still have a lower G-R than 40% control.

After 7 days at 95°C loose mix aging, all RA mixes and control mixes exceed the crack warning, and two control mixes are approaching the crack limit at 600 kPa. 6006 and 6007 show higher G-R values than 40% control blends, and other RA blends show results comparable to controls. This is an indication of the decreasing effect of RA after aging. Only 6003 shows lower G-R values compared to controls, indicating better crack resistance.

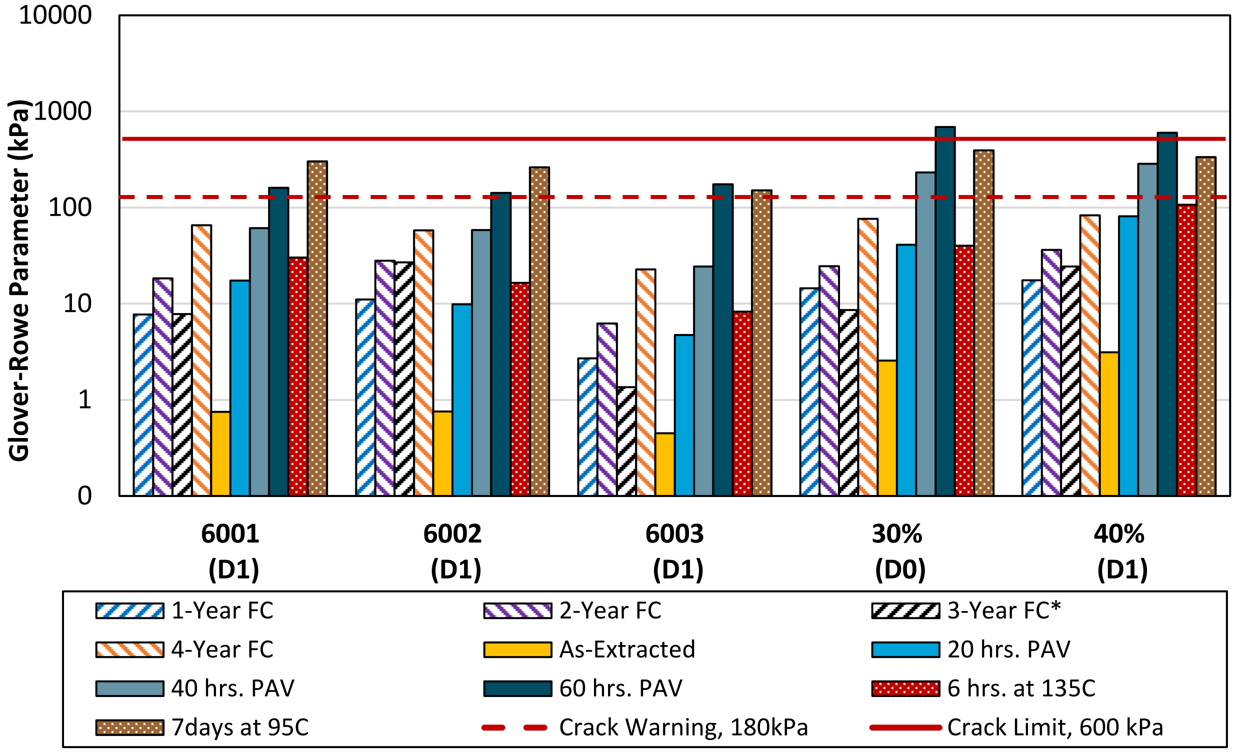

Figure 6-27: G-R Parameter for Day 1 RA Sections and Controls

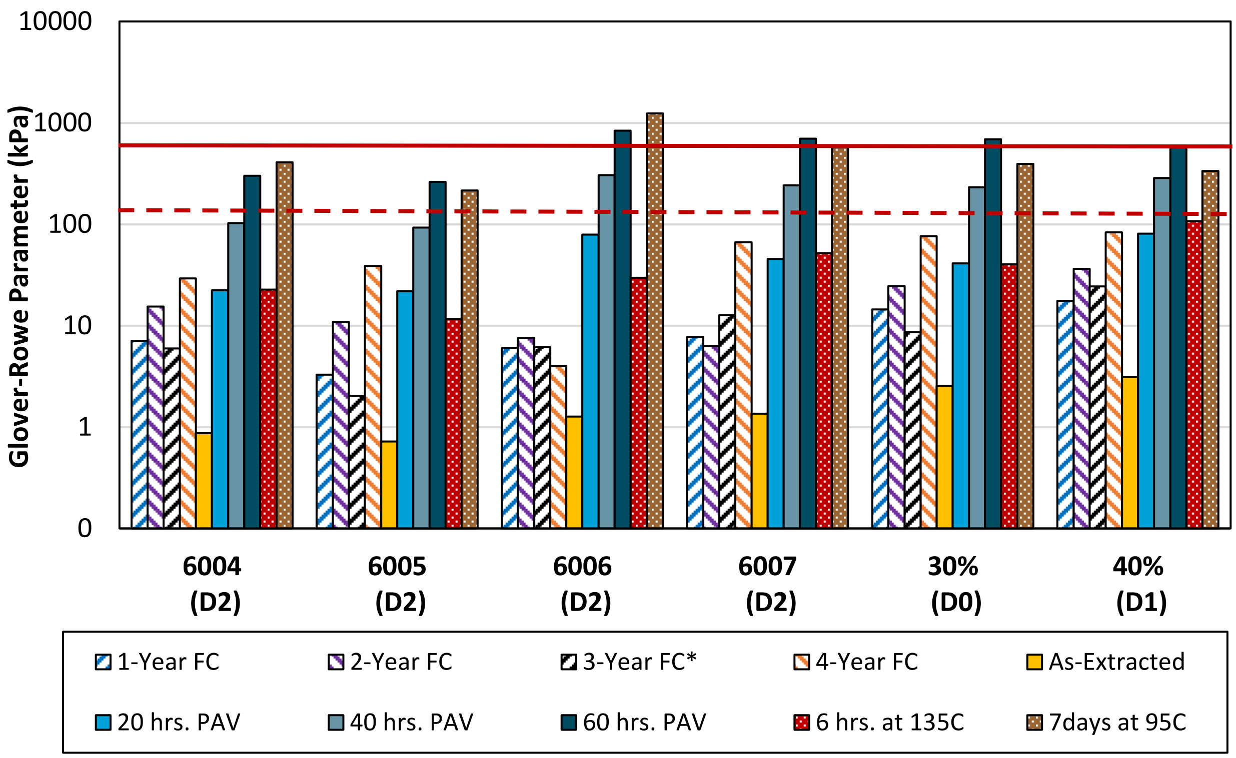

Figure 6-28: G-R Parameter for Day 2 RA Sections and 2 Controls

6.3.3 Chemical Compositions

Compositional changes for lab and field-aged, recovered binders are presented for % Asphaltenes and Colloidal Index in **Figure 6-29** and Figure 6-30. For binders recovered from loose mix then aged for multiple PAV cycles the % Asphaltenes are initially lower for the RA sections relative to the controls. After 40 hours PAV aging all values are similar. The 6 hrs. at 135°C loose mix aging condition matches the as-extracted binder after 40-hours PAV aging or falls between 20-hour and 40-hour PAV aging for all RA sections and the 40% control. Loose mixed aged results for the 30% control most closely match 20-hour PAV aged material. For the field cores, 1-year had lower asphaltenes and higher Colloidal Index relative the 6 hrs. at 135°C loose mix aged material for all sections except 6003, in which the Colloidal Index was equal to the aged loose mix. The magnitude of difference varied for each test section. An increase in asphaltenes and corresponding decrease in colloidal index between 1-year and 2-year Field Cores was observed for all sections except 6001 where the change was negligible.

For the 4-year field cores, the chemical composition of the 30% and 40% control cores showed similarity. This is evidenced by their comparable asphaltene ratios and colloidal indexes and is even consistent over the 1~4-year field cores. 6003 shows lower asphaltene ratios and higher colloidal indices than the control mixes.

After 7 days of 95°C loose mix aging, the material results agree well with the 60-hour PAV aging for two controls and all RA sections except 6002. The 40% control mix showed slightly more asphaltene and lower colloidal index than 30% control. All Day 1 RA mixtures showed higher asphaltenes ratio and lower colloidal index than control mixes.

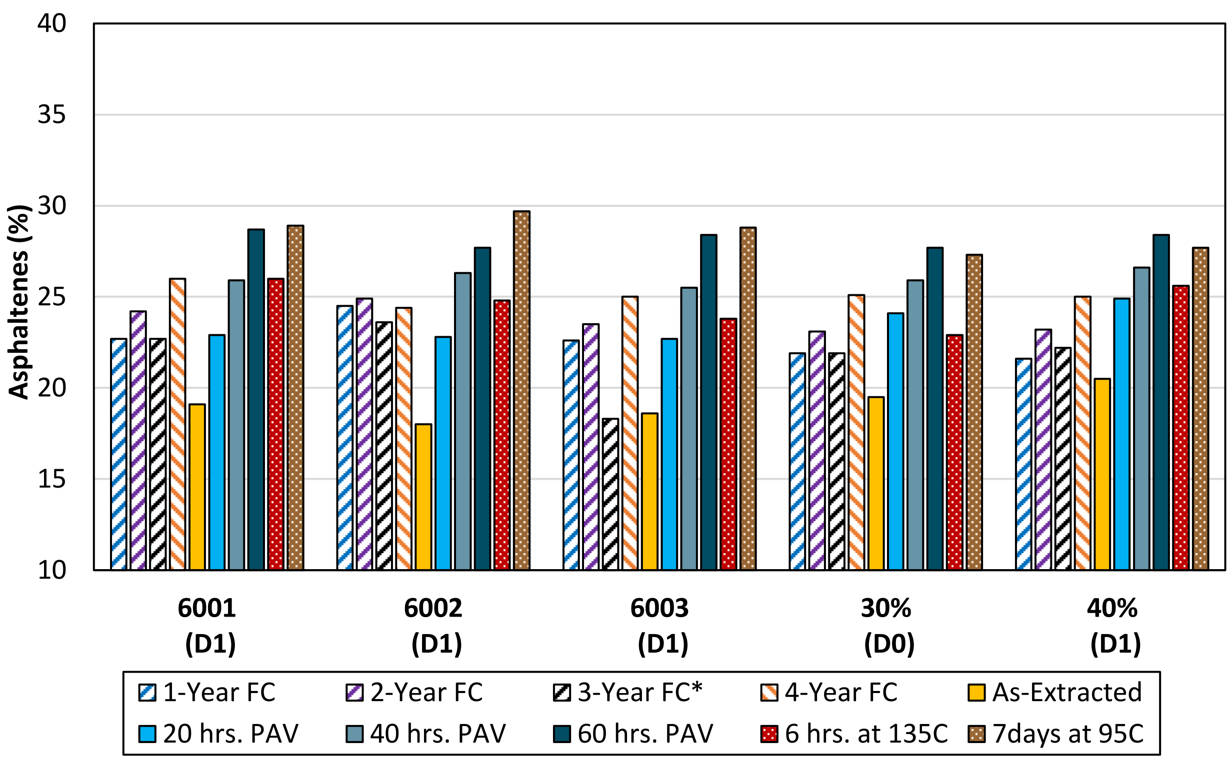

Figure 6-29: % Asphaltenes for Day 1 Control and RA Sections

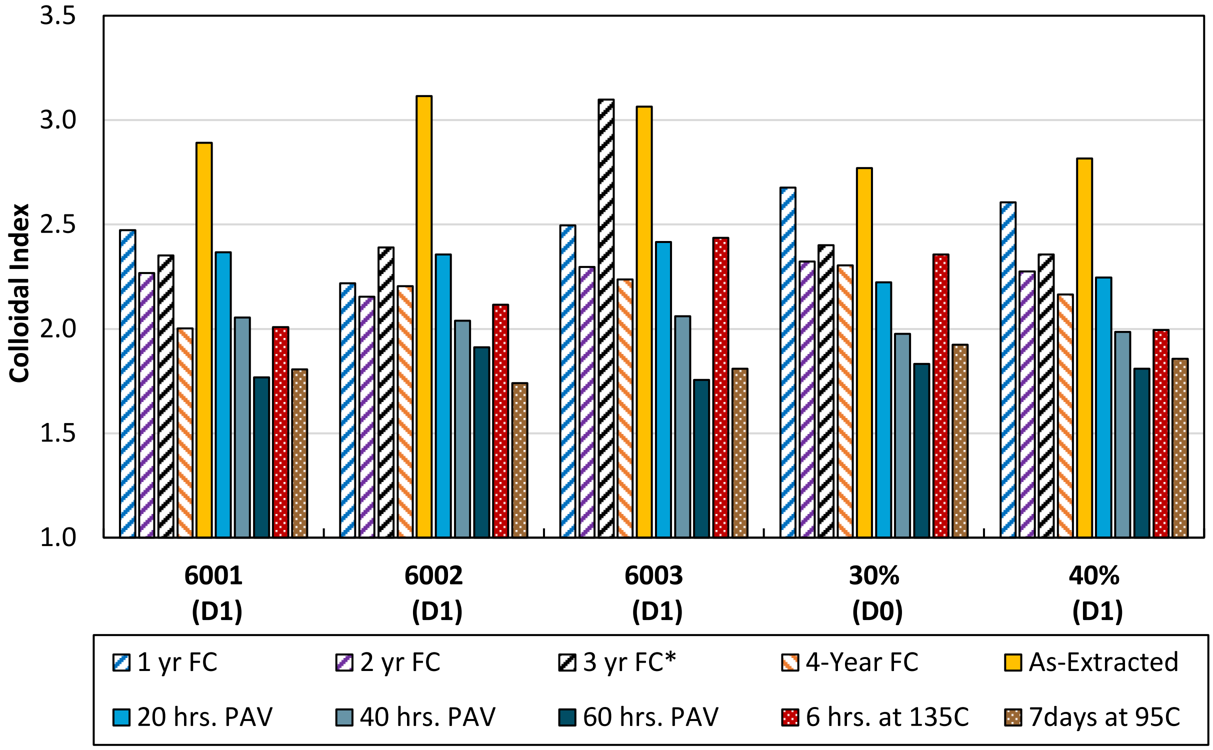

Figure 6-30: Colloidal Index for Day 1 Control and RA Sections

Percent asphaltene and Colloidal Index plots for the Day-2 lab and field aged samples are presented in **Figure 6-31** and **Figure 6-32**. For the as-extracted binder, the percent asphaltenes for the control mixes are lower than the RA mixes across all PAV aging conditions, with the highest values observed for RA sections 6006 and 6007. With extended aging levels the differentiation between sections 6006 and 6007 increases. Similar trends were observed for the Colloidal Index where a higher % asphaltenes corresponds to lower Colloidal Index values. In general, the 6 hrs. at 135°C loose mix aging condition most closely matches 20-hour PAV for both parameters studied. For the 30% control section and RA sections 6004 and 6005 both %asphaltenes and Colloidal Index of 1,2 and 3- year field cores compare well with the 6-hour aged loose mix. For sections 6006, 6007 and 40% control both field parameters are less than (%asphaltenes) or greater than (Colloidal Index) the result after 6-hour loose mix aging, indicating that the aging experienced in the field for these sections is less than aging that occurred during laboratory conditioning.

The chemical composition of 3 years field cores* show mix 6004 and 6005 have similar asphaltene ratio and colloidal index with two control mixes. 6006 and 6007 field cores have higher asphaltene ratio and lower colloidal index than the control mixes. The chemical composition after 7 days at 95°C loose mix aging matches well with the 60-hours PAV aging for both parameters. All RA sections show higher asphaltene ratio and lower colloidal index than the control mixes.

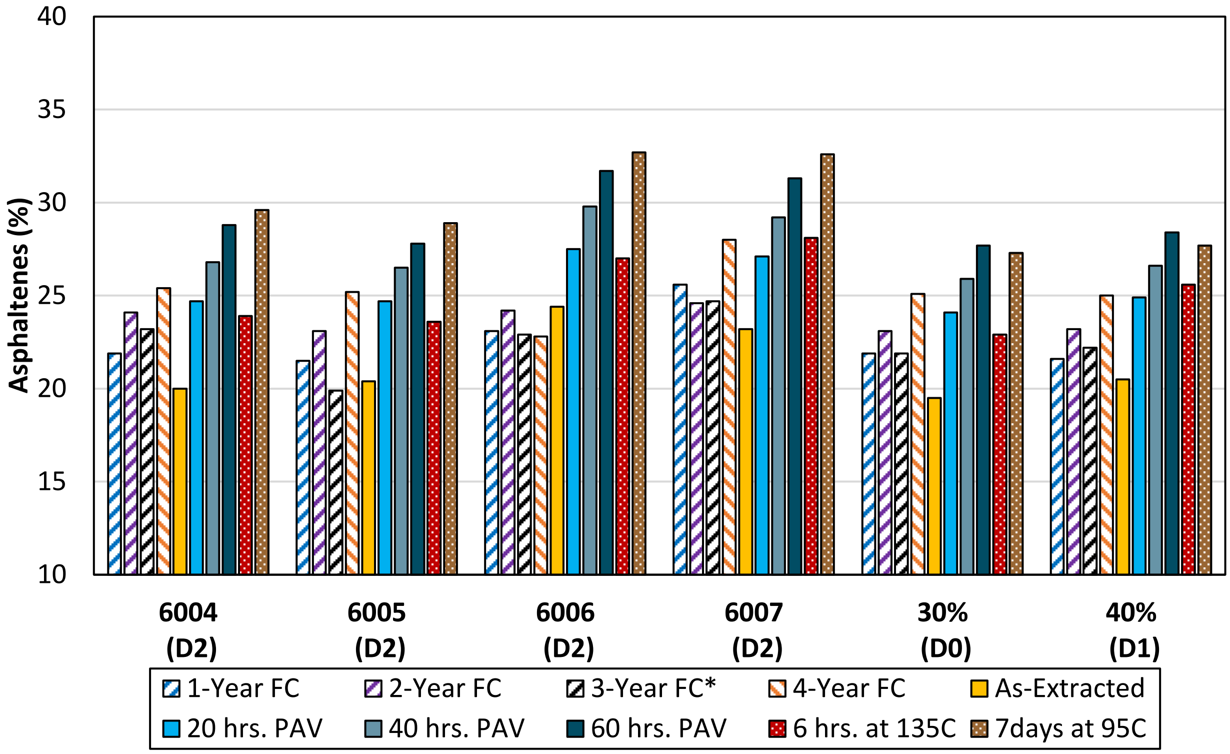

Figure 6-31: % Asphaltenes for Day 2 Control and RA Sections

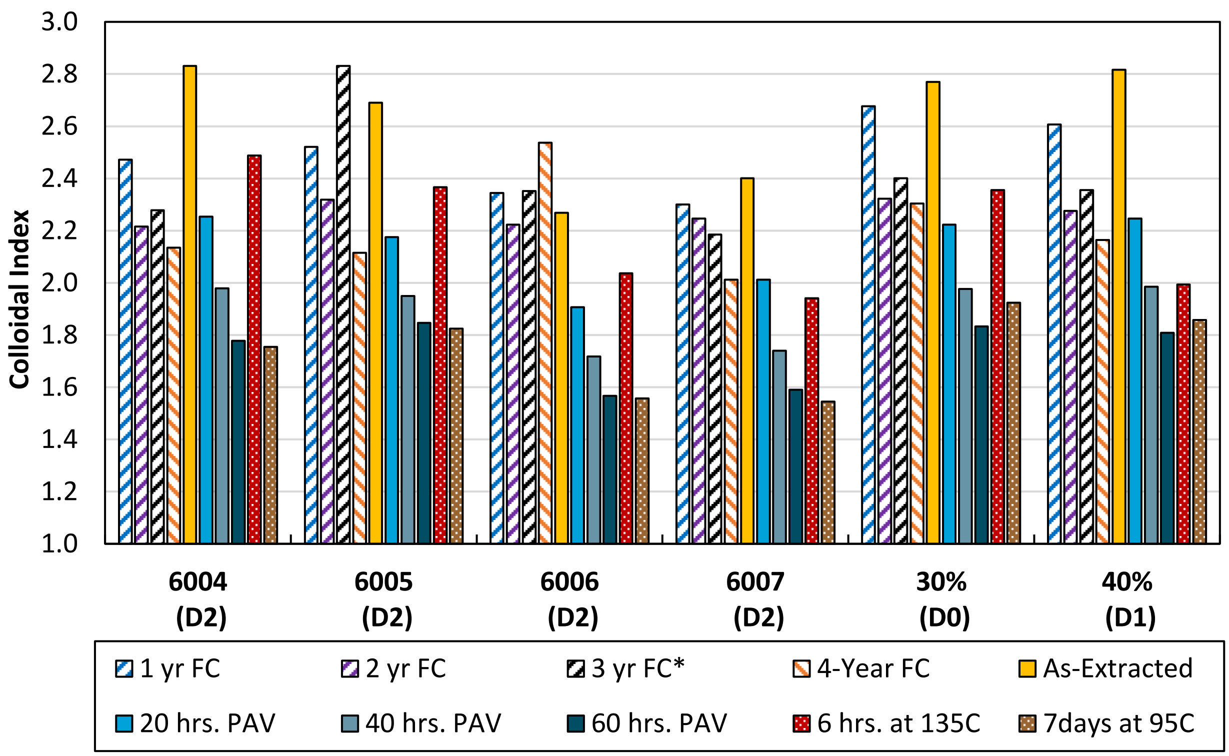

Figure 6-32: Colloidal Index for Day 2 Control and RA Sections

Carbonyl Ratio and Carbonyl + Sulfoxide Ratio determined from FTIR are presented in **Figure 6-33** and **Figure 6-34.** For these figures Year 0 corresponds to the as-extracted binder from the loose mix sampled during construction, Years 1 and 2 correspond to results from Field Cores. In both plots a substantial increase in carbonyl or carbonyl + sulfoxide ratio from year 0 to Year 1 or Year 2 field cores was observed for the control sections and RA sections 6001 – 6005. Both ratios for RA sections 6006 and 6007 started high at Year 0 and remained high for the subsequent sampling times.

For 4-year field cores, only 6002, 6003, 6007, 40% control shows an increased carbonyl ratios ratio and carbonyl + sulfoxide ratio than the 2-year field cores. Furthermore, when examining RA sections, they consistently showed higher values than the control mixes. This increase can be attributed to the inclusion of RA, which boosts the initial content of both carbonyl and sulfoxide in the binder. After 7 days at 95 C mix aging, the FTIR parameters increased to the levels that close to "as extracted" + 60 PAV aging for 6002, 6003, 6004, 6005 and two control mixes. Future work will merge this data set with the rheological testing data presented and explore relationships between rheological parameters and compositional data from SARA and FTIR analysis.

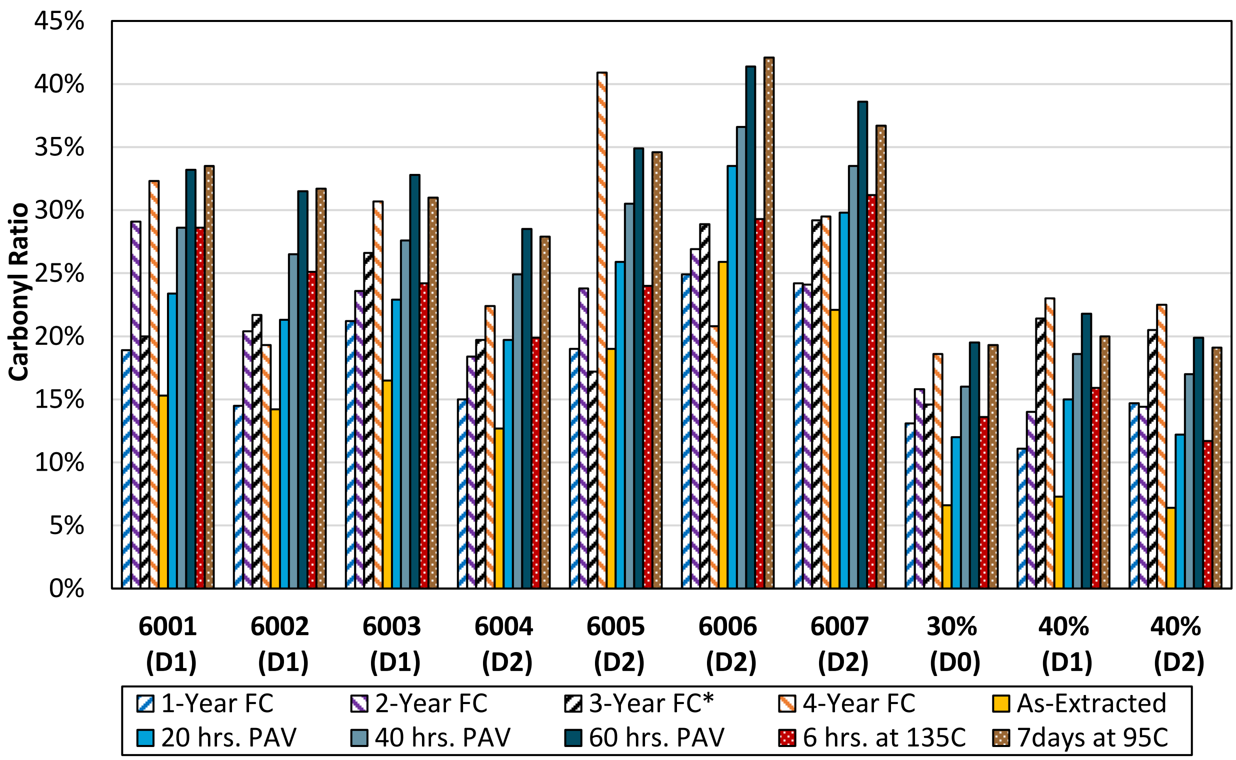

Figure 6-33: Carbonyl Ratio – All Control and RA Sections

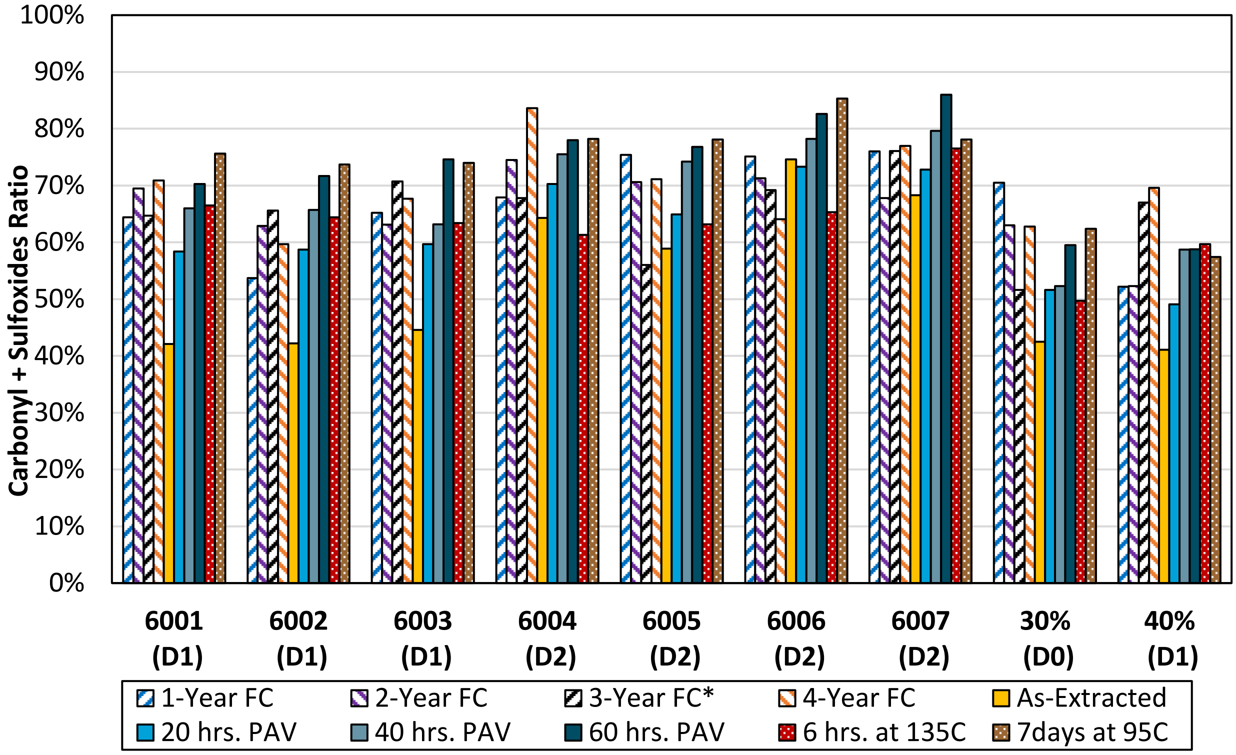

Figure 6-34: Carbonyl + Sulfoxides – All Control and RA Sections

Chapter 7: Mixture Test Results

This chapter summarizes the results of the mixture testing conducted throughout this project. The scope of testing materials encompassed plant-produced mix, laboratory-aged loose mix, and field cores collected over a four-year period, providing a thorough understanding of the mixture's properties.

7.1 Complex Modulus Test Results

This section presents the results of dynamic modulus ($|E^*|$) and phase angle (δ) derived from four replicate specimens at various aging conditions. The data is fitted and shifted into master curves and each curve is adjusted to an air void level of 7%.

7.1.1 Master Curves of Control Mixtures

Figure 7.1 below shows a direct comparison of 30% and 40% Day 1 control mixes for the field cores over 4 years and 3 loose mix aging conditions. The general trend between the 4 years of field aging and RPM aging shows that the control mixes gain higher stiffness and lower peak phase angle values with aging. Comparing between the mixes, both control mixes exhibit comparable dynamic modulus and phase angle master curves during the early stages of field aging (1 to 4 years) and under RPM lab aging conditions. However, as aging progresses, the 40% control mix demonstrates a slightly higher dynamic modulus than the 30% control mix, particularly noticeable in the 4-year field core and the 7-day, 95°C LTA condition. This suggests that higher RAP content contributes to increased stiffness of the asphalt mixture after extensive aging.

After 6 hours of 135°C LTA conditioning, the stiffness and phase angle of both control mixes are found to be comparable to those of the 1-year field cores at mid and high frequencies. This suggests that LTA conditioning at 135°C for 6 hours simulates approximately one year of field aging, thereby replicating the changes in the asphalt mixture after one year of in-service conditions.

After 7 days of LTA conditioning at 95°C, the 30% control mix shows higher stiffness and lower phase angle than the 40% control mix. While both mixes show significantly higher stiffness and reduced phase angles compared to the 4-year field cores. This result indicates that LTA conditioning at 95°C significantly enhances the aging effect beyond that observed during four years of field aging.

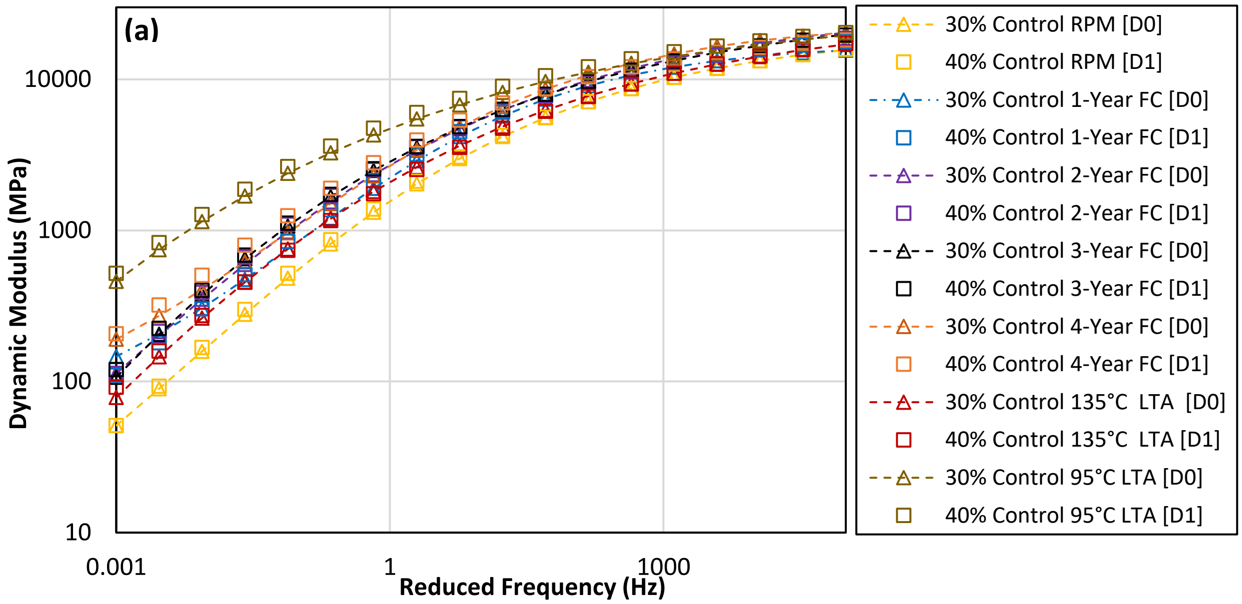
(a)
Dynamic Modulus (MPa)
10000
1000
100
10
0.001
1
1000
Reduced Frequency (Hz)
30% Control RPM [D0]
40% Control RPM [D1]
30% Control 1-Year FC [D0]
40% Control 1-Year FC [D1]
30% Control 2-Year FC [D0]
40% Control 2-Year FC [D1]
30% Control 3-Year FC [D0]
40% Control 3-Year FC [D1]
30% Control 4-Year FC [D0]
40% Control 4-Year FC [D1]
30% Control 135°C LTA [D0]
40% Control 135°C LTA [D1]
30% Control 95°C LTA [D0]
40% Control 95°C LTA [D1]

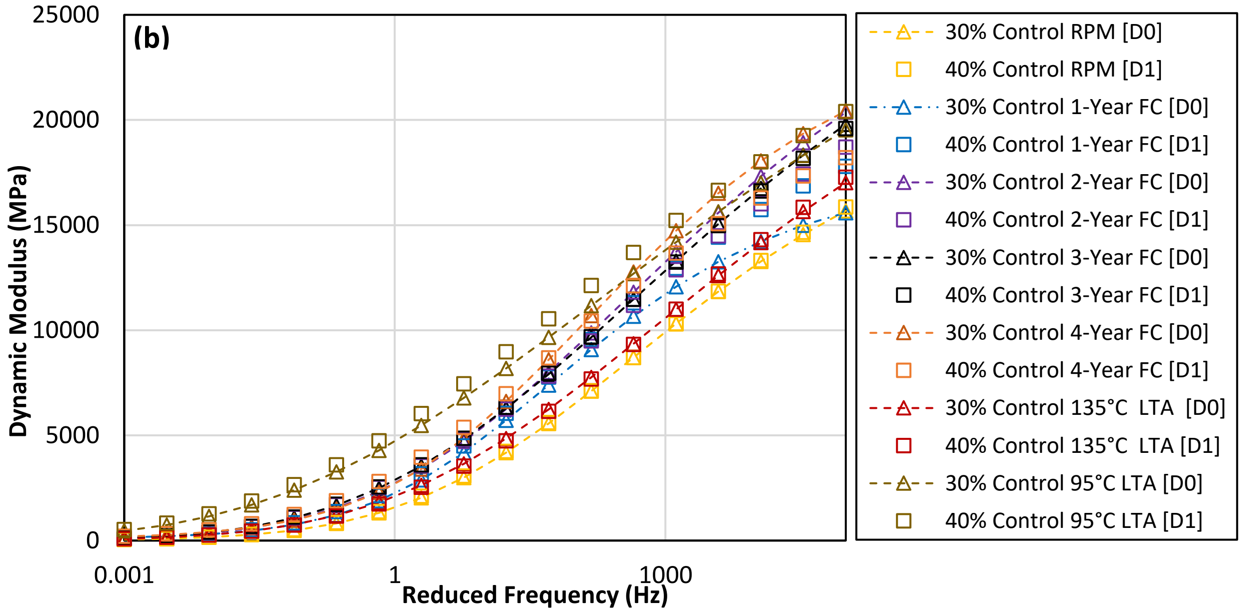
(b)
Dynamic Modulus (MPa)
25000
20000
15000
10000
5000
0
0.001
1
1000
Reduced Frequency (Hz)
30% Control RPM [D0]
40% Control RPM [D1]
30% Control 1-Year FC [D0]
40% Control 1-Year FC [D1]
30% Control 2-Year FC [D0]
40% Control 2-Year FC [D1]
30% Control 3-Year FC [D0]
40% Control 3-Year FC [D1]
30% Control 4-Year FC [D0]
40% Control 4-Year FC [D1]
30% Control 135°C LTA [D0]
40% Control 135°C LTA [D1]
30% Control 95°C LTA [D0]
40% Control 95°C LTA [D1]

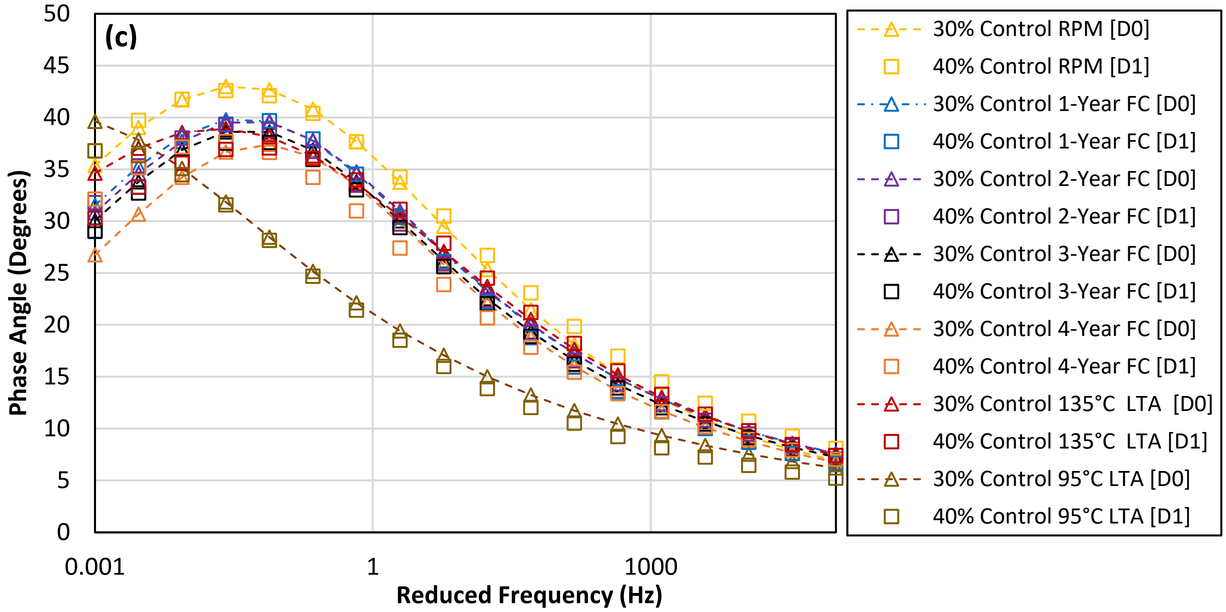

Figure 7-1 Master Curves of (a) Dynamic Modulus (Linear Scale) (b) Dynamic Modulus (Logarithmic Scale) and (c) Phase Angle for All Control Mixtures (Ref. 21.1°C)

7.1.2 Master Curves of Field Cores and Long-term Aged Mixes

Table 7-1 below summarizes the differences in dynamic modulus and phase angle properties of the RA mixtures as compared to the control mixes the under different laboratory and field aging conditions All master curves can be found in the Appendix.

In terms of 4-year field cores, 40% RAP Control displays a higher dynamic modulus and a lower phase angle than the 30% RAP Control at both low and intermediate frequencies. When compared to the 30% RAP Control, most RA field cores exhibit lower stiffness and higher phase angles; however, 6002 and 6007 show dynamic modulus and phase angle values comparable to those of the 30% RAP Control. Relative to the 40% RAP Control, all RA field cores demonstrate lower dynamic moduli and higher phase angles. This observation suggests that most recycling agents still effectively soften the aged binder present in the RAP and enhance the mixture's relaxation properties through four years of field aging.

After 135 °C long term aging, the two control mixtures show comparable dynamic modulus and phase angle, indicating comparable stiffness and relaxation properties. Sections 6006 and 6007 demonstrate statistically significant higher dynamic modulus and lower phase angles compared to the control mixes, which may indicate increased susceptibility to severe cracking. 6001 and 6003 show slightly lower modulus and higher phase angles relative to the controls, which points to the RA's positive effect on enhancing cracking resistance. Other RA mixes display properties that generally align with those of the control mixes, suggesting the effect of the RA diminishes after LTA.

After 7 days at 95°C LTA, the 40% RAP Control mix shows slightly higher modulus and lower phase angle values compared to the 30% Control. RA mixes 6004 and 6007 show properties comparable to both control mixes, suggesting a diminished effect of the RAs in terms of enhancing cracking resistance. In contrast, most other RA mixtures still exhibit slightly lower dynamic modulus and higher phase angle values than both control mixtures, indicating improved stiffness and relaxation properties which may enhance cracking resistance.

The data suggests that RAs generally lead to a reduction in dynamic modulus and an increase in phase angle which could be beneficial in terms of improving the cracking resistance. This improvement was observed across both laboratory and field aging scenarios in the short term; however, some RA mixes lose the benefits with the longer-term field aging or lab aging. Both loose mix aging protocols—6 hours at 135°C and 7 days at 95°C—indicate that RAs 6004 and 6007 lose their effectiveness over time. Conversely, the 3-year and 4-year field core analyses uniquely identify RA 6002 as diminishing in effectiveness. This suggests that the 4-year field core duration may not be sufficient to differentiate the long-term impacts of RAs.

Table 7-1: Summary of the Effect of RAs on Dynamic Modulus and Phase Angle

Properties Compared to Corresponding Control Mix			30% Control with same aging level	40% Control (D1) with same aging level
Decrease in Dynamic Modulus (|E*|)	Lab Aged	RPM	All RA Mixes	All RA Mixes
		LTA, 6hrs. at 135C	All except 6004 6005 6007	All except 6004 6005 6007
		LTA, 7days at 95C	All except 6004 6006 6007	All except 6007
	In-situ Aged	1-Year FC	All except 6002	All except 6002
		2-Year FC	All	All
		3-Year FC	All except 6002	All except 6002
		4-Year FC	All except 6002	All except 6002
Increase in Phase Angle	Lab Aged	RPM	All RA Mixes	All RA Mixes
		LTA, 6hrs. at 135C	All except 6004 6005 6006 6007	All except 6004 6005 6007
		LTA, 7days at 95C	All except 6006 6007	All except 6006 6007
	In-situ Aged	1-Year FC	All RA Mixes	All RA Mixes
		2-Year FC	All except 6001 6002 6007	All RA Mixture
		3-Year FC	6003 6004 6005	All except 6002
		4-Year FC	All except 6002	All except 6002

7.1.3 Glover Rowe Mixture Parameter

Figure 7-2 shows G-R_m values calculated to assess the cracking resistance based on the combination of stiffness and relaxation. Field cores 6002, 6006, and 6007 exhibit values that are either comparable to or greater than the 30% control mix over a duration of 4 years. All RA mixtures have consistently lower values than those of the 40% control mixes over all four years. This suggests that all seven recycling agents enhance the cracking resistance of the field cores compared to the 40% Control. Mix 6003 has a notable distinction, characterized by a lower G-R_m parameter in comparison to the other RA mixes.

After 6 hours at 135C LTA, only the mixes 6001, 6002, and 6003 RA mixes from day 1 consistently exhibit reduced G-R_m values compared to the control. After 7 days at 95C LTA, it is shown that the majority of RA still exhibit lower G-R_m values compared to the two control formulations. Nevertheless, compounds 6006 and 6007 deviate from this pattern as they have more pronounced cracking characteristics in comparison to the control compounds.

The percentage change in RPM indicates that 6001 exhibit lower susceptibility to aging for both field cores and lab aged loose mix. It is shown that its resistance to cracking does not undergo significant changes with aging.

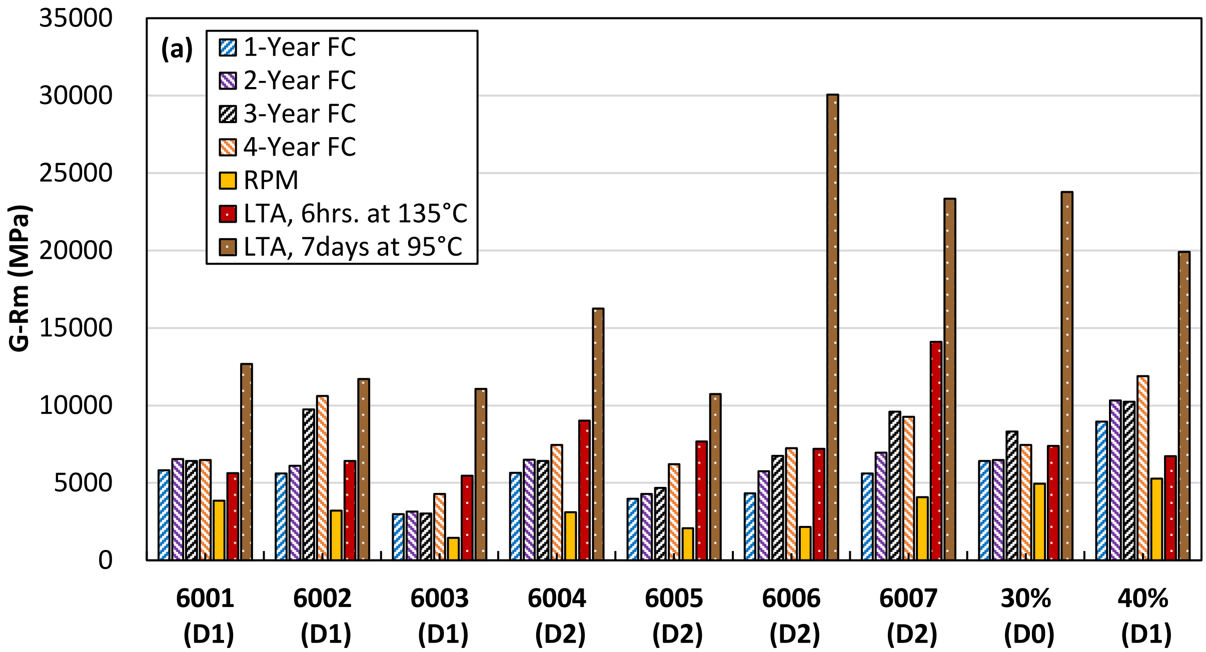

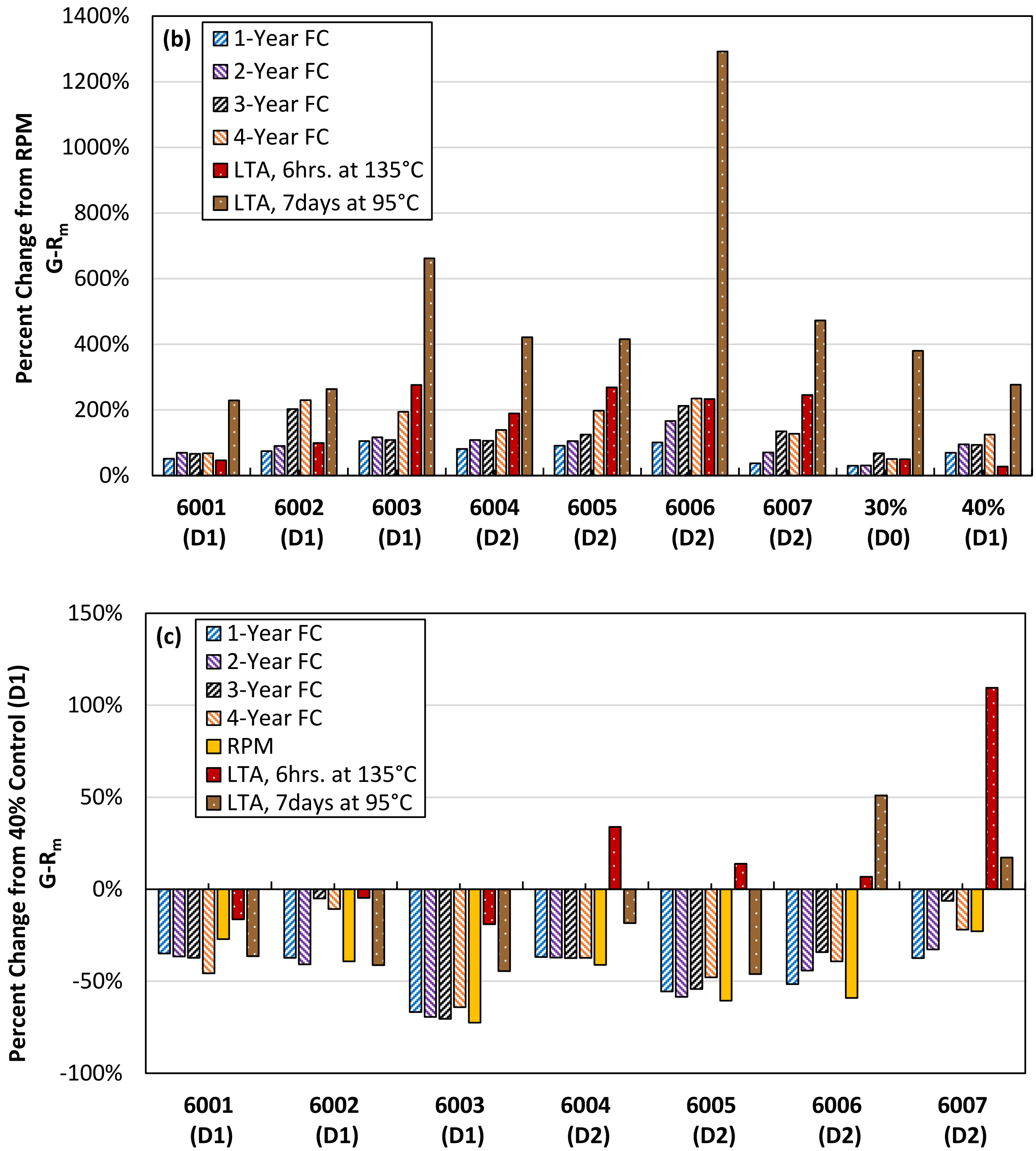

Figure 7-2 Analysis of G-R_m Parameter and its Changes. (a) G-R_m Parameter Values, (b) Percent Change in G-R_m with Aging, (c) Percent Change in G-R_m due to RA (Temperature=20°C; Frequency=5Hz)

7.2 Direct Tension cycle Fatigue Testing Results

Figure 7-3 and **Figure 7-4** shows the measured D^R and S_{app} values with aging measured from the DTCF test. Each column represents an average of 4 replicates, and the error bar represents one standard deviation interval from the mean. The field cores and 6 hours at 135C LTA exhibit a similar or slightly reduced D^R as field aging years progress or lab aging procedures advance. However, the changes in the field cores are not as significant as those observed with S_{app}, and in contrast, 7 days at 95C LTA caused a significant decrease in both D^R and S_{app} from the RPM condition. This indicates that the four-year field core and 6 hours at 135C LTA are not enough to differentiate the significant changes in mixture fatigue properties. Also, the different trends observed for the D^R and S_{app} parameters can be attributed to the different theoretical bases for the development of the parameters. The D^R parameter is calculated primarily based on the reduction of the pseudo stiffness of a specimen during the test. Thus, it is more related to the damage tolerance of the asphalt mixture. The S_{app} parameter is calculated based on the dissipated energy of the specimen with an increase of cycles (and it does incorporate mix stiffness); therefore, it is more representative of the trade-off between the applied stress and strain, material stiffness, and relaxation capability.

Statistical analysis of the field cores indicates that the 30% control and the 40% control FC exhibit comparable D^R over the 4-year period. However, the 40% Control exhibits a lower S_{app} than the 30% Control FC over the same period. With the exception of FC 6003, which exhibited comparable results with the 40% Control, all RA treated 4-year FCs exhibited higher D^R and S_{app} values than the 40% Control, indicating that RA still exhibited a minor improvement in fatigue properties.

For the RPM specimens, the control mixture 40% control exhibited slightly higher S_{app} values than the 30% control mixture. The fatigue cracking properties of RA mixtures 6001, 6002, 6003, and 6005 have been found to be significantly improved when compared to the corresponding 40% control mixtures. This is indicated by the higher DR values observed in the RA mixtures. In terms of the S_{app} parameter, all RA mixtures exhibited S_{app} values that fell between those of the 40% control and the 30% control mixtures.

After the 6-hour LTA at 135°C, the control mixture (40% Control) exhibited significantly higher values than the 30% Control mixture for both parameters. The RA mixtures (6002, 6003, and 6005) demonstrated significantly enhanced fatigue properties, exhibiting higher values for both D^R and S_{app} parameter than the corresponding 40% Control mixture and the 30% Control mixture.

After 7 days LTA at 95°C, the D^R values for the 40% Control are higher than 30% control mixes. The majority of RA mixtures, with the exception of the 6007 mix, exhibit higher DR values than 30% and 40% Control. Mixtures 6003, 6004, 6005, and 6006 exhibit higher S_{app} values than the 30% and 40% control.

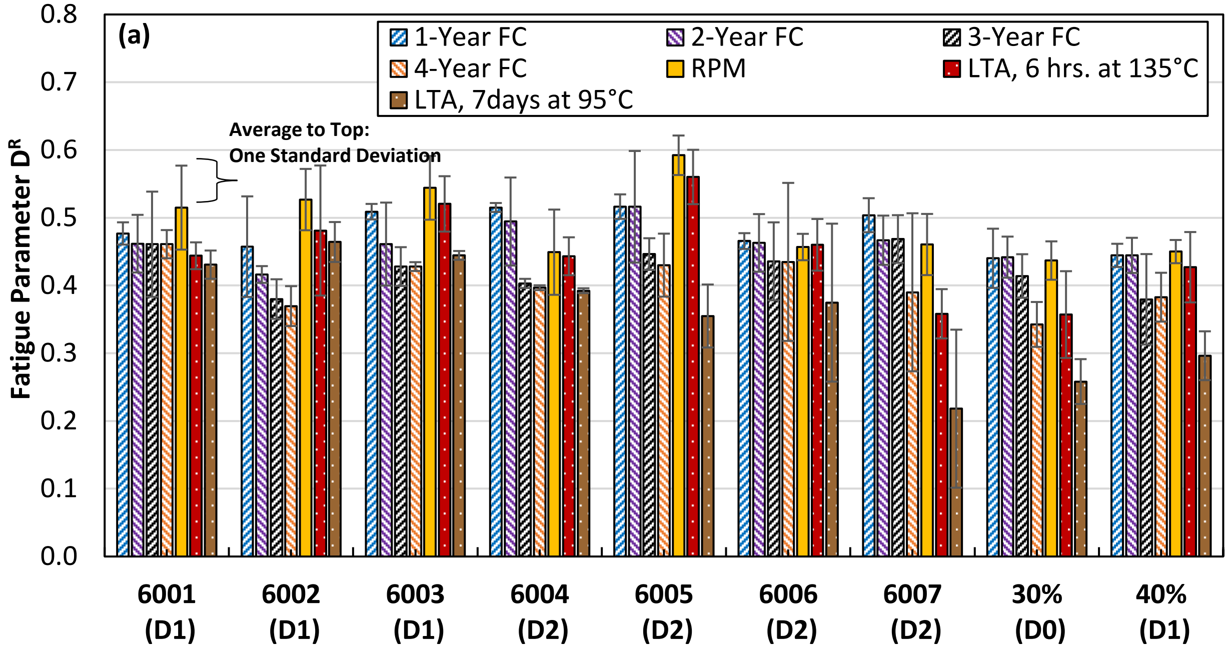

(a)
1-Year FC
2-Year FC
3-Year FC
4-Year FC
RPM
LTA, 6 hrs. at 135°C
LTA, 7days at 95°C
Average to Top:
One Standard Deviation
Fatigue Parameter D^R
0.8
0.7
0.6
0.5
0.4
0.3
0.2
0.1
0.0
6001 (D1)
6002 (D1)
6003 (D1)
6004 (D2)
6005 (D2)
6006 (D2)
6007 (D2)
30% (D0)
40% (D1)

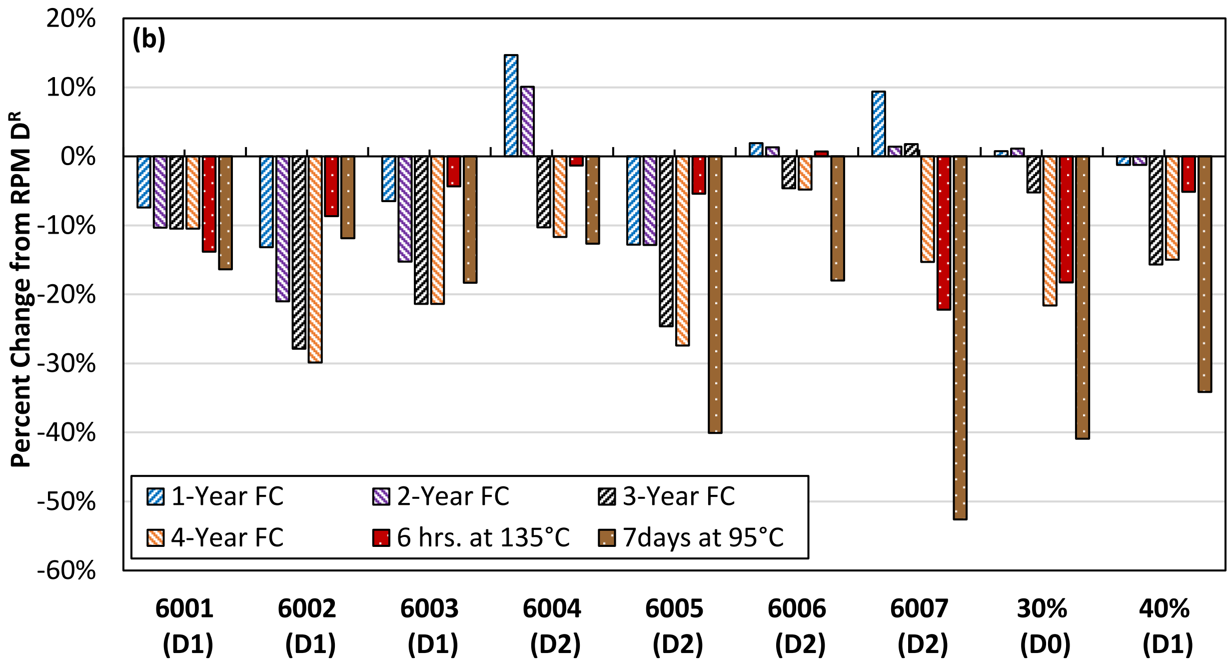

(b)
Percent Change from RPM D^R
20%
10%
0%
-10%
-20%
-30%
-40%
-50%
-60%
1-Year FC
2-Year FC
3-Year FC
4-Year FC
6 hrs. at 135°C
7days at 95°C
6001 (D1)
6002 (D1)
6003 (D1)
6004 (D2)
6005 (D2)
6006 (D2)
6007 (D2)
30% (D0)
40% (D1)

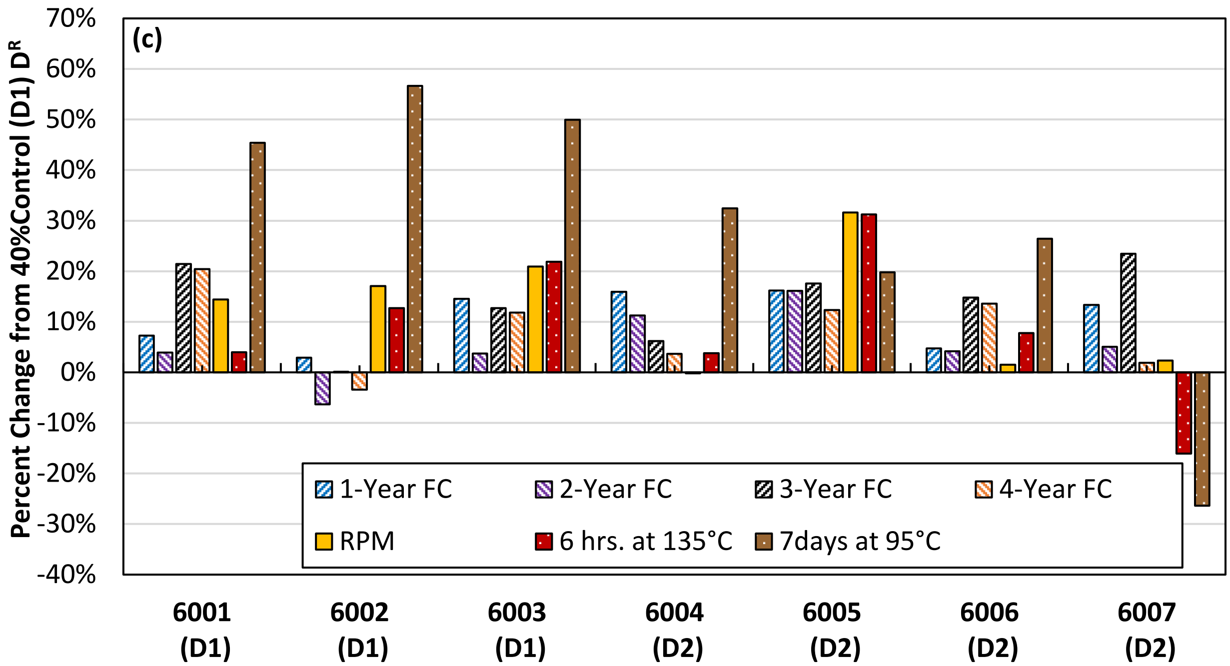

Figure 7-3 Fatigue Cracking Parameter G^R and its Changes. (a) G^R Parameter Values, (b) Percent Change in G^R with Aging, (c) Percent Change in G^R due to RA

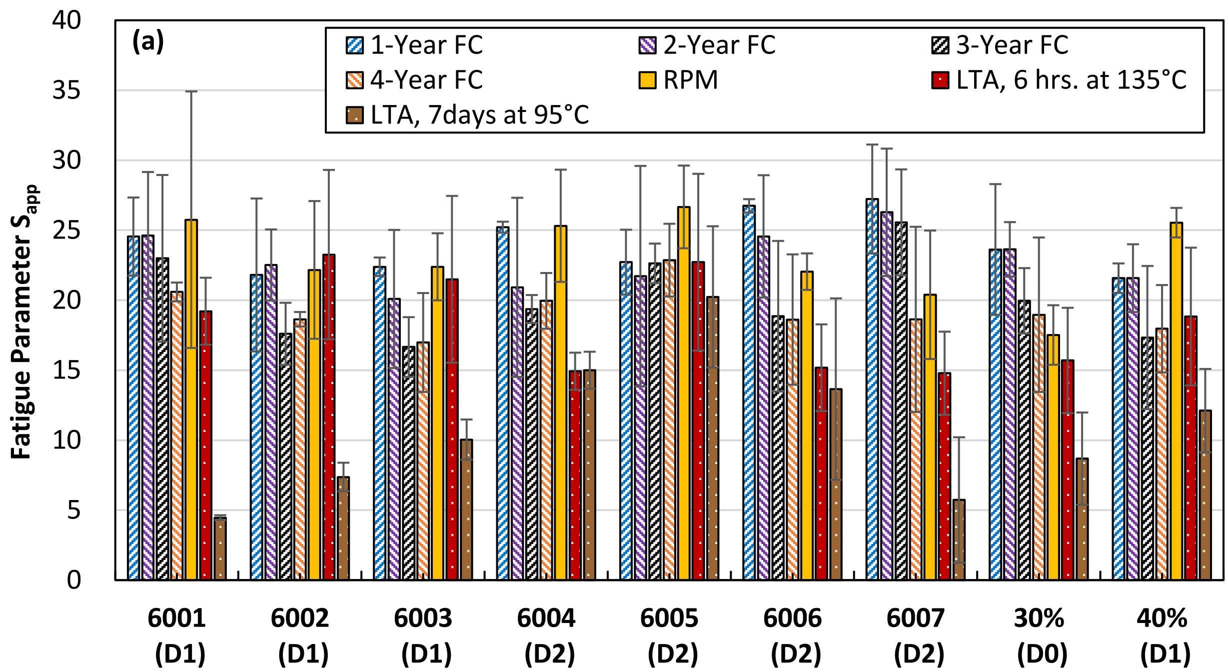

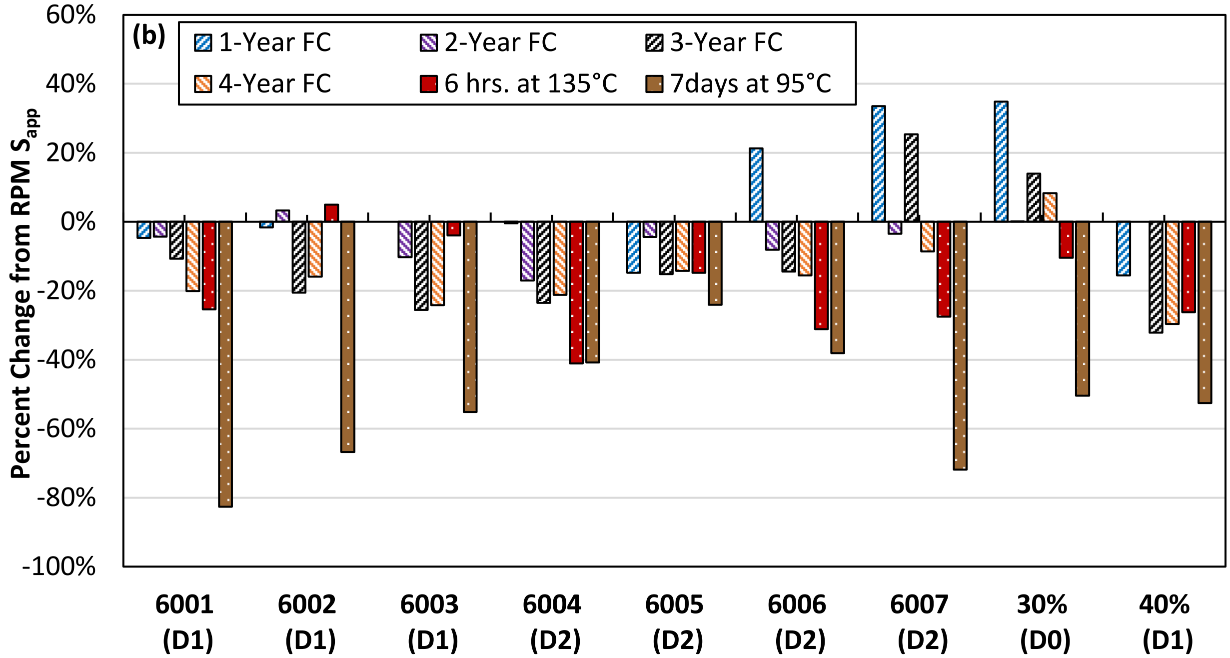

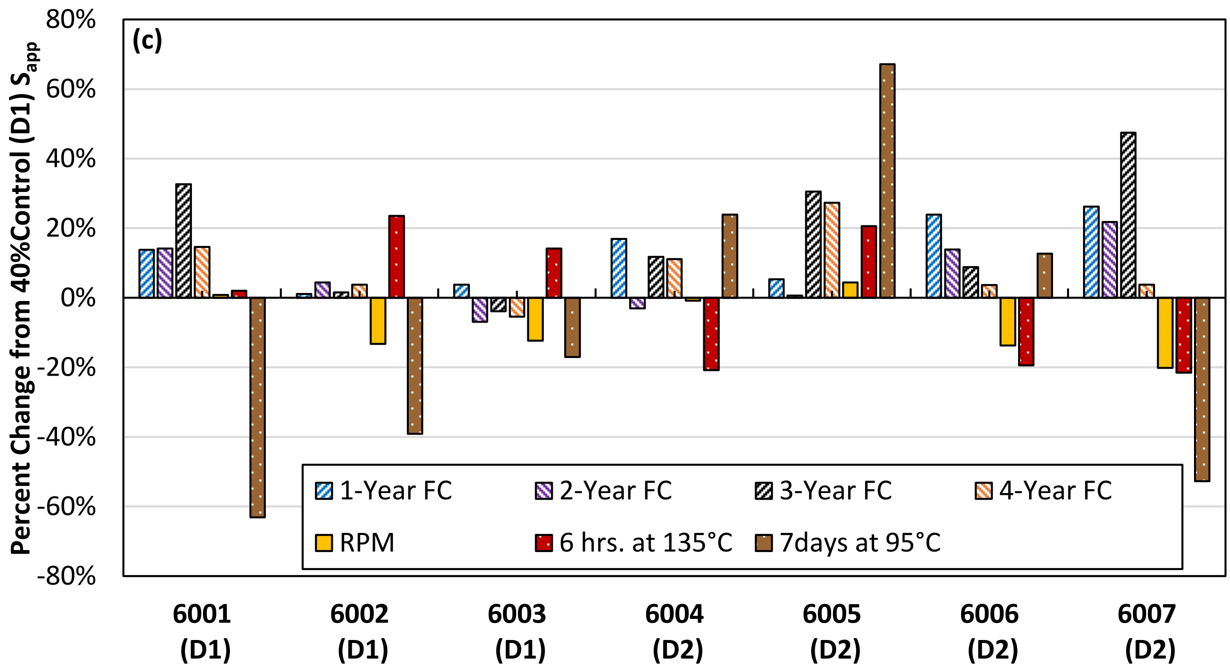

Figure 7-4 Fatigue Cracking Parameter S_{app} and its Changes. (a) S_{app} Parameter Values, (b) Percent Change in S_{app} with Aging, (c) Percent Change in S_{app} due to RA

7.3 Disk-shaped Compact Tension Test

Figure 7-6 and **Figure 7-7** below show the G_f, *FST* and *PPI* values with aging calculated from the DCT testing. Each bar for RPM and 6 hrs. at 135°C LTA aged mixtures show an average of 12 replicates, and each bar for seven days at 95°C LTA mixtures show an average of 4 replicates. The error bar represents one standard deviation. G_f results show that except for the 6005 mixes, which reaches the typically used threshold value of 400 J/m^2, all study mixtures fall below the threshold for RPM and two LTA aging levels. There is not a consistent trend concerning the change of G_f and *FST* value with aging. In contrast, the *PPI* parameters captured a general decrease of cracking resistance caused by both six hrs. at 135°C LTA and seven days at 95°C LTA.

In the case of RPM mixes, the 40% control mixture exhibits superior cracking resistance in terms of all three parameters compared to the 30% control mixture. Upon comparison of the RA-treated mixtures to the two control mixtures, most RA mixtures demonstrate comparable.G_f and *FST* values with the 30% Control mixture. However, the 6005 mixture exhibits an enhanced improvement in low-temperature cracking properties compared to the 40% Control mixture. The *PPI* results indicate that the 6005-mix performed superior to the 40% Control. At the same time, most RA mixtures demonstrated *PPI* values that fell between those of the 30% Control and 40% Control.

After 6 hrs. at 135°C LTA, 40% Control has a comparable result with 30% and 40% Control. Mixtures 6005 and 6006 have shown better low-temperature fracture resistance than control mixtures in all three parameters. At the same time, all other RA-treated mixes show comparable properties to those of controls.

After 7 days at 95°C LTA, the 40% D2 control displays significantly higher values than the other 30% control mixtures. The comparison between the mixtures shows that only the 6001 and 6005 mixtures have better-cracking properties than the 40% Control mixture. Overall, the *PPI* indicates a more consistent and sensitive trend to aging and RA inclusion than G_f and FST.

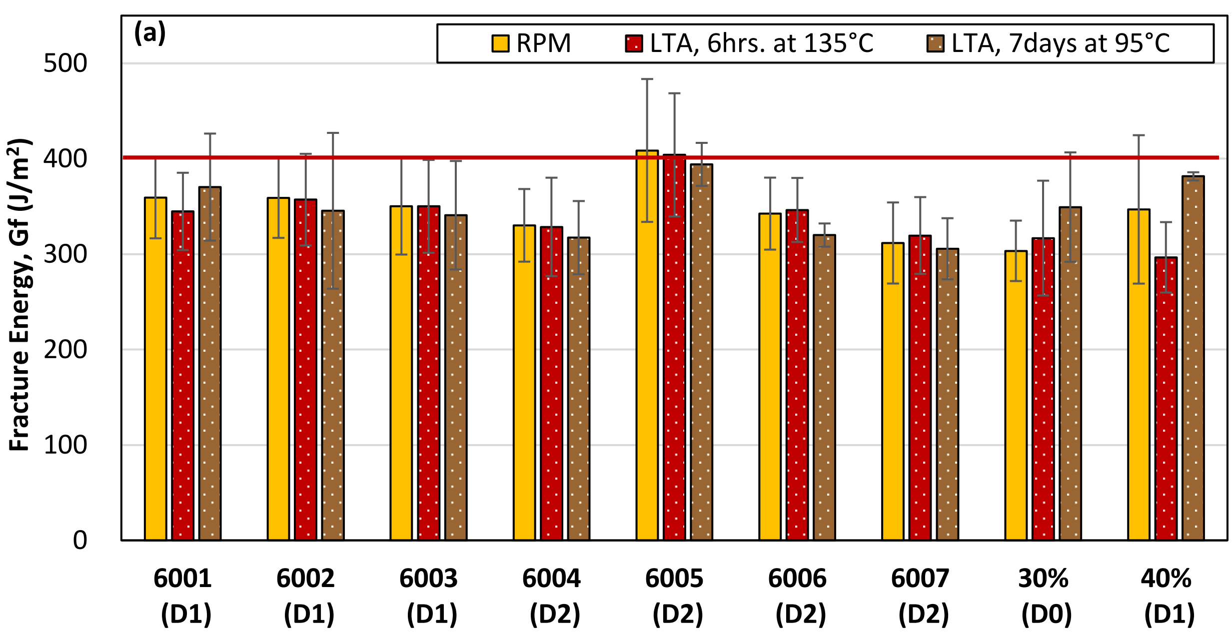

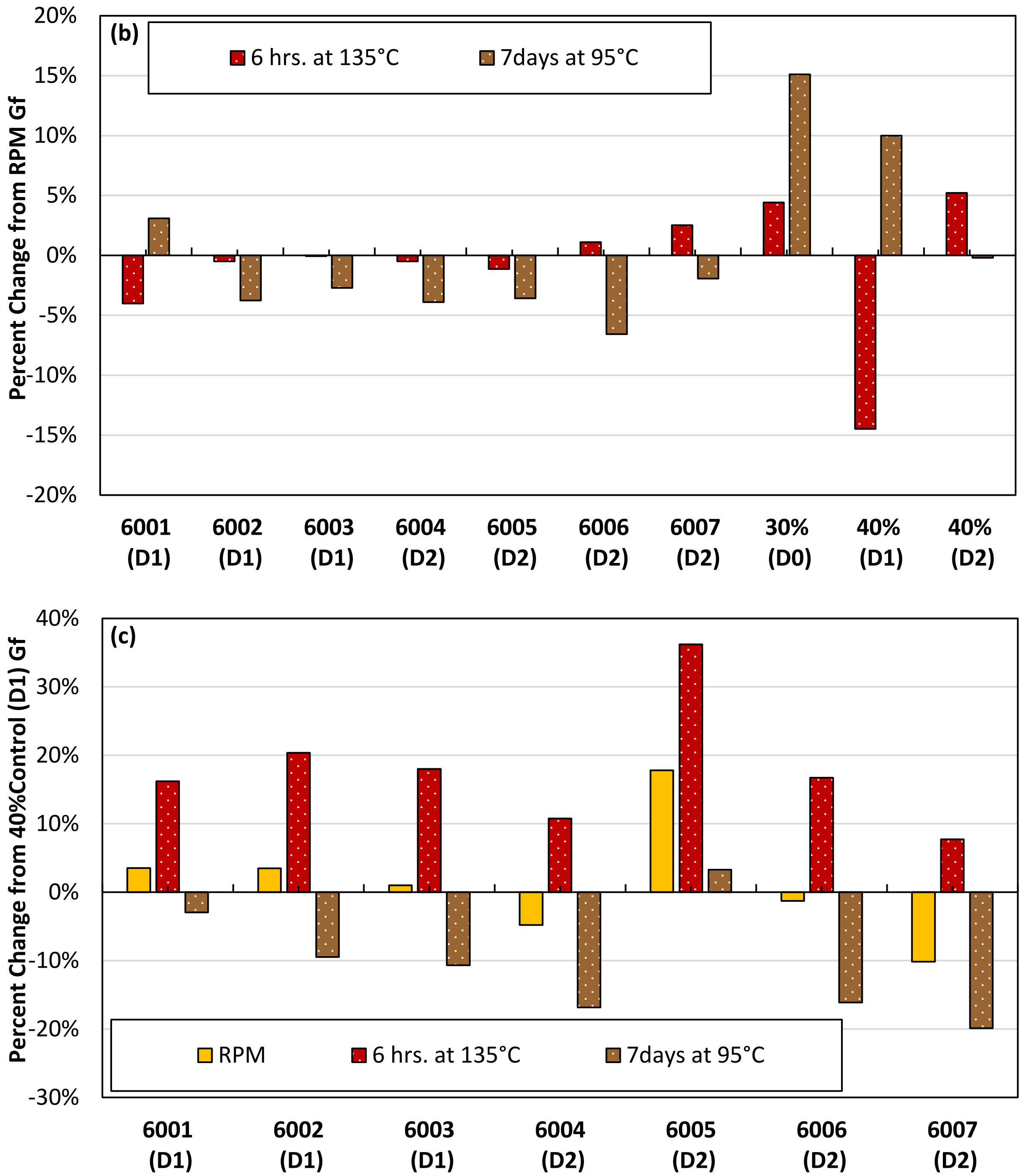

Figure 7-5 Cracking Parameter Fracture Energy and its Changes. (a) Fracture Energy Values, (b) Percent Change in Fracture Energy with Aging, (c) Percent Change in Fracture Energy due to RA

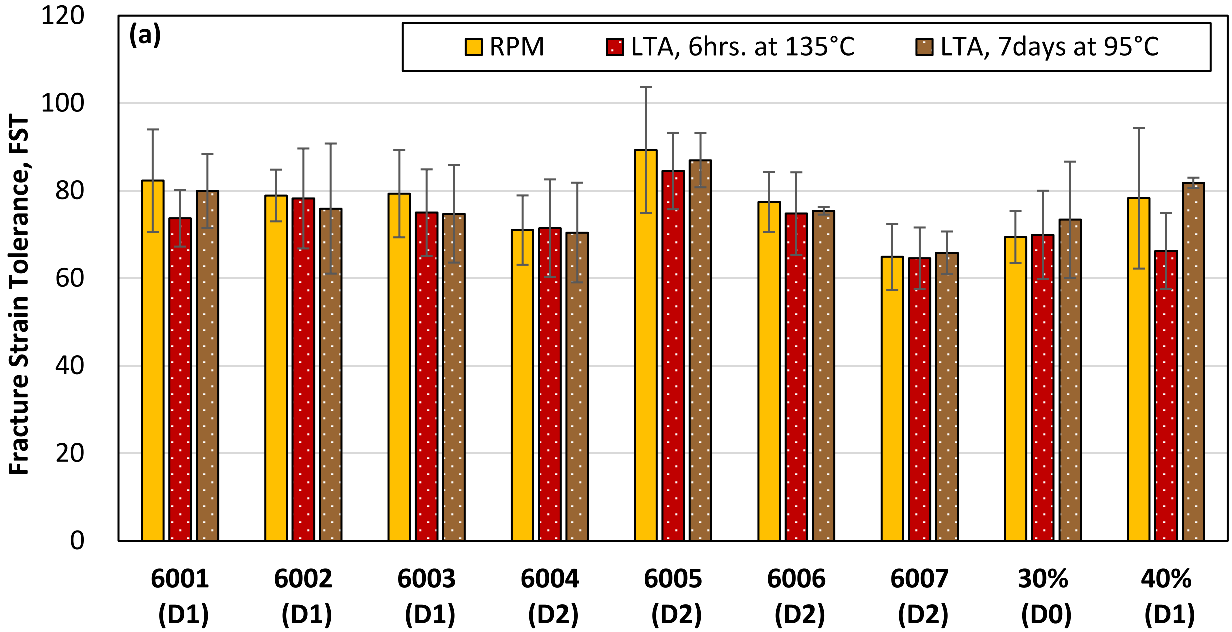
(a)
RPM
LTA, 6hrs. at 135°C
LTA, 7days at 95°C
Fracture Strain Tolerance, FST
120
100
80
60
40
20
0
6001 (D1)
6002 (D1)
6003 (D1)
6004 (D2)
6005 (D2)
6006 (D2)
6007 (D2)
30% (D0)
40% (D1)

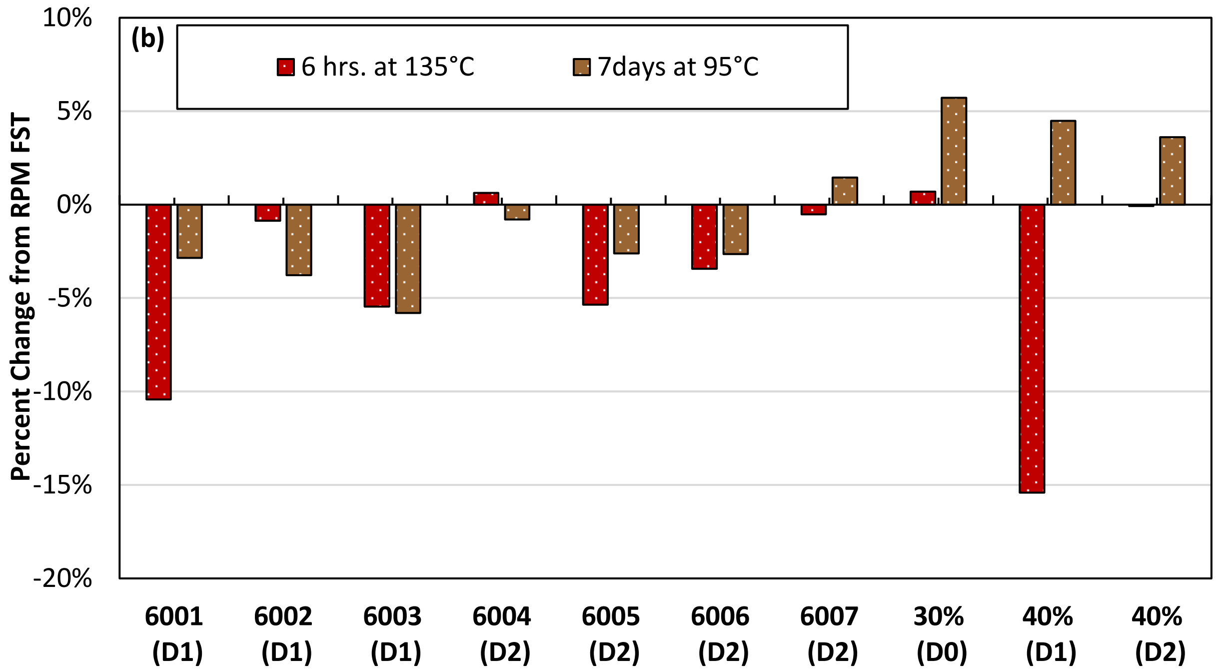
(b)
6 hrs. at 135°C
7days at 95°C
Percent Change from RPM FST
10%
5%
0%
-5%
-10%
-15%
-20%
6001 (D1)
6002 (D1)
6003 (D1)
6004 (D2)
6005 (D2)
6006 (D2)
6007 (D2)
30% (D0)
40% (D1)
40% (D2)

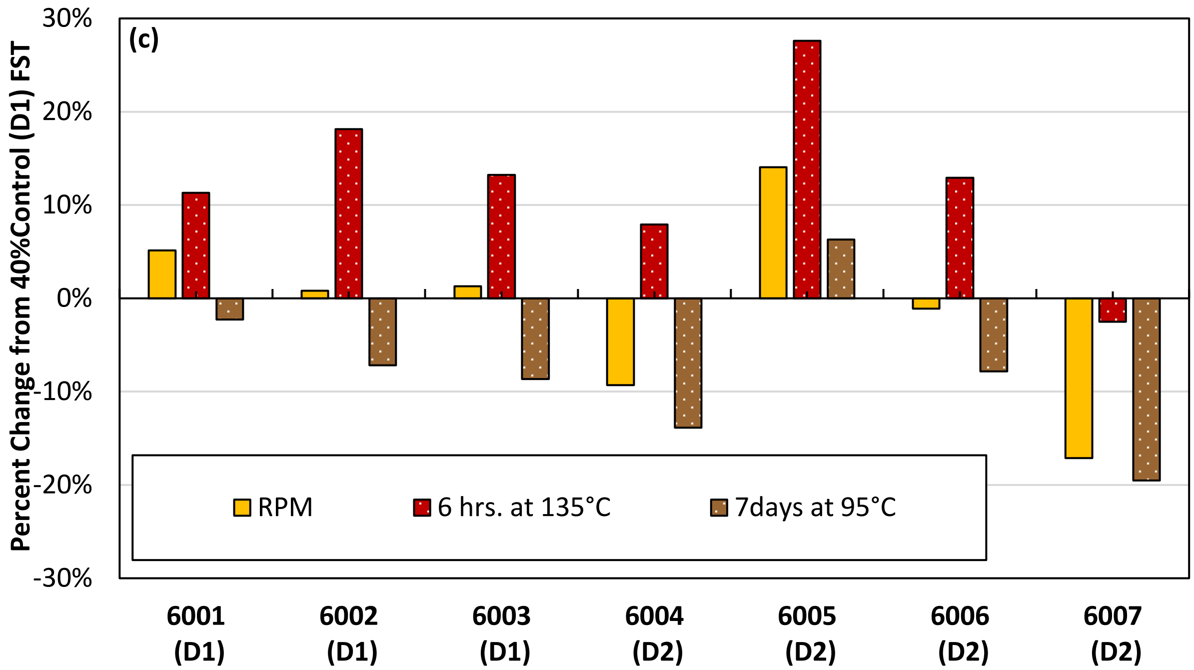

Figure 7-6 Cracking Parameter FST and its Changes. (a) FST Values, (b) Percent Change in FST with Aging, (c) Percent Change in FST due to RA

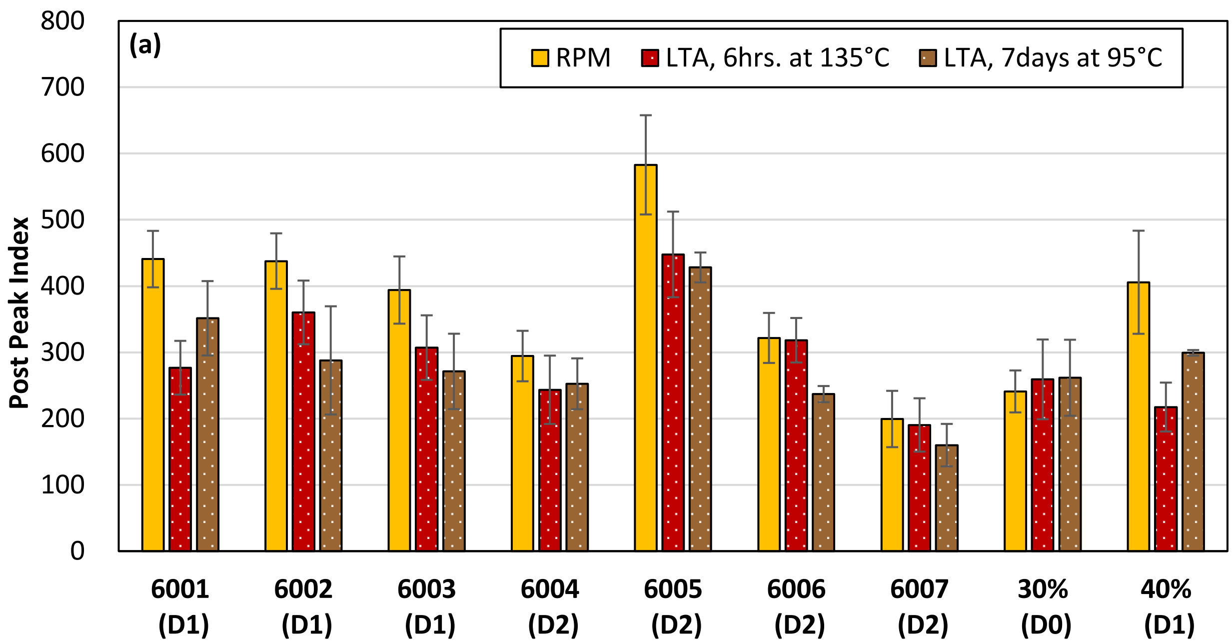

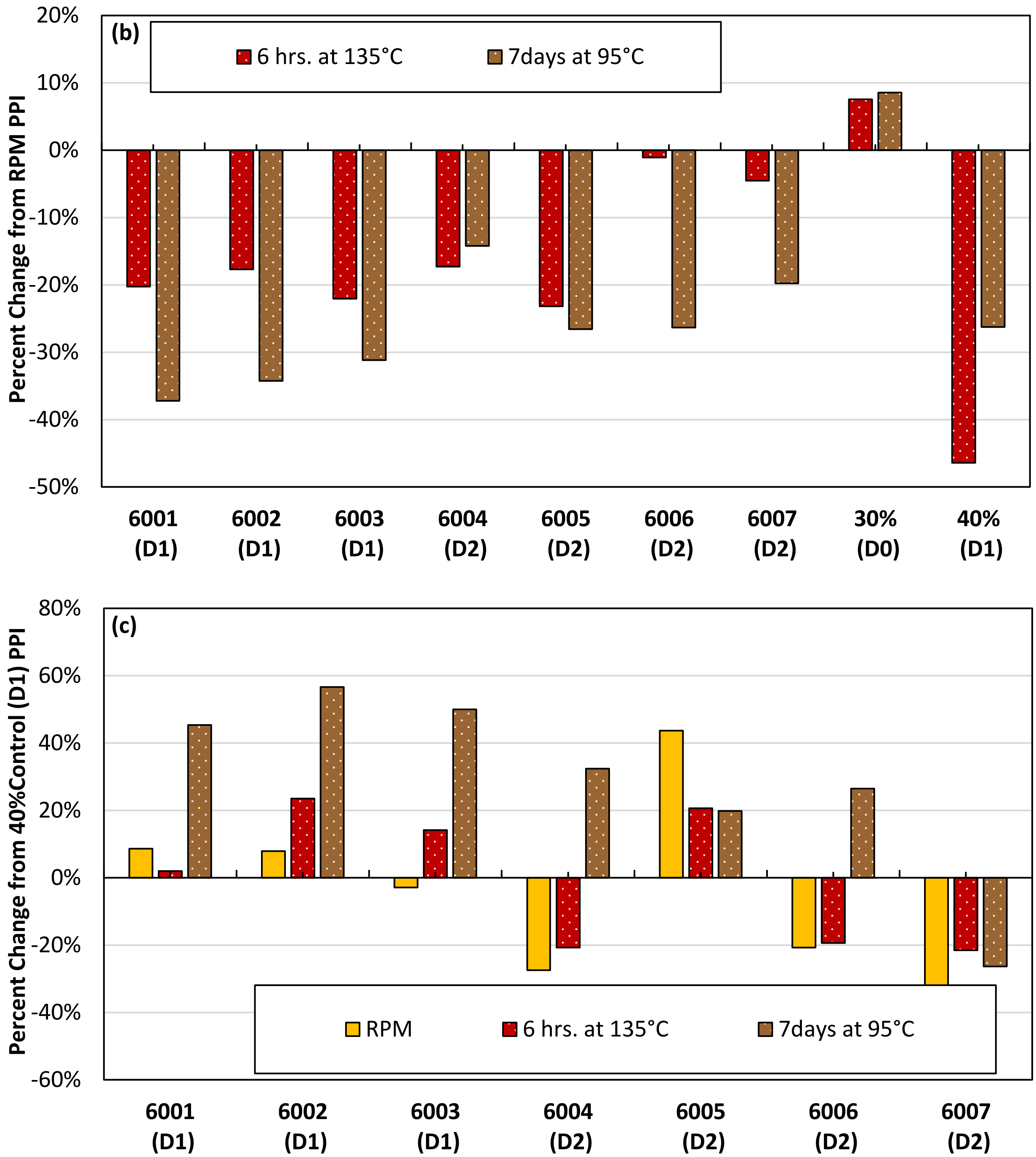

Figure 7-7 Cracking Parameter PPI and its Changes. (a) PPI Parameter Values, (b) Percent Change in PPI with Aging, (c) Percent Change in PPI due to RA

7.4 Illinois Flexibility Index Test

Figure 7-8 and **Figure 7-9** shows the G_f values, FI values and the percentage decline in FI values for the research mixes as determined by the Illinois Flexibility Index SCB (I-FIT) test at various laboratory mix aging levels. The 3 days at 95°C LTA* aging protocol is applied immediately to the compacted specimens, as the star "*" shows. All other lab aging protocols are applied on the loose mixes. One standard deviation from the mean is represented by the error bars. Each of the three experimental LTA conditioning methods results in a considerable decrease in FI. All 2-Yr FC, RPM mixtures, 6 hrs. at 135°C and 3 days at 95°C mixture aging meet the FI=4 criterion. The 30% control mixture in the RPM condition has a greater FI than the two 40% control mixes. The FI values of combinations 6001, 6003, 6004, 6005, and 6006 are substantially greater than those of their 30% and 40% control mixtures. Regarding statistics, mixtures 6002 and 6007 are similar to their respective 40% and 30% control compounds.

After 6 hrs. at 135°C LTA, the 30% control blend had a higher FI value than the 40% control blend average after six hours at 135°C LTA, suggesting improved cracking resistance. The 40% control mixtures and the 30% control mixture (6002 is comparable to the 30% control) have much lower FI values than the RA mixtures. All RA mixes and 30% Control, except 40% Control, satisfy the criteria of FI=4.

After 3 days at 95°C LTA*on compacted samples, mixture 6007 has comparable FI with two control mixtures after three days at 95°C LTA*on compiled samples. Despite this, all other mixtures exhibit better cracking resistance than the control mixtures.

After 7 days at 95°C LTA, every mixture shows a notable decline in FI and fail the cracking criteria. Comparable FI values are shown from RPM and two control mixes. While all other RA mixes exhibit higher FI than the control mixtures, mixtures 6006 and 6007 match the FI values with both of the control mixtures. This suggests that even after LTA, the RA is still improvising the cracking resistance.

A comparison of the aging protocol and field cores with FI values shows that 6 hours at 135°C LTA is insufficient to achieve the same level of aging as more than 2-years FC. Conditioning for three days at 95°C LTA* on compacted specimens can usually match a 2-year FC. 7 days at 95°C LTA will age the loose mix considerably more than 3-year FC.

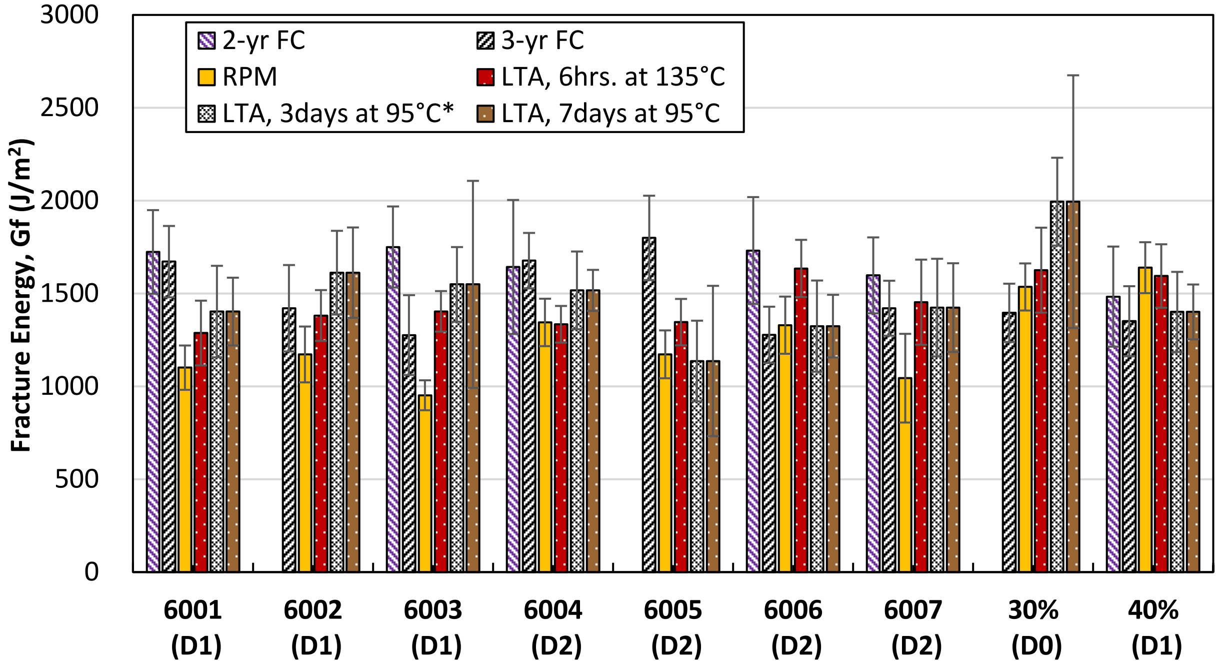

Figure 7-8 Fracture Energy G_f Measured from I-FIT test

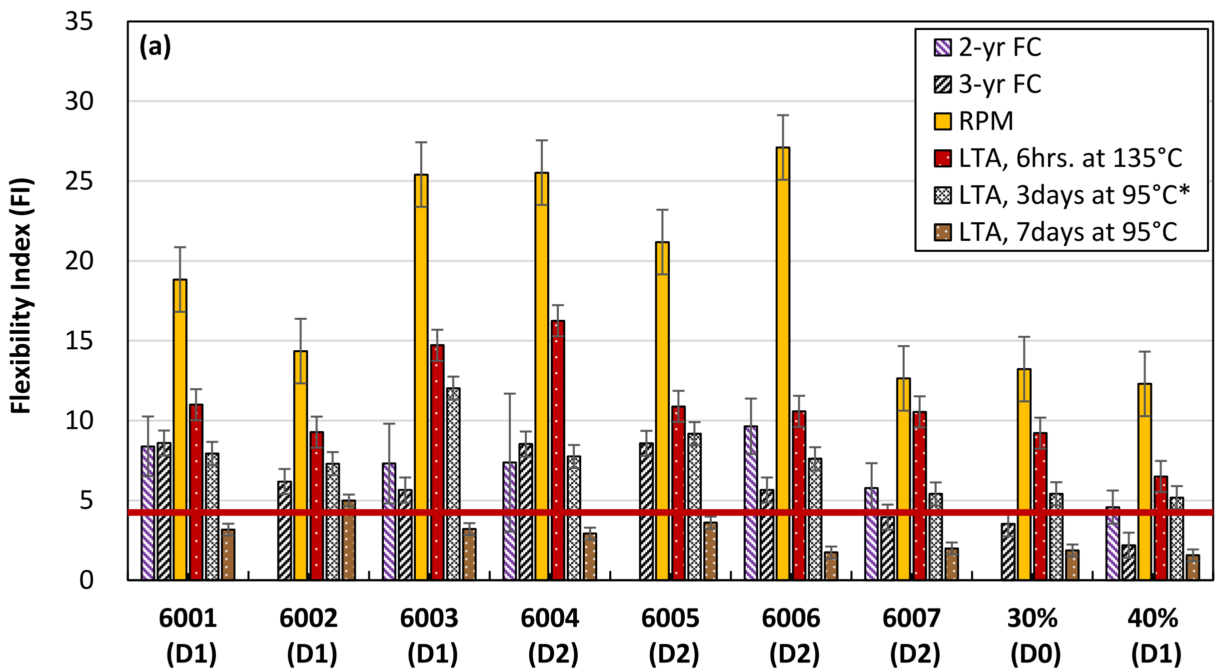

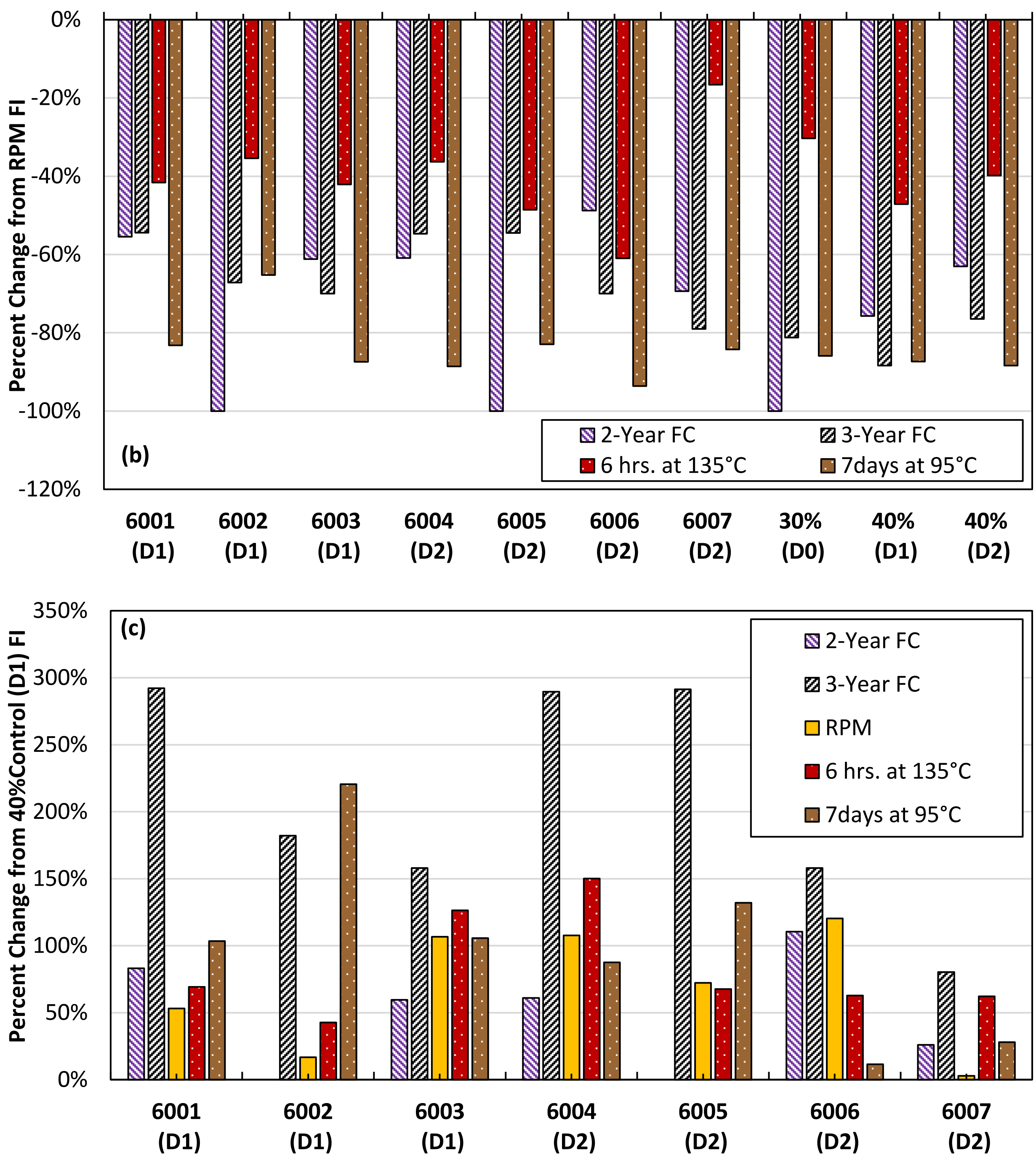

Figure 7-9 Cracking Parameter FI and its Changes. (a) FI Parameter Values, (b) Percent Change in FI with Aging, (c) Percent Change in FI due to RA

7.5 Cracking Tolerance Test

Figure 7-10 below shows the CT_{Index} values and the percent decrease in CT_{Index} values with aging, respectively. The error bars show one standard deviation. There is no statistical difference in CT_{Index}

value for the control mixtures in RPM condition. Mixtures 6001, 6003, 6004 and 6005 have significantly higher CT_{Index} values than their respective 40% control mixture and 30% control mixture.

After 6 hrs. at 135°C LTA, there is no statistical difference between the three control mixtures. Except for mixtures 6006 and 6007, RA mixtures show significant improvement in CT_{Index} value over the corresponding 40% control mixtures as well as the 30% control mixture. As shown in **Figure 6-7 (b)**, mixtures 6006 and 6007 show a larger change in CT_{Index} values with aging as compared to the control mixtures, indicating the higher aging susceptibility. The change in mixture 6004 is comparable with 40% control mixture while other RA mixtures generally have smaller changes with aging than all three control mixtures.

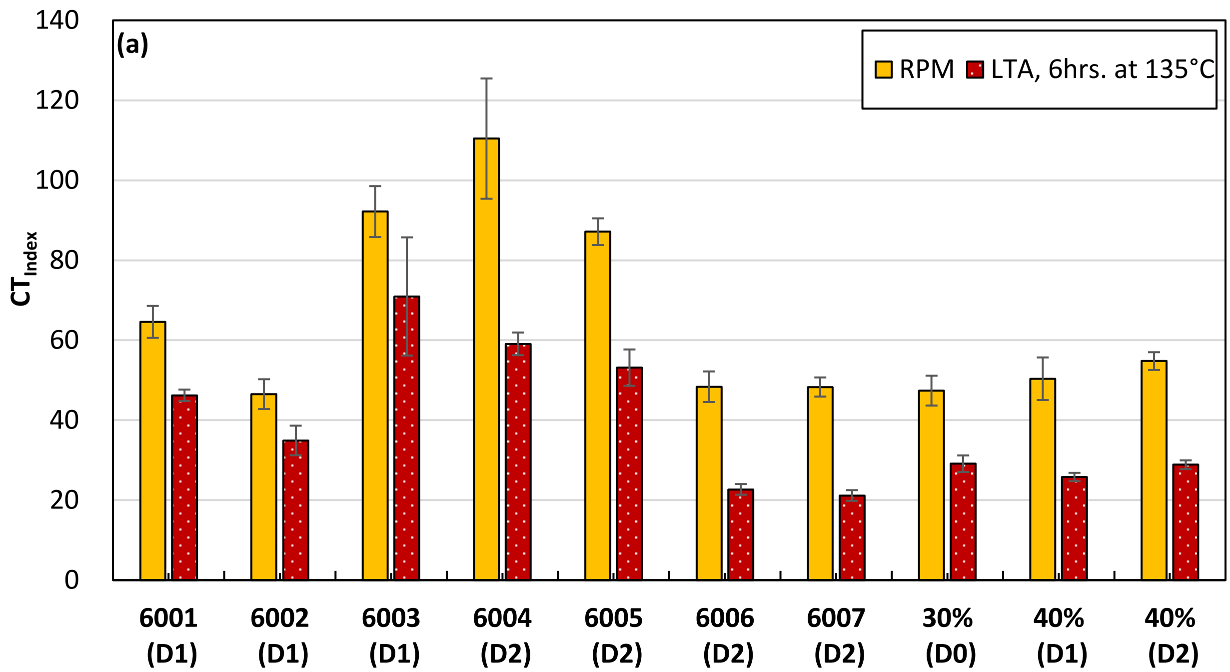

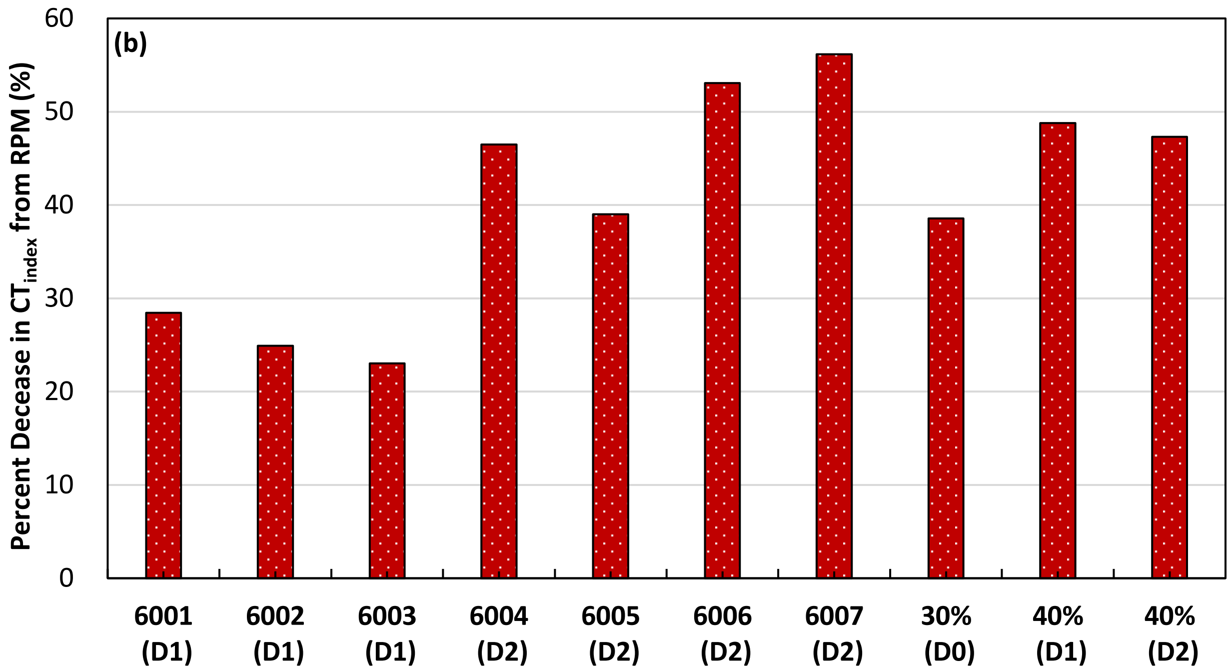

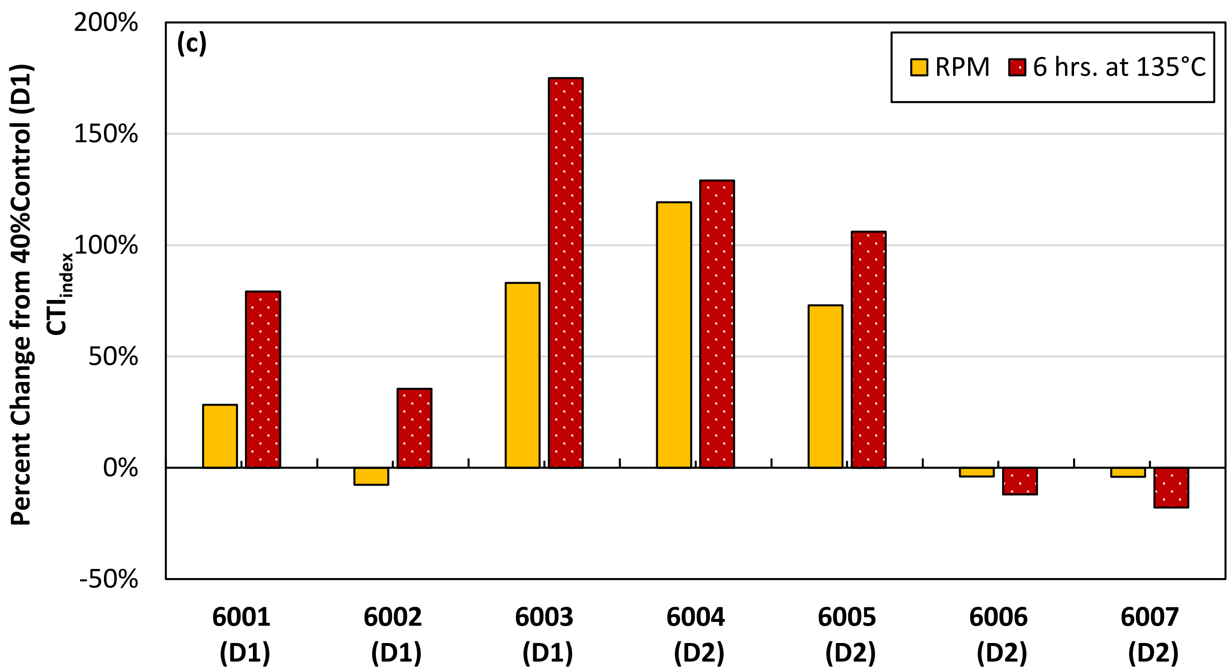

Figure 7-10 (a) CT_{Index} Values; and (b) Percent Decrease in CT_{Index} Values with Aging (c) Percent Change in RA Section Respect to 40% Day1 Control

7.6 Tensile Strength Ratio Test

Figure 7-11 below shows the wet and dry indirect tensile strength values with different aging conditions for the study mixtures. The 6 hrs. at 135°C LTA results for 6004 and 6006 have not been provided to the research team. For the RPM specimens, there is a statistically significant difference between the control mixtures and RA mixtures. All RA mixtures have a lower tensile strength than 30% and the corresponding 40% mixture, indicating the softening effect to the RA agents. All mixtures have a substantially lower wet tensile strength, indicating the deterioration of the strength with the moisture conditioning. After 6 hrs. at 135°C LTA condition, control mixture 40% has a significantly higher value than the 30% control mixture for both parameters. All LTA mixtures (except 6005) have a higher tensile strength value after aging.

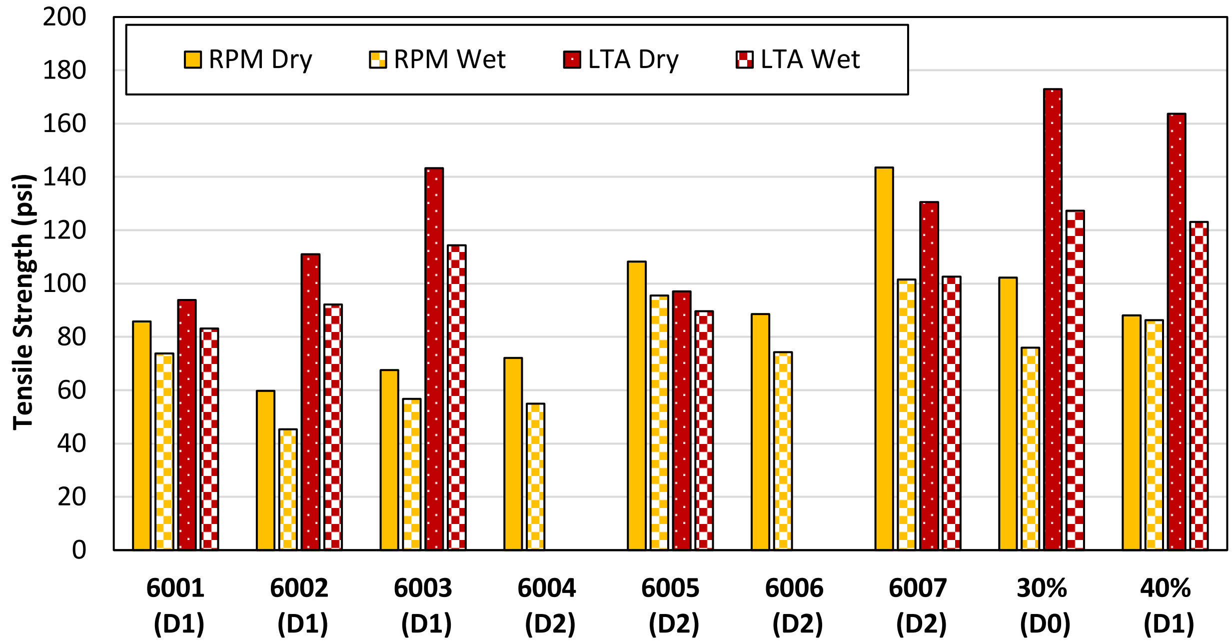

Figure 7-11 Before/After Moisture Conditioning Indirect Tensile Strength with Aging Condition

Figure 7-12 below shows the percent difference in TSR value with aging for the different study mixtures. The 40% control mixture passes the TSR threshold value of 80% for RPM condition, while none of the control mixture meets the requirement after LTA. The 30% control mixture has a lower TSR value as compared to the 40% control mixture for both aging conditions, indicating the higher RAP content may contribute to the lower moisture resistance of these mixtures. This can be related to the fact that the aggregate in the recycled materials is covered and protected by the aged binder and the bond between aggregate and aged binder is stronger than those between aggregate and base binder, making the recycled mixture less vulnerable to moisture damage. Mixtures with RAs (except 6002) generally have the TSR values that fall between the 30% control mixture and corresponding 40% control mixture in RPM condition. There is not a clear trend showing the change of TSR value with increase of aging condition. After 6 hrs. at 135°C LTA, all RA mixtures except have higher TSR values than all control mixtures. The RA treated mixtures have smaller change in TSR value with aging than the 40% control mixture.

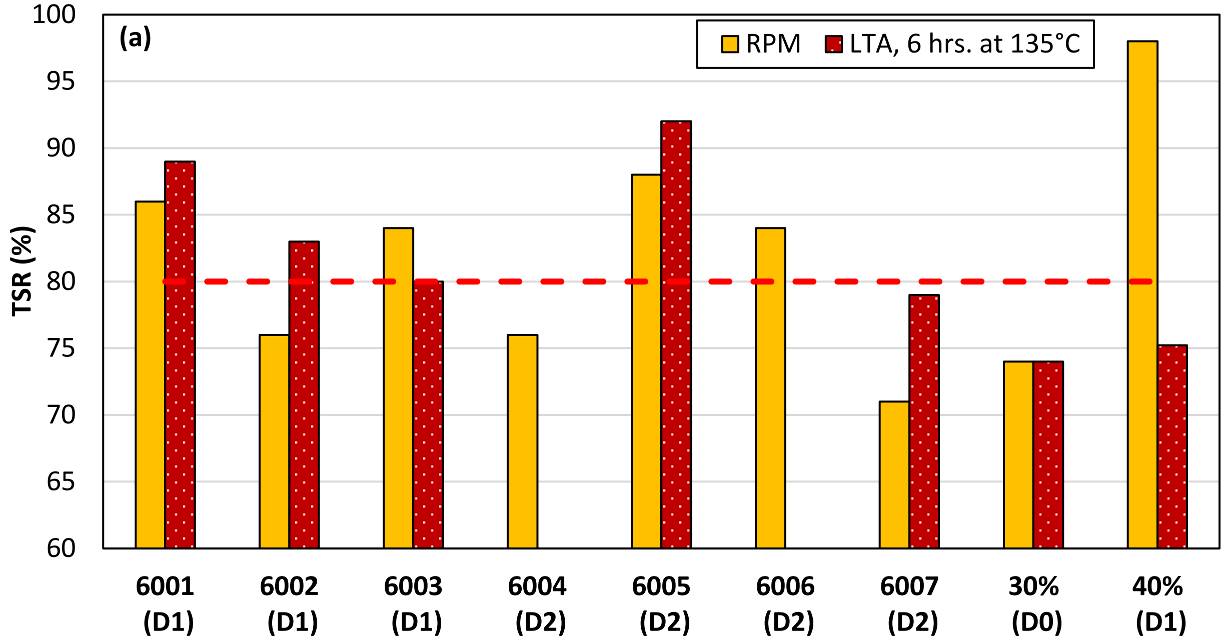

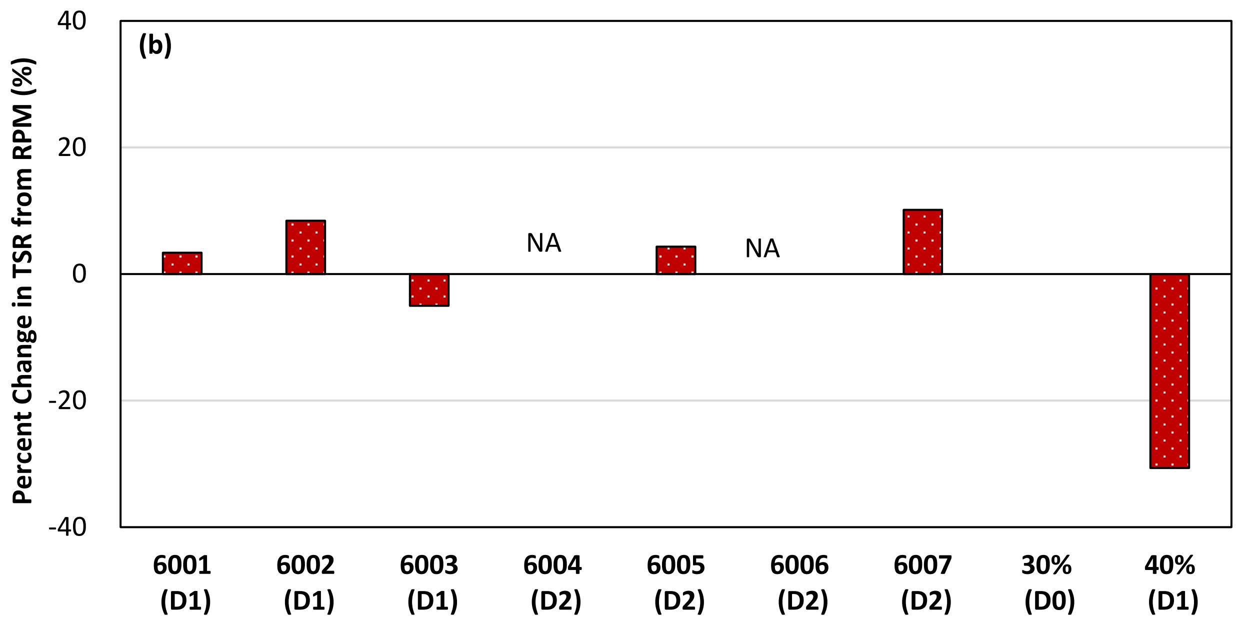

Figure 7-12 (a) TSR Values; and (b) Change in TSR Values with Aging Condition

7.7 Hamburg Wheel Tracking Test

Figure 7-13 shows the HWTT results in terms of the number of passes to reach 12.5mm rut depth for the study mixtures in the RPM, with error bars representing the measurements from two replicates. Only the 6007, 30% and 40% control mixtures meet the threshold value of 10,000 passes at 12.5mm rut depth. Comparing the control mixtures, the 30% control mixture has lower number of passes to the

12.5mm rut depth than 40% control mixture. Generally, mixtures with RAs (except for 6007) have substantially lower number of passes to the 12.5mm rut depth value, indicating significant deterioration of the rutting performance at the RA dosages used in this study. This indicates RA, when diffusing in the mix, may cause a softening effect on the base binder. As this portion of the binder changes its stiffness, the overall mastic phase becomes softer and results in higher rutting susceptibility.

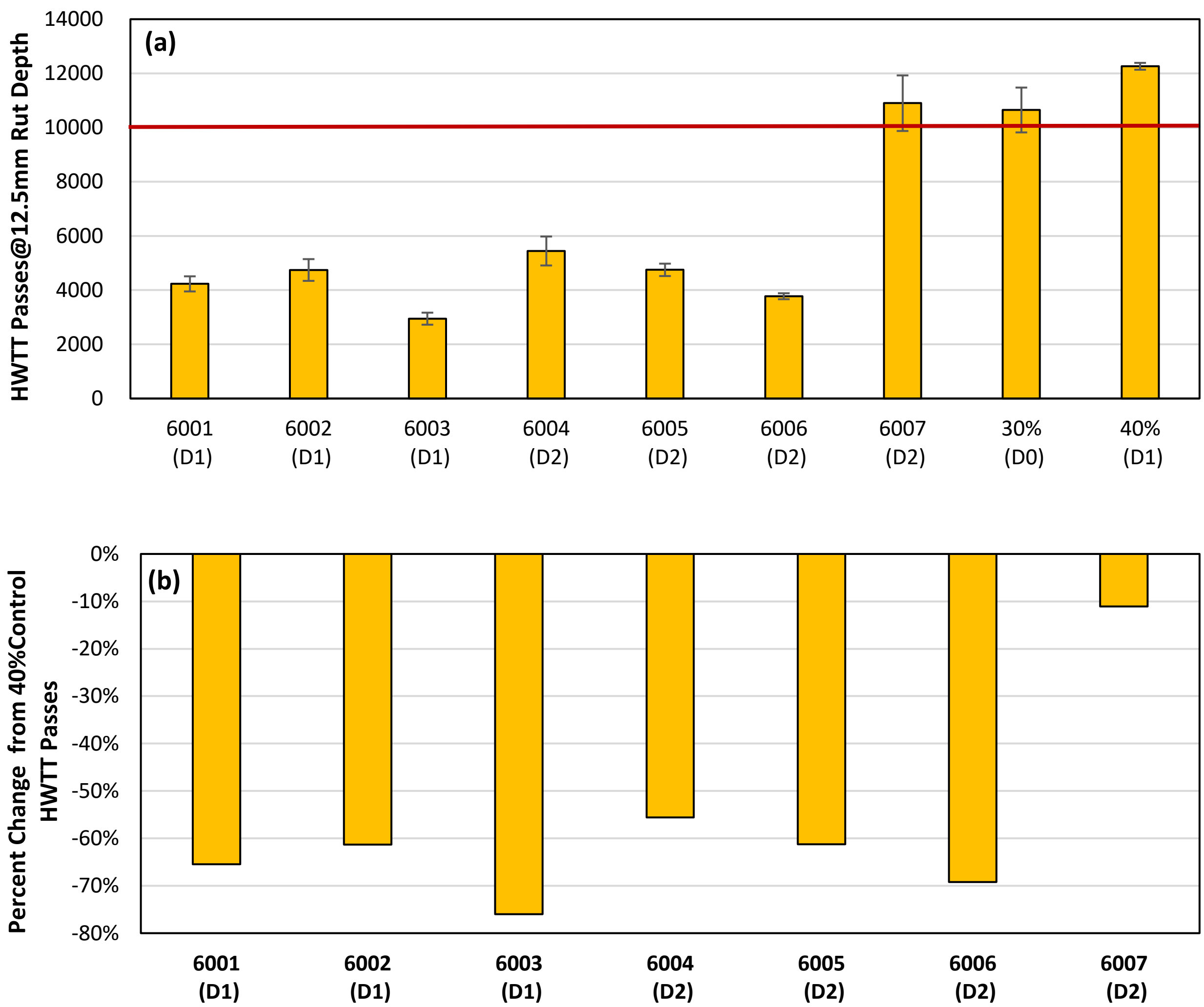

Figure 7-13 (a) Number of Passes to 12.5mm Rut Depth from Hamburg Wheel Track Testing (HWTT) (b) Change in Passes Values due to RA

Figure 7-14 shows the SIP values for the study mixtures measured from the HWTT test. There is a statistical difference between the three control mixtures with 40% control mixture indicating the best moisture resistance with the highest SIP value. The RA mixtures, except for 6007, have significantly lower SIP values than the 30% and 40% control mixtures, indicating the study RAs may drastically deteriorate the moisture resistance at the dosages used in the study. Similar trends can be observed for the LC_{SN} parameter, as shown in **Figure 7-15.**

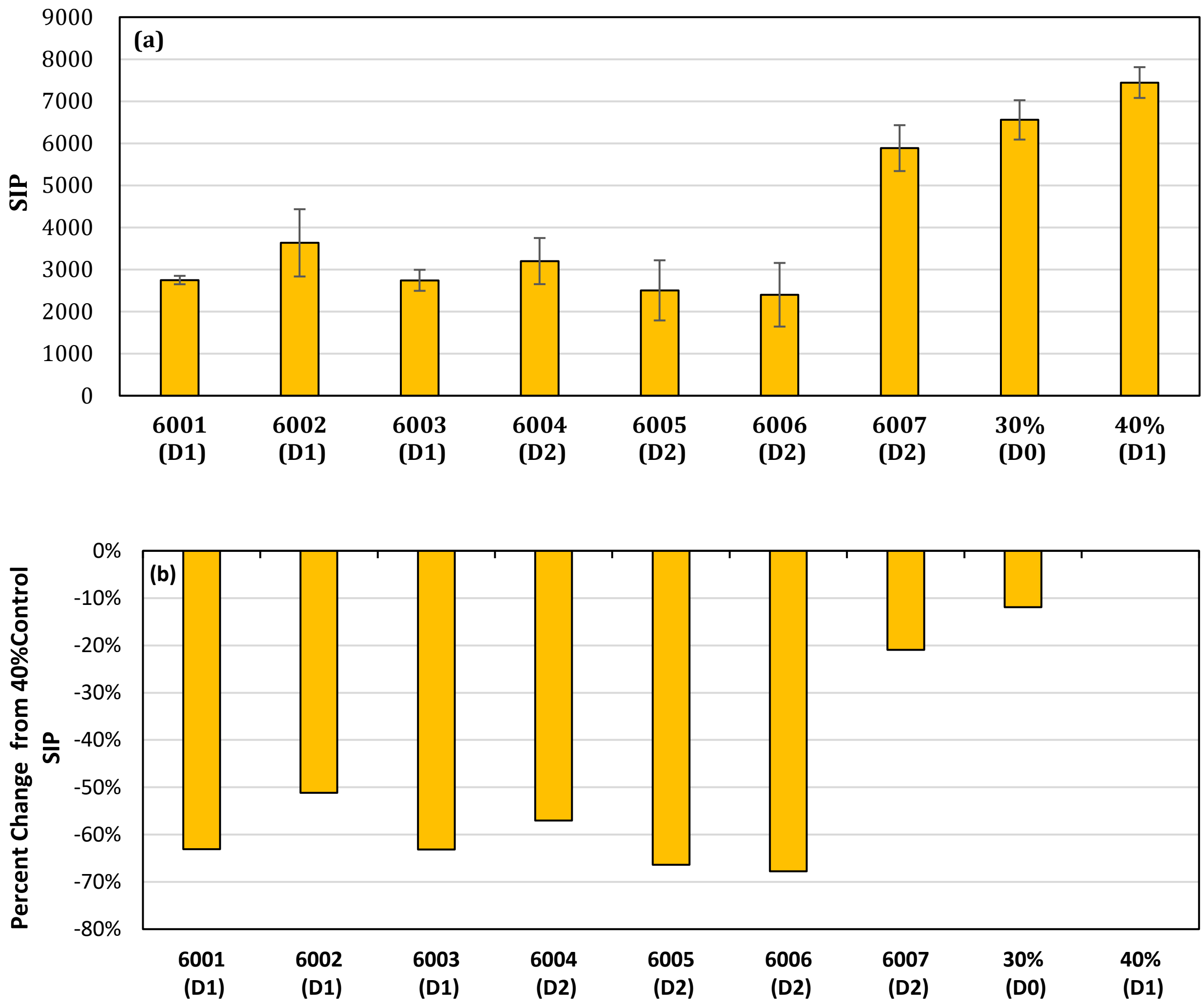

Figure 7-14 (a) SIP from Hamburg Wheel Track Testing (HWTT) (b) Change in SIP due to RA

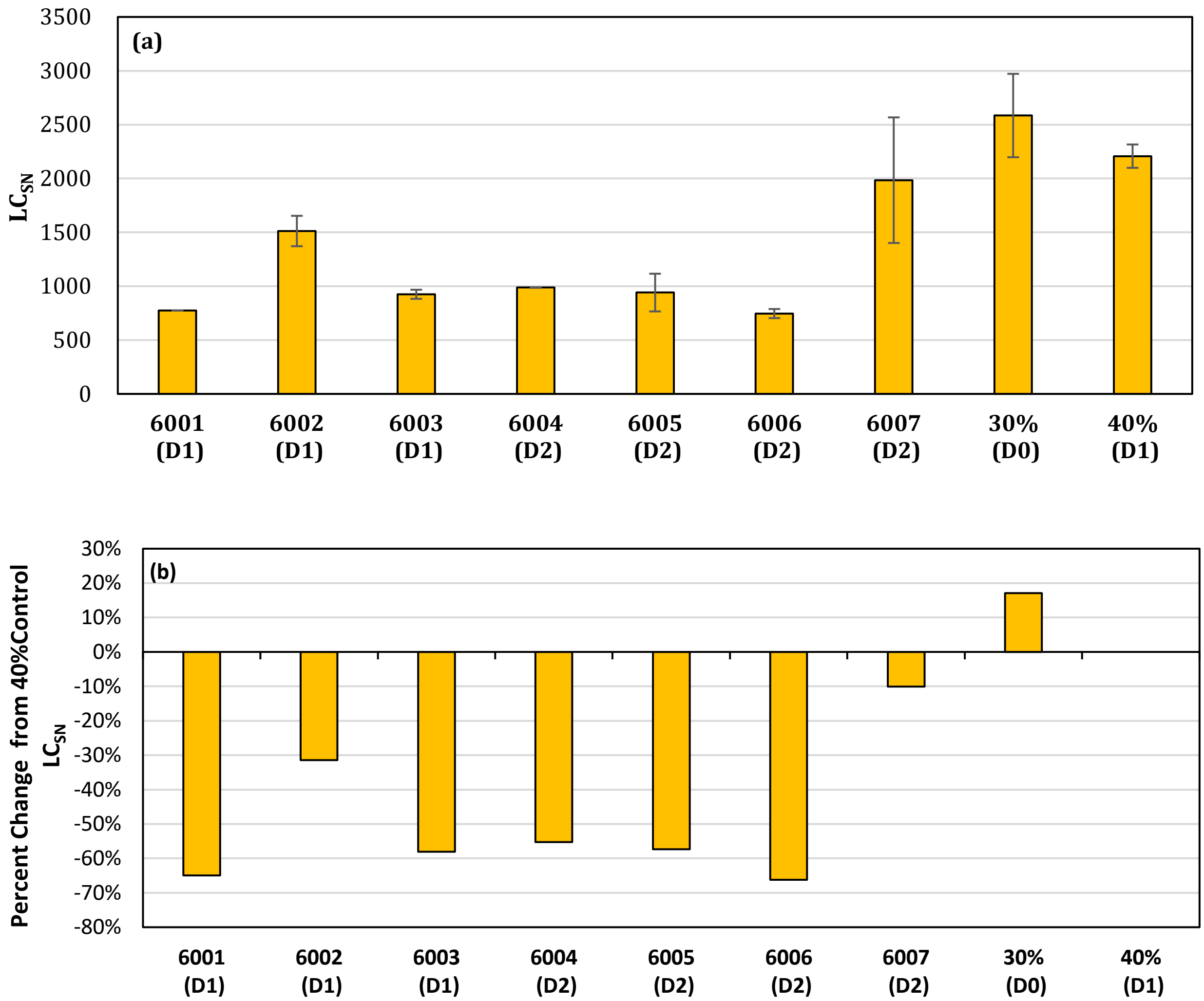

Figure 7-15 (a) LC_{SN} from Hamburg Wheel Track Testing (HWTT) (b) Change in LC_{SN} Values due to RA

Chapter 8: Pavement Performance Evaluation and Correlation Analysis

In this chapter, the field performance of each pavement test section represented by riding quality, cracking, and rutting data collected from regular surveys is presented. In addition, the correlations between various laboratory test indices and field performance are evaluated in terms of different laboratory aging protocols (PAV Aging Levels and Loose Mix Aging Levels).

8.1 Field Performance

MnDOT collected data on the number of transverse cracks, accumulative length of transverse cracking, International Roughness Index (IRI), and rutting depth on the study sections. The available data includes cracking measurements for 4 years and 3 years of ride quality and rutting data. MnDOT indicates that all test sections are generally in good condition with no serious issues or distress noted. By the end of the fourth year in service, the only type of distress that can be noticed during the on-site examination is transverse cracking. Given this scenario, the Pavement Condition Index (PCI) is not suitable for evaluating the test sections in this project as a comprehensive characterization of different types of distress. Instead, a pavement condition parameter is used to evaluate only one specific distress. The deduct value and transverse cracking performance index are adopted as indicators of transverse cracking performance, as outlined in section 4.3.

Figure 8-1 shows the transverse cracking distress observed on the test sections over 4 years. The 40% D1 control section shows the most degradation in terms of both the quantity and length of transverse cracking and the 30% control section shows the least. All the RA sections fall between the two control sections.

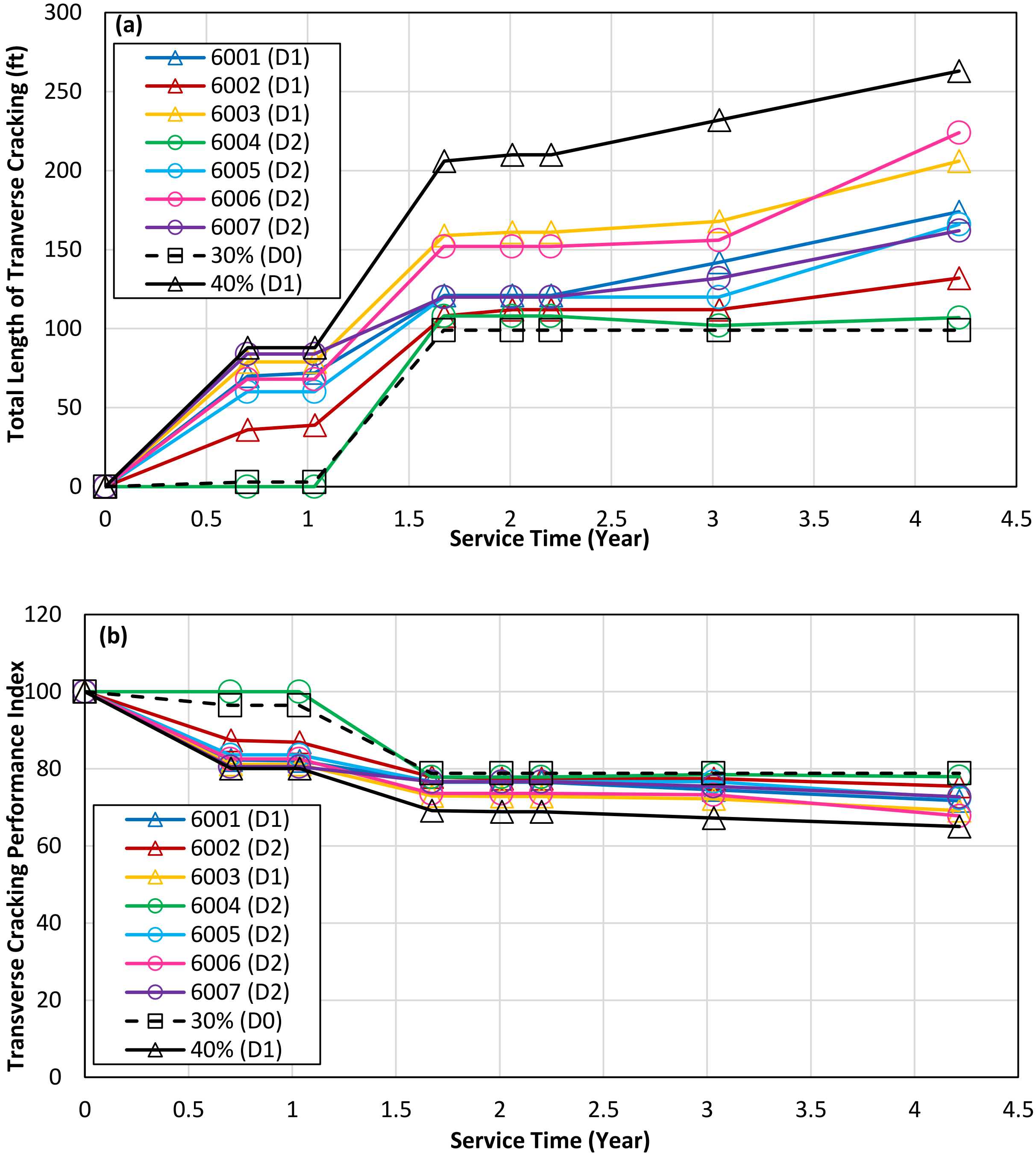
(a)
Total Length of Tranverse Cracking (ft)
Service Time (Year)
6001 (D1)
6002 (D1)
6003 (D1)
6004 (D2)
6005 (D2)
6006 (D2)
6007 (D2)
30% (D0)
40% (D1)
(b)
Transverse Cracking Performance Index
Service Time (Year)
6001 (D1)
6002 (D2)
6003 (D1)
6004 (D2)
6005 (D2)
6006 (D2)
6007 (D2)
30% (D0)
40% (D1)

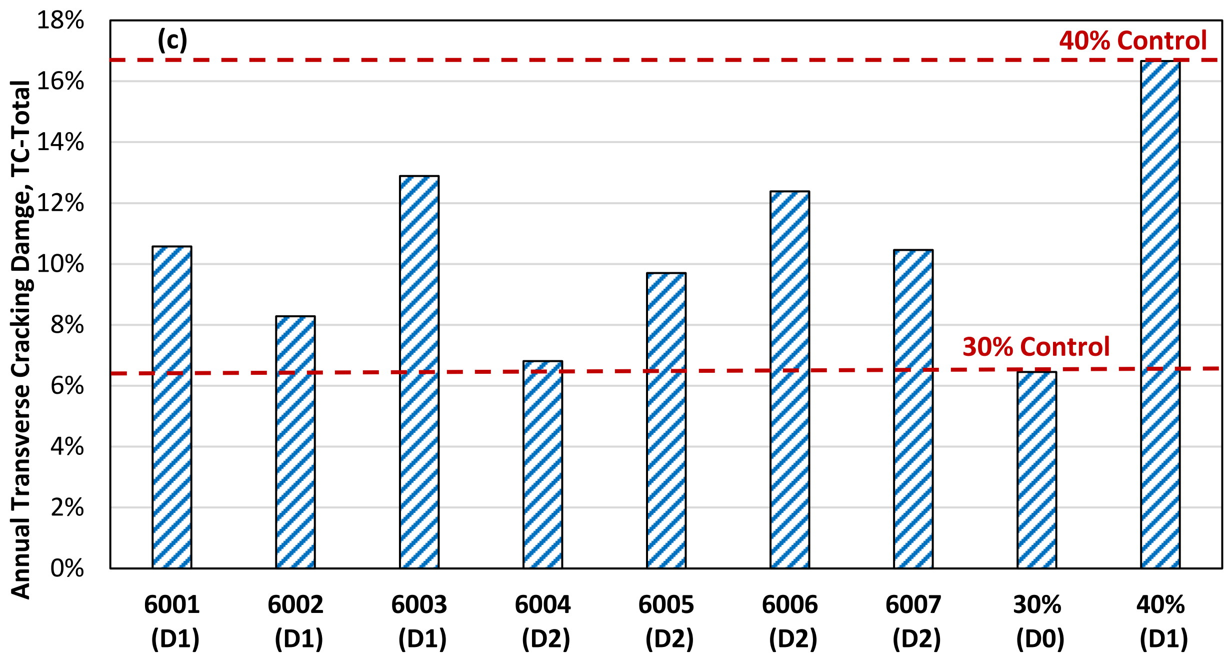

Figure 8-1 Transverse Cracking Performance for 4 Years of Service. (a) Accumulative length of Transverse Cracking, (b) Transverse Cracking Performance Index, (c) Annual Transverse Cracking Damage (TC-Total)

Figure 8-2 shows the IRI results of the test sections over three years. All test sections have IRI values below the threshold of 95 in/mile set forth by the Federal Highway Administration, which defines a pavement in "good" condition as having an IRI below this value. The IRI values show a small increase over the first two years with a gradually increase in IRI values over the initial two years after construction, which then begins to increase after approximately two and a half years. The 30% control consistency shows a slightly higher IRI than the 40% control section. After three years of service, section 6007 has a slightly higher IRI section 6006 has a slightly lower IRI than all other sections. The majority of other RA sections exhibit similar IRI with 30% control and the 40% control sections after three years of service. **Figure 8-2 (d)** shows the change in the International Roughness Index (IRI) over three years, demonstrating the increase in pavement roughness during the service period. The 30% control section shows a slightly lesser increase in roughness compared to the 40% control section, as expected. Notably, Section 6004 exhibits significantly better resistance to roughness increase than the control sections.

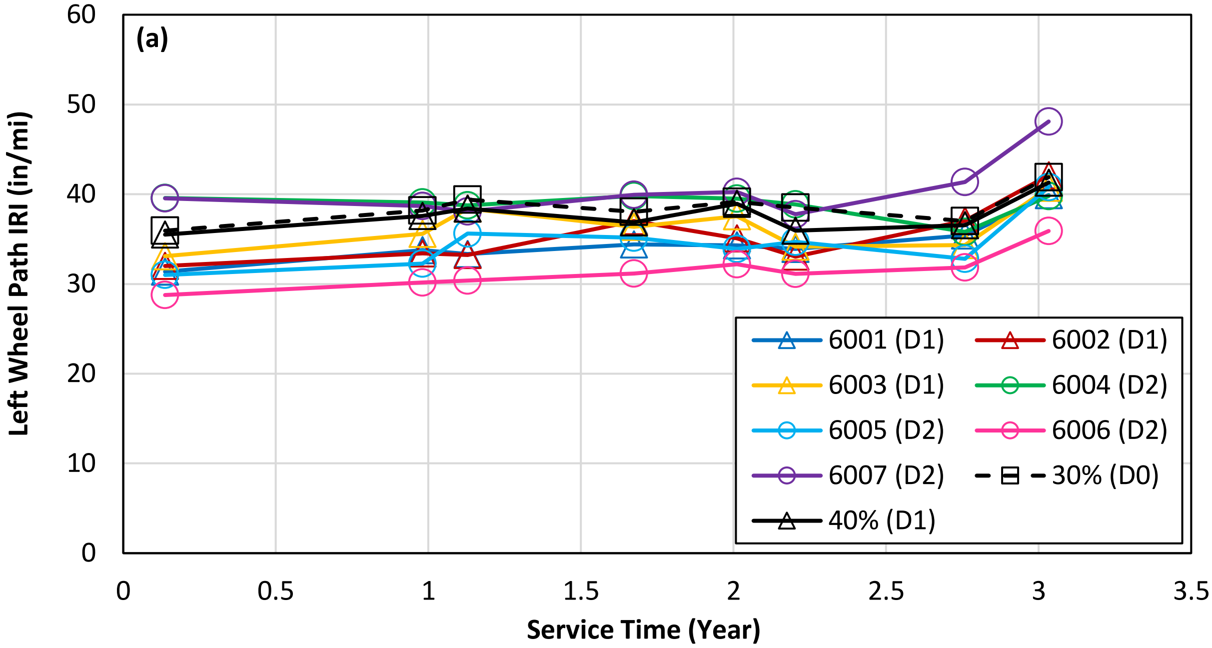
(a)
Left Wheel Path IRI (in/mi)
Service Time (Year)
60
50
40
30
20
10
0
0
0.5
1
1.5
2
2.5
3
3.5
6001 (D1)
6002 (D1)
6003 (D1)
6004 (D2)
6005 (D2)
6006 (D2)
6007 (D2)
30% (D0)
40% (D1)

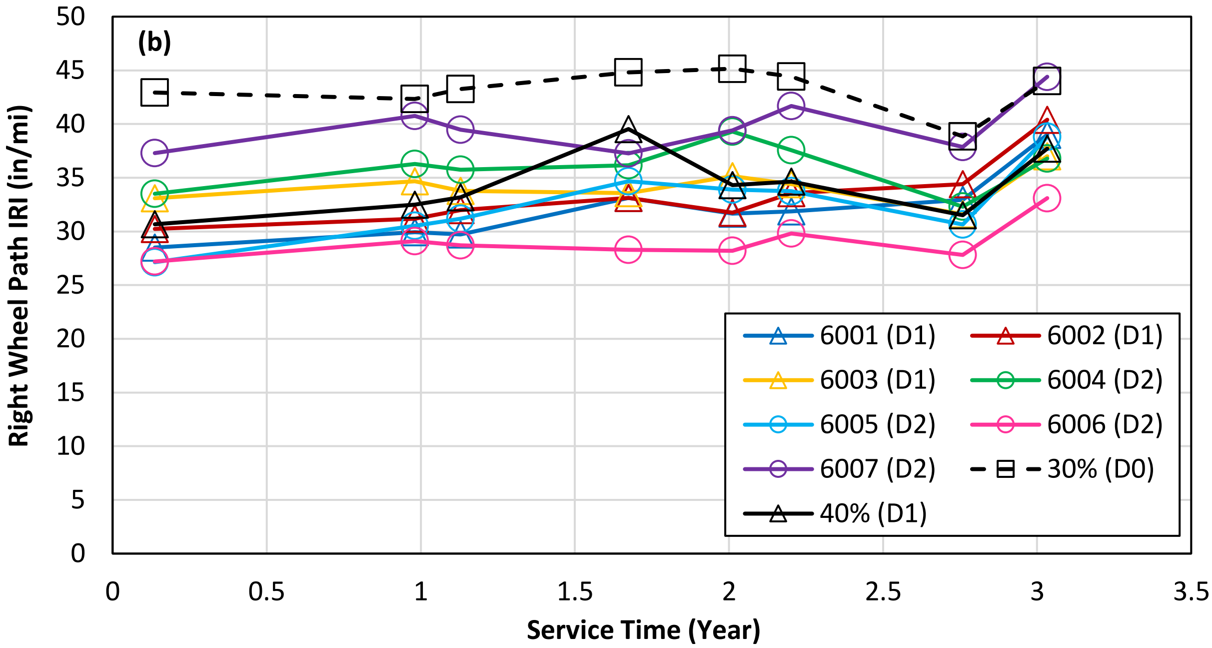
(b)
Right Wheel Path IRI (in/mi)
Service Time (Year)
50
45
40
35
30
25
20
15
10
5
0
0
0.5
1
1.5
2
2.5
3
3.5
6001 (D1)
6002 (D1)
6003 (D1)
6004 (D2)
6005 (D2)
6006 (D2)
6007 (D2)
30% (D0)
40% (D1)

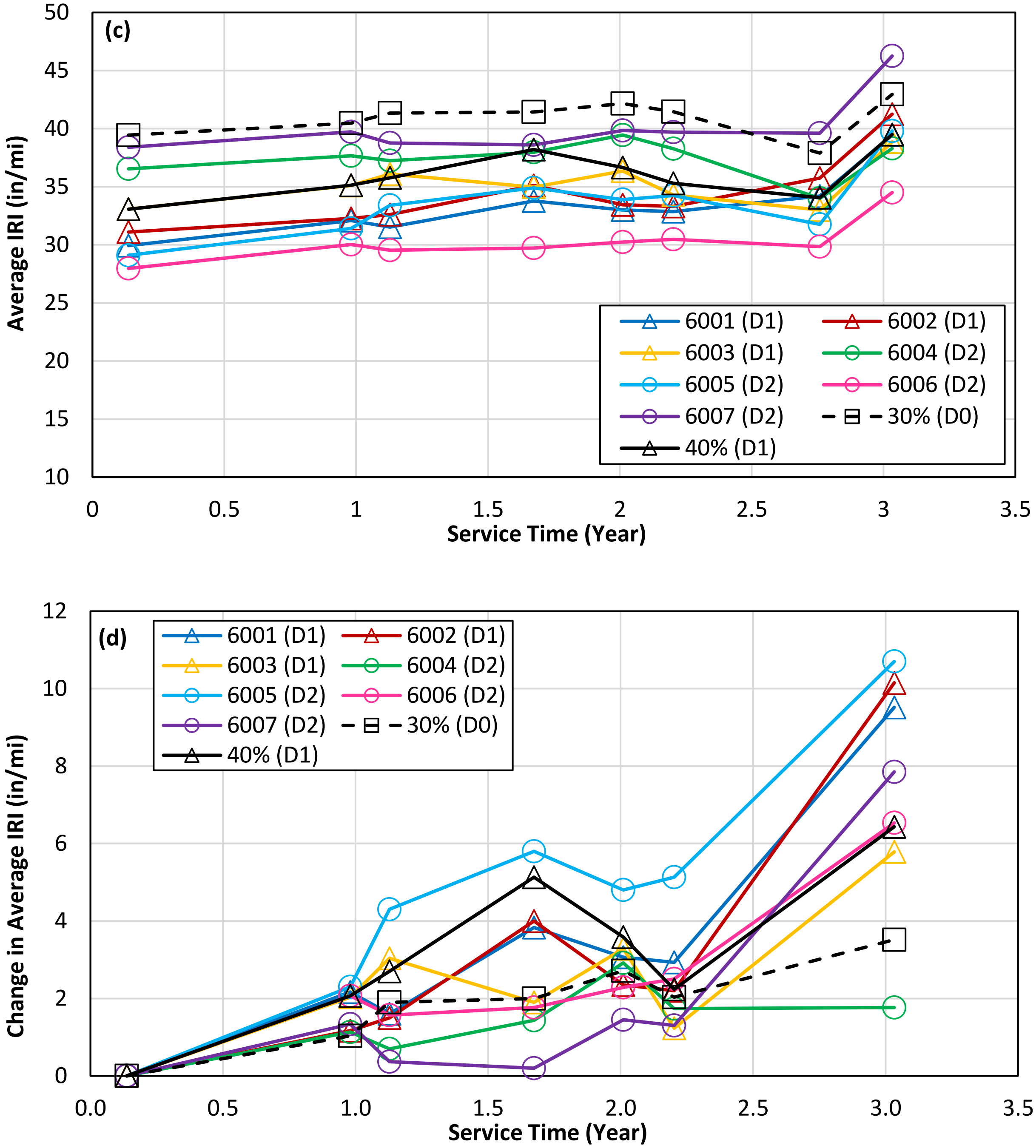

Figure 8-2 International Roughness Index. (a) IRI of Left Wheel Path, (b) IRI of Right Wheel Path, (c) Average IRI of Two Wheel Paths, (d) Change in Average IRI over 3 Years

Figure 8-3 shows the rutting depth observed over a three-year period for the nine test sections. Overall, the rutting of all test sections is minimal, with all sections performing similarly and remaining well below the intervention threshold of 12.5mm for critical rutting performance.

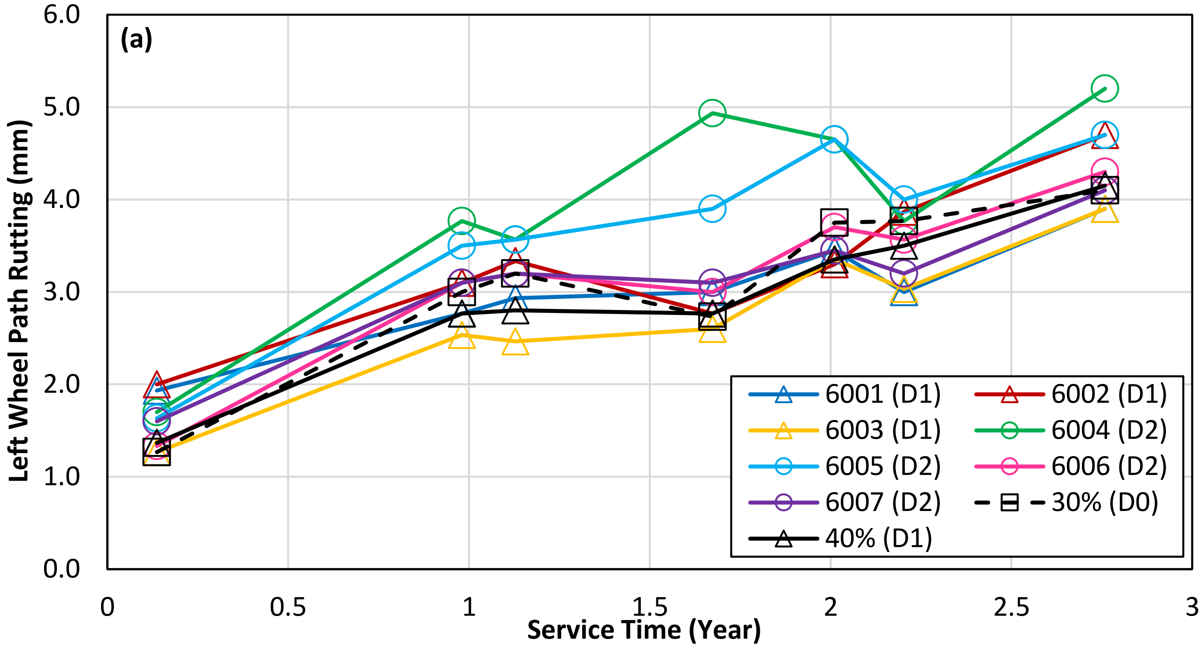
(a)
Left Wheel Path Rutting (mm)
Service Time (Year)
6001 (D1)
6002 (D1)
6003 (D1)
6004 (D2)
6005 (D2)
6006 (D2)
6007 (D2)
30% (D0)
40% (D1)

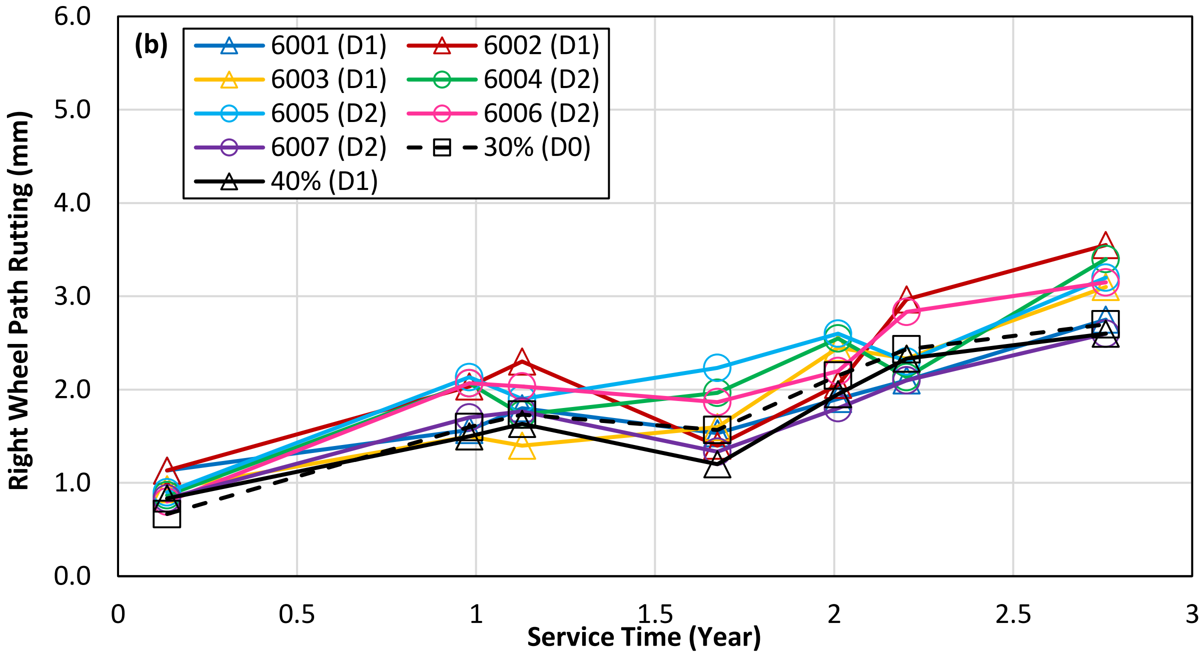
(b)
Right Wheel Path Rutting (mm)
Service Time (Year)
6001 (D1)
6002 (D1)
6003 (D1)
6004 (D2)
6005 (D2)
6006 (D2)
6007 (D2)
30% (D0)
40% (D1)

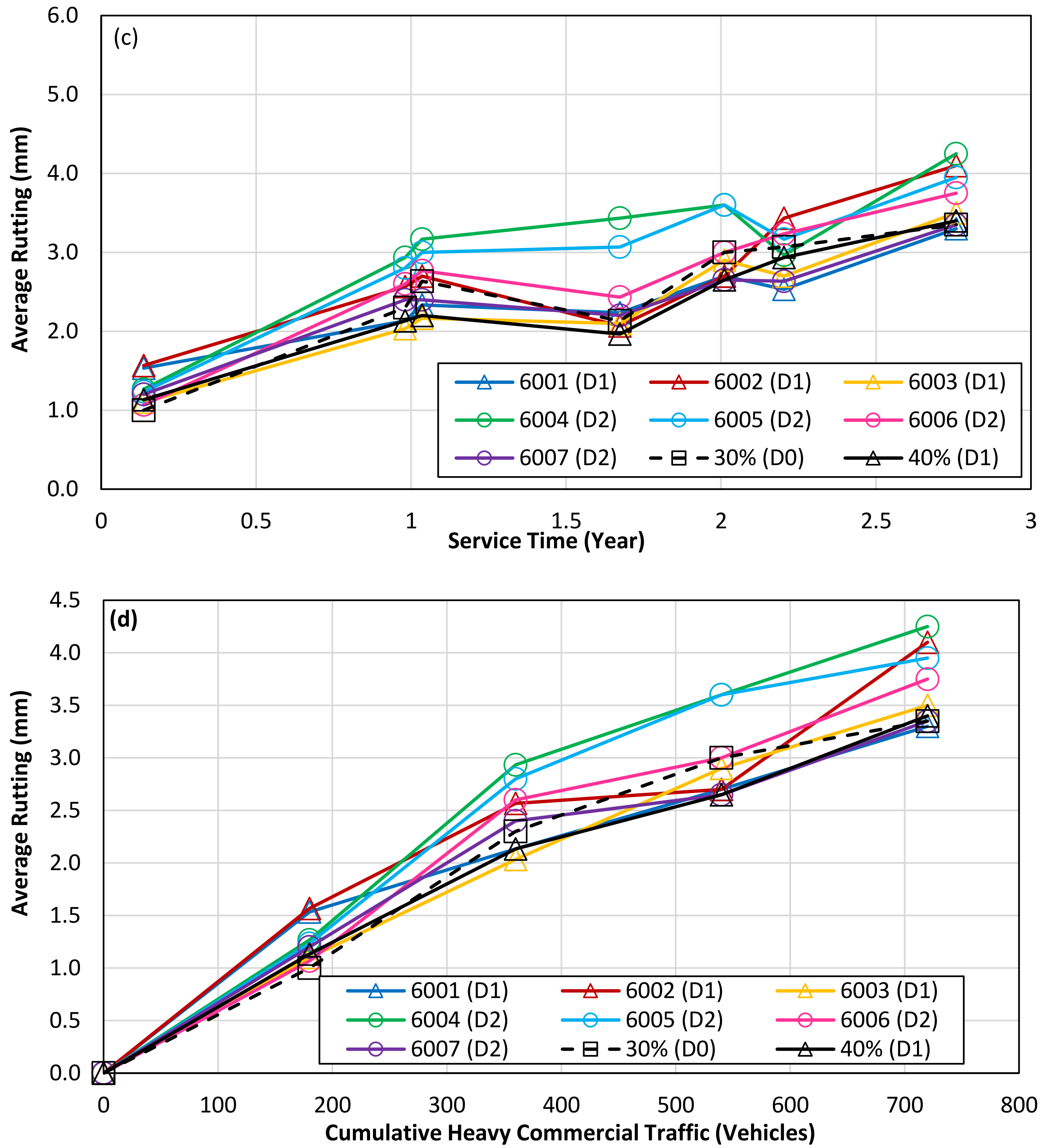

Figure 8-3 Rut Depth (a) Rut Depth of Left Wheel Path, (b) Rut Depth of Right Wheel Path, (c) Average Rut Depth of Two Wheel Paths (d) Rut Depth Change with Heavy Traffic

8.2 Simulated Pavement Performance

The FlexPAVE™ software is utilized to predicting the long-term pavement performance with respect to fatigue cracking over a 20-year service period. The climate data is determined based on the project site in Emily, MN. The viscoelastic and fatigue material characteristics of the wearing course were determined using complex modulus test and DTCF test, respectively. The material properties entered for the 9 cases were RPM material and 4-Year FC. The simulation then analyzed the fatigue damage under long-term cyclic loading.

Figure 8-4 **(a)** and **(b)** below show the FlexPAVE^{TM} predicted fatigue total damage in the pavement structure over time, using RPM and 4-Year FC data, respectively. **Figure 8-5** shows the predicted fatigue damage for each at the end of the 20 years. The amount of fatigue damage in all sections is similar for the analysis with both RPM and 4-Year data.

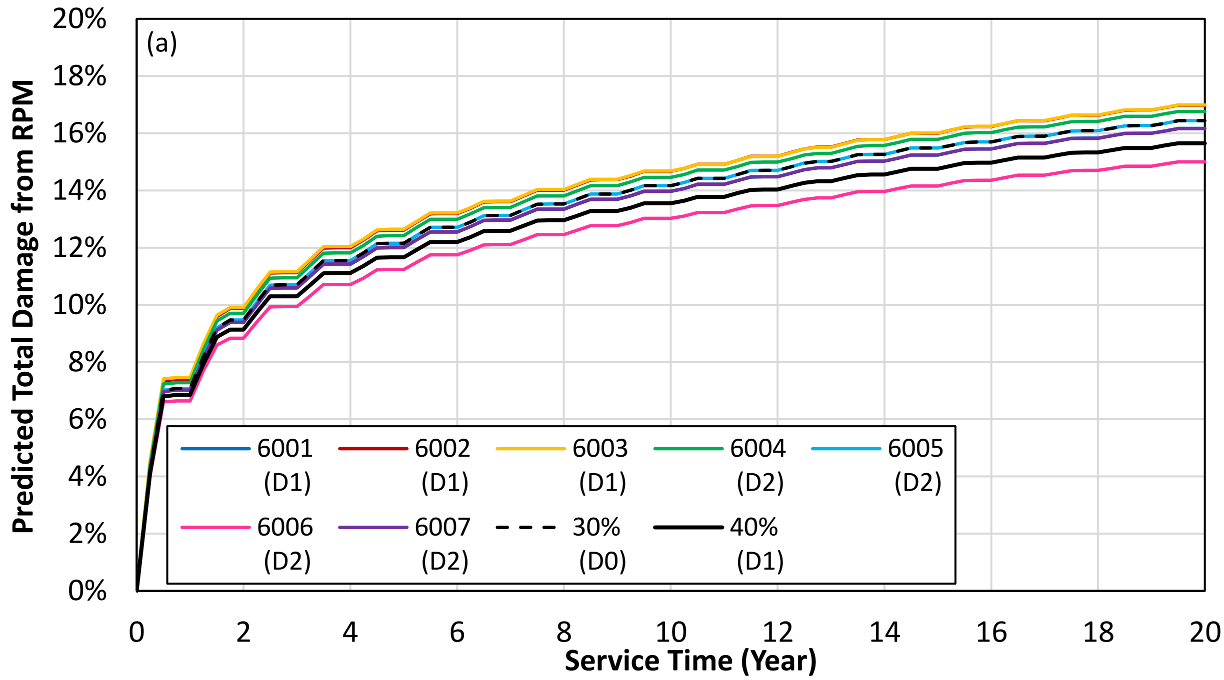

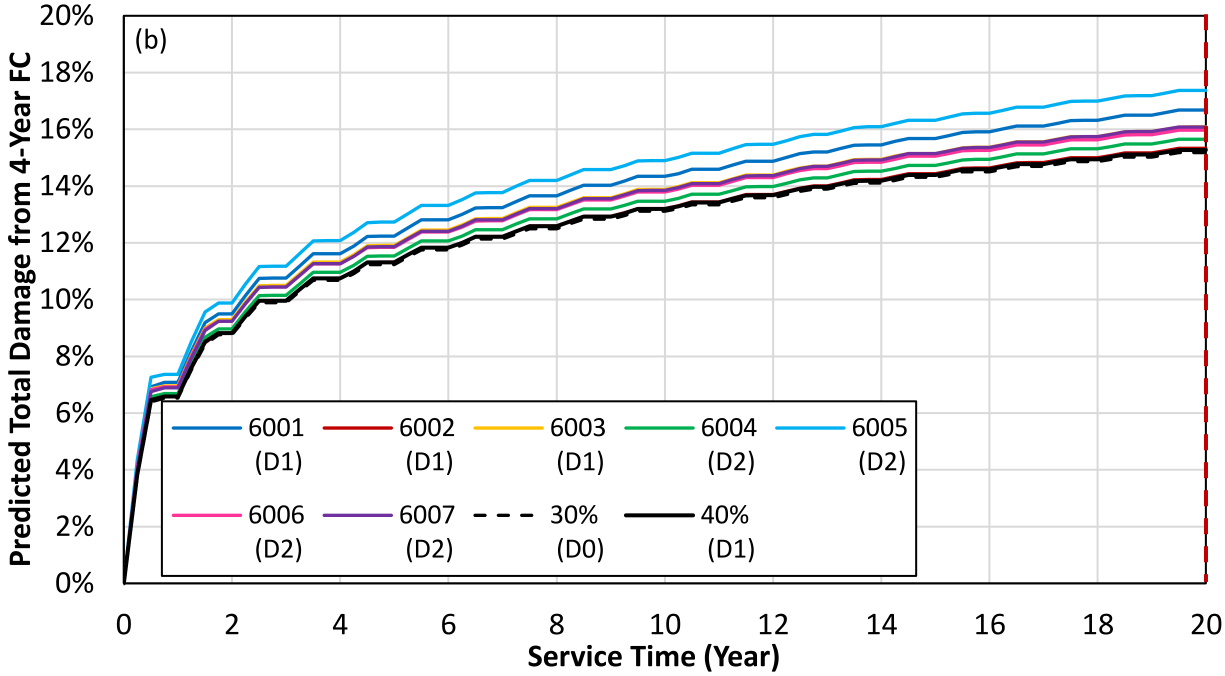

Figure 8-4 Predicted Total Damage of Pavement with Service Time. (a) Based on the Reheated Plan Mix, (b) Based on the 4-Year FC

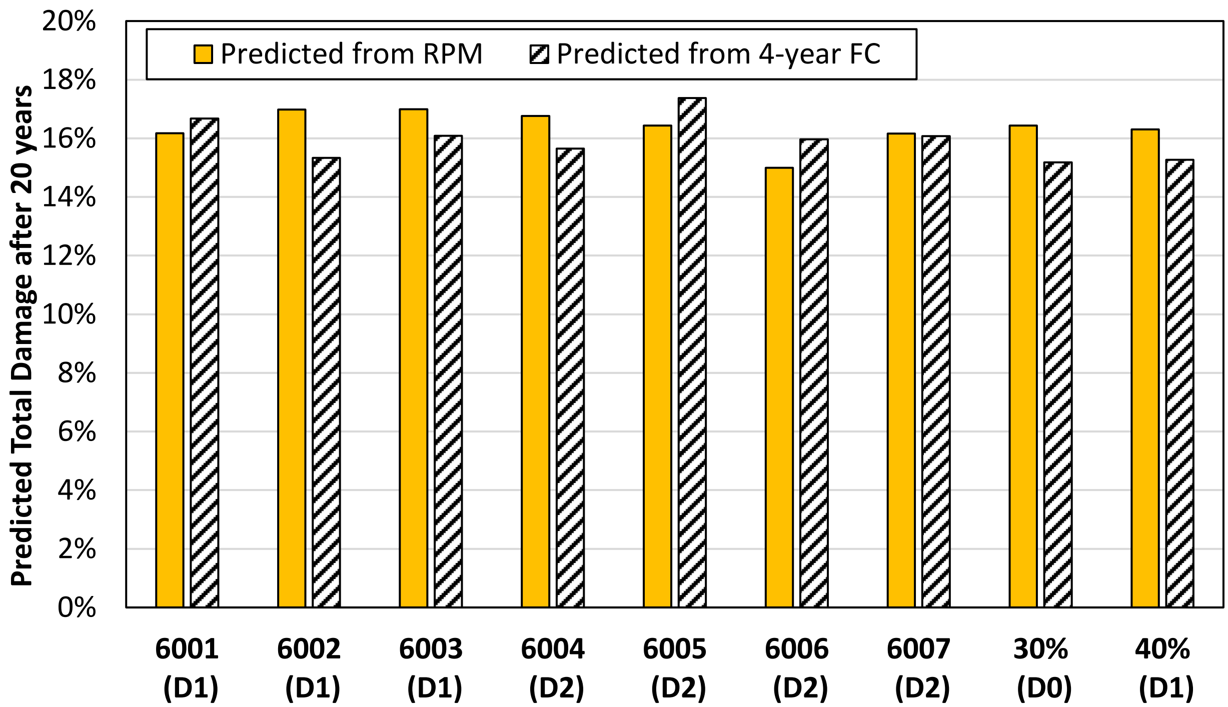

Figure 8-5 Comparison of Predicted Total Damage of Pavement at Year 2039

8.3 Comparison of Field Performance and Field Core Properties

In this section, binder and mixture laboratory test results from the field cores are correlated with field performance over a period of 1 to 4 years. The purpose of this analysis is to identify promising laboratory characterization methods and field performance evaluation indices. Furthermore, the interaction between laboratory and field results will be investigated in order to acquire insight into the detection of promising relationships under field aging. Subsequently, the promising relationship can be applied in the following section, where the material parameters with each laboratory aging protocols were correlated to the overall 4-year field performance.

8.3.1 Correlation between Field Core and Field Performance

Figure 8-6 below shows the Pearson correlation scatter plot matrix between representative field core mixture test parameters and field performance, along with all pairwise scatter plots illustrating each relationship. The scatter plot visually explores correlations and relationships between multiple variables in a dataset. Each cell below the diagonal displays a scatter plot, with different colors like blue, purple, black and yellow scatter representing 1~4-year aging conditions respectively. The cells above the diagonal feature correlation coefficient heat map, ranging from -1 to 1, color-coded from blue (negative correlation) to red (positive correlation), where the size of each circle within these cells indicates the strength of the correlation; larger circles denote stronger relationships. The focus of this analysis is to investigate the lab-field correlation. Thus, the correlations within different binder parameters and the correlations within different performances are not the focus of this study, so those slots are shaded. The significant lab-field correlations (Pearson correlation coefficients>0.65) are marked with green squares to help identify the most important observation between field performance and test variables.

When comparing the mixture properties, the positive and negative signs of the coefficients reveal meaningful relationships with field cracking performance: higher G-R_m values or lower fatigue parameters are associated with more severe field cracking parameters. In terms of field laboratory cracking performance indices, TC-Total, Deduct Value and Surface Rating generally show good correlation with laboratory deduct values. And Sapp generally shows significant correlation with all three cracking performance indices. The G-R_m show a higher correlation with pavement roughness than the fatigue parameters, with a trend that higher G-R_m lead to severe roughness result.

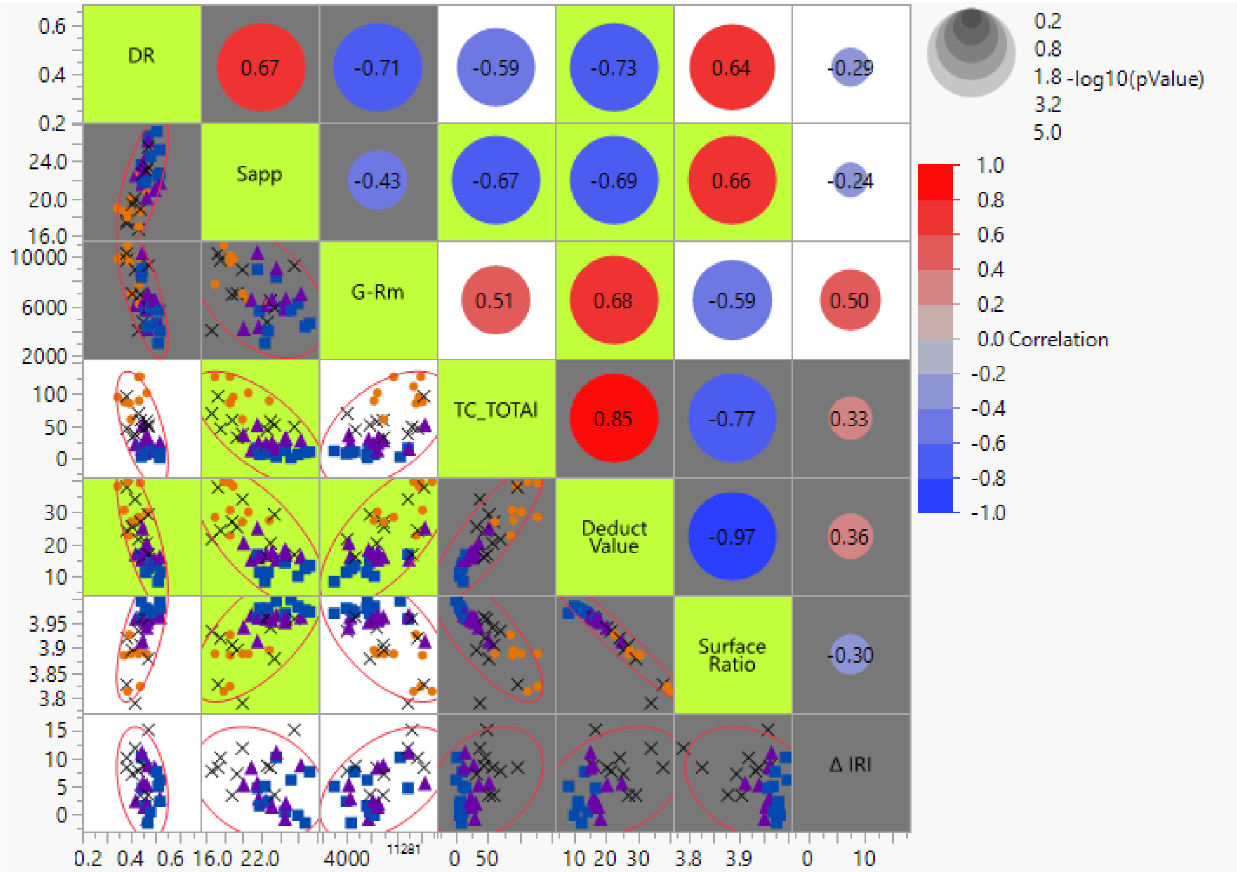

Figure 8-6 Correlation Significance Matrix with Scatter Plots for Field Core Properties and Field Performance

8.3.2 Correlation between Recovered Field Core Binder Properties and Field Performance

Figure 8-7 below shows the Pearson correlation coefficients between the rheological properties of extracted and recovered binder from field cores and field performance. The results indicate that binder rheological properties have a strong higher correlation with field cracking performance while having a low correlation with pavement roughness performance. The two binder cracking resistance parameters, ΔTc and G-R, show comparatively good correlations with crack density, TC-total and, Deduct Value. The other rheological parameters, ΔTc, glassy modulus, cross-over modulus, and R-value have significant correlations with TC-total. This indicates that higher ΔTc and lower G-R values generally correlate with better field thermal cracking performance.

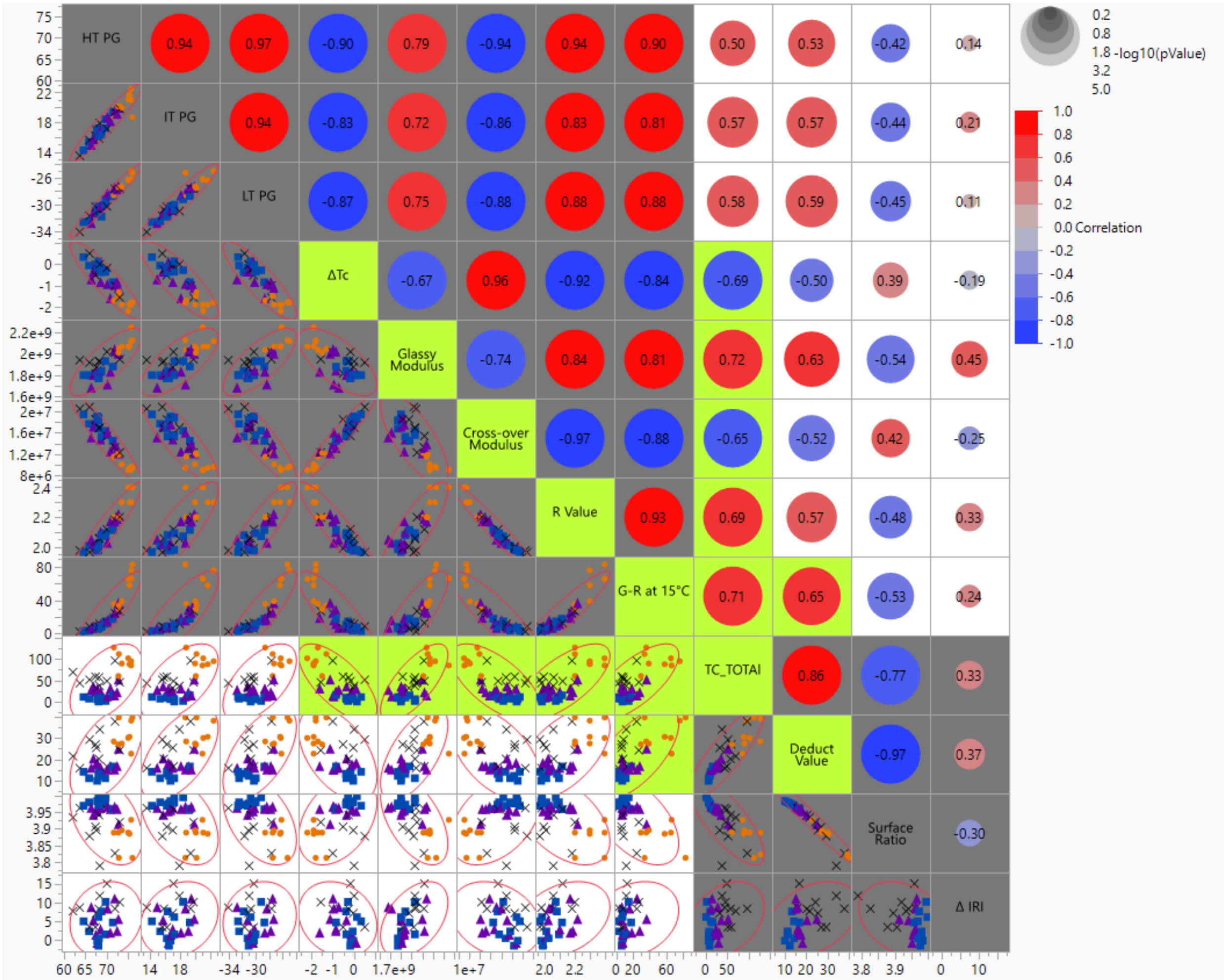

Figure 8-7 Correlation Significance Matrix with Scatter Plots for Field Core Binder Rheology and Field Performance

Figure 8-8 below shows the Pearson correlation coefficients between field performance and the chemical composition of the extracted and recovered binders from field cores. The results indicate that resin and aromatic content have potential correlations with field thermal cracking performance. The analysis indicates that the field core with higher %resin and lower %aromatics may have more severe thermal cracking performance. Despite these two parameters, all other chemical composition parameters didn't show promising correlations with field cracking performance and roughness.

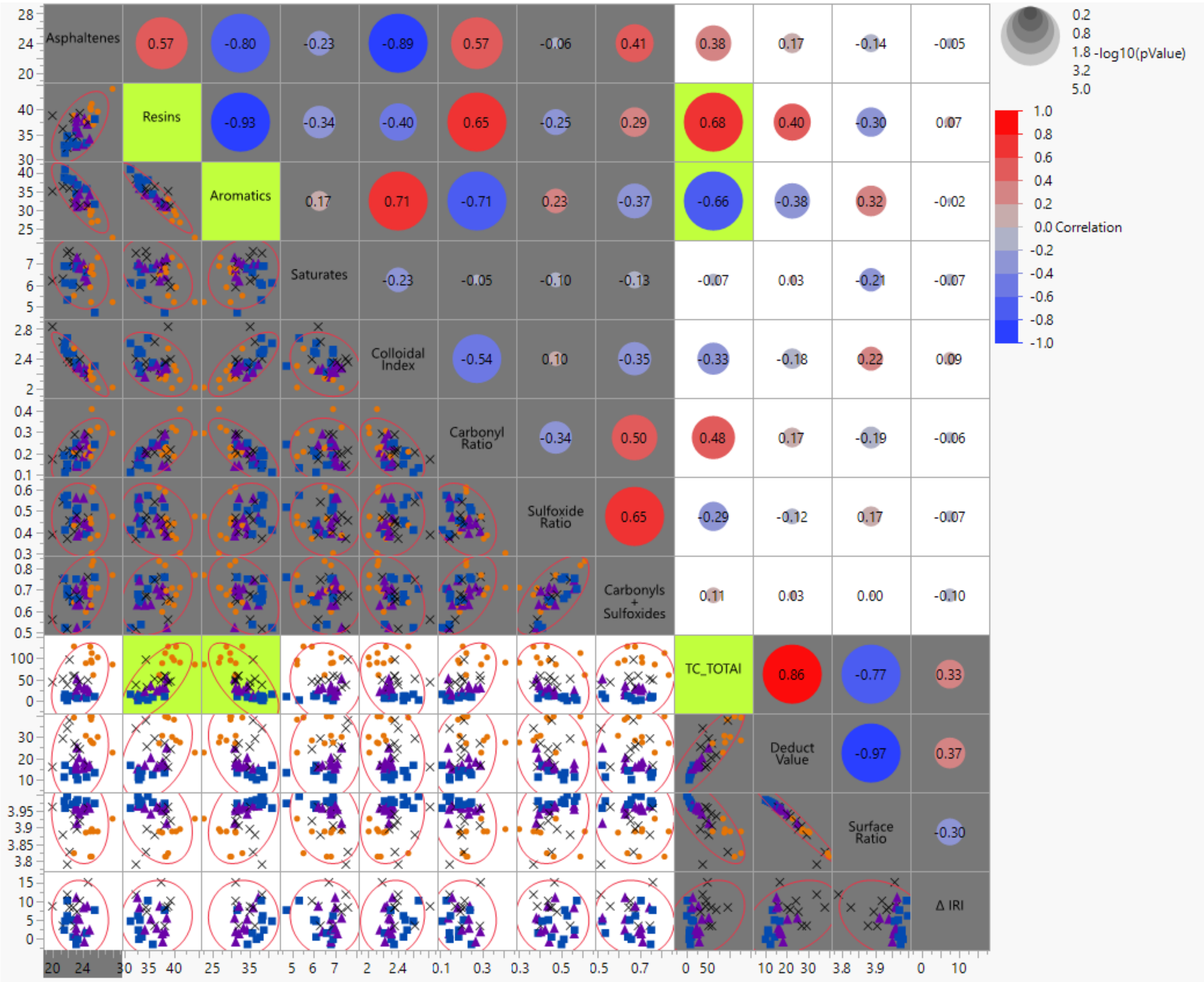

Figure 8-8 Correlation Significance Matrix with Scatter Plots for Field Core Binder Chemical Composition and Field Performance

In general, in terms of lab testing material properties, the D^R, S_{app}, and G-R_m parameters from mixture testing, and ΔTc, G-R, Aromaticity Index, and Carbonyl Ratio from binder testing, show good correlation with field performance (Deduct Value and Surface Rating) based on the correlation analysis of all 4-year field cores. Although the Colloidal Index and Carbonyl Ratio did not perform as well, they are still considered for inclusion. These parameters will be selected and used as evaluation methods in the correlation analysis between lab-aged material and field performance.

8.4 Comparison of Field Performance and Lab-Aged Material Properties

The further correlation analysis evaluates which lab protocols or methods best simulate real-world pavement deterioration and effectively assesses the long-term performance of the studied RAs. The material properties with each laboratory aging protocol are correlated to the overall 4-year field performance in this section. This approach serves the main objective of the research, which is to evaluate long-term effectiveness with accelerated aging protocols in the laboratory.

Based on the lab-field correlation analysis of field cores presented in Section 8.3, TC-Total, Deduct Value, and MnDOT Surface Rating have been selected as the overall cracking performance indices for the 4-year period. For ride quality, the change in IRI (ΔIRI) from the initial value is used to characterize long-term overall roughness performance. Given that the observed rutting depths are extremely low, correlations were not performed.

8.4.1 Correlation between Extracted Binder Properties and Long-Term Field Performance

Table 8-1 shows the Pearson correlation coefficients between field performance indices and binder properties. **Table 8-2** below shows the Pearson Correlation Coefficients between field performance indices and properties of PAV aged binders that extracted from unaged loose mixes. In correlation analysis for field cracking performance, The Surface Rating and Deduct Value indices consistently correlate well with multiple binder properties, which is consistent with observations of laboratory-field correlations in field cores, thus also reaffirming their potential in field performance assessment. The TC-total generally shows lower correlations with binder properties and does not perform as strongly as the observation on the field cores.

Based on the correlation analysis on lab properties, it is evident that certain parameters consistently show strong correlations with field performance to date. Specifically, the G-R parameter exhibits robust correlations with Deduct Value and Surface Rating across all aging protocols, indicating potential in predicting field cracking performance. The LTPG also demonstrates strong correlations with Deduct Value and Surface Rating, especially under PAV aging protocols, making it another potential indicator of field performance. The ΔTc and R values also shows moderate correlations with field performance indices with RPM and 9 days at 95°C protocols but do not perform as strongly as G-R and LTPG under the PAV aging. Further examination of the coefficients' sign and relationship shows that the higher G-R values or warmer LTPG lead to higher deducted value and lower Surface Rating. These findings suggest that G-R, and IT PG are the potential promising parameters for correlating lab-aged binder properties with field performance. As a result, these parameters should be prioritized in further analyses to refine aging protocols and better simulate real-world pavement conditions.

Table 8-1: Pearson Coefficients between Field Performance and Rheological Properties for Loose Mix Aged Recovered Binder

DSR Binder Properties	Field Performance at Aging Protocols											
	RPM				6 hrs at 135C				9 days at 95C			
	TC-T	DV	SR	ΔIRI	TC-T	DV	SR	ΔIRI	TC-T	DV	SR	ΔIRI
HT PG	0.0	0.0	-0.1	0.0	0.3	0.1	-0.1	0.1	-0.2	0.4	-0.4	-0.2
IT PG	0.2	0.5	-0.5	-0.4	0.3	0.4	-0.4	-0.3	0.1	0.6	-0.4	-0.4
LT PG	0.2	0.5	-0.6	-0.5	0.3	0.5	-0.6	-0.5	-0.1	0.5	-0.5	-0.8
ΔTc	0.1	0.6	-0.4	-0.1	-0.5	-0.2	0.2	-0.3	0.6	0.4	-0.4	-0.3
Glassy Mod.	0.3	0.7	-0.5	-0.4	0.2	0.2	-0.3	0.4	0.1	0.7	-0.7	-0.1
Cross-over Mod.	-0.1	-0.1	0.2	-0.1	-0.2	0.2	-0.1	-0.5	0.6	0.2	-0.2	-0.2
R Value	0.3	0.5	-0.5	-0.1	0.2	-0.1	0.1	0.5	-0.5	0.0	0.0	0.1
G-R at 15°C	0.5	0.7	-0.7	-0.3	0.6	0.3	-0.3	0.0	-0.3	0.4	-0.5	-0.6

Table 8-2: Pearson Coefficients between Field Performance and Rheological Properties for PAV Aged Recovered Binder

DSR Binder Properties	Field Performance at Aging Protocols											
	As-Extracted x 20 hrs. PAV				As-Extracted x 40 hrs. PAV				As-Extracted x 60 hrs. PAV			
	TC-T	DV	SR	ΔIRI	TC-T	DV	SR	ΔIRI	TC-T	DV	SR	ΔIRI
HT PG	0.2	0.4	-0.4	-0.3	0.2	0.5	-0.5	-0.3	0.2	0.4	-0.5	-0.3
IT PG	0.2	0.5	-0.5	-0.4	0.3	0.5	-0.6	-0.5	0.2	0.4	-0.5	-0.6
LT PG	0.2	0.5	-0.5	-0.5	0.2	0.6	-0.6	-0.6	0.2	0.5	-0.6	-0.7
ΔTc	-0.3	-0.3	0.2	0.2	-0.1	0.0	0.1	0.0	-0.2	-0.1	0.1	-0.2
Glassy Mod.	-0.3	-0.2	0.1	0.4	0.3	0.6	-0.4	0.1	0.3	0.3	-0.4	-0.1
Cross-over Mod.	-0.3	-0.3	0.3	-0.1	-0.1	-0.3	0.3	-0.1	-0.2	-0.4	0.4	0.0
R Value	0.1	0.2	-0.2	0.3	0.3	0.4	-0.3	0.1	0.3	0.3	-0.4	0.0
G-R at 15°C	0.6	0.6	-0.5	-0.2	0.4	0.6	-0.6	-0.3	0.2	0.4	-0.5	-0.3

Table 8-3 and **Table 8-4** below show the Pearson correlation coefficients between the binder chemical composition parameters and field performance for extracted binders with PAV cycles and extracted binders from the loose mixes, respectively. In the correlation analysis for field performance, the cracking indices Surface Rating and Deduct Value and the roughness indices ΔIRI correlate well with SARA at long-term mix aging levels, but not well for PAV aging protocols.

In the correlation analysis for different aging protocols, SARA fraction results show low correlation with long-term field performance at short-term mixture aging RPM and all PAV binder aging levels. However, SARA Friction shows a good correlation with crack and roughness field performance at mixture aging levels in terms of % resin, Paraffinic Index and Aromaticity Index. FT-IR test results show good correlations with field cracking performance for both mix and binder long-term aging protocols.

Comparison of compositional parameters shows that the sulfoxide ratio and carbonyl + sulfoxides are the most promising indicators for predicting field performance, particularly for cracking indices. These parameters consistently show strong negative correlations with TC-T, DV, and SR over several aging protocols, becoming particularly significant at the long-term aging levels: 6 h at 135°C and 9 days at 95°C, as well as 20 and 40 h. PAV. Percent Resins and Aromaticity Index from SARA analysis also show significant correlations, but only under two long-term mix aging levels.

Table 8-3: Pearson Coefficients between Field Performance and Chemical Composition Parameters for Loose Mix Aged Recovered Binder

Binder Properties		Field Performance at Aging Protocols											
		RPM				6 hrs at 135C				9 days at 95C			
		TC-T	DV	SR	ΔIRI	TC-T	DV	SR	ΔIRI	TC-T	DV	SR	ΔIRI
SARA)	Asphaltenes	0.1	-0.1	0.1	0.1	0.2	-0.4	0.4	0.5	-0.2	-0.5	0.5	0.3
	Resins	0.0	-0.2	0.1	0.1	-0.3	-0.7	0.8	0.4	-0.1	-0.2	0.1	0.5
	Aromatics	0.0	0.2	0.0	-0.1	0.0	0.6	-0.6	-0.6	0.1	0.4	-0.3	-0.4
	Saturates	-0.6	-0.1	-0.2	0.3	0.4	0.5	-0.4	0.4	0.4	0.6	-0.4	-0.5
	Colloidal Index	0.0	0.2	0.0	-0.1	-0.3	0.1	-0.2	-0.6	0.1	0.5	-0.5	-0.3
	Paraffinic Index	0.1	-0.2	0.1	0.1	-0.1	-0.6	0.6	0.4	-0.1	-0.4	0.4	0.4
	Aromaticity Index	0.0	0.2	0.0	-0.1	0.0	0.6	-0.7	-0.6	0.1	0.4	-0.3	-0.5
	Stability Index	0.1	-0.1	0.1	0.1	0.2	-0.3	0.4	0.5	-0.1	-0.5	0.5	0.3
FT-IR	Carbonyl Ratio	-0.1	-0.6	0.6	0.5	-0.1	-0.7	0.7	0.7	-0.2	-0.6	0.6	0.6
	Sulfoxide Ratio	-0.3	-0.3	0.1	-0.2	0.1	-0.5	0.5	0.2	-0.7	-0.4	0.2	-0.4
	Carbonyls + Sulfoxides	-0.3	-0.5	0.4	0.1	-0.1	-0.8	0.8	0.6	-0.4	-0.7	0.6	0.4

Table 8-4: Correlation coefficients between PAV aged binder properties and field performance

Binder Properties		Field Performance at Aging Protocols											
		20 hrs. PAV				40 hrs. PAV				60 hrs. PAV			
		TC-T	DV	SR	ΔIRI	TC-T	DV	SR	ΔIRI	TC-T	DV	SR	ΔIRI
SARA	Asphaltenes	0.0	-0.2	0.1	0.1	0.0	-0.2	0.2	0.1	0.1	-0.3	0.3	0.1
	Resins	0.7	0.2	-0.1	0.1	0.6	0.2	0.0	0.2	0.8	0.4	0.0	0.3
	Aromatics	-0.5	-0.1	0.0	-0.1	-0.4	-0.1	0.0	-0.2	-0.6	-0.1	-0.1	-0.3
	Saturates	-0.2	0.3	-0.3	0.2	-0.2	0.2	-0.5	-0.3	0.1	0.0	-0.2	-0.3
	Colloidal Index	0.0	0.1	0.0	-0.1	0.0	0.2	-0.1	-0.1	-0.1	0.3	-0.2	0.0
	Paraffinic Index	0.5	0.1	0.0	0.1	0.4	0.1	0.0	0.2	0.6	0.2	0.1	0.2
	Aromaticity Index	-0.5	-0.1	0.0	-0.1	-0.4	-0.1	0.0	-0.2	-0.6	-0.1	-0.1	-0.3
	Stability Index	0.0	-0.1	0.0	0.1	0.0	-0.2	0.2	0.1	0.1	-0.3	0.2	0.1
FT-IR	Carbonyl Ratio	-0.1	-0.6	0.6	0.5	-0.1	-0.6	0.7	0.6	-0.1	-0.7	0.7	0.6
	Sulfoxide Ratio	-0.7	-0.4	0.2	-0.5	-0.4	-0.6	0.5	0.1	-0.6	-0.6	0.4	-0.4
	Carbonyls + Sulfoxides	-0.4	-0.7	0.6	0.2	-0.3	-0.7	0.7	0.4	-0.4	-0.8	0.7	0.3

8.4.2 Correlation between Lab-Aged Mixture Properties and Long-Term Field Performance

Table 8-5 shows the Pearson Correlation Coefficients between various lab aged mixture properties and field performance indices at different aging levels. The general observation on field performance indices and aging levels shows the Deduct Value and Surface Rating have good correlation with certain mixture properties. Similarly, the field roughness performance, marked by changes in the International Roughness Index (ΔIRI), consistently correlates strongly with fatigue parameters, low-temperature cracking, and moisture resistance. It indicates that the overall cracking resistance captured in fatigue resistance, thermal cracking and moisture test have potential effect on the surface roughness of RA treated overlay.

In comparing aging protocols, RPM appears to be particularly effective in correlating field cracking performance with various parameters such as G-R_m, DR, DCT-PPI and TSR. In contrast, long-term aging protocols—6 hours at 135°C and 9 days at 95°C—do not generally show improved correlations for most mixture properties, with the notable exception of the FI from the I-FIT test. This index exhibits a stronger correlation with field conditions under both extended aging protocols than with the RPM, highlighting its potential utility in predicting long-term field performance. Specifically, after aging for 6 hours at 135°C aging, the FI, D^R and DCT-G_f exhibit a fairly good correlation with field cracking performance. After 7 days at 95°C LTA, G-R_m, FI, and D^R show a good correlation with field cracking performance.

Table 8-5: Correlation coefficients between loose mix aged mixture properties and field performance

Binder Properties		Field Performance at Aging Protocols											
		RPM				6 hrs. at 135C				9 days at 95C			
		TC-T	DV	SR	ΔIRI	TC-T	DV	SR	ΔIRI	TC-T	DV	SR	ΔIRI
Intermediate. Temperature Cracking	G-R_m	0.1	0.6	-0.6	-0.4	-0.3	-0.3	0.2	-0.2	0.2	0.5	-0.6	-0.5
	IFIT-FI	-0.1	-0.3	0.3	0.0	-0.5	-0.7	0.5	-0.1	-0.4	-0.5	0.5	0.6
	CT_{Index}	0.1	-0.4	0.4	0.2	-0.2	-0.5	0.4	0.0	NA	NA	NA	NA
Fatigue	D^R	-0.1	-0.6	0.6	0.8	0.1	-0.4	0.5	0.5	0.0	-0.3	0.4	0.4
	S_{app}	0.1	-0.4	0.5	0.5	0.2	-0.2	0.3	0.7	0.0	0.0	0.0	-0.1
Low Temperature Cracking	DCT-G_f	0.1	-0.3	0.5	0.7	-0.3	-0.5	0.5	0.6	0.3	0.1	0.0	0.6
	DCT-FST	0.2	-0.1	0.3	0.7	-0.2	-0.3	0.3	0.6	0.4	0.1	0.0	0.6
	DCT-PPI	0.1	-0.5	0.6	0.9	-0.2	-0.2	0.3	0.7	0.1	0.0	0.1	0.5
Moisture	TSR	-0.3	-0.6	0.6	0.8	0.8	0.5	-0.1	0.1	NA	NA	NA	NA

Chapter 9: Conclusions and Recommendations

This research project focused on testing and analysis of asphalt materials with different RA products to assess their impact on long-term performance. The main objective of this project was to evaluate how RAs impact various properties of asphalt mixtures containing RAP, as well as how the properties of the RA treated asphalt materials change over time. The study included field test sections with 40% RAP mixtures treated with seven different RAs and control sections containing 30% and 40% RAP. A comprehensive set of binder and mixture tests were conducted at various laboratory aging levels and on field cores taken annually over four years. The subsequent subsections provide summary tables, figures, and key findings based on the discussion and analysis presented in the previous chapters. Recommendations are also provided for future work.

The primary purpose of using RAs is to improve cracking resistance of mixtures with RAP. Therefore, the improvement in cracking resistance is a key focus when evaluating the effectiveness of RAs. The relationship shown in Equation 9.1 expresses the percent change in an index property due to the inclusion of RAs as compared to the control material. This approach to quantify effectiveness allows the effectiveness of RAs to be compared across different parameters and aging scales.

$$RA\ Effectiveness = \left(\frac{Index_{RA} - Index_{Control}}{Index_{Control}}\right) \times 100\% \tag{9.1}$$

9.1 Evaluation of RA Effect on Asphalt Binder

This section presents a comprehensive summary of the rheological properties, chemical composition, and functional groups as well as the change of these properties with different aging conditions. The evaluations are made by comparing the RA sections with respect to 40% Day 1 control. Numerous anomalies related to the rheological properties, chemical composition, and aging susceptibility of the 40% Day 2 control have been noted in previous sections of this report that could potentially bias the comparisons. The tables in this section summarize the sections that showed an improvement in properties over the controls. RA sections 6001-6007 have been labeled as 1, 2, 3, etc. The numbers in each cell identify the RA sections that showed improvement relative to 40% control for that property.

Improvement for each of the summarized parameters was defined as follows:

- Performance Grading
    - High temperature PG: Lower continuous grade (i.e., softening).
    - Intermediate temperature PG: Lower continuous grade.
    - Low temperature PG: Lower continuous grade.
- Rheological Parameters
    - R-Value: Lower R-Values represent better relaxation properties.
    - Glover Rowe (G-R): Lower value.
    - ΔT_c: Higher value, cracking risk increases as ΔT_c becomes more negative.
- Chemical Compositions
    - Colloidal Index: Higher value.
    - Carbonyl Ratio & Carbonyl + Sulfoxide Ratio: Lower value.

9.1.1 In-line sampled binder:

Table 6.1 below provides an overall summary of the effects of various RAs on the measured properties as compared to the base binders. The key findings are listed after the table.

Table 9-1 Summary of the RA Materials Showing Improvement Over Base Binders for In-line Sampled Binder Properties (numbers in table correspond to section numbers, 1 = 6001, 2 = 6002, etc.)

Properties/Parameters Compared to Corresponding Base Binder		Ori. Binder	Ori. Binder + RTFO	Ori. Binder + 40 hr PAV
Performance Grade (DSR)	PG	All	All	All
Rheological Properties (DSR)	R-value	All except for 5	All	All
	ΔTc	All	All	All
	G-R	All	All	All
Colloidal Index (SARA)	CI	All except for 7	All except for 7	All except for 1, 7
Functional Group Indices (FTIR)	Carbonyl ratio	None	None	None
	Sulfoxide ratio	All except for 4	All except for 4, 5	All except for 4, 5, 6

- All RA binders (6001-6007) met the project requirement of decreasing the PGLT of the base binder (-28°C) to -34°C. However, the PGHT for all the RA modified binders dropped 8-12°C (almost equivalent of two high-temperature performance grades) as compared to the base binder.
- The base binders sampled on the two production days (O1 and O2) generally have very similar properties. The base binder N (6007) has slightly different measured rheological parameters than the other two base binders.
- All RA binders (6001-6007) generally show improved rheological parameters as compared to the respective base binders after each aging condition (unaged, RTFO and 20 hrs. PAV).
- All RA binders (6001-6007) generally have a higher colloidal index and carbonyl ratio than the base binders at all aging conditions. RA binders 6004 and 6005 have a higher sulfoxide ratio than the base binder at all aging conditions.

9.1.2 Binders extracted and recovered from Production Mix

Table 9-3 and **Table 9-3** below provide an overall summary of the effects of different RAs on the measured performance grade, rheological properties, and chemical composition compared to the control materials.

Table 9-2 Summary of RA Materials Showing Improvement over Control Materials for Recovered Binder Properties after PAV Aging Cycles (numbers in table correspond to section numbers, 1 = 6001, 2 = 6002, etc.)

Comparison		Rec. Binder		Rec. Binder + 20 hr PAV		Rec. Binder + 40 hr PAV		Rec. Binder + 60 hr PAV	
Control Mixture		30% RAP	40% RAP	30% RAP	40% RAP	30% RAP	40% RAP	30% RAP	40% RAP
Performance Grade	PGHT	1,2,3,4,5	1,2,3,4,5	1,2,3,4,5	1,2,3,4,5,7	1,2,3,4,5	1,2,3,4,5,7	1,2,3,4,5	1,2,3,4,5,6
	PGIT	1,2,3,4,5,6	1,2,3,4,5,6	1,2,3,4,5,7	1,2,3,4,5,7	1,2,3,4,5,7	1,2,3,4, 5, 7	1, 2, 3, 4, 5, 7	1, 2, 3, 4, 5, 7
	PGLT	1,2,3,4,5,7	1,2,3,4,5,7	1,2,3,4,5,7	1,2,3,4,5,7	1,2,3,4,5	1,2,3,4,5,7	1,2,3,4,5,7	1,2,3,4,5
Rheological Properties	R-Value	1,2,3,4	1,2,3,4,5,7	2,3,4	All	1,2,3,4,5,6	1,2,3,4,5,6	1,2,3,4	1,2,3,4,5,6
	G-R	All	All	1,2,3,4,5	All	1,2,3,4,5	1,2,3,4,5,7	1,2,3,4,5	1,2,3,4,5
	ΔT_c	1,2,3	1,2,3,5	1,2,3	1,2,3,4,5	1,2,3	1,2,3,4,5	1,2,3,4	1,2,3,4
Chemical Composition	Colloidal Index	1,2,3,4	1,2,3,4	1,2,3,4	1,2,3,4	1,2,3,4	1,2,3	2,5	2,5
	Carbonyl Ratio	None	None	None	None	None	None	None	None
	Carbonyl + Sulfoxide Ratio	None	None	None	None	None	None	None	None

Table 9-3 Summary of RA Materials Showing Improvement over Control Materials for Recovered Binder Properties from Field Cores and Lab Aged Mixture (numbers in table correspond to section numbers, 1 = 6001, 2 = 6002, etc.)

Comparison		Field Core Yr 1		Field Core Yr 2		Field Core Yr 3*		Field Core Yr 4		6hrs. at 135C Loose Mix Aged		7days. at 95C Loose Mix Aged	
Control Mixture		30% RAP	40% RAP	30% RAP	40% RAP	30% RAP	40% RAP	30% RAP	40% RAP	30% RAP	40% RAP	30% RAP	40% RAP
Performance Grade	PGHT	All	All	1,3,4,5,6,7	1,3,4,5,6,7	1,3,4,5,6	1,3,4,5,6,7	1,2,3,4,5,6	1,2,3,4,5,6	1,2,3,4,5	All	3,5	3,5
	PHIT	All	All	All	All	1,3,4,5,6	1,3,4,5,6,7	All	All	All	All	1,3,5	3,5
	PGLT	All	All	All	All	1,3,4,5	1,3,4,5,6,7	All	All	All	All	1,3,5	3,5
Rheological Properties	R-Value	1,3,4,5,6	1,2,3,4,5,6	3,4,6,7	3,4,6,7	3,4,5,6	1,3,4,5,6	3,4,6	3,4,5,6	3,4	1,2,3,4,5	3	3,5
	G-R	All	All	All	All	1,3,4,5,6	1,2,3,4,5,6	1,2,3,4,5,6	1,2,3,4,5,6	1,2,3,4,5	All	1,2,3,4,5	1,2,3,4,5
	ΔT_c	1,3,4,5,6	All	2,3,4,5,6,7	2,3,4,5,6,7	1,3,4,5,6,7	1,3,4,5,6,7	3,4,6	3,4,6	1,3,4,5	1,2,3,4,5	3	3
Chemical Composition	Colloidal Index	None	None	1,3,5	1,3,5	3,5	3,5	3,6	6	3,4,5	1,2,3,4,5,6	None	5
	Carbonyl Ratio	None	None	All	All	All	1,4,5	All	2,4,6	None	None	None	None
	Carbonyl + Sulfoxide Ratio	None	None	None	None	None	2,5	2	2,3,6	None	None	None	None

**: Extracted and recovered from the test specimens.*

The comparison summarized in Table 9-2 provides a straightforward assessment of the effectiveness of RAs under the various aging conditions studied. The key findings are listed below:

- 60-hour PAV aging represents a higher level of aging than is currently required for product certification and was more extreme than the lab and field mix aging conditions studied to date.
- Overall sections 6001-6005 showed improvement relative to the controls for PG and R-Value. In most cases the improvements noted were consistent in comparison with both the 30% and 40% RAP controls.
- For durability parameters, the relevant comparisons are after the 40-hour and 60-hour PAV aging conditions. Results for all sections were below cracking warning/failure limits at less severe aging conditions.
- After extended aging the ΔT_c parameter was more discriminating as sections 6005 and 6007 were not identified as resulting in improvement in some cases. ΔT_c also eliminated Section 6004 and 6005 from the 30% RAP comparison after 40-hour PAV.
- Regarding composition, only the Colloidal Index provides a meaningful comparison. The Colloidal Index identified less RAs providing improvement, particularly at more severe aging. Data presented previously showed a broad range of initial Colloidal Index values that decreased with aging. After 60-hour PAV aging, most Colloidal Index values for controls and most RA modified binders were the same.
- The combined summary of chemical and physical properties demonstrated that binders with similar composition had different rheological/durability properties. Introduction of RAs causes an increase in carbonyl ratio and carbonyl +sulfoxide ratio relative to the controls. This was observed previously in stratification of the data sets when plotted against PAV aging time or a rheological parameter. Numerically, these ratios will not be lower than the controls for the RAs studied. However, the control and RA modified binders changed at similar rates with aging, particularly for carbonyl ratio.

Table 9-3 provides the comparison for laboratory aged loose mix (6 hours at 135°C) and field cores (Year 1 & 2).

- Overall, most of the RA sections resulted in improvements particularly for rheological and durability properties. The results are consistent with the concept that aging is needed to differentiate between RAs and the control.
- The RA sections were initially formulated at least one PG grade colder than the control, this softening effect remained through the field aging experienced to date. The data also suggested that the 6 hours 135°C loose mix aging procedure was not sufficient to differentiate RAs and the controls for the mixes used in this project.

9.1.3 Long-Term Evaluation of RA Effectiveness

Figure 9-1 to **Figure 9-3** show how the effectiveness of the 7 RAs studied changes with aging using representative binder parameters. Within each figure, the plots in the first row show the RA effectiveness with respect to the 30% control, and those in the second row are with respect to the 40% control. Positive values indicate improvement of the property with respect to the controls.

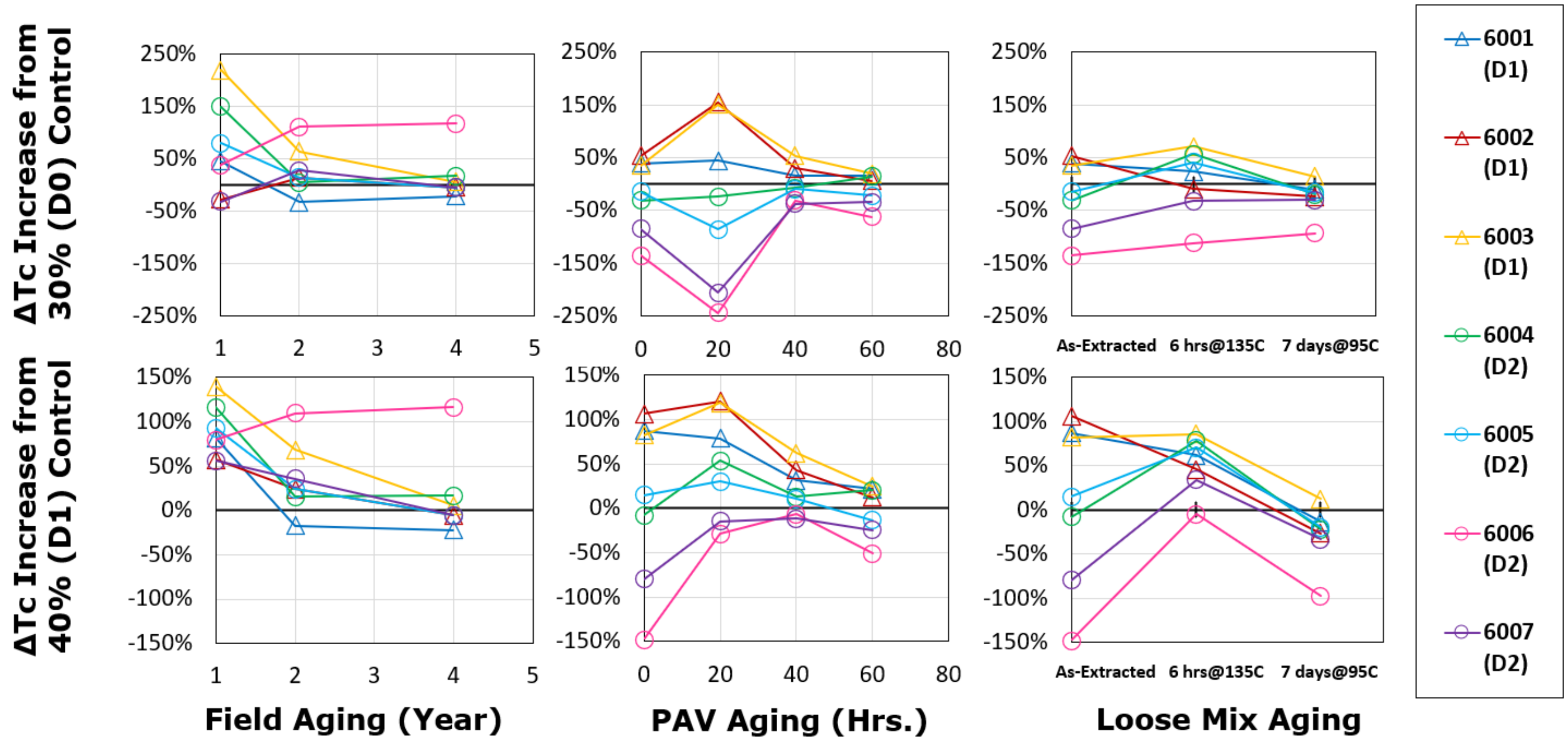

Figure 9-1 RA Effectiveness on ΔTc Parameter with Aging

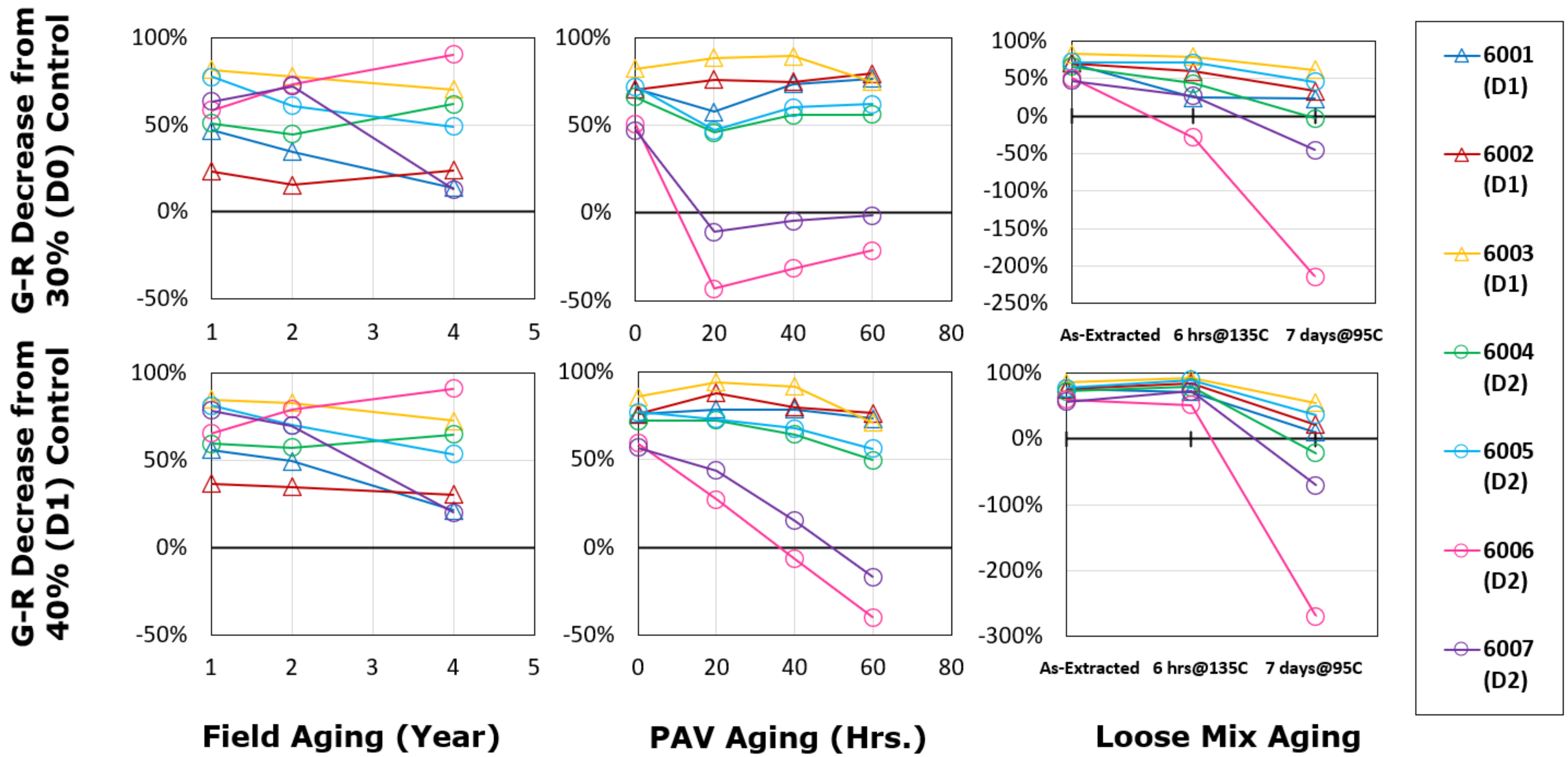

Figure 9-2 RA Effectiveness on G-R Parameter with Aging

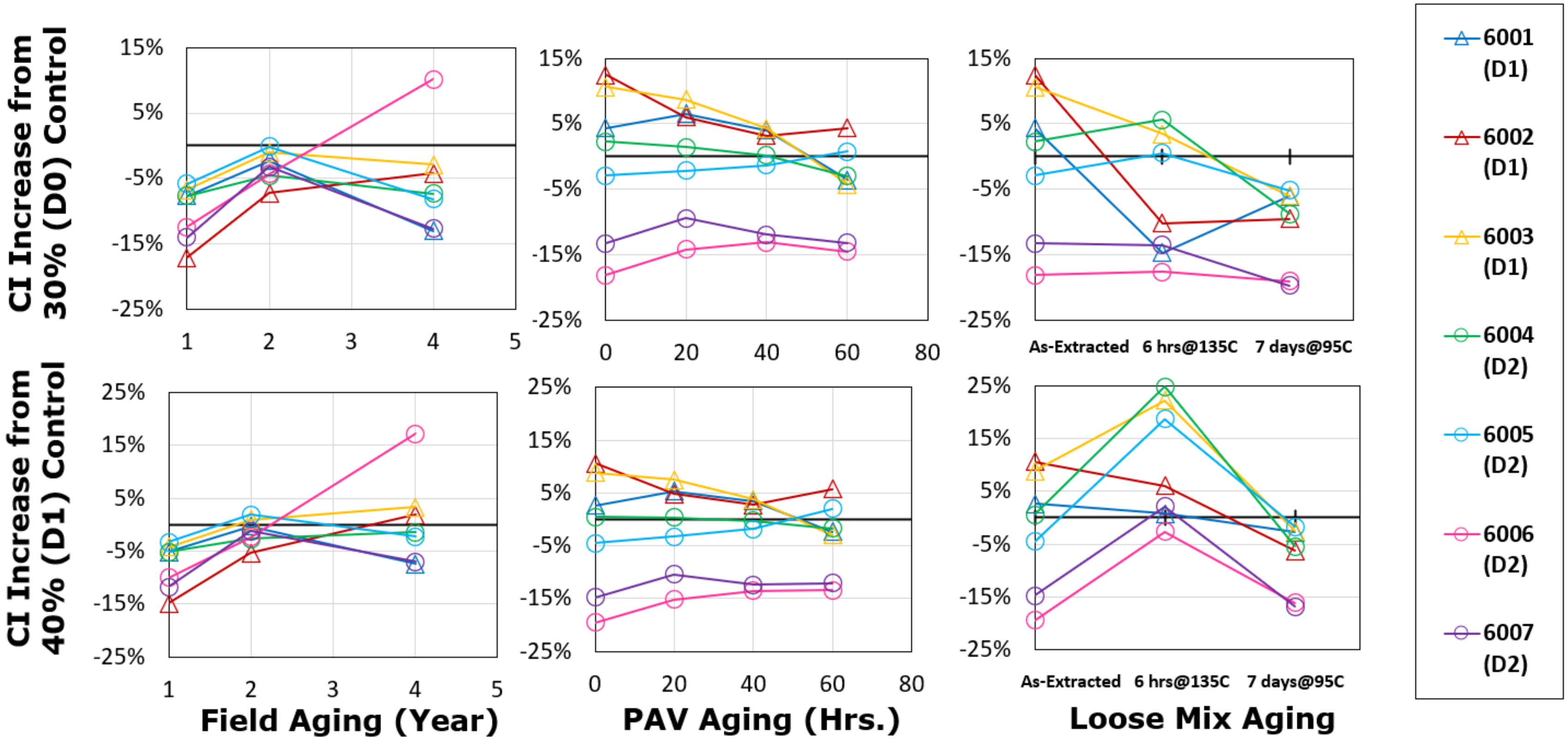

Figure 9-3 RA Effectiveness on Colloidal Index Parameter with Aging

9.2 Evaluation of RA Effect on Asphalt Mixture

The laboratory testing campaign included reheated plant produced mixtures, plant produced mixtures with laboratory conditioning of loose mixture for 6 hours at 135°C and 7 days at 95°C, and field cores taken from the test sections each year over 4 years of service. Testing includes the mixture E* test for rheological characterization, DTCF test for fatigue evaluation, TSR test for moisture susceptibility evaluation, and SCB (I-FIT) test, CT-Index and DCT test for investigation of the mixture fracture behavior at low and intermediate temperatures. In addition, the HWTT test was conducted for rutting characterization on the unaged mixtures.

9.2.1 RA Effect on Field Cores:

This subsection provides summary tables, figures, and key findings from the analysis of the mixture test results discussed in the previous chapters. **Table 9-4** illustrates that the RA mixtures have improved rheological properties, intermediate-temperature cracking, and fatigue properties when compared to the control mixtures at various aging levels. The summary table evaluates the effectiveness of RA at different aging levels by comparing the properties of the RA mixtures to those of the 30% control and 40% Day 1 control mixtures

- Rheological Parameters
  - Stiffness: Softer dynamic modulus.
  - Relaxation Capability: Higher phase angle modulus at intermediate temperature.
- Intermediate-temperature Cracking
  - Glover Rowe Mixture ($G\text{-}R_m$): Lower $G\text{-}R_m$ values.
- Fatigue Properties
  - D^R and S_{app} Parameter: Lower values.

Table 9-4 below provides an overall summary for the effects of various RAs on the measured properties of field cores, compared to the control field cores. The findings suggest that incorporating RAs typically enhanced the resistance of the mixtures to intermediate temperature cracking and fatigue cracking. This improvement can be attributed to the softening of the stiffness and the increased relaxation capability of the mixtures. However, after the field aging to the fourth year, the beneficial impact of some RAs on cracking property diminishes. These observations are particularly noteworthy in relation to the relaxation capacity, $G\text{-}R_m$, and fatigue parameters.

Table 9-4 Summary of RA Materials Showing Improvement over Control Materials for Field Core Properties (numbers in table correspond to section numbers, 1 = 6001, 2 = 6002, etc.)

Comparison		1-Year FC		2-Year FC		3-Year FC		4-Year FC	
Control field core		30% RAP	40% RAP	30% RAP	40% RAP	30% RAP	40% RAP	30% RAP	40% RAP
Rheological properties	Stiffness	1,3,4, 5,6,7	All	1,3,4, 5,6,7	1,3,4, 5,6,7	1,3,4,5,6	All	1,3,4, 5,6	1,3,4,5,6,7
	Relaxation Capability	1,3,4, 5,6,7	All	1,3,4,5,6	All	1,3,4,5	All	1,3,5	1,3,4,5,6
Intermediate-temperature cracking	G-Rm	All	All	All	All	All	All	1,3,4,5,6	All
Fatigue properties	DR	All	1,3,4, 5,6,7	1,3,4, 5,6,7	1,3,4,5,6,7	1,3,5, 6,7	1,3,4, 5,6,7	All	1,3,4,5,6,7
	Sapp	4,5,6,7	All	1,6,7	1,4,6,7	1,5,7	1,4,5, 6,7	1,4,5	1,4,5

9.2.2 RA Effect on Mixtures

Table 9-5 below summarizes the effects of various RAs on the asphalt mixes under different loose mix aging conditions.

Table 9-5 Summary of RA Materials Showing Improvement over Control Materials for Mixture Properties (numbers in table correspond to section numbers, 1 = 6001, 2 = 6002, etc.)

Comparison		RPM		6 hrs. at 135°C LTA		7days at 95°C LTA.	
Control Mixture		30% RAP	40% RAP	30% RAP	40% RAP	30% RAP	40% RAP
Rheological Properties	Stiffness	All	All	1,2,3	1,2,3,6	1,2,3,4,5	1,2,3,4,5
	Relaxation Capability	All	All	1,2,3	1,2,3	1,2,3,4,5	1,2,3,4,5,7
Intermediate-temperature Cracking	G-Rm	All	All	1,2,3	1,2,3,6	1,2,3,4,5,7	1,2,3,4,5
	CT Index	1,3,4,5	1,3, 4, 5	1,2,3,4,5	1,2,3,4,5	NA[1]	NA
	FI	1,2,3,4,5,6	All	1,3,4,5,6,7	All	1,2,3,4,5	1,2,3,4,5
Fatigue Properties	DR	All	All	All	All	All	1,3,4,5,6,7
	Sapp	1,2,5,7	1,2,4,5,6,7	1,2,3,4,5,6	1,2,3,4,5,6	4,5,6,7	All
Low-temperature Cracking	Gf	All	5	All	All	1,2,5	5
	FST	1,2,3,4,5,6	1,5	1,2,3,5	1,2,3,4,5,6	1,2,3,4,5,6	1,2,3,4,5,6
	PPI	1,2,3,4,5,6	1,2,5	1,2,3,5,6	1,2,3,4,5,6	1,2,5	1,5
Rutting	HWTT Passes	7	None	NA		NA	
Moisture Resistance	TSR	1,2,3,5,7	1,2,3,5,7	1,2,3,4,5,6	5	NA	NA

Under the RPM condition, the results indicate that the inclusion of RAs generally improves the rheological properties of the aged mix in terms of stiffness and relaxation capability. The medium- and low-temperature

[1] NA: testing not conducted

fracture resistance as measured by G-R_m, CT_{index}, FI and PPI, and moisture resistance is consistently improved. The results indicate that the inclusion of RAs generally improves all the cracking properties of the mixture. With the long-term aging, all the cracking properties indicate that the RA materials lose some of their effectiveness.

- **Rheological Properties**: all RA materials demonstrate improved stiffness and relaxation properties over the control sections under RPM conditions. However, RA 6006 and 6007 exhibit a loss in effectiveness after long-term aging. RA 6001, 6002, and 6003 consistently show improvements over the control under both aging protocols. Conversely, RA 6004 and 6005 improve under the 7-day at 95°C LTA protocol, but their effectiveness diminishes under the 6-hour at 135°C LTA condition.
- **Intermediate-Temperature Fracture and Fatigue Resistance:** Most RA sections, except for 6002 and 6007, show improvement over the control under RPM conditions. After long-term aging, RA 6006 and 6007 lose their effectiveness. Meanwhile, RA 6001, 6002, 6003, 6004, and 6005 continue to exhibit improvements over the controls, aligning with the observations of rheological properties.
- **Low-Temperature Fracture Properties:** The 30% and 40% RAP controls display significantly different results. Under RPM conditions, most RA sections, except for 6007, demonstrate enhanced fracture properties compared to the 30% RAP control. After long-term aging, RA 6001, 6002, 6003, and 6005 consistently show improvement over the controls under the 6-hour at 135°C LTA condition. Furthermore, RA 6001 and 6005 continue to show consistent improvement over controls after the 7-day at 95°C LTA.

9.2.3 RA Effect on Field Performance

Table 9-6 provides a summary of the effects of various reclaimed asphalts (RAs) on pavement performance over time, spanning from 1 to 4 years. It highlights that the 30% RAP control section outperforms all RA-treated sections in terms of cracking resistance over four years, whereas the 40% RAP control section exhibits more severe cracking than all RA sections. In terms of rutting, there was a short-term reduction in performance due to the softening effect of RA; however, specific RA-treated sections, such as 6003 and 6007, demonstrated better rutting resistance than both control sections after four years. Additionally, parts of RA (6001, 6002, 6003, and 6005) improved the ride quality, showing lower International Roughness Index (IRI) values than the control sections over three years, likely due to enhanced crack resistance, which contributed to smoother surface conditions. Despite these improvements, it is noted that the overall transverse cracking resistance, although improved over the 40% RAP control, did not reach the performance levels of the 30% RAP control. Furthermore, the overall riding quality and rutting performance remained in very good condition, with the sections far from requiring maintenance. It is important to note that the RAs were only applied in the 1.5-inch wearing course at the top of the testing sections, which significantly influences surface performance measurements like IRI. However, the transverse cracking performance, influenced by factors like thermal and reflective cracking, depends on the entire pavement structure and the material properties of all layers, not just the wearing course.

Table 9-6 Summary of RA Materials Showing Improvement over Control Materials for Pavement Performance (numbers in table correspond to section numbers, 1 = 6001, 2 = 6002, etc.)

Comparison		1-Year FC		2-Year FC		3-Year FC		4-Year FC	
Control Pavement Section		30% RAP	40% RAP	30% RAP	40% RAP	30% RAP	40% RAP	30% RAP	40% RAP
Cracking Performance	Length of Cracking	None	1,2,3, 5,6,7	None	All	None	All	None	All
	Transverse Cracking Index	None	All	None	1,2,3, 5,6,7	None	1,2,3, 5,6,7	None	1,2,3, 5,6,7
Rutting Performance	Rutting Depth	1,3,7	None	1,3,7	None	None	None		
Riding Quality	IRI	All	1,2,3, 5,6	All	1,2,3, 5,6	6	1,2,3, 4,5,6		

9.2.4 Long-Term Evaluation of RA Effectiveness

Figure 9-4 to Figure 9-6 show how the effectiveness of the 7 RAs studied changes over time on representative parameters for rheological properties, intermediate-temperature, and low-temperature fracture properties, respectively. Within each subplot, the two plots in the first row show the RA effectiveness with respect to the 30% control and the second plots with respect to the 40% control. The plots in the left column show the effectiveness over field aging time, while the plots in the right column show the RA effectiveness over laboratory aging protocols. The horizontal axis represents the performance level of 30% RAP or 40% RAP control, when the curves show positive values indicates the improvement on the properties.

Figure 9-4 shows that RA effectiveness on rheological properties remains relatively stable over 4 years although 6002 and 6007 are approaching the controls, indicating consistent performance in real-world conditions. In contrast, laboratory aging at both LTA protocols shows a significant decline in RA effectiveness. This suggests that 4 years of field aging is not enough to substantially differentiate RA rheological properties. This observation highlights the need to consider increasing the field monitoring time when evaluating the long-term performance of RAs in pavement rheological properties.

Figure 9-5 and Figure 9-6 show the RA effectiveness on intermediate-temperature and low-temperature fracture properties, respectively. The results indicate that the RA effectiveness on the intermediate-temperature fracture generally does not decrease with aging. However, some RA will lose effectiveness on low-temperature fracture properties after 7 days at 95°C aging protocols.

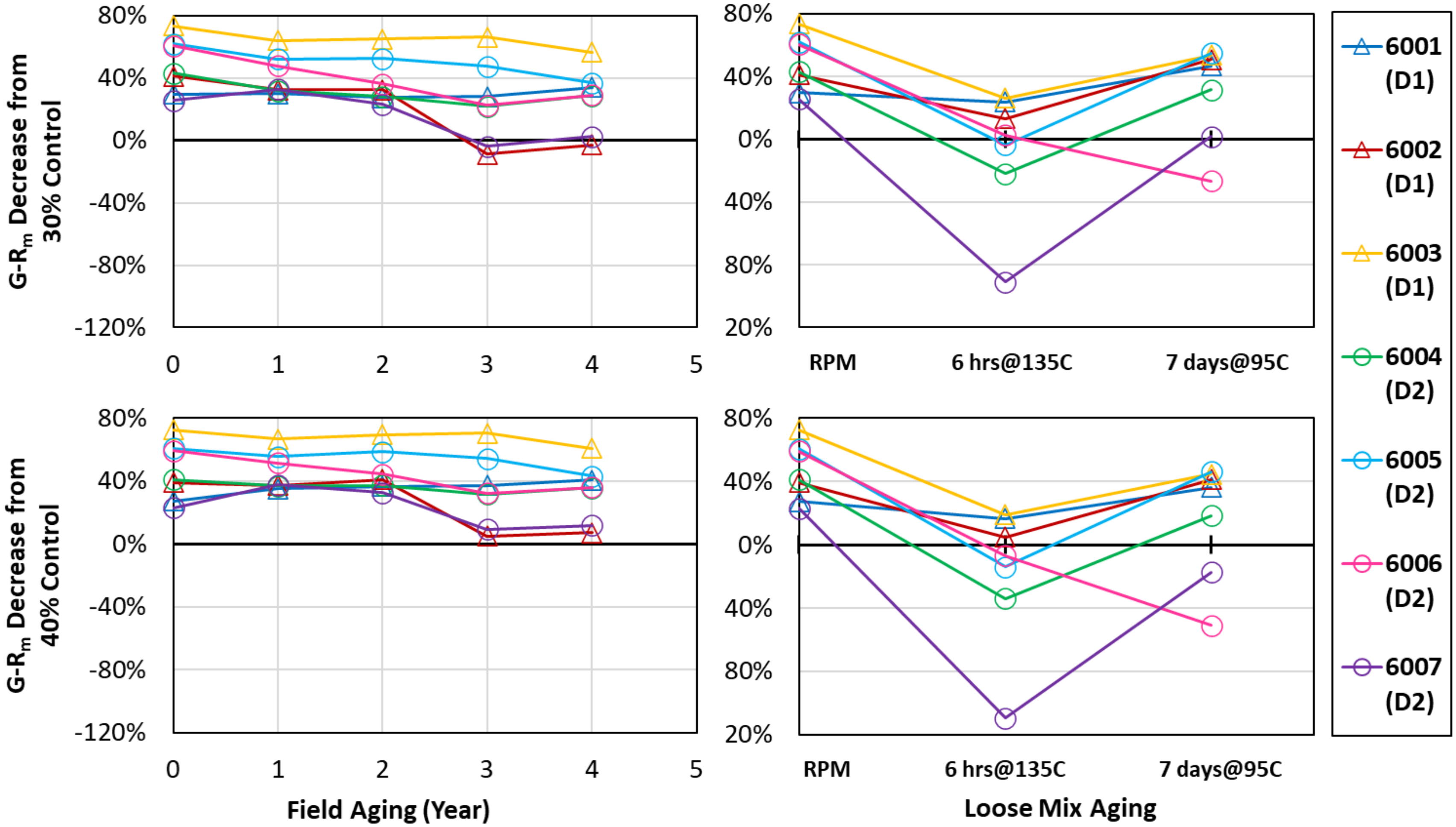

Figure 9-4 RA Effectiveness on G-R_m Parameter with Aging

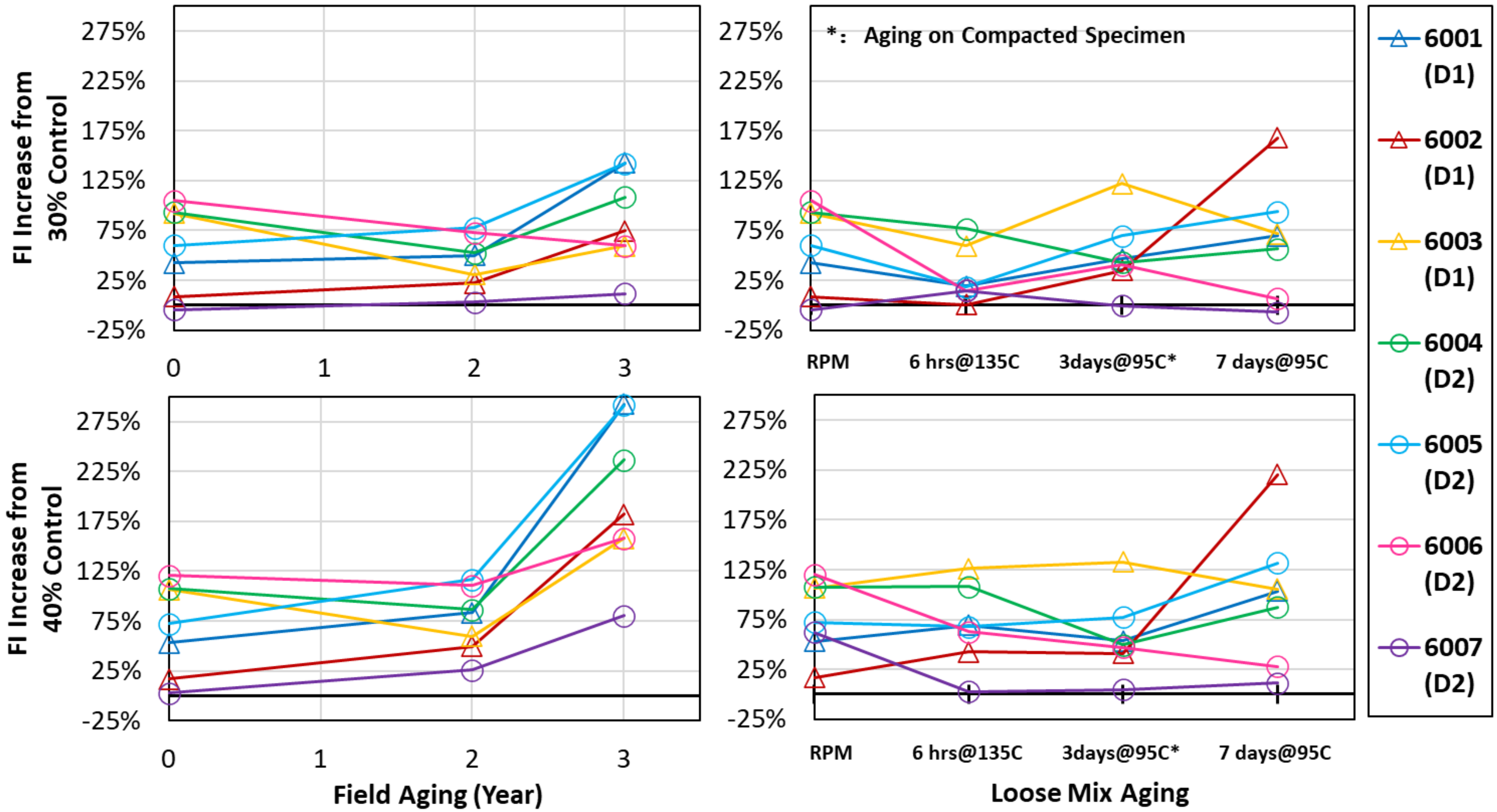

Figure 9-5 RA Effectiveness on FI Parameter with Aging

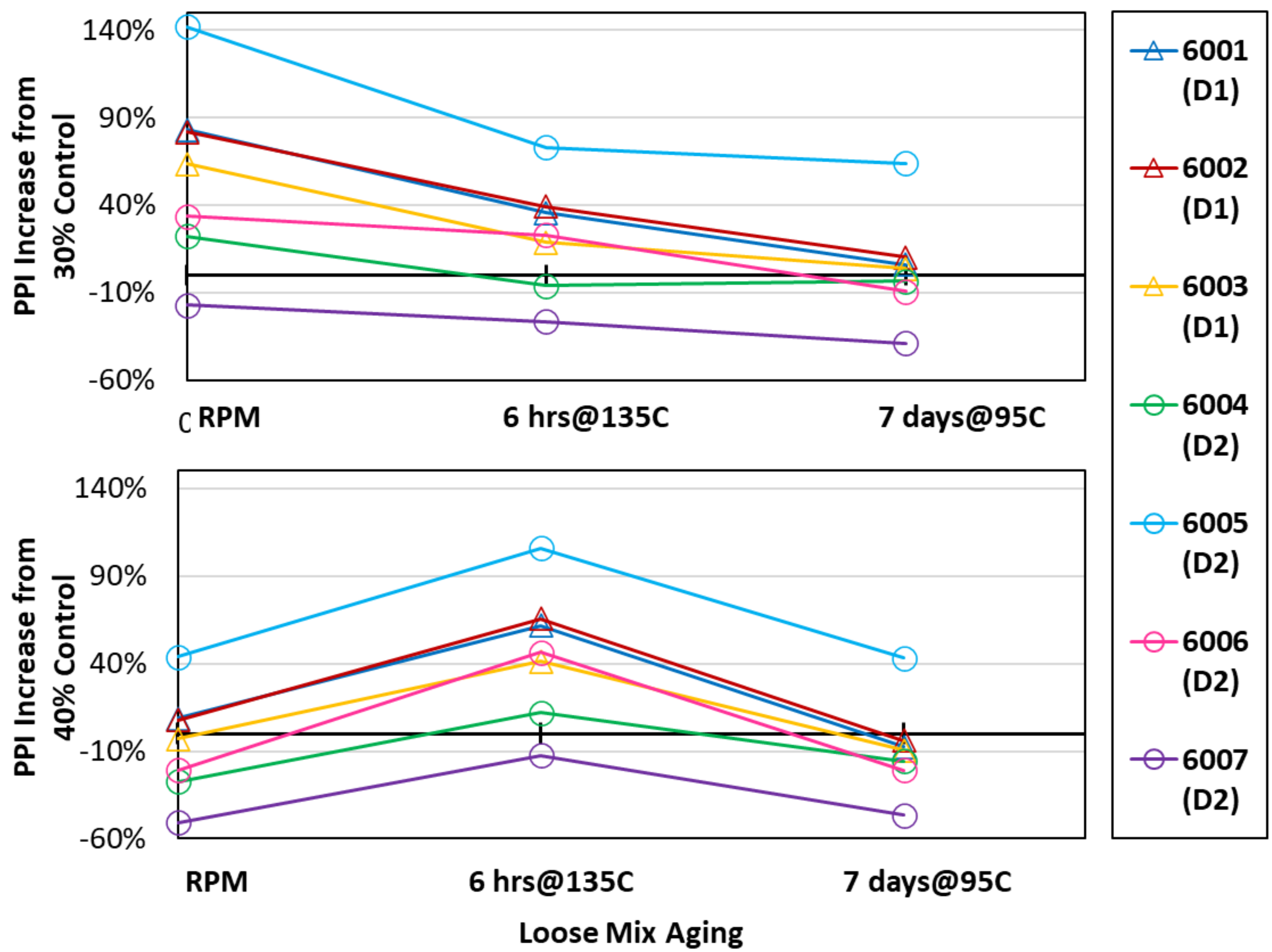

Figure 9-6 RA Effectiveness on PPI Parameter with Aging

9.3 Key Findings

Significant findings from this research include a detailed examination of the effects of reclaimed asphalt (RA) on binder properties, mixture properties, and field performance. The study shows that all RAs exhibit improved rheological properties in 1-year field cores. However, the benefits of RA diminish with field aging, and after four years, some RAs show comparable properties with controls. It is noted that RAs inherently have higher carbonyl ratios than controls, and this baseline ratio varies among different RAs.

In terms of mixture properties, the inclusion of RA enhances both rheological properties and fracture and fatigue crack resistance initially. These benefits decrease with both laboratory and field aging. After four years or extended aging of loose mixes, some RAs lose their improvement in crack resistance and perform comparably to the 30% control.

Regarding field performance, distress in the first four years is primarily composed of transverse cracking. Only a few instances of longitudinal cracking appeared in the fourth year. The ride quality and rutting values are minimal. Based on four years of collected cracking performance data, all RAs have demonstrated some improvement in transverse crack resistance compared to the 40% RAP control, but they have not reached the performance level of the 30% control. While all RAs show slightly higher rut depths than control sections, the degradation in ride quality and rutting after four years is not significant enough for a comparative analysis. Overall, four years of field data are insufficient to clearly differentiate performance among different RAs.

With respect to long-term aging protocols, the trend of laboratory aging results is consistent with field observations, as RA-treated mixes show a gradual reduction in cracking properties over time, indicating a diminishing effectiveness of RAs. With respect to the laboratory aging protocols, the 6 hours at 135°C loose mix protocol approximates the aging effects typically observed after approximately 2 to 4 years in the field. In contrast, the 7 days at 95°C loose mix protocol results in more severe aging than that observed with 4 years of field aging.

Regarding Lab-Field Correlations, both the monitored mixture cracking parameter D^R, S_{app} and G-R_m from field cores show a fairly good correlation with field cracking performance. Among binder properties, the cracking properties ΔT_c and G-R parameter, as well as rheological properties like R-Value and glassy modulus, outperform PG grading and exhibit a more significant correlation with field thermal cracking performance. Compared to the physical binder properties, chemical composition parameters show less correlation with field performance. However, %resin and %aromatics demonstrate potential correlation with thermal cracking performance.

The main distress type in the first four years for the studied test sections is transverse cracking, with longitudinal cracking expected to accumulate in the following years. The long-term effects of RAs on pavement rutting and roughness remain unclear. Therefore, extended field performance monitoring is required to effectively distinguish performance between RA sections in terms of different performance (thermal cracking, fatigue cracking, rutting and roughness). This extended monitoring will also facilitate the identification of reliable testing parameters and laboratory aging protocols that best simulate actual field conditions. Extended field performance data will be crucial in differentiating the long-term effects of various RAs and improving the reliability of lab-field correlations for predicting pavement performance.

References

Adams, J., Elwardany, M., Planche, J-P. Boysen, R. & Rovani, J.}, (2019). Diagnostic techniques for various asphalt refining and modification methods. *Energy Fuels,* 33(4*:* 2680-2698. https://doi.org/10.1021/acs.energyfuels.8b03738.

Ali, H., & Mohammadafzali, M. (2015). *Long-term aging of recycled binders* (No. BDV29 Two 977-01). Florida. Dept. of Transportation. Research Center. https://rosap.ntl.bts.gov/view/dot/29514

Anderson, M. (1991). Using the multiple-stress creep-recovery (MSCR) test. Paper presented at the Association of Modified Asphalt Producers Annual Meeting, Savannah, GA, February 2–3, Avon, OH. (Paper available online to members)

Anderson, M., King, G., Hanson, D., & Blankenship, P. (2011). Evaluation of the Relationship between Asphalt Binder Properties and Non-Load Related Cracking. *Journal of the Association of Asphalt Paving Technologists*, 615-663.

Andriescu, A., & Hesp, S. A. (2009). Time–temperature superposition in rheology and ductile failure of asphalt binders. *International Journal of. Pavement Engineering., 10*(4) 229–240.

Andriescu, A., Iliuta, S., Hesp, S.A., & Youtchef, J.S. (2004). Essential and Plastic Works of Ductile Fracture in Asphalt Binders and Mixtures. *Proceedings of the. Canadian Technical Asphalt Association, 49,* 93–121.

Apostolidis, P., Liu, X., Erkens, S., & Scarpas, A. (2019) Evaluation of epoxy modification in bitumen, *Construction and Building Materials,* 208: 361-368, ISSN 0950-0618, https://doi.org/10.1016/j.conbuildmat.2019.03.013.

Arámbula-Mercado, E., Kaseer, F., Martin, A. E., Yin, F., & Cucalon, L. G. (2018). Evaluation of recycling agent dosage selection and incorporation methods for asphalt mixtures with high RAP and RAS contents. *Construction and Building Materials*, 158, 432-442.

Arnold, T. (2017). What's in Your Asphalt? *Public Roads, 2017* (Sept.), 14–19.

Barborak, R. C., Coward, C. E., & Lee, R. E. (2016). Detection and estimation of re-refined engine oil bottoms in asphalt binders: Texas Department of Transportation's approach with wavelength dispersive x-ray fluorescence spectroscopy. *Transportation Research Record*, *2574*(1), 48-56. https://doi.org/10.3141/2574-05

Barghabany, P., Zhang, J., Mohammad, L., Cooper, S., & Cooper, S. (2022). Effect of laboratory aging levels on asphalt binder chemical/rheological properties and fracture resistance of asphalt mixtures. *Journal of Materials in Civil Engineering, 34* (3) https://doi.org/10.1061/(ASCE)MT.1943-5533.0004126

Canto, L. B., Mantovani, G. L., Deazevedo, E. R., Bonagamba, T. J., Hage, E., & Pessan, L. A. (2006). Molecular characterization of styrene-butadiene-styrene block copolymers (SBS) by GPC, NMR, and FTIR. *Polymer Bulletin*, *57*(4), 513-524.

Carpenter, S. H., & Wolosick, J. R. (1980). Modifier influence in the characterization of hot-mix recycled material. *Transportation research record*, (777). Transportation Research Board, National Research Council, Washington, DC, pp. 15-22

Chen, M., Leng, B., Wu, S., & Sang, Y. (2014). Physical, chemical and rheological properties of waste edible vegetable oil rejuvenated asphalt binders. *Construction and Building materials*, *66*, 286-298.

Christensen, D. W., & Tran, N. (2022). *Relationships Between the Fatigue Properties of Asphalt Binders and the Fatigue Performance of Asphalt Mixtures.* Washington, D.C.: National Academy of Sciences.

Christensen, D., Mensching, D., Rowe, G., Anderson, R. M., Hanz, A., Reinke, G., & Anderson, D. (2019). Past, present, and future of asphalt binder rheological parameters: Synopsis of 2017 Technical Session 307 at the 96th Annual Meeting of the Transportation Research Board. *Transportation Research Circular*, (E-C241).

Churchill, E. V., Amirkhanian, S. N., & Burati Jr, J. L. (1995). HP-GPC characterization of asphalt aging and selected properties. *Journal Of Materials in Civil Engineering*, *7*(1), 41-49.

Claudy, P., Letoffe, J. M., King, G. N., & Plancke, J. P. (1992). Characterization of asphalts cements by thermomicroscopy and differential scanning calorimetry: Correlation to classic physical properties. *Fuel Science & Technology International*, *10*(4-6), 735-765.

Claudy, P., Letoffe, J. M., King, G. N., Planche, J. P., & Brule, B. (1991). Characterization of paving asphalts by differential scanning calorimetry. *Fuel Science & Technology International*, *9*(1), 71-92.

Clopotel, C. S., Velasquez, R., Bahia, H. U., Pérez-Jiménez, F., Miró, R., & Botella, R. (2012). Relationship between binder and mixture damage resistance at intermediate and low temperatures. *Transportation Research Record*, 2293(1), 39-47. https://doi.org/10.3141/2293-05

Cong, P., Guo, X., & Mei, L. (2020). Investigation on rejuvenation methods of aged SBS modified asphalt binder. *Fuel*, *279*, 118556.

Cong, P., Wang, J., Zhou, Z., & Zhang, H. (2020) Preparation of rejuvenating agent and property evaluation of rejuvenated SBS modified asphalt binders, *Construction and Building Materials*, 233, 117911.

Cotterell, B., & Reddel, J. K.. (1977). Essential Work of Plane Stress Fracture. *International Journal of Fracture 13*(3) 267–277.

Daly, W. H., Negulescu, I., & Balamurugan, S. S. (2013). *Implementation of GPC Characterization of Asphalt Binders at Louisiana Materials Laboratory* (No. FHWA/LA. 13/505). Louisiana. Dept. of Transportation and Development.

Daryaee, D., Habibpour, M., Gulzar, S., & Underwood, B. S. (2021). Combined effect of waste polymer and rejuvenator on performance properties of reclaimed asphalt binder. *Construction and Building Materials*, *268*, 121059.

Derjaguin, B.V., Muller, V.M., & Toporov, Y.P. (1975) Effect of contact deformations on the adhesion of particles, *Journal of Colloid and Interface Science*: 53(2): 314-326, ISSN 0021-9797, https://doi.org/10.1016/0021-9797(75)90018-1.

DiBenedetto, A.T. (1987), Prediction of the glass transition temperature of polymers: A model based on the principle of corresponding states. *Journal of Polymer Science, Part B: Polymer Physics* 25: 1949-1969. https://doi.org/10.1002/polb.1987.090250914.

Dourado, E. R., Simao, R. A., & Leite, L. F. M. (2012). Mechanical properties of asphalt binders evaluated by atomic force microscopy. *Journal of Microscopy*, *245*(2), 119-128.

Elkashef, m., Williams, R.C. & Cochran, E.W. (2019) Thermal and cold flow properties of bio-derived rejuvenators and their impact on the properties of rejuvenated asphalt binders, *Thermochimica Acta* 671: 48-53, ISSN 0040-6031, https://doi.org/10.1016/j.tca.2018.11.011.

Elwardany, M. D., Planche, J.-P., & Adams, J. J. (2019). Determination of binder glass transition and crossover temperatures using 4-mm plates on a dynamic shear rheometer. *Transportation Research Record*, 2673(10): 247-260. https://doi.org/10.1177/0361198119849571.

Epps Martin, A., Kaseer, F., Arámbula-Mercado, E., Bajaj, A., Cucalon, L. G., Yin, F., Chowdhury, A, Epps, J., Glover, C., Hajj, E.Y., Morian, N., Daniel, J.S., Oshone, M., Rahbar-Rastegar, R., Ogbo, C. & King, G. (2020). *Evaluating the Effects of Recycling Agents on Asphalt Mixtures with High RAS and RAP Binder Ratios (NCHRP Research Report 927)*. Washington, DC: The National Academies Press. https://doi.org/10.17226/25749.

Epps, J. A., & Holmgreen, R. J. (1980). *Design of Recycled Asphalt Concrete Mixtures (Report 214-22).* Texas Transportation Institute: College Station, Texas https://static.tti.tamu.edu/tti.tamu.edu/documents/214-22.pdf

Erskine, J. A. Hesp, S.A. & Kaveh, F (2012). Another look at accelerated aging of asphalt cements in the pressure aging vessel (P5EE-202) *in Proceedings of the 5th Eurasphalt and Eurobitume Congress,* Istanbul, Turkey.

Feng, Z. G., Bian, H. J., Li, X. J., & Yu, J. Y. (2016). FTIR analysis of UV aging on bitumen and its fractions. *Materials and Structures*, *49*, 1381-1389.

Fischer, H., Stadler, H., & Erina, N. (2013). Quantitative temperature-depending mapping of mechanical properties of bitumen at the nanoscale using the AFM operated with PeakForce TappingTM mode. *Journal of Microscopy*, *250*(3), 210-217.

Geng, J., Li, H., & Sheng, Y. (2014). Changing regularity of SBS in the aging process of polymer modified asphalt binder based on GPC analysis. *International Journal of Pavement Research and Technology*, *7*(1), 77.

Gong, M., Yang, J., Zhang, J., Zhu, H., & Tong, T. (2016). Physical–chemical properties of aged asphalt rejuvenated by bio-oil derived from biodiesel residue. *Construction and Building Materials*, *105*, 35-45..

Gulmine, J. V., Janissek, P. R., Heise, H. M., & Akcelrud, L. (2002). Polyethylene characterization by FTIR. *Polymer testing*, *21*(5), 557-563.

Hansen, K., Newcomb, D., & Cervarich, M. (2011). Asphalt tops the charts for environmental stewardship-again. *HMAT: Hot Mix Asphalt Technology*, *16*(5).

Haghshenas, H.F., Nabizadeh, H., Kim, Y-R., & Santosh, K. (2016) Research on high-RAP asphalt mixtures with rejuvenators and WMA additives, *Nebraska Department of Roads Research Report*. Report SPR-P1(15) M016.

Hanz, A., & Reinke, G. (2016, August). Extended Aging of RAS Mixes with Rejuvenator. In *Binder expert Task Group Meeting* (pp. 1-41).

Harrison, I. R., Wang, G., & Hsu, T. C. (1992). *A differential scanning calorimetry study of asphalt binders* (No. SHRP-A/UFR-92-612), Washington, DC: National Academy of Sciences

Hesp, S. A., & Shurvell, H. F. (2010). X-ray fluorescence detection of waste engine oil residue in asphalt and its effect on cracking in service. *International Journal of Pavement Engineering*, *11*(6), 541-553.

Hesp, S. A., Iliuta, S., & Shirokoff, J. W. (2007). Reversible aging in asphalt binders. *Energy & Fuels*, *21*(2), 1112-1121.

Hesp, S., Johnson, K-A., Mcewan, R., Kumar, S., Samy, S., K., Ritchie, S., & Thomas, M. (2014). Effect of ten commercial warm mix additives on the quality and durability of cold lake asphalt cement. *International Journal of Pavements*, *13* (1), 1–11.

Hintz, C., Velasquez, R., Johnson, C., & Bahia, H. (2011). Modification and validation of linear amplitude sweep test for binder fatigue specification. *Transportation Research Record*, *2207*(1), 99-106.

Hofko, B., et al. (2017). Repeatability and sensitivity of FTIR ATR spectral analysis methods for bituminous binders, *Materials and Structures*, 50(3), pp.1-15.

Holmgreen Jr, R. J., Epps, J. A., Little, D. N., & Button, J. A. (1982). Recycling agents for recycled bituminous binders-executive summary. Final report Sep 78-Dec 80 (No. PB-83-168823). Texas Transportation Inst., College Station (USA).

Horan, B. (2011). Multiple stress creep recovery (MSCR) Task Force. Paper presented at the Southeastern Asphalt User/Producer Group (SEAUPG) Meeting, Savannah, GA, November 11–17.

Hossain, Z., Roy, S., & Rashid, F. (2020). Microscopic examination of rejuvenated binders with high reclaimed asphalts. *Construction and Building Materials*, *257*, 119490.

Huang, W., Guo, Y., Zheng, Y., Ding, Q., Sun, C., Yu, J., Zhu, M & Yu, H. (2021). Chemical and rheological characteristics of rejuvenated bitumen with typical rejuvenators. *Construction and Building Materials*, *273*, 121525

Im, S., & Zhou, F. (2014). *Field performance of RAS test sections and laboratory investigation of impact of rejuvenators on engineering properties of RAP/RAS mixes* (No. FHWA/TX-14/0-6614-3). Texas. Dept. of Transportation. Research and Technology Implementation Office. https://rosap.ntl.bts.gov/view/dot/27281/dot_27281_DS1.pdf

Jahangir, R., Little, D., & Bhasin, A. (2015). Evolution of asphalt binder microstructure due to tensile loading determined using AFM and image analysis techniques. *International Journal of Pavement Engineering*, *16*(4), 337-349.

Jiménez-Mateos, J. M., Quintero, L. C., & Rial, C. (1996). Characterization of petroleum bitumens and their fractions by thermogravimetric analysis and differential scanning calorimetry. *Fuel*, *75*(15), 1691-1700.

Johnson, K. A. N., & Hesp, S. A. (2014). Effect of waste engine oil residue on quality and durability of SHRP materials reference library binders. *Transportation research record*, *2444*(1), 102-109.

Kamal, M. R., & Sourour, S. (1973). Kinetics and thermal characterization of thermoset cure. *Polymer Engineering & Science*, *13*(1), 59-64.

Kandhal, P. S., & Mallick, R. B. (1998). Chapter 7: Hot Mix Asphalt Recycling (Materials and Mix Design) in Pavement Recycling Guidelines for State and Local Governments: Participants Reference Book. (FHWA-SA-98,0*42*. https://rosap.ntl.bts.gov/view/dot/33835

Kari, W. J. (1980). Prevention And Control of Reflective Cracking, Introduction and Definition. In *Proceedings Association of Asphalt Paving Technologists* (Vol. 49, p. 267).

Karki, P., & Zhou, F. (2016). Effect of rejuvenators on rheological, chemical, and aging properties of asphalt binders containing recycled binders. *Transportation Research Record*, 2574(1), 74-82.

Karlsson, R., & Isacsson, U. (2003). Application of FTIR-ATR to characterization of bitumen rejuvenator diffusion. *Journal of Materials in Civil Engineering*, *15*(2), 157-165.

Karlsson, R., Isacsson, U., & Ekblad, J. (2007). Rheological characterisation of bitumen diffusion. *Journal of materials science*, *42*, 101-108.

Kaseer, F., Cucalon, L. G., Arámbula-Mercado, E. D. I. T. H., Martin, A. E., & Epps, J. (2018). Practical tools for optimizing recycled materials content and recycling agent dosage for improved short-and long-term performance of rejuvenated binder blends and mixtures. *Journal of the Association of Asphalt Paving Technologists,* 87, 513-550.

Kaskow, J., van Poppelen, S., & Hesp, S. A. (2018). Methods for the quantification of recycled engine oil bottoms in performance-graded asphalt cement. *Journal of Materials in Civil Engineering*, *30*(2), 04017269.

Kim, S. S. (2005). Direct measurement of asphalt binder thermal cracking. *Journal of Materials in Civil Engineering*, *17*(6), 632-639.

Kim, S. S. (2010). *Asphalt binder cracking device to reduce low-temperature asphalt pavement cracking* (No. FHWA-HIF-11-029). Federal Highway Administration (US).

Kim, S.S. (2007). *Development of an Asphalt Binder Cracking Device*. Washington, DC: IDEA Program, Transportation Research Board.

Kim, Y. R., Haghshenas, H., Nabizadeh, H., & Santosh, K. (2016). *Research on High-RAP Asphalt Mixtures with Rejuvenators and WMA Additives* (No. SPR-P1 (15) M016). Nebraska. Dept. of Roads.

Kriz, P., Stastna, J., & Zanzotto, L. (2008). Glass transition and phase stability in asphalt binders. *Road Materials and Pavement Design*, *9*(sup1), 37-65, https://doi.org/10.1080/14680629.2008.9690158

Kudva, R. A., Keskkula, H., & Paul, D. R. (1998). Compatibilization of nylon 6/ABS blends using glycidyl methacrylate/methyl methacrylate copolymers. *Polymer*, *39*(12), 2447-2460. https://doi.org/10.1016/S0032-3861(97)00583-1

Lamontagne, J., Durrieu, F., Planche, J. P., Mouillet, V., & Kister, J. (2001). Direct and continuous methodological approach to study the ageing of fossil organic material by infrared microspectrometry imaging: application to polymer modified bitumen. *Analytica chimica acta*, *444*(2), 241-250.

Le Guern, M., Chailleux, E., Farcas, F., Dreessen, S., & Mabille, I. (2010). Physico-chemical analysis of five hard bitumens: Identification of chemical species and molecular organization before and after artificial aging. *Fuel*, *89*(11), 3330-3339.

Lee, T. C., Terrel, R. L., & Mahoney, J. P. (1983). Test for efficiency of mixing of recycled asphalt paving mixtures, *Transportation Research Record* (No. 911), https://onlinepubs.trb.org/Onlinepubs/trr/1983/911/911-007.pdf.

Lei, Z., Bahia, H., & Yi-qiu, T. (2015). Effect of bio-based and refined waste oil modifiers on low temperature performance of asphalt binders. *Construction and building materials*, *86*, 95-100.

Lima, F. S. G., & Leite, L. F. M. (2004). Determination of asphalt cement properties by near infrared spectroscopy and chemometrics. *Petroleum Science and technology*, *22*(5-6), 589-600.

Lin, P. S., Wu, T. L., Chang, C. W., & Chou, B. Y. (2011). Effects of recycling agents on aged asphalt binders and reclaimed asphalt concrete. *Materials and structures*, 44, 911-921.

Little, D. H., Holmgreen Jr, R. J., & Epps, J. A. (1981). Effect of recycling agents on the structural performance of recycled asphalt concrete materials. In *Association of asphalt paving technologists proceedings* (Vol. 50).

Loeber, L., Muller, G., Morel, J., & Sutton, O. (1998). Bitumen in colloid science: A chemical, structural and rheological approach. *Fuel*, *77*(13), 1443-1450.

Loeber, L., Sutton, O., Morel, J. V. J. M., Valleton, J. M., & Muller, G. (1996). New direct observations of asphalts and asphalt binders by scanning electron microscopy and atomic force microscopy. *Journal of microscopy*, 182(1), 32-39.

Ma, Y., Hu, W., Polaczyk, P.A., Han, B., Xiao, R., Zhang, M. & Huang, B. (2020) Rheological and aging characteristics of the recycled asphalt binders with different rejuvenator incorporation methods, *Journal of Cleaner Production*, 262: 121249, ISSN 0959-6526, https://doi.org/10.1016/j.jclepro.2020.121249.

Mansourkhaki A, Ameri M, Habibpour M, & Underwood B. S., (2020) Relations between colloidal indices and low-temperature properties of reclaimed binder modified with softer binder, oil-rejuvenator and polybutadiene rubber. *Construction and Building Materials*, 239, 117800, https://doi.org/10.1016/j.conbuildmat.2019.117800.

Marsac, M., et al. (2014). Potential and limits of FTIR methods for reclaimed asphalt characterization, *Materials and Structures*. 47(8), pp.1273-1286.

Masson, J. F., Leblond, V., & Margeson, J. (2006). Bitumen morphologies by phase-detection atomic force microscopy. *Journal of microscopy*, *221*(1), 17-29.

Masson, J. F., Leblond, V., Margeson, J., & Bundalo-Perc, S. (2007). Low-temperature bitumen stiffness and viscous paraffinic nano-and micro-domains by cryogenic AFM and PDM. *Journal of microscopy*, *227*(3), 191-202.

Menapace, I., Masad, E., Papavassilieu & Kassem, E. (2015). Evaluation of aging in asphalt cores at room temperature using low field nuclear magnetic resonance. In A. Nikolaides (Ed.), *Bituminous Mixtures and Pavements VI* (p. 395), CRC Press. https://doi.org/10.1201/b18538

Menapace, I., Masad, E., Papavassiliou, G., & Kassem, E. (2016). Evaluation of ageing in asphalt cores using low-field nuclear magnetic resonance. *International Journal of Pavement Engineering*, *17*(10), 847-860.

Mercado, E. A., Martin, A. E., & Kaseer, F. (2018). Case study on balancing mixtures with high recycled materials contents. In *Advances in Materials and Pavement Prediction* (pp. 239-242). CRC Press.

Miknis, F. P., & Michon, L. C. (1998). Some applications of nuclear magnetic resonance imaging to crumb rubber modified asphalts. *Fuel*, *77*(5), 393-397.

Mogawer, W. S., Booshehrian, A., Vahidi, S., & Austerman, A. J. (2013). Evaluating the effect of rejuvenators on the degree of blending and performance of high RAP, RAS, and RAP/RAS mixtures. Road Materials and Pavement Design, 14(sup2), 193-213.

Mohammadafzali, M., Ali, H., Musselman, J. A., Sholar, G. A., & Rilko, W. A. (2017). Aging of rejuvenated asphalt binders. *Advances in Materials Science and Engineering*, *2017*(1), 8426475.

Moraes M.B., Pereira R.B., Simão R.A., & Leite L.F. 2010). High temperature AFM study of CAP 30/45 pen grade bitumen, *Journal of Microscopy*: 239 (1) 46–53.

Morea, F., Marcozzi, R., & Castaño, G. (2012). Rheological properties of asphalt binders with chemical tensoactive additives used in Warm Mix Asphalts (WMAs). *Construction and Building Materials*, *29*, 135-141.

Muñoz, J. F., Balachandran, C., Yao, Y., Shastry, A., Perry, L., Beyene, M. A., & Arnold, T. (2018). Forensic investigation of the cause (s) of slippery ultra-thin bonded wearing course of an asphalt pavement: influence of binder content. *International Journal of Pavement Engineering,* 19(7), 593-600.

Nahar, S. N., Schmets, A. J. M., Schitter, G., & Scarpas, A. (2014, June). Quantitative nanomechanical property mapping of bitumen micro-phases by peak-force atomic force microscopy. In *12th ISAP Conference on Asphalt Pavements* (Vol. 30).

National Academies of Sciences, Engineering, and Medicine (2020) *Evaluating the Effects of Recycling Agents on Asphalt Mixtures with High RAS and RAP Binder Ratios*. Washington, DC: The National Academies Press. https://doi.org/10.17226/25749.

Newcomb, D. E., & Epps, J. A. (1981). *Asphalt recycling technology: Literature review and research plan. Final Report*. New Mexico Univ., Albuquerque. Engineering Research Inst.

Newcomb, D. E., Nusser, B. J., Kiggundu, B. M., & Zallen, D. M. (1984). Laboratory study of the effects of recycling modifiers on aged asphalt cement. *Transportation Research Record*, (968).

Oliver, J. W. (2009). Changes in the chemical composition of Australian bitumens. *Road Materials and Pavement Design*, *10*(3), 569-586.

Oliver, J. W. H., (1974). Diffusion of Oils in Asphalts. *Industrial & Engineering Chemistry Product Research and Development, 13*(1) 76–82.

O'Sullivan, K. A. (2011). *Rejuvenation of reclaimed asphalt pavement (RAP) in hot mix asphalt recycling with high RAP content* (Doctoral dissertation, Worcester Polytechnic Institute).

Oyekunle, L. O. (2006). Certain relationships between chemical composition and properties of petroleum asphalts from different origin. *Oil & Gas Science and Technology-Revue de l'IFP*, *61*(3), 433-441..

Paliukaite, M., Assuras, M., Hesp, S.A.M. (2016). Effect of recycled engine oil bottoms on the ductile failure properties of straight and polymer-modified asphalt cements. *Construction and Building Materials, 126:* 190–196, ISSN 0950-0618, https://doi.org/10.1016/j.conbuildmat.2016.08.156

Paliukaitė, M., Assuras, M., Silva, S. C., Ding, H., Gotame, Y., Nie, Y., Ubaid, I & Hesp, S. A. (2017). Implementation of the double-edge-notched tension test for asphalt cement acceptance. *Transportation in Developing Economies*, *3*, 1-10. https://doi.org/10.1007/s40890-017-0034-0

Paliukaite, M., Vaitkus, A., & Zofka, A. (2014). Evaluation of bitumen fractional composition depending on the crude oil type and production technology. In *Environmental engineering. Proceedings of the international conference on environmental engineering. ICEE* (Vol. 9, p. 1). Vilnius Gediminas Technical University, Department of Construction Economics & Property.

Pasandín, A. R., Pérez, I., Gómez-Meijide, B., & Pérez-Barge, N. (2015). The effect of hydrated lime on the bond between asphalt and recycled concrete aggregates. *Petroleum Science and Technology*, *33*(10), 1141-1148.

Pauli, A. T. & J. F. Branthaver. (1999). Rheological and compositional definitions of compatibility as they relate to the colloidal model of asphalt and residua. In American Chemical Society Division of Petroleum Chemistry*, Petroleum Preprints, 44*, 190–193.

Petersen, J. C. (2009). A review of the fundamentals of asphalt oxidation: chemical, physicochemical, physical property, and durability relationships. *Transportation research circular*, (E-C140).

Pieri, N., Jacquot, F., Mille, G., Planche, J. P., & Kister, J. (1996). GC-MS identification of biomarkers in road asphalts and in their parent crude oils. Relationships between crude oil maturity and asphalt reactivity towards weathering. *Organic geochemistry*, *25*(1-2), 51-68.

Planche, J. P., Claudy, P. M., Létoffé, J. M., & Martin, D. (1998). Using thermal analysis methods to better understand asphalt rheology. *Thermochimica acta*, *324*(1-2), 223-227.

Polacco, G., Filippi, S., Paci, M., Giuliani, F., & Merusi, F. (2012). Structural and rheological characterization of wax modified bitumens. *Fuel*, *95*, 407-416.

Rebelo, L. M., De Sousa, J. S., Abreu, A. S., Baroni, M. P. M. A., Alencar, A. E. V., Soares, S. A., ... & Soares, J. B. (2014). Aging of asphaltic binders investigated with atomic force microscopy. *Fuel*, *117*, 15-25.

Rathore, M., Zaumanis, M., & Haritonovs, V. (2019, November). Asphalt recycling technologies: a review on limitations and benefits. In *IOP Conference Series: Materials Science and Engineering* (Vol. 660, No. 1, p. 012046). IOP Publishing.

Redelius, P., & Soenen, H. (2015). Relation between bitumen chemistry and performance. *Fuel*, *140*, 34-43.

Reinke, G., & Hanz, A. (2018). Evaluation of Two Comparative Test Projects in Minnesota and the Relationship Between Binder Composition, Binder Aging, and In-Service Mixture Performance. *Relationships of Laboratory Mixture Aging to Asphalt Mixture Performance*, 64.

Rigg, A., Duff, A., Nie, Y., Somuah, M., Tetteh, N., & Hesp, S. A. (2017). Non-isothermal kinetic analysis of reversible ageing in asphalt cements. *Road Materials and Pavement Design*, *18*(sup4), 185-210. https://doi.org/10.1080/14680629.2017.1389070

Rodriguez-Fernandez, I., Lastra-Gonzalez, P., Indacoechea-Vega, I., & Castro-Fresno, D. (2019). Recyclability potential of asphalt mixes containing reclaimed asphalt pavement and industrial by-products. *Construction and Building Materials*, *195*, 148-155.

Rodriguez-Fernández, I., Lastra-González, P., Jato-Espino, D., & Indacoechea-Vega, I. (2019). Design for the maximization of the amount of Reclaimed Asphalt Pavement (RAP) and by-products in asphalt mixtures. In *Pavement and Asset Management* (pp. 501-506). CRC Press.

Romberg, J. W., Nesmith, S. D., & Traxler, R. N. (1959). Some Chemical Aspects of the Components of Asphalt. *Journal of Chemical and Engineering Data*, *4*(2), 159-161.

Rostler, F. S., & White, R. M. (1959). Fraction Componentes of Asphalts. In *American Society for Testing and Materials: Third Pacific Area Meeting. Philadelphia*.

Roy, S. (2018). *Evaluation of moisture susceptibility of asphalt binders using Atomic Force Microscopy (AFM)*. Arkansas State University.

Roy, S., & Hossain, Z. (2021). Use of molecular-level dissipated energy of asphalt binders to predict moisture effects on pavements. *International Journal of Pavement Engineering*, *22*(11), 1351-1362. https://doi.org/10.1080/10298436.2019.1685670.

Schmets, A., Kringos, N., Pauli, T., Redelius, P., & Scarpas, T. (2010). On the existence of wax-induced phase separation in bitumen. *International Journal of Pavement Engineering*, *11*(6), 555-563.

Shen, J., Nomura, K., & Kinoshita, S. (2002). Performance-based approach for determining optimum rejuvenator content in hot mix recycling. *Journal Of Pavement Engineering, JSCE*, *7*, 1-28.

Shen, J., Huang, B., & Hachiya, Y. (2004). Validation of performance-based method for determining rejuvenator content in HMA. *International Journal of Pavement Engineering*, *5*(2), 103-109.

Shen, J., Amirkhanian, S. N., & Lee, S. J. (2007). HP-GPC characterization of rejuvenated aged CRM binders. *Journal of Materials in Civil Engineering*, *19*(6), 515-522.

Sias, J. E., Dave, E. V., Zhang, R., & Rahbar-Rastegar, R. (2019). *Incorporating impact of aging on cracking performance of mixtures during design* (No. FHWA-NH-RD-26962O). University of New Hampshire. Department of Civil and Environmental Engineering.

Siegel, J. A., Fisher, J., Gilna, C., Spadafora, A., & Krupp, D. (1985). Fluorescence of petroleum products I. Three-dimensional fluorescence plots of motor oils and lubricants. *Journal of Forensic Sciences*, *30*(3), 741-759.

Sui, C., Farrar, M. J., Harnsberger, P. M., Tuminello, W. H., & Turner, T. F. (2011). New low-temperature performance-grading method: Using 4-mm parallel plates on a dynamic shear rheometer. *Transportation Research Record*, *2207*(1), 43-48.

Sui, C., Farrar, M., Tuminello, W., & Turner, T. F. (2010). New Technique for Measuring Low-Temperature Properties of Asphalt Binders with Small Amounts of Material. *Transportation Research Record, Journal of the Transportation Research Board, 2179*, 23-28.

Thomas, W. H., & Tester, H. E. (1933, July). The Effect of Paraffin Wax in Asphaltic Bitumen and Its Estimation. In *World Petroleum Congress* (pp. WPC-204). WPC.

Tran, N. H., Taylor, A., & Willis, R. (2012). *Effect of Rejuvenator on Performance Properties of HMA Mixtures With High RAP and RAS Contents*. *NCAT report*, *1*, 12-15.

Traxler, R. N., & Romberg, J. W. (1952). Asphalt, a colloidal material. *Industrial & Engineering Chemistry*, *44*(1), 155-158.

Turner, T. F., & Branthaver, J. F. (1997). DSC studies of asphalts and asphalt components. In A. M. Usmani (ed.) *Asphalt science and technology*, (pp. 59-101) CRC Press, ISBN 9780429181450.

Veeraragavan, R. K. (2016). An investigation of the performance of hot mix asphalt (HMA) binder course materials with high percentage of reclaimed asphalt pavement (RAP) and rejuvenators. *Worcester Polytechnic Institute*.

Wang, S., Wang, Q., Wu, X., & Zhang, Y. (2015). Asphalt modified by thermoplastic elastomer based on recycled rubber. *Construction and Building Materials*, *93*, 678-684.

Wang, S., Yuan, C., & Jiaxi, D. (2014). Crumb tire rubber and polyethylene mutually stabilized in asphalt by screw extrusion. *Journal of Applied Polymer Science*, *131*(23).

Wang, F., Wang, Z., Li, C., Xiao, Y., Wu, S., & Pan, P. (2017). The rejuvenating effect in hot asphalt recycling by mortar transfer ratio and image analysis. *Materials*, *10*(6), 574.

Wang, Z., Li, J., Zhang, Z., Jia, M., & Yang, J. (2020). Formulation of a new warm-mix recycling agent and its rejuvenating effect on aged asphalt. *Construction and Building Materials*, *262*, 120804. https://doi.org/10.1016/j.conbuildmat.2020.120804

Willis, J. R., Taylor, A., Tran, N. H., Kluttz, B., & Timm, D. H. (2012). Laboratory evaluation of high polymer plant-produced mixtures. *Road Materials and Pavement Design*, *13*(sup1), 260-280.Willis, J. R., Turner, P., Julian, G., Taylor, A. J., Tran, N., & Padula, F. (2012). *Effects of changing virgin binder grade and content on RAP mixture properties. NCAT Report*, (12-03).

Xu, M., & Zhang, Y. (2020). Study of rejuvenators dynamic diffusion behavior into aged asphalt and its effects. *Construction and Building Materials*, *261*, 120673.

Yan, J., Zhang, Z., Zhu, H., Li, F., & Liu, Q. (2014). Experimental study of hot recycled asphalt mixtures with high percentages of reclaimed asphalt pavement and different recycling agents. *Journal of Testing and Evaluation*, *42*(5), 1183-1190.

Yao, H., Dai, Q., You, Z., Ye, M., & Yap, Y. K. (2016). Rheological properties, low-temperature cracking resistance, and optical performance of exfoliated graphite nanoplatelets modified asphalt binder. *Construction and Building Materials*, *113*, 988-996.

Zaumanis, M., Mallick, R. B., & Frank, R. (2013). Evaluation of rejuvenator's effectiveness with conventional mix testing for 100% reclaimed Asphalt pavement mixtures. *Transportation research record*, *2370*(1), 17-25.

Zaumanis, M., Mallick, R. B., & Frank, R. (2014a). 100% Recycled hot mix asphalt: A review and analysis. *Resources, Conservation and Recycling*, 92, 230-245.

Zaumanis, M., Mallick, R.B., Poulikakos, L. & Frank, R. (2014b) Influence of six rejuvenators on the performance properties of Reclaimed Asphalt Pavement (RAP) binder and 100% recycled asphalt mixtures, *Construction and Building Materials* 71, 538-550, ISSN 0950-0618, https://doi.org/10.1016/j.conbuildmat.2014.08.073.

Zaumanis, M., Mallick, R. B., & Frank, R. (2015). Evaluation of different recycling agents for restoring aged asphalt binder and performance of 100% recycled asphalt. *Materials and Structures*, 48, 2475-2488.

Zelelew, H., Paugh, C., & Corrigan, M. R. (2011). Warm-mix asphalt laboratory permanent deformation performance in State of Pennsylvania: Case study (No. 11-2784). Paper presented at the *90th* Transportation Research Board Annual Meeting, January 23–27, Washington, DC.

Zhang, R. (2020). *Evaluation and Identification of Cracking Susceptibility of Asphalt Binders and Mixtures by Incorporation of Effects of Aging on Performance* (Doctoral dissertation, University of New Hampshire), https://scholars.unh.edu/cgi/viewcontent.cgi?article=3536&context=dissertation.

Zhang, R., Sias, J. E., Dave, E. V., & Rahbar-Rastegar, R. (2019). Impact of aging on the viscoelastic properties and cracking behavior of asphalt mixtures. *Transportation Research Record*, *2673*(6), 406-415, https://doi.org/10.1177/0361198119846473.

Zhang, R., You, Z., Wang, H., Ye, M., Yap, Y. K., & Si, C. (2019). The impact of bio-oil as rejuvenator for aged asphalt binder. *Construction and Building Materials*, *196*, 134-143, https://doi.org/10.1016/j.conbuildmat.2018.10.168.

Zhao, S., Huang, B., Shu, X., & Woods, M. E. (2015). Quantitative characterization of binder blending: How much recycled binder is mobilized during mixing? *Transportation Research Record*, *2506*(1), 72-80, https://doi.org/10.3141/2506-08.

Zhou, F., Mogawer, W., Li, H., Andriescu, A., & Copeland, A. (2013). Evaluation of fatigue tests for characterizing asphalt binders. *Journal of Materials in Civil Engineering*, *25*(5), 610-617.

Zhou, F., Im, S., Morton, D., Lee, R., Hu, S., & Scullion, T. (2015). Rejuvenator characterization, blend characteristics, and proposed mix design method. *Journal of the Association of Asphalt Paving Technologists, 84*, 675-704.

Zhou, H., Wang, Z., Zhu, Y., Li, Q., Zou, H. J., Qu, H. Y., Chen, Y. R. & Du, Y. P. (2013). Quantitative determination of trace metals in high-purity silicon carbide powder by laser ablation inductively coupled plasma mass spectrometry without binders. *Spectrochimica Acta Part B: Atomic Spectroscopy*, *90*, 55-60, https://doi.org/10.1016/j.sab.2013.10.003.

Zhu, H., Xu, G., Gong, M., & Yang, J. (2017). Recycling long-term-aged asphalts using bio-binder/plasticizer-based rejuvenator. *Construction and Building Materials*, *147*, 117-129.

Ziari, H., Moniri, A., Bahri, P., & Saghafi, Y. (2019). The effect of rejuvenators on the aging resistance of recycled asphalt mixtures. *Construction and Building Materials*, *224*, 89-98.

Appendix A: Mix Designs and Individual Testing Result

DEPARTMENT OF TRANSPORTATION

BITUMINOUS PLANT MIX DESIGN REPORT

District 3A Materials Lab
7694 Industrial Park Rd.
Baxter, MN 56425
Phone: 218-828-5755
Fax: 218-828-5816

 # 3A-2019-169

Date: 8/16/2019

THIS MIX DESIGN REPORT IS NOT VALID UNTIL PLANT NO. INDICATED BELOW IS CERTIFIED.

ENGINEER	FOR
PROJECT NUMBER	
CONTRACTOR SIGN.	

SPEC	2360 AFT
SPEC YEAR	2019
MIX TYPE	SPWEB340
AC GRADE	PER PROPOSAL

THIS MIXTURE HAS BEEN REVIEWED FOR VOLUMETRIC PROPERTIES ONLY, IT DOES NOT ASSURE THAT FIELD PLACEMENT AND COMPACTION REQUIREMENTS HAVE BEEN MET.

PLANT NO. **AB BASE 4** - **2019** JOB MIX FORMULA

Begin With Test Number

SP	WE	301
- -	- -	- - -

AFT Properties

Pbe	4.6
SA	26.4
Adj. AFT	8.8

Sieve Size (mm)	(in.)	Composite Formula	Broad Band		For Information Only Virgin Formula PERCENT PASSING
25.0	(1)			–	
19.0	(3/4)	100	100	– 100	
12.5	(1/2)	99	85	– 100	
9.5	(3/8)	86	35	– 90	
4.75	(#4)	67	30	– 80	
2.36	(#8)	57	25	– 65	
1.18	(#16)	45		–	
0.600	(#30)	30		–	
0.300	(#50)	13		–	
0.150	(#100)	6		–	
0.075	(#200)	3.4	2.0	– 7.0	
Spec. Voids		4.0	3.0	– 5.0	
% AC		4.9 (TOTAL)	4.5		%AC (NEW) 3.5

TM # 3A-TM19-0058 Indicates a Gyratory Density of 150.0 (lbs/ft3) at 60 Design Gyrations
Use of anti-strip required: No

%	Pit	Source of Material	Total Sp. G	Minus #4 % Passing	Minus #4 Sp. G
34 %	18145	Andrews Ba Sand 3A-BA19-0198	2.658	95 %	2.658
6 %	18145	Andrews 1/2" Rock old pile 3A-BA19-0196	2.752	8 %	2.752
14 %	18145	Andrews Class "D" 3A-BA19-0206	2.709	86 %	2.709
16 %	18145	Andrews 1/2" Rock new pile 3A-BA19-0205	2.752	1 %	2.752
%				%	
%				%	
%				%	
30 %	18145	TH 6 Millings 3A-BR19-0028	2.667	74 %	2.667
		Mix Aggregate Specific Gravity at the Listed Percentages =	**2.688**		**2.671**

Remarks

Mix Design Reviewed by:

Thomas J. Boser

Mix Design Specialist

3A-2019-169 Ver. 2

cc: Dist Mat'ls Eng. - Sara Johnson
Contractor - ANDERSON BROS.

Figure A--1 Mix Design for 30% RAP Mixture

DEPARTMENT OF TRANSPORTATION

BITUMINOUS PLANT MIX DESIGN REPORT

District 3A Materials Lab
7694 Industrial Park Rd.
Baxter, MN 56425
Phone: 218-828-5755
Fax: 218-828-5816

3A-2019-184

Date: 8/26/2019

THIS MIX DESIGN REPORT IS NOT VALID UNTIL PLANT NO. INDICATED BELOW IS CERTIFIED.

ENGINEER	FOR
PROJECT NUMBER	
CONTRACTOR SIGN.	

SPEC	2360 AFT
SPEC YEAR	2019
MIX TYPE	SPWEA340
AC GRADE	PER PROPOSAL

THIS MIXTURE HAS BEEN REVIEWED FOR VOLUMETRIC PROPERTIES ONLY, IT DOES NOT ASSURE THAT FIELD PLACEMENT AND COMPACTION REQUIREMENTS HAVE BEEN MET.

PLANT NO. AB BASE 4 - 2019 JOB MIX FORMULA

Begin With Test Number

SP	WE	301
- -	- -	- - -

AFT Properties

Pbe	4.6
SA	26.3
Adj. AFT	8.9

Sieve Size (mm)	(In.)	Composite Formula	Broad Band		For Information Only Virgin Formula PERCENT PASSING
25.0	(1)				
19.0	(3/4)				
12.5	(1/2)	100	100	100	
9.5	(3/8)	85	85	100	
4.75	(#4)	65	60	90	
2.36	(#8)	55	45	70	
1.18	(#16)	44			
0.600	(#30)	29			
0.300	(#50)	13			
0.150	(#100)	6			
0.075	(#200)	3.6	2.0	7.0	
Spec. Voids		4.0	3.0	5.0	
% AC		4.9 (TOTAL)	4.5		%AC (NEW) 3.0

TM # 3A-TM19-0068 Indicates a Gyratory Density of 150.0 (lbs/ft3) at 60 Design Gyrations
Use of anti-strip required: No

%	Pit	Source of Material	Total Sp. G	Minus #4 % Passing	Minus #4 Sp. G
26 %	18145	Andrews Ba Sand 3A-BA19-0198	2.658	95 %	2.658
4 %	18144	Taylor 1/2" Rock 3A-BA19-0176	2.721	3 %	2.721
12 %	18145	Andrews Class "D" 3A-BA19-0206	2.709	86 %	2.709
18 %	18145	Andrews 1/2" Rock new pile 3A-BA19-0205	2.752	1 %	2.752
%				%	
%				%	
%				%	
40 %	18145	TH 6 Millings 3A-BR19-0028	2.667	74 %	2.667
		Mix Aggregate Specific Gravity at the Listed Percentages =	2.687		2.670

Remarks

Mix Design Reviewed by:

Thomas J. Boser

Thomas J. Boser

Mix Design Specialist

3A-2019-184 Ver. 1

cc: Dist Mat'ls Eng. - Sara Johnson
Contractor - ANDERSON BROS.

Figure A--2 Mix Design for 40% RAP Mixture

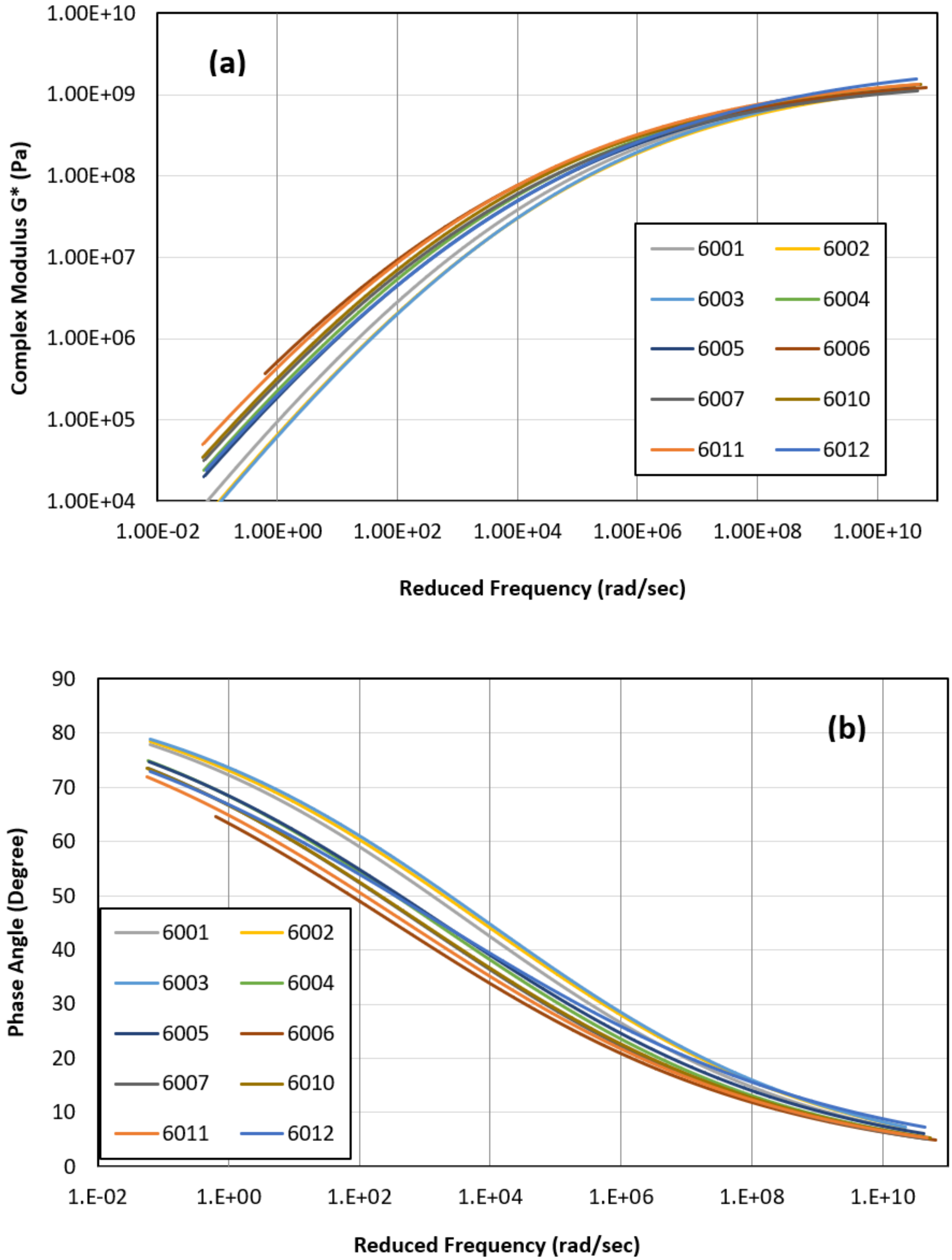

Figure A-3 Master Curves of (a) Complex Modulus and (b) Phase Angle for As-extracted Binders (Ref. 25°C)

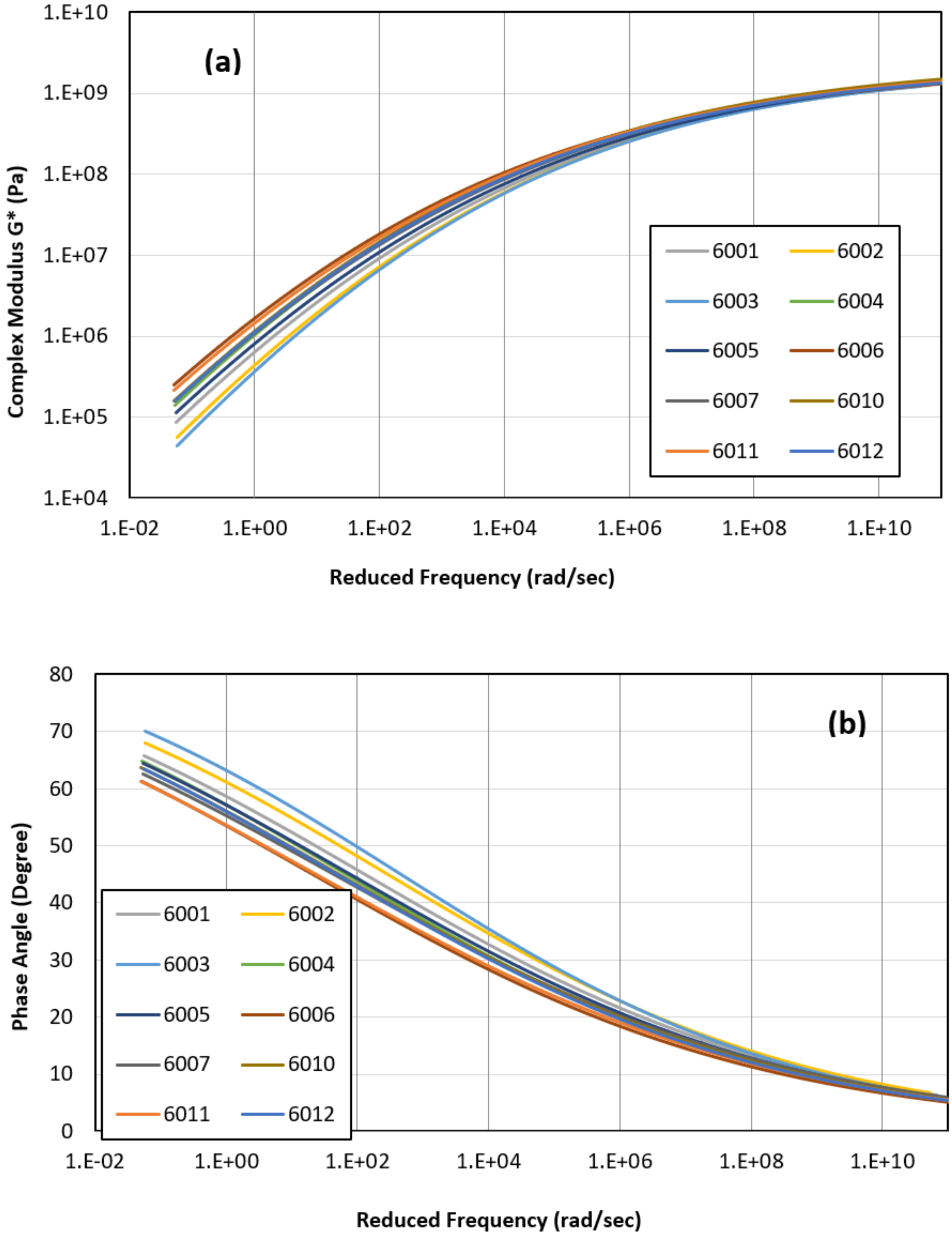

Figure A-4 Master Curves of (a) Complex Modulus and (b) Phase Angle for20 hrs. PAV Aged Binders (Ref. 25°C)

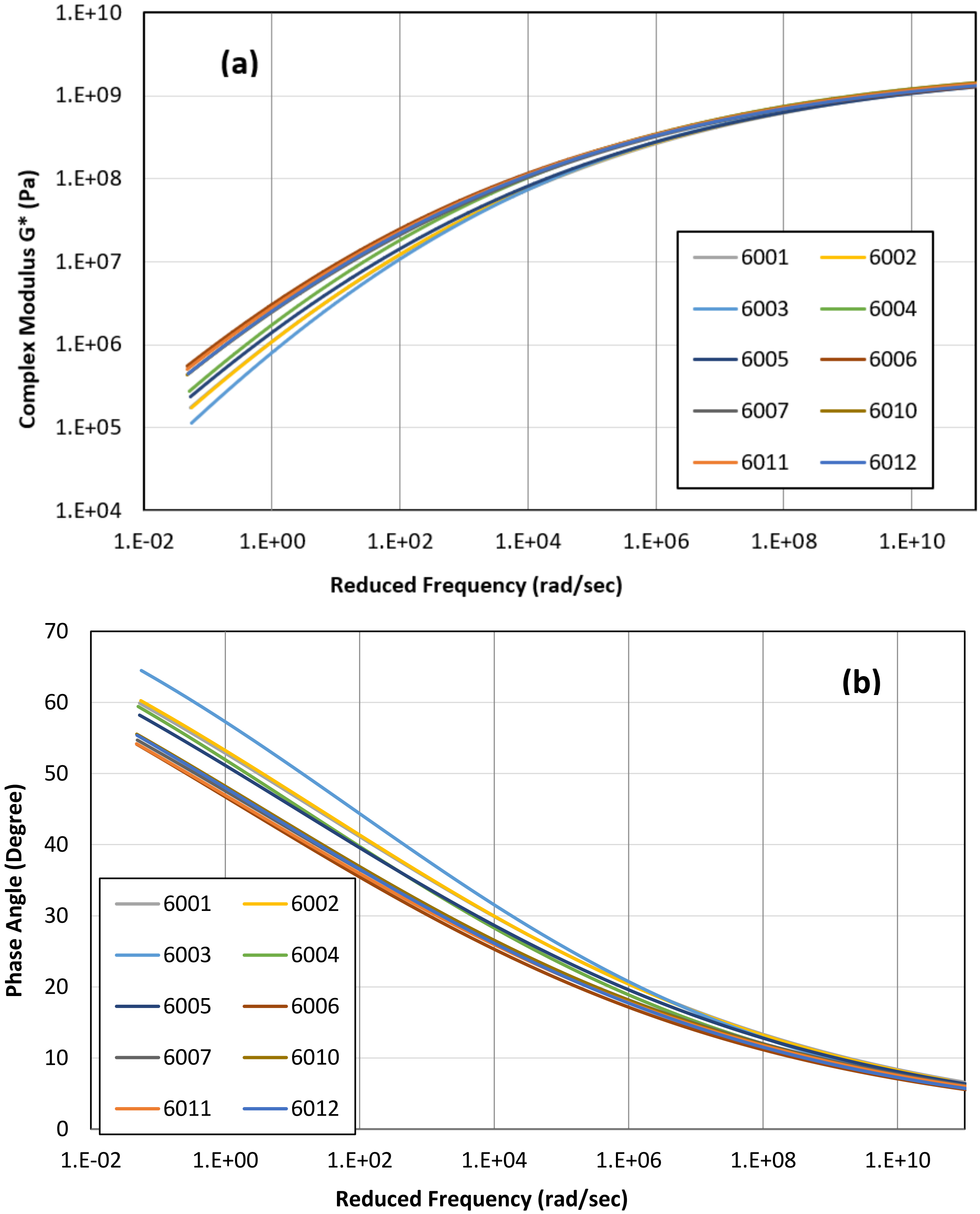

Figure A-5 Master Curves of (a) Complex Modulus and (b) Phase Angle for 40 hrs. PAV Aged Binders (Ref. 25°C)

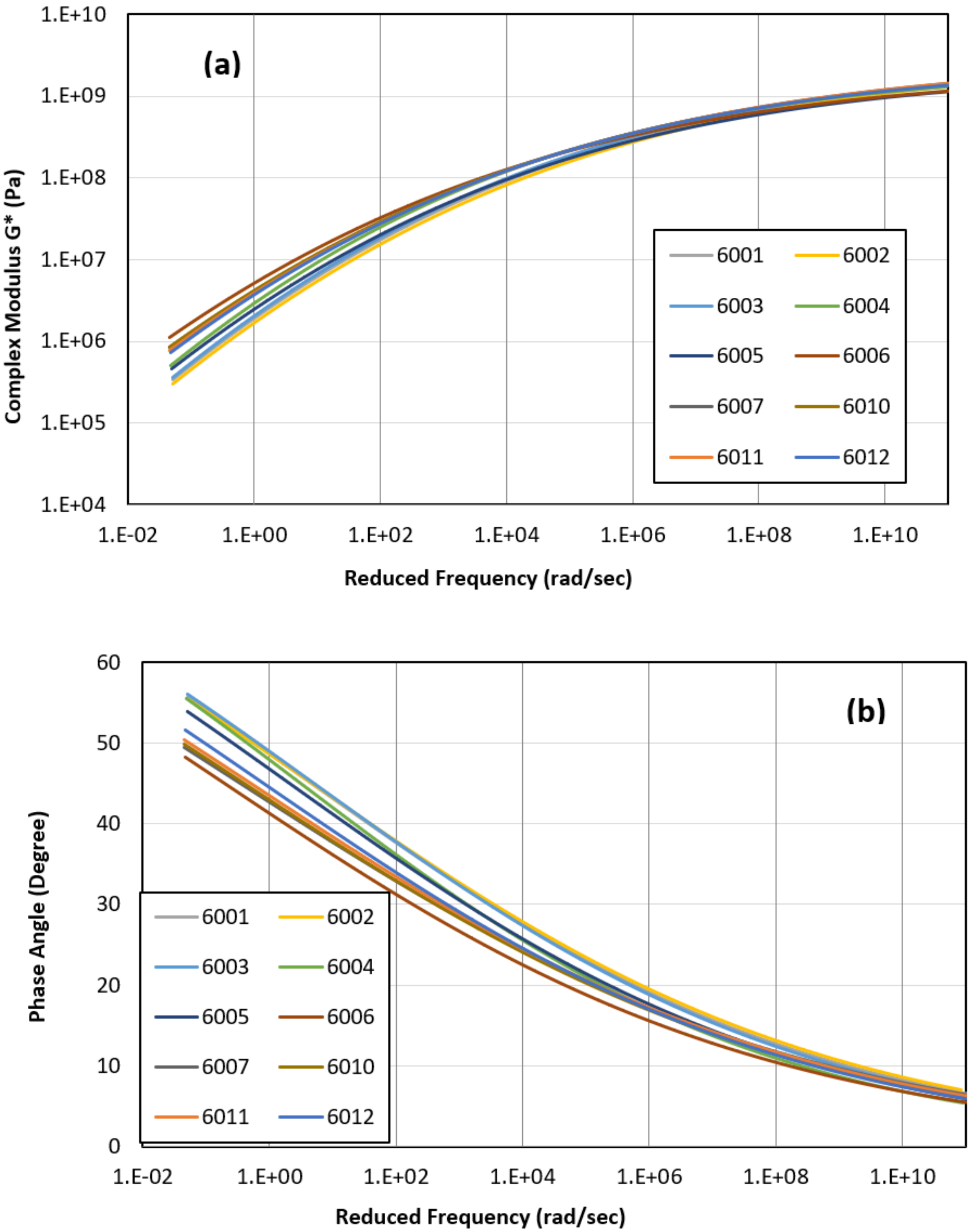

Figure A-6 Master Curves of (a) Complex Modulus and (b) Phase Angle for 60 hrs. PAV Aged Binders (Ref. 25°C)

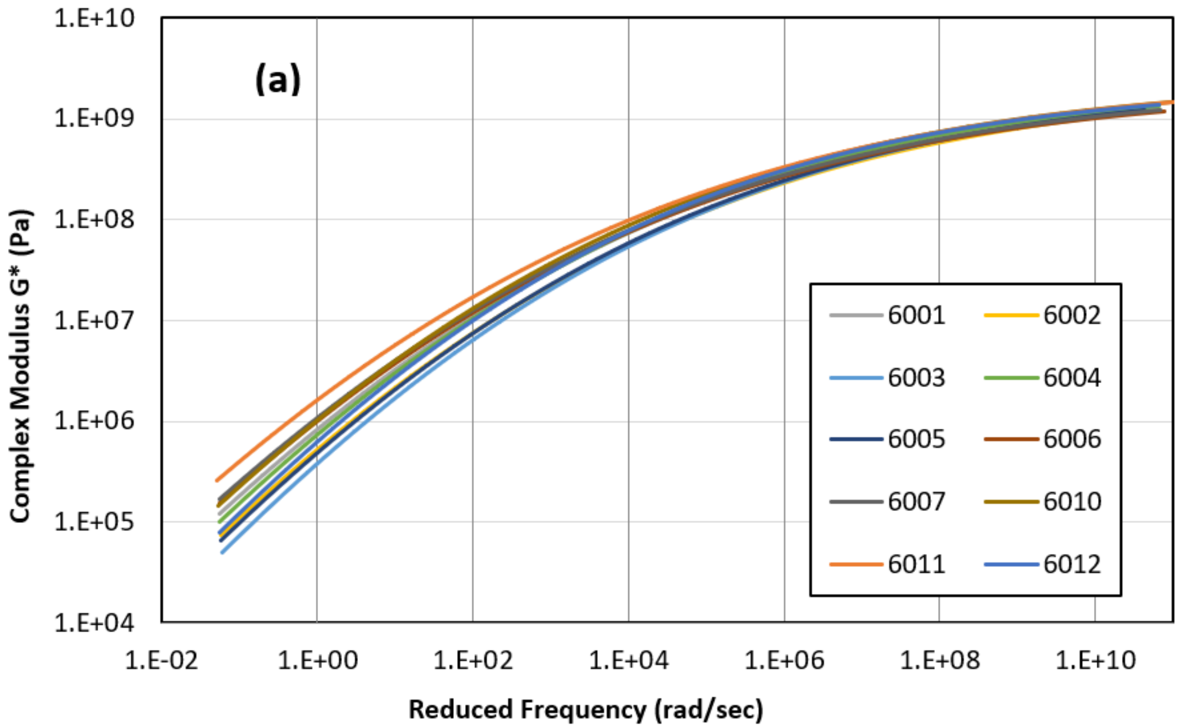

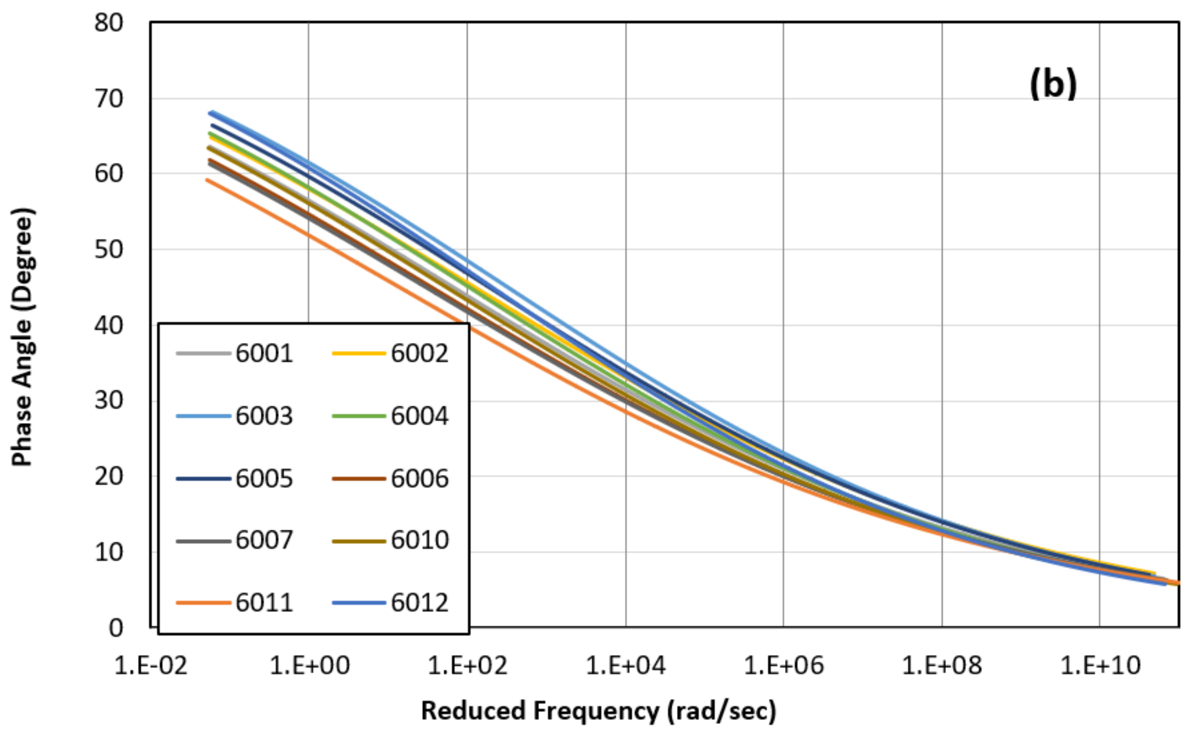

Figure A-7 Master Curves of (a) Complex Modulus and (b) Phase Angle for Loose Mix Aged 6 hrs. at 135°C Binders (Ref. 25°C)

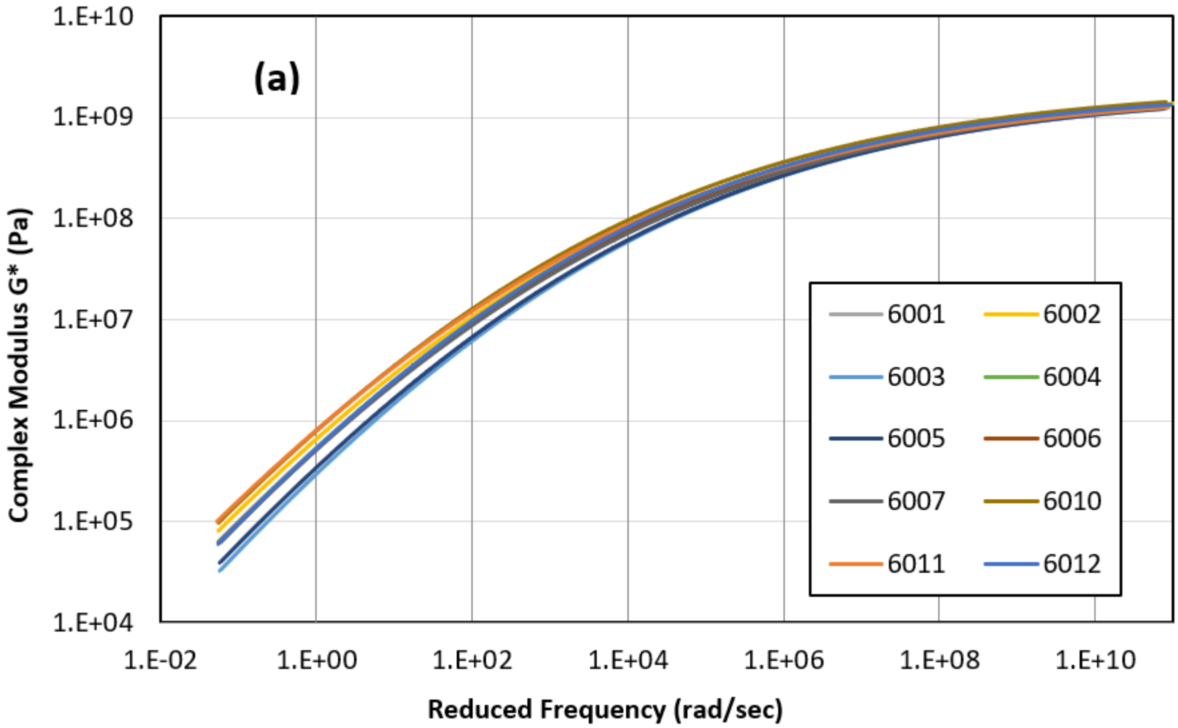

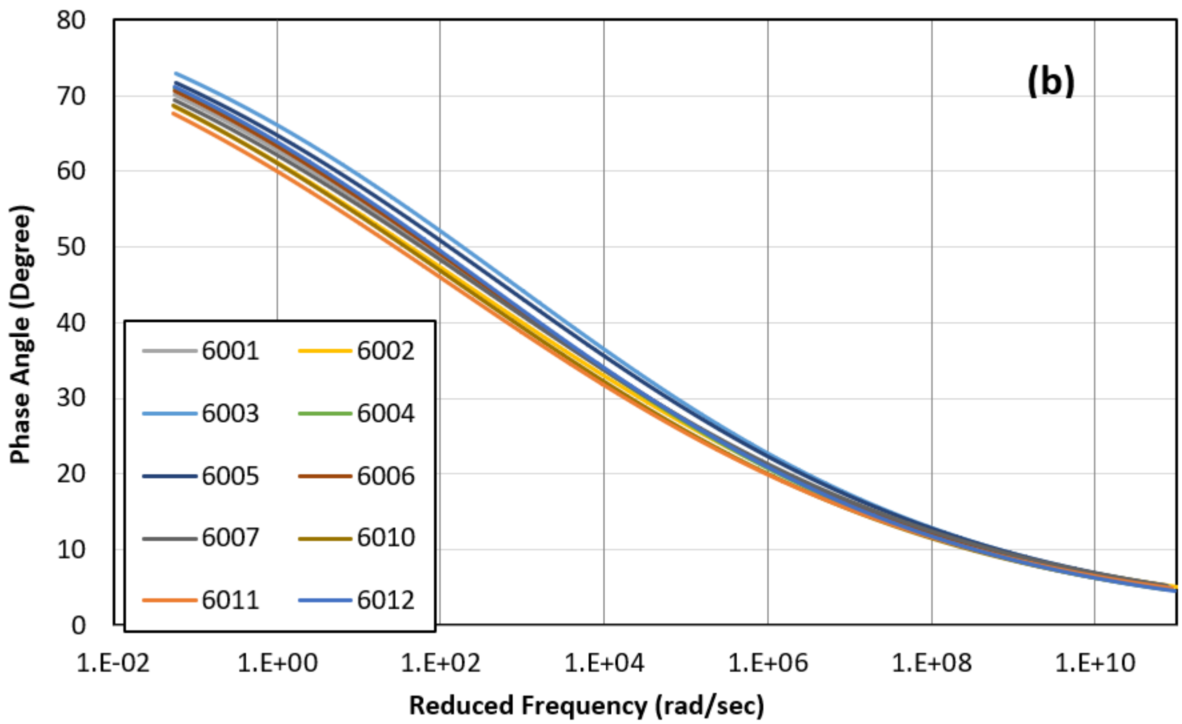

Figure A--8 Master Curves of (a) Complex Modulus and (b) Phase Angle for Year 1 Field Cores (Ref. 25°C)

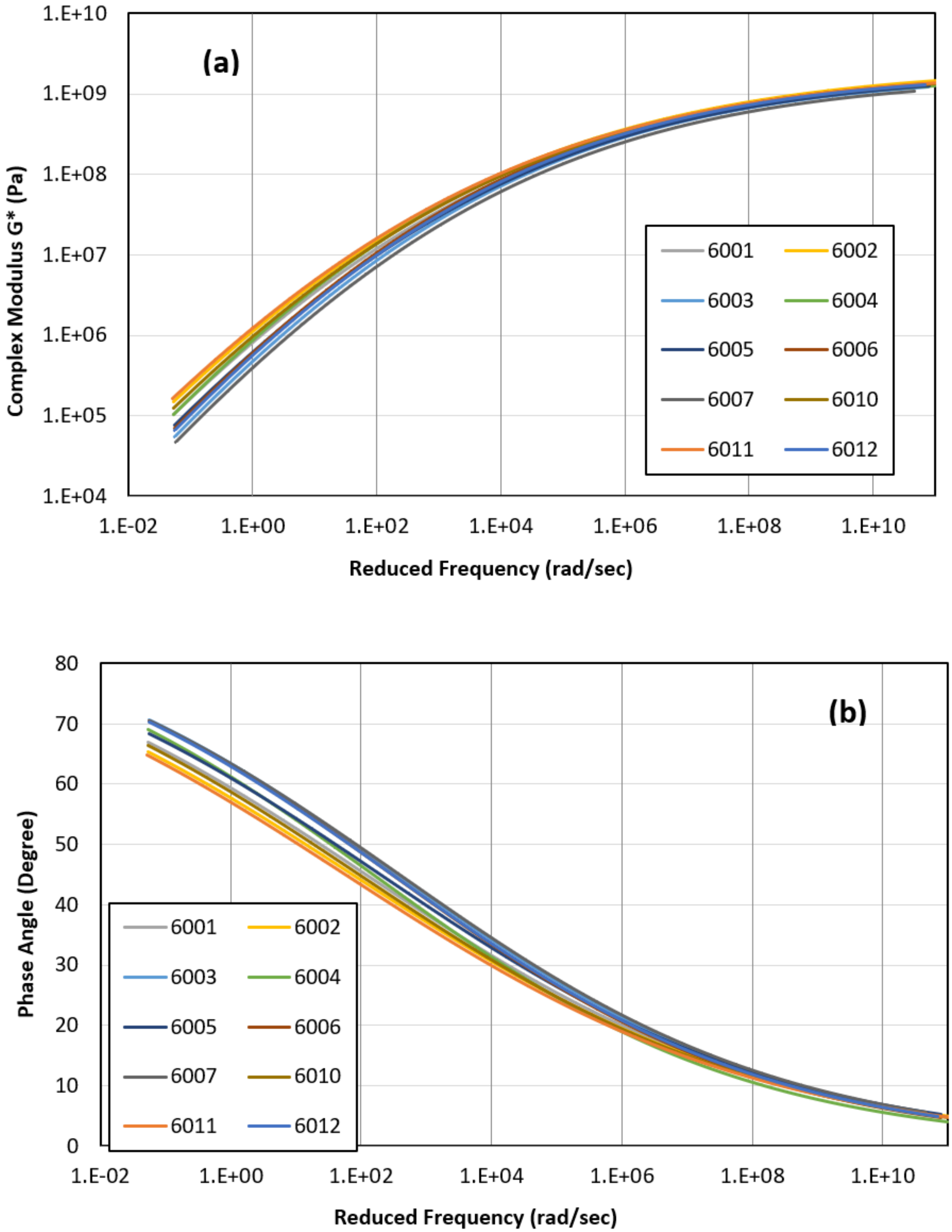

Figure A-9 Master Curves of (a) Complex Modulus and (b) Phase Angle for Year 2 Field Cores (Ref. 25°C)

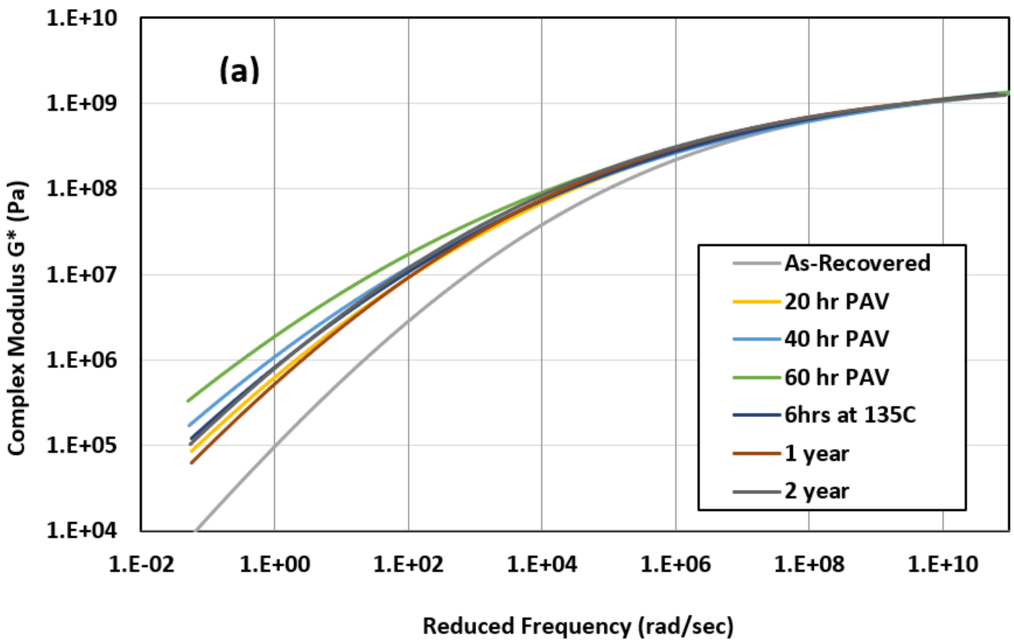

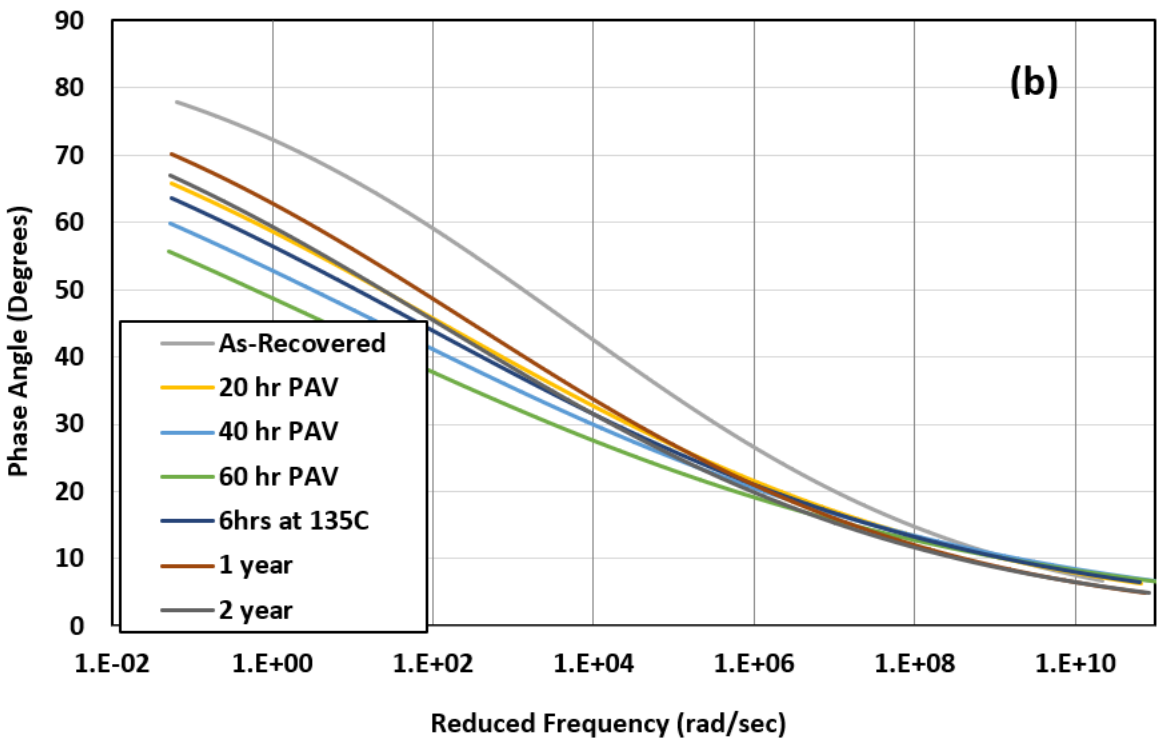

Figure A-10 Master Curves of (a) Complex Modulus and (b) Phase Angle for Section 6001 – All Aging Conditions (Ref. 25°C)

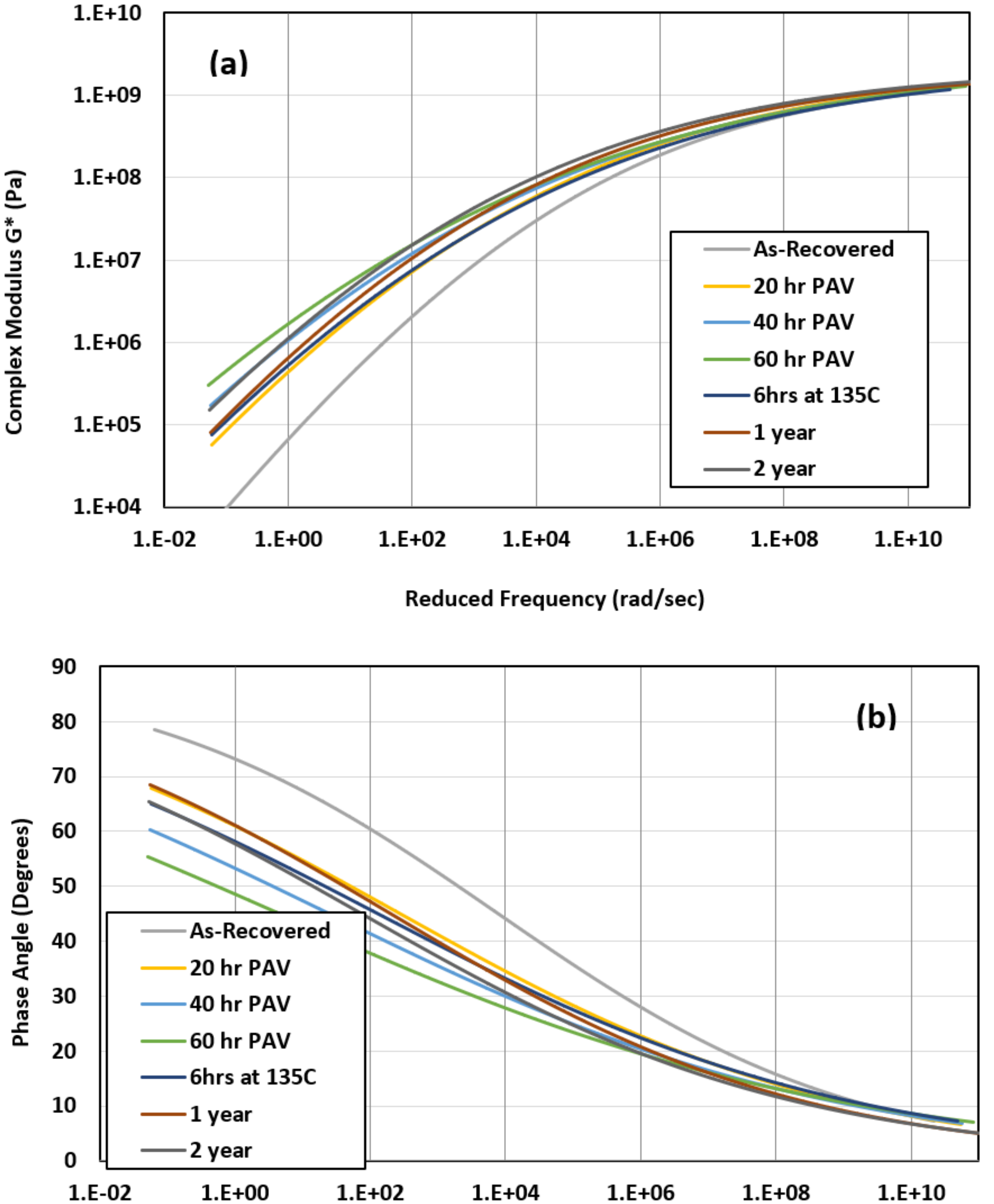

Figure A-11 Master Curves of (a) Complex Modulus and (b) Phase Angle for Section 6002 – All Aging Conditions (Ref. 25°C)

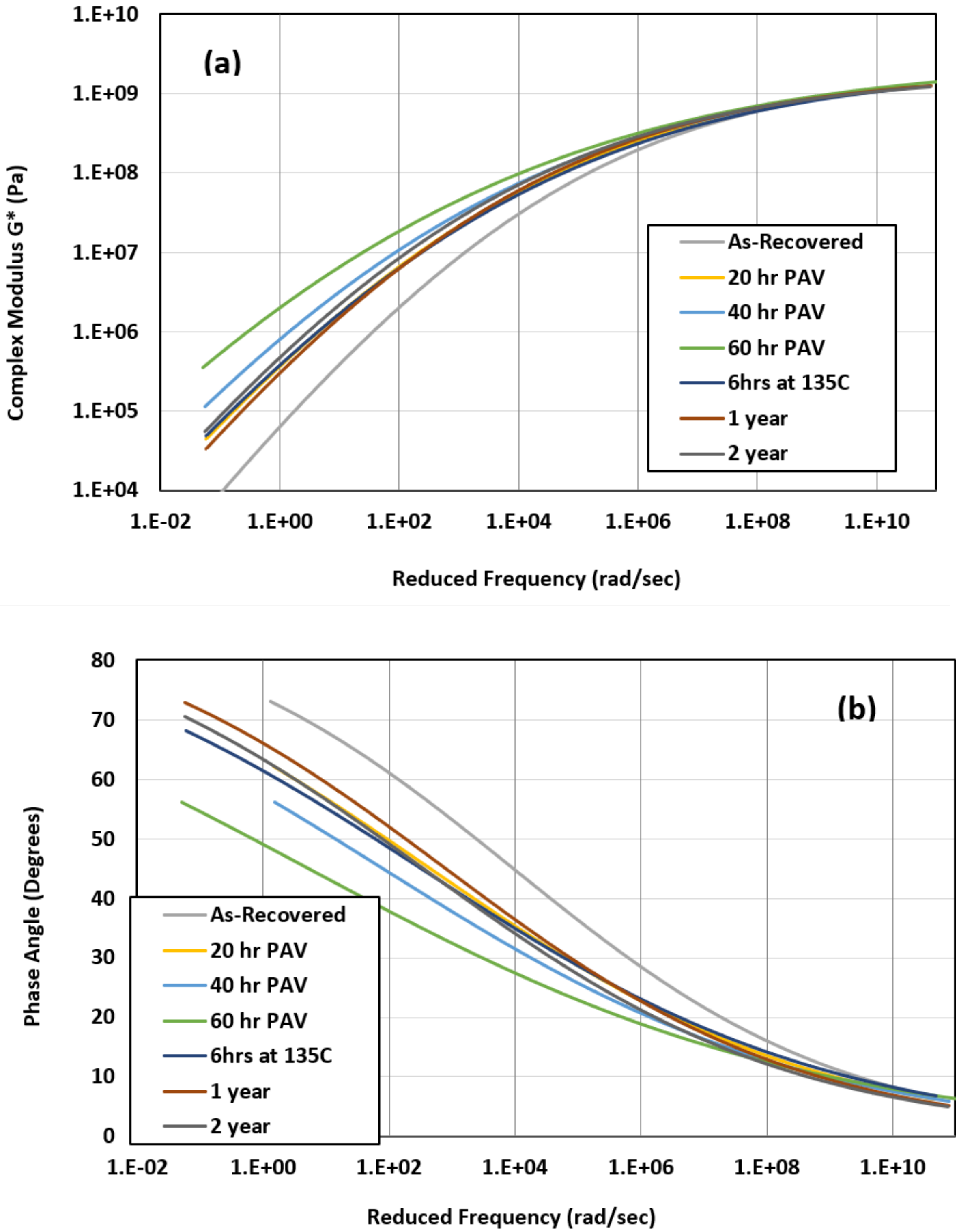

Figure A-12 Master Curves of (a) Complex Modulus and (b) Phase Angle for Section 6003 – All Aging Conditions (Ref. 25°C)

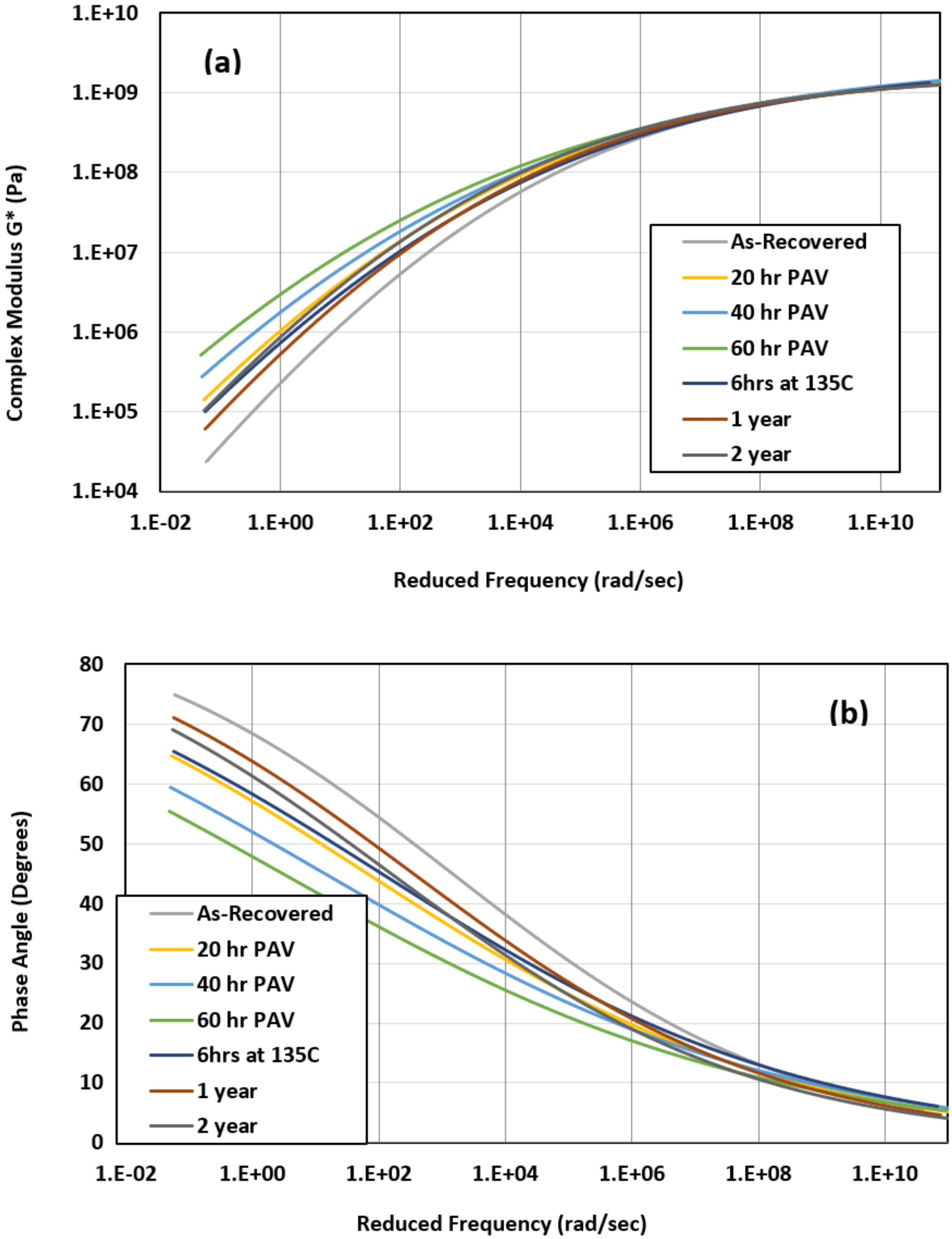

Figure A-13 Master Curves of (a) Complex Modulus and (b) Phase Angle for Section 6004 – All Aging Conditions (Ref. 25°C)

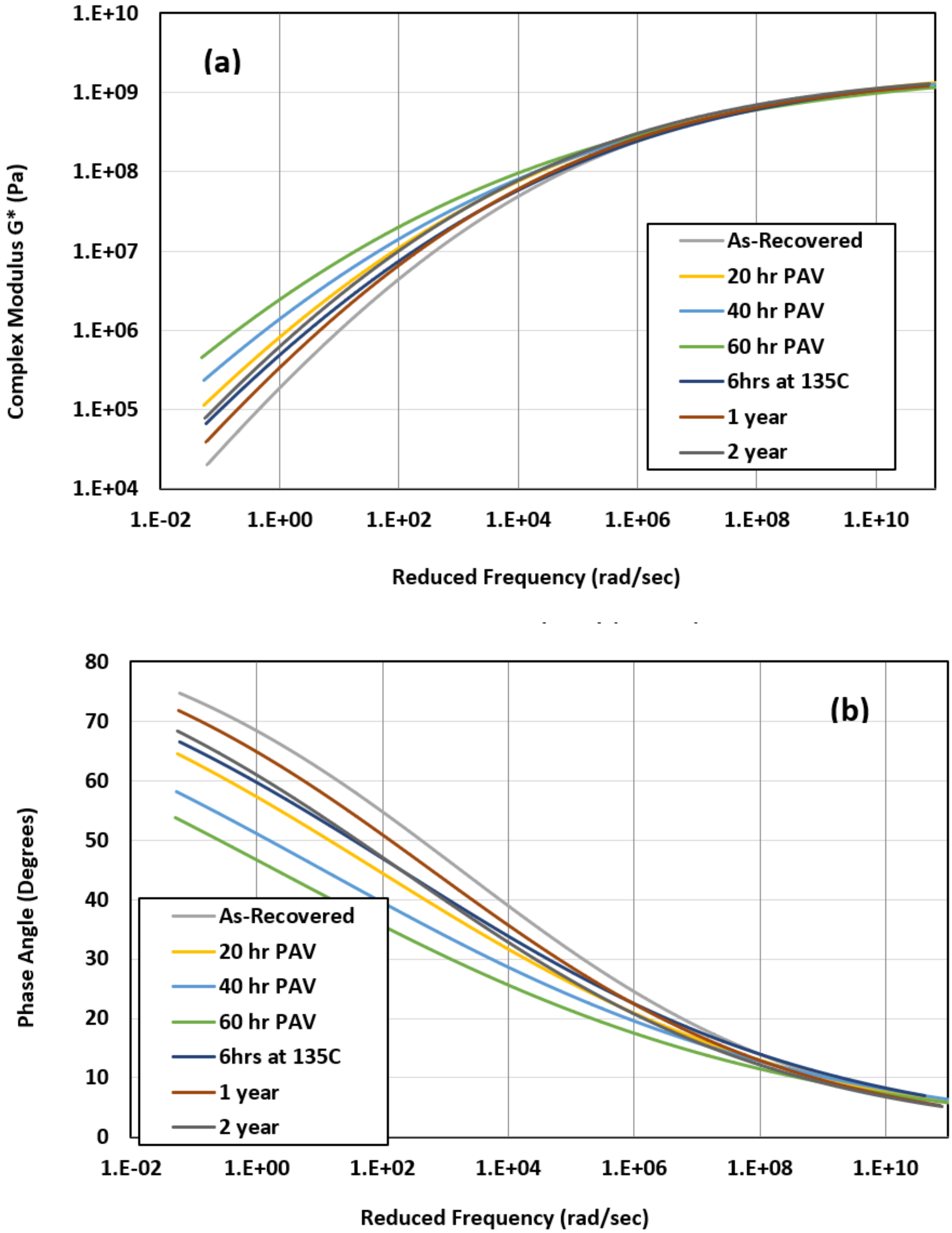

Figure A-14 Master Curves of (a) Complex Modulus and (b) Phase Angle for Section 6005 – All Aging Conditions (Ref. 25°C)

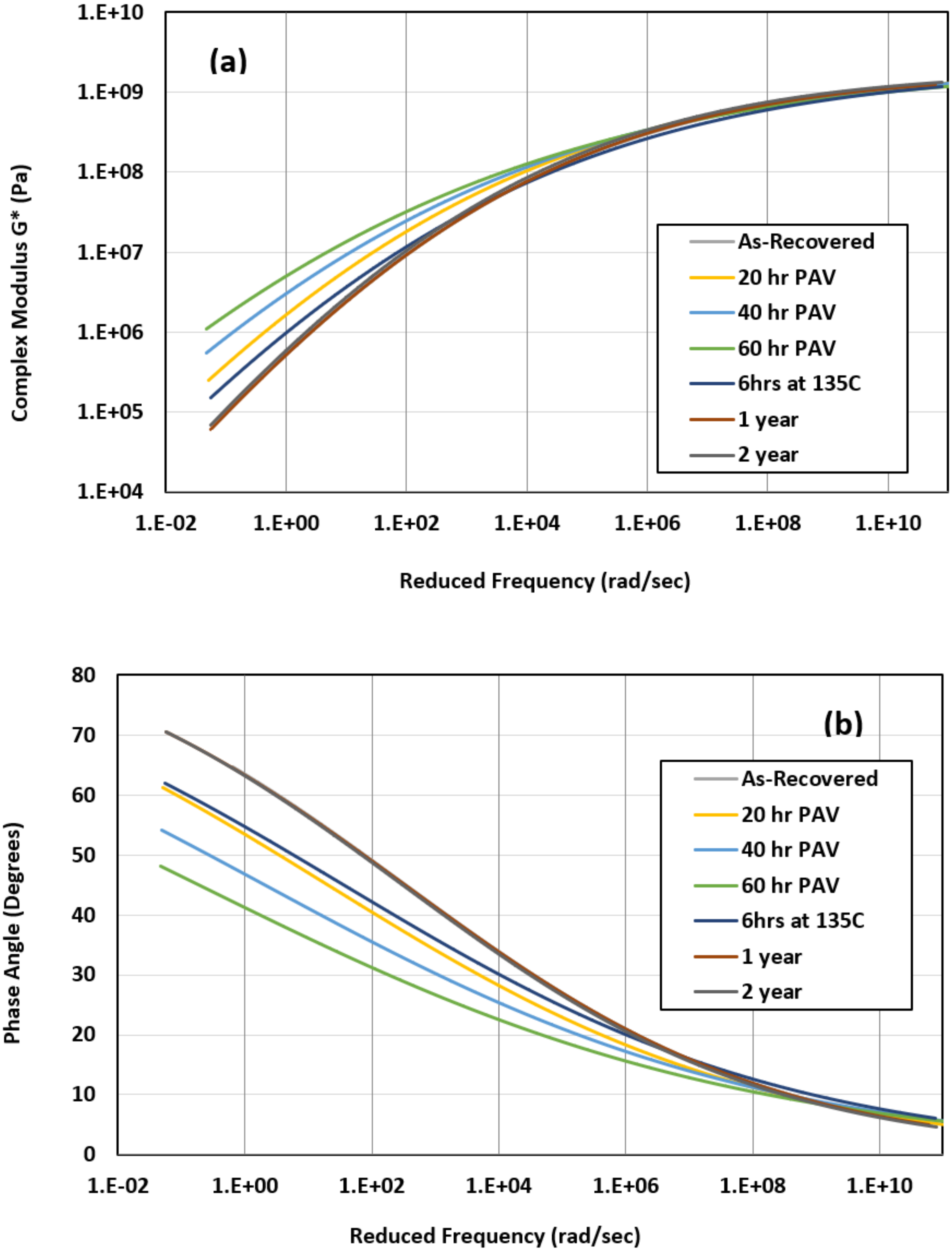

Figure A-15 Master Curves of (a) Complex Modulus and (b) Phase Angle for Section 6006 – All Aging Conditions (Ref. 25°C)

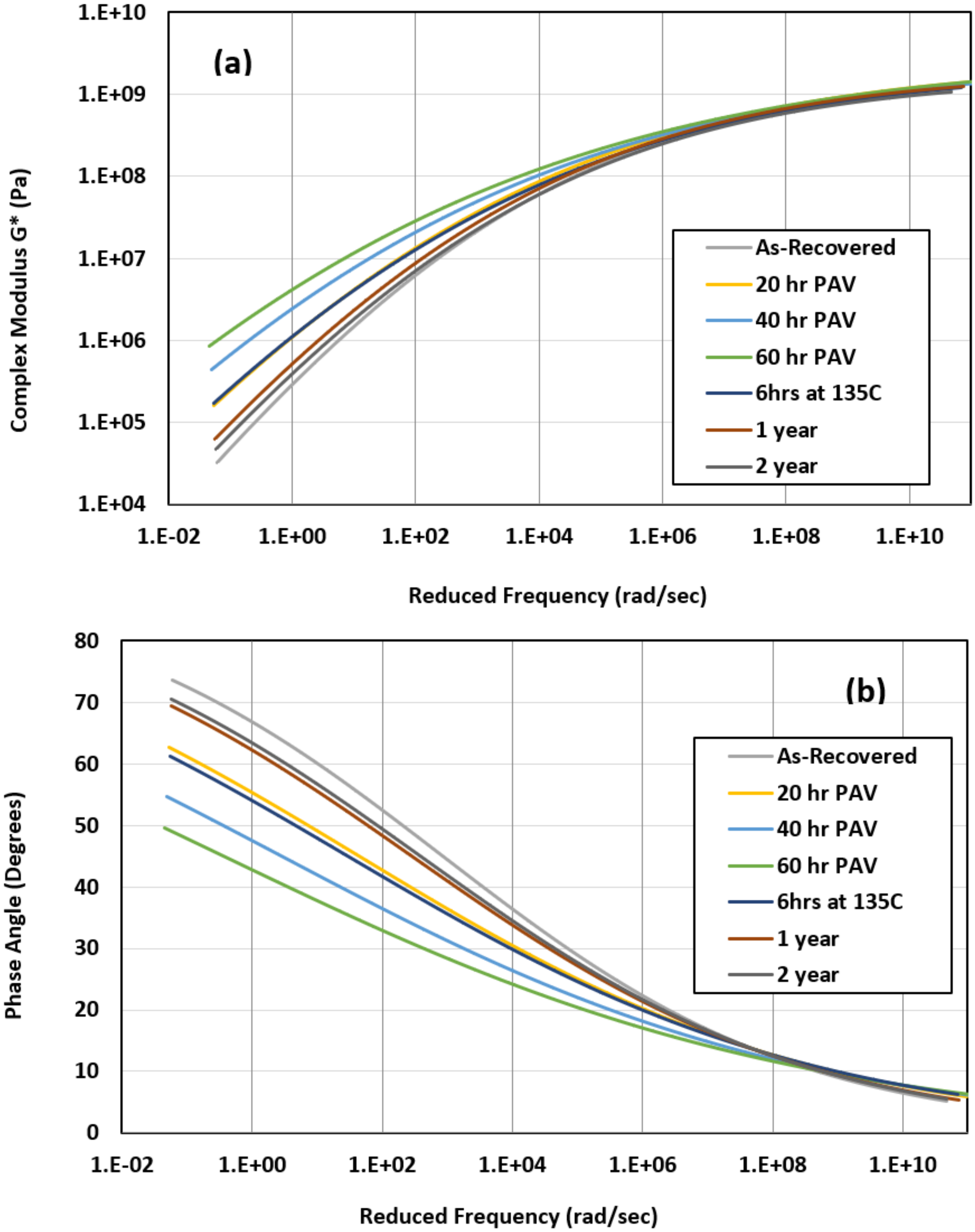

Figure A-16 Master Curves of (a) Complex Modulus and (b) Phase Angle for Section 6007 – All Aging Conditions (Ref. 25°C)

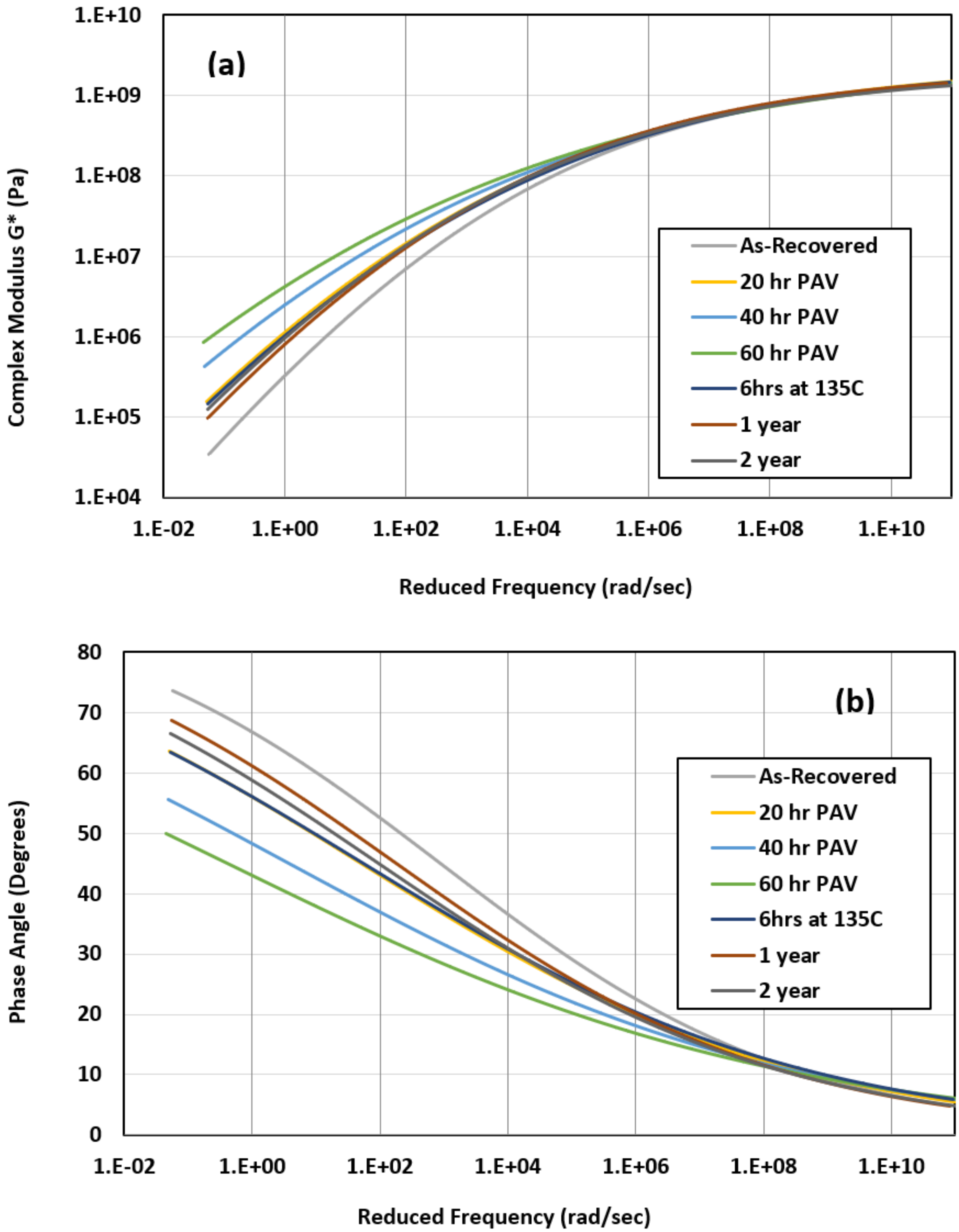

Figure A-17 Master Curves of (a) Complex Modulus and (b) Phase Angle for Section 6010 – All Aging Conditions (Ref. 25°C)

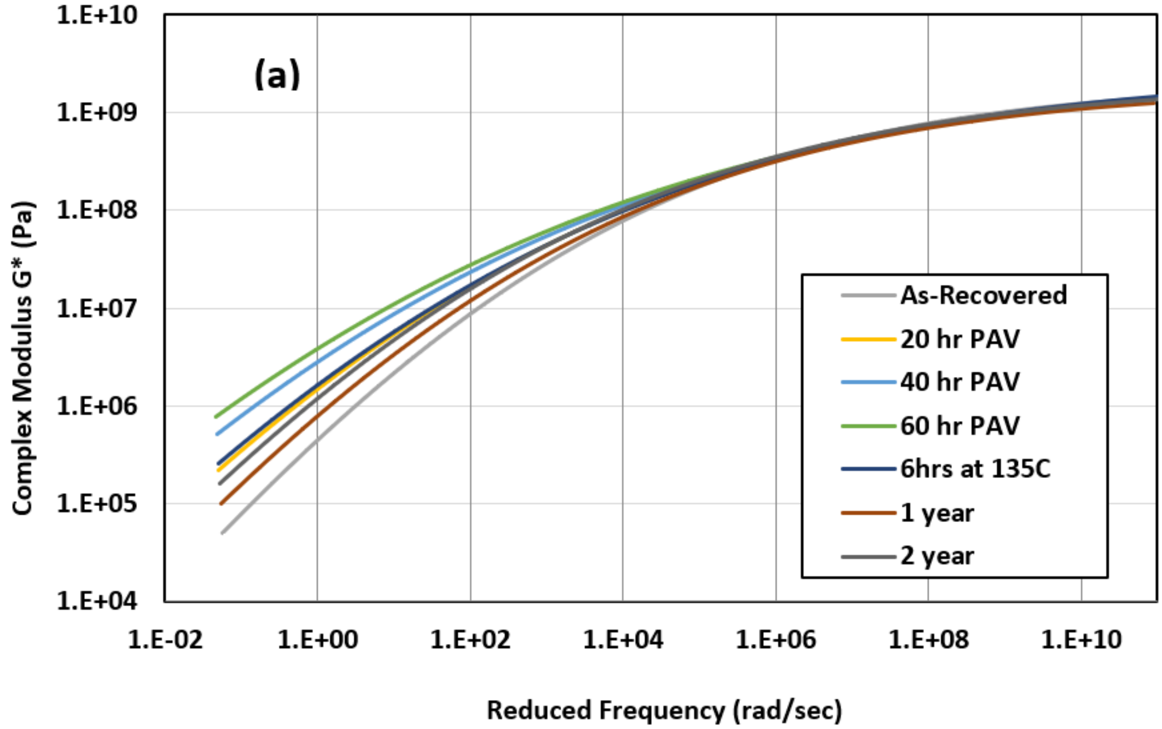

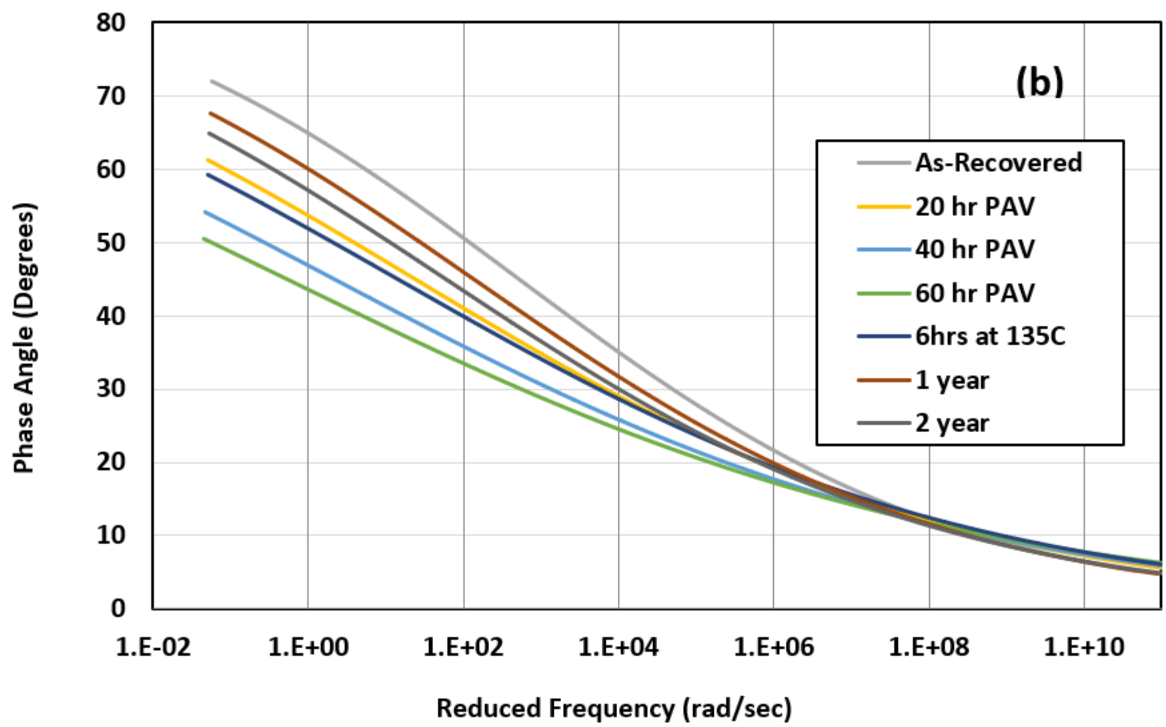

Figure A-18 Master Curves of (a) Complex Modulus and (b) Phase Angle for Section 6011 – All Aging Conditions (Ref. 25°C)

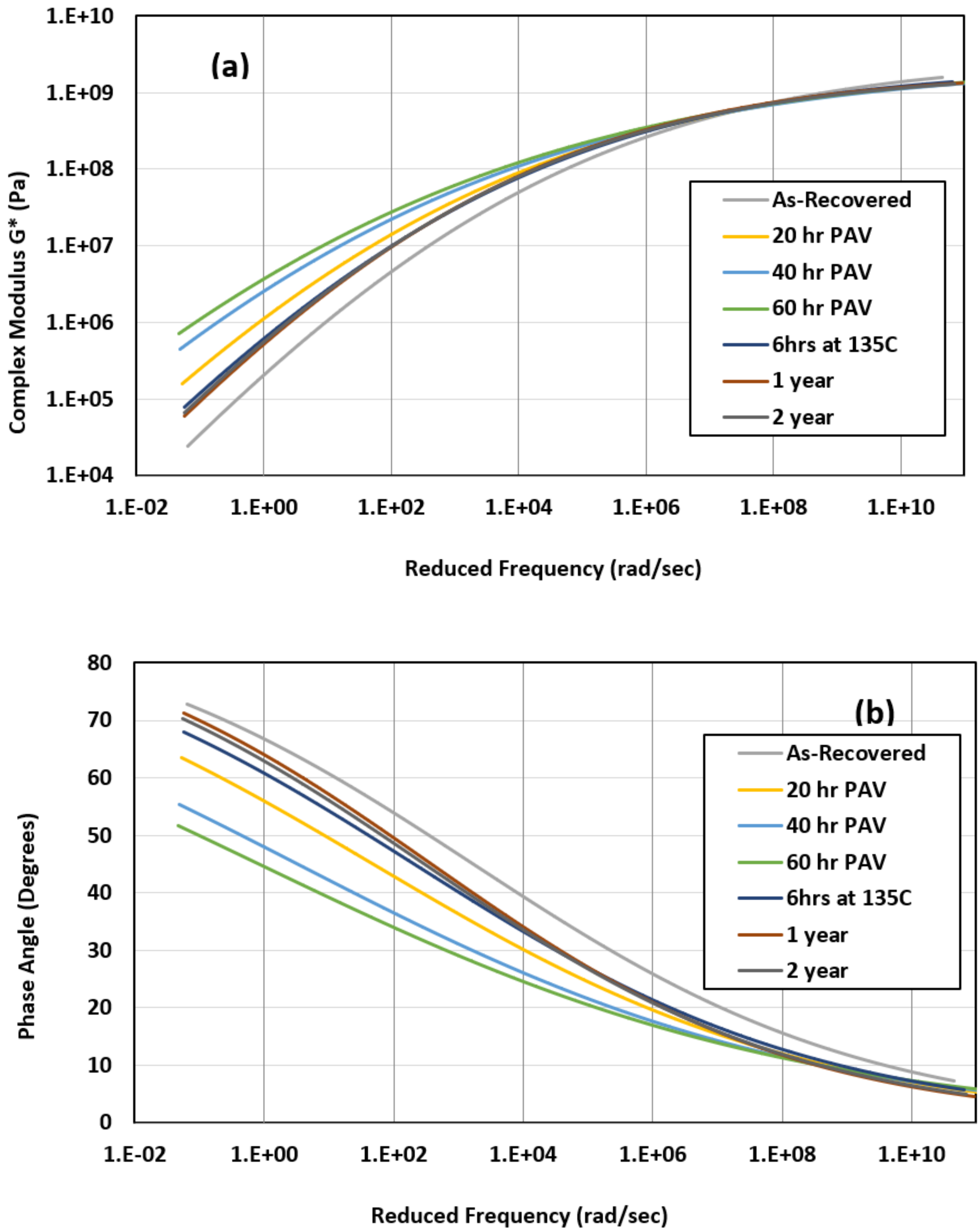

Figure A-19 Master Curves of (a) Complex Modulus and (b) Phase Angle for Section 6012 – All Aging Conditions (Ref. 25°C)

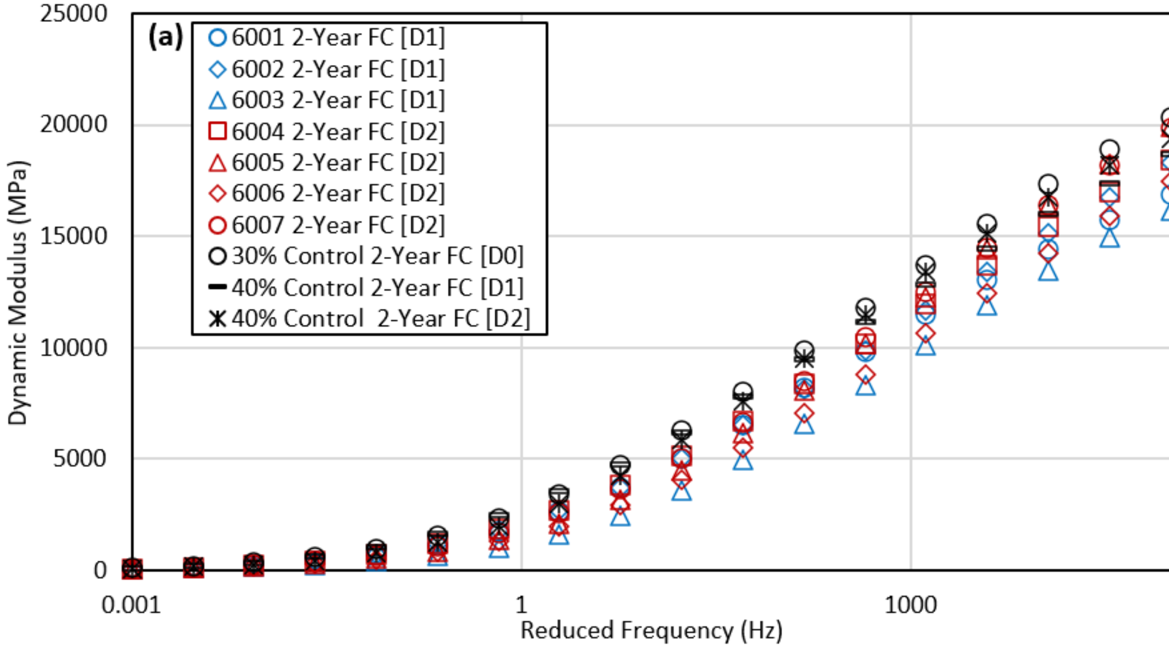

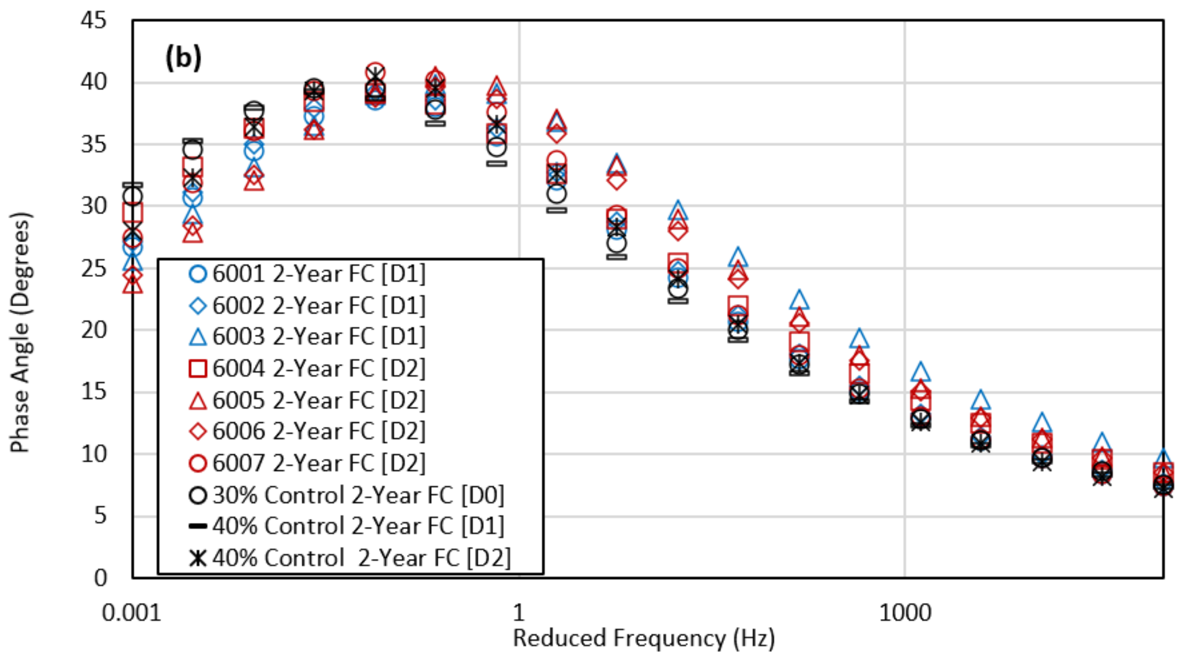

Figure A-20 Master Curves of (a) Dynamic Modulus (Logarithmic Scale) and (b) Phase Angle for 2-Year Field Core Mixtures (Ref. 21.1°C)

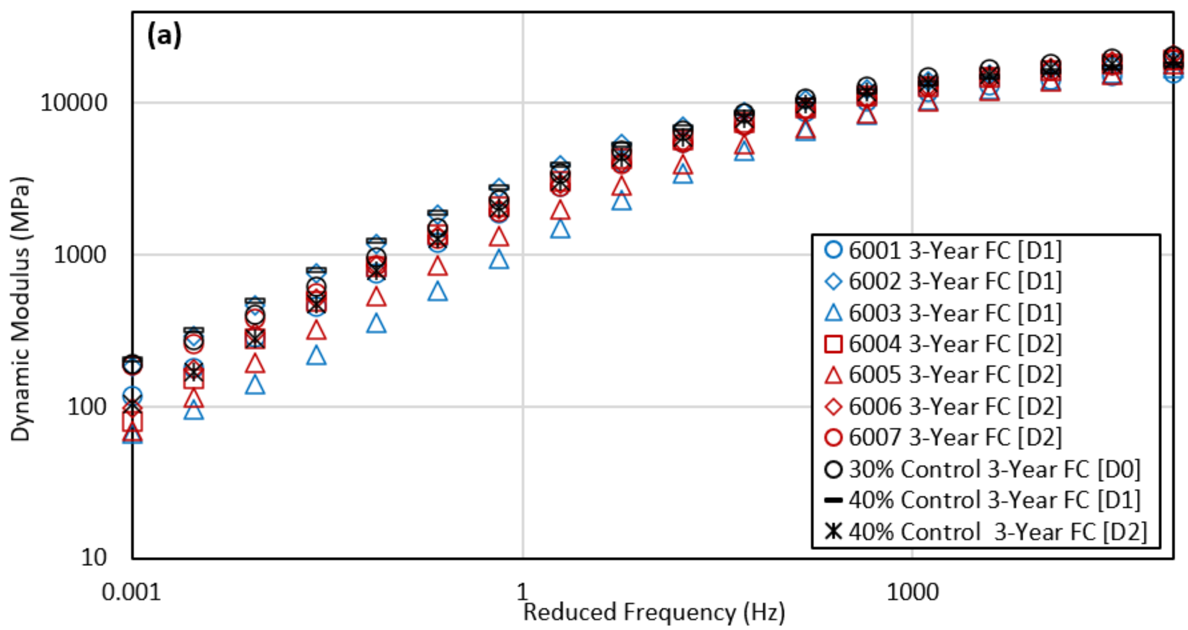
(a)
10000
1000
100
10
Dynamic Modulus (MPa)
0.001
1
1000
Reduced Frequency (Hz)
6001 3-Year FC [D1]
6002 3-Year FC [D1]
6003 3-Year FC [D1]
6004 3-Year FC [D2]
6005 3-Year FC [D2]
6006 3-Year FC [D2]
6007 3-Year FC [D2]
30% Control 3-Year FC [D0]
40% Control 3-Year FC [D1]
40% Control 3-Year FC [D2]

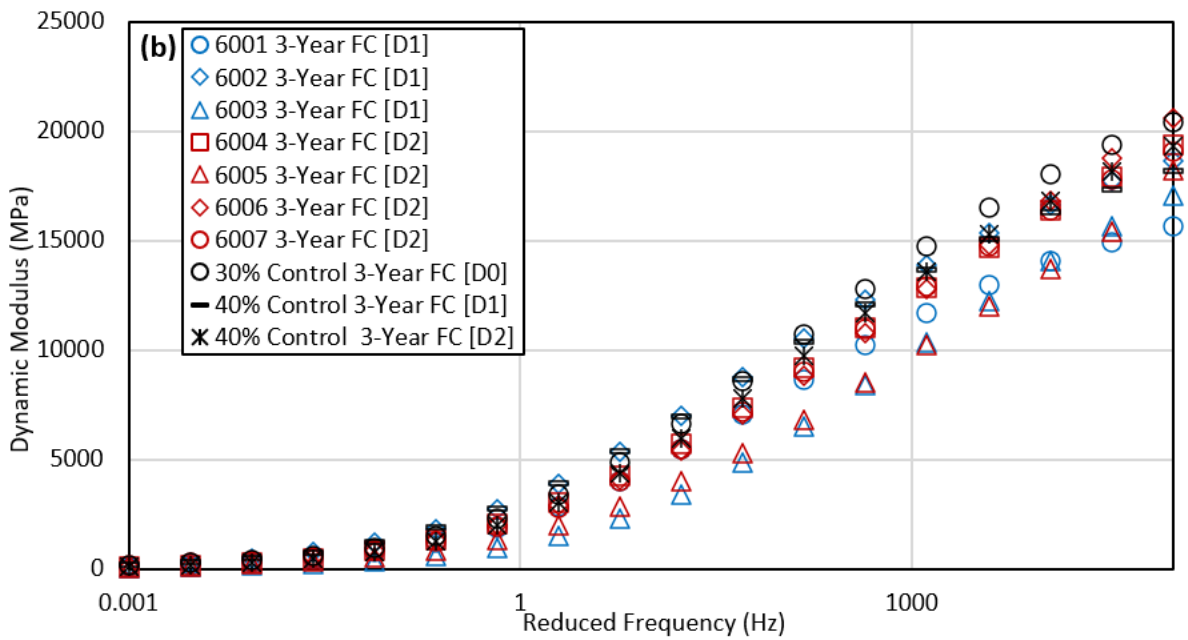
(b)
25000
20000
15000
10000
5000
0
Dynamic Modulus (MPa)
0.001
1
1000
Reduced Frequency (Hz)
6001 3-Year FC [D1]
6002 3-Year FC [D1]
6003 3-Year FC [D1]
6004 3-Year FC [D2]
6005 3-Year FC [D2]
6006 3-Year FC [D2]
6007 3-Year FC [D2]
30% Control 3-Year FC [D0]
40% Control 3-Year FC [D1]
40% Control 3-Year FC [D2]

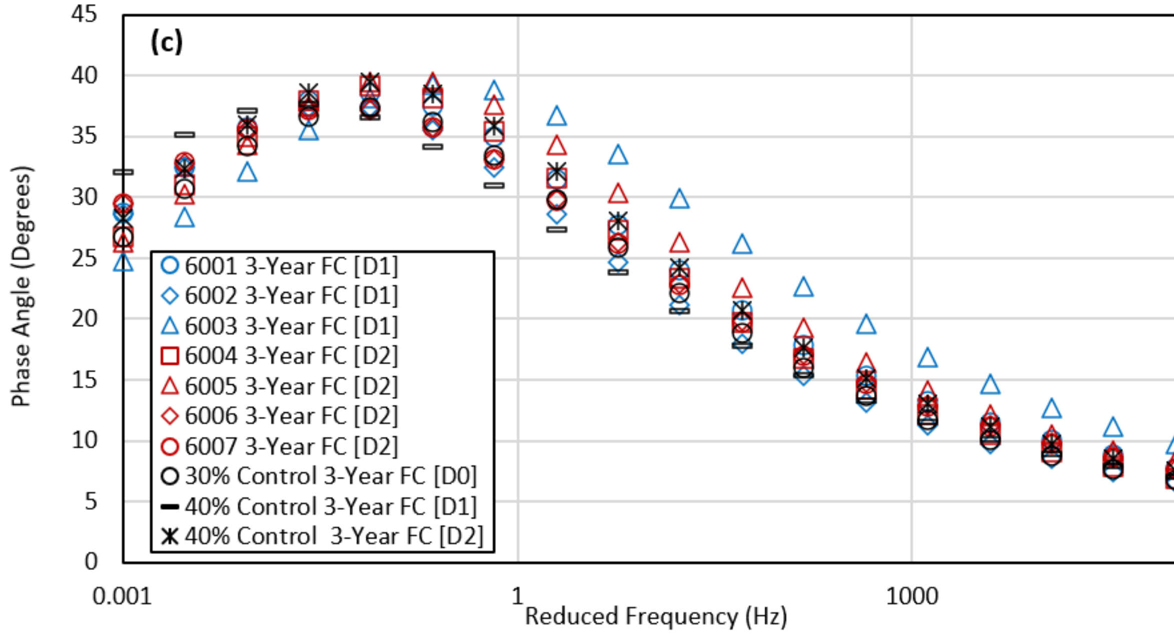

Figure A-21 Master Curves of (a) Dynamic Modulus (Linear Scale) (b) Dynamic Modulus (Logarithmic Scale) and (c) Phase Angle for 3-Year Field Core Mixtures (Ref. 21.1°C)

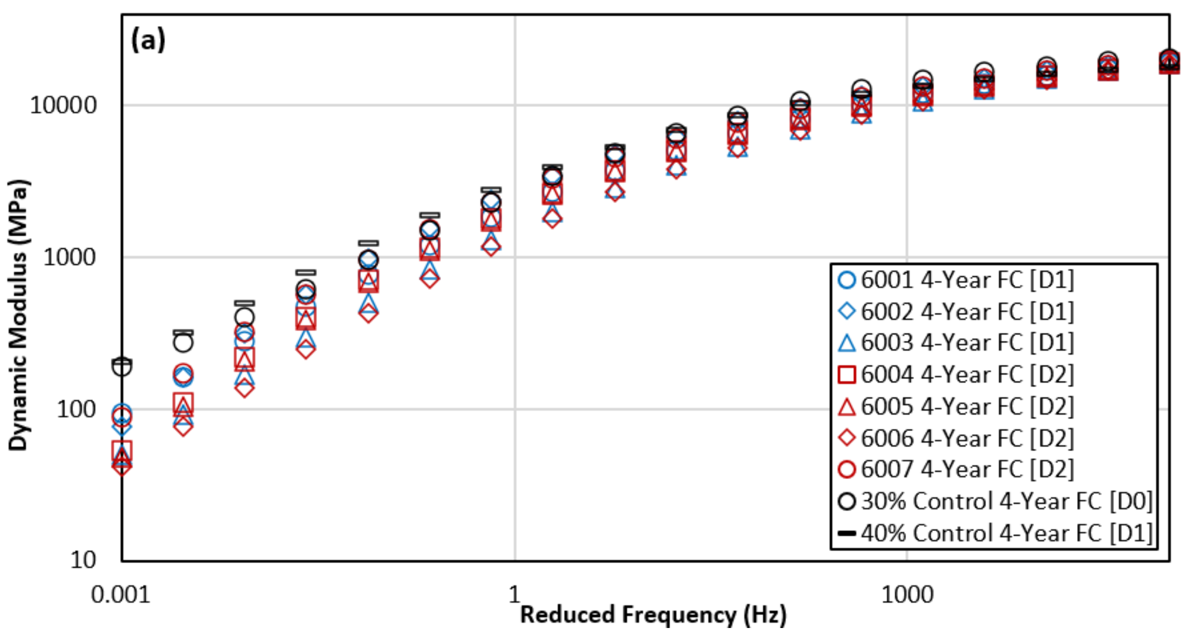

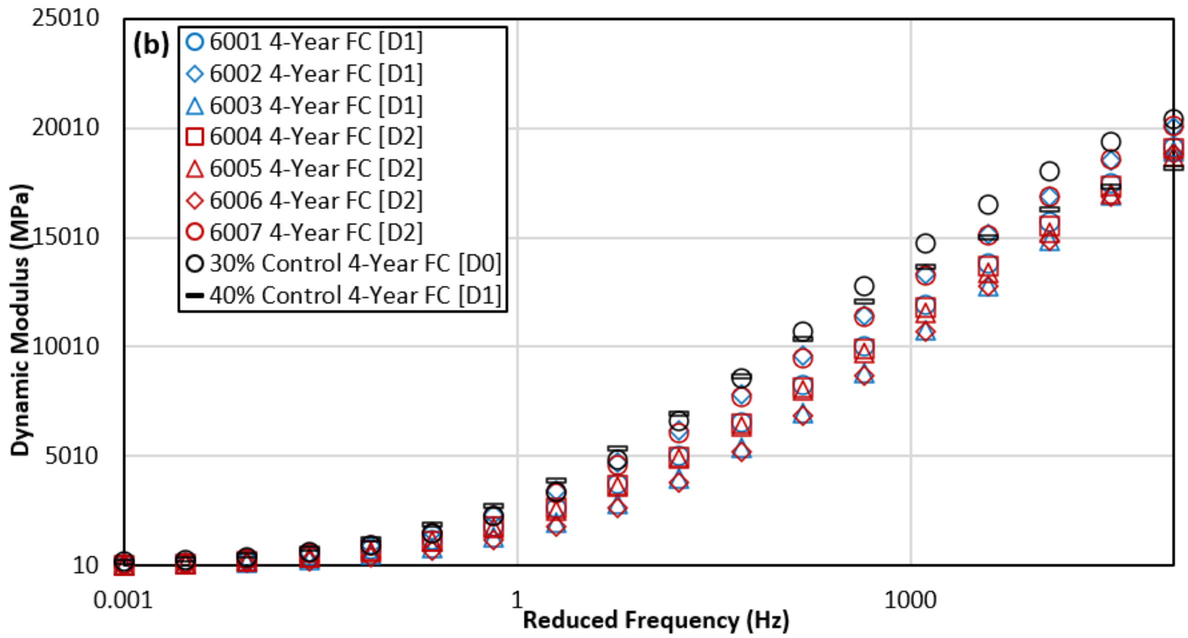

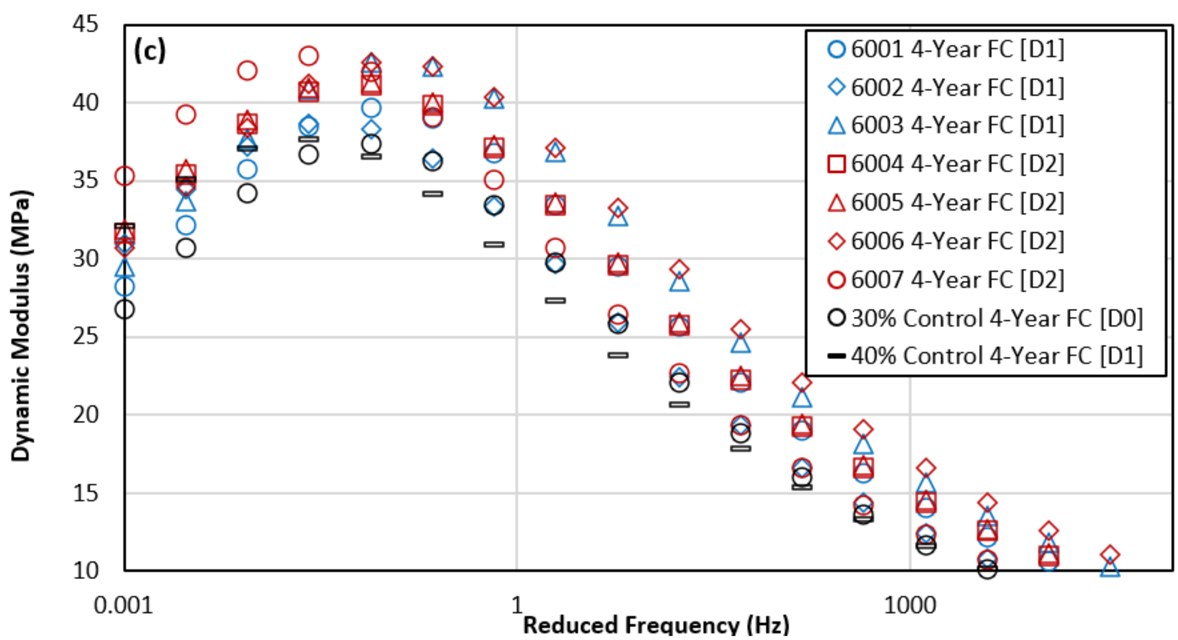

Figure A-22 Master Curves of (a) Dynamic Modulus (Linear Scale) (b) Dynamic Modulus (Logarithmic Scale) and (c) Phase Angle for 3-Year Field Core Mixtures (Ref. 21.1°C)

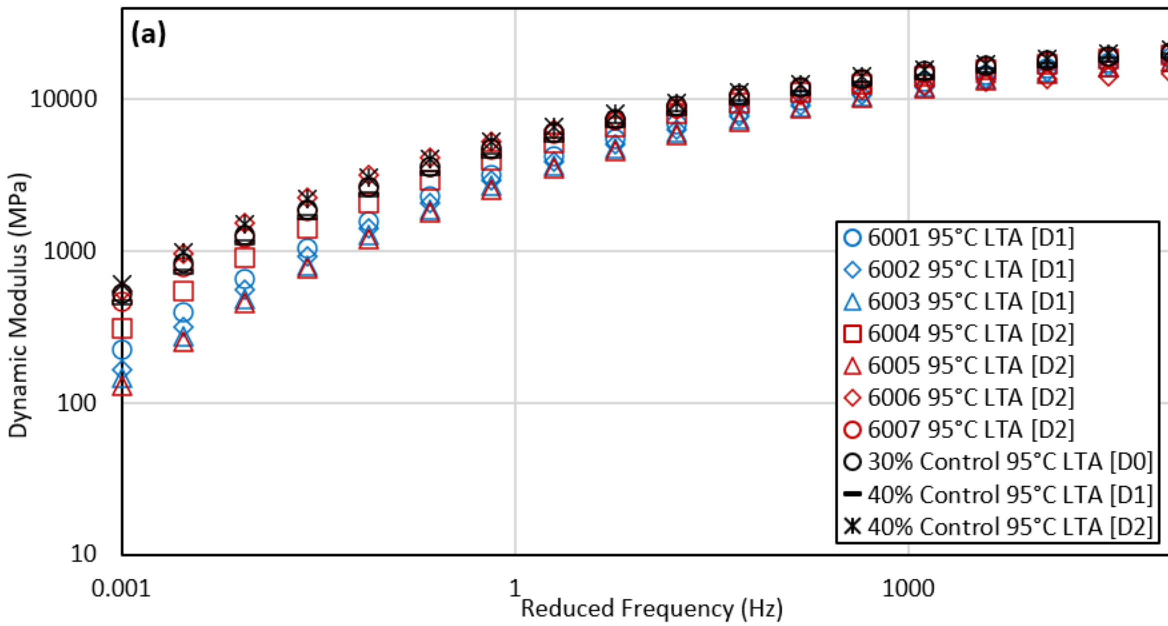

(a)
Dynamic Modulus (MPa)
10000
1000
100
10
0.001
1
1000
Reduced Frequency (Hz)
6001 95°C LTA [D1]
6002 95°C LTA [D1]
6003 95°C LTA [D1]
6004 95°C LTA [D2]
6005 95°C LTA [D2]
6006 95°C LTA [D2]
6007 95°C LTA [D2]
30% Control 95°C LTA [D0]
40% Control 95°C LTA [D1]
40% Control 95°C LTA [D2]

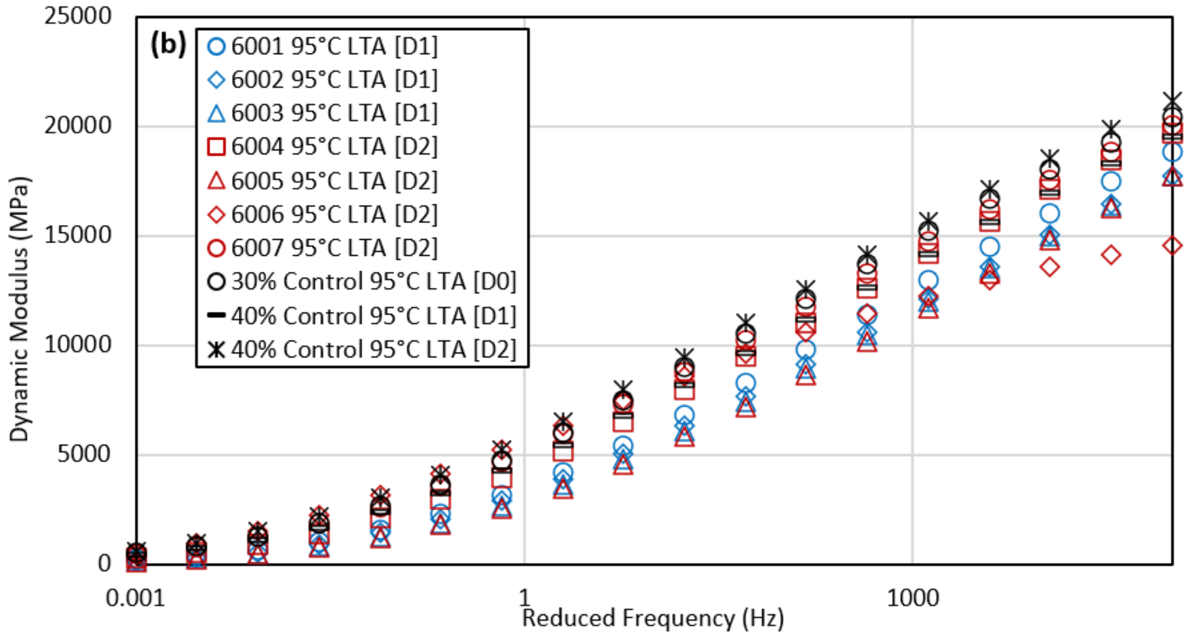

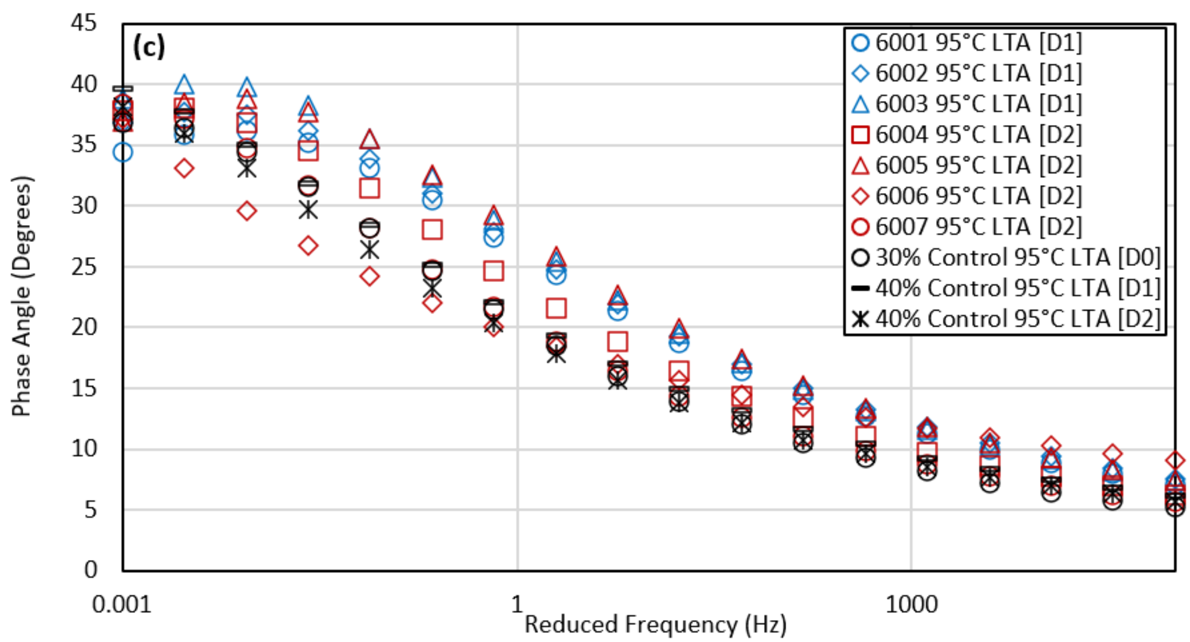

Figure A-23 Master Curves of (a) Dynamic Modulus (Linear Scale) (b) Dynamic Modulus (Logarithmic Scale) and (c) Phase Angle for 7day at 95°C Loose Mix LTA (Ref. 21.1°C)

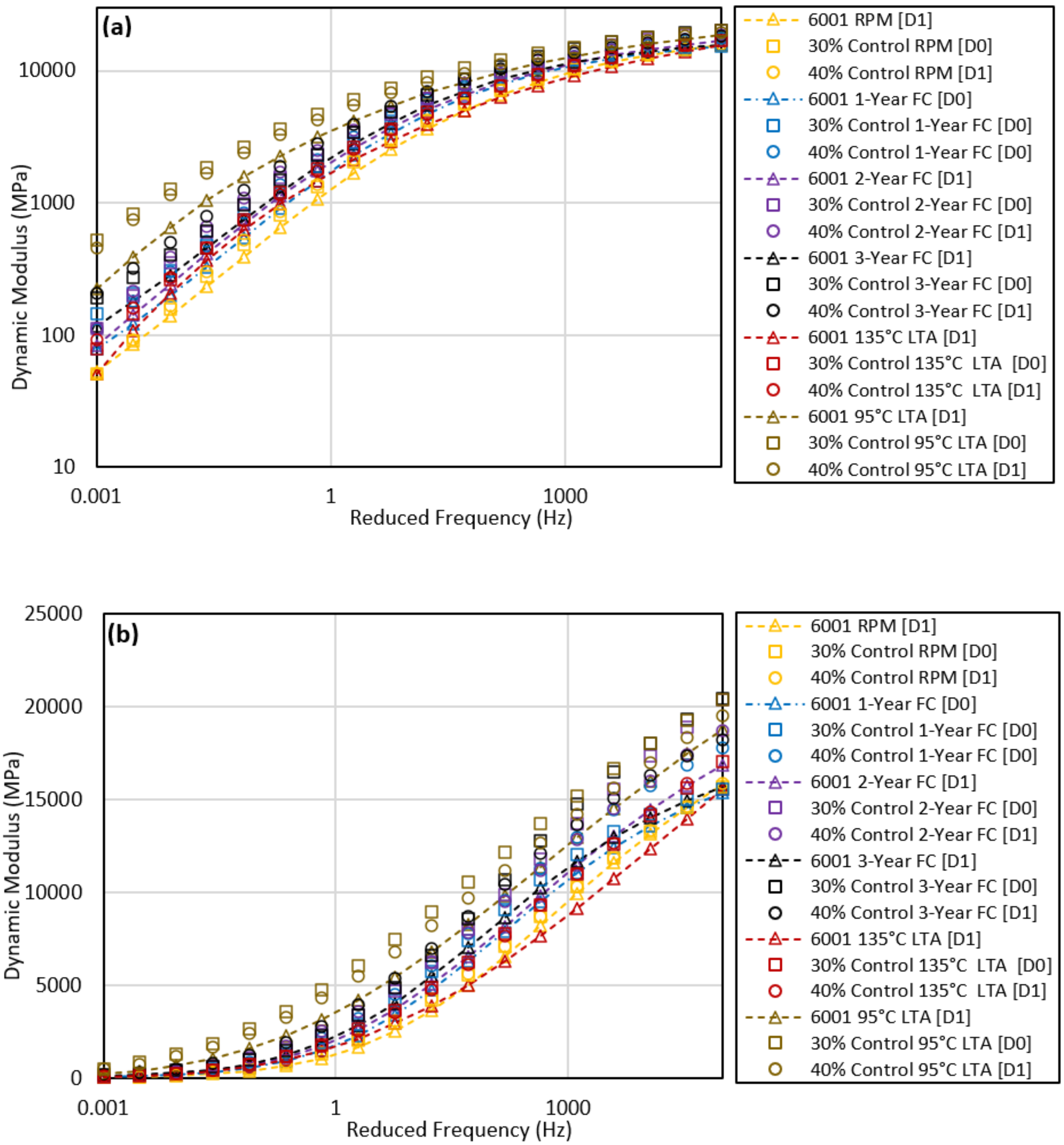
(a)
Dynamic Modulus (MPa)
10000
1000
100
10
0.001
1
1000
Reduced Frequency (Hz)
6001 RPM [D1]
30% Control RPM [D0]
40% Control RPM [D1]
6001 1-Year FC [D0]
30% Control 1-Year FC [D0]
40% Control 1-Year FC [D0]
6001 2-Year FC [D1]
30% Control 2-Year FC [D0]
40% Control 2-Year FC [D1]
6001 3-Year FC [D1]
30% Control 3-Year FC [D0]
40% Control 3-Year FC [D1]
6001 135°C LTA [D1]
30% Control 135°C LTA [D0]
40% Control 135°C LTA [D1]
6001 95°C LTA [D1]
30% Control 95°C LTA [D0]
40% Control 95°C LTA [D1]
(b)
Dynamic Modulus (MPa)
25000
20000
15000
10000
5000
0
0.001
1
1000
Reduced Frequency (Hz)
6001 RPM [D1]
30% Control RPM [D0]
40% Control RPM [D1]
6001 1-Year FC [D0]
30% Control 1-Year FC [D0]
40% Control 1-Year FC [D0]
6001 2-Year FC [D1]
30% Control 2-Year FC [D0]
40% Control 2-Year FC [D1]
6001 3-Year FC [D1]
30% Control 3-Year FC [D0]
40% Control 3-Year FC [D1]
6001 135°C LTA [D1]
30% Control 135°C LTA [D0]
40% Control 135°C LTA [D1]
6001 95°C LTA [D1]
30% Control 95°C LTA [D0]
40% Control 95°C LTA [D1]

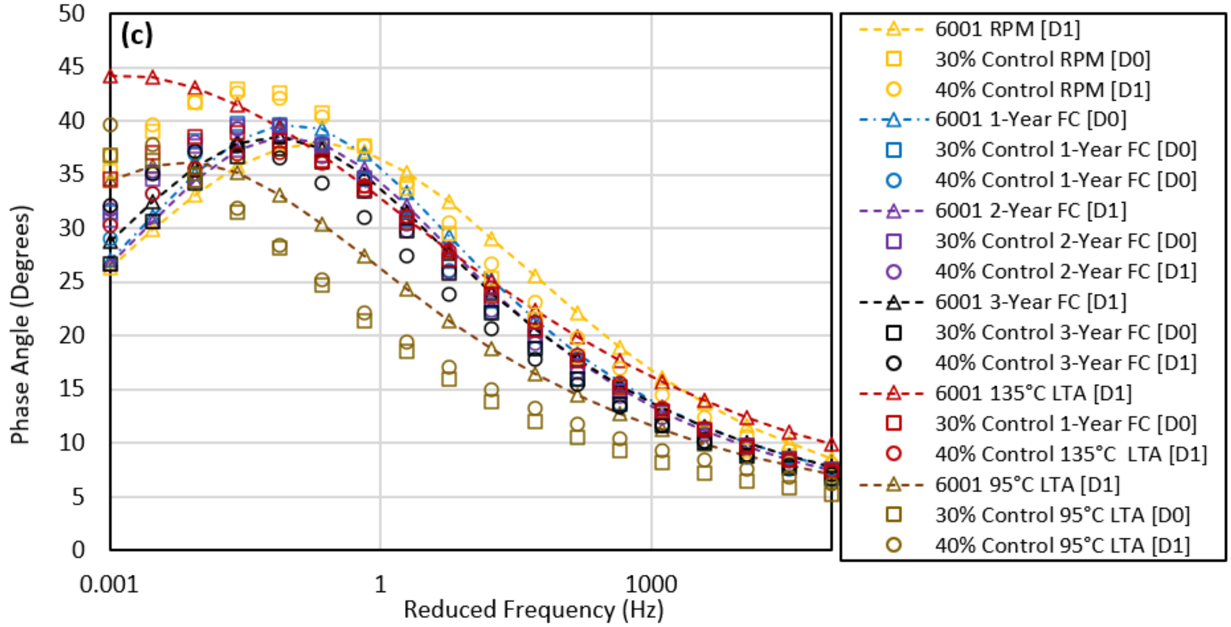

Figure A-24 Master Curves of (a) Dynamic Modulus (Linear Scale) (b) Dynamic Modulus (Logarithmic Scale) and (c) Phase Angle for 6001 Mixture with Different Aging Conditions (Ref. 21.1°C)

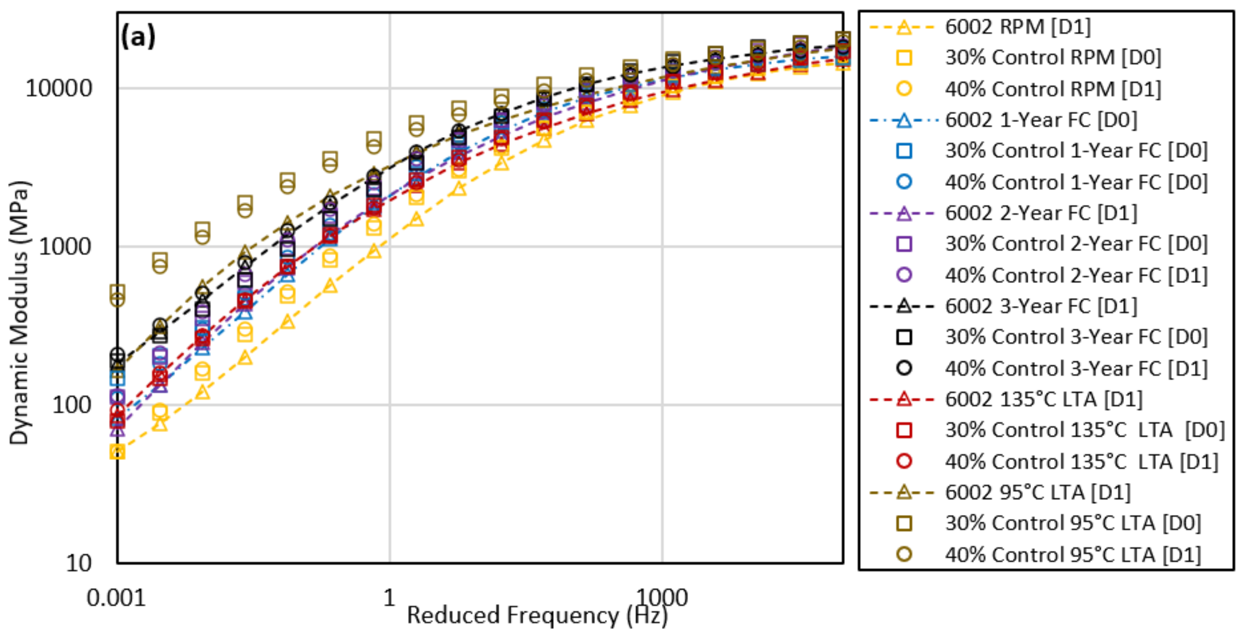

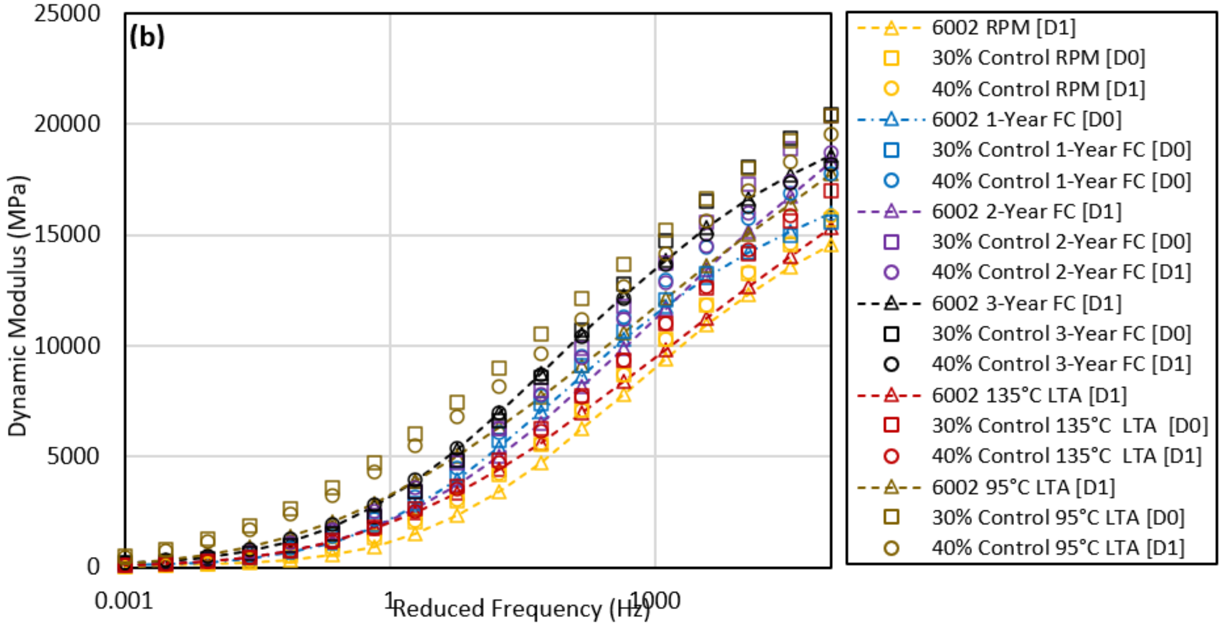

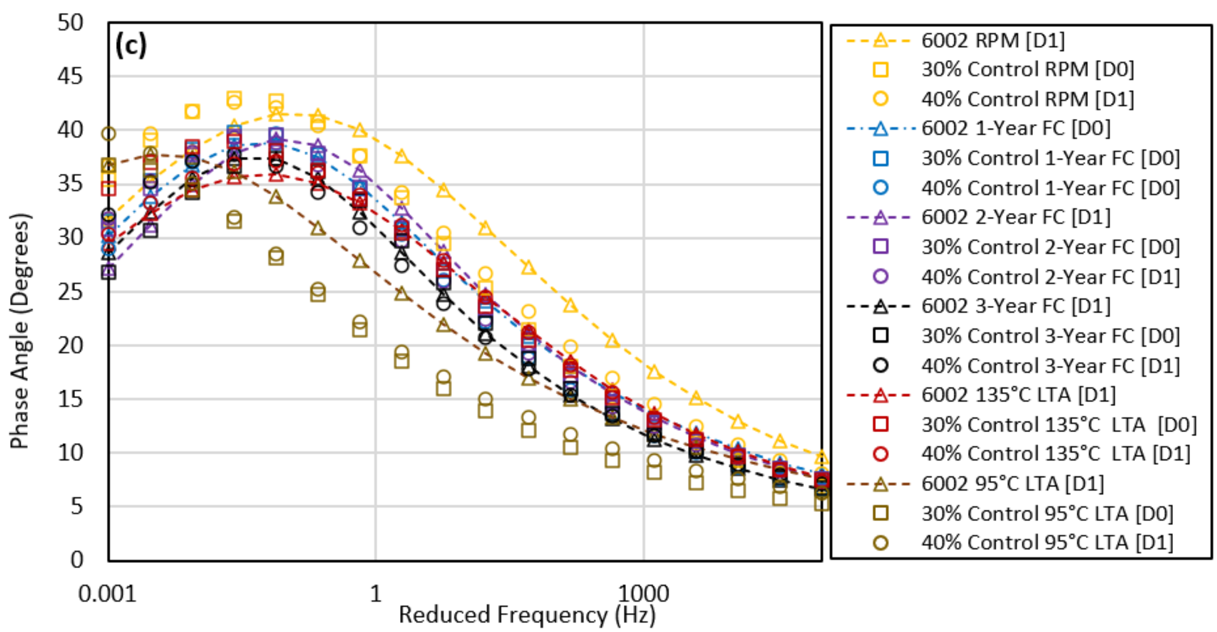

Figure A-25 Master Curves of (a) Dynamic Modulus (Linear Scale) (b) Dynamic Modulus (Logarithmic Scale) and (c) Phase Angle for 6002 Mixture with Different Aging Conditions (Ref. 21.1°C)

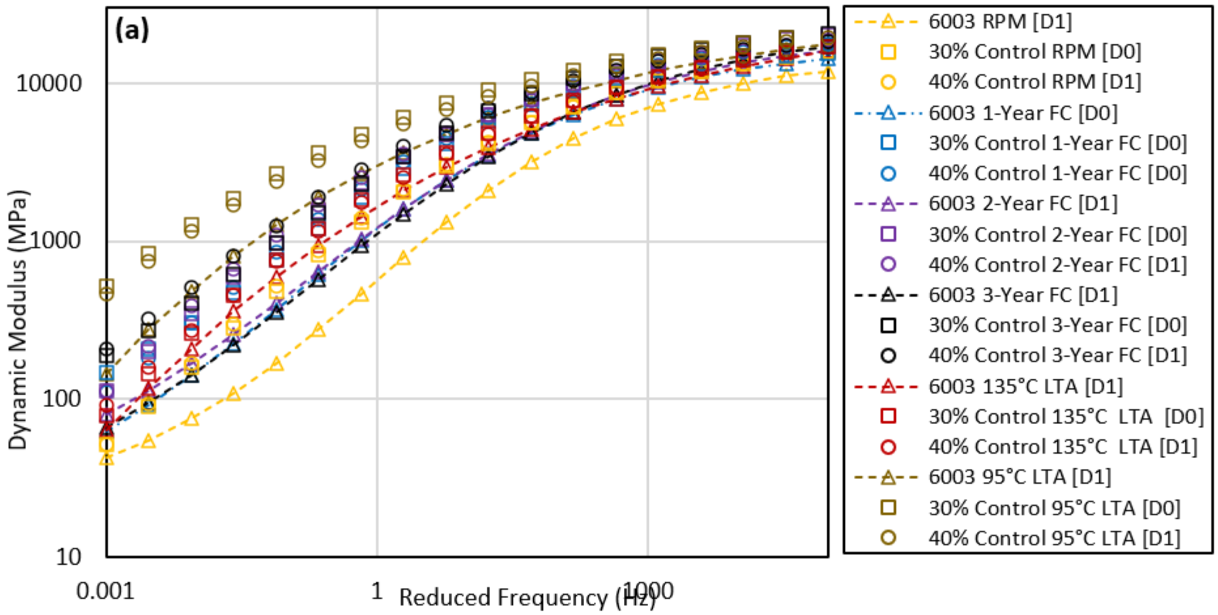
(a)
Dynamic Modulus (MPa)
10000
1000
100
10
0.001
1
1000
Reduced Frequency (Hz)
6003 RPM [D1]
30% Control RPM [D0]
40% Control RPM [D1]
6003 1-Year FC [D0]
30% Control 1-Year FC [D0]
40% Control 1-Year FC [D0]
6003 2-Year FC [D1]
30% Control 2-Year FC [D0]
40% Control 2-Year FC [D1]
6003 3-Year FC [D1]
30% Control 3-Year FC [D0]
40% Control 3-Year FC [D1]
6003 135°C LTA [D1]
30% Control 135°C LTA [D0]
40% Control 135°C LTA [D1]
6003 95°C LTA [D1]
30% Control 95°C LTA [D0]
40% Control 95°C LTA [D1]

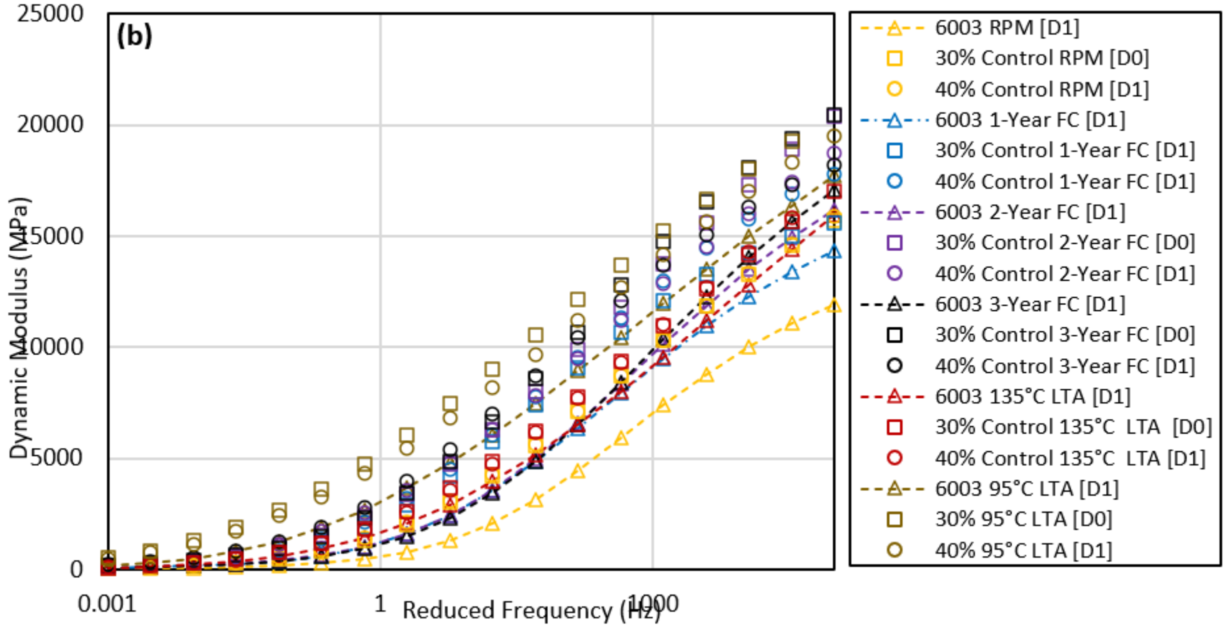
(b)
Dynamic Modulus (MPa)
25000
20000
15000
10000
5000
0
0.001
1
1000
Reduced Frequency (Hz)
6003 RPM [D1]
30% Control RPM [D0]
40% Control RPM [D1]
6003 1-Year FC [D1]
30% Control 1-Year FC [D1]
40% Control 1-Year FC [D1]
6003 2-Year FC [D1]
30% Control 2-Year FC [D0]
40% Control 2-Year FC [D1]
6003 3-Year FC [D1]
30% Control 3-Year FC [D0]
40% Control 3-Year FC [D1]
6003 135°C LTA [D1]
30% Control 135°C LTA [D0]
40% Control 135°C LTA [D1]
6003 95°C LTA [D1]
30% 95°C LTA [D0]
40% 95°C LTA [D1]

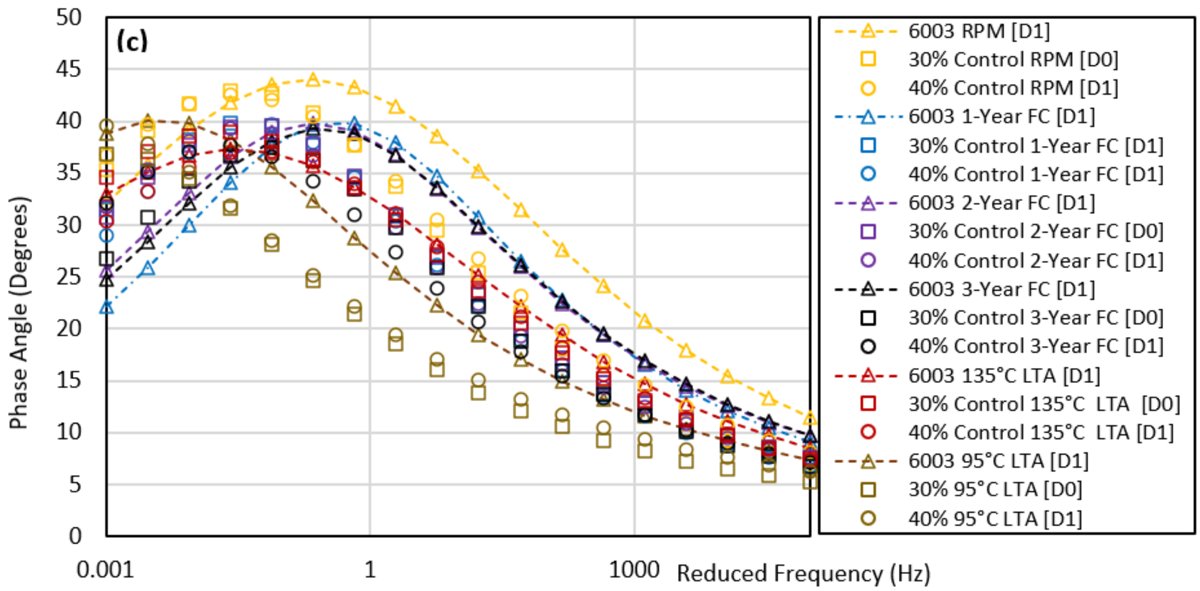

Figure A-26 Master Curves of (a) Dynamic Modulus (Linear Scale) (b) Dynamic Modulus (Logarithmic Scale) and (c) Phase Angle for 6003 Mixture with Different Aging Conditions (Ref. 21.1°C)

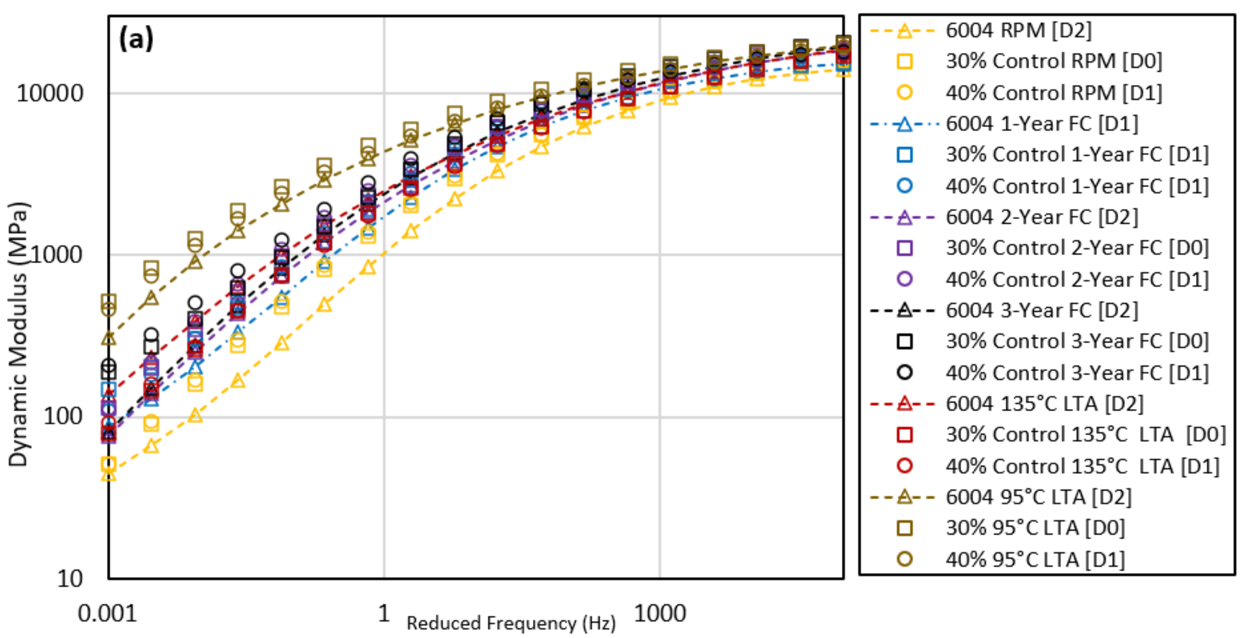

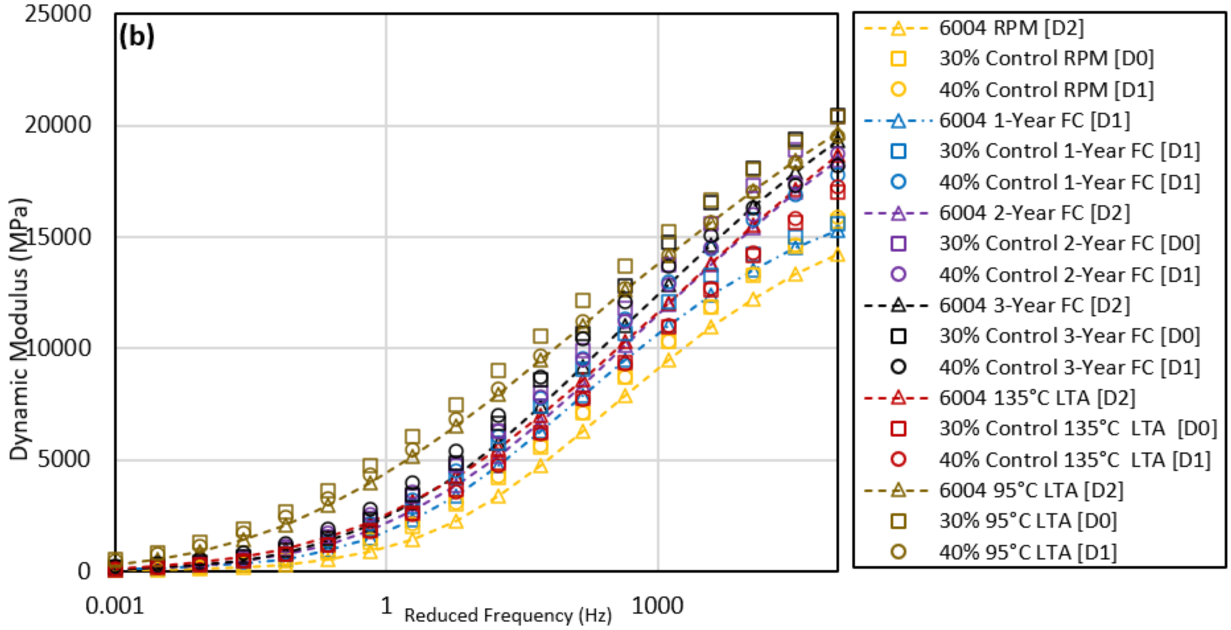

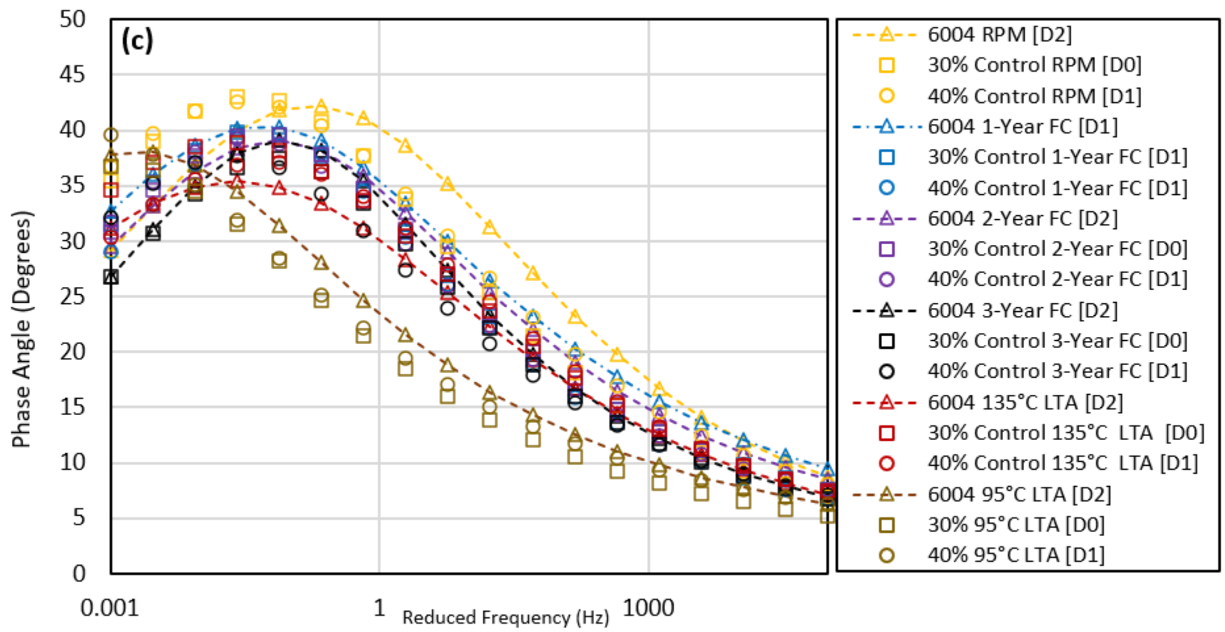

Figure A-27 Master Curves of (a) Dynamic Modulus (Linear Scale) (b) Dynamic Modulus (Logarithmic Scale) and (c) Phase Angle for 6004 Mixture with Different Aging Conditions (Ref. 21.1°C)

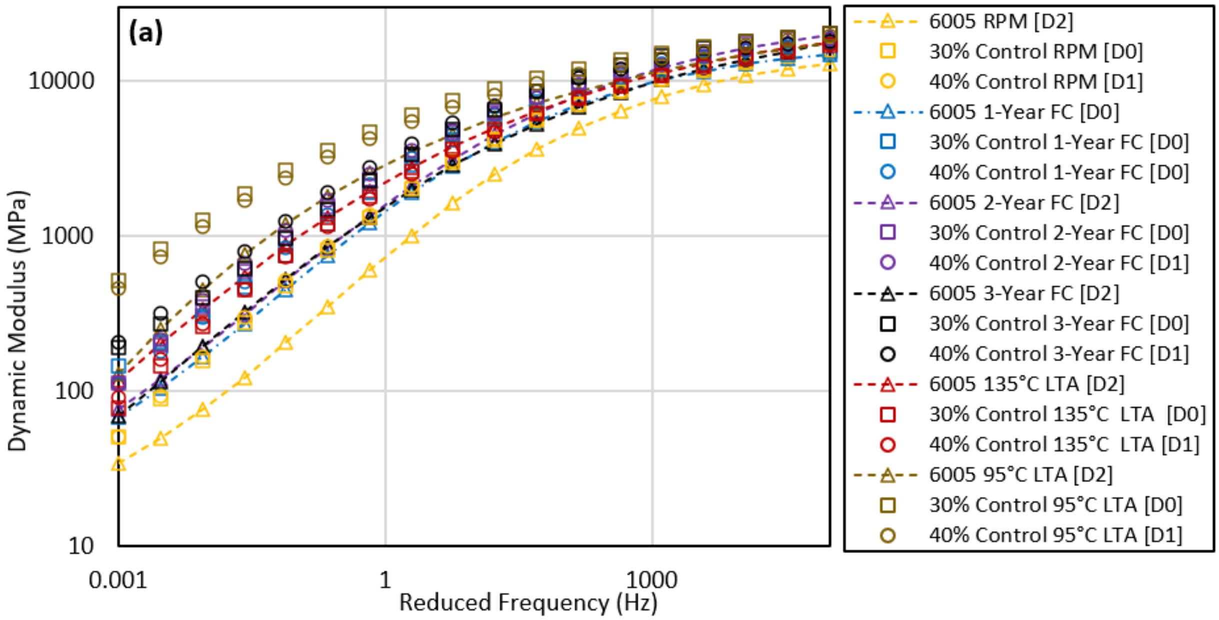
(a)
Dynamic Modulus (MPa)
10
100
1000
10000
0.001
1
1000
Reduced Frequency (Hz)
6005 RPM [D2]
30% Control RPM [D0]
40% Control RPM [D1]
6005 1-Year FC [D0]
30% Control 1-Year FC [D0]
40% Control 1-Year FC [D0]
6005 2-Year FC [D2]
30% Control 2-Year FC [D0]
40% Control 2-Year FC [D1]
6005 3-Year FC [D2]
30% Control 3-Year FC [D0]
40% Control 3-Year FC [D1]
6005 135°C LTA [D2]
30% Control 135°C LTA [D0]
40% Control 135°C LTA [D1]
6005 95°C LTA [D2]
30% Control 95°C LTA [D0]
40% Control 95°C LTA [D1]

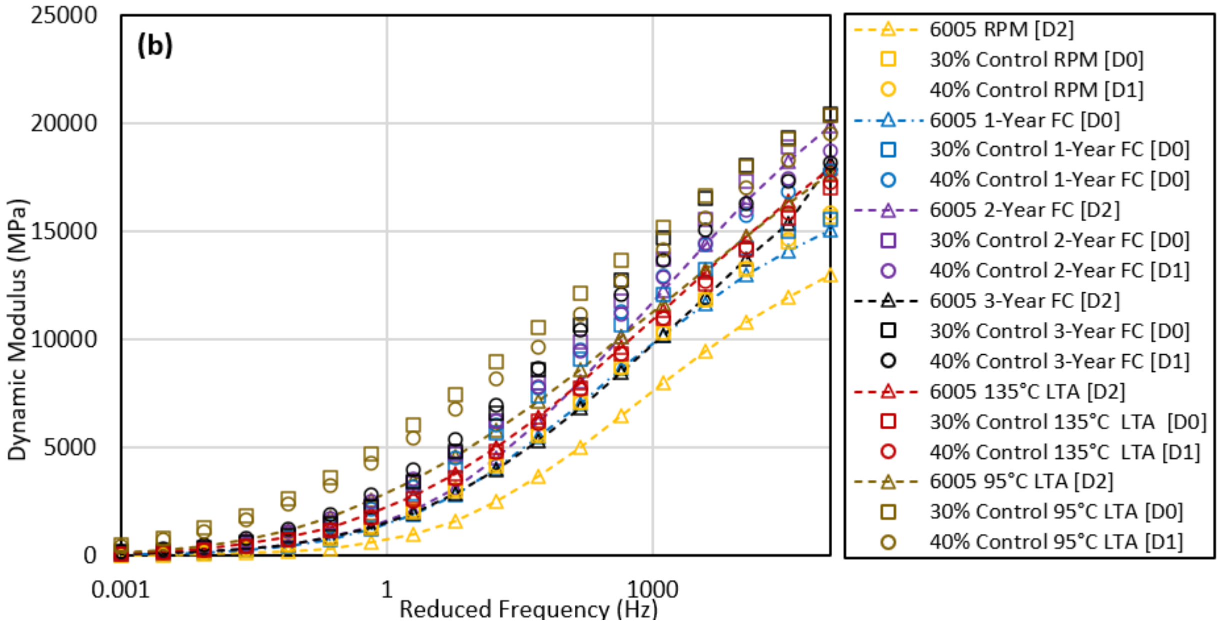
(b)
Dynamic Modulus (MPa)
0
5000
10000
15000
20000
25000
0.001
1
1000
Reduced Frequency (Hz)
6005 RPM [D2]
30% Control RPM [D0]
40% Control RPM [D1]
6005 1-Year FC [D0]
30% Control 1-Year FC [D0]
40% Control 1-Year FC [D0]
6005 2-Year FC [D2]
30% Control 2-Year FC [D0]
40% Control 2-Year FC [D1]
6005 3-Year FC [D2]
30% Control 3-Year FC [D0]
40% Control 3-Year FC [D1]
6005 135°C LTA [D2]
30% Control 135°C LTA [D0]
40% Control 135°C LTA [D1]
6005 95°C LTA [D2]
30% Control 95°C LTA [D0]
40% Control 95°C LTA [D1]

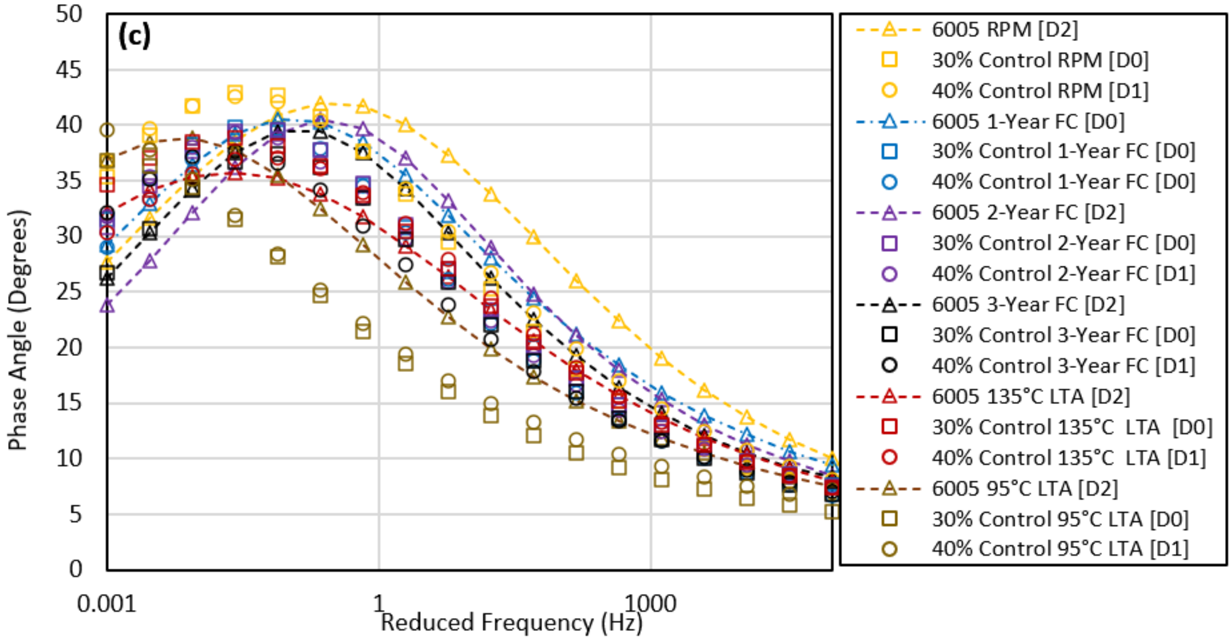

Figure A-28 Master Curves of (a) Dynamic Modulus (Linear Scale) (b) Dynamic Modulus (Logarithmic Scale) and (c) Phase Angle for 6005 Mixture with Different Aging Conditions (Ref. 21.1°C)

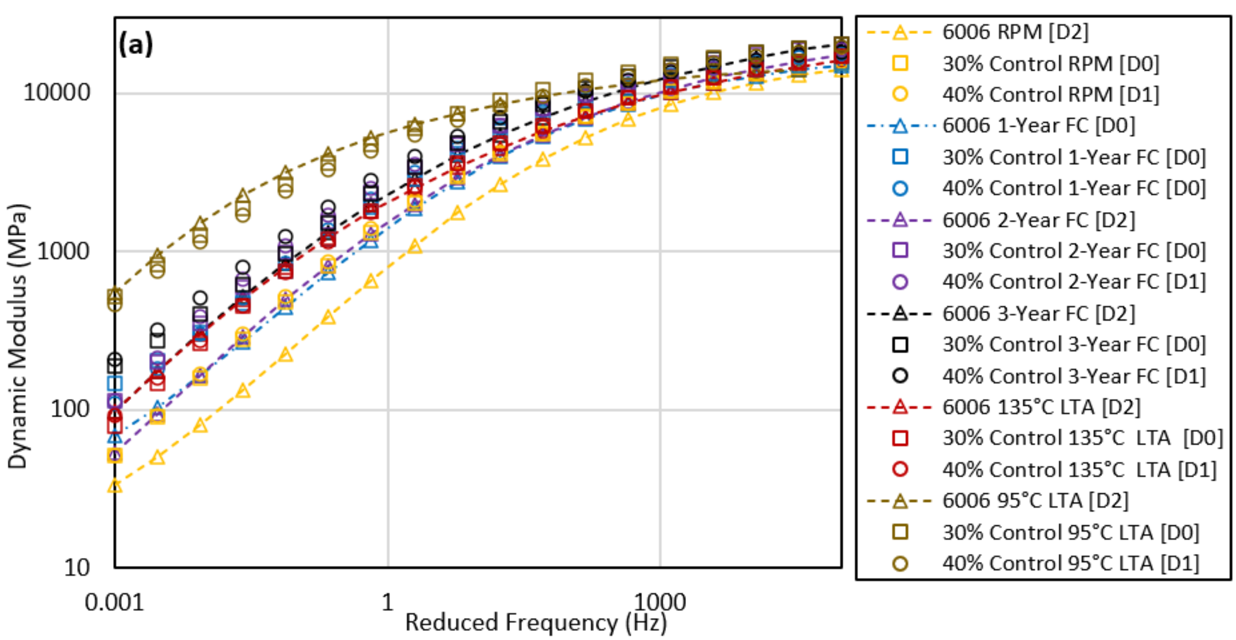

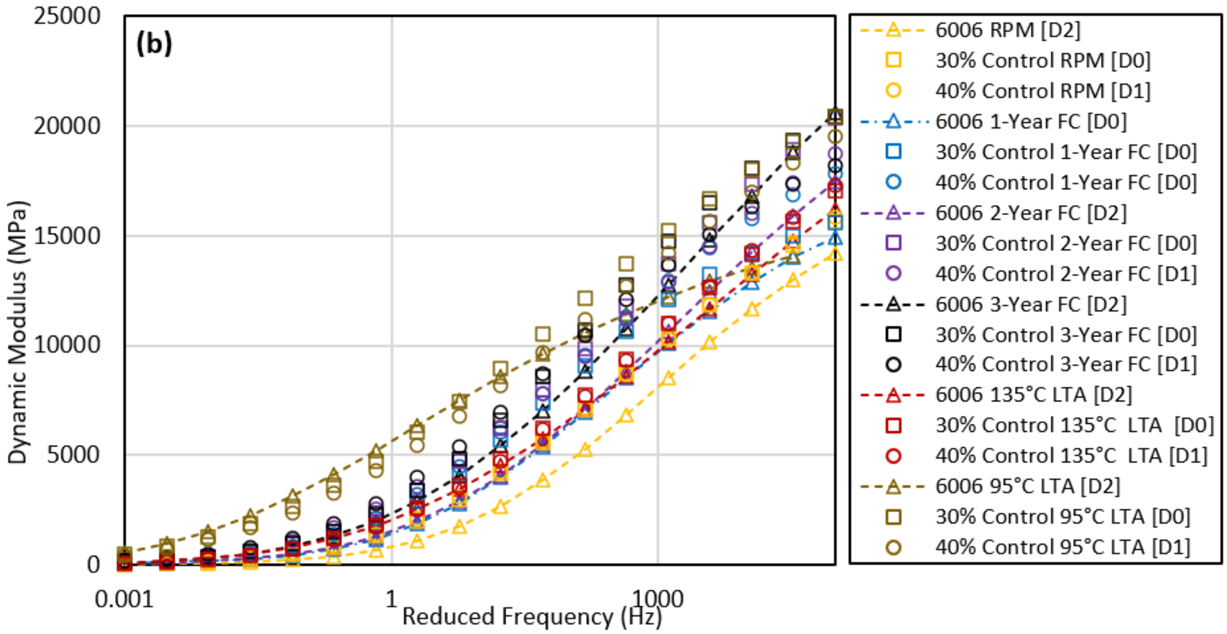

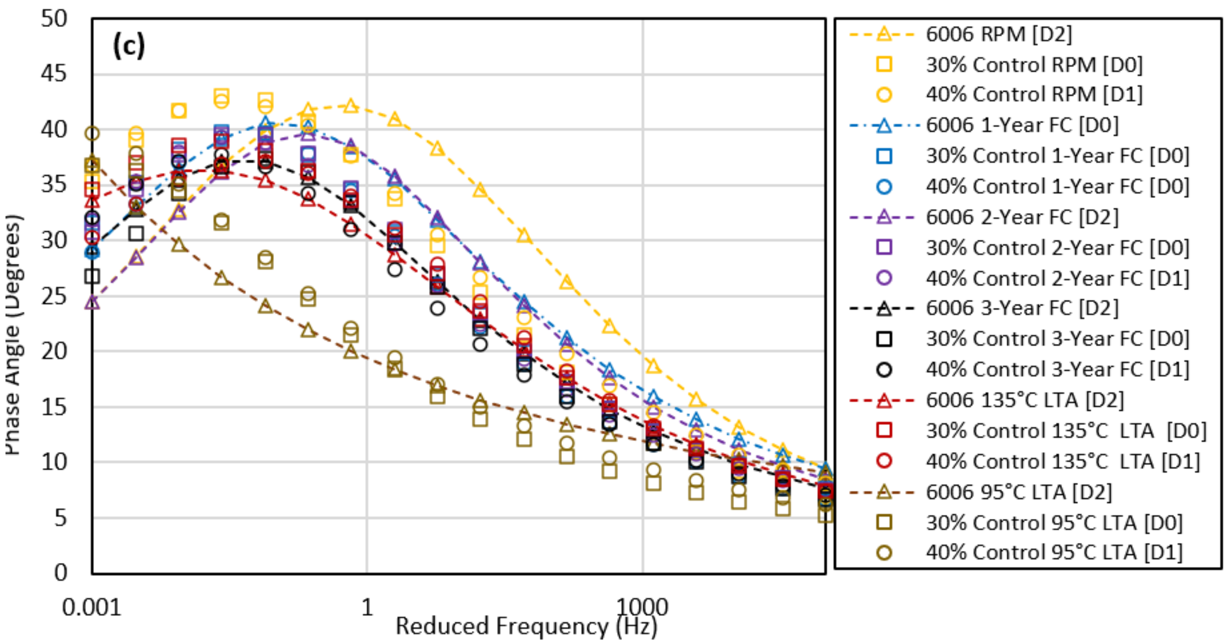

Figure A-29 Master Curves of (a) Dynamic Modulus (Linear Scale) (b) Dynamic Modulus (Logarithmic Scale) and (c) Phase Angle for 6006 Mixture with Different Aging Conditions (Ref. 21.1°C)

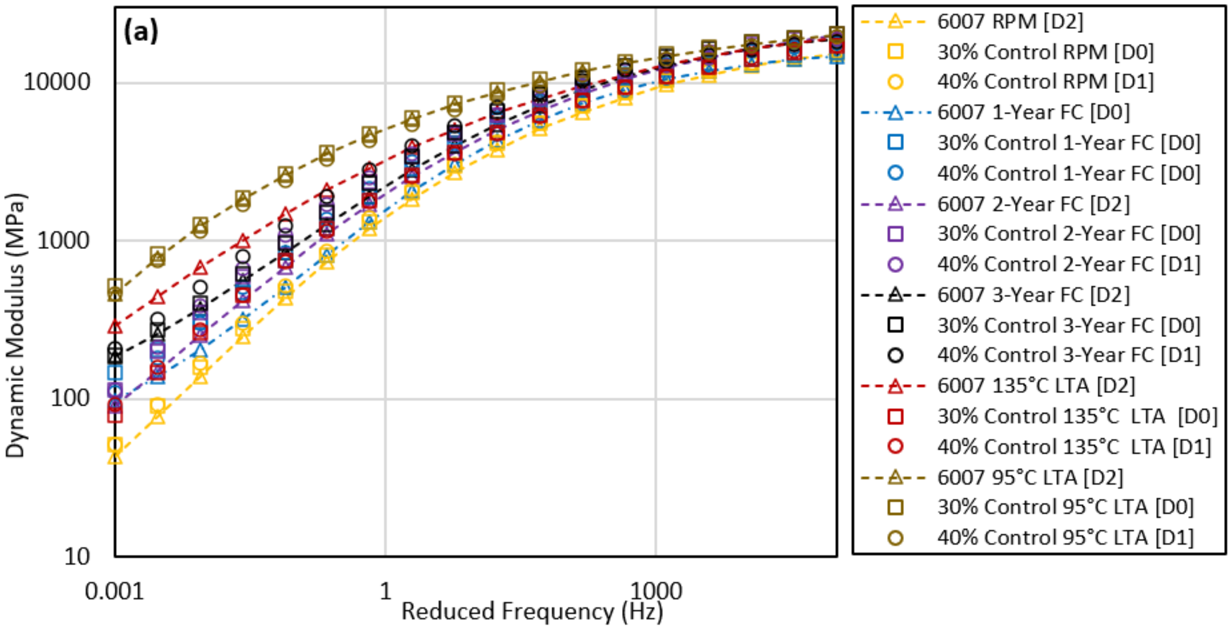
(a)
10000
1000
100
10
0.001
1
1000
Reduced Frequency (Hz)
Dynamic Modulus (MPa)
6007 RPM [D2]
30% Control RPM [D0]
40% Control RPM [D1]
6007 1-Year FC [D0]
30% Control 1-Year FC [D0]
40% Control 1-Year FC [D0]
6007 2-Year FC [D2]
30% Control 2-Year FC [D0]
40% Control 2-Year FC [D1]
6007 3-Year FC [D2]
30% Control 3-Year FC [D0]
40% Control 3-Year FC [D1]
6007 135°C LTA [D2]
30% Control 135°C LTA [D0]
40% Control 135°C LTA [D1]
6007 95°C LTA [D2]
30% Control 95°C LTA [D0]
40% Control 95°C LTA [D1]

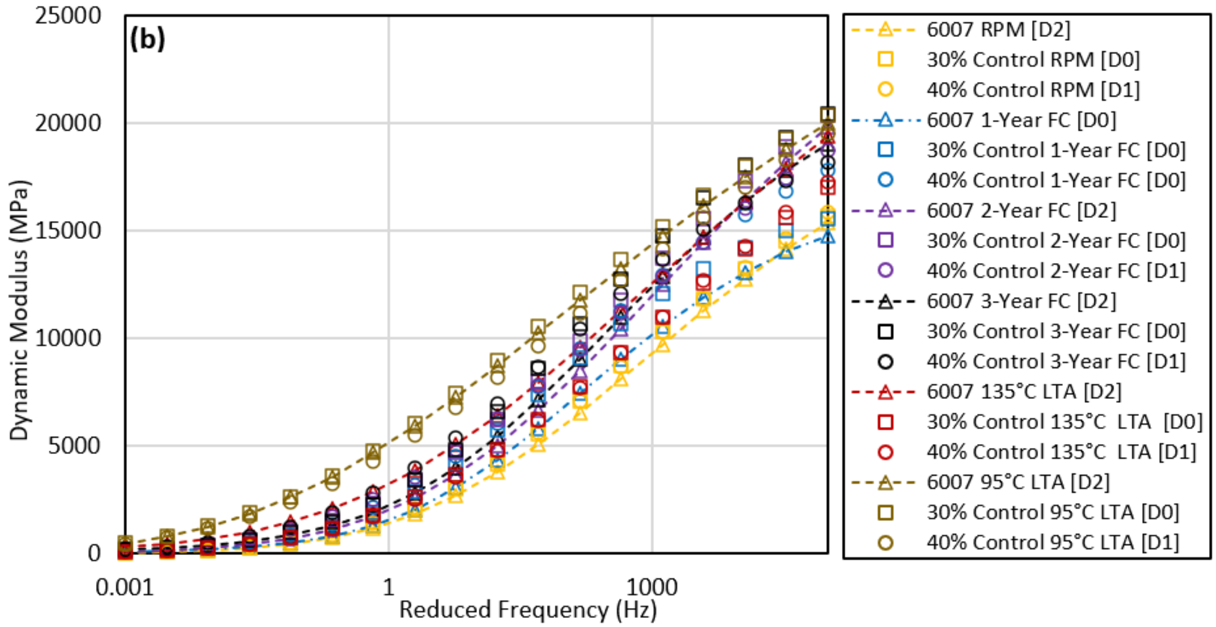
(b)
25000
20000
15000
10000
5000
0
0.001
1
1000
Reduced Frequency (Hz)
Dynamic Modulus (MPa)
6007 RPM [D2]
30% Control RPM [D0]
40% Control RPM [D1]
6007 1-Year FC [D0]
30% Control 1-Year FC [D0]
40% Control 1-Year FC [D0]
6007 2-Year FC [D2]
30% Control 2-Year FC [D0]
40% Control 2-Year FC [D1]
6007 3-Year FC [D2]
30% Control 3-Year FC [D0]
40% Control 3-Year FC [D1]
6007 135°C LTA [D2]
30% Control 135°C LTA [D0]
40% Control 135°C LTA [D1]
6007 95°C LTA [D2]
30% Control 95°C LTA [D0]
40% Control 95°C LTA [D1]

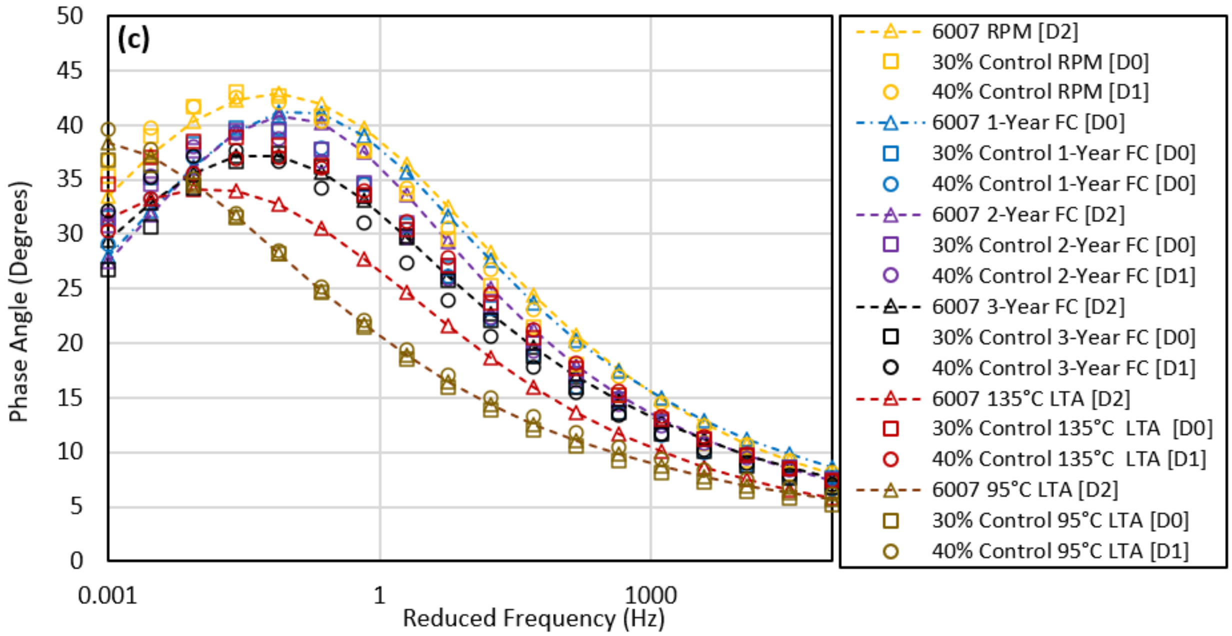

Figure A-30 Master Curves of (a) Dynamic Modulus (Linear Scale) (b) Dynamic Modulus (Logarithmic Scale) and (c) Phase Angle for 6007 Mixture with Different Aging Conditions (Ref. 21.1°C)

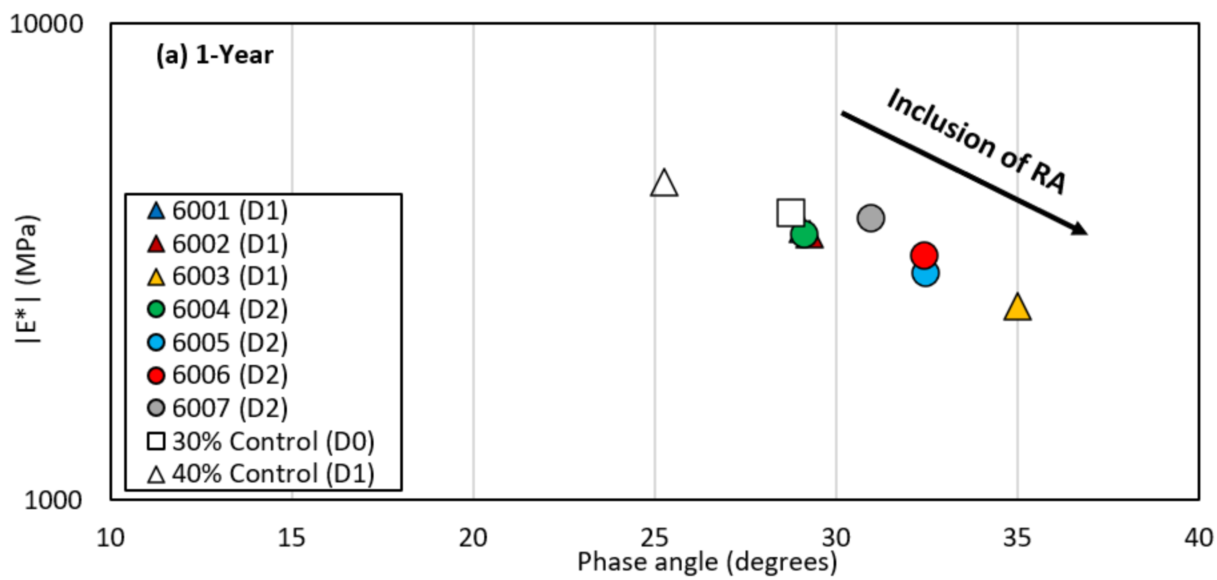

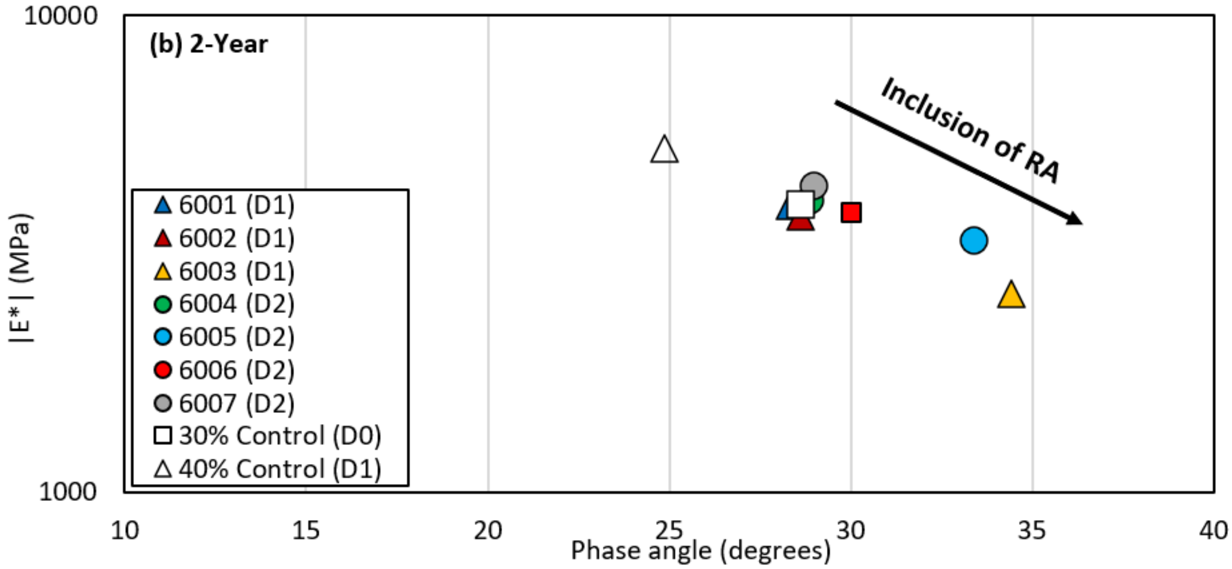
(b) 2-Year
Inclusion of RA
|E*| (MPa)
10000
1000
Phase angle (degrees)
10
15
20
25
30
35
40
6001 (D1)
6002 (D1)
6003 (D1)
6004 (D2)
6005 (D2)
6006 (D2)
6007 (D2)
30% Control (D0)
40% Control (D1)

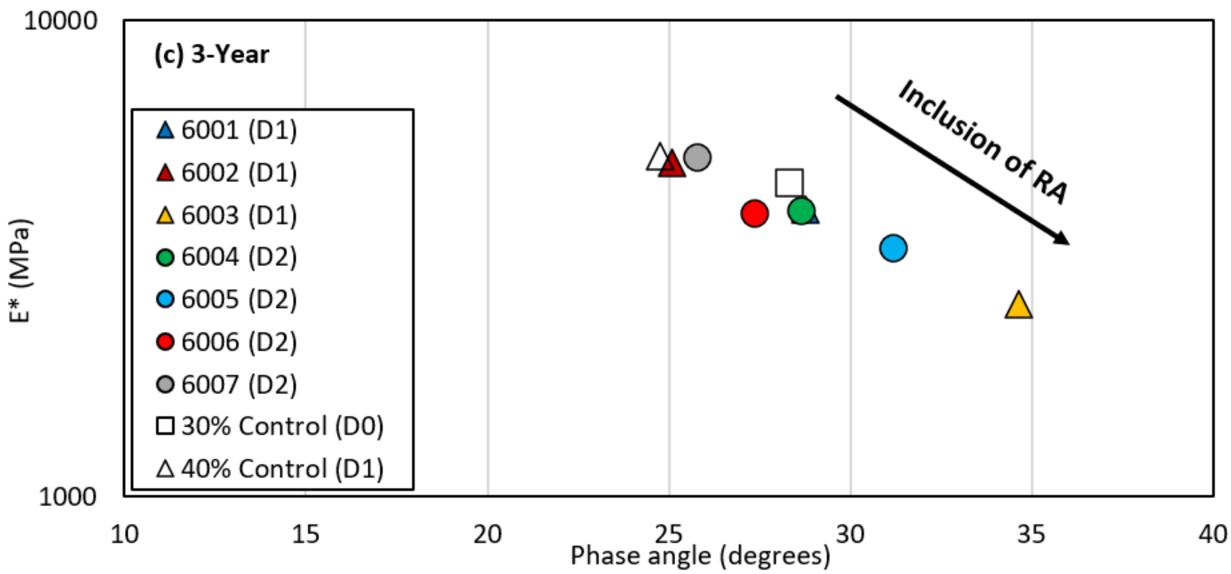
(c) 3-Year
Inclusion of RA
E* (MPa)
10000
1000
Phase angle (degrees)
10
15
20
25
30
35
40
6001 (D1)
6002 (D1)
6003 (D1)
6004 (D2)
6005 (D2)
6006 (D2)
6007 (D2)
30% Control (D0)
40% Control (D1)

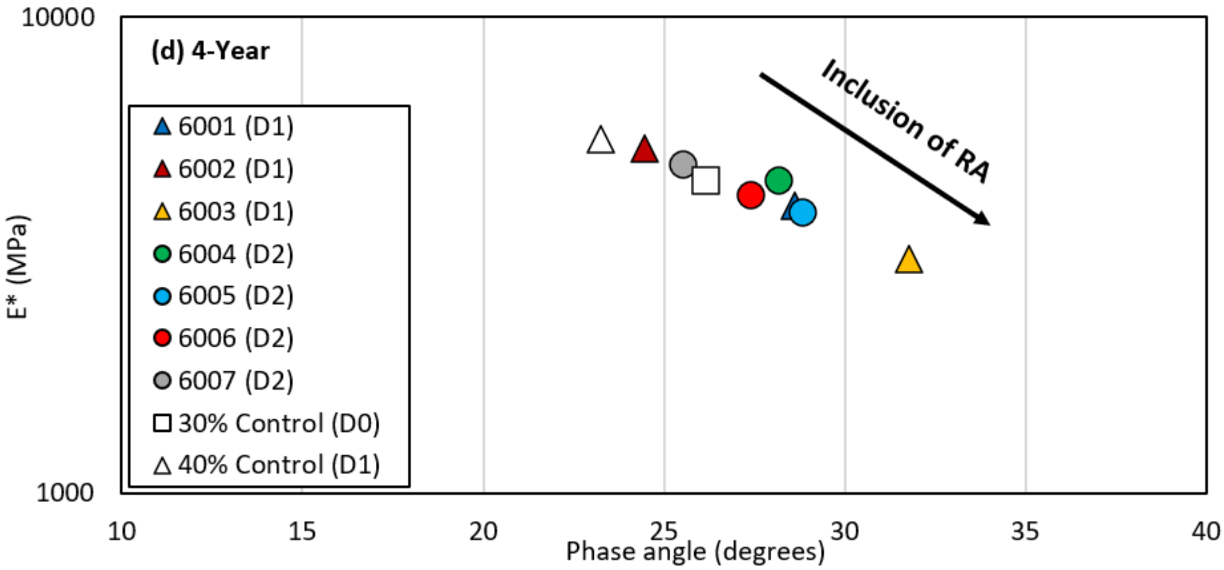

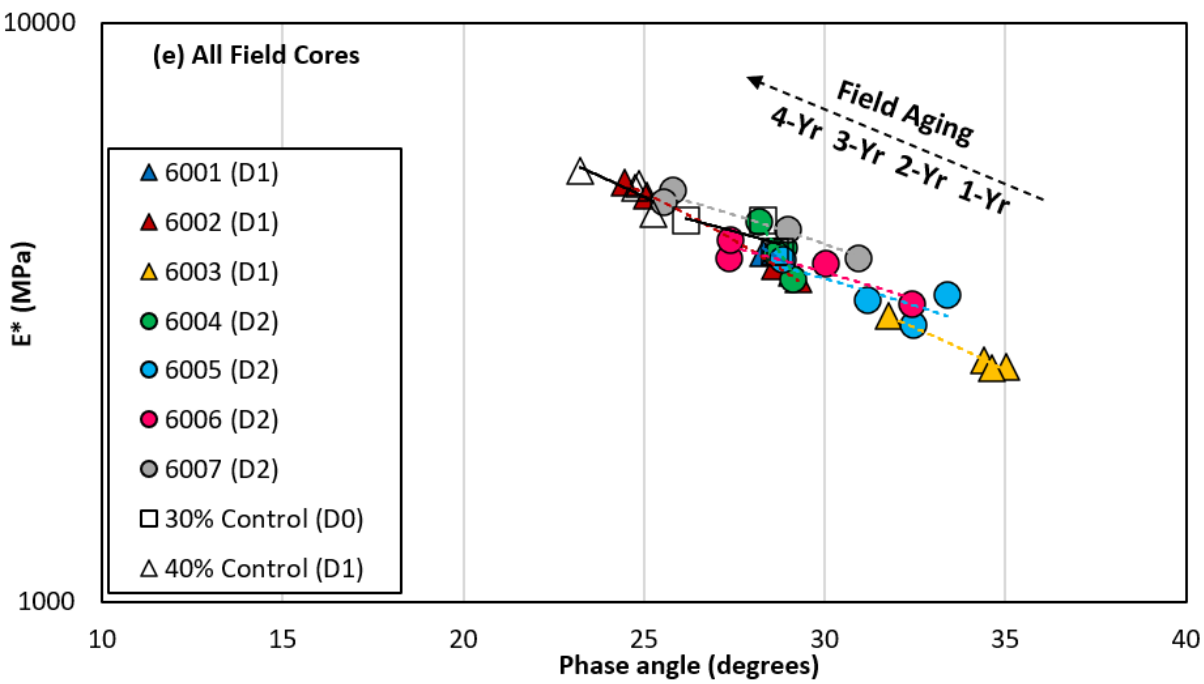

Figure A-31 Mixture Black Space Plot for Field Cores; (a) 1-Year FC, (b) 2-Year FC, (c) 3-Year FC, (d) 4-Year FC (e) All Field Cores (Temperature=20°C; Frequency=5Hz)

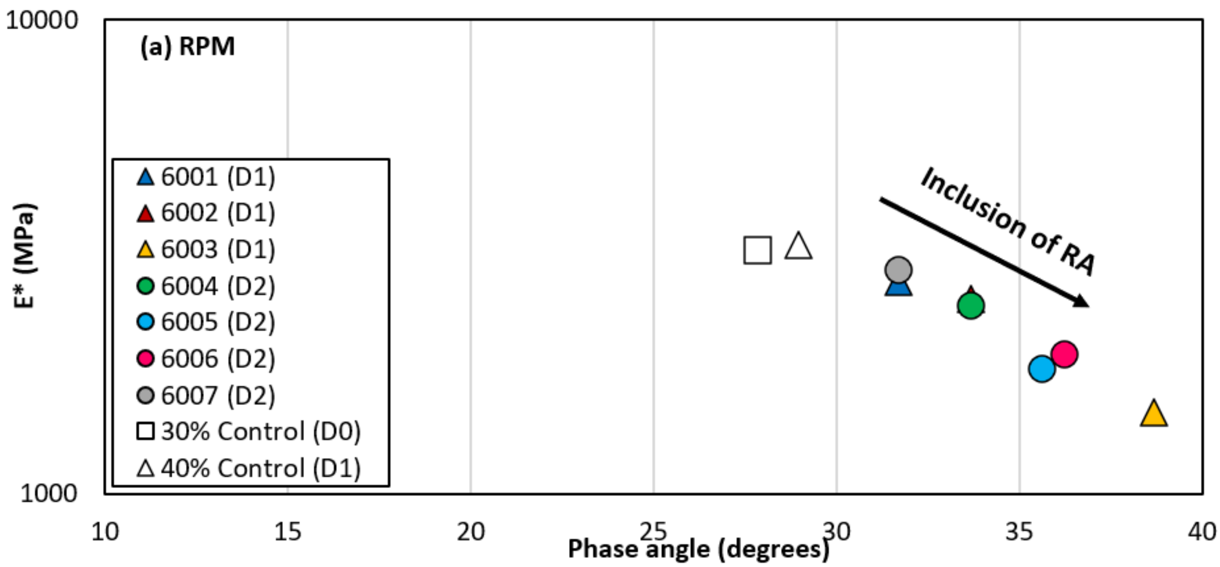
(a) RPM
E* (MPa)
Phase angle (degrees)
Inclusion of RA
6001 (D1)
6002 (D1)
6003 (D1)
6004 (D2)
6005 (D2)
6006 (D2)
6007 (D2)
30% Control (D0)
40% Control (D1)
10000
1000
10
15
20
25
30
35
40

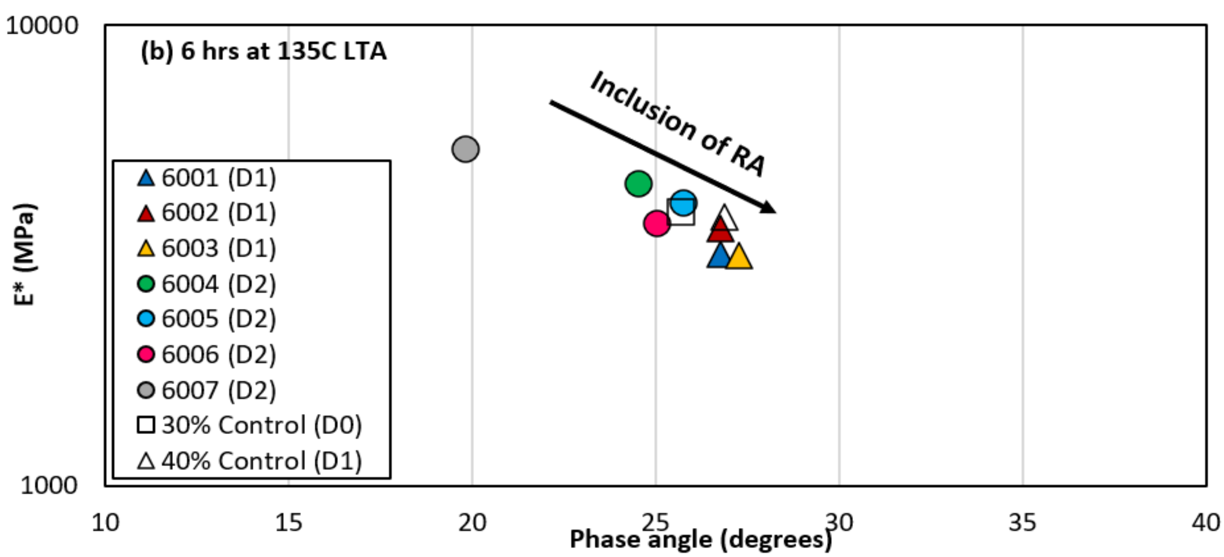
(b) 6 hrs at 135C LTA
E* (MPa)
Phase angle (degrees)
Inclusion of RA
6001 (D1)
6002 (D1)
6003 (D1)
6004 (D2)
6005 (D2)
6006 (D2)
6007 (D2)
30% Control (D0)
40% Control (D1)
10000
1000
10
15
20
25
30
35
40

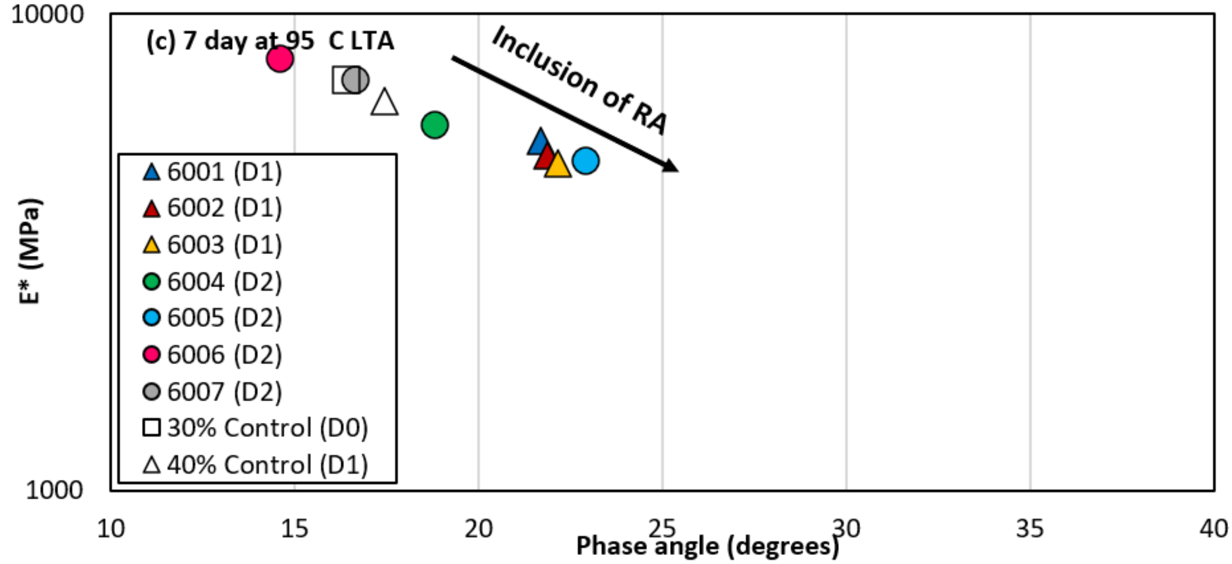

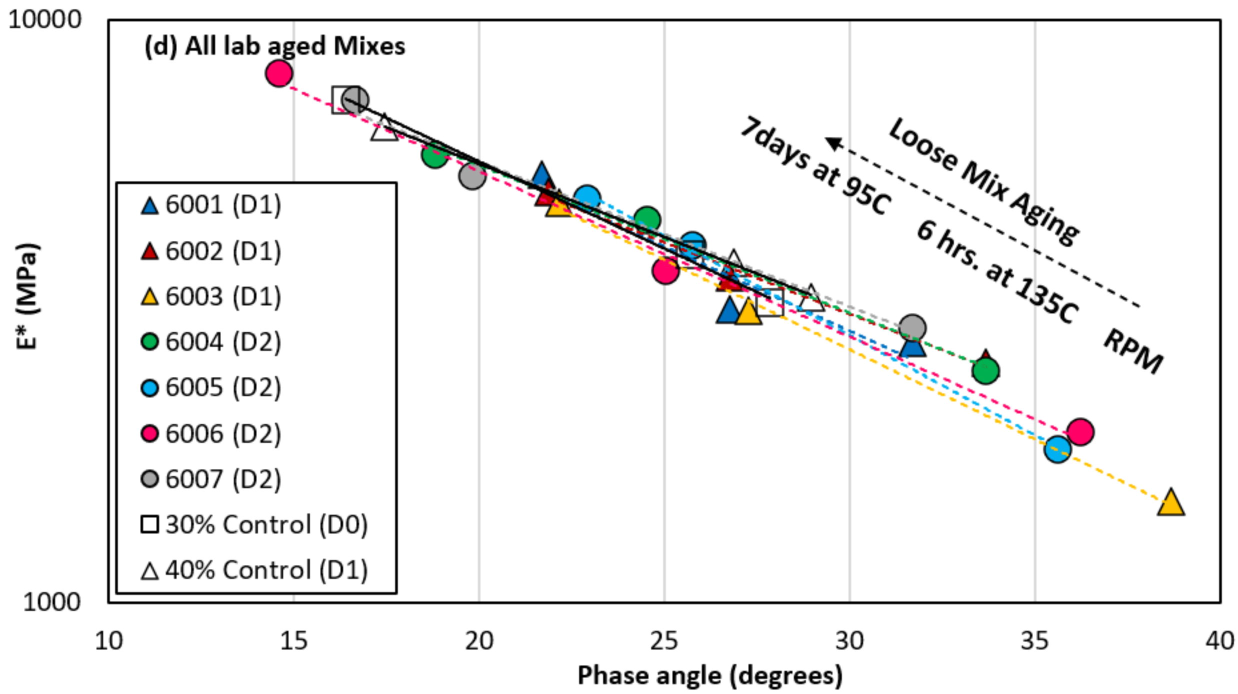

Figure A-32 Mixture Black Space Plot for Lab Aged Mixtures; (a) RPM, (b) 6 hrs. at 135C LTA, (c) 7 day at 95 C LTA, (d) All Lab aged mixes (Temperature=20°C; Frequency=5Hz)

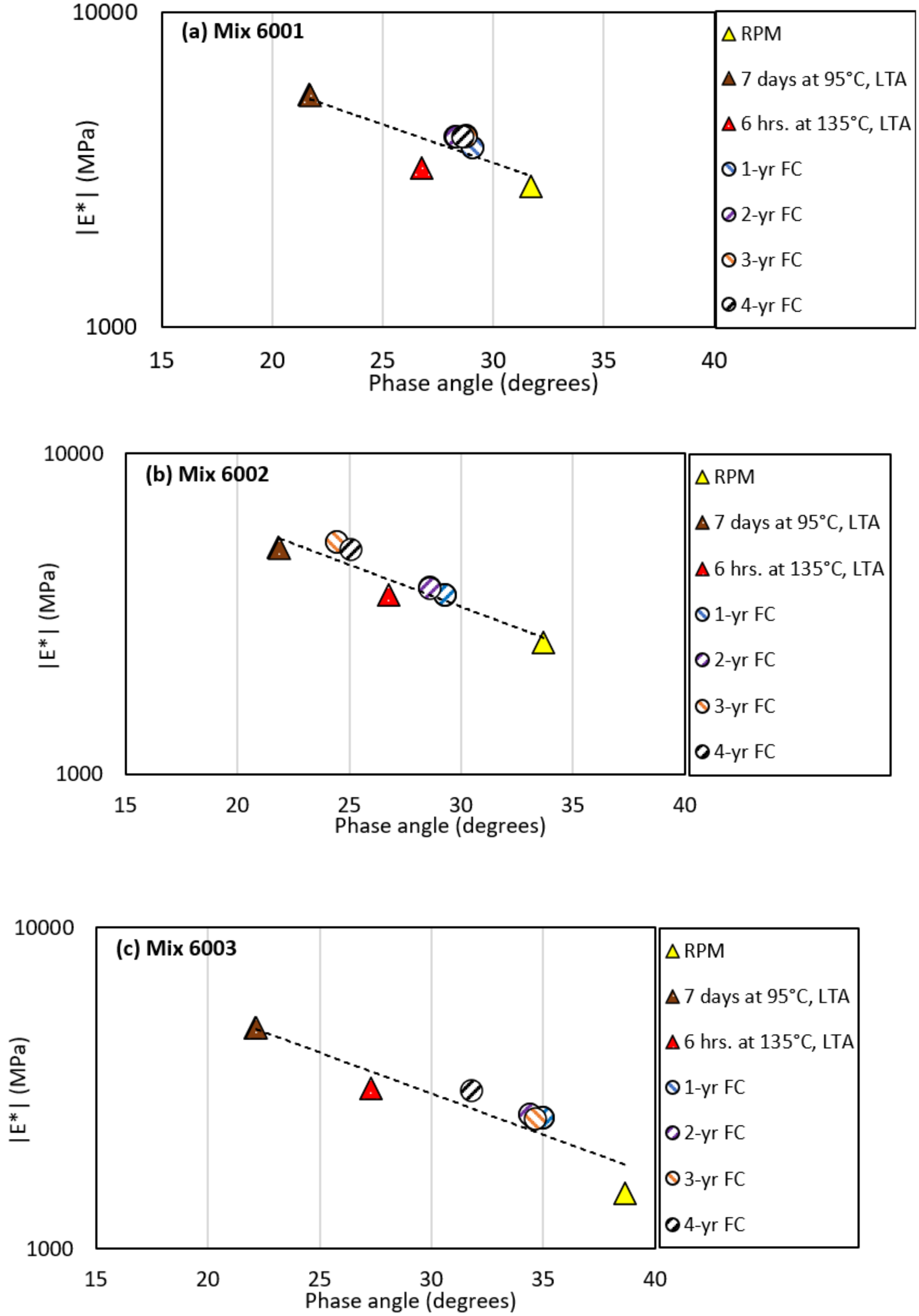

Figure A-33 Black Space Analysis of D1 RA Mixtures. (a) 6001 Mix (b) 6002 Mix (c) 6003 Mix

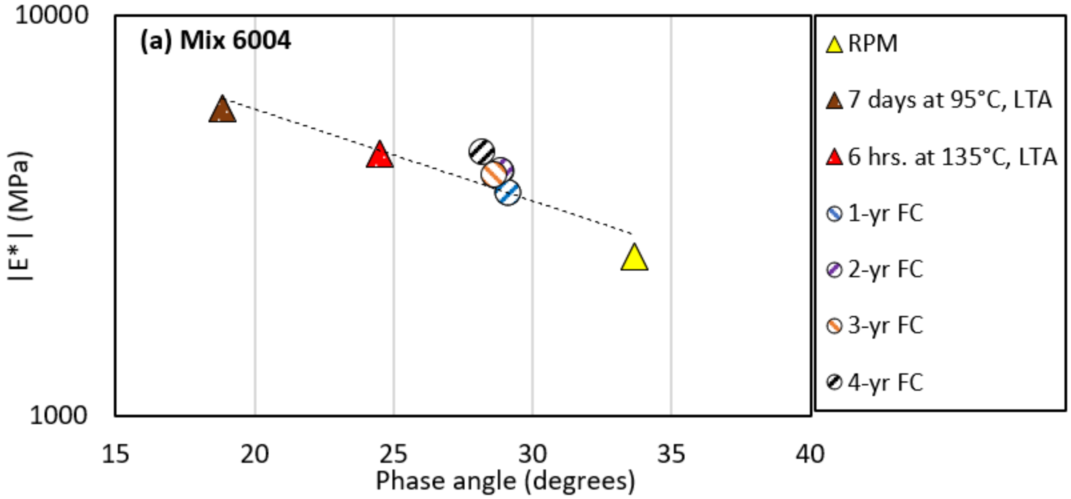
(a) Mix 6004
10000
1000
|E*| (MPa)
15
20
25
30
35
40
Phase angle (degrees)
RPM
7 days at 95°C, LTA
6 hrs. at 135°C, LTA
1-yr FC
2-yr FC
3-yr FC
4-yr FC

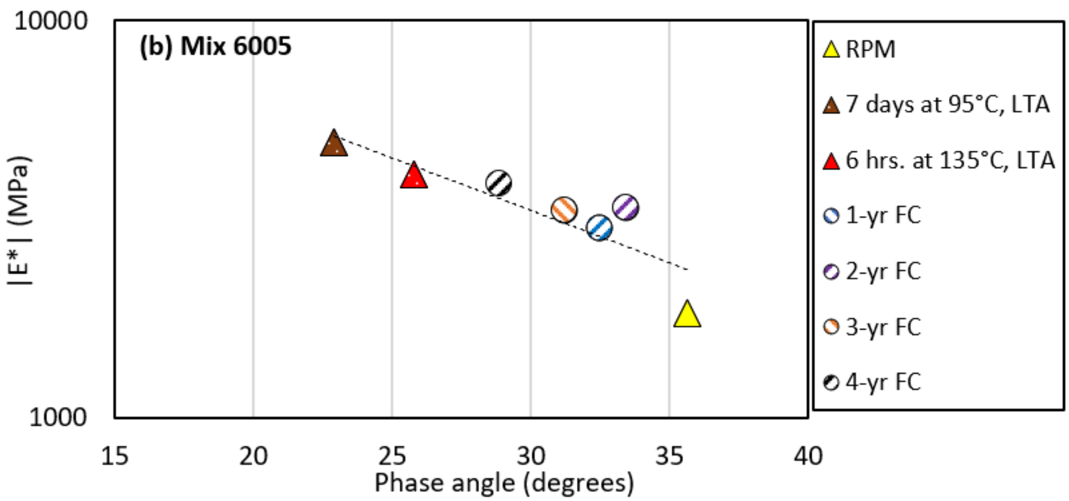
(b) Mix 6005
10000
1000
|E*| (MPa)
15
20
25
30
35
40
Phase angle (degrees)
RPM
7 days at 95°C, LTA
6 hrs. at 135°C, LTA
1-yr FC
2-yr FC
3-yr FC
4-yr FC

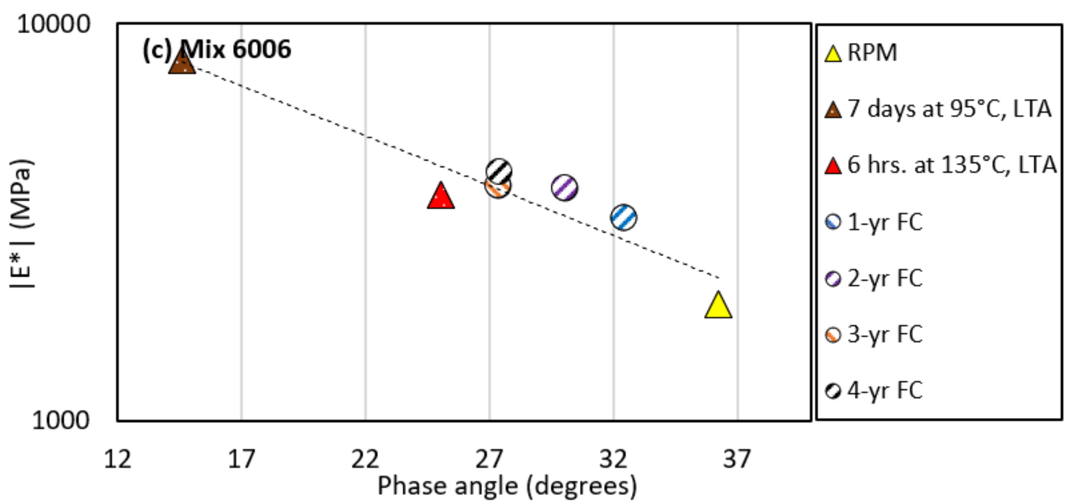
(c) Mix 6006
10000
1000
|E*| (MPa)
12
17
22
27
32
37
Phase angle (degrees)
RPM
7 days at 95°C, LTA
6 hrs. at 135°C, LTA
1-yr FC
2-yr FC
3-yr FC
4-yr FC

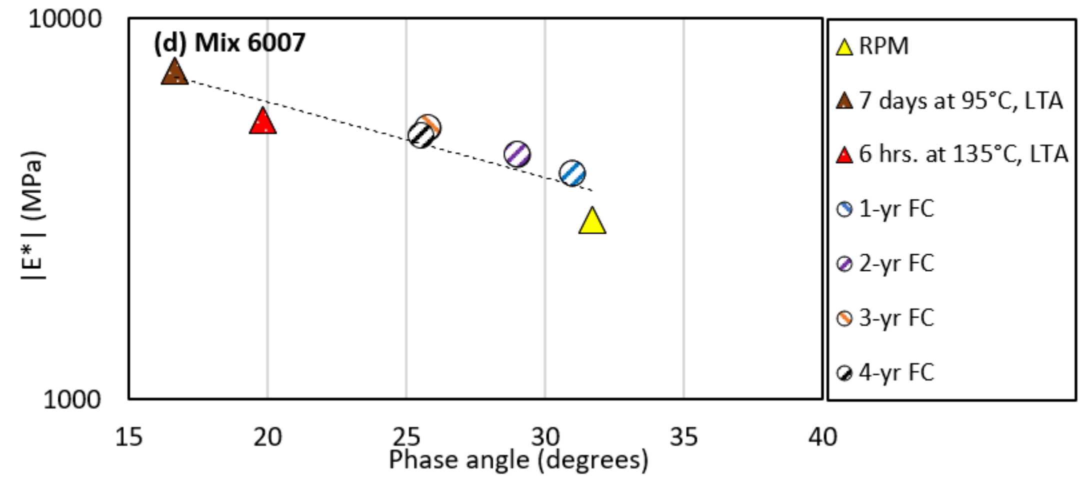

Figure A-34 Black Space Analysis of D2 RA Mixtures. (a) 6004 Mix (b) 6005 Mix (c) 6006 Mix (d) 6007 Mix

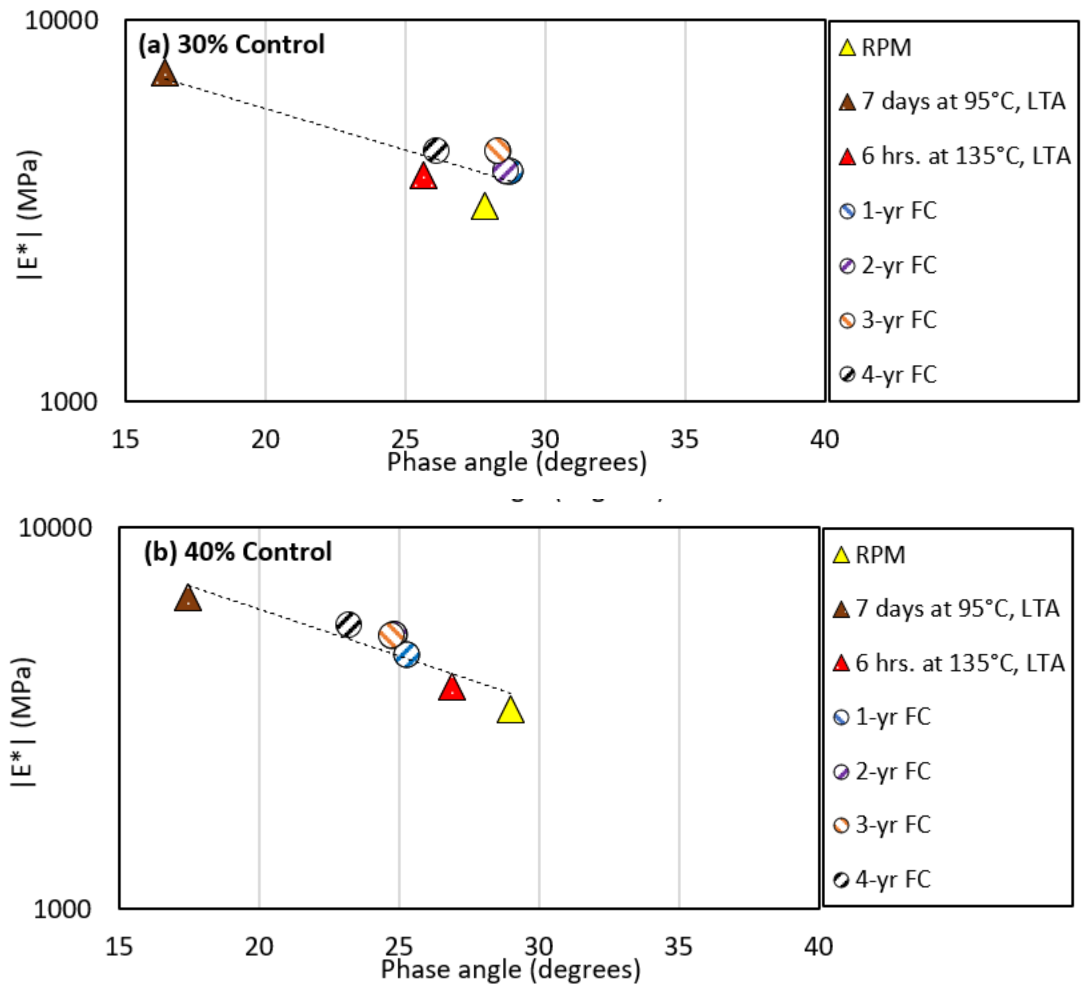

Figure A-35 Black Space Analysis Control Mixes (a) 30% Control Mix (b) 40% Control Mix

Table A-1: Summary of SARA and FTIR Results – Sections 6001–- 6004

Section	Aging	SARA Fractions					FTIR		
		Asphaltenes	Resins	Cyclics	Saturates	CI	Carbonyl Ratio	Sulfoxide Ratio	Carbonyls + Sulfoxides
6001	As-Recovered	19.1	38.7	35.6	6.6	2.891	0.153	0.268	0.421
	20 hr PAV	22.9	42.6	27.7	6.8	2.367	0.234	0.35	0.584
	40 hr PAV	25.9	41	26.2	6.8	2.055	0.286	0.374	0.66
	60 hr PAV	28.7	39.1	24.7	7.4	1.767	0.332	0.371	0.703
6002	As-Recovered	18	34.7	41	6.3	3.115	0.142	0.28	0.422
	20 hr PAV	22.8	36.7	33.5	7	2.356	0.213	0.374	0.587
	40 hr PAV	26.3	38.5	28.6	6.6	2.04	0.265	0.392	0.657
	60 hr PAV	27.7	39	26.6	6.6	1.913	0.315	0.402	0.717
6003	As-Recovered	18.6	35	40.4	6	3.065	0.165	0.281	0.446
	20 hr PAV	22.7	39.1	31.7	6.6	2.416	0.229	0.368	0.597
	40 hr PAV	25.5	39.1	28.3	7.2	2.061	0.276	0.356	0.632
	60 hr PAV	28.4	38.4	25.3	7.9	1.755	0.328	0.418	0.746
6004	As-Recovered	20	40.6	33.3	6.1	2.831	0.127	0.516	0.643
	20 hr PAV	24.7	39	30.2	6	2.254	0.197	0.506	0.703
	40 hr PAV	26.8	37.9	28.6	6.8	1.979	0.249	0.506	0.755
	60 hr PAV	28.8	37.3	26.7	7.2	1.778	0.285	0.495	0.78
6005	As-Recovered	20.4	39.5	33.4	6.7	2.69	0.19	0.399	0.589
	20 hr PAV	24.7	38	30.5	6.8	2.175	0.259	0.39	0.649
	40 hr PAV	26.5	38.2	27.9	7.4	1.95	0.305	0.437	0.742
	60 hr PAV	27.8	39.5	25.3	7.3	1.846	0.349	0.419	0.768

Table A-2: Summary of SARA and FTIR Results – Sections 6006-6012

Section	Aging	SARA Fractions					FTIR		
		Asphaltenes	Resins	Cyclics	Saturates	CI	Carbonyl Ratio	Sulfoxide Ratio	Carbonyls + Sulfoxides
6006	As-Recovered	24.4	44.3	25.1	6.2	2.268	0.259	0.487	0.746
	20 hr PAV	27.5	44	21.6	6.9	1.907	0.335	0.398	0.733
	40 hr PAV	29.8	44.9	18.3	7	1.717	0.366	0.416	0.782
	60 hr PAV	31.7	42.3	18.8	7.3	1.567	0.414	0.412	0.826
6007	As-Recovered	23.2	43.2	27.4	6.2	2.401	0.221	0.462	0.683
	20 hr PAV	27.1	40.8	26	6.1	2.012	0.298	0.43	0.728
	40 hr PAV	29.2	40.5	23	7.3	1.74	0.335	0.461	0.796
	60 hr PAV	31.3	38.4	23	7.3	1.591	0.386	0.474	0.86
6010	As-Recovered	19.5	38.8	34.6	7	2.77	0.066	0.359	0.425
	20 hr PAV	24.1	38	30.9	6.9	2.223	0.12	0.396	0.516
	40 hr PAV	25.9	37.7	28.7	7.7	1.976	0.16	0.363	0.523
	60 hr PAV	27.7	36.5	28.2	7.6	1.833	0.195	0.4	0.595
6011	As-Recovered	20.5	39.9	33.9	5.7	2.817	0.073	0.338	0.411
	20 hr PAV	24.9	44.3	24.9	5.9	2.247	0.15	0.341	0.491
	40 hr PAV	26.6	41.6	24.9	6.9	1.985	0.186	0.401	0.587
	60 hr PAV	28.4	43	21.4	7.2	1.809	0.218	0.37	0.588
6012	As-Recovered	18.4	34.4	41.3	5.9	3.115	0.064	0.293	0.357
	20 hr PAV	22.6	38.4	32	7	2.378	0.122	0.394	0.516
	40 hr PAV	25.7	39	27.9	7.5	2.015	0.17	0.314	0.484
	60 r PAV	27.6	38.5	26.6	7.3	1.865	0.199	0.417	0.616